CALCIUM AND HEART FAILURE: FROM BENCH TO BEDSIDE

EDITED BY: Elisabetta Cerbai, Alessandro Mugelli and Daniel M. Johnson
PUBLISHED IN: Frontiers in Physiology and Frontiers in Pharmacology

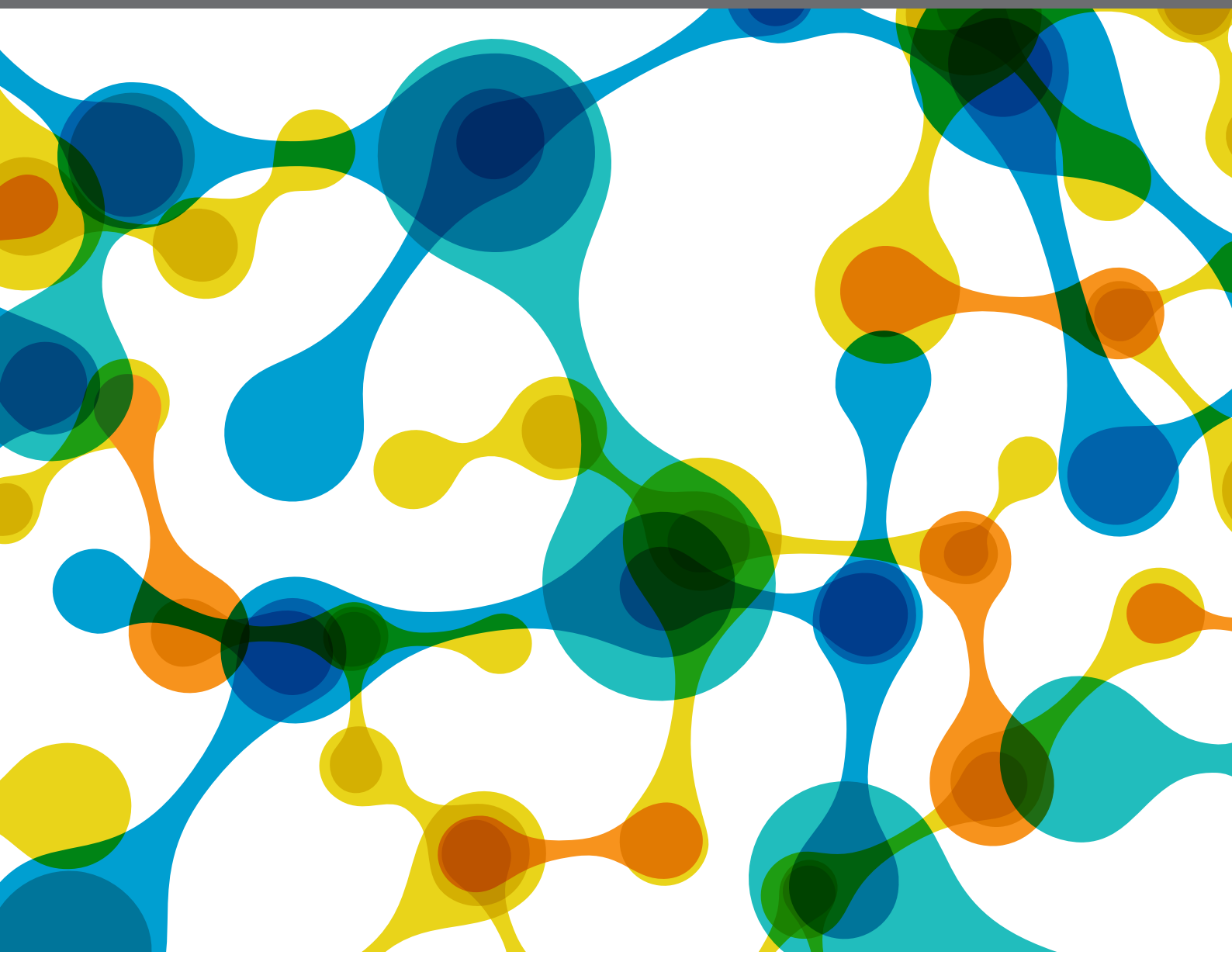

frontiers Research Topics

frontiers

ISSN 1664-8714
ISBN 978-2-88976-554-6
DOI 10.3389/978-2-88976-554-6

About Frontiers

Frontiers is more than just an open-access publisher of scholarly articles: it is a pioneering approach to the world of academia, radically improving the way scholarly research is managed. The grand vision of Frontiers is a world where all people have an equal opportunity to seek, share and generate knowledge. Frontiers provides immediate and permanent online open access to all its publications, but this alone is not enough to realize our grand goals.

Frontiers Journal Series

The Frontiers Journal Series is a multi-tier and interdisciplinary set of open-access, online journals, promising a paradigm shift from the current review, selection and dissemination processes in academic publishing. All Frontiers journals are driven by researchers for researchers; therefore, they constitute a service to the scholarly community. At the same time, the Frontiers Journal Series operates on a revolutionary invention, the tiered publishing system, initially addressing specific communities of scholars, and gradually climbing up to broader public understanding, thus serving the interests of the lay society, too.

Dedication to Quality

Each Frontiers article is a landmark of the highest quality, thanks to genuinely collaborative interactions between authors and review editors, who include some of the world's best academicians. Research must be certified by peers before entering a stream of knowledge that may eventually reach the public - and shape society; therefore, Frontiers only applies the most rigorous and unbiased reviews.
Frontiers revolutionizes research publishing by freely delivering the most outstanding research, evaluated with no bias from both the academic and social point of view. By applying the most advanced information technologies, Frontiers is catapulting scholarly publishing into a new generation.

What are Frontiers Research Topics?

Frontiers Research Topics are very popular trademarks of the Frontiers Journals Series: they are collections of at least ten articles, all centered on a particular subject. With their unique mix of varied contributions from Original Research to Review Articles, Frontiers Research Topics unify the most influential researchers, the latest key findings and historical advances in a hot research area! Find out more on how to host your own Frontiers Research Topic or contribute to one as an author by contacting the Frontiers Editorial Office: frontiersin.org/about/contact

CALCIUM AND HEART FAILURE: FROM BENCH TO BEDSIDE

Topic Editors:
Elisabetta Cerbai, University of Florence, Italy
Alessandro Mugelli, University of Florence, Italy
Daniel M. Johnson, The Open University, United Kingdom

Citation: Cerbai, E., Mugelli, A., Johnson, D. M., eds. (2022). Calcium and Heart Failure: From Bench to Bedside. Lausanne: Frontiers Media SA.
doi: 10.3389/978-2-88976-554-6

Table of Contents

frontiers in Physiology

ORIGINAL RESEARCH
published: 11 May 2021
doi: 10.3389/fphys.2021.656516

Role of Reduced Sarco-Endoplasmic Reticulum Ca^{2+}-ATPase Function on Sarcoplasmic Reticulum Ca^{2+} Alternans in the Intact Rabbit Heart

*Lianguo Wang[1], Rachel C. Myles[2], I-Ju Lee[1], Donald M. Bers[1] and Crystal M. Ripplinger[1]**

[1] Department of Pharmacology, School of Medicine, University of California, Davis, Davis, CA, United States, [2] Institute of Cardiovascular and Medical Sciences, University of Glasgow, Glasgow, United Kingdom

Sarcoplasmic reticulum (SR) Ca^{2+} cycling is tightly regulated by ryanodine receptor (RyR) Ca^{2+} release and sarco-endoplasmic reticulum Ca^{2+}-ATPase (SERCA) Ca^{2+} uptake during each excitation–contraction coupling cycle. We previously showed that RyR refractoriness plays a key role in the onset of SR Ca^{2+} alternans in the intact rabbit heart, which contributes to arrhythmogenic action potential duration (APD) alternans. Recent studies have also implicated impaired SERCA function, a key feature of heart failure, in cardiac alternans and arrhythmias. However, the relationship between reduced SERCA function and SR Ca^{2+} alternans is not well understood. Simultaneous optical mapping of transmembrane potential (V_m) and SR Ca^{2+} was performed in isolated rabbit hearts ($n = 10$) using the voltage-sensitive dye RH237 and the low-affinity Ca^{2+} indicator Fluo-5N-AM. Alternans was induced by rapid ventricular pacing. SERCA was inhibited with cyclopiazonic acid (CPA; 1–10 μM). SERCA inhibition (1, 5, and 10 μM of CPA) resulted in dose-dependent slowing of SR Ca^{2+} reuptake, with the time constant (*tau*) increasing from 70.8 ± 3.5 ms at baseline to 85.5 ± 6.6, 129.9 ± 20.7, and 271.3 ± 37.6 ms, respectively ($p < 0.05$ vs. baseline for all doses). At fast pacing frequencies, CPA significantly increased the magnitude of SR Ca^{2+} and APD alternans, most strongly at 10 μM (pacing cycle length = 220 ms: SR Ca^{2+} alternans magnitude: 57.1 ± 4.7 vs. 13.4 ± 8.9 AU; APD alternans magnitude 3.8 ± 1.9 vs. 0.2 ± 0.19 AU; $p < 0.05$ 10 μM of CPA vs. baseline for both). SERCA inhibition also promoted the emergence of spatially discordant alternans. Notably, at all CPA doses, alternation of SR Ca^{2+} release occurred prior to alternation of diastolic SR Ca^{2+} load as pacing frequency increased. Simultaneous optical mapping of SR Ca^{2+} and V_m in the intact rabbit heart revealed that SERCA inhibition exacerbates pacing-induced SR Ca^{2+} and APD alternans magnitude, particularly at fast pacing frequencies. Importantly, SR Ca^{2+} release alternans always occurred before the onset of SR Ca^{2+} load alternans. These findings suggest that even in settings of diminished SERCA function, relative refractoriness of RyR Ca^{2+} release governs the onset of intracellular Ca^{2+} alternans.

Keywords: sarco-endoplasmic reticulum Ca^{2+}-ATPase, sarcoplasmic reticulum Ca^{2+}, optical mapping, alternans, arrhythmia

OPEN ACCESS

Edited by:
Daniel M. Johnson, The Open University, United Kingdom

Reviewed by:
Christopher O'Shea, University of Birmingham, United Kingdom
Kenneth Laurita, Case Western Reserve University, United States
Antonio Zaza, University of Milano-Bicocca, Italy

****Correspondence:***
Crystal M. Ripplinger
cripplinger@ucdavis.edu

Specialty section:
This article was submitted to Cardiac Electrophysiology, a section of the journal Frontiers in Physiology

Received: *20 January 2021*
Accepted: *29 March 2021*
Published: *11 May 2021*

Citation:
Wang L, Myles RC, Lee I-J, Bers DM and Ripplinger CM (2021) Role of Reduced Sarco-Endoplasmic Reticulum Ca^{2+}-ATPase Function on Sarcoplasmic Reticulum Ca^{2+} Alternans in the Intact Rabbit Heart. Front. Physiol. 12:656516. doi: 10.3389/fphys.2021.656516

INTRODUCTION

In mammalian hearts, Ca^{2+} release from and reuptake into the sarcoplasmic reticulum (SR) is tightly regulated for proper excitation–contraction coupling (ECC) (Bers, 2002a). At steady state, during each ECC cycle, Ca^{2+} is released from the SR through ryanodine receptors (RyRs) during systole, and the same amount of Ca^{2+} is taken back up by the sarco-endoplasmic reticulum Ca^{2+}-ATPase (SERCA) pump during diastole. At rapid rates, beat-to-beat alternation in the amount of Ca^{2+} released from the SR has been demonstrated to underlie the development of repolarization alternans (Chudin et al., 1999; Diaz et al., 2004; Goldhaber et al., 2005; Picht et al., 2006; Laurita and Rosenbaum, 2008; Bayer et al., 2010; Alvarez-Lacalle et al., 2013), which can lead to lethal ventricular arrhythmias in patients (Gehi et al., 2005; Verrier et al., 2011). Several recent studies have shown that RyR function and expression play a key role in the onset of Ca^{2+} alternans (Kornyeyev et al., 2012; Wang et al., 2014; Zhong et al., 2016; Sun et al., 2018; Zhong et al., 2018). For example, using optical mapping of free intra-SR Ca^{2+} in the intact rabbit heart, we showed that as heart rate increases, SR Ca^{2+} release begins to alternate without appreciable changes in diastolic SR Ca^{2+} load, suggesting that refractoriness of RyR Ca^{2+} release governs the onset of alternans (Wang et al., 2014). Indeed, in that study, sensitizing RyR with low-dose caffeine delayed the onset and reduced the magnitude of SR Ca^{2+} and resulting action potential (AP) duration (APD) alternans (Wang et al., 2014). Several recent studies in mouse hearts and myocytes have revealed that either reduced expression or loss of function of RyR exacerbates intracellular Ca^{2+} alternans (Zhong et al., 2016; Sun et al., 2018), whereas gain of function in RyR reduces Ca^{2+} alternans (Kornyeyev et al., 2012; Sun et al., 2018). However, the relationship between reduced SERCA function, as occurs in failing hearts, and SR Ca^{2+} alternans is not as straightforward.

Impaired SERCA function occurs in heart failure (HF) (Sakata et al., 2007; Kawase et al., 2008; Jessup et al., 2011; Zsebo et al., 2014) and is known to potentiate intracellular Ca^{2+} alternans, presumably due to insufficient Ca^{2+} reuptake during diastole and subsequent alternation of SR Ca^{2+} load (Wilson et al., 2009). Because SR Ca^{2+} release is steeply dependent on SR Ca^{2+} load (Bers, 2001, 2002a, 2014), insufficient Ca^{2+} reuptake and beat-to-beat alternation in SR Ca^{2+} load could therefore cause alternation of SR Ca^{2+} release (Diaz et al., 2004; Xie et al., 2008; Zhou et al., 2016). Indeed, detailed mechanistic studies in isolated cardiomyocytes have confirmed this mechanism (Diaz et al., 2004). Studies in failing hearts have also shown that decreased SERCA expression or activity is associated with Ca^{2+} alternans, and overexpression of the cardiac SERCA pump can suppress Ca^{2+} alternans (Wan et al., 2005; Cutler et al., 2009, 2012). On the other hand, mathematical simulations suggest that severely reducing the activity of SERCA may actually suppress rather than promote Ca^{2+} alternans (Weiss et al., 2006; Qu et al., 2013, 2016). Indeed, a recent experimental study confirmed that severe pharmacological inhibition of SERCA suppressed alternans, but promoting SERCA function via phospholamban knock-out had only a minor effect on Ca^{2+} alternans in both wild-type and RyR loss-of-function mice (Sun et al., 2018). A recent study in the rat heart shows that atrial SERCA overexpression or inhibition had no effect on cardiac alternans (Nassal et al., 2015). These conflicting observations suggest that the effect of altered SERCA activity on the genesis of SR Ca^{2+} alternans is complex and warrants further investigation.

To address the role of reduced SERCA function in contributing to SR Ca^{2+} alternans and subsequent arrhythmogenic APD alternans, we performed optical mapping of free intra-SR Ca^{2+} concomitantly with transmembrane potential (V_m) in intact rabbit hearts. We assessed the impact of reduced SERCA function using cyclopiazonic acid (CPA), a SERCA inhibitor (Szentesi et al., 2004), on SR Ca^{2+} alternans and evaluated whether alternans were driven by beat-to-beat changes in SR Ca^{2+} release and/or diastolic SR Ca^{2+} load. We also determined the relationship between pacing frequency and degree of SERCA inhibition on resulting SR Ca^{2+} and APD alternans magnitude.

Abbreviations: AP, action potential; APD, action potential duration; APD_{80}, action potential duration at 80% repolarization; $Ca^{2+}{}_i$, intracellular Ca^{2+}; $[Ca^{2+}]_{SR}$, intra-sarcoplasmic reticulum free Ca^{2+}; CICR, Ca^{2+}-induced Ca^{2+} release; CPA, cyclopiazonic acid; CV, conduction velocity; ECC, excitation–contraction coupling; ECG, electrocardiogram; I_{Ca}, L-type Ca^{2+} current; LV, left ventricle; NCX, Na^+–Ca^{2+} exchanger; PCL, pacing cycle length; RyR, ryanodine receptor; S1, cycle length of pacing drive train; S2, cycle length of premature pacing stimulus; SERCA, sarco-endoplasmic reticulum Ca^{2+}-ATPase; SR, sarcoplasmic reticulum; V_m, transmembrane potential; VT/VF, ventricular tachycardia/fibrillation.

MATERIALS AND METHODS

Ethical Approval

All procedures involving animals were approved by the Animal Care and Use Committee of the University of California, Davis (Reference No. 20991), and adhered to the Guide for the Care and Use of Laboratory Animals published by the National Institutes of Health (NIH Publication N0. 85-23, revised 2011). Male New Zealand White rabbits (3.0–3.5 kg, $n = 10$; Charles River Laboratories) were housed on a 12 h light–dark cycle and given access to food and water *ad libitum*.

Whole-Heart Langendorff Perfusion

Rabbit hearts were Langendorff-perfused as described previously (Wang et al., 2014, 2015; Murphy et al., 2017). Briefly, rabbits were administered heparin (1,000 units IV) and were anesthetized with pentobarbital sodium (50 mg/kg IV). After deep anesthesia was achieved, evidenced by lack of eye-blink and foot withdrawal reflexes, a median sternotomy was performed with a vertical midline incision from the substernal notch to the xiphoid process. Hearts were rapidly removed and placed in 200 ml of ice-cold cardioplegia solution (composition in mmol/L: NaCl 110, $CaCl_2$ 1.2, KCl 16, $MgCl_2$ 16, and $NaHCO_3$ 10). Following cannulation of the aorta, Langendorff perfusion was initiated with oxygenated (95% O_2, 5% CO_2) Tyrode's solution of the following composition (in mmol/L): NaCl 128.2, $CaCl_2$ 1.3, KCl 4.7, $MgCl_2$ 1.05, NaH_2PO_4 1.19,

$NaHCO_3$ 20, and glucose 11.1 (pH 7.4 ± 0.05). The perfusate was pumped from a reservoir with 2 L of Tyrode's solution through an in-line filter and two bubble traps before passing via the cannula to the heart and then recirculated from the perfusion chamber back to the reservoir and re-gassed. Flow rate (∼30 ml/min) was adjusted to maintain a perfusion pressure of 60–70 mmHg. The heart was securely positioned supine in the perfusion chamber. The perfusion apparatus was temperature controlled with heated baths used for the perfusate and a water-jacketed perfusion chamber. Two Ag/AgCl disc electrodes were positioned in the bath to record an electrocardiogram (ECG) analogous to a lead I configuration. A bipolar pacing electrode was positioned on the base of the left ventricular (LV) epicardium.

Dual Optical Mapping of SR Ca^{2+} and V_m

Optical mapping of intra-SR free [Ca^{2+}] and transmembrane potential (V_m) was performed as previously described in detail (Wang et al., 2014, 2015; Murphy et al., 2017; Wang and Ripplinger, 2019). After a 10-min equilibration period, blebbistatin (Tocris Bioscience, Ellisville, MO; 10–20 μM) was added to the perfusate to reduce energy demands of the heart during dye loading (Wengrowski et al., 2013) and to eliminate motion artifact during optical recordings (Fedorov et al., 2007). Hearts were then switched to a recirculating perfusate (200 ml) and loaded by retrograde perfusion with Tyrode's solution containing Fluo-5N, acetoxymethyl ester (Fluo-5N AM; 5 μM, dissolved in dimethyl sulfoxide and Pluronic F-127, 20% wt/vol, Invitrogen; Carlsbad, CA, United States) for 60 min at room temperature (Kornyeyev et al., 2010), followed by 15 min washout at 37°C to remove residual Fluo-5N AM. Hearts were subsequently stained with the voltage-sensitive dye RH237 [Invitrogen, Carlsbad, CA, United States; 50 μl of 1 mg/ml in dimethyl sulfoxide (DMSO)]. All experiments were performed at 37°C.

The anterior epicardial surface was excited using LED light sources centered at 470 nm (Mightex, Pleasanton, CA, United States) and bandpass filtered from 475 to 495 nm (Semrock, Rochester, NY, United States). The emitted fluorescence was collected through a THT-macroscope (SciMedia) and split with a dichroic mirror at 545 nm (Omega, Brattleboro, VT, United States). The longer wavelength moiety, containing the V_m signal, was longpass filtered at 700 nm; and the shorter wavelength moiety, containing the SR Ca^{2+} signal, was bandpass filtered with a 32-nm filter centered at 518 nm (Omega, Brattleboro, VT, United States). The emitted fluorescence signals were recorded using two CMOS cameras (MiCam Ultima-L, SciMedia, Costa Mesa, CA, United States) with a sampling rate of 0.5–1 kHz and 100 × 100 pixels with a field of view of 31 × 31 mm.

Experimental Protocol

Baseline electrophysiological parameters were determined during LV epicardial pacing at a pacing cycle length (PCL) of 300 ms using a 2-ms pulse at twice the diastolic threshold. To induce alternans, the PCL was decremented in 20-ms steps. The effects of pharmacological SERCA inhibition were determined by adding CPA (1–10 μM) to the perfusate. Relative refractoriness of RyR Ca^{2+} release was measured as recovery of SR Ca^{2+} release with a single extra-stimulus (S1–S2 pacing protocol).

Data Analysis and Statistics

Data analysis was performed using two commercially available analysis programs (*BV_Analyze*, Brainvision, Tokyo, Japan; and *Optiq*, Cairn, United Kingdom) and a free optical mapping analysis software ElectroMap (O'Shea et al., 2019). V_m and SR Ca^{2+} datasets were spatially aligned (using heart images from each camera obtained during white light illumination) and processed with a Gaussian spatial filter (radius 3 pixels). For both APs and SR Ca^{2+} transients, activation time was determined at 50% of the maximal amplitude (or time at 50% of nadir for SR Ca^{2+}). For APs, repolarization time at 80% return to baseline was used to calculate APD (APD_{80}). SERCA function was quantified using the time constant (τ) of a single exponential fit to the recovery portion of the SR Ca^{2+} trace (from 5 to 90% recovery).

The spectral method, which has been used clinically for detecting micro-volt T-wave alternans (Verrier et al., 2011), was used to detect the presence of significant APD and SR Ca^{2+} alternans as previously described (Myles et al., 2011). The spectral method was chosen due to its high sensitivity and relative immunity to noise. Briefly, at each pacing frequency, APs or SR Ca^{2+} transients from a ∼4-s recording were aligned in time using the pacing artifact as a reference point, resulting in a two-dimensional matrix of signals, $AP(n,t)$, where n is the beat number and t is time. A fast Fourier transform (FFT) was used to compute the power spectra across beats for each t, and the spectra were summed. The alternans magnitude was then defined as the resulting amplitude of the summed spectra at 0.5 cycles/beat. This approach allowed us to determine if an area within the mapping field of view was experiencing significant APD or SR Ca^{2+} alternans (greater than the background noise levels) as well as the spatial extent of significant alternans. A magnitude of ≥ 2 was used as the minimum threshold for significant APD or SR Ca^{2+} alternans, corresponding to a beat-to-beat change in APD_{90} ≥ 5 ms or beat-to-beat change in SR Ca^{2+} release amplitude ≥ 5%, respectively.

To more precisely differentiate between the onset of diastolic SR Ca^{2+} load alternans and SR Ca^{2+} release alternans, quantification of the SR Ca^{2+} transient was also performed, as previously described (Wang et al., 2014). The amplitude of SR Ca^{2+} release alternans was calculated as 1 minus the ratio of the average small beat (S) release amplitude to the average large beat (L) release amplitude (1 - S/L) during a 1- to 2-s recording. The amplitude of diastolic SR Ca^{2+} load alternans was calculated as the average difference between diastolic levels (D) of S and L beats divided by the average L amplitude (D/L) during a 1- to 2-s recording. Data are expressed as mean ± standard deviation (SD) and were compared using a one-way ANOVA with Bonferroni *post-hoc* test for multiple groups or a Student *t*-test when

only two groups were compared. $p < 0.05$ was considered statistically significant.

RESULTS

Effects of Sarco-Endoplasmic Reticulum Ca^{2+}-ATPase Inhibition on V_m and Sarcoplasmic Reticulum Ca^{2+}

To determine the role of SERCA function on V_m and SR Ca^{2+}, increasing doses of CPA, a specific SERCA inhibitor (Seidler et al., 1989; Szentesi et al., 2004), were added to the perfusate, while simultaneous imaging of RH237 (V_m) and Fluo-5N (SR Ca^{2+}) was performed at 300-ms PCL (**Figures 1A,B**). As expected, CPA (1, 5, and 10 μM) prolonged APD (**Figure 1C**) and decreased the relative amplitude of the normalized SR Ca^{2+} transient in a dose-dependent manner (**Figure 1D**). These findings are consistent with previous observations in adult guinea pig ventricular myocytes in the presence of CPA (Szentesi et al., 2004). Furthermore, CPA tended to increase the SR Ca^{2+} time to nadir (indicative of SR Ca^{2+} release, **Figure 1E**) and caused a dose-dependent increase in SR Ca^{2+} reuptake time (*tau*, **Figure 1F**), with *tau* increasing from 70.8 ± 3.5 ms at baseline to 85.5 ± 6.6, 129.9 ± 20.7, and 271.3 ± 37.6 ms ($p < 0.05$ vs. baseline for all doses). CPA did not impact mean conduction velocity (CV: 54.9 ± 1.6 cm/s at baseline vs. 54.8 ± 4.6, 54.7 ± 3.2, and 53.8 ± 2.8 cm/s for 1, 5, and 10 μM, p = NS). The marked prolongation of APD in the presence of CPA suggests that alterations in SR Ca^{2+} reuptake feed back onto V_m to influence AP dynamics, potentially due to a reduction in Ca^{2+}-dependent inactivation of L-type Ca^{2+} current (I_{CaL}) and consequent increased I_{CaL} during the AP plateau.

Sarco-Endoplasmic Reticulum Ca^{2+}-ATPase Inhibition Worsens Pacing-Induced Action Potential Duration and Sarcoplasmic Reticulum Ca^{2+} Alternans

To induce alternans, hearts were paced by decrementing the PCL. Consistent with previous reports, SERCA inhibition (1 and 5 μM of CPA) increased the incidence and magnitude of both APD and SR Ca^{2+} alternans (Wan et al., 2005; Nivala et al., 2015; Weinberg, 2016). Example maps of the alternans magnitude at two PCLs are shown in **Figures 2A,B**, along with corresponding optical V_m and SR Ca^{2+} traces (**Figures 2C,D**). Consistent with our previous studies, significant SR Ca^{2+} alternans emerged prior to the onset of APD alternans (i.e., at longer PCLs) (Wang et al., 2014). In the example shown, at baseline, SR Ca^{2+} alternans was induced at PCL = 220 ms without significant APD alternans (**Figures 2B,D**, top vs. bottom left traces). CPA at 1 and 5 μM dose-dependently shifted the alternans threshold to a longer PCL and increased the magnitude of both APD and SR Ca^{2+} alternans. Indeed, when the alternans magnitude was quantified at PCL = 220 ms, the magnitude of both APD and SR Ca^{2+} alternans tended to increase in a dose-dependent manner (**Figures 3A,B**). However, detailed analysis of SR Ca^{2+} kinetics and the frequency dependence of alternans revealed more complex behaviors.

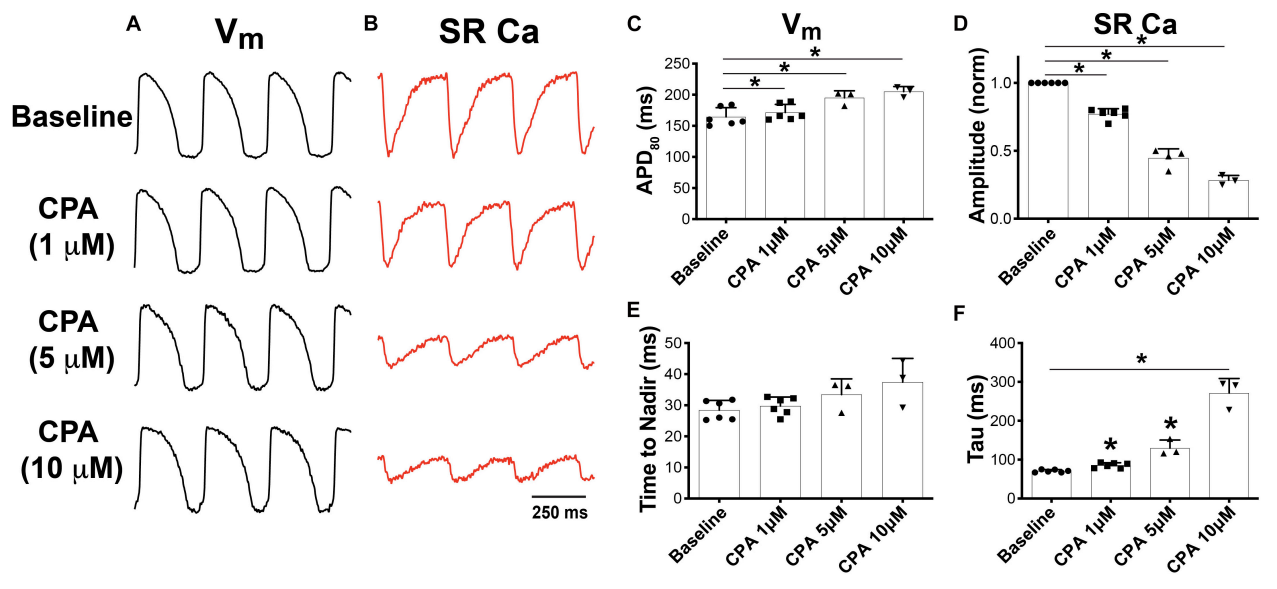

FIGURE 1 | Dual optical mapping of V_m **(A)** and sarcoplasmic reticulum (SR) Ca^{2+} **(B)** during sarco-endoplasmic reticulum Ca^{2+}-ATPase (SERCA) inhibition with cyclopiazonic acid (CPA) and pacing at a pacing cycle length (PCL) of 300 ms. CPA caused a dose-dependent increase in APD_{80} **(C)** and decrease in normalized SR Ca^{2+} transient amplitude **(D)**. CPA tended to prolong the time to nadir of SR Ca^{2+} release **(E)** and significantly prolonged SR Ca^{2+} reuptake time (*tau*, **F**). Mean ± SD. N = 3–6 (*$p < 0.05$ vs. baseline).

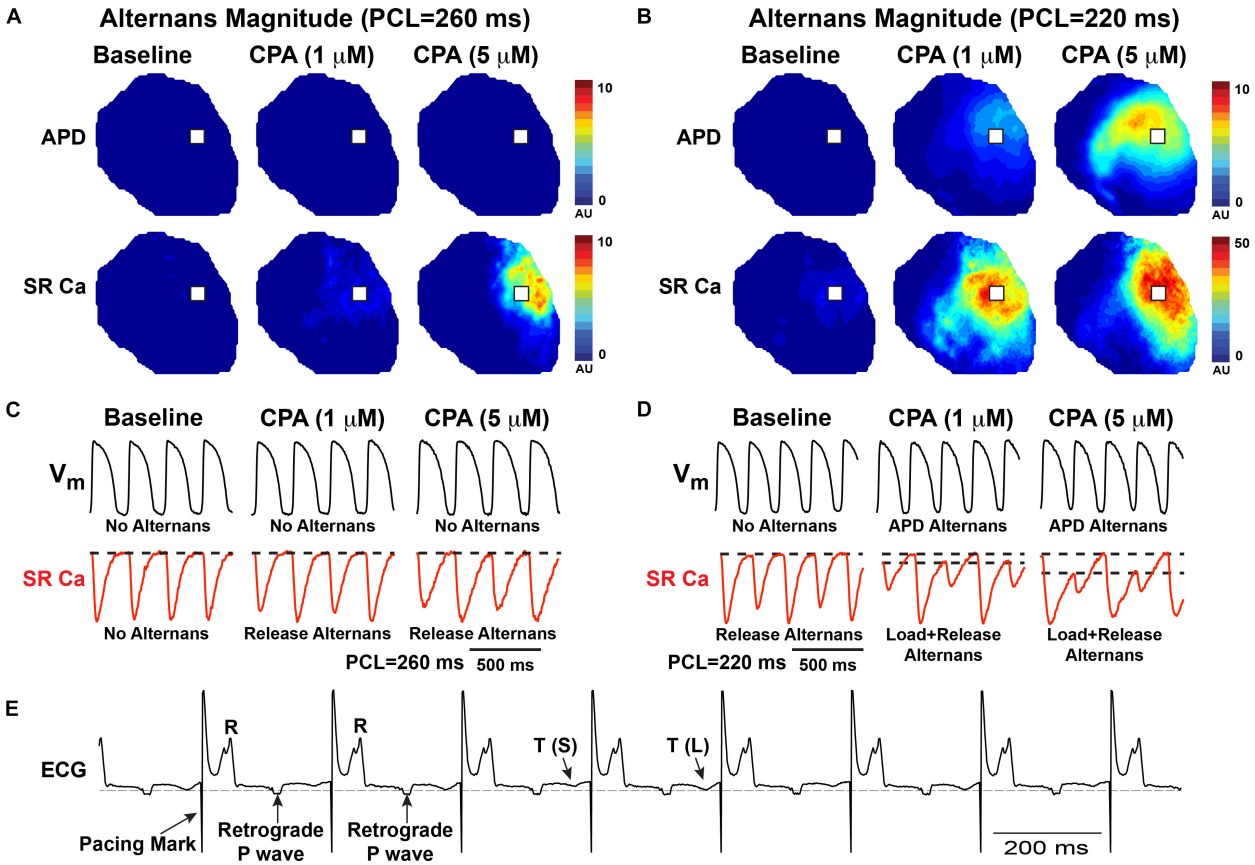

FIGURE 2 | Both action potential duration (APD) and sarcoplasmic reticulum (SR) Ca^{2+} alternans progressively worsen with increased pacing frequency as shown by the alternans magnitude maps **(A,B)** and in example optical traces **(C,D)** from the location indicated with a white box in **(A,B)**. In this example, cyclopiazonic acid (CPA) (1–5 μM) caused a dose-dependent increase in the magnitude of SR Ca^{2+} and APD alternans and an increase in the pacing cycle length (PCL) at which alternans occurred. **(E)** Example ECG showing T-wave alternans—small (S) vs. large (L) T-wave.

Effects of Sarco-Endoplasmic Reticulum Ca^{2+}-ATPase Inhibition on Sarcoplasmic Reticulum Ca^{2+} Load and Release Alternans

Although spectral analysis allows for sensitive detection of both APD and SR Ca^{2+} alternans, it does not differentiate SR Ca^{2+} diastolic load from release alternans. To more precisely investigate the role of SERCA inhibition, detailed quantification of the SR Ca^{2+} transient was performed as shown in **Figures 3C–F**. We have previously shown in the normal heart that SR Ca^{2+} release alternans always occur at slower PCLs, prior to the onset of SR Ca^{2+} load alternans, indicating the prominent role of RyR refractoriness in governing the onset of alternans (Wang et al., 2014). Our working hypothesis was that SERCA inhibition with CPA would lead to insufficient SR Ca^{2+} reuptake during diastole, causing alternation of diastolic SR Ca^{2+} load, and that load and release alternans may therefore emerge simultaneously. Contrary to this hypothesis, at all doses of CPA, alternation of SR Ca^{2+} release occurred prior to the onset of any detectable alternation in SR Ca^{2+} load (**Figures 2C,D**, **3E–G**). Interestingly, high-dose CPA (10 μM) tended to suppress both load and release alternans at slower pacing frequencies (**Figures 3C,E–G**) but caused larger magnitude load and release alternans at faster pacing frequencies (similar to 5 μM of CPA, **Figures 3E,F**). Yet even with high-dose CPA, significant SR Ca^{2+} release alternans occurred before the onset of detectable SR Ca^{2+} load alternans (**Figure 3G**), suggesting that RyR refractoriness plays a key role in the genesis of cardiac alternans, even when SERCA function is significantly reduced. Indeed, at the lower $[Ca^{2+}]_{SR}$ associated with CPA-dependent SERCA inhibition, the RyR refractory period might be prolonged, opposite to the shortening of refractoriness at very high $[Ca^{2+}]_{SR}$ levels (Bers, 2002b).

Sarco-Endoplasmic Reticulum Ca^{2+}-ATPase Inhibition Increases Relative Ryanodine Receptor Refractoriness

To determine if SERCA inhibition modifies relative RyR refractoriness and recovery of SR Ca^{2+} release, an S1–S2 pacing protocol was performed with low-dose (1 μM) CPA (**Figure 4A**). At S1 = 300 ms, there was no SR Ca^{2+} alternans at baseline or

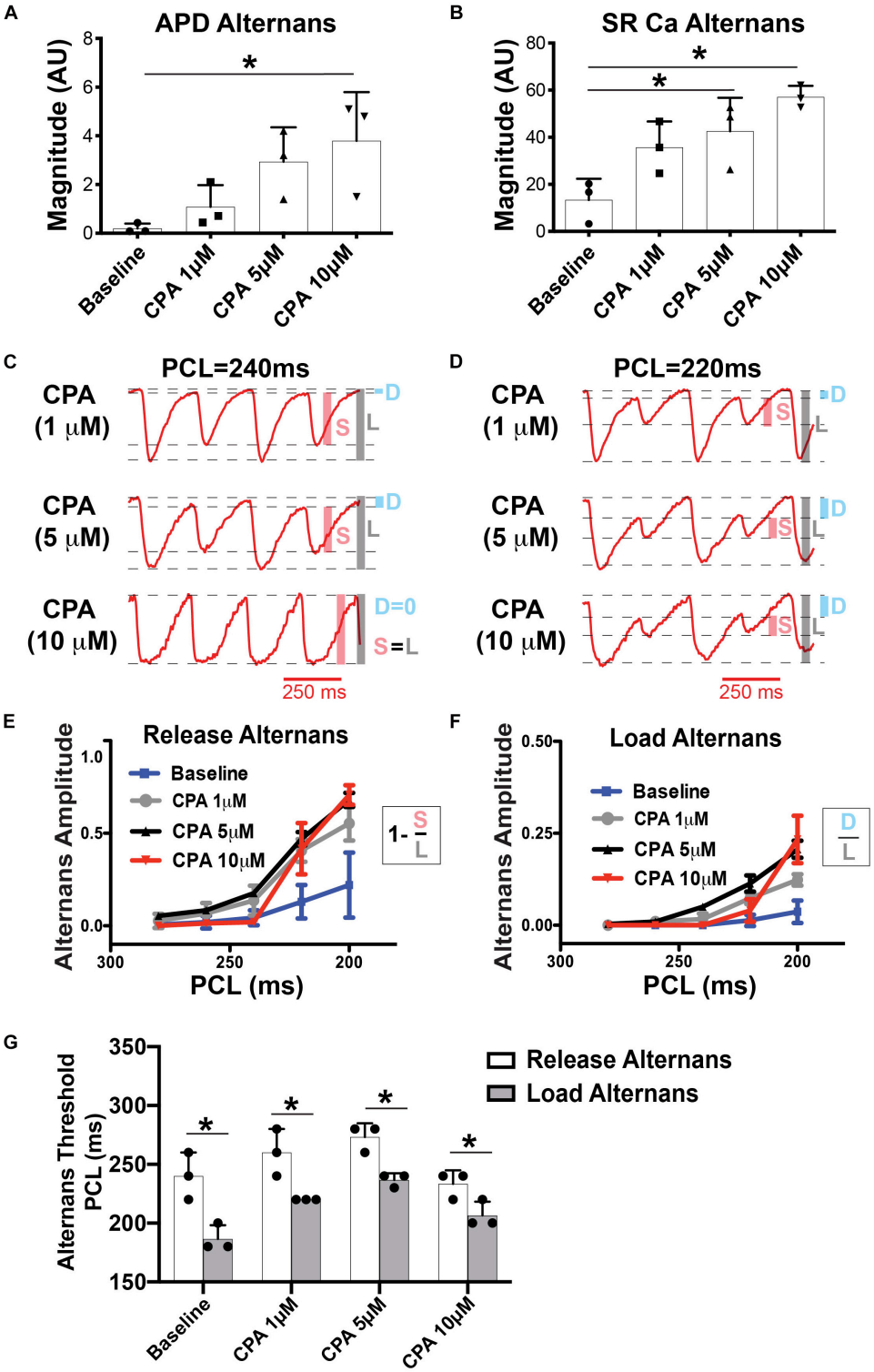

FIGURE 3 | At pacing cycle length (PCL) = 220 ms, cyclopiazonic acid (CPA) increased the magnitude of both action potential duration (APD) **(A)** and sarcoplasmic reticulum (SR) Ca^{2+} **(B)** alternans. Mean ± SD. $N = 3$ (*$p < 0.05$ vs. Baseline). **(C,D)** Example SR Ca^{2+} traces at a slower **(C)** and faster **(D)** PCL. High-dose CPA (10 μM) tended to decrease alternans magnitude at slower rates, while increasing alternans magnitude at faster rates. **(E,F)** Quantification of release **(E)** and load **(F)** alternans according to the equations indicated. Shaded bars in **(C,D)** show approximate measurements for calculations in **(E,F)**. S, small; L, large; D, diastolic level. **(G)** Under all conditions, release alternans emerged at a longer PCL than load alternans. Mean ± SD. $N = 3$ (*$p < 0.05$ vs. corresponding threshold for release alternans).

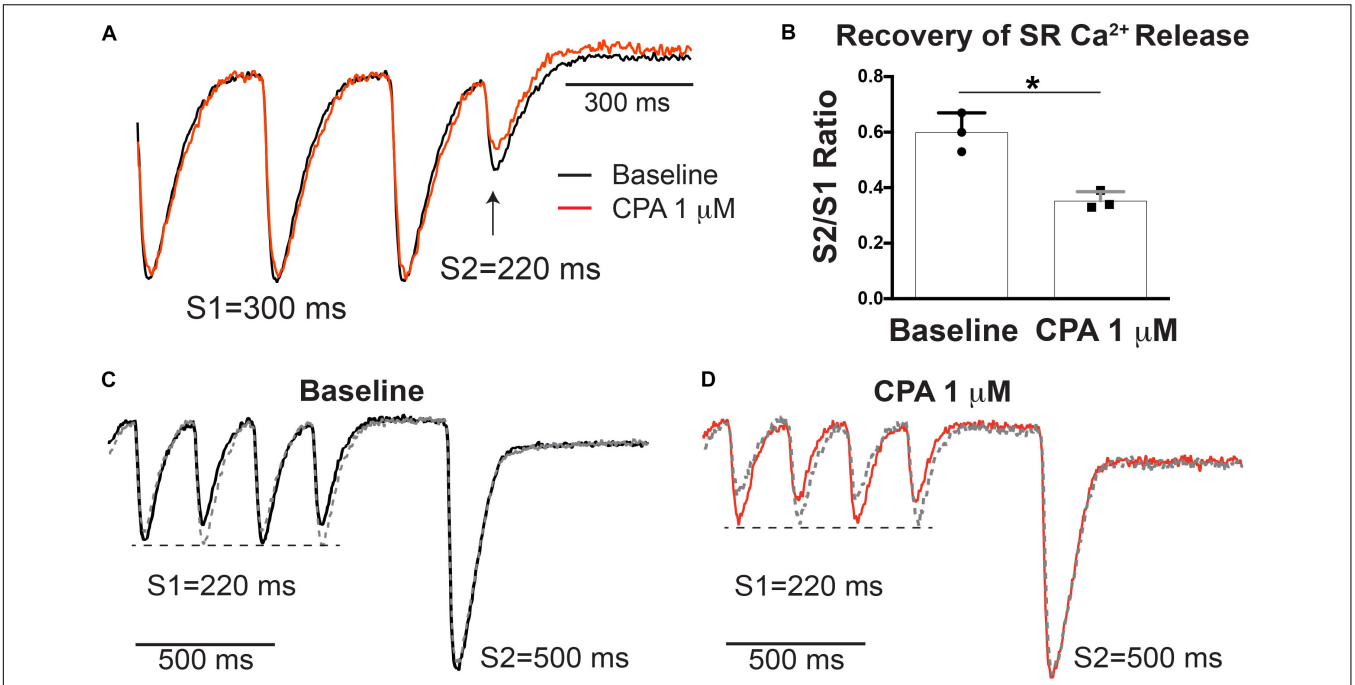

FIGURE 4 | Sarco-endoplasmic reticulum Ca^{2+}-ATPase (SERCA) inhibition with cyclopiazonic acid (CPA) increased relative ryanodine receptor (RyR) refractoriness **(A)**. **(B)** S2/S1 ratio (S1 = 300, S2 = 220 ms) was significantly decreased with 1 μM of CPA. Mean ± SD. $N = 3$ (*$p < 0.05$ vs. baseline). **(C,D)** Alternative S1–S2 protocol in which alternans was induced at S1 = 220 ms and a longer S2 (500 ms) was applied. The pacing protocol was repeated so that the last S1 was either a small (solid) or large (dashed) release. A similarly large sarcoplasmic reticulum (SR) Ca^{2+} release occurred after a large or small release at baseline **(C)** and following 1 μM of CPA **(D)**, indicating similar SR Ca^{2+} load after small and large beats.

with low-dose CPA, but there is incomplete recovery of SR Ca^{2+} release at S2 = 220 ms in both groups (**Figure 4A**). Notably, 1 μM of CPA caused a stronger suppression of the S2-induced SR Ca^{2+} release when normalized to the S1 release (S2/S1 ratio, **Figure 4B**), consistent with a prolongation in relative RyR refractoriness upon SERCA inhibition. An alternative S1–S2 protocol was also performed, where the S1 train at a shorter PCL (220 ms) induces SR Ca^{2+} alternans, followed by a long S2 pause to ensure more complete RyR recovery (**Figures 4C,D**). This protocol was repeated so that the longer S2 interval occurred after both large and small SR Ca^{2+} release. In response to the long S2 interval, a similar amplitude SR Ca^{2+} release occurred, regardless of the amplitude of SR Ca^{2+} release at the last S1 beat (large or small), indicating that SR Ca^{2+} content does not appreciably alternate from beat to beat and that at this pacing frequency, availability of RyR for Ca^{2+} release is a key contributor to alternans both with and without CPA.

Sarco-Endoplasmic Reticulum Ca^{2+}-ATPase Inhibition Promotes Spatially Discordant Alternans

Further investigation of spatial alternans dynamics shows that CPA also promoted an earlier emergence of spatially discordant alternans. **Figure 5A** illustrates the emergence of SR Ca^{2+} alternans with increasing doses of CPA and progressively faster PCLs. Spatial discordance occurs when a clear nodal line is observed (5 μM of CPA at 200 ms and 10 μM of CPA at 220 and 200 ms) and was confirmed by assessing alternans phase (**Figure 5B**). The pacing threshold for emergence of spatial discordance increased with increasing doses of CPA (**Figure 5C**), and in all cases, spatial discordance of both APD and SR Ca^{2+} alternans occurred at the same PCL. The fact that pacing thresholds for spatial discordance are the same for APD and SR Ca^{2+} indicates that V_m and SR Ca^{2+} remain in-phase with each other (long APD corresponds to larger SR Ca^{2+} transient and *vice versa*) even when the heart is spatially out-of-phase (long APD and large SR Ca^{2+} transient in one location; short APD and smaller SR Ca^{2+} transient in another location). Spatially discordant alternans are known to create very large gradients in repolarization, setting the stage for unidirectional conduction block and the induction of reentry (Pastore et al., 1999; Walker and Rosenbaum, 2005; Hayashi et al., 2007; Wilson and Rosenbaum, 2007).

DISCUSSION

Using dual optical mapping of V_m and SR Ca^{2+}, we show that modest inhibition of SERCA increases relative RyR refractoriness and worsens pacing-induced SR Ca^{2+} and APD alternans. Importantly, even under conditions of SERCA inhibition, SR Ca^{2+} release alternans always occurred prior to the onset of appreciable SR Ca^{2+} load alternans or APD alternans. Severe inhibition of SERCA function with high-dose CPA tended to suppress SR Ca^{2+} alternans at slower pacing but worsened

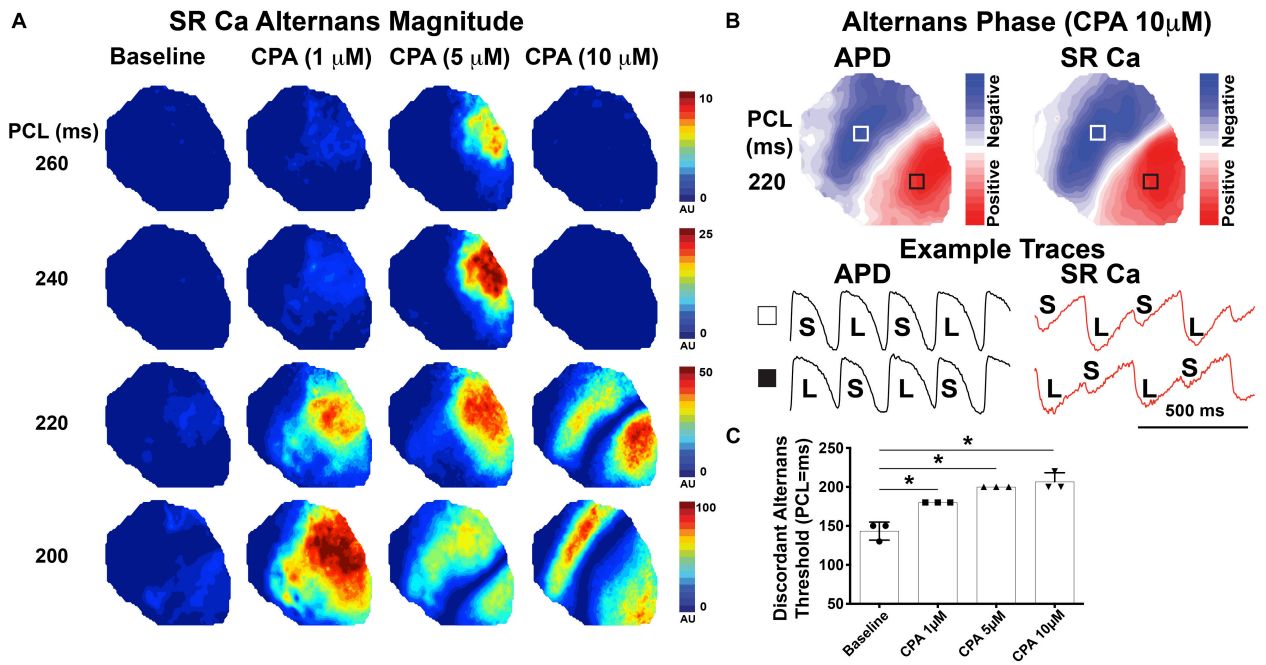

FIGURE 5 | Inhibition of sarco-endoplasmic reticulum Ca^{2+}-ATPase (SERCA) with cyclopiazonic acid (CPA) promoted the emergence of spatially discordant alternans at slower pacing cycle lengths (PCL). **(A)** Magnitude of sarcoplasmic reticulum (SR) Ca^{2+} alternans at progressively faster PCLs. Spatial discordance emerges at 220-ms PCL for 10 μM of CPA and at 200-ms PCL for 5 μM CPA, while baseline and 1 μM of CPA remain spatially concordant over the PCLs shown. **(B)** Alternans phase with the nodal line indicated in white where alternans transitions from small:large to large:small. Optical V_m and SR Ca^{2+} traces are from the regions indicated with white and black boxes. **(C)** Pacing threshold for the induction of spatial discordance was significantly increased with CPA. Mean ± SD. $N = 3$ ($^*p < 0.05$ vs. baseline).

alternans at faster pacing frequencies. All doses of CPA also promoted the emergence of spatial discordance. While these data demonstrate that both SERCA and RyR function are key players, the fact that significant SR Ca^{2+} release alternans always occurs before the onset of SR Ca^{2+} load alternans suggests that encroachment on RyR refractoriness *per se* predominates as the initiator of Ca^{2+} transients alternans. Furthermore, we find that slowed SR Ca^{2+} uptake and lower SR Ca^{2+} content shift that refractoriness threshold to longer PCLs.

Simultaneous Mapping of V_m and Sarcoplasmic Reticulum Ca^{2+} in the Intact Heart

We previously developed methodology using the voltage-sensitive dye, RH237, and low-affinity Ca^{2+} indicator, Fluo-5N AM, to map V_m and SR Ca^{2+} simultaneously in the intact heart (Wang et al., 2014, 2015; Murphy et al., 2017). Fluo-5N has a dissociation constant (K_d) around 400 μM and therefore exhibits minimal fluorescence in the cytosol compared to the SR lumen, where the Ca^{2+} content is at or near the millimolar range. Thus, SR Ca^{2+} dynamics can be assessed independently from transmembrane Ca^{2+} flux. Both fluorescent indicators are excited with blue light (488 nm), and the emission wavelengths are split and recorded on two separate high-speed detectors, allowing for precise beat-to-beat mapping of V_m and SR Ca^{2+} dynamics at high spatial and temporal resolutions (Wang et al., 2014). As shown in **Figure 1**, in addition to expected prolongation of SR Ca^{2+} reuptake (*tau*), SERCA inhibition also dose-dependently prolonged APD and decreased the relative amplitude of SR Ca^{2+} release. Decreased SR Ca^{2+} transient amplitude is suggestive of decreased SR Ca^{2+} content, which would be expected with SERCA inhibition; however, Fluo-5N Ca^{2+} signals are uncalibrated, and therefore, signal amplitudes can only be used to ascertain relative differences.

Impact of Sarco-Endoplasmic Reticulum Ca^{2+}-ATPase Inhibition on V_m and Sarcoplasmic Reticulum Ca^{2+} Alternans

Under normal conditions and stable heart rate, diastolic SR Ca^{2+} load varies little from beat to beat, indicating a precise balance between RyR Ca^{2+} release and SERCA reuptake during each ECC cycle. We have previously shown in normal rabbit hearts that as heart rate increases, beat-to-beat alternation of SR Ca^{2+} release occurs prior to appreciable alternation of SR Ca^{2+} load and that relative refractoriness of RyR governs the onset of arrhythmogenic alternans (Wang et al., 2014). However, SERCA function has also been implicated in cardiac alternans, particularly in HF where SERCA expression or activity is reduced and alternans severity is increased (Wan et al., 2005; Cutler et al., 2009, 2012). The objective of the present study was to test the relatively straightforward hypothesis that SERCA inhibition with CPA would worsen alternans and would do so via insufficient SR

Ca^{2+} reuptake during diastole, causing alternation of diastolic SR Ca^{2+} load, and that load and release alternans may therefore emerge simultaneously. While CPA did indeed worsen alternans, release alternans still preceded load alternans, causing us to reject this simple explanatory hypothesis.

One consistent and somewhat unexpected finding of the present study was that SR Ca^{2+} release *always* alternated prior to any discernable alternation in diastolic SR Ca^{2+} load under all conditions assessed (**Figures 2**, **3G**). Therefore, even though SR Ca^{2+} reuptake was impaired and slowed with CPA, insufficient diastolic SR refilling by itself does not appear to be a primary driver of alternans onset. A mechanistic clue was that even mild SERCA inhibition slowed the relative recovery of RyR Ca^{2+} release measured with an S1–S2 protocol (**Figure 4**), and increased RyR refractoriness is consistent with increased alternans magnitude. The magnitude and recovery of RyR Ca^{2+} release are known to be highly dependent on SR Ca^{2+} load, and although we assume that SERCA inhibition decreases SR Ca^{2+} content, we cannot measure absolute SR Ca^{2+} concentration with our method. However, recent data indicate that the *velocity* of SR Ca^{2+} refilling may affect SR Ca^{2+} release restitution, independent of SR Ca^{2+} load (Cely-Ortiz et al., 2020), and this mechanism may also be involved here.

At lower doses (1 and 5 μM), CPA tended to increase the magnitude of SR Ca^{2+} and APD alternans, as well as increase the PCL at which alternans first emerged (**Figures 2**, **3**). High-dose (10 μM) CPA, however, tended to reduce alternans at slow PCLs but worsened alternans at fast PCLs (**Figures 3**, **5**). These somewhat conflicting effects raise an important question of how severely reduced SERCA function suppresses SR Ca^{2+} alternans at slower pacing (e.g., PCL = 240–260 ms) and yet promotes SR Ca^{2+} alternans at faster pacing (e.g., PCL = 200–220 ms). One possible explanation is that greatly impaired SERCA function (by ∼75% based on refilling *tau* values in **Figure 1F**) may reduce SR Ca^{2+} content and release dramatically (Millet et al., 2021), especially when the pacing frequency is slow, masking alternans at slower rates. However, as pacing frequency increases, SR Ca^{2+} load also increases (Wang et al., 2014), which in turn would increase the magnitude of SR Ca^{2+} release and make alternans more apparent. Alternatively, rapid pacing may cause diastolic cytosolic Ca^{2+} elevation, which in turn triggers Ca^{2+}-calmodulin-dependent inactivation of RyR and, consequently, an imbalance of SR Ca^{2+} release and reuptake (Wei et al., 2020). Thus, the role of SERCA activity in either suppressing or promoting SR Ca^{2+} alternans may depend on relative changes in SR Ca^{2+} content at various pacing frequencies.

Moreover, the overall magnitude of *intracellular* Ca^{2+} alternans will also depend on transmembrane Ca^{2+} flux (i.e., I_{CaL}) and intracellular Ca^{2+} concentration, which were not assessed here but are also dependent on SERCA and RyR activity. Indeed, a previous study in the isolated rabbit working heart showed that the relationship between SERCA activity and whole heart mechanical function is highly non-linear and also involves significant changes in intracellular Ca^{2+} flux (Elliott et al., 2012). Furthermore, it should be noted that in HF, the degree of SERCA impairment varies with disease stage and etiology (Sen et al., 2000) and that restoring the SERCA pump function in HF is not always beneficial (Zhang et al., 2010).

Impact of Sarco-Endoplasmic Reticulum Ca^{2+}-ATPase Inhibition on Spatially Discordant Alternans

SERCA inhibition also caused spatially discordant alternans to occur at slower pacing frequencies (**Figure 5**). We propose that there is likely a continuum of mechanisms responsible for the onset and progression of alternans. RyR refractoriness is first encroached upon (which as shown in the present study can be indirectly modulated by SERCA activity). This leads to the emergence of SR Ca^{2+} release alternans. As heart rate increases, diastolic SR Ca^{2+} load also begins to alternate, which further augments SR Ca^{2+} release alternans. APD alternans also begins to emerge in this regime. At even faster heart rates, dynamical mechanisms, such as APD and CV restitution, may contribute to spatial discordance and subsequent ventricular tachycardia/fibrillation (VT/VF). The results of this study suggest that simply changing SR Ca^{2+} regulation can shift this entire continuum of mechanisms, in this case, to occur at slower pacing frequencies. Consistent with previous studies, we posit that dynamical mechanisms (i.e., APD or CV restitution) likely still govern the onset of spatial discordance (Wilson and Rosenbaum, 2007). Although CPA did not slow CV, it did prolong APD (due to feedback between SR Ca^{2+} and V_m, **Figure 1**). Prolongation of APD will result in shorter diastolic intervals and APD restitution may therefore be invoked at slower pacing frequencies, thereby promoting spatial discordance.

Sarcoplasmic Reticulum Ca^{2+}/V_m Coupling

SR Ca^{2+} dynamics can impact APD, as shown in **Figure 1**, where CPA dose-dependently prolonged APD. Indeed, reduced SR Ca^{2+} release can slow Ca^{2+}-dependent inactivation (CDI) of I_{CaL}, which would tend to prolong APD. However, a smaller Ca^{2+} transient also tends to reduce the magnitude of inward Na^+–Ca^{2+} exchange current (I_{NCX}), which would tend to shorten APD. Therefore, the net change in APD is a balance between these two mechanisms. The fact that CPA prolongs APD suggests that the net effect of reduced SERCA function (vs. normal SERCA function) on APD is via reduced CDI of I_{CaL}. This may seem somewhat at odds with the positive SR Ca^{2+}/V_m coupling observed during alternans (large SR Ca^{2+} transient corresponds to long APD, **Figures 2**, **5**). However, in the case of beat-to-beat changes in the Ca^{2+} transient, intrinsic SERCA function is the same during large and small beats, and in this case, inward I_{NCX} depends directly on $[Ca]_i$ and predominates over I_{Ca} inactivation on APD.

CONCLUSION

These findings shed new light on the role of SR Ca^{2+} in the progression from normal rhythms to arrhythmogenic

cardiac alternans. While SERCA inhibition caused SR Ca^{2+} and subsequent APD alternans to appear at longer PCLs, this was not directly due to altered diastolic $[Ca^{2+}]_{SR}$. However, the reduced SERCA function and consequent lower SR Ca^{2+} load prolonged RyR refractoriness, which is how alternans is promoted by SERCA inhibition. Indeed, SR Ca^{2+} release alternans occurred prior to SR Ca^{2+} load alternans under all conditions, and that can lead secondarily to load alternans, APD alternans, and ultimately spatial discordance. These findings may provide important insight into underlying mechanisms governing alternans onset and severity in failing hearts, where reduced SERCA function is a common phenotype.

LIMITATIONS

This study assessed mechanisms of SR Ca^{2+} and APD alternans but did not specifically address susceptibility to VT/VF nor how SERCA inhibition with CPA may alter VT/VF dynamics. This remains an important area for future study. Although we did not observe appreciable changes in diastolic SR Ca^{2+} load prior to the onset of SR Ca^{2+} release alternans, it is possible that very small changes in diastolic SR Ca^{2+} occur at the luminal side of RyR and govern release. Our imaging approach does not have the spatial resolution nor sensitivity to definitively rule this out.

DATA AVAILABILITY STATEMENT

The raw data supporting the conclusions of this article will be made available by the authors, without undue reservation.

ETHICS STATEMENT

The animal study was reviewed and approved by the UC Davis Institutional Animal Care and Use Committee.

AUTHOR CONTRIBUTIONS

LW and CR conceived the study, designed and conducted experiments, analyzed data, generated figures, and wrote the manuscript. IL analyzed, reviewed and interpreted data, and edited the manuscript. RM and DB contributed to study conception and design, critically reviewed and interpreted data, and edited the manuscript. All authors have reviewed the data and approved the final manuscript.

FUNDING

This study was supported by the National Institutes of Health R01 HL111600 (CR) and P01 HL141084 (CR and DB) and by the Wellcome Trust 105907/Z/14/Z (RM).

REFERENCES

Alvarez-Lacalle, E., Cantalapiedra, I. R., Penaranda, A., Cinca, J., Hove-Madsen, L., and Echebarria, B. (2013). Dependency of calcium alternans on ryanodine receptor refractoriness. *PLoS One* 8:e55042. doi: 10.1371/journal.pone.0055042

Bayer, J. D., Narayan, S. M., Lalani, G. G., and Trayanova, N. A. (2010). Rate-dependent action potential alternans in human heart failure implicates abnormal intracellular calcium handling. *Heart Rhythm.* 7, 1093–1101. doi: 10.1016/j.hrthm.2010.04.008

Bers, D. M. (2001). *Excitation-Contraction Coupling and Cardiac Contractile Force*. Dordrecht: Kluwer Academic.

Bers, D. M. (2002a). Cardiac excitation-contraction coupling. *Nature* 415, 198–205.

Bers, D. M. (2002b). Sarcoplasmic reticulum Ca release in intact ventricular myocytes. *Front. Biosci.* 7:d1697–d1711.

Bers, D. M. (2014). Cardiac sarcoplasmic reticulum calcium leak: basis and roles in cardiac dysfunction. *Annu. Rev. Physiol.* 76, 107–127. doi: 10.1146/annurev-physiol-020911-153308

Cely-Ortiz, A., Felice, J. I., Diaz-Zegarra, L. A., Valverde, C. A., Federico, M., Palomeque, J., et al. (2020). Determinants of Ca2+ release restitution: insights from genetically altered animals and mathematical modeling. *J. Gen. Physiol.* 152:e201912512.

Chudin, E., Goldhaber, J., Garfinkel, A., Weiss, J., and Kogan, B. (1999). Intracellular Ca(2+) dynamics and the stability of ventricular tachycardia. *Biophys. J.* 77, 2930–2941. doi: 10.1016/s0006-3495(99)77126-2

Cutler, M. J., Wan, X., Laurita, K. R., Hajjar, R. J., and Rosenbaum, D. S. (2009). Targeted SERCA2a gene expression identifies molecular mechanism and therapeutic target for arrhythmogenic cardiac alternans. *Circ. Arrhythm. Electrophysiol.* 2, 686–694. doi: 10.1161/circep.109.863118

Cutler, M. J., Wan, X., Plummer, B. N., Liu, H., Deschenes, I., Laurita, K. R., et al. (2012). Targeted sarcoplasmic reticulum Ca2+ ATPase 2a gene delivery to restore electrical stability in the failing heart. *Circulation* 126, 2095–2104. doi: 10.1161/circulationaha.111.071480

Diaz, M. E., O'neill, S. C., and Eisner, D. A. (2004). Sarcoplasmic reticulum calcium content fluctuation is the key to cardiac alternans. *Circ. Res.* 94, 650–656. doi: 10.1161/01.res.0000119923.64774.72

Elliott, E. B., Kelly, A., Smith, G. L., and Loughrey, C. M. (2012). Isolated rabbit working heart function during progressive inhibition of myocardial SERCA activity. *Circ. Res.* 110, 1618–1627. doi: 10.1161/circresaha.111.262337

Fedorov, V. V., Lozinsky, I. T., Sosunov, E. A., Anyukhovsky, E. P., Rosen, M. R., Balke, C. W., et al. (2007). Application of blebbistatin as an excitation-contraction uncoupler for electrophysiologic study of rat and rabbit hearts. *Heart Rhythm.* 4, 619–626. doi: 10.1016/j.hrthm.2006.12.047

Gehi, A. K., Stein, R. H., Metz, L. D., and Gomes, J. A. (2005). Microvolt T-wave alternans for the risk stratification of ventricular tachyarrhythmic events: a meta-analysis. *J. Am. Coll. Cardiol.* 46, 75–82. doi: 10.1016/j.jacc.2005.03.059

Goldhaber, J. I., Xie, L. H., Duong, T., Motter, C., Khuu, K., and Weiss, J. N. (2005). Action potential duration restitution and alternans in rabbit ventricular myocytes: the key role of intracellular calcium cycling. *Circ. Res.* 96, 459–466. doi: 10.1161/01.res.0000156891.66893.83

Hayashi, H., Shiferaw, Y., Sato, D., Nihei, M., Lin, S. F., Chen, P. S., et al. (2007). Dynamic origin of spatially discordant alternans in cardiac tissue. *Biophys. J.* 92, 448–460. doi: 10.1529/biophysj.106.091009

Jessup, M., Greenberg, B., Mancini, D., Cappola, T., Pauly, D. F., Jaski, B., et al. (2011). Calcium upregulation by percutaneous administration of gene therapy in cardiac disease (CUPID): a phase 2 trial of intracoronary gene therapy of sarcoplasmic reticulum Ca2+-ATPase in patients with advanced heart failure. *Circulation* 124, 304–313. doi: 10.1161/circulationaha.111.022889

Kawase, Y., Ly, H. Q., Prunier, F., Lebeche, D., Shi, Y., Jin, H., et al. (2008). Reversal of cardiac dysfunction after long-term expression of SERCA2a by gene transfer in a pre-clinical model of heart failure. *J. Am. Coll. Cardiol.* 51, 1112–1119. doi: 10.1016/j.jacc.2007.12.014

Kornyeyev, D., Petrosky, A. D., Zepeda, B., Ferreiro, M., Knollmann, B., and Escobar, A. L. (2012). Calsequestrin 2 deletion shortens the refractoriness of Ca(2)(+) release and reduces rate-dependent Ca(2)(+)-alternans in intact mouse hearts. *J. Mol. Cell Cardiol.* 52, 21–31. doi: 10.1016/j.yjmcc.2011.09.020

Kornyeyev, D., Reyes, M., and Escobar, A. L. (2010). Luminal Ca(2+) content regulates intracellular Ca(2+) release in subepicardial myocytes of intact beating mouse hearts: effect of exogenous buffers. *Am. J. Physiol. Heart Circ. Physiol.* 298, H2138–H2153.

Laurita, K. R., and Rosenbaum, D. S. (2008). Cellular mechanisms of arrhythmogenic cardiac alternans. *Prog. Biophys. Mol. Biol.* 97, 332–347. doi: 10.1016/j.pbiomolbio.2008.02.014

Millet, J., Aguilar-Sanchez, Y., Kornyeyev, D., Bazmi, M., Fainstein, D., Copello, J. A., et al. (2021). Thermal modulation of epicardial Ca2+ dynamics uncovers molecular mechanisms of Ca2+ alternans. *J. Gen. Physiol.* 153:e202012568.

Murphy, S. R., Wang, L., Wang, Z., Domondon, P., Lang, D., Habecker, B. A., et al. (2017). beta-Adrenergic inhibition prevents action potential and calcium handling changes during regional myocardial ischemia. *Front. Physiol.* 8:630. doi: 10.3389/fphys.2017.00630

Myles, R. C., Burton, F. L., Cobbe, S. M., and Smith, G. L. (2011). Alternans of action potential duration and amplitude in rabbits with left ventricular dysfunction following myocardial infarction. *J. Mol. Cell Cardiol.* 50, 510–521. doi: 10.1016/j.yjmcc.2010.11.019

Nassal, M. M., Wan, X., Laurita, K. R., and Cutler, M. J. (2015). Atrial SERCA2a overexpression has no affect on cardiac alternans but promotes arrhythmogenic SR Ca2+ triggers. *PLoS One* 10:e0137359. doi: 10.1371/journal.pone.0137359

Nivala, M., Song, Z., Weiss, J. N., and Qu, Z. (2015). T-tubule disruption promotes calcium alternans in failing ventricular myocytes: mechanistic insights from computational modeling. *J. Mol. Cell Cardiol.* 79, 32–41. doi: 10.1016/j.yjmcc.2014.10.018

O'Shea, C., Holmes, A. P., Yu, T. Y., Winter, J., Wells, S. P., Correia, J., et al. (2019). ElectroMap: high-throughput open-source software for analysis and mapping of cardiac electrophysiology. *Sci. Rep.* 9:1389.

Pastore, J. M., Girouard, S. D., Laurita, K. R., Akar, F. G., and Rosenbaum, D. S. (1999). Mechanism linking T-wave alternans to the genesis of cardiac fibrillation. *Circulation* 99, 1385–1394. doi: 10.1161/01.cir.99.10.1385

Picht, E., Desantiago, J., Blatter, L. A., and Bers, D. M. (2006). Cardiac alternans do not rely on diastolic sarcoplasmic reticulum calcium content fluctuations. *Circ. Res.* 99, 740–748. doi: 10.1161/01.res.0000244002.88813.91

Qu, Z., Liu, M. B., and Nivala, M. (2016). A unified theory of calcium alternans in ventricular myocytes. *Sci. Rep.* 6:35625.

Qu, Z., Nivala, M., and Weiss, J. N. (2013). Calcium alternans in cardiac myocytes: order from disorder. *J. Mol. Cell Cardiol.* 58, 100–109. doi: 10.1016/j.yjmcc.2012.10.007

Sakata, S., Lebeche, D., Sakata, N., Sakata, Y., Chemaly, E. R., Liang, L. F., et al. (2007). Restoration of mechanical and energetic function in failing aortic-banded rat hearts by gene transfer of calcium cycling proteins. *J. Mol. Cell Cardiol.* 42, 852–861. doi: 10.1016/j.yjmcc.2007.01.003

Seidler, N. W., Jona, I., Vegh, M., and Martonosi, A. (1989). Cyclopiazonic acid is a specific inhibitor of the Ca2+-ATPase of sarcoplasmic reticulum. *J. Biol. Chem.* 264, 17816–17823. doi: 10.1016/s0021-9258(19)84646-x

Sen, L., Cui, G., Fonarow, G. C., and Laks, H. (2000). Differences in mechanisms of SR dysfunction in ischemic vs. idiopathic dilated cardiomyopathy. *Am. J. Physiol. Heart Circ. Physiol.* 279, H709–H718.

Sun, B., Wei, J., Zhong, X., Guo, W., Yao, J., Wang, R., et al. (2018). The cardiac ryanodine receptor, but not sarcoplasmic reticulum Ca(2+)-ATPase, is a major determinant of Ca(2+) alternans in intact mouse hearts. *J. Biol. Chem.* 293, 13650–13661. doi: 10.1074/jbc.ra118.003760

Szentesi, P., Pignier, C., Egger, M., Kranias, E. G., and Niggli, E. (2004). Sarcoplasmic reticulum Ca2+ refilling controls recovery from Ca2+-induced Ca2+ release refractoriness in heart muscle. *Circ. Res.* 95, 807–813.

Verrier, R. L., Klingenheben, T., Malik, M., El-Sherif, N., Exner, D. V., Hohnloser, S. H., et al. (2011). Microvolt T-wave alternans physiological basis, methods of measurement, and clinical utility–consensus guideline by International Society for Holter and Noninvasive Electrocardiology. *J. Am. Coll. Cardiol.* 58, 1309–1324.

Walker, M. L., and Rosenbaum, D. S. (2005). Cellular alternans as mechanism of cardiac arrhythmogenesis. *Heart Rhythm.* 2, 1383–1386. doi: 10.1016/j.hrthm.2005.09.009

Wan, X., Laurita, K. R., Pruvot, E. J., and Rosenbaum, D. S. (2005). Molecular correlates of repolarization alternans in cardiac myocytes. *J. Mol. Cell Cardiol.* 39, 419–428. doi: 10.1016/j.yjmcc.2005.06.004

Wang, L., De Jesus, N. M., and Ripplinger, C. M. (2015). Optical mapping of intra-sarcoplasmic reticulum Ca2+ and transmembrane potential in the langendorff-perfused rabbit heart. *J. Vis. Exp.* 103:53166.

Wang, L., Myles, R. C., De Jesus, N. M., Ohlendorf, A. K., Bers, D. M., and Ripplinger, C. M. (2014). Optical mapping of sarcoplasmic reticulum Ca2+ in the intact heart: ryanodine receptor refractoriness during alternans and fibrillation. *Circ. Res.* 114, 1410–1421. doi: 10.1161/circresaha.114.302505

Wang, L., and Ripplinger, C. M. (2019). "Optical mapping of sarcoplasmic reticulum Ca2+ and transmembrane potential in the intact heart: insights into Ca2+−mediated arrhythmias," in *Cardiac Mapping*, eds M. Shenasa, G. Hindricks, D. J. Callans, J. M. Miller, and M. E. Josephson (Hoboken, NJ: John Wiley & Sons Ltd), 313. doi: 10.1002/9781119152637.ch23

Wei, J., Yao, J., Belke, D., Guo, W., Zhong, X., Sun, B., et al. (2020). Ca(2+)-CaM dependent inactivation of RyR2 Underlies Ca(2+) alternans in intact heart. *Circ Res.* 128, e63–e83.

Weinberg, S. H. (2016). Impaired sarcoplasmic reticulum calcium uptake and release promote electromechanically and spatially discordant alternans: a computational study. *Clin. Med. Insights Cardiol.* 10, 1–15.

Weiss, J. N., Karma, A., Shiferaw, Y., Chen, P. S., Garfinkel, A., and Qu, Z. (2006). From pulsus to pulseless: the saga of cardiac alternans. *Circ. Res.* 98, 1244–1253. doi: 10.1161/01.res.0000224540.97431.f0

Wengrowski, A. M., Kuzmiak-Glancy, S., Jaimes, R. III, and Kay, M. W. (2013). NADH changes during hypoxia, ischemia, and increased work differ between isolated heart preparations. *Am. J. Physiol. Heart Circ. Physiol.* 306, H529–H537.

Wilson, L. D., Jeyaraj, D., Wan, X., Hoeker, G. S., Said, T. H., Gittinger, M., et al. (2009). Heart failure enhances susceptibility to arrhythmogenic cardiac alternans. *Heart Rhythm.* 6, 251–259. doi: 10.1016/j.hrthm.2008.11.008

Wilson, L. D., and Rosenbaum, D. S. (2007). Mechanisms of arrythmogenic cardiac alternans. *Europace* 9(Suppl. 6), vi77–vi82.

Xie, L. H., Sato, D., Garfinkel, A., Qu, Z., and Weiss, J. N. (2008). Intracellular Ca alternans: coordinated regulation by sarcoplasmic reticulum release, uptake, and leak. *Biophys. J.* 95, 3100–3110. doi: 10.1529/biophysj.108.130955

Zhang, T., Guo, T., Mishra, S., Dalton, N. D., Kranias, E. G., Peterson, K. L., et al. (2010). Phospholamban ablation rescues sarcoplasmic reticulum Ca(2+) handling but exacerbates cardiac dysfunction in CaMKIIdelta(C) transgenic mice. *Circ. Res.* 106, 354–362. doi: 10.1161/circresaha.109.207423

Zhong, X., Sun, B., Vallmitjana, A., Mi, T., Guo, W., Ni, M., et al. (2016). Suppression of ryanodine receptor function prolongs Ca2+ release refractoriness and promotes cardiac alternans in intact hearts. *Biochem. J.* 473, 3951–3964. doi: 10.1042/bcj20160606

Zhong, X., Vallmitjana, A., Sun, B., Xiao, Z., Guo, W., Wei, J., et al. (2018). Reduced expression of cardiac ryanodine receptor protects against stress-induced ventricular tachyarrhythmia, but increases the susceptibility to cardiac alternans. *Biochem. J.* 475, 169–183. doi: 10.1042/bcj20170631

Zhou, X., Bueno-Orovio, A., Orini, M., Hanson, B., Hayward, M., Taggart, P., et al. (2016). In vivo and in silico investigation into mechanisms of frequency dependence of repolarization alternans in human ventricular cardiomyocytes. *Circ. Res.* 118, 266–278. doi: 10.1161/circresaha.115.307836

Zsebo, K., Yaroshinsky, A., Rudy, J. J., Wagner, K., Greenberg, B., Jessup, M., et al. (2014). Long-term effects of AAV1/SERCA2a gene transfer in patients with severe heart failure: analysis of recurrent cardiovascular events and mortality. *Circ. Res.* 114, 101–108. doi: 10.1161/circresaha.113.302421

Conflict of Interest: The authors declare that the research was conducted in the absence of any commercial or financial relationships that could be construed as a potential conflict of interest.

frontiers in Physiology

REVIEW
published: 09 September 2021
doi: 10.3389/fphys.2021.718404

The Physiology and Pathophysiology of T-Tubules in the Heart

*Ingunn E. Setterberg[1,2], Christopher Le[1,2†], Michael Frisk[1,2†], Harmonie Perdreau-Dahl[1,2], Jia Li[1,2] and William E. Louch[1,2]**

[1] Institute for Experimental Medical Research, Oslo University Hospital and University of Oslo, Oslo, Norway, [2] KG Jebsen Centre for Cardiac Research, University of Oslo, Oslo, Norway

In cardiomyocytes, invaginations of the sarcolemmal membrane called t-tubules are critically important for triggering contraction by excitation-contraction (EC) coupling. These structures form functional junctions with the sarcoplasmic reticulum (SR), and thereby enable close contact between L-type Ca^{2+} channels (LTCCs) and Ryanodine Receptors (RyRs). This arrangement in turn ensures efficient triggering of Ca^{2+} release, and contraction. While new data indicate that t-tubules are capable of exhibiting compensatory remodeling, they are also widely reported to be structurally and functionally compromised during disease, resulting in disrupted Ca^{2+} homeostasis, impaired systolic and/or diastolic function, and arrhythmogenesis. This review summarizes these findings, while highlighting an emerging appreciation of the distinct roles of t-tubules in the pathophysiology of heart failure with reduced and preserved ejection fraction (HFrEF and HFpEF). In this context, we review current understanding of the processes underlying t-tubule growth, maintenance, and degradation, underscoring the involvement of a variety of regulatory proteins, including junctophilin-2 (JPH2), amphiphysin-2 (BIN1), caveolin-3 (Cav3), and newer candidate proteins. Upstream regulation of t-tubule structure/function by cardiac workload and specifically ventricular wall stress is also discussed, alongside perspectives for novel strategies which may therapeutically target these mechanisms.

Keywords: t-tubules, dyad, cardiomyocyte, calcium homeostasis, heart failure

OPEN ACCESS

Edited by:
Daniel M. Johnson,
The Open University, United Kingdom

Reviewed by:
Jessica Caldwell,
University of California, Davis, United States
Leonardo Sacconi,
University of Florence, Italy
Fabien Brette,
Institut National de la Santé et de la Recherche Médicale (INSERM), France

****Correspondence:***
William E. Louch
w.e.louch@medisin.uio.no

† These authors have contributed equally to this work

Specialty section:
This article was submitted to Cardiac Electrophysiology, a section of the journal Frontiers in Physiology

Received: *31 May 2021*
Accepted: *07 July 2021*
Published: *09 September 2021*

Citation:
Setterberg IE, Le C, Frisk M, Perdreau-Dahl H, Li J and Louch WE (2021) The Physiology and Pathophysiology of T-Tubules in the Heart. Front. Physiol. 12:718404. doi: 10.3389/fphys.2021.718404

T-TUBULE STRUCTURE AND FUNCTION

Forceful contraction of the heart requires coordinated contraction of cardiac muscle cells, called cardiomyocytes. Within these cells, electrical excitation during the action potential is linked to cell shortening by a process known as excitation-contraction (EC) coupling. In mammalian heart, this process is made possible by membrane invaginations called t-tubules which propagate the action

Abbreviations: CICR, Ca^{2+}-induced Ca^{2+} release; Cav-3, Caveolin-3; CRU, Ca^{2+} release unit; DAD, Delayed afterdepolarization; EAD, Early afterdepolarization; EC coupling, Excitation-contraction coupling; HF, Heart failure; HFpEF, Heart failure with preserved ejection fraction; HFrEF, Heart failure with reduced ejection fraction; JPH2, Junctophilin-2; LTCC, L-type Ca^{2+} channel; miR-24, microRNA-24; MG53, Mitsugumin 53; NEXN, Nexilin; NCX, Sodium-calcium exchanger 1; PKC, Protein kinase C; RyR, Ryanodine Receptor; SR, Sarcoplasmic Reticulum; Tcap, Titin cap/Telethonin.

potential into the cell interior. Critical in normal cardiac physiology and importantly disrupted during disease, t-tubules have been the focus of considerable research focus in the past decades. This review will summarize this progress and outline future perspectives, with particular attention given to potential roles of t-tubules as therapeutic targets.

Structural Overview

Retzius (1881) first suggested t-tubules' existence in 1881 after he noted that muscle cells exhibit a quick inward spread of electrical depolarization ("negative variation"). Thereafter, the first visual evidence of t-tubules was provided by Nyström (1897), who found that India ink entered rabbit heart muscle in a transverse pattern. In 1957, with the help of electron microscopy, Lindner (1957) clearly described t-tubule structures in dog ventricular cardiomyocytes. Subsequent studies from both skeletal and cardiac muscle revealed that t-tubules serve to rapidly conduct electrical excitation and facilitate communication with the sarcoplasmic reticulum (SR) (Huxley and Taylor, 1955; Cheng et al., 1996), thereby playing a central role in EC coupling. More recently, the advent of newer techniques, such as three-dimensional (3D) electron microscopy, super-resolution microscopy, and ion-conductance microscopy have provided ever greater detail in current understanding of t-tubule biology (Gu et al., 2002; Hayashi et al., 2009; Pinali et al., 2013; Crossman et al., 2017; Frisk et al., 2021).

A schematic overview of cardiomyocyte t-tubule structure is provided in **Figure 1**. Originally named transverse tubules, the majority of these structures are indeed oriented transversely across the cell, in a well-organized network along the Z-lines (Lindner, 1957; McNutt, 1975; Kostin et al., 1998). However, a fraction of tubules is positioned along the cardiomyocyte's longitudinal axis, extending into the A-band of the sarcomere (Simpson, 1965; Forssmann and Girardier, 1970; Sperelakis and Rubio, 1971; Forbes and Sperelakis, 1976; Soeller and Cannell, 1999; Pinali et al., 2013). In an effort to accurately describe this arrangement, and include both populations of t-tubules, some have referred to the overall network as the transverse-axial tubule system (TATS) (Sperelakis and Rubio, 1971; Forbes and Sperelakis, 1976). In rat cardiomyocytes, the proportions of transverse and longitudinal t-tubules are estimated at 60 and 40%, respectively (Soeller and Cannell, 1999), although as noted below there are large species differences. In addition to variation in overall orientation, t-tubules also exhibit non-uniform branching, tortuosity, bulges, and folds (Jayasinghe et al., 2012; Hong et al., 2014), and the lumen diameter of the t-tubules varies from 20 to 450 nm (Soeller and Cannell, 1999). These narrow dimensions of the t-tubules are believed to restrict solute movement compared to the extracellular environment, with important physiological consequences (Swift et al., 2006; Kong et al., 2018b; Uchida and Lopatin, 2018). However, a recent publication demonstrated that there is significant deformation of t-tubules throughout the cardiomyocyte contractile cycle. During contraction, extracellular solution is thus actively pumped in and out of the t-tubular compartment in a rate-dependent manner, counteracting geometrical diffusion constraints, and representing a new form of t-tubule functional autoregulation which has been hitherto underappreciated (Rog-Zielinska et al., 2021b).

There are considerable species differences in t-tubule density and organization (Soeller and Cannell, 1999). Indeed, depending on species, t-tubules constitute 0.8–3.6% of the total cell volume, and 21–64% of the total sarcolemma (Stewart and Page, 1978; Severs et al., 1985; Bers, 2002; Hayashi et al., 2009). In smaller species with higher heart rates (mouse and rat), t-tubule arrangement is the most complex, with denser, more branched and thinner structures than large mammals (rabbit, pig, and human) (Soeller and Cannell, 1999; Cannell et al., 2006; Savio-Galimberti et al., 2008; Jayasinghe et al., 2012; Kong et al., 2018b). Mouse cardiomyocytes also exhibit smaller t-tubule openings, and thus it has been proposed that t-tubular solute movement is more restricted in these cells than in larger species (Kong et al., 2018b). T-tubule topology also varies across the different heart chambers. While t-tubule structure is reported to be similarly well-organized in both left and right ventricle (Tidball et al., 1991; Chen et al., 2013; Guo et al., 2013), there is greater variance reported in the atria. Although t-tubules have been identified in atrial myocytes in both small (rat) (Frisk et al., 2014) and larger mammals (pig, dog, sheep, cow, horse, and human) (Dibb et al., 2009; Lenaerts et al., 2009; Richards et al., 2011; Frisk et al., 2014; Arora et al., 2017), studies in rat and pig indicated that only a minority of atrial cells contain tubular structures (Frisk et al., 2014; Gadeberg et al., 2016). When they are present in atrial cells, t-tubules are considerably less developed than those present in ventricular myocytes, with generally lower density and often a more longitudinal orientation (Dibb et al., 2009; Lenaerts et al., 2009; Smyrnias et al., 2010; Richards et al., 2011; Frisk et al., 2014; Glukhov et al., 2015; Gadeberg et al., 2016; Arora et al., 2017). Notably, t-tubule density is reported to be higher in the atria's epicardium than in the endocardium (Frisk et al., 2014). Although not yet closely examined, there may also be intra-chamber variability in t-tubule structure, as lower t-tubule density has been reported in the apex than other regions of the left ventricle (Wright et al., 2018; Frisk et al., 2021).

Functional Overview

As central players in EC-coupling, t-tubule structure is closely linked to contractile function. T-tubules carry the action potential (AP) deep into the cell interior, and the resulting depolarization of the t-tubular membrane leads to opening of voltage-gated L-type Ca^{2+} channels (LTCCs, $Ca_v1.2$; see **Figure 1**). This influx of Ca^{2+} from the extracellular space triggers a larger amount of Ca^{2+} release from the SR through ryanodine receptors (RyRs); a process called Ca^{2+}-induced Ca^{2+} release (CICR) (Fabiato, 1983; Bers, 2002). Binding of the released Ca^{2+} to the myofilaments results in the contraction of the cell, and thus the whole heart. Thereafter, relaxation occurs as Ca^{2+} is recycled into the SR by the SR Ca^{2+}-ATPase (SERCA), or extruded from the cell by the Na^+/Ca^{2+} exchanger (NCX), and to a lesser extent, the sarcolemmal Ca^{2+} ATPase (Louch et al., 2012).

The presence of a dense and well-organized t-tubule network ensures synchronous Ca^{2+} release across the cell. This is particularly apparent in mouse and rat ventricular cardiomyocytes, due to the robust presence of these structures

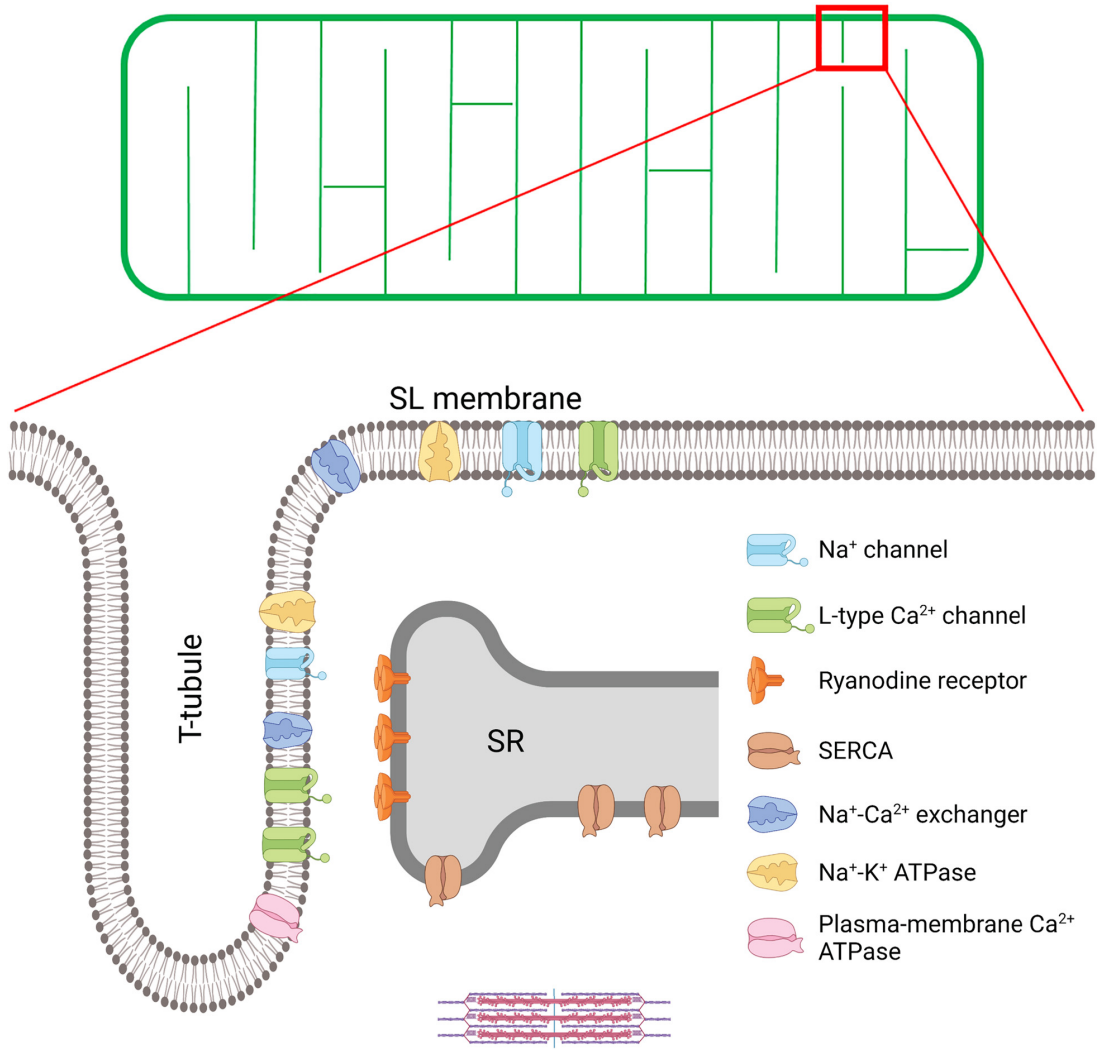

FIGURE 1 | T-tubule structure and key proteins involved in excitation-contraction (EC) coupling in the cardiomyocyte. A schematic overview of the t-tubule network is provided in the upper panel, while an enlargement of the indicated region is provided below to illustrate positioning of EC coupling proteins. EC coupling is initiated as Na^+ channels are opened, and the cell membrane depolarizes during the action potential. This depolarization triggers the opening of voltage-gated L-type Ca^{2+}-channels (LTCCs) in the t-tubules, and subsequent Ca^{2+}-induced Ca^{2+} release from the SR through the opening of Ryanodine Receptors (RyRs). This process occurs at specialized junctions called dyads, where LTCCs and RyRs are in close proximity. After released Ca^{2+} binds to the myofilaments to trigger contraction, Ca^{2+} is recycled into the SR by the sarco-endoplasmic reticulum ATPase (SERCA), and removed from the cell by the Na^+-Ca^{2+} exchanger (NCX) and the plasma-membrane Ca^{2+} ATPase. NCX activity is critically regulated by Na^+ levels, set by the Na^+ channel and the Na^+-K^+ ATPase within t-tubules. Created with BioRender.com.

(Heinzel et al., 2002; Louch et al., 2006; Song et al., 2006). However, in larger animals, such as pig, less synchronous Ca^{2+} release has been linked to the lower cardiomyocyte t-tubule density (Heinzel et al., 2002, 2008). Similarly, in atrial cells with a less developed t-tubule network, the Ca^{2+} transient is less synchronous, with a wave-like propagation of released Ca^{2+} from the periphery toward the cell interior (Frisk et al., 2014). This dyssynchronous pattern of Ca^{2+} release can be reproduced by experimentally detubulating cardiomyocytes (Louch et al., 2004; Brette et al., 2005).

Triggering of Ca^{2+} release from the SR requires its close alignment with the t-tubule membrane at "dyads" (**Figure 1**), and close proximity between LTCCs and RyRs (Sun et al., 1995). While EM data have historically indicated that the dyadic cleft measures only ≈12 nm across (Takeshima et al., 2000), recent data have suggested that the true dimensions may be even more narrow (<10 nm), and that artifactual expansion of the cleft could have occurred in earlier work as a result of sample fixation procedures (Rog-Zielinska et al., 2021a). Consistent dyadic dimensions are ensured by junctophilin-2 (JPH2) which stabilizes the membranes, but also functionally interacts with both RyRs and LTCCs (Jiang et al., 2016; Munro et al., 2016; Reynolds et al., 2016; Gross et al., 2021). Insight into the precise positioning of these dyadic proteins has been made possible

by new advances in super-resolution microscopy, including STED (Wagner et al., 2012), 3d STORM (Shen et al., 2019), and DNA-PAINT techniques (Jayasinghe et al., 2018; Sheard et al., 2019). For example, nanoscale visualization of RyRs has shown that these proteins are organized into clusters containing an average of 9–14 channels (Baddeley et al., 2009; Jayasinghe et al., 2018; Shen et al., 2019). Tight packing of RyRs within these clusters is thought to synchronize their gating (Marx et al., 2001; Sobie et al., 2006). At the larger scale, RyR clusters that are in close proximity have been predicted to cooperate as a Ca^{2+} release unit (CRU), or a "super-cluster," with released Ca^{2+} jumping between nearby clusters to produce a Ca^{2+} spark (Sobie et al., 2006; Baddeley et al., 2009; Louch et al., 2013; Kolstad et al., 2018). CRUs are estimated to contain an average of between 18 and 23 RyRs (Shen et al., 2019), and this composition is a key factor in determining Ca^{2+} spark frequency and amplitude (Xie et al., 2019).

On the t-tubule side of the dyad, LTCCs are localized opposite RyR clusters. LTCCs also form clusters, with sizes estimated to be about 67% of those reported for RyRs (Scriven et al., 2010). Exciting new data indicate that the interaction between LTCCs facilitates Ca^{2+} influx *via* coupled gating of the channels (Dixon et al., 2015). Recently, Ito and colleagues found that β-adrenergic receptor activation augments LTCC abundance and promotes enhanced channel interaction, thereby amplifying Ca^{2+} influx *via* a protein kinase A-dependent pathway (Ito et al., 2019). NCX localization in dyads remains a controversial topic (Scriven et al., 2000; Thomas et al., 2003), but it is reported that at least a fraction of NCX is colocalized with RyRs (Mohler et al., 2005; Jayasinghe et al., 2009; Schulson et al., 2011; Wang et al., 2014; **Figure 1**). While the main function of NCX is extrusion of Ca^{2+} during relaxation (Louch et al., 2012), numerous reports have suggested that Ca^{2+} entry *via* NCX can also act in "reverse mode" to trigger SR Ca^{2+} release (Sipido et al., 1997; Henderson et al., 2004; Lines et al., 2006; Larbig et al., 2010). This mechanism is proposed to follow Na^{+} influx during the rising phase of the action potential, which creates driving force for NCX-mediated Ca^{2+} entry.

Besides ion channels, such as the LTCC and NCX, the t-tubular membrane is also enriched in molecules which critically regulate their structure and function. Notable examples are amphiphysin-2 (BIN1), junctophilin-2 (JPH2), and caveolin-3 (Cav-3) (**Figure 1**), which are involved in functions spanning t-tubule growth, t-tubule microdomain formation, and regulation of LTCC and RyR localization and activity. A detailed discussion of these important t-tubule regulators will be made in the following sections.

T-TUBULE REMODELING

T-Tubule Remodeling Throughout Life

The process of t-tubule development varies between species (Ziman et al., 2010; Louch et al., 2015; Jones et al., 2018). In species such as cow, guinea pig, sheep and human, t-tubules have been found in the fetal stages of development (Forbes and Sperelakis, 1976; Sheldon et al., 1976; Forsgren and Thornell, 1981; Brook et al., 1983; Kim et al., 1992). A recent study in sheep specified that t-tubule development started at a late fetal stage (108 days out of 145 days), with further maturation occurring after birth (Munro and Soeller, 2016). In contrast, t-tubules only appear postnatally in mouse, rat, rabbit, and cat cardiomyocytes (Hirakow et al., 1980; Hoerter et al., 1981; Gotoh, 1983; Ziman et al., 2010; Hamaguchi et al., 2013; Lipsett et al., 2019). In rats, t-tubules appear gradually and become visible around 4–9 days after birth (Ziman et al., 2010; Mackova et al., 2017; Lipsett et al., 2019), with an initial appearance at the cell surface as sparse openings along Z-spines, with a rudimentary internal structure that is largely longitudinal in orientation (**Figure 2**). During further development, t-tubule density strikingly increases, with a re-orientation into a clear striated pattern at roughly 20 days of age, and a progressively more dominant presence of transverse over longitudinal elements (Ziman et al., 2010; Louch et al., 2015; Mackova et al., 2017; **Figure 2**). This process continues until surprisingly late stages of postnatal development (Oyehaug et al., 2013).

It is noteworthy that the heart exhibits robust contractile function at early embryonic stages of development in the absence of t-tubules (Brand, 2003). Since these embryonic myocytes are quite thin, EC coupling is sufficiently supported by U-shaped propagation of the Ca^{2+} transient from the surface of the cells to the interior (Rapila et al., 2008; Korhonen et al., 2010), reminiscent of Ca^{2+} release patterns observed in detubulated myocytes described above. This pattern of Ca^{2+} release is initiated at the cell surface, where LTCCs and RyRs are co-localized before birth (Snopko et al., 2008), and propagated by RyRs assembled on SR extensions positioned at intervals of 2 μm (de Diego et al., 2008; Rapila et al., 2008). These internal RyR clusters continue to be assembled along Z-lines as t-tubules arrive, and dyadic pairings with LTCCs are quickly formed (Ziman et al., 2010; Lipsett et al., 2019). Thus, dyadic functionality is rapidly attained once these structures are formed, allowing progressive increases in Ca^{2+} release efficiency with further maturation (Ziman et al., 2010; Lipsett et al., 2019).

Recent data suggest that the aging heart may exhibit reversal of the processes of dyadic assembly that take place during development. Aging is associated with reduced cardiomyocyte contractility, especially in males (Grandy and Howlett, 2006; Feridooni et al., 2015), and these changes are linked to reduction in cardiomyocyte t-tubule density (Kong et al., 2018a; Lyu et al., 2021). An accompanying reduction of t-tubule Ca^{2+} current density during aging has also been linked to loss of a cav-3-dependent mechanism that augments t-tubular Ca^{2+} current density (Kong et al., 2018a).

T-Tubule Remodeling During Heart Failure

Heart failure (HF) is a leading cause of death worldwide. It is therefore of great importance to understand the different mechanisms underlying this condition, to facilitate discovery of novel treatment targets. HF can be divided into two main entities; HF with reduced ejection fraction (HFrEF) and HF with preserved ejection fraction (HFpEF). HFrEF describes a state where the cardiac muscle is unable to contract adequately, leaving

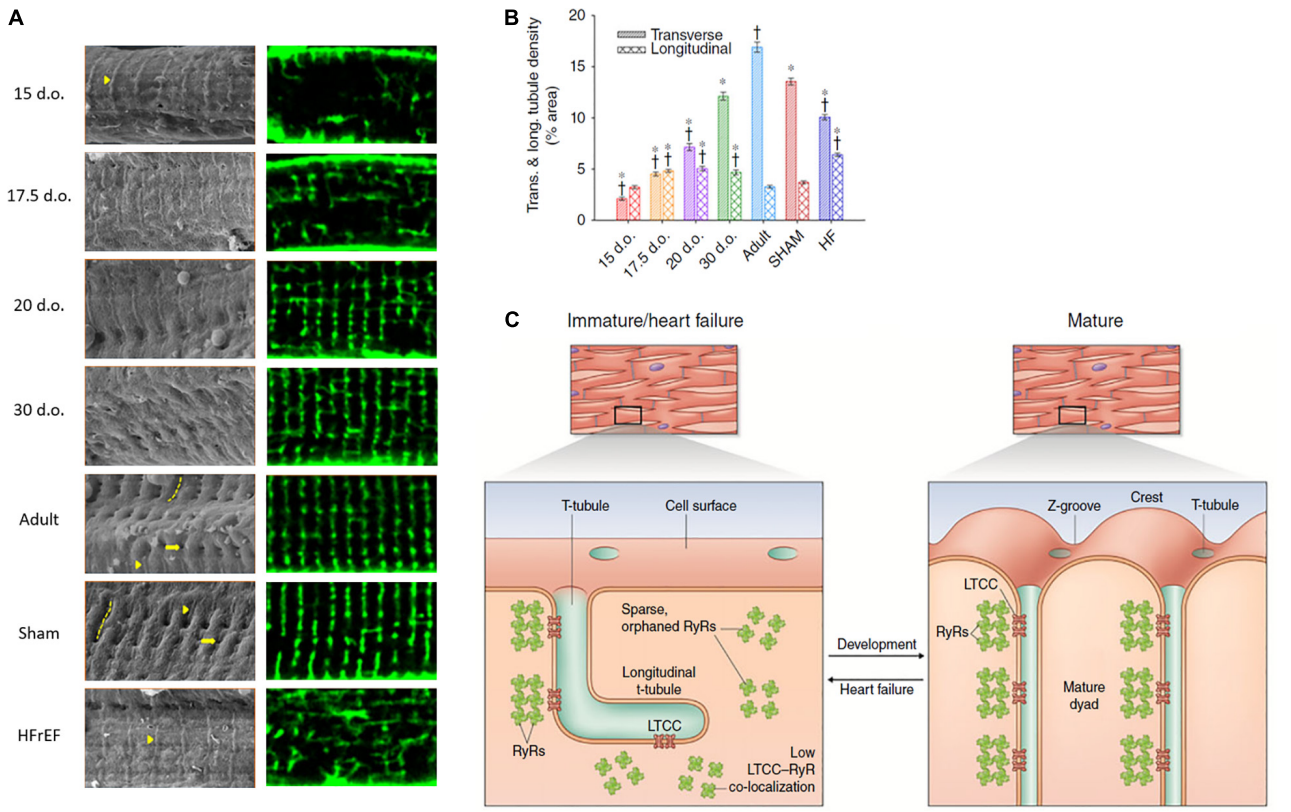

FIGURE 2 | Changes in cardiomyocyte surface topography and dyadic organization in the developing and HFrEF rat heart. **(A)** Left panels: Scanning electron micrographs show the appearance of Z-spines (arrowheads) from an early time point during development and their re-appearance during post-infarction HFrEF. Z-grooves (dashed lines) and t-tubule openings (arrows) appear gradually during development and are lost in HFrEF. Right panels: temporally matched confocal captures of internal t-tubules (di-8-ANEPPS staining). **(B)** Quantification of these t-tubule signals illustrates an organizational shift from a predominantly longitudinal to largely transverse orientation during maturation, but reversion to an immature phenotype during HFrEF. **(C)** Structural parallels between developing and failing myocytes include not only t-tubule structure, but also similarly sparse arrangements of RyRs that exhibit low co-localization with LTCCs. d.o., days old. $^{*}P < 0.05$ vs. adult in same category, $^{\dagger}P < 0.05$ vs. SHAM in same category. Reproduced from Lipsett et al. (2019) with permission.

the heart unable to meet the body's oxygen demand. This state is associated with ventricular dilation, thinning of ventricular walls and high wall stress. HFpEF, on the contrary, is predominantly linked to cardiac hypertrophy, wall thickening, and maintained wall stress (Pieske et al., 2019). Although, ejection fraction is preserved in this condition, compromised cardiac chamber relaxation and filling yields impaired cardiac output. Hence, both HF entities are severe diseases with 2-year mortality rates between 14 and 19% (Lam et al., 2018).

HFrEF mechanisms have been extensively investigated, and numerous studies in a range of species and disease etiologies have linked disease progression to alterations in t-tubule structure and function (Jones et al., 2018; **Figure 3**). Typically this remodeling includes reduced t-tubule density (Maron et al., 1975; Heinzel et al., 2008; Swift et al., 2008; Wei et al., 2010; Wu et al., 2011, 2012; Xie et al., 2012; Ibrahim et al., 2013; Frisk et al., 2021; Yamakawa et al., 2021), including a lower density of transversely oriented tubules (Louch et al., 2006, 2013; Song et al., 2006; Swift et al., 2008; Ibrahim et al., 2010, 2013; Wei et al., 2010; van Oort et al., 2011; Wu et al., 2011; Lyon et al., 2012; Wagner et al., 2012; Xie et al., 2012; Oyehaug et al., 2013; Frisk et al., 2021). Based on this finding, it has often been claimed that t-tubules are "lost" in HFrEF. However, recent work has indicated that the t-tubule frame may in fact be maintained in this condition, although cell size increases (Frisk et al., 2021). Thus, the observed decrease in t-tubule density is suggested to reflect a lack of adaptive remodeling to meet the developing cellular hypertrophy, rather than a degradation of t-tubule structure *per se*. Further complicating the picture is the observation that t-tubule remodeling in HFrEF frequently includes an increased fraction of longitudinally oriented tubules (Kaprielian et al., 2000; Louch et al., 2006, 2013; Song et al., 2006; Sachse et al., 2012; Swift et al., 2012; Wagner et al., 2012; Oyehaug et al., 2013; Frisk et al., 2016, 2021), t-tubule dilation (Maron et al., 1975; Schaper et al., 1991; Kostin et al., 1998; Kaprielian et al., 2000; Lyon et al., 2012; Pinali et al., 2017), loss of tubule openings at the cell surface (Lyon et al., 2009; Lipsett et al., 2019), and the appearance of broad t-tubule "sheets" (Pinali et al., 2017; Seidel et al., 2017a; Fiegle et al., 2020). The animal models employed in these examinations have included myocardial infarction (Louch et al., 2006; Swift et al., 2008; Lyon et al., 2009; Wagner et al., 2012; Oyehaug et al., 2013; Crocini et al., 2014; Frisk et al.,

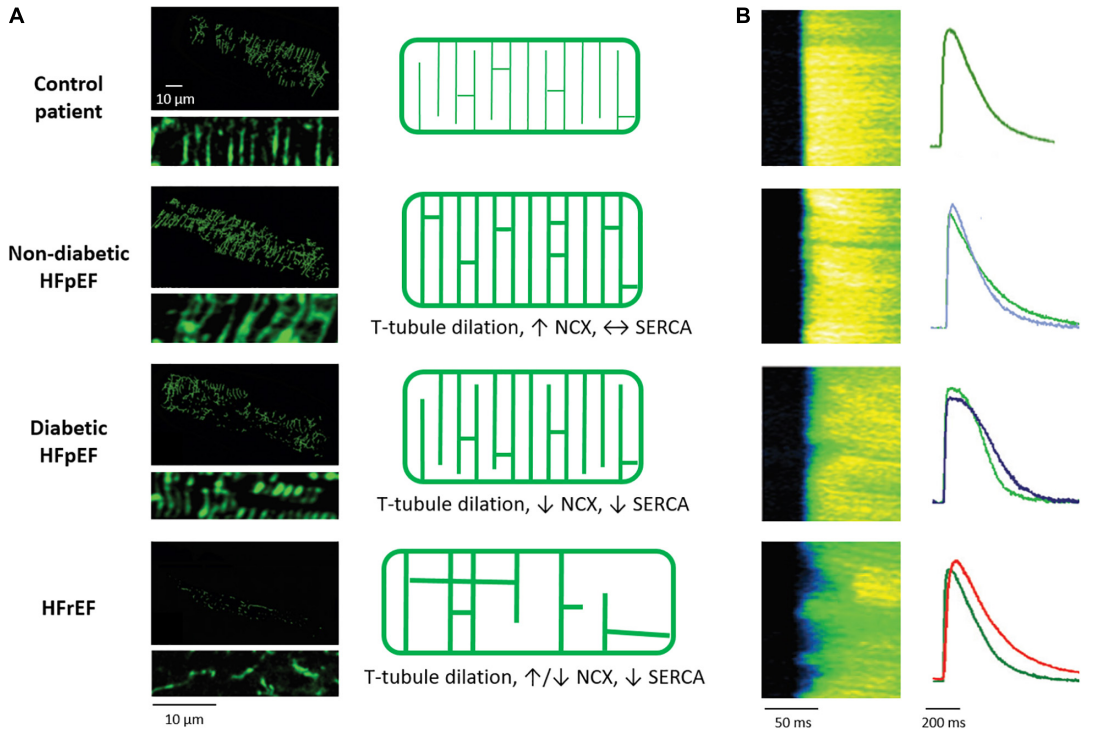

FIGURE 3 | Alterations in cardiomyocyte t-tubule structure and Ca^{2+} release in different HF entities. **(A)** Left panels: 3D reconstructions and 2D zoom-ins of t-tubules imaged in human cardiac biopsies (wheat germ agglutinin staining). Healthy individuals are compared with HFpEF patients, with and without diabetes mellitus, and HFrEF patients. As illustrated in the schematics (right panels), t-tubule density is unchanged in diabetic HFpEF, increased in non-diabetic HFpEF, and decreased in HFrEF. In all HF entities, t-tubules dilate. However, whereas t-tubule remodeling is accompanied by increased NCX and SERCA function in non-diabetic HFpEF, Ca^{2+} removal by these proteins is decreased in diabetic HFpEF and HFrEF. **(B)** T-tubule disruption promotes dyssynchronous and slowed Ca^{2+} release in rats with HFrEF but not HFpEF, while slowed Ca^{2+} removal promotes diastolic dysfunction in diabetic HFpEF and HFrEF. For each disease state, representative Ca^{2+} transients (right panels) are presented with comparison to a control cardiomyocyte (green) for the individual rat models. Micrographs and Ca^{2+} transients are reproduced from Frisk et al. (2021) with permission.

2016, 2021; Sanchez-Alonso et al., 2016; Schobesberger et al., 2017; Lipsett et al., 2019), aortic stenosis (Wei et al., 2010; Ibrahim and Terracciano, 2013; Pinali et al., 2013; Caldwell et al., 2014), hypertension (Song et al., 2006; Xie et al., 2012; Shah et al., 2014; Singh et al., 2017), tachycardia (He et al., 2001; Balijepalli et al., 2003; Caldwell et al., 2014), and diabetes (Stolen et al., 2009; Ward and Crossman, 2014). Similar disruption of t-tubule structure has also been reported during chronic ischemia (Heinzel et al., 2008) and atrial fibrillation (Lenaerts et al., 2009). Notably, t-tubule remodeling is not limited to the left ventricle, as comparable alterations have been reported in the right ventricle (Wei et al., 2010; Xie et al., 2012) and atrial cells as well (Melnyk et al., 2002; Dibb et al., 2009; Lenaerts et al., 2009; Wakili et al., 2010; Richards et al., 2011). In disease models with a non-uniform myocardial affliction, such as myocardial infarction, there are reports that t-tubule remodeling exhibits a spatial gradient, with the most marked changes occurring proximal to the infarcted myocardium (Frisk et al., 2016; Pinali et al., 2017; Wang et al., 2018). Perhaps most importantly, examinations in human tissue (Crossman et al., 2015; Frisk et al., 2021) broadly concur with the findings described in animal disease models, as reviewed in Louch et al. (2010b), Ibrahim et al. (2011), Guo et al. (2013), and Hong and Shaw (2017).

T-tubule disorganization during HFrEF causes spatial dissociation between key players in EC coupling, most notably LTCCs and RyRs. This rearrangement leads to the formation of "orphaned" RyRs which are no longer co-localized with t-tubules (Louch et al., 2006; Song et al., 2006; **Figure 2C**). A resulting de-synchronization of the Ca^{2+} transient occurs, as Ca^{2+} release from orphaned RyRs can only be triggered after diffusion of Ca^{2+} from intact dyads (He et al., 2001; Balijepalli et al., 2003; Cannell et al., 2006; Kemi et al., 2011; Xie et al., 2012; Louch et al., 2013). Ca^{2+} release dyssynchrony is further augmented in failing cells by reduced SR Ca^{2+} content (Oyehaug et al., 2013). The net result of this de-synchronized Ca^{2+} transient is slowed and reduced magnitude of contraction; a hallmark of HFrEF (Louch et al., 2010b).

Impaired efficiency of CICR is not only linked to reorganized t-tubules and orphaned RyRs, but also a reduced ability of t-tubules to trigger Ca^{2+} release where they are present. This deficit is at least partly attributable to reduced t-tubular LTCC current (Bryant et al., 2015; Sanchez-Alonso et al., 2016; Lipsett et al., 2019). Reduced L-type current has, in turn, been linked to altered localization of LTCCs, but also changes in AP configuration, that prevent optimal channel recruitment (Sah et al., 2002; Louch et al., 2010a). Interesting

data have suggested that there is also impairment of AP propagation into some t-tubules in failing cardiomyocytes, resulting in desynchronization of Ca^{2+} release (Crocini et al., 2014). Continuing work has suggested that this loss of electrical activation may be caused by constriction of t-tubule geometry in this condition (Scardigli et al., 2017; Uchida and Lopatin, 2018).

Recent work has indicated that loss of t-tubule functionality during HFrEF additionally stems from alterations on the SR side of the dyad. We observed "dispersion" of RyRs in MI-induced HFrEF, characterized by break-up of RyR clusters into smaller sub-clusters (Kolstad et al., 2018; **Figure 2C**). Functionally, we observed that this dispersion was associated with increased "silent" Ca^{2+} leak, not visible as sparks. Furthermore, we found that larger multi-cluster CRUs exhibited low fidelity Ca^{2+} spark generation. When successfully triggered, sparks in failing cells displayed slow kinetics as Ca^{2+} spread across dispersed CRUs. Previous work performed by us and others demonstrated that sparks occur almost exclusively at t-tubules (Brette et al., 2005; Meethal et al., 2007; Louch et al., 2013), suggesting that CRU dispersion and slow sparks solely occur at intact dyads. Thus, t-tubule and CRU remodeling may occur independently. Ultimately, it seems likely that t-tubule and CRU disruption have additive effects, yielding even more marked de-synchronization and slower SR Ca^{2+} release (Kolstad et al., 2018).

Importantly, not all dyadic changes during HFrEF are detrimental. For example, at early stages of disease, longitudinal tubules appear before transverse elements have disappeared (Louch et al., 2006). LTCCs are co-localized with RyRs at longitudinal dyads, allowing these structures to actively release Ca^{2+} (Lipsett et al., 2019). Thus, their early growth following the initiating insult (for example myocardial infarction or induction of aortic banding) is thought to be compensatory (Mork et al., 2007). At later time points, contractile function declines as transverse elements are lost, supporting that this latter type of remodeling is a direct cause of HFrEF (Wei et al., 2010; Shah et al., 2014).

Heart Failure With Preserved Ejection Fraction

The above discussion has highlighted convincing evidence that disrupted t-tubule structure and Ca^{2+} homeostasis are a root cause of HFrEF. However, approximately 50% of HF patients exhibit HFpEF (Lekavich et al., 2015), and the mechanisms underlying this disease entity are merely beginning to be unraveled. Recent evidence from our group indicates that a distinct form of subcellular remodeling occurs in this condition. Using patient biopsies we observed that, conversely to HFrEF, cardiomyocytes from HFpEF individuals exhibited increased t-tubule density (**Figure 3A**), and a positive correlation between t-tubule density and the severity of *in vivo* diastolic dysfunction (Frisk et al., 2021). Higher t-tubule densities resulted from a combination of t-tubule dilation and proliferation, consistent with adaptive remodeling. These data contribute to growing evidence that t-tubules have compensatory capacity, as similar increases in t-tubule density have been reported during physiological hypertrophy following exercise training (Kemi et al., 2011). In this sense, t-tubule growth during concentric, non-dilatory hypertrophy may be viewed as a continuation of processes set in motion during development. Importantly, functional data support such a compensatory role, as cardiomyocytes obtained from hypertensive and ischemic rat models of HFpEF revealed maintained Ca^{2+} release and reuptake despite decreased SERCA protein levels (**Figure 3B**). Marked phosphorylation of the SERCA inhibitory protein phospholamban was identified as the key motif for unchanged diastolic Ca^{2+} homeostasis (Frisk et al., 2021). Other studies examining Dahl salt sensitive rats and aorta banded rats with impaired cardiac relaxation have reported similar maintenance of t-tubule structure and Ca^{2+} homeostasis (Roe et al., 2017; Curl et al., 2018; Kilfoil et al., 2020).

HFpEF includes a set of patients with diverse etiologies, including those suffering from cardiac ischemia or hypertension, as noted above, but also diabetes (Lekavich et al., 2015). In contrast to other disease etiologies, diabetic HFpEF appears to negatively affect both t-tubule integrity and Ca^{2+} handling. Indeed, we observed that HFpEF patients and animal models with diabetes exhibited less compensatory t-tubule growth than their non-diabetic counterparts, as t-tubule density was merely maintained (Frisk et al., 2021; **Figure 3A**). We hypothesize that this reduced capacity for adaptive remodeling may be related to abnormal caveolin-3 and/or phospoinositol-3 kinase expression and activity, since cholesterol, fatty acid and phosphoinositide composition of the sarcolemmal membrane are altered during diabetes (Russell et al., 2017). As discussed later, decreased autophagy might also play a role (Hsu et al., 2016; Seidel et al., 2019). Despite less adaptive t-tubule remodeling, systolic Ca^{2+} release was observed to be quite well-maintained in diabetic HFpEF. However, diastolic dysfunction in this condition was linked to impairment of diastolic Ca^{2+} homeostasis, caused by reduced activity of both SERCA and NCX (Frisk et al., 2021; **Figure 3B**). Accumulating evidence has indicated that the reduced NCX activity in diabetic HFpEF may be related to elevated cytosolic Na^+ levels, which reduce the driving force for t-tubular Ca^{2+} removal. This Na^+ accumulation has in turn been linked to increased activity of the Na^+-glucose co-transporter 1 (Lambert et al., 2015; Frisk et al., 2021) and/or the Na^+-H^+-exchanger (Jaquenod De Giusti et al., 2019). Thus, there appears to be impairment of diastolic Ca^{2+} homeostasis in diabetic HFpEF, which includes detrimental alterations in t-tubule function.

While investigations of HFpEF mechanisms are ongoing, the above studies present an emerging view that t-tubule structure remains adequate to maintain near-normal SR Ca^{2+} release in this condition. This striking difference from the cardiomyocyte phenotype linked to HFrEF is perhaps not surprising. In addition to the aforementioned differences in chamber remodeling, HFrEF is primarily associated with activation of the renin-angiotensin- aldosterone system and stretch-mediated signaling pathways, while inflammation, endothelial dysfunction, and alteration of the extracellular matrix are key components of HFpEF (Paulus and Tschope, 2013). Perhaps most importantly, established therapies for HFrEF, such as neurohumoral blockage, have proven ineffective

for treatment of HFpEF (Paulus and Tschope, 2013). Thus, there appears to be a growing consensus that management of HFpEF will require novel strategies, and that these therapies may be best directed at non-cardiomyocyte alterations occurring in the endothelium and/or extracellular matrix.

Consequences for Arrhythmia

Alterations in t-tubule structure and function during HF not only impact systolic and diastolic function, but also have complex consequences for arrhythmia generation (Orchard et al., 2013). HFrEF is frequently associated with increased RyR "leak," which can be exacerbated by SR Ca^{2+} overload during β-adrenergic stimulation (Dridi et al., 2020). Extrusion of this spontaneously released Ca^{2+} by NCX triggers an inward, depolarizing current. If this current occurs during the downstroke of the action potential, an early afterdepolarization (EAD) results, while delayed afterdepolarizations (DADs) are triggered by spontaneous Ca^{2+} release between beats (Orchard et al., 2013). How would t-tubule remodeling during HFrEF affect these processes? As noted above, t-tubule reorganization in this disease results in the formation of orphaned RyRs. However, Ca^{2+} sparks occur mostly at intact dyads where t-tubules are present, and only to a much lesser degree at orphaned RyRs (Brette et al., 2005; Meethal et al., 2007; Louch et al., 2013). In the event that spontaneous release does occur at an orphaned RyR, an EAD or DAD would be less likely to occur because NCX is more distally located (Biesmans et al., 2011; Edwards and Louch, 2017). On the other hand, propagation of spontaneously released Ca^{2+} as a wave is more likely to occur, since distally localized NCX does not draw Ca^{2+} away from the wavefront. Recent data have painted a more complex picture that considers also the relationship between Ca^{2+} release and LTCC activity. Less Ca^{2+}-dependent inactivation of LTCCs, due to displaced (orphaned) RyRs, and resulting increased Ca^{2+} influx has been predicted to contribute to SR Ca^{2+} overload (Shiferaw et al., 2020). Thus, t-tubule remodeling may make spontaneous Ca^{2+} release more likely in HFrEF, while at the same time attenuating the link between these events and EADs/DADs.

T-tubule remodeling also has complex implications for EADs triggered by channel reopening. Phase-2 EADs initiated by LTCCs may be favored in HFrEF, as L-type current is redistributed to the cell surface (Sanchez-Alonso et al., 2016; Loucks et al., 2018). This increase in LTCC open probability has been linked to calcium-calmodulin kinase II-dependent phosphorylation of the channel, which augments window current (Sanchez-Alonso et al., 2016), but also phosphorylation by protein kinase A, based on the presence of β2 adrenergic receptors and phosphodiesterases (Loucks et al., 2018). Conversely, loss of LTCCs and NCX in t-tubules, and their respective currents, may shorten the AP making phase-2 EADs less likely, but Na^{+} channel re-activation and phase-3 EADs more likely (Orchard et al., 2013; Edwards and Louch, 2017). A shorter AP, and accompanying reduction in refractory period, also increases the chance of re-entrant arrhythmia (Herring et al., 2019). In addition to changes in ion channel expression and regulation, Hong and colleagues have provided evidence that alterations in the geometry of the t-tubules themselves can promote the occurrence of EADs (Hong et al., 2014). They observed that intricate folding of the t-tubule lumen creates a microenvironment with slowed ion diffusion. Upon loss of these membrane folds, more rapid exchange of ions between the t-tubule lumen and extracellular space was linked to prolonged action potential duration, and the generation of EADs and arrhythmia (Hong et al., 2014). This interesting observation raises the possibility that t-tubule dilation observed during HFrEF and HFpEF (**Figure 3A**) may also have arrhythmogenic consequences.

Finally, growing evidence supports that t-tubule remodeling during HFrEF can promote pro-arrhythmic alternans. Two mathematical modeling studies have linked spatially discordant alternans to the increased fraction of orphaned RyRs that yield a phase of secondary release following Ca^{2+} diffusion from intact dyads (Li et al., 2012; Song et al., 2018). Jiang et al. (2014) suggested that there is, however, an intermediate range of t-tubule remodeling where this phenomenon occurs. Thus, failing ventricular myocytes and healthy atrial myocytes are likely susceptible to this mechanism of alternans, while failing atrial myocytes may be less prone due to their very low t-tubule densities (Jiang et al., 2014). Importantly, since Ca^{2+}-voltage coupling is an additional determinant of alternans generation (Gaeta et al., 2009), the susceptibility of failing myocytes to alternans is expected to be complicated by changes in AP configuration. Interrogating and integrating these mechanisms will be an important topic of future work.

EMERGING T-TUBULE REGULATORS

The above sections have highlighted a growing consensus that t-tubule remodeling is a key trigger for reduced contractility and arrhythmia in HFrEF. This understanding has led to a concerted effort to reveal the processes that control t-tubule structure in both health and disease. We review the emerging findings from this work in the following sections.

Workload

Accumulating evidence has indicated that ventricular workload plays a key role in regulating t-tubule structure. Pioneering work by the Terraciano group was the first to indicate that the loss of t-tubules during HFrEF could be directly triggered by the elevated ventricular workload (reviewed in Ibrahim and Terracciano, 2013). In their work, failing hearts were unloaded by heterotopic transplantation into healthy animals, resulting in rescue of t-tubular structure (Ibrahim et al., 2012). Similar approaches to unloading of the failing heart either pharmacologically (Chen et al., 2012; Xie et al., 2012; Huang et al., 2016) or *via* resynchronization therapy (Sachse et al., 2012; Lichter et al., 2014) have similarly shown improved cardiac function linked to restoration of t-tubules. Interestingly, unloading of healthy hearts promoted loss of t-tubules (Ibrahim et al., 2012). These findings support the notion that there is an optimal range of loads necessary to maintain t-tubule integrity (Ibrahim et al., 2015).

Workload is a broad term, and ongoing efforts are aimed at revealing the precise critical mechanical stimuli which control t-tubule structure. The dilated, thin-walled ventricle leads to elevated ventricular wall stress in HFrEF, and this appears to be

a critical mechanical signal. Indeed, when we examined regional differences across the post-infarction rat heart we observed a correlation between wall stress and t-tubule disruption. This remodeling included significant t-tubule disruption near the infarct, where thinning of the myocardium markedly increases wall stress, together with locally impaired Ca^{2+} homeostasis and *in vivo* systolic and diastolic dysfunction (Frisk et al., 2016; Roe et al., 2019). *Ex vivo* studies supported this direct role of wall stress in the regulation of t-tubular structure. A likely implication of this wall stress-t-tubule relationship is in differentiating the pathophysiology of HFrEF and HFpEF, since as noted above, HFpEF is associated with concentric remodeling and maintained wall stress, and maintained t-tubule density (Frisk et al., 2021).

How does mechanical overload lead to the t-tubule loss? What are the associated mechanosensors and signaling pathways? While the precise mechanisms continue to be investigated, titin may be of importance, as it plays a key role in cardiomyocyte mechanotransduction by regulating interactions between the extracellular matrix and sarcomeres (Linke, 2008). Telethonin, or titin cap (TCap), a stretch-sensitive protein located in the Z-disc of cardiomyocytes, also integrates mechanical signals (Ibrahim and Terracciano, 2013; Ibrahim et al., 2013). Indeed, TCap knockout mice exhibited progressive disruption of the t-tubules during development (Ibrahim et al., 2013), and TCap downregulation is reported in HFrEF (Lyon et al., 2012). Furthermore, increased Tcap expression was associated with recovery of t-tubules during reverse remodeling induced by SERCA2a gene therapy (Lyon et al., 2012). While further studies are needed to examine the interplay between myocardial load, expression of Tcap, and t-tubule organization, this protein is viewed as a promising therapeutic target (Roe et al., 2015).

Other studies have linked membrane-mediated mechanosensation by stretch-activated channels, integrins, proteoglycans and angiotensin II type I receptors to activation of a variety of pathways, including MAPK, AKT, calcineurin-NFAT, and microRNA-24 (miR-24) (Lammerding et al., 2004; Dostal et al., 2014). Of these, it should be noted that miR-24 is a member of the miR23a-27a-24-2 cluster, which is upregulated in HF (Xu et al., 2012). Xu et al. (2012) observed that overexpression of miR-24 disrupted dyadic structure, and reduced CICR efficiency. This group also found that miR-24 suppression protected against HFrEF progression (Li et al., 2013).

As Jones et al. (2018) discussed in their recent review article, elevated workload and wall stress regulate not only cardiomyocyte remodeling, but also the extracellular matrix. Interestingly, recent evidence indicates that fibrosis occurs within t-tubules in HFrEF, but not in HFpEF where wall stress is maintained (Crossman et al., 2017; Frisk et al., 2021). Crossman and colleagues in fact detected fibroblast filopodia within the t-tubules of HFrEF hearts, suggesting a mechanism for local collagen production (Crossman et al., 2017). Although the consequences of this collagen deposition are unclear, it is proposed that accompanying stiffening of the membrane might mark the t-tubule for degradation (Louch and Nattel, 2017). In apparent support of this hypothesis, it should be noted that in the post-infarcted heart, the most marked t-tubule loss occurs in regions proximal to the infarct, where the fibrosis is most pronounced (Frisk et al., 2016; Seidel et al., 2017b). Fibrosis is expected to impair mechanosignaling, and new data indicate that this might occur within t-tubules themselves during stretch and contraction (Dyachenko et al., 2009; McNary et al., 2011). Such a role is suggestive of t-tubules having a self-regulating feature.

In summary of the above discussion, it appears to be no coincidence that the vast majority of present HFrEF therapies relieve symptoms and delay disease progression by reducing the workload of the heart, and specifically the physical stress placed on the ventricular wall (Cohn, 1996; Tarzia et al., 2016; Berliner and Bauersachs, 2017; Schmitto et al., 2018; Vaidya and Dhamoon, 2019). However, there is great potential for improvement. For example, wall stress and t-tubule structure might be longitudinally tracked as biomarkers, aimed at optimizing ventricular load. Future treatment strategies could also be envisioned which directly inhibit the mechanosensing that signals t-tubule remodeling.

Insight From Developing Cardiomyocytes

In the quest to unravel signaling pathways involved in triggering subcellular remodeling in HFrEF, newfound attention has turned to the importance of the fetal gene program. Indeed, our group has recently observed striking similarities between developing and diseased cardiomyocytes (**Figure 2**). Structurally, these similarities include a disorganized and predominantly longitudinal t-tubule configuration in both types of cells. There also appear to be similarities in dyadic configuration, as these junctions are progressively "packed" with LTCCs and RyRs in developing cardiomyocytes and "unpacked" in HFrEF, consistent with a "last in, first out" paradigm (Lipsett et al., 2019). However, even though immature and failing cardiomyocytes share rather similar subcellular structure, functional differences were observed. For example, while dyads were observed to effectively trigger Ca^{2+} release from early developmental states, impaired release Ca^{2+} release was noted along t-tubules in failing cells (Lipsett et al., 2019). Thus, it is unlikely that there is a complete reversion of subcellular structure/function to an immature state in this disease.

The above observations suggest that subcellular remodeling during HFrEF progression likely shares signaling mechanisms with the developing heart, which may include fetal genes that are reactivated in disease, and/or adult genes that are suppressed (Rajabi et al., 2007; Louch et al., 2015; **Figure 4**). Until recently, however, these signals and cardiomyocyte developmental biology in general have been rather under-investigated. This has changed as interest in the generation of stem cell-derived cardiomyocytes and myocardium has come to the forefront, and included an ever-expanding use of human induced pluripotent stem cells (iPSCs). Most early work on iPSC-derived cardiomyocytes generated cells with quite immature features, including a round instead of rod shape, lack of t tubules, poor cooperation of LTCCs and RyRs, and dyssynchronous Ca^{2+} transients with delayed Ca^{2+} release occurring in the cell center. More recently, however, improved differentiation has been achieved by treating iPSCs with hormones thought

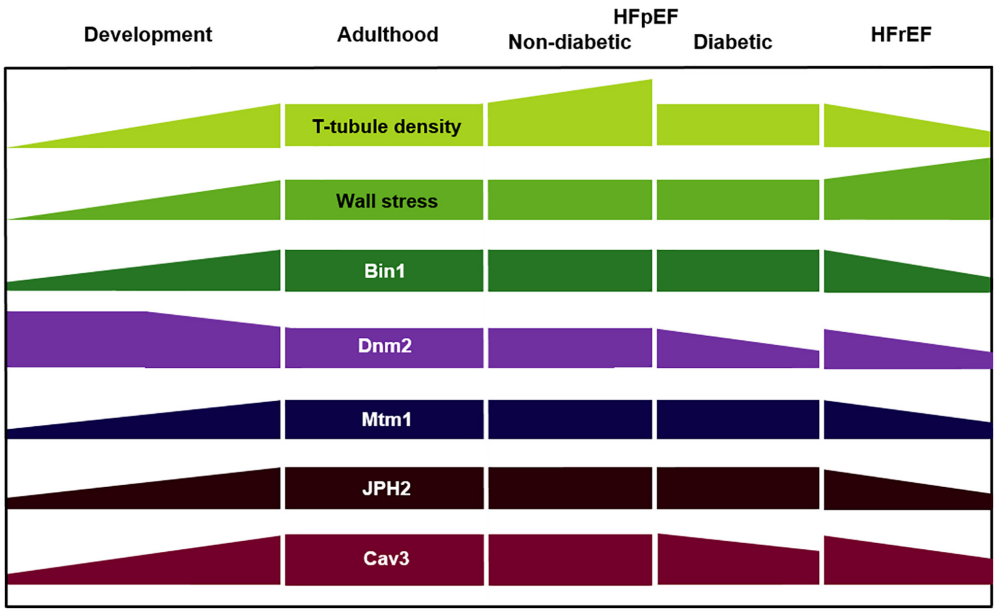

FIGURE 4 | Key regulators of t-tubule structure during development, adulthood, and heart failure of various etiologies. HFpEF, heart failure with preserved ejection fraction; HFrEF, heart failure with reduced ejection fraction; Dnm2, dynamin-2; Mtm1, myotubularin-1; JPH2, junctophilin-2; Cav3, caveolin-3.

critical for cardiac maturation. Parikh et al. (2017) observed that supplementing the culture medium with thyroid and glucocorticoid hormones, followed by single-cell culture on a Matrigel mattress, stimulated rudimentary t-tubule development and functional coupling of LTCCs and RyRs. Similarly, Huang et al. (2020) documented t-tubule formation close to z-lines in iPSC-derived cardiomyocytes treated with thyroid hormone, dexamethasone, and insulin-like growth factor-1 in both 2D and 3D culture conditions. It is noteworthy that both of these studies included a cellular environment which provided mechanical cues, reinforcing the view expressed above that t-tubule growth and maintenance are highly workload-sensitive. Indeed, even without hormone treatment, Silbernagel et al. (2020) found that reshaping single iPSC-CMs in rectangular 3D-micro-scaffolds triggered t tubule formation and improved Ca^{2+} handling. Ronaldson-Bouchard et al. (2018) on the other hand, co-cultured hiPSC-CMs with human cardiac fibroblasts, exposed the developing tissue to mechanical load, and gradually increased electrical stimulation. With this method, the authors observed an impressive degree of cellular maturation, including transversely oriented t-tubules, functional Ca^{2+} handling, and adult-like gene expression profiles. This progress has given credence to the application of iPSC-derived cardiomyocytes for human cardiac disease modeling, drug development, and eventually, engineered cardiac tissue which may be suitable for *in vivo* implantation.

BIN1 and Its Partners

In addition to the broader t-tubule regulatory processes described above, several specific proteins have been attributed roles in dyadic structure and function. Of these, BIN1 has received particular attention. This membrane sensing and bending protein has been identified as a key regulator of t-tubule structure assembly and maintenance in both developing and diseased hearts (Lee et al., 2002; Muller et al., 2003; Hong et al., 2010, 2014; see **Figure 4**). However, understanding of these roles has been complicated by the fact that BIN1 is expressed in several tissue- and species-specific isoforms. Early work suggested that the presence of exon 11 is required to induce tubulogenesis (Lee et al., 2002; Kojima et al., 2004), and exon 11-containing BIN1 isoforms expressed in rat, sheep, and human myocardium have indeed been observed to induce t-tubule formation (Caldwell et al., 2014; De La Mata et al., 2019; Lawless et al., 2019; Li L. L. et al., 2020). However, other studies have reported that exon 11 is dispensable for t-tubule development (Prokic et al., 2020), and shown that the mouse heart expresses four BIN1 splice variants which do not contain this motif (BIN1, BIN1+13, BIN1+17, and BIN1+13+17) (Forbes and Sperelakis, 1976; Hong et al., 2014). In addition to gross t-tubule biogenesis, there may also be isoform-specific roles in determining their fine structure and function. Hong and colleagues reported that isoform BIN1+13+17 creates microdomains by folding the tubular inner membrane (Hong et al., 2014), and attracts phosphorylated RyRs on the SR membrane (Fu et al., 2016). Since BIN1 also anchors microtubules transporting LTCCs, in a process known as targeted delivery (Hong et al., 2012b; De La Mata et al., 2019), an emerging view is that this protein serves as a master regulator of dyadic structure and function. Consistent with this paradigm, genetic knockout of BIN1 has been shown to be embryonically lethal (Muller et al., 2003).

Accumulating data have identified BIN1 as a culprit in cardiac pathology, with its downregulation linked to decreased t-tubule

density in HFrEF (Caldwell et al., 2014; Hong et al., 2014; **Figure 4**). An associated reduction in t-tubule folding has also been predicted to augment diffusion of ions within individual t-tubules which, as noted above, may predispose for cardiac arrhythmias (Hong et al., 2014). Furthermore, given BIN1's proposed role in trafficking of LTCCs and RyRs to the dyad, it seems highly plausible that "unpacking" of these proteins during HFrEF progression may be linked to declining BIN1 levels (Manfra et al., 2017). These findings indicate that BIN1 may serve as a therapeutic target in HFrEF, and preclinical data support this view. Treating mice with isoproterenol-induced HFrEF with adenoviral BIN1 overexpression was shown to attenuate hypertrophy, increase t-tubular microfolding, normalize SERCA2a distribution, and decrease the LTCC-RyR nearest neighbor distance (Liu Y. et al., 2020). This group additionally showed that BIN1 transduction rescued pre-existing global cardiac global dysfunction following aortic banding (Li J. et al., 2020). Beyond BIN1 overexpression as a therapeutic alternative, it appears that this protein may even serve as a biomarker. With normal, continuous turnover of BIN1 from dyads in healthy human patients, high levels of BIN1 are maintained in the blood. Thus, lowering of BIN1 levels has been linked to HF and arrhythmia (Hong et al., 2012a), including HFpEF disease severity and hospitalization risk (Nikolova et al., 2018), and HFrEF-associated risk of cardiovascular events (Hitzeman et al., 2020).

Given the exciting basic science and clinical data described above, more thorough investigation of BIN1's protein partners seems warranted. Evidence from skeletal muscle has indicated that BIN1's interaction with dynamin-2 (Dnm2) critically regulates tubulogenesis (Lee et al., 2002; Picas et al., 2014). This membrane-bound GTPase mediates membrane fission of clathrin-coated pits and plays a central role in membrane and vesicle trafficking (Gonzalez-Jamett et al., 2013). Dnm2 knockdown was found to rescue perinatal death in Bin1 knockout mice, and to normalize t-tubule formation and muscle function in animals with myopathies caused by Bin1 mutations (Tasfaout et al., 2017). An inhibitory role of Dnm2 in tubulogenesis was further supported by the observation that increasing its expression disrupts Bin1-induced tubulation in skeletal muscle (Gibbs et al., 2014).

A key aspect of Bin1's function appears to be its ability to cluster phosphoinositides (PIs), in particular PI4, $5P_2$ (Lee et al., 2002). The dominant precursors of this phosphoinositide are PI and PI5P, which are created through the actions of the PI3P phosphatase myotubularin-1 (MTM1) (Ketel et al., 2016). This protein is expressed in most tissues, where it regulates endolysosomal sorting and trafficking by controlling PI expression patterns (Ketel et al., 2016; **Figure 5**, yellow arrows). Exciting data from the skeletal muscle field indicate that Bin1-mediated tubulogenesis is dependent on MTM1's phosphatase activity, as MTM1 expression levels predict the extent of t-tubule biogenesis (Al-Qusairi and Laporte, 2011; Royer et al., 2013). Although MTM1's role in t-tubule formation in cardiomyocytes is not yet resolved, PIs are indeed thought to be important for maintaining t-tubule integrity (Wu et al., 2011) and MTM1

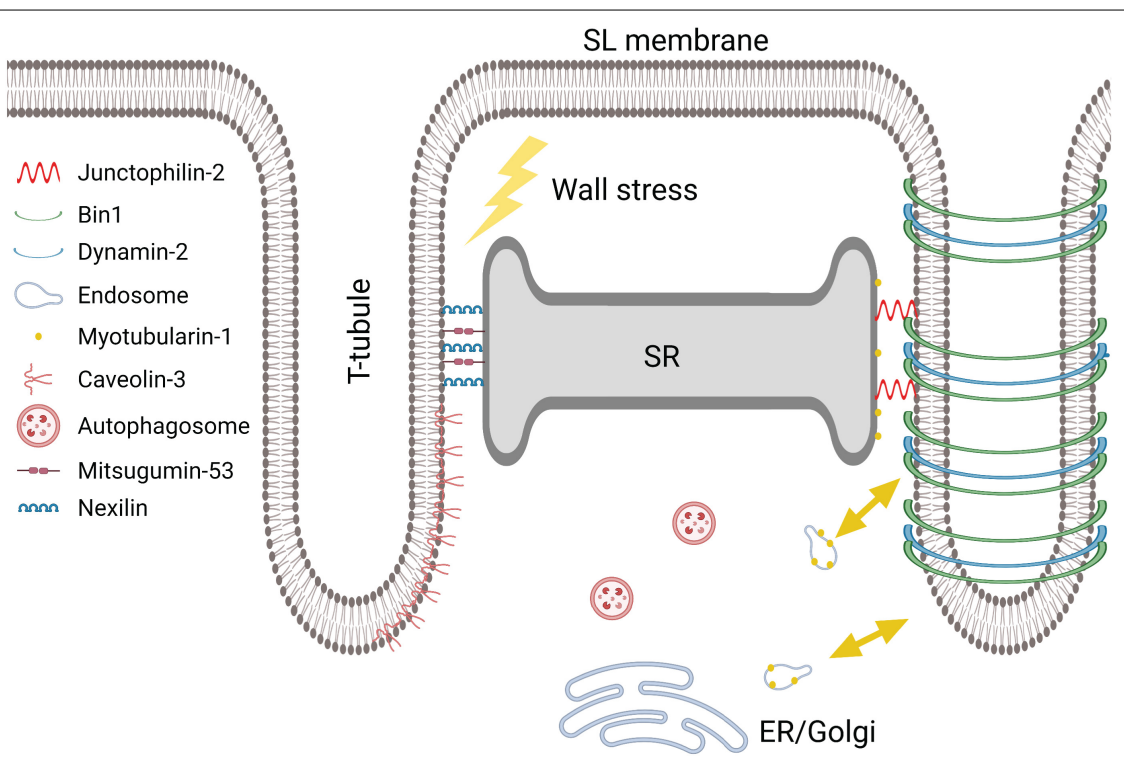

FIGURE 5 | Proposed proteins and pathways involved in dyadic biogenesis, maintenance, and disruption. Created with BioRender.com.

dysregulation can induce dilated cardiomyopathy (Agrawal et al., 2014). Collectively, an emerging view is that balanced expression and activity of Bin1, Dnm2 and MTM1 are crucial for controlling tubule growth and maintenance (**Figures 4**, **5**).

Junctophilin-2

As noted in the first chapter, JPH2 is a membrane anchoring protein, important for connecting the sarcolemma and its t-tubules to the SR in the dyad (Takeshima et al., 2000; Minamisawa et al., 2004; Han et al., 2013; Beavers et al., 2014; **Figure 5**). In this capacity, JPH2 maintains dyadic dimensions, and efficient crosstalk between LTCCs and RyRs. Importantly, JPH2 also interacts with both LTCCs and RyRs (Jiang et al., 2016; Reynolds et al., 2016), although the precise nature of these connections is not completely understood.

As with BIN1, JPH2 has been shown to play a key role in the development of t-tubules and dyads, both pre- and postnatally (Ziman et al., 2010; Munro and Soeller, 2016; **Figure 4**). This function is enabled by the membrane on receptor nexus (MORN) motif of JPH2, which allows anchoring to the t-tubule membrane, while the carboxy terminal is secured within the lumen of the SR (Nishi et al., 2000; Takeshima et al., 2000). The role of JPH2 in forming dyads is supported by the parallel appearance of JPH2 and t-tubules along z-lines in advance of developing t-tubules (Ziman et al., 2010). Furthermore, in mouse studies, reduced expression of JPH2 has been found to prevent t-tubule growth or result in an immature longitudinal configuration (Chen et al., 2013; Reynolds et al., 2013), consistent with a role of JPH2 in anchoring transverse, but not longitudinal elements (Chen et al., 2013). When JPH2 is fully knocked out in mice, it results in embryonic mortality, suggesting that it is required for dyad formation at the surface of the cell, even before the development of t-tubules starts (Takeshima et al., 2000; Franzini-Armstrong et al., 2005; Jones et al., 2018).

In adult failing cardiomyocytes, declining expression of JPH2 has been linked to t-tubule remodeling and disrupted dyads (Minamisawa et al., 2004; Xu et al., 2007; Wei et al., 2010; Landstrom et al., 2011; Chen et al., 2012; Xie et al., 2012; Zhang et al., 2014; Frisk et al., 2016; **Figure 4**). A causative role of JPH2 as a promoter of this remodeling is supported by studies showing that overexpression of JPH2 protects against t-tubule degradation, abnormal SR Ca^{2+} release, and HFrEF (Guo et al., 2014; Reynolds et al., 2016).

Emerging data support the role of JPH2 as a regulator of dyadic proteins. JPH2 overexpression was reported to result in the formation of larger RyR clusters within CRUs (Munro et al., 2016), while Wang et al. (2014) observed a reduction in RyR and NCX co-localization following JPH2 knockdown. JPH2 binding to RyRs may directly stabilize the channel's function, as JPH2 knockdown induced RyR hyperactivity (van Oort et al., 2011), while overexpression inhibited Ca^{2+} sparks (Munro et al., 2016). JPH2 is also reported to modulate LTCC activity, which has important implications for L-type current in HFrEF, where JPH2 expression is lowered (Jiang et al., 2016). Interestingly, recent data from Gross et al. (2021) indicate that the "Joining Region" of JPH2 may exert direct effects on the localization of LTCC in t-tubules, indicating that not only the presence of JPH2 but specifically JPH2-LTCC binding is necessary for maintenance of dyadic integrity and Ca^{2+} homeostasis.

What causes JPH2 changes during disease? A suggested mechanism for suppression of JPH2 expression is *via* upregulation of microRNA-24 (miR-24), as Xu et al. (2012) showed that a miR-24 antagomir protected against JPH2 downregulation and associated changes in t-tubule architecture. Mislocalization of JPH2 in the failing heart has also been reported, and linked to reorganization of the microtubules necessary for its delivery to dyads (Zhang et al., 2014; Prins et al., 2016).

Calpain cleavage of JPH2 is believed to be one of the mechanisms behind its downregulation, as first reported in mouse models of reversible heart failure (Guo et al., 2015), and ischemia-reperfusion injury (Wu et al., 2014). Furthermore, Wang et al. (2018) demonstrated increased calpain-mediated JPH2 cleavage in several mouse HFrEF models (myocardial infarction, transaortic banding, and chronic isoproterenol infusion), and found that inhibition of calpain partially restored both JPH2 expression levels and t-tubular density. These authors also observed that in a dual overexpression model of calpain and JPH2, JPH2 expression was only transiently maintained, and that subsequent deterioration in t-tubules and higher risk of cardiac death temporally correlated with declining JPH2 levels. Interestingly, contrasting reports also indicate that two different cleavage products of JPH2 may relocate to the nucleus, and attenuate (Guo et al., 2018b), or exacerbate cardiomyocyte stress responses (Lahiri et al., 2020).

Finally, the function of JPH2 has been shown to be dependent on its phosphorylation status (Guo et al., 2015), which is in turn regulated by "striated muscle preferentially expressed protein kinase" (SPEG). SPEG is downregulated in HFrEF, and loss of SPEG-dependent phosphorylation of JPH2 is suggested to promote t-tubule disruption (Quick et al., 2017).

Taken together, there is an abundance of evidence to support that JPH2 is a critical regulator of dyadic assembly and maintenance, and that this function extends far beyond a passive role in anchoring membrane positions. Thus, JPH2 is a promising target for future therapies.

Caveolin-3

Cav-3 is known to play a key role in the formation of t-tubules and caveolae (Parton et al., 1997; **Figures 4**, **5**). However, as with other dyadic regulators, emerging data suggest that decreased expression of Cav-3 has important functional consequences in the failing heart. Data from the Orchard group have shown that Cav-3 knockout mice exhibit cardiac dysfunction, associated with t-tubule reorganization and decreased LTCC current density (Bryant et al., 2018b). In another study, this group found that pressure overload in mice triggered loss of t-tubular Ca^{2+} current density and impairment of Ca^{2+} release, linked to lowered levels at Cav-3 (Bryant et al., 2018a). Interestingly, follow-up work with Cav-3 overexpressing mice exposed to pressure overload showed cardioprotective effects linked to maintained t-tubular Ca^{2+} current (Kong et al., 2019). Of note, these protective effects may also be linked to associations between Cav-3 and JPH2,

as Cav-3 overexpression reportedly stabilizes JPH2, and thus t-tubules (Minamisawa et al., 2004).

Autophagy

Recent work has identified a role of autophagy in regulating the assembly and disassembly of cardiac t-tubules (**Figure 5**). First, dexamethasone, a synthetic glucocorticoid, was shown to aid t-tubule growth in stem cell-derived cardiomyocytes (Parikh et al., 2017), and knockout of cardiac glucocorticoid receptors was found to induce heart failure and disturbances in Ca^{2+} handling (Oakley et al., 2013). However, it wasn't until Seidel and colleagues (Seidel et al., 2019) recently examined the t-tubule network in glucocorticoid receptor knockout mice that the former results were linked to autophagy. Here they demonstrated that t-tubule loss caused by glucocorticoid receptor knockout can be rescued by treatment with dexamethasone, and that this is associated with upregulation of the autophagy markers LC3BII and p62. Furthermore, treatment with rapamycin, an autophagy enhancer, reproduced the findings with dexamethasone treatment. Conversely, treatment with chloroquine and bafilomycin A1 (autophagy blockers) exacerbated detrimental effects on t-tubules (Seidel et al., 2019). In line with these findings, it has also been shown that a high-fat diet, and diabetes, induce apoptosis and cardiac alterations through inhibition of autophagy (Hsu et al., 2016).

Nexilin

Very recently, several studies from the Chen group have identified an exciting new dyadic regulator, called Nexilin (NEXN) (**Figure 5**). Previously known as an actin-binding and Z-disk protein, NEXN was shown to be critical to the formation of dyadic membranes, as myocytes from knockout animals did not develop t-tubules and exhibited early postnatal cardiomyopathy and lethality (Liu et al., 2019). Furthermore, conditional knockout of NEXN in adult cardiomyocytes resulted in a remodeling of t-tubule structure that was highly reminiscent of HFrEF, with loss of transverse t-tubules and an increased proportion of longitudinal elements (Spinozzi et al., 2020). The authors additionally reported that NEXN interacts with both JPH2 and RyRs, and that its loss results in decreased expression of these and other dyadic proteins, and accompanying impairment of Ca^{2+} homeostasis (Liu et al., 2019; Spinozzi et al., 2020). These findings are of considerable interest, as nexilin mutations are linked to cardiopathy in mice and humans (Hassel et al., 2009; Wang H. et al., 2010; Haas et al., 2015; Liu C. et al., 2020). Further work is required to determine the exact mechanism by which NEXN grows and maintains dyads, and whether NEXN alterations occur in acquired HFrEF. In this regard, it is noteworthy that NEXN expression levels were found to be maintained in HFrEF patients (Chen et al., 2018).

Mitsugumin 53

The muscle-specific membrane repair protein mitsugumin 53 (MG53) is an up and coming t-tubule regulator (Kitmitto et al., 2019; **Figure 5**). This "wound-healing" protein is part of the tripartite motif family (TRIM), and is often referred to as TRIM72. Wang X. et al. (2010) were the first to identify MG53 as critical for maintaining cardiomyocyte sarcolemmal stability. The sarcolemmal membrane of the cardiomyocyte is the first line of defense against external stresses, such as oxygen and nutrient deprivation, inflammation and oxidative stress, and indeed, loss of sarcolemmal viability is a key step in cell death *via* necrosis (Kitmitto et al., 2019). Regulatory injury-repair proteins, such as MG53, are thus important for the integrity of both the sarcolemma and the cell as a whole. A new study suggests that while MG53 is not necessary for the development or maintenance of t-tubules during health, it may crucially preserve their integrity and function when the heart is placed under pathological stress (Zhang et al., 2017). When an injury or defect appears in the cell membrane, MG53 travels to the injury site and "plugs the hole," by re-sealing the membrane (Cooper and McNeil, 2015). MG53 coordinates this role through interplay with caveolaer proteins (Kitmitto et al., 2019). He et al. (2012) found that elevated expression of MG53 improved heart function and augmented membrane repair capacity. While these authors did not specifically link these findings to changes in t-tubule structure/function, such effects seem likely based on the well-established role of declining t-tubule integrity in disease.

Protein Kinase C

Protein kinase C (PKC) activation has been implicated in t-tubule remodeling in a recent study by Guo et al. (2018a), where the authors found a transient elevation in PKC activity in the days following transaortic banding. Inhibition of PKC during this period ameliorated subsequent t-tubule remodeling and heart failure development. It was shown that the increase in PKC coincided with a transient biphasic mode of actin depolymerization and repolarization, and that PKC inhibition abolished this response. Furthermore, the use of various inhibitors or stabilizers of F-actin polymers seemed to protect the t-tubule system after aortic banding, indicating that the sudden biphasic response is detrimental to t-tubule integrity. Blocking stretch-activated channels diminished the PKC-mediated effect on t-tubules, implicating these channels in mechanosensitive regulation of t-tubule structure downstream of PKC. These exciting findings are consistent with a growing appreciation for the importance of workload in regulating t-tubule structure, but are the first to implicate a role of PKC and actin filament dynamics in these processes.

Integrated Understanding of T-Tubule Regulators

The above discussion has highlighted recent work implicating a plethora of proteins involved in the growth and maintenance of t-tubules and their remodeling during disease. How should we make sense of this increasingly complex array of proteins? Are there shared, overarching signaling pathways which coordinate changing protein expression patterns? We believe that changing physical stress experienced by the myocardium

is at least one such signal. Indeed, when viewed from a mechanosensatory viewpoint we can see that many of the proposed t-tubule regulators can be functionally clustered together. For example, several of these proteins have proposed roles in mechanosensing at the cell membrane (PKC *via* stretch-activated channels) or Z-disks (T-Cap), or are linked to the mechanosensitive process of actin polymerization (BIN1, Nexilin, and PKC). A perhaps somewhat distinct group of t-tubule regulatory proteins appears to be focused on maintenance of the membrane itself, and notably includes Mtm1, BIN1, and the general autophagic and endocytic processes. It is less clear that these processes are mechanosensitive in cardiomyocytes, and we might rather speculate that the changing metabolic environment of the diseased heart is an overarching signal that regulates membrane integrity.

Despite promising results from rodent studies, it seems unlikely that targeting of only a single t-tubule regulator would be sufficient to therapeutically protect t-tubule structure in humans. Rather, we believe that new interventions should instead be aimed at the overarching signals and functional groups of proteins described above. For example, upregulating expression of JPH2 has been suggested as an approach to maintain dyadic structure during HFrEF (Reynolds et al., 2016). However, we expect that this approach would yield only temporary benefits since JPH2 downregulation is itself driven by elevated workload (Frisk et al., 2016), and thus the persistence of these mechanical cues would continue to signal detrimental changes in JPH2 and other mechanosensitive proteins. Indeed, it is notable that existing therapeutics for HFrEF act largely to alleviate cardiac workload, and thus are expected to normalize expression of a spectrum of key mechanosensitive t-tubule regulators. As an alternative approach, we speculate that more precisely interrupting the processes of mechanosensation at the levels of the cardiomyocyte membrane and/or cytoskeleton could be broadly beneficial in the treatment of HFrEF patients.

CONCLUSION AND SUMMARY

This review has summarized our growing appreciation for the role of t-tubules and dyads as critical regulators of cardiomyocyte Ca^{2+} homeostasis, and thus systolic and diastolic function of the heart as a working organ. The discussion has highlighted a consensus view that t-tubule remodeling is a key mechanism contributing to disrupted Ca^{2+} handling and contractility in HFrEF, and a likely contributor to arrythmogenesis, but that distinct forms of remodeling occur during HFpEF. We have described a wealth of evidence indicating key roles of dyadic proteins JPH2, BIN1, and Cav-3, but also newer players and signaling pathways which hold promise. We believe that several current HFrEF therapies preserve t-tubule structure and cardiac function by normalizing expression of these proteins, and that this involves relief of the high workload that drives dyadic disruption. We anticipate that improved safeguarding of t-tubule integrity will serve as a basis for future HFrEF therapy.

AUTHOR CONTRIBUTIONS

All authors contributed to the writing of the article and development of the figures.

FUNDING

This work was financially supported by the European Union's Horizon 2020 Research and Innovation Programme (Consolidator grant, WL) under grant agreement No. 647714, the Norwegian Research Council (WL and MF), the South-Eastern Norway Regional Health Authority (WL and MF), the KG Jebsen Centre for Cardiac Research (WL and CL), the Norwegian Institute for Public Health (MF and JL), and the University of Oslo (IS).

REFERENCES

Agrawal, P. B., Pierson, C. R., Joshi, M., Liu, X., Ravenscroft, G., Moghadaszadeh, B., et al. (2014). SPEG interacts with myotubularin, and its deficiency causes centronuclear myopathy with dilated cardiomyopathy. *Am. J. Hum. Genet.* 95, 218–226. doi: 10.1016/j.ajhg.2014.07.004

Al-Qusairi, L., and Laporte, J. (2011). T-tubule biogenesis and triad formation in skeletal muscle and implication in human diseases. *Skelet. Muscle* 1:26. doi: 10.1186/2044-5040-1-26

Arora, R., Aistrup, G. L., Supple, S., Frank, C., Singh, J., Tai, S., et al. (2017). Regional distribution of T-tubule density in left and right atria in dogs. *Heart Rhythm* 14, 273–281. doi: 10.1016/j.hrthm.2016.09.022

Baddeley, D., Jayasinghe, I. D., Lam, L., Rossberger, S., Cannell, M. B., and Soeller, C. (2009). Optical single-channel resolution imaging of the ryanodine receptor distribution in rat cardiac myocytes. *Proc. Natl. Acad. Sci. U.S.A.* 106, 22275–22280. doi: 10.1073/pnas.0908971106

Balijepalli, R. C., Lokuta, A. J., Maertz, N. A., Buck, J. M., Haworth, R. A., Valdivia, H. H., et al. (2003). Depletion of T-tubules and specific subcellular changes in sarcolemmal proteins in tachycardia-induced heart failure. *Cardiovasc. Res.* 59, 67–77.

Beavers, D. L., Landstrom, A. P., Chiang, D. Y., and Wehrens, X. H. (2014). Emerging roles of junctophilin-2 in the heart and implications for cardiac diseases. *Cardiovasc. Res.* 103, 198–205. doi: 10.1093/cvr/cvu151

Berliner, D., and Bauersachs, J. (2017). Current drug therapy in chronic heart failure: the new guidelines of the European society of cardiology (ESC). *Korean Circ. J.* 47, 543–554. doi: 10.4070/kcj.2017.0030

Bers, D. M. (2002). Cardiac excitation-contraction coupling. *Nature* 415, 198–205.

Biesmans, L., Macquaide, N., Heinzel, F. R., Bito, V., Smith, G. L., and Sipido, K. R. (2011). Subcellular heterogeneity of ryanodine receptor properties in ventricular myocytes with low T-tubule density. *PLoS One* 6:e25100. doi: 10.1371/journal.pone.0025100

Brand, T. (2003). Heart development: molecular insights into cardiac specification and early morphogenesis. *Dev. Biol.* 258, 1–19. doi: 10.1016/s0012-1606(03)00112-x

Brette, F., Despa, S., Bers, D. M., and Orchard, C. H. (2005). Spatiotemporal characteristics of SR Ca^{2+} uptake and release in detubulated rat ventricular myocytes. *J. Mol. Cell. Cardiol.* 39, 804–812. doi: 10.1016/j.yjmcc.2005.08.005

Brook, W. H., Connell, S., Cannata, J., Maloney, J. E., and Walker, A. M. (1983). Ultrastructure of the myocardium during development from early fetal life to adult life in sheep. *J. Anat.* 137(Pt 4), 729–741.

Bryant, S. M., Kong, C. H. T., Watson, J. J., Gadeberg, H. C., James, A. F., Cannell, M. B., et al. (2018a). Caveolin 3-dependent loss of t-tubular I_{Ca} during

hypertrophy and heart failure in mice. *Exp. Physiol.* 103, 652–665. doi: 10.1113/ep086731

Bryant, S. M., Kong, C. H. T., Watson, J. J., Gadeberg, H. C., Roth, D. M., Patel, H. H., et al. (2018b). Caveolin-3 KO disrupts t-tubule structure and decreases t-tubular I_{Ca} density in mouse ventricular myocytes. *Am. J. Physiol. Heart Circ. Physiol.* 315, H1101–H1111.

Bryant, S. M., Kong, C. H., Watson, J., Cannell, M. B., James, A. F., and Orchard, C. H. (2015). Altered distribution of I_{Ca} impairs Ca release at the t-tubules of ventricular myocytes from failing hearts. *J. Mol. Cell. Cardiol.* 86, 23–31. doi: 10.1016/j.yjmcc.2015.06.012

Caldwell, J. L., Smith, C. E., Taylor, R. F., Kitmitto, A., Eisner, D. A., Dibb, K. M., et al. (2014). Dependence of cardiac transverse tubules on the BAR domain protein amphiphysin II (BIN-1). *Circ. Res.* 115, 986–996. doi: 10.1161/circresaha.116.303448

Cannell, M. B., Crossman, D. J., and Soeller, C. (2006). Effect of changes in action potential spike configuration, junctional sarcoplasmic reticulum micro-architecture and altered t-tubule structure in human heart failure. *J. Muscle Res. Cell Motil.* 27, 297–306. doi: 10.1007/s10974-006-9089-y

Chen, B., Guo, A., Zhang, C., Chen, R., Zhu, Y., and Hong, J. (2013). Critical roles of junctophilin-2 in T-tubule and excitation-contraction coupling maturation during postnatal development. *Cardiovasc. Res.* 100, 54–62. doi: 10.1093/cvr/cvt180

Chen, B., Li, Y., Jiang, S., Xie, Y. P., Guo, A., Kutschke, W., et al. (2012). beta-Adrenergic receptor antagonists ameliorate myocyte T-tubule remodeling following myocardial infarction. *FASEB J.* 26, 2531–2537. doi: 10.1096/fj.11-199505

Chen, C. Y., Caporizzo, M. A., Bedi, K., Vite, A., Bogush, A. I., Robison, P., et al. (2018). Suppression of detyrosinated microtubules improves cardiomyocyte function in human heart failure. *Nat. Med.* 24, 1225–1233. doi: 10.1038/s41591-018-0046-2

Cheng, H., Lederer, M. R., Lederer, W. J., and Cannell, M. B. (1996). Calcium sparks and $[Ca^{2+}]_i$ waves in cardiac myocytes. *Am. J. Physiol.* 270, C148–C159.

Cohn, J. N. (1996). The management of chronic heart failure. *N. Engl. J. Med.* 335, 490–498.

Cooper, S. T., and McNeil, P. L. (2015). Membrane repair: mechanisms and pathophysiology. *Physiol. Rev.* 95, 1205–1240. doi: 10.1152/physrev.00037.2014

Crocini, C., Coppini, R., Ferrantini, C., Yan, P., Loew, L. M., Tesi, C., et al. (2014). Defects in T-tubular electrical activity underlie local alterations of calcium release in heart failure. *Proc. Natl. Acad. Sci. U.S.A.* 111, 15196–15201. doi: 10.1073/pnas.1411557111

Crossman, D. J., Shen, X., Jullig, M., Munro, M., Hou, Y., Middleditch, M., et al. (2017). Increased collagen within the transverse tubules in human heart failure. *Cardiovasc. Res.* 113, 879–891. doi: 10.1093/cvr/cvx055

Crossman, D. J., Young, A. A., Ruygrok, P. N., Nason, G. P., Baddelely, D., Soeller, C., et al. (2015). T-tubule disease: relationship between t-tubule organization and regional contractile performance in human dilated cardiomyopathy. *J. Mol. Cell. Cardiol.* 84, 170–178. doi: 10.1016/j.yjmcc.2015.04.022

Curl, C. L., Danes, V. R., Bell, J. R., Raaijmakers, A. J. A., Ip, W. T. K., Chandramouli, C., et al. (2018). Cardiomyocyte functional etiology in heart failure with preserved ejection fraction is distinctive-a new preclinical model. *J. Am. Heart Assoc.* 7:e007451.

de Diego, C., Chen, F., Xie, L. H., Dave, A. S., Thu, M., Rongey, C., et al. (2008). Cardiac alternans in embryonic mouse ventricles. *Am. J. Physiol. Heart Circ. Physiol.* 294, H433–H440.

De La Mata, A., Tajada, S., O'Dwyer, S., Matsumoto, C., Dixon, R. E., Hariharan, N., et al. (2019). BIN1 induces the formation of T-Tubules and adult-like Ca^{2+} release units in developing cardiomyocytes. *Stem Cells* 37, 54–64. doi: 10.1002/stem.2927

Dibb, K. M., Clarke, J. D., Horn, M. A., Richards, M. A., Graham, H. K., Eisner, D. A., and Trafford, A. W. (2009). Characterization of an extensive transverse tubular network in sheep atrial myocytes and its depletion in heart failure. *Circ. Heart Fail.* 2, 482–489. doi: 10.1161/circheartfailure.109.852228

Dixon, R. E., Moreno, C. M., Yuan, C., Opitz-Araya, X., Binder, M. D., Navedo, M. F., et al. (2015). Graded Ca^{2+}/calmodulin-dependent coupling of voltage-gated CaV1.2 channels. *eLife* 4:e05608.

Dostal, D. E., Feng, H., Nizamutdinov, D., Golden, H. B., Afroze, S. H., Dostal, J. D., et al. (2014). Mechanosensing and regulation of cardiac function. *J. Clin. Exp. Cardiol.* 5:314.

Dridi, H., Kushnir, A., Zalk, R., Yuan, Q., Melville, Z., and Marks, A. R. (2020). Intracellular calcium leak in heart failure and atrial fibrillation: a unifying mechanism and therapeutic target. *Nat. Rev. Cardiol.* 17, 732–747. doi: 10.1038/s41569-020-0394-8

Dyachenko, V., Husse, B., Rueckschloss, U., and Isenberg, G. (2009). Mechanical deformation of ventricular myocytes modulates both TRPC6 and Kir2.3 channels. *Cell Calcium* 45, 38–54. doi: 10.1016/j.ceca.2008.06.003

Edwards, A. G., and Louch, W. E. (2017). Species-dependent mechanisms of cardiac arrhythmia: a cellular focus. *Clin. Med. Insights Cardiol.* 1:1179546816686061.

Fabiato, A. (1983). Calcium-induced release of calcium from the cardiac sarcoplasmic reticulum. *Am. J. Physiol.* 245, C1–C14.

Feridooni, H. A., Dibb, K. M., and Howlett, S. E. (2015). How cardiomyocyte excitation, calcium release and contraction become altered with age. *J. Mol. Cell. Cardiol.* 83, 62–72. doi: 10.1016/j.yjmcc.2014.12.004

Fiegle, D. J., Schober, M., Dittrich, S., Cesnjevar, R., Klingel, K., Volk, T., et al. (2020). Severe T-System remodeling in pediatric viral myocarditis. *Front. Cardiovasc. Med.* 7:624776. doi: 10.3389/fcvm.2020.624776

Forbes, M. S., and Sperelakis, N. (1976). The presence of transverse and axial tubules in the ventricular myocardium of embryonic and neonatal guinea pigs. *Cell Tissue Res.* 166, 83–90. doi: 10.1007/bf00215127

Forsgren, S., and Thornell, L. E. (1981). The development of Purkinje fibres and ordinary myocytes in the bovine fetal heart. An ultrastructural study. *Anat. Embryol.* 162, 127–136. doi: 10.1007/bf00306485

Forssmann, W. G., and Girardier, L. (1970). A study of the T system in rat heart. *J. Cell Biol.* 44, 1–19. doi: 10.1083/jcb.44.1.1

Franzini-Armstrong, C., Protasi, F., and Tijskens, P. (2005). The assembly of calcium release units in cardiac muscle. *Ann. N. Y. Acad. Sci.* 1047, 76–85. doi: 10.1196/annals.1341.007

Frisk, M., Koivumaki, J. T., Norseng, P. A., Maleckar, M. M., Sejersted, O. M., and Louch, W. E. (2014). Variable t-tubule organization and Ca^{2+} homeostasis across the atria. *Am. J. Physiol. Heart Circ. Physiol.* 307, H609–H620.

Frisk, M., Le, C., Shen, X., Roe, A. T., Hou, Y., and Manfra, O. (2021). Etiology-dependent impairment of diastolic cardiomyocyte calcium homeostasis in heart failure with preserved ejection fraction. *J. Am. Coll. Cardiol.* 77, 405–419.

Frisk, M., Ruud, M., Espe, E. K., Aronsen, J. M., Roe, A. T., Zhang, L., et al. (2016). Elevated ventricular wall stress disrupts cardiomyocyte t-tubule structure and calcium homeostasis. *Cardiovasc. Res.* 112, 443–451. doi: 10.1093/cvr/cvw111

Fu, Y., Shaw, S. A., Naami, R., Vuong, C. L., Basheer, W. A., Guo, X., et al. (2016). Isoproterenol promotes rapid ryanodine receptor movement to bridging integrator 1 (BIN1)-organized dyads. *Circulation* 133, 388–397. doi: 10.1161/circulationaha.115.018535

Gadeberg, H. C., Bond, R. C., Kong, C. H., Chanoit, G. P., Ascione, R., Cannell, M. B., et al. (2016). Heterogeneity of T-Tubules in pig hearts. *PLoS One* 11:e0156862. doi: 10.1371/journal.pone.0156862

Gaeta, S. A., Bub, G., Abbott, G. W., and Christini, D. J. (2009). Dynamical mechanism for subcellular alternans in cardiac myocytes. *Circ. Res.* 105, 335–342. doi: 10.1161/circresaha.109.197590

Gibbs, E. M., Davidson, A. E., Telfer, W. R., Feldman, E. L., and Dowling, J. J. (2014). The myopathy-causing mutation DNM2-S619L leads to defective tubulation in vitro and in developing zebrafish. *Dis. Model. Mech.* 7, 157–161.

Glukhov, A. V., Balycheva, M., Sanchez-Alonso, J. L., Ilkan, Z., Alvarez-Laviada, A., and Bhogal, N. (2015). Direct evidence for microdomain-specific localization and remodeling of functional L-Type calcium channels in rat and human atrial myocytes. *Circulation* 132, 2372–2384. doi: 10.1161/circulationaha.115.018131

Gonzalez-Jamett, A. M., Momboisse, F., Haro-Acuna, V., Bevilacqua, J. A., Caviedes, P., and Cardenas, A. M. (2013). Dynamin-2 function and dysfunction along the secretory pathway. *Front. Endocrinol. (Lausanne)* 4:126. doi: 10.3389/fendo.2013.00126

Gotoh, T. (1983). Quantitative studies on the ultrastructural differentiation and growth of mammalian cardiac muscle cells. The atria and ventricles of the cat. *Acta Anat.* 115, 168–177. doi: 10.1159/000145687

Grandy, S. A., and Howlett, S. E. (2006). Cardiac excitation-contraction coupling is altered in myocytes from aged male mice but not in cells from aged female mice. *Am. J. Physiol. Heart Circ. Physiol.* 291, H2362–H2370.

Gross, P., Johnson, J., Romero, C. M., Eaton, D. M., Poulet, C., Sanchez-Alonso, J., et al. (2021). Houser, interaction of the joining region in junctophilin-2 with

the L-Type Ca^{2+} channel is pivotal for cardiac dyad assembly and intracellular Ca^{2+} dynamics. *Circ. Res.* 128, 92–114.

Gu, Y., Gorelik, J., Spohr, H. A., Shevchuk, A., Lab, M. J., and Harding, S. E. (2002). High-resolution scanning patch-clamp: new insights into cell function. *FASEB J.* 16, 748–750. doi: 10.1096/fj.01-1024fje

Guo, A., Chen, R., Wang, Y., Huang, C. K., Chen, B., Kutschke, W., et al. (2018a). Transient activation of PKC results in long-lasting detrimental effects on systolic $[Ca^{2+}]_i$ in cardiomyocytes by altering actin cytoskeletal dynamics and T-tubule integrity. *J. Mol. Cell. Cardiol.* 115, 104–114. doi: 10.1016/j.yjmcc.2018.01.003

Guo, A., Hall, D., Zhang, C., Peng, T., Miller, J. D., Kutschke, W., et al. (2015). Molecular determinants of calpain-dependent cleavage of Junctophilin-2 protein in cardiomyocytes. *J. Biol. Chem.* 290, 17946–17955. doi: 10.1074/jbc.m115.652396

Guo, A., Wang, Y., Chen, B., Wang, Y., Yuan, J., Zhang, L., et al. (2018b). E-C coupling structural protein junctophilin-2 encodes a stress-adaptive transcription regulator. *Science* 362:eaan3303. doi: 10.1126/science.aan3303

Guo, A., Zhang, C., Wei, S., Chen, B., and Song, L. S. (2013). Emerging mechanisms of T-tubule remodelling in heart failure. *Cardiovasc. Res.* 98, 204–215. doi: 10.1093/cvr/cvt020

Guo, A., Zhang, X., Iyer, V. R., Chen, B., Zhang, C., Kutschke, W. J., et al. (2014). Overexpression of junctophilin-2 does not enhance baseline function but attenuates heart failure development after cardiac stress. *Proc. Natl. Acad. Sci. U.S.A.* 111, 12240–12245. doi: 10.1073/pnas.1412729111

Haas, J., Frese, K. S., Peil, B., Kloos, W., Keller, A., Nietsch, R., et al. (2015). Atlas of the clinical genetics of human dilated cardiomyopathy. *Eur. Heart J.* 36, 1123–1135.

Hamaguchi, S., Kawakami, Y., Honda, Y., Nemoto, K., Sano, A., Namekata, I., et al. (2013). Developmental changes in excitation-contraction mechanisms of the mouse ventricular myocardium as revealed by functional and confocal imaging analyses. *J. Pharmacol. Sci.* 123, 167–175. doi: 10.1254/jphs.13099fp

Han, J., Wu, H., Wang, Q., and Wang, S. (2013). Morphogenesis of T-tubules in heart cells: the role of junctophilin-2. *Sci. China Life Sci.* 56, 647–652. doi: 10.1007/s11427-013-4490-4

Hassel, D., Dahme, T., Erdmann, J., Meder, B., Huge, A., Stoll, M., et al. (2009). Nexilin mutations destabilize cardiac Z-disks and lead to dilated cardiomyopathy. *Nat. Med.* 15, 1281–1288. doi: 10.1038/nm.2037

Hayashi, T., Martone, M. E., Yu, Z., Thor, A., Doi, M., Holst, M. J., et al. (2009). Three-dimensional electron microscopy reveals new details of membrane systems for Ca^{2+} signaling in the heart. *J. Cell Sci.* 122, 1005–1013. doi: 10.1242/jcs.028175

He, B., Tang, R. H., Weisleder, N., Xiao, B., Yuan, Z., Cai, C., et al. (2012). Enhancing muscle membrane repair by gene delivery of MG53 ameliorates muscular dystrophy and heart failure in delta-Sarcoglycan-deficient hamsters. *Mol. Ther.* 20, 727–735. doi: 10.1038/mt.2012.5

He, J., Conklin, M. W., Foell, J. D., Wolff, M. R., Haworth, R. A., Coronado, R., et al. (2001). Reduction in density of transverse tubules and L-type Ca^{2+} channels in canine tachycardia-induced heart failure. *Cardiovasc. Res.* 49, 298–307. doi: 10.1016/s0008-6363(00)00256-x

Heinzel, F. R., Bito, V., Biesmans, L., Wu, M., Detre, E., von Wegner, F., et al. (2008). Remodeling of T-tubules and reduced synchrony of Ca^{2+} release in myocytes from chronically ischemic myocardium. *Circ. Res.* 102, 338–346. doi: 10.1161/circresaha.107.160085

Heinzel, F. R., Bito, V., Volders, P. G., Antoons, G., Mubagwa, K., and Sipido, K. R. (2002). Spatial and temporal inhomogeneities during Ca^{2+} release from the sarcoplasmic reticulum in pig ventricular myocytes. *Circ. Res.* 91, 1023–1030. doi: 10.1161/01.res.0000045940.67060.dd

Henderson, S. A., Goldhaber, J. I., So, J. M., Han, T., Motter, C., Ngo, A., et al. (2004). Functional adult myocardium in the absence of Na^+-Ca^{2+} exchange: cardiac-specific knockout of NCX1. *Circ. Res.* 95, 604–611. doi: 10.1161/01.res.0000142316.08250.68

Herring, N., Kalla, M., and Paterson, D. J. (2019). The autonomic nervous system and cardiac arrhythmias: current concepts and emerging therapies. *Nat. Rev. Cardiol.* 16, 707–726. doi: 10.1038/s41569-019-0221-2

Hirakow, R., Gotoh, T., and Watanabe, T. (1980). Quantitative studies on the ultrastructural differentiation and growth of mammalian cardiac muscle cells. I. The atria and ventricles of the rat. *Acta Anat.* 108, 144–152. doi: 10.1159/000145293

Hitzeman, T. C., Xie, Y., Zadikany, R. H., Nikolova, A. P., Baum, R., Caldaruse, A. M., et al. (2020). cBIN1 score (CS) identifies ambulatory HFrEF patients and predicts cardiovascular events. *Front. Physiol.* 11:503. doi: 10.3389/fphys.2020.00503

Hoerter, J., Mazet, F., and Vassort, G. (1981). Perinatal growth of the rabbit cardiac cell: possible implications for the mechanism of relaxation. *J. Mol. Cell. Cardiol.* 13, 725–740. doi: 10.1016/0022-2828(81)90255-8

Hong, T. T., Cogswell, R., James, C. A., Kang, G., Pullinger, C. R., Malloy, M. J., et al. (2012a). Plasma BIN1 correlates with heart failure and predicts arrhythmia in patients with arrhythmogenic right ventricular cardiomyopathy. *Heart Rhythm* 9, 961–967. doi: 10.1016/j.hrthm.2012.01.024

Hong, T. T., Smyth, J. W., Chu, K. Y., Vogan, J. M., Fong, T. S., Jensen, B. C., et al. (2012b). BIN1 is reduced and Cav1.2 trafficking is impaired in human failing cardiomyocytes. *Heart Rhythm* 9, 812–820. doi: 10.1016/j.hrthm.2011.11.055

Hong, T. T., Smyth, J. W., Gao, D., Chu, K. Y., Vogan, J. M., Fong, T. S., et al. (2010). BIN1 localizes the L-type calcium channel to cardiac T-tubules. *PLoS Biol.* 8:e1000312. doi: 10.1371/journal.pbio.1000312

Hong, T., and Shaw, R. M. (2017). Cardiac T-Tubule microanatomy and function. *Physiol. Rev.* 97, 227–252. doi: 10.1152/physrev.00037.2015

Hong, T., Yang, H., Zhang, S. S., Cho, H. C., Kalashnikova, M., Sun, B., et al. (2014). Cardiac BIN1 folds T-tubule membrane, controlling ion flux and limiting arrhythmia. *Nat. Med.* 20, 624–632. doi: 10.1038/nm.3543

Hsu, H. C., Chen, C. Y., Lee, B. C., and Chen, M. F. (2016). High-fat diet induces cardiomyocyte apoptosis via the inhibition of autophagy. *Eur. J. Nutr.* 55, 2245–2254. doi: 10.1007/s00394-015-1034-7

Huang, C. K., Chen, B. Y., Guo, A., Chen, R., Zhu, Y. Q., Kutschke, W., et al. (2016). Sildenafil ameliorates left ventricular T-tubule remodeling in a pressure overload-induced murine heart failure model. *Acta Pharmacol. Sin.* 37, 473–482. doi: 10.1038/aps.2016.13

Huang, C. Y., Peres Moreno Maia-Joca, R., Ong, C. S., Wilson, I., DiSilvestre, D., Tomaselli, G. F., et al. (2020). Enhancement of human iPSC-derived cardiomyocyte maturation by chemical conditioning in a 3D environment. *J. Mol Cell. Cardiol.* 138, 1–11. doi: 10.1016/j.yjmcc.2019.10.001

Huxley, A. F., and Taylor, R. E. (1955). Function of Krause's membrane. *Nature* 176:1068.

Ibrahim, M., Al Masri, A., Navaratnarajah, M., Siedlecka, U., Soppa, G. K., Moshkov, A., et al. (2010). Prolonged mechanical unloading affects cardiomyocyte excitation-contraction coupling, transverse-tubule structure, and the cell surface. *FASEB J.* 24, 3321–3329. doi: 10.1096/fj.10-156638

Ibrahim, M., and Terracciano, C. M. (2013). Reversibility of T-tubule remodelling in heart failure: mechanical load as a dynamic regulator of the T-tubules. *Cardiovasc. Res.* 98, 225–232. doi: 10.1093/cvr/cvt016

Ibrahim, M., Gorelik, J., Yacoub, M. H., and Terracciano, C. M. (2011). The structure and function of cardiac t-tubules in health and disease. *Proc. Biol. Sci.* 278, 2714–2723. doi: 10.1098/rspb.2011.0624

Ibrahim, M., Kukadia, P., Siedlecka, U., Cartledge, J. E., Navaratnarajah, M., Tokar, S., et al. (2012). Cardiomyocyte Ca^{2+} handling and structure is regulated by degree and duration of mechanical load variation. *J. Cell. Mol. Med.* 16, 2910–2918. doi: 10.1111/j.1582-4934.2012.01611.x

Ibrahim, M., Nader, A., Yacoub, M. H., and Terracciano, C. (2015). Manipulation of sarcoplasmic reticulum Ca^{2+} release in heart failure through mechanical intervention. *J. Physiol.* 593, 3253–3259. doi: 10.1113/jp270446

Ibrahim, M., Siedlecka, U., Buyandelger, B., Harada, M., Rao, C., Moshkov, A., et al. (2013). A critical role for Telethonin in regulating t-tubule structure and function in the mammalian heart. *Hum. Mol. Genet.* 22, 372–383.

Ito, D. W., Hannigan, K. I., Ghosh, D., Xu, B., Del Villar, S. G., and Xiang, Y. K. (2019). beta-adrenergic-mediated dynamic augmentation of sarcolemmal CaV 1.2 clustering and co-operativity in ventricular myocytes. *J. Physiol.* 597, 2139–2162. doi: 10.1113/jp277283

Jaquenod De Giusti, C., Blanco, P. G., Lamas, P. A., Carrizo Velasquez, F., Lofeudo, J. M., Portiansky, E. L., et al. (2019). Carbonic anhydrase II/sodium-proton exchanger 1 metabolon complex in cardiomyopathy of ob(-/-) type 2 diabetic mice. *J. Mol. Cell. Cardiol.* 136, 53–63. doi: 10.1016/j.yjmcc.2019.09.005

Jayasinghe, I. D., Cannell, M. B., and Soeller, C. (2009). Organization of ryanodine receptors, transverse tubules, and sodium-calcium exchanger in rat myocytes. *Biophys. J.* 97, 2664–2673. doi: 10.1016/j.bpj.2009.08.036

Jayasinghe, I., Clowsley, A. H., Lin, R., Lutz, T., Harrison, C., Green, E., et al. (2018). True molecular scale visualization of variable clustering properties of ryanodine receptors. *Cell Rep.* 22, 557–567. doi: 10.1016/j.celrep.2017.12.045

Jayasinghe, I., Crossman, D., Soeller, C., and Cannell, M. (2012). Comparison of the organization of T-tubules, sarcoplasmic reticulum and ryanodine receptors in rat and human ventricular myocardium. *Clin. Exp. Pharmacol. Physiol.* 39, 469–476. doi: 10.1111/j.1440-1681.2011.05578.x

Jiang, M., Zhang, M., Howren, M., Wang, Y., Tan, A., Balijepalli, R. C., et al. (2016). JPH-2 interacts with Ca_i-handling proteins and ion channels in dyads: contribution to premature ventricular contraction-induced cardiomyopathy. *Heart Rhythm* 13, 743–752. doi: 10.1016/j.hrthm.2015.10.037

Jiang, Y., Tanaka, H., Matsuyama, T. A., Yamaoka, Y., and Takamatsu, T. (2014). Pacing-induced non-uniform Ca^{2+} dynamics in rat atria revealed by rapid-scanning confocal microscopy. *Acta Histochem. Cytochem.* 47, 59–65. doi: 10.1267/ahc.14014

Jones, P. P., MacQuaide, N., and Louch, W. E. (2018). Dyadic plasticity in cardiomyocytes. *Front. Physiol.* 9:1773. doi: 10.3389/fphys.2018.01773

Kaprielian, R. R., Stevenson, S., Rothery, S. M., Cullen, M. J., and Severs, N. J. (2000). Distinct patterns of dystrophin organization in myocyte sarcolemma and transverse tubules of normal and diseased human myocardium. *Circulation* 101, 2586–2594. doi: 10.1161/01.cir.101.22.2586

Kemi, O. J., Hoydal, M. A., Macquaide, N., Haram, P. M., Koch, L. G., Britton, S. L., et al. (2011). The effect of exercise training on transverse tubules in normal, remodeled, and reverse remodeled hearts. *J. Cell Physiol.* 226, 2235–2243. doi: 10.1002/jcp.22559

Ketel, K., Krauss, M., Nicot, A. S., Puchkov, D., Wieffer, M., Muller, R., et al. (2016). A phosphoinositide conversion mechanism for exit from endosomes. *Nature* 529, 408–412. doi: 10.1038/nature16516

Kilfoil, P. J., Lotteau, S., Zhang, R., Yue, X., Aynaszyan, S., Solymani, R. E., et al. (2020). Distinct features of calcium handling and beta-adrenergic sensitivity in heart failure with preserved versus reduced ejection fraction. *J. Physiol.* 598, 5091–5108. doi: 10.1113/jp280425

Kim, H. D., Kim, D. J. I, Lee, J., Rah, B. J., Sawa, Y., and Schaper, J. (1992). Human fetal heart development after mid-term: morphometry and ultrastructural study. *J. Mol. Cell. Cardiol.* 24, 949–965. doi: 10.1016/0022-2828(92)91862-y

Kitmitto, A., Baudoin, F., and Cartwright, E. J. (2019). Cardiomyocyte damage control in heart failure and the role of the sarcolemma. *J. Muscle Res. Cell Motil.* 40, 319–333. doi: 10.1007/s10974-019-09539-5

Kojima, C., Hashimoto, A., Yabuta, I., Hirose, M., Hashimoto, S., Kanaho, Y., et al. (2004). Regulation of Bin1 SH3 domain binding by phosphoinositides. *EMBO J.* 23, 4413–4422. doi: 10.1038/sj.emboj.7600442

Kolstad, T. R., van den Brink, J., MacQuaide, N., Lunde, P. K., Frisk, M., Aronsen, J. M., et al. (2018). Ryanodine receptor dispersion disrupts Ca^{2+} release in failing cardiac myocytes. *eLife* 7:e39427.

Kong, C. H. T., Bryant, S. M., Watson, J. J., Gadeberg, H. C., Roth, D. M., Patel, H. H., et al. (2018a). The effects of aging on the regulation of T-Tubular I_{Ca} by caveolin in mouse ventricular myocytes. *J. Gerontol. A Biol. Sci. Med. Sci.* 73, 711–719. doi: 10.1093/gerona/glx242

Kong, C. H. T., Bryant, S. M., Watson, J. J., Roth, D. M., Patel, H. H., Cannell, M. B., et al. (2019). Cardiac-specific overexpression of caveolin-3 preserves t-tubular I_{Ca} during heart failure in mice. *Exp. Physiol.* 104, 654–666. doi: 10.1113/ep087304

Kong, C. H. T., Rog-Zielinska, E. A., Kohl, P., Orchard, C. H., and Cannell, M. B. (2018b). Solute movement in the t-tubule system of rabbit and mouse cardiomyocytes. *Proc. Natl. Acad. Sci. U.S.A.* 115, E7073–E7080.

Korhonen, T., Rapila, R., Ronkainen, V. P., Koivumaki, J. T., and Tavi, P. (2010). Local Ca^{2+} releases enable rapid heart rates in developing cardiomyocytes. *J. Physiol.* 588, 1407–1417. doi: 10.1113/jphysiol.2009.185173

Kostin, S., Scholz, D., Shimada, T., Maeno, Y., Mollnau, H., Hein, S., et al. (1998). The internal and external protein scaffold of the T-tubular system in cardiomyocytes. *Cell Tissue Res.* 294, 449–460. doi: 10.1007/s004410051196

Lahiri, S. K., Quick, A. P., Samson-Couterie, B., Hulsurkar, M., Elzenaar, I., van Oort, R. J., et al. (2020). Nuclear localization of a novel calpain-2 mediated junctophilin-2 C-terminal cleavage peptide promotes cardiomyocyte remodeling. *Basic Res. Cardiol.* 115:49.

Lam, C. S. P., Gamble, G. D., Ling, L. H., Sim, D., Leong, K. T. G., Yeo, P. S. D., et al. (2018). Mortality associated with heart failure with preserved vs. reduced ejection fraction in a prospective international multi-ethnic cohort study. *Eur. Heart J.* 39, 1770–1780. doi: 10.1093/eurheartj/ehy005

Lambert, R., Srodulski, S., Peng, X., Margulies, K. B., Despa, F., and Despa, S. (2015). Intracellular Na^+ concentration ($[Na^+]_i$) is elevated in diabetic hearts due to enhanced Na^+-Glucose cotransport. *J. Am. Heart Assoc.* 4:e002183.

Lammerding, J., Kamm, R. D., and Lee, R. T. (2004). Mechanotransduction in cardiac myocytes. *Ann. N. Y. Acad. Sci.* 1015, 53–70. doi: 10.1196/annals.1302.005

Landstrom, A. P., Kellen, C. A., Dixit, S. S., van Oort, R. J., Garbino, A., Weisleder, N., et al. (2011). Junctophilin-2 expression silencing causes cardiocyte hypertrophy and abnormal intracellular calcium-handling. *Circ. Heart Fail.* 4, 214–223. doi: 10.1161/circheartfailure.110.958694

Larbig, R., Torres, N., Bridge, J. H., Goldhaber, J. I., and Philipson, K. D. (2010). Activation of reverse Na^+-Ca^{2+} exchange by the Na^+ current augments the cardiac Ca^{2+} transient: evidence from NCX knockout mice. *J. Physiol.* 588, 3267–3276. doi: 10.1113/jphysiol.2010.187708

Lawless, M., Caldwell, J. L., Radcliffe, E. J., Smith, C. E. R., Madders, G. W. P., Hutchings, D. C., et al. (2019). Phosphodiesterase 5 inhibition improves contractile function and restores transverse tubule loss and catecholamine responsiveness in heart failure. *Sci. Rep.* 9:6801.

Lee, E., Marcucci, M., Daniell, L., Pypaert, M., Weisz, O. A., Ochoa, G. C., et al. (2002). Amphiphysin 2 (Bin1) and T-tubule biogenesis in muscle. *Science* 297, 1193–1196. doi: 10.1126/science.1071362

Lekavich, C. L., Barksdale, D. J., Neelon, V., and Wu, J. R. (2015). Heart failure preserved ejection fraction (HFpEF): an integrated and strategic review. *Heart Fail. Rev.* 20, 643–653. doi: 10.1007/s10741-015-9506-7

Lenaerts, I., Bito, V., Heinzel, F. R., Driesen, R. B., Holemans, P., D'Hooge, J., et al. (2009). Ultrastructural and functional remodeling of the coupling between Ca^{2+} influx and sarcoplasmic reticulum Ca^{2+} release in right atrial myocytes from experimental persistent atrial fibrillation. *Circ. Res.* 105, 876–885. doi: 10.1161/circresaha.109.206276

Li, J., Agvanian, S., Zhou, K., Shaw, R. M., and Hong, T. (2020). Exogenous cardiac bridging Integrator 1 benefits mouse hearts with pre-existing pressure overload-induced heart failure. *Front. Physiol.* 11:708. doi: 10.3389/fphys.2020.00708

Li, L. L., Guo, Q. J., Lou, H. Y., Liang, J. H., Yang, Y., Xing, X., et al. (2020). Nanobar array assay revealed complementary roles of BIN1 splice isoforms in cardiac T-Tubule morphogenesis. *Nano Lett.* 20, 6387–6395. doi: 10.1021/acs.nanolett.0c01957

Li, Q., O'Neill, S. C., Tao, T., Li, Y., Eisner, D., and Zhang, H. (2012). Mechanisms by which cytoplasmic calcium wave propagation and alternans are generated in cardiac atrial myocytes lacking T-tubules-insights from a simulation study. *Biophys. J.* 102, 1471–1482. doi: 10.1016/j.bpj.2012.03.007

Li, R. C., Tao, J., Guo, Y. B., Wu, H. D., Liu, R. F., Bai, Y., et al. (2013). In vivo suppression of microRNA-24 prevents the transition toward decompensated hypertrophy in aortic-constricted mice. *Circ. Res.* 112, 601–605. doi: 10.1161/circresaha.112.300806

Lichter, J. G., Carruth, E., Mitchell, C., Barth, A. S., Aiba, T., Kass, D. A., et al. (2014). Remodeling of the sarcomeric cytoskeleton in cardiac ventricular myocytes during heart failure and after cardiac resynchronization therapy. *J. Mol. Cell. Cardiol.* 72, 186–195. doi: 10.1016/j.yjmcc.2014.03.012

Lindner, E. (1957). [Submicroscopic morphology of the cardiac muscle]. *Z. Zellforsch. Mikrosk. Anat. (Vienna, Austria: 1948)* 45, 702–746.

Lines, G. T., Sande, J. B., Louch, W. E., Mork, H. K., Grottum, P., and Sejersted, O. M. (2006). Contribution of the Na^+/Ca^{2+} exchanger to rapid Ca^{2+} release in cardiomyocytes. *Biophys. J.* 91, 779–792. doi: 10.1529/biophysj.105.072447

Linke, W. A. (2008). Sense and stretchability: the role of titin and titin-associated proteins in myocardial stress-sensing and mechanical dysfunction. *Cardiovasc. Res.* 77, 637–648.

Lipsett, D. B., Frisk, M., Aronsen, J. M., Norden, E. S., Buonarati, O. R., Cataliotti, A., et al. (2019). Cardiomyocyte substructure reverts to an immature phenotype during heart failure. *J. Physiol.* 59, 1833–1853. doi: 10.1113/jp277273

Liu, C., Spinozzi, S., Chen, J. Y., Fang, X., Feng, W., Perkins, G., et al. (2019). Nexilin is a new component of junctional membrane complexes required for cardiac T-Tubule formation. *Circulation* 140, 55–66. doi: 10.1161/circulationaha.119.039751

Liu, C., Spinozzi, S., Feng, W., Chen, Z., Zhang, L., Zhu, S., et al. (2020). Homozygous G650del nexilin variant causes cardiomyopathy in mice. *JCI Insight* 5:e138780.

Liu, Y., Zhou, K., Li, J., Agvanian, S., Caldaruse, A. M., Shaw, S., et al. (2020). In mice subjected to chronic stress, exogenous cBIN1 preserves calcium-handling machinery and cardiac function. *JACC Basic Transl. Sci.* 5, 561–578. doi: 10.1016/j.jacbts.2020.03.006

Louch, W. E., and Nattel, S. (2017). T-tubular collagen: a new player in mechanosensing and disease? *Cardiovasc. Res.* 113, 839–840. doi: 10.1093/cvr/cvx091

Louch, W. E., Bito, V., Heinzel, F. R., Macianskiene, R., Vanhaecke, J., Flameng, W., et al. (2004). Reduced synchrony of Ca^{2+} release with loss of T-tubules-a comparison to Ca^{2+} release in human failing cardiomyocytes. *Cardiovasc. Res.* 62, 63–73. doi: 10.1016/j.cardiores.2003.12.031

Louch, W. E., Hake, J., Jolle, G. F., Mork, H. K., Sjaastad, I., Lines, G. T., et al. (2010a). Control of Ca^{2+} release by action potential configuration in normal and failing murine cardiomyocytes. *Biophys. J.* 99, 1377–1386. doi: 10.1016/j.bpj.2010.06.055

Louch, W. E., Hake, J., Mork, H. K., Hougen, K., Skrbic, B., and Ursu, D. (2013). Slow Ca^{2+} sparks de-synchronize Ca^{2+} release in failing cardiomyocytes: evidence for altered configuration of Ca^{2+} release units? *J. Mol. Cell. Cardiol.* 58, 41–52. doi: 10.1016/j.yjmcc.2013.01.014

Louch, W. E., Koivumaki, J. T., and Tavi, P. (2015). Calcium signalling in developing cardiomyocytes: implications for model systems and disease. *J. Physiol.* 593, 1047–1063. doi: 10.1113/jphysiol.2014.274712

Louch, W. E., Mork, H. K., Sexton, J., Stromme, T. A., Laake, P., Sjaastad, I., et al. (2006). T-tubule disorganization and reduced synchrony of Ca^{2+} release in murine cardiomyocytes following myocardial infarction. *J. Physiol.* 574, 519–533. doi: 10.1113/jphysiol.2006.107227

Louch, W. E., Sejersted, O. M., and Swift, F. (2010b). There goes the neighborhood: pathological alterations in T-tubule morphology and consequences for cardiomyocyte Ca^{2+} handling. *J. Biomed. Biotechnol.* 2010:503906.

Louch, W. E., Stokke, M. K., Sjaastad, I., Christensen, G., and Sejersted, O. M. (2012). No rest for the weary: diastolic calcium homeostasis in the normal and failing myocardium. *Physiology (Bethesda)* 27, 308–323. doi: 10.1152/physiol.00021.2012

Loucks, A. D., O'Hara, T., and Trayanova, N. A. (2018). Degradation of T-Tubular microdomains and altered cAMP compartmentation lead to emergence of arrhythmogenic triggers in heart failure myocytes: an in silico study. *Front. Physiol.* 9:1737. doi: 10.3389/fphys.2018.01737

Lyon, A. R., MacLeod, K. T., Zhang, Y., Garcia, E., Kanda, G. K., Lab, M. J., et al. (2009). Loss of T-tubules and other changes to surface topography in ventricular myocytes from failing human and rat heart. *Proc. Natl. Acad. Sci. U.S.A.* 106, 6854–6859. doi: 10.1073/pnas.0809777106

Lyon, A. R., Nikolaev, V. O., Miragoli, M., Sikkel, M. B., Paur, H., Benard, L., et al. (2012). Plasticity of surface structures and beta(2)-adrenergic receptor localization in failing ventricular cardiomyocytes during recovery from heart failure. *Circ. Heart Fail.* 5, 357–365. doi: 10.1161/circheartfailure.111.964692

Lyu, Y., Verma, V. K., Lee, Y., Taleb, I., Badolia, R., Shankar, T. S., et al. (2021). Remodeling of t-system and proteins underlying excitation-contraction coupling in aging versus failing human heart. *NPJ Aging Mech. Dis.* 7:16.

Mackova, K., Zahradnikova, A. Jr., Hotka, M., Hoffmannova, B., Zahradnik, I., and Zahradnikova, A. (2017). Calcium release-dependent inactivation precedes formation of the tubular system in developing rat cardiac myocytes. *Eur. Biophys. J.* 46, 691–703. doi: 10.1007/s00249-017-1249-z

Manfra, O., Frisk, M., and Louch, W. E. (2017). Regulation of cardiomyocyte t-tubular structure: opportunities for therapy. *Curr. Heart Fail. Rep.* 14, 167–178. doi: 10.1007/s11897-017-0329-9

Maron, B. J., Ferrans, V. J., and Roberts, W. C. (1975). Ultrastructural features of degenerated cardiac muscle cells in patients with cardiac hypertrophy. *Am. J. Pathol.* 79, 387–434.

Marx, S. O., Gaburjakova, J., Gaburjakova, M., Henrikson, C., Ondrias, K., and Marks, A. R. (2001). Coupled gating between cardiac calcium release channels (ryanodine receptors). *Circ. Res.* 88, 1151–1158. doi: 10.1161/hh1101.091268

McNary, T. G., Bridge, J. H., and Sachse, F. B. (2011). Strain transfer in ventricular cardiomyocytes to their transverse tubular system revealed by scanning confocal microscopy. *Biophys. J.* 100, L53–L55.

McNutt, N. S. (1975). Ultrastructure of the myocardial sarcolemma. *Circ. Res.* 37, 1–13. doi: 10.1161/01.res.37.1.1

Meethal, S. V., Potter, K. T., Redon, D., Munoz-del-Rio, A., Kamp, T. J., Valdivia, H. H., et al. (2007). Structure-function relationships of Ca spark activity in normal and failing cardiac myocytes as revealed by flash photography. *Cell Calcium* 41, 123–134. doi: 10.1016/j.ceca.2006.05.006

Melnyk, P., Zhang, L., Shrier, A., and Nattel, S. (2002). Differential distribution of Kir2.1 and Kir2.3 subunits in canine atrium and ventricle. *Am. J. Physiol. Heart Circ. Physiol.* 283, H1123–H1133.

Minamisawa, S., Oshikawa, J., Takeshima, H., Hoshijima, M., Wang, Y., Chien, K. R., et al. (2004). Junctophilin type 2 is associated with caveolin-3 and is down-regulated in the hypertrophic and dilated cardiomyopathies. *Biochem. Biophys. Res. Commun.* 325, 852–856. doi: 10.1016/j.bbrc.2004.10.107

Mohler, P. J., Davis, J. Q., and Bennett, V. (2005). Ankyrin-B coordinates the Na/K ATPase, Na/Ca exchanger, and $InsP_3$ receptor in a cardiac T-tubule/SR microdomain. *PLoS Biol.* 3:e423. doi: 10.1371/journal.pbio.0030423

Mork, H. K., Sjaastad, I., Sande, J. B., Periasamy, M., Sejersted, O. M., and Louch, W. E. (2007). Increased cardiomyocyte function and Ca^{2+} transients in mice during early congestive heart failure. *J. Mol. Cell. Cardiol.* 43, 177–186. doi: 10.1016/j.yjmcc.2007.05.004

Muller, A. J., Baker, J. F., DuHadaway, J. B., Ge, K., Farmer, G., Donover, P. S., et al. (2003). Targeted disruption of the murine Bin1/Amphiphysin II gene does not disable endocytosis but results in embryonic cardiomyopathy with aberrant myofibril formation. *Mol. Cell. Biol.* 23, 4295–4306. doi: 10.1128/mcb.23.12.4295-4306.2003

Munro, M. L. I, Jayasinghe, D., Wang, Q., Quick, A., Wang, W., Baddeley, D., et al. (2016). Junctophilin-2 in the nanoscale organisation and functional signalling of ryanodine receptor clusters in cardiomyocytes. *J. Cell Sci.* 129, 4388–4398.

Munro, M. L., and Soeller, C. (2016). Early transverse tubule development begins in utero in the sheep heart. *J. Muscle Res. Cell. Motil.* 37, 195–202. doi: 10.1007/s10974-016-9462-4

Nikolova, A. P., Hitzeman, T. C., Baum, R., Caldaruse, A. M., Agvanian, S., Xie, Y., et al. (2018). Association of a novel diagnostic biomarker, the plasma cardiac bridging Integrator 1 score, with heart failure with preserved ejection fraction and cardiovascular hospitalization. *JAMA Cardiol.* 3, 1206–1210. doi: 10.1001/jamacardio.2018.3539

Nishi, M., Mizushima, A., Nakagawara, K., and Takeshima, H. (2000). Characterization of human junctophilin subtype genes. *Biochem. Biophys. Res. Commun.* 273, 920–927. doi: 10.1006/bbrc.2000.3011

Nyström, G. (1897). Über die lymphbahnen des Herzens. *Arch. Anat. Physiol. (Anat. Abt.)* 12, 361–378.

Oakley, R. H., Ren, R., Cruz-Topete, D., Bird, G. S., Myers, P. H., Boyle, M. C., et al. (2013). Essential role of stress hormone signaling in cardiomyocytes for the prevention of heart disease. *Proc. Natl. Acad. Sci. U.S.A.* 110, 17035–17040. doi: 10.1073/pnas.1302546110

Orchard, C. H., Bryant, S. M., and James, A. F. (2013). Do t-tubules play a role in arrhythmogenesis in cardiac ventricular myocytes? *J. Physiol.* 591, 4141–4147. doi: 10.1113/jphysiol.2013.254540

Oyehaug, L., Loose, K. O., Jolle, G. F., Roe, A. T., Sjaastad, I., Christensen, G., et al. (2013). Synchrony of cardiomyocyte Ca^{2+} release is controlled by T-tubule organization, SR Ca^{2+} content, and ryanodine receptor Ca^{2+} sensitivity. *Biophys. J.* 104, 1685–1697. doi: 10.1016/j.bpj.2013.03.022

Parikh, S. S., Blackwell, D. J., Gomez-Hurtado, N., Frisk, M., Wang, L., Kim, K., et al. (2017). Thyroid and glucocorticoid hormones promote functional t-tubule development in human-induced pluripotent stem cell-derived cardiomyocytes. *Circ. Res.* 121, 1323–1330. doi: 10.1161/circresaha.117.311920

Parton, R. G., Way, M., Zorzi, N., and Stang, E. (1997). Caveolin-3 associates with developing T-tubules during muscle differentiation. *J. Cell Biol.* 136, 137–154. doi: 10.1083/jcb.136.1.137

Paulus, W. J., and Tschope, C. (2013). A novel paradigm for heart failure with preserved ejection fraction: comorbidities drive myocardial dysfunction and remodeling through coronary microvascular endothelial inflammation. *J. Am. Coll. Cardiol.* 62, 263–271.

Picas, L., Viaud, J., Schauer, K., Vanni, S., Hnia, K., Fraisier, V., et al. (2014). BIN1/M-Amphiphysin2 induces clustering of phosphoinositides to recruit its downstream partner dynamin. *Nat. Commun.* 5:5647.

Pieske, B., Tschope, C., de Boer, R. A., Fraser, A. G., Anker, S. D., Donal, E., et al. (2019). How to diagnose heart failure with preserved ejection fraction: the

HFA-PEFF diagnostic algorithm: a consensus recommendation from the Heart Failure Association (HFA) of the European society of cardiology (ESC). *Eur. Heart J.* 40, 3297–3317. doi: 10.1093/eurheartj/ehz641

Pinali, C., Bennett, H., Davenport, J. B., Trafford, A. W., and Kitmitto, A. (2013). Three-dimensional reconstruction of cardiac sarcoplasmic reticulum reveals a continuous network linking transverse-tubules: this organization is perturbed in heart failure. *Circ. Res.* 113, 1219–1230. doi: 10.1161/circresaha.113.301348

Pinali, C., Malik, N., Davenport, J. B., Allan, L. J., Murfitt, L., Iqbal, M. M., et al. (2017). Post-myocardial infarction T-tubules form enlarged branched structures with dysregulation of Junctophilin-2 and Bridging Integrator 1 (BIN-1). *J. Am. Heart Assoc.* 6:e004834.

Prins, K. W., Asp, M. L., Zhang, H., Wang, W., and Metzger, J. M. (2016). Microtubule-mediated misregulation of Junctophilin-2 underlies T-Tubule disruptions and calcium mishandling in mdx Mice. *JACC Basic Transl. Sci.* 1, 122–130. doi: 10.1016/j.jacbts.2016.02.002

Prokic, I., Cowling, B. S., Kutchukian, C., Kretz, C., Tasfaout, H., Gache, V., et al. (2020). Differential physiological roles for BIN1 isoforms in skeletal muscle development, function and regeneration. *Dis. Model. Mech.* 13:dmm044354.

Quick, A. P., Wang, Q., Philippen, L. E., Barreto-Torres, G., Chiang, D. Y., Beavers, D., et al. (2017). SPEG (Striated Muscle Preferentially Expressed Protein Kinase) is essential for cardiac function by regulating junctional membrane complex activity. *Circ. Res.* 120, 110–119. doi: 10.1161/circresaha.116.309977

Rajabi, M., Kassiotis, C., Razeghi, P., and Taegtmeyer, H. (2007). Return to the fetal gene program protects the stressed heart: a strong hypothesis. *Heart Fail. Rev.* 12, 331–343. doi: 10.1007/s10741-007-9034-1

Rapila, R., Korhonen, T., and Tavi, P. (2008). Excitation-contraction coupling of the mouse embryonic cardiomyocyte. *J. Gen. Physiol.* 132, 397–405. doi: 10.1085/jgp.200809960

Retzius, G. (1881). Zur Kenntnis der quergestreiften Muskelfaser. *Biol. Untersuch.* 1, 1–26.

Reynolds, J. O., Chiang, D. Y., Wang, W., Beavers, D. L., Dixit, S. S., Skapura, D. G., et al. (2013). Junctophilin-2 is necessary for T-tubule maturation during mouse heart development. *Cardiovasc. Res.* 100, 44–53. doi: 10.1093/cvr/cvt133

Reynolds, J. O., Quick, A. P., Wang, Q., Beavers, D. L., Philippen, L. E., and Showell, J. (2016). Junctophilin-2 gene therapy rescues heart failure by normalizing RyR2-mediated Ca^{2+} release. *Int. J. Cardiol.* 225, 371–380. doi: 10.1016/j.ijcard.2016.10.021

Richards, M. A., Clarke, J. D., Saravanan, P., Voigt, N., Dobrev, D., Eisner, D. A., et al. (2011). Transverse tubules are a common feature in large mammalian atrial myocytes including human. *Am. J. Physiol. Heart Circ. Physiol.* 301, H1996–H2005.

Roe, A. T., Aronsen, J. M., Skardal, K., Hamdani, N., Linke, W. A., Danielsen, H. E., et al. (2017). Increased passive stiffness promotes diastolic dysfunction despite improved Ca^{2+} handling during left ventricular concentric hypertrophy. *Cardiovasc. Res.* 113, 1161–1172. doi: 10.1093/cvr/cvx087

Roe, A. T., Frisk, M., and Louch, W. E. (2015). Targeting cardiomyocyte Ca^{2+} homeostasis in heart failure. *Curr. Pharm. Des.* 21, 431–448. doi: 10.2174/1381612821041204124129

Roe, A. T., Ruud, M., Espe, E. K., Manfra, O., Longobardi, S., Aronsen, J. M., et al. (2019). Regional diastolic dysfunction in post-infarction heart failure: role of local mechanical load and SERCA expression. *Cardiovasc. Res.* 115, 752–764. doi: 10.1093/cvr/cvy257

Rog-Zielinska, E. A., Moss, R., Kaltenbacher, W., Greiner, J., Verkade, P., Seemann, G., et al. (2021a). Nano-scale morphology of cardiomyocyte t-tubule/sarcoplasmic reticulum junctions revealed by ultra-rapid high-pressure freezing and electron tomography. *J. Mol. Cell. Cardiol.* 153, 86–92. doi: 10.1016/j.yjmcc.2020.12.006

Rog-Zielinska, E. A., Scardigli, M., Peyronnet, R., Zgierski-Johnston, C. M., Greiner, J., Madl, J., et al. (2021b). Beat-by-Beat cardiomyocyte t-tubule deformation drives tubular content exchange. *Circ. Res.* 128, 203–215. doi: 10.1161/circresaha.120.317266

Ronaldson-Bouchard, K., Ma, S. P., Yeager, K., Chen, T., Song, L., Sirabella, D., et al. (2018). Advanced maturation of human cardiac tissue grown from pluripotent stem cells. *Nature* 556, 239–243. doi: 10.1038/s41586-018-0016-3

Royer, B., Hnia, K., Gavriilidis, C., Tronchere, H., Tosch, V., and Laporte, J. (2013). The myotubularin-amphiphysin 2 complex in membrane tubulation and centronuclear myopathies. *EMBO Rep.* 14, 907–915. doi: 10.1038/embor.2013.119

Russell, J., Du Toit, E. F., Peart, J. N., Patel, H. H., and Headrick, J. P. (2017). Myocyte membrane and microdomain modifications in diabetes: determinants of ischemic tolerance and cardioprotection. *Cardiovasc. Diabetol.* 16:155.

Sachse, F. B., Torres, N. S., Savio-Galimberti, E., Aiba, T., Kass, D. A., Tomaselli, G. F., et al. (2012). Subcellular structures and function of myocytes impaired during heart failure are restored by cardiac resynchronization therapy. *Circ. Res.* 110, 588–597. doi: 10.1161/circresaha.111.257428

Sah, R., Ramirez, R. J., and Backx, P. H. (2002). Modulation of Ca^{2+} release in cardiac myocytes by changes in repolarization rate: role of phase-1 action potential repolarization in excitation-contraction coupling. *Circ. Res.* 90, 165–173. doi: 10.1161/hh0202.103315

Sanchez-Alonso, J. L., Bhargava, A., O'Hara, T., Glukhov, A. V., Schobesberger, S., Bhogal, N., et al. (2016). Microdomain-specific modulation of L-Type calcium channels leads to triggered ventricular arrhythmia in heart failure. *Circ. Res.* 119, 944–955. doi: 10.1161/circresaha.116.308698

Savio-Galimberti, E., Frank, J., Inoue, M., Goldhaber, J. I., Cannell, M. B., Bridge, J. H., et al. (2008). Novel features of the rabbit transverse tubular system revealed by quantitative analysis of three-dimensional reconstructions from confocal images. *Biophys. J.* 95, 2053–2062. doi: 10.1529/biophysj.108.130617

Scardigli, M., Crocini, C., Ferrantini, C., Gabbrielli, T., Silvestri, L., Coppini, R., et al. (2017). Quantitative assessment of passive electrical properties of the cardiac T-tubular system by FRAP microscopy. *Proc. Natl. Acad. Sci. U.S.A.* 114, 5737–5742. doi: 10.1073/pnas.1702188114

Schaper, J., Froede, R., Hein, S., Buck, A., Hashizume, H., Speiser, B., et al. (1991). Impairment of the myocardial ultrastructure and changes of the cytoskeleton in dilated cardiomyopathy. *Circulation* 83, 504–514. doi: 10.1161/01.cir.83.2.504

Schmitto, J. D., Krabatsch, T., Damme, L., and Netuka, I. (2018). Less invasive HeartMate 3 left ventricular assist device implantation. *J. Thorac. Dis.* 10, S1692–S1695.

Schobesberger, S., Wright, P., Tokar, S., Bhargava, A., Mansfield, C., Glukhov, A. V., et al. (2017). T-tubule remodelling disturbs localized beta2-adrenergic signalling in rat ventricular myocytes during the progression of heart failure. *Cardiovasc. Res.* 113, 770–782. doi: 10.1093/cvr/cvx074

Schulson, M. N., Scriven, D. R., Fletcher, P., and Moore, E. D. (2011). Couplons in rat atria form distinct subgroups defined by their molecular partners. *J. Cell Sci.* 124, 1167–1174. doi: 10.1242/jcs.080929

Scriven, D. R., Asghari, P., Schulson, M. N., and Moore, E. D. (2010). Analysis of Cav1.2 and ryanodine receptor clusters in rat ventricular myocytes. *Biophys. J.* 99, 3923–3929. doi: 10.1016/j.bpj.2010.11.008

Scriven, D. R., Dan, P., and Moore, E. D. (2000). Distribution of proteins implicated in excitation-contraction coupling in rat ventricular myocytes. *Biophys. J.* 79, 2682–2691. doi: 10.1016/s0006-3495(00)76506-4

Seidel, T., Fiegle, D. J., Baur, T. J., Ritzer, A., Nay, S., Heim, C., et al. (2019). Glucocorticoids preserve the t-tubular system in ventricular cardiomyocytes by upregulation of autophagic flux. *Basic Res. Cardiol.* 114:47. doi: 10.3390/cells9010047

Seidel, T., Navankasattusas, S., Ahmad, A., Diakos, N. A., Xu, W. D., Tristani-Firouzi, M., et al. (2017a). Sheet-like remodeling of the transverse tubular system in human heart failure impairs excitation-contraction coupling and functional recovery by mechanical unloading. *Circulation* 135, 1632–1645. doi: 10.1161/circulationaha.116.024470

Seidel, T., Sankarankutty, A. C., and Sachse, F. B. (2017b). Remodeling of the transverse tubular system after myocardial infarction in rabbit correlates with local fibrosis: a potential role of biomechanics. *Prog. Biophys. Mol. Biol.* 130, 302–314. doi: 10.1016/j.pbiomolbio.2017.07.006

Severs, N. J., Slade, A. M., Powell, T., Twist, V. W., and Jones, G. E. (1985). Morphometric analysis of the isolated calcium-tolerant cardiac myocyte. Organelle volumes, sarcomere length, plasma membrane surface folds, and intramembrane particle density and distribution. *Cell Tissue Res.* 240, 159–168.

Shah, S. J., Aistrup, G. L., Gupta, D. K., O'Toole, M. J., Nahhas, A. F., Schuster, D., et al. (2014). Ultrastructural and cellular basis for the development of abnormal myocardial mechanics during the transition from hypertension to heart failure. *Am. J. Physiol. Heart Circ. Physiol.* 306, H88–H100.

Sheard, T. M. D., Hurley, M. E., Colyer, J., White, E., Norman, R., Pervolaraki, E., et al. (2019). Three-dimensional and chemical mapping of intracellular signaling nanodomains in health and disease with enhanced expansion microscopy. *ACS Nano* 13, 2143–2157.

Sheldon, C. A., Friedman, W. F., and Sybers, H. D. (1976). Scanning electron microscopy of fetal and neonatal lamb cardiac cells. *J. Mol. Cell. Cardiol.* 8, 853–862. doi: 10.1016/0022-2828(76)90068-7

Shen, X., van den Brink, J., Hou, Y., Colli, D., Le, C., Kolstad, T. R., et al. (2019). 3D dSTORM imaging reveals novel detail of ryanodine receptor localization in rat cardiac myocytes. *J. Physiol.* 597, 399–418. doi: 10.1113/jp277360

Shiferaw, Y., Aistrup, G. L., Louch, W. E., and Wasserstrom, J. A. (2020). Remodeling promotes proarrhythmic disruption of calcium homeostasis in failing atrial myocytes. *Biophys. J.* 118, 476–491. doi: 10.1016/j.bpj.2019.12.012

Silbernagel, N., Korner, A., Balitzki, J., Jaggy, M., Bertels, S., Richter, B., et al. (2020). Shaping the heart: structural and functional maturation of iPSC-cardiomyocytes in 3D-micro-scaffolds. *Biomaterials* 227:119551. doi: 10.1016/j.biomaterials.2019.119551

Simpson, F. O. (1965). The transverse tubular system in mammalian myocardial cells. *Am. J. Anat.* 117, 1–17. doi: 10.1002/aja.1001170102

Singh, J. K., Barsegyan, V., Bassi, N., Marszalec, W., Tai, S., Mothkur, S., et al. (2017). T-tubule remodeling and increased heterogeneity of calcium release during the progression to heart failure in intact rat ventricle. *Physiol. Rep.* 5:e13540. doi: 10.14814/phy2.13540

Sipido, K. R., Maes, M., and Van de Werf, F. (1997). Low efficiency of Ca^{2+} entry through the Na(+)-Ca^{2+} exchanger as trigger for Ca^{2+} release from the sarcoplasmic reticulum. A comparison between L-type Ca^{2+} current and reverse-mode Na(+)-Ca^{2+} exchange. *Circ. Res.* 81, 1034–1044. doi: 10.1161/01.res.81.6.1034

Smyrnias, I., Mair, W., Harzheim, D., Walker, S. A., Roderick, H. L., and Bootman, M. D. (2010). Comparison of the T-tubule system in adult rat ventricular and atrial myocytes, and its role in excitation-contraction coupling and inotropic stimulation. *Cell Calcium* 47, 210–223. doi: 10.1016/j.ceca.2009.10.001

Snopko, R. M., Ramos-Franco, J., Di Maio, A., Karko, K. L., Manley, C., Piedras-Renteria, E., et al. (2008). Ca^{2+} sparks and cellular distribution of ryanodine receptors in developing cardiomyocytes from rat. *J. Mol. Cell. Cardiol.* 44, 1032–1044. doi: 10.1016/j.yjmcc.2008.03.015

Sobie, E. A., Guatimosim, S., Gomez-Viquez, L., Song, L. S., Hartmann, H., Saleet Jafri, M., et al. (2006). The Ca^{2+} leak paradox and rogue ryanodine receptors: SR Ca 2+ efflux theory and practice. *Prog. Biophys. Mol. Biol.* 90, 172–185. doi: 10.1016/j.pbiomolbio.2005.06.010

Soeller, C., and Cannell, M. B. (1999). Examination of the transverse tubular system in living cardiac rat myocytes by 2-photon microscopy and digital image-processing techniques. *Circ. Res.* 84, 266–275. doi: 10.1161/01.res.84.3.266

Song, L. S., Sobie, E. A., McCulle, S., Lederer, W. J., Balke, C. W., and Cheng, H. (2006). Orphaned ryanodine receptors in the failing heart. *Proc. Natl. Acad. Sci. U.S.A.* 103, 4305–4310. doi: 10.1073/pnas.0509324103

Song, Z., Liu, M. B., and Qu, Z. (2018). Transverse tubular network structures in the genesis of intracellular calcium alternans and triggered activity in cardiac cells. *J. Mol. Cell. Cardiol.* 114, 288–299. doi: 10.1016/j.yjmcc.2017.12.003

Sperelakis, N., and Rubio, R. (1971). An orderly lattice of axial tubules which interconnect adjacent transverse tubules in guinea-pig ventricular myocardium. *J. Mol. Cell. Cardiol.* 2, 211–220. doi: 10.1016/0022-2828(71)90054-x

Spinozzi, S., Liu, C., Chen, Z., Feng, W., Zhang, L., Ouyang, K., et al. (2020). Nexilin is necessary for maintaining the transverse-axial tubular system in adult cardiomyocytes. *Circ. Heart Fail.* 13:e006935.

Stewart, J. M., and Page, E. (1978). Improved stereological techniques for studying myocardial cell growth: application to external sarcolemma, T system, and intercalated disks of rabbit and rat hearts. *J. Ultrastruct. Res.* 65, 119–134. doi: 10.1016/s0022-5320(78)90050-3

Stolen, T. O., Hoydal, M. A., Kemi, O. J., Catalucci, D., Ceci, M., Aasum, E., et al. (2009). Interval training normalizes cardiomyocyte function, diastolic Ca^{2+} control, and SR Ca^{2+} release synchronicity in a mouse model of diabetic cardiomyopathy. *Circ. Res.* 105, 527–536. doi: 10.1161/circresaha.109.199810

Sun, X. H., Protasi, F., Takahashi, M., Takeshima, H., Ferguson, D. G., and Franzini-Armstrong, C. (1995). Molecular architecture of membranes involved in excitation-contraction coupling of cardiac muscle. *J. Cell Biol.* 129, 659–671. doi: 10.1083/jcb.129.3.659

Swift, F., Birkeland, J. A., Tovsrud, N., Enger, U. H., Aronsen, J. M., Louch, W. E., et al. (2008). Altered Na^+/Ca^{2+}-exchanger activity due to downregulation of Na^+/K^+-ATPase alpha$_2$-isoform in heart failure. *Cardiovasc. Res.* 78, 71–78. doi: 10.1093/cvr/cvn013

Swift, F., Franzini-Armstrong, C., Oyehaug, L., Enger, U. H., Andersson, K. B., Christensen, G., et al. (2012). Extreme sarcoplasmic reticulum volume loss and compensatory T-tubule remodeling after Serca2 knockout. *Proc. Natl. Acad. Sci. U.S.A.* 109, 3997–4001. doi: 10.1073/pnas.1120172109

Swift, F., Stromme, T. A., Amundsen, B., Sejersted, O. M., and Sjaastad, I. (2006). Slow diffusion of K^+ in the T tubules of rat cardiomyocytes. *J. Appl. Physiol. (1985)* 101, 1170–1176. doi: 10.1152/japplphysiol.00297.2006

Takeshima, H., Komazaki, S., Nishi, M., Iino, M., and Kangawa, K. (2000). Junctophilins: a novel family of junctional membrane complex proteins. *Mol. Cell* 6, 11–22. doi: 10.1016/s1097-2765(00)00003-4

Tarzia, V., Di Giammarco, G., Di Mauro, M., Bortolussi, G., Maccherini, M., Tursi, V., et al. (2016). From bench to bedside: can the improvements in left ventricular assist device design mitigate adverse events and increase survival? *J. Thorac. Cardiovasc. Surg.* 151, 213–217. doi: 10.1016/j.jtcvs.2015.09.107

Tasfaout, H., Buono, S., Guo, S., Kretz, C., Messaddeq, N., Booten, S., et al. (2017). Antisense oligonucleotide-mediated Dnm2 knockdown prevents and reverts myotubular myopathy in mice. *Nat. Commun.* 8:15661.

Thomas, M. J., Sjaastad, I., Andersen, K., Helm, P. J., Wasserstrom, J. A., Sejersted, O. M., et al. (2003). Localization and function of the Na^+/Ca^{2+}-exchanger in normal and detubulated rat cardiomyocytes. *J. Mol. Cell. Cardiol.* 35, 1325–1337. doi: 10.1016/j.yjmcc.2003.08.005

Tidball, J. G., Cederdahl, J. E., and Bers, D. M. (1991). Quantitative analysis of regional variability in the distribution of transverse tubules in rabbit myocardium. *Cell Tissue Res.* 264, 293–298. doi: 10.1007/bf00313966

Uchida, K., and Lopatin, A. N. (2018). Diffusional and electrical properties of T-Tubules are governed by their constrictions and dilations. *Biophys. J.* 114, 437–449. doi: 10.1016/j.bpj.2017.11.3742

Vaidya, Y., and Dhamoon, A. S. (2019). *StatPearls*. Treasure Island (FL): StatPearls Publishing StatPearls Publishing LLC.

van Oort, R. J., Garbino, A., Wang, W., Dixit, S. S., Landstrom, A. P., Gaur, N., et al. (2011). Disrupted junctional membrane complexes and hyperactive ryanodine receptors after acute junctophilin knockdown in mice. *Circulation* 123, 979–988. doi: 10.1161/circulationaha.110.006437

Wagner, E., Lauterbach, M. A., Kohl, T., Westphal, V., Williams, G. S., and Steinbrecher, J. H. (2012). Stimulated emission depletion live-cell super-resolution imaging shows proliferative remodeling of T-tubule membrane structures after myocardial infarction. *Circ. Res.* 111, 402–414.

Wakili, R., Yeh, Y. H., Yan Qi, X., Greiser, M., Chartier, D., Nishida, K., et al. (2010). Multiple potential molecular contributors to atrial hypocontractility caused by atrial tachycardia remodeling in dogs. *Circ. Arrhythm. Electrophysiol.* 3, 530–541.

Wang, H., Li, Z., Wang, J., Sun, K., Cui, Q., Song, L., et al. (2010). Mutations in NEXN, a Z-disc gene, are associated with hypertrophic cardiomyopathy. *Am. J. Hum. Genet.* 87, 687–693.

Wang, W., Landstrom, A. P., Wang, Q., Munro, M. L., Beavers, D., Ackerman, M. J., et al. (2014). Reduced junctional Na^+/Ca^{2+}-exchanger activity contributes to sarcoplasmic reticulum Ca^{2+} leak in junctophilin-2-deficient mice. *Am. J. Physiol. Heart Circ. Physiol.* 307, H1317–H1326.

Wang, X., Xie, W., Zhang, Y., Lin, P., Han, L., Han, P., et al. (2010). Cardioprotection of ischemia/reperfusion injury by cholesterol-dependent MG53-mediated membrane repair. *Circ. Res.* 107, 76–83.

Wang, Y., Chen, B., Huang, C. K., Guo, A., Wu, J., Zhang, X., et al. (2018). Targeting calpain for heart failure therapy: implications from multiple murine models. *JACC Basic Transl. Sci.* 3, 503–517.

Ward, M. L., and Crossman, D. J. (2014). Mechanisms underlying the impaired contractility of diabetic cardiomyopathy. *World J. Cardiol.* 6, 577–584. doi: 10.4330/wjc.v6.i7.577

Wei, S., Guo, A., Chen, B., Kutschke, W., Xie, Y. P., Zimmerman, K., et al. (2010). T-tubule remodeling during transition from hypertrophy to heart failure. *Circ. Res.* 107, 520–531. doi: 10.1161/circresaha.109.212324

Wright, P. T., Bhogal, N. K., Diakonov, I., Pannell, L. M. K., Perera, R. K., and Bork, N. I. (2018). Cardiomyocyte membrane structure and cAMP compartmentation produce anatomical variation in beta2AR-cAMP responsiveness in murine hearts. *Cell Rep.* 23, 459–469. doi: 10.1016/j.celrep.2018.03.053

Wu, C. Y., Chen, B., Jiang, Y. P., Jia, Z., Martin, D. W., Liu, S., et al. (2014). Calpain-dependent cleavage of junctophilin-2 and T-tubule remodeling in a mouse model of reversible heart failure. *J. Am. Heart Assoc.* 3: e000527.

Wu, C. Y., Jia, Z., Wang, W., Ballou, L. M., Jiang, Y. P., Chen, B., et al. (2011). PI3Ks maintain the structural integrity of T-tubules in cardiac myocytes. *PLoS One* 6:e24404. doi: 10.1371/journal.pone.0024404

Wu, H. D., Xu, M., Li, R. C., Guo, L., Lai, Y. S., Xu, S. M., et al. (2012). Ultrastructural remodelling of Ca^{2+} signalling apparatus in failing heart cells. *Cardiovasc. Res.* 95, 430–438. doi: 10.1093/cvr/cvs195

Xie, Y. P., Chen, B., Sanders, P., Guo, A., Li, Y., Zimmerman, K., et al. (2012). Sildenafil prevents and reverses transverse-tubule remodeling and Ca^{2+} handling dysfunction in right ventricle failure induced by pulmonary artery hypertension. *Hypertension* 59, 355–362. doi: 10.1161/hypertensionaha.111.180968

Xie, Y., Yang, Y., Galice, S., Bers, D. M., and Sato, D. (2019). Size matters: ryanodine receptor cluster size heterogeneity potentiates calcium waves. *Biophys. J.* 116, 530–539. doi: 10.1016/j.bpj.2018.12.017

Xu, M., Wu, H. D., Li, R. C., Zhang, H. B., Wang, M., Tao, J., et al. (2012). Mir-24 regulates junctophilin-2 expression in cardiomyocytes. *Circ. Res.* 111, 837–841. doi: 10.1161/circresaha.112.277418

Xu, M., Zhou, P., Xu, S. M., Liu, Y., Feng, X., Bai, S. H., et al. (2007). Intermolecular failure of L-type Ca^{2+} channel and ryanodine receptor signaling in hypertrophy. *PLoS Biol* 5:e21. doi: 10.1371/journal.pbio.0050021

Yamakawa, S., Wu, D., Dasgupta, M., Pedamallu, H., Gupta, B., Modi, R., et al. (2021). Role of t-tubule remodeling on mechanisms of abnormal calcium release during heart failure development in canine ventricle. *Am. J. Physiol. Heart Circ. Physiol.* 320, H1658–H1669.

Zhang, C., Chen, B., Guo, A., Zhu, Y., Miller, J. D., Gao, S., et al. (2014). Microtubule-mediated defects in junctophilin-2 trafficking contribute to myocyte transverse-tubule remodeling and Ca^{2+} handling dysfunction in heart failure. *Circulation* 129, 1742–1750. doi: 10.1161/circulationaha.113.008452

Zhang, C., Chen, B., Wang, Y., Guo, A., Tang, Y., Khataei, T., et al. (2017). MG53 is dispensable for T-tubule maturation but critical for maintaining T-tubule integrity following cardiac stress. *J. Mol. Cell. Cardiol.* 112, 123–130. doi: 10.1016/j.yjmcc.2017.08.007

Ziman, A. P., Gomez-Viquez, N. L., Bloch, R. J., and Lederer, W. J. (2010). Excitation-contraction coupling changes during postnatal cardiac development. *J. Mol. Cell. Cardiol.* 48, 379–386. doi: 10.1016/j.yjmcc.2009.09.016

Conflict of Interest: The authors declare that the research was conducted in the absence of any commercial or financial relationships that could be construed as a potential conflict of interest.

Publisher's Note: All claims expressed in this article are solely those of the authors and do not necessarily represent those of their affiliated organizations, or those of the publisher, the editors and the reviewers. Any product that may be evaluated in this article, or claim that may be made by its manufacturer, is not guaranteed or endorsed by the publisher.

frontiers in Physiology

CORRECTION
published: 26 October 2021
doi: 10.3389/fphys.2021.790227

Corrigendum: The Physiology and Pathophysiology of T-Tubules in the Heart

Ingunn E. Setterberg[1,2], *Christopher Le*[1,2†], *Michael Frisk*[1,2†], *Harmonie Perdreau-Dahl*[1,2], *Jia Li*[1,2] *and William E. Louch*[1,2*]

[1] Institute for Experimental Medical Research, Oslo University Hospital and University of Oslo, Oslo, Norway, [2] KG Jebsen Centre for Cardiac Research, University of Oslo, Oslo, Norway

Keywords: t-tubules, dyad, cardiomyocyte, calcium homeostasis, heart failure

OPEN ACCESS

Approved by:
Frontiers Editorial Office, Frontiers Media SA, Switzerland

***Correspondence:**
William E. Louch
w.e.louch@medisin.uio.no

†These authors have contributed equally to this work

Specialty section:
This article was submitted to Cardiac Electrophysiology, a section of the journal Frontiers in Physiology

Received: *06 October 2021*
Accepted: *07 October 2021*
Published: *26 October 2021*

Citation:
Setterberg IE, Le C, Frisk M, Perdreau-Dahl H, Li J and Louch WE (2021) Corrigendum: The Physiology and Pathophysiology of T-Tubules in the Heart. Front. Physiol. 12:790227. doi: 10.3389/fphys.2021.790227

A Corrigendum on

The Physiology and Pathophysiology of T-Tubules in the Heart
Setterberg, I. E., Le, C., Frisk, M., Perdreau-Dahl, H., Li, J., and Louch, W. E. (2021). Front. Physiol. 12:718404. doi: 10.3389/fphys.2021.718404

Harmonie Perdreau-Dahl was not included as an author in the published article. The corrected Author Contributions Statement appears below.

AUTHOR CONTRIBUTIONS

All authors contributed to the writing of the article and development of the figures.

The authors apologize for this error and state that this does not change the scientific conclusions of the article in any way. The original article has been updated.

frontiers in Physiology

REVIEW
published: 08 October 2021
doi: 10.3389/fphys.2021.734210

RyR2 and Calcium Release in Heart Failure

*Jean-Pierre Benitah, Romain Perrier, Jean-Jacques Mercadier, Laetitia Pereira and Ana M. Gómez**

Signaling and Cardiovascular Pathophysiology—UMR-S 1180, INSERM, Université Paris-Saclay, Châtenay-Malabry, France

Heart Failure (HF) is defined as the inability of the heart to efficiently pump out enough blood to maintain the body's needs, first at exercise and then also at rest. Alterations in Ca^{2+} handling contributes to the diminished contraction and relaxation of the failing heart. While most Ca^{2+} handling protein expression and/or function has been shown to be altered in many models of experimental HF, in this review, we focus in the sarcoplasmic reticulum (SR) Ca^{2+} release channel, the type 2 ryanodine receptor (RyR2). Various modifications of this channel inducing alterations in its function have been reported. The first was the fact that RyR2 is less responsive to activation by Ca^{2+} entry through the L-Type calcium channel, which is the functional result of an ultrastructural remodeling of the ventricular cardiomyocyte, with fewer and disorganized transverse (T) tubules. HF is associated with an elevated sympathetic tone and in an oxidant environment. In this line, enhanced RyR2 phosphorylation and oxidation have been shown in human and experimental HF. After several controversies, it is now generally accepted that phosphorylation of RyR2 at the Calmodulin Kinase II site (S2814) is involved in both the depressed contractile function and the enhanced arrhythmic susceptibility of the failing heart. Diminished expression of the FK506 binding protein, FKBP12.6, may also contribute. While these alterations have been mostly studied in the left ventricle of HF with reduced ejection fraction, recent studies are looking at HF with preserved ejection fraction. Moreover, alterations in the RyR2 in HF may also contribute to supraventricular defects associated with HF such as sinus node dysfunction and atrial fibrillation.

Keywords: ryanodine receptor, heart failure, calcium, excitation contraction coupling, sinus node, atrial fibrillation

OPEN ACCESS

Edited by:
Daniel M. Johnson,
The Open University, United Kingdom

Reviewed by:
Bjorn C. Knollmann,
Vanderbilt University, United States
Shanna Hamilton,
The Ohio State University, United States

****Correspondence:***
Ana M. Gómez
ana-maria.gomez@inserm.fr

Specialty section:
This article was submitted to Cardiac Electrophysiology, a section of the journal Frontiers in Physiology

Received: *30 June 2021*
Accepted: *30 August 2021*
Published: *08 October 2021*

Citation:
Benitah J-P, Perrier R, Mercadier J-J, Pereira L and Gómez AM (2021) RyR2 and Calcium Release in Heart Failure. Front. Physiol. 12:734210. doi: 10.3389/fphys.2021.734210

INTRODUCTION

Heart failure (HF) is one of the major causes of death worldwide. It is characterized by the failure of the cardiac pump to maintain a sufficient blood flow to oxygenize and carry nutrients to the whole body. According to left ventricular systolic function, HF has been divided into two major groups: HF with reduced ejection fraction (HFrEF) and HF with preserved ejection fraction (HFpEF). HFrEF generally occurs after cardiac injury (myocardial infarction) or under chronic stress (hypertension), leading to the alteration of contractile function of the heart. It is now well established that alteration of cardiomyocyte Ca^{2+} homeostasis plays a critical role in the development of the pathology, leading to cardiac remodeling, failure of the cardiac pump, and cardiac arrhythmias.

Ca^{2+} plays a key role in cardiomyocyte contraction. In each heartbeat, the membrane depolarization during an action potential (AP) activates L-type Ca^{2+} channels (LTCC), which are located in the sarcolemma and are more concentrated at the transverse (T) tubules (**Figure 1**).

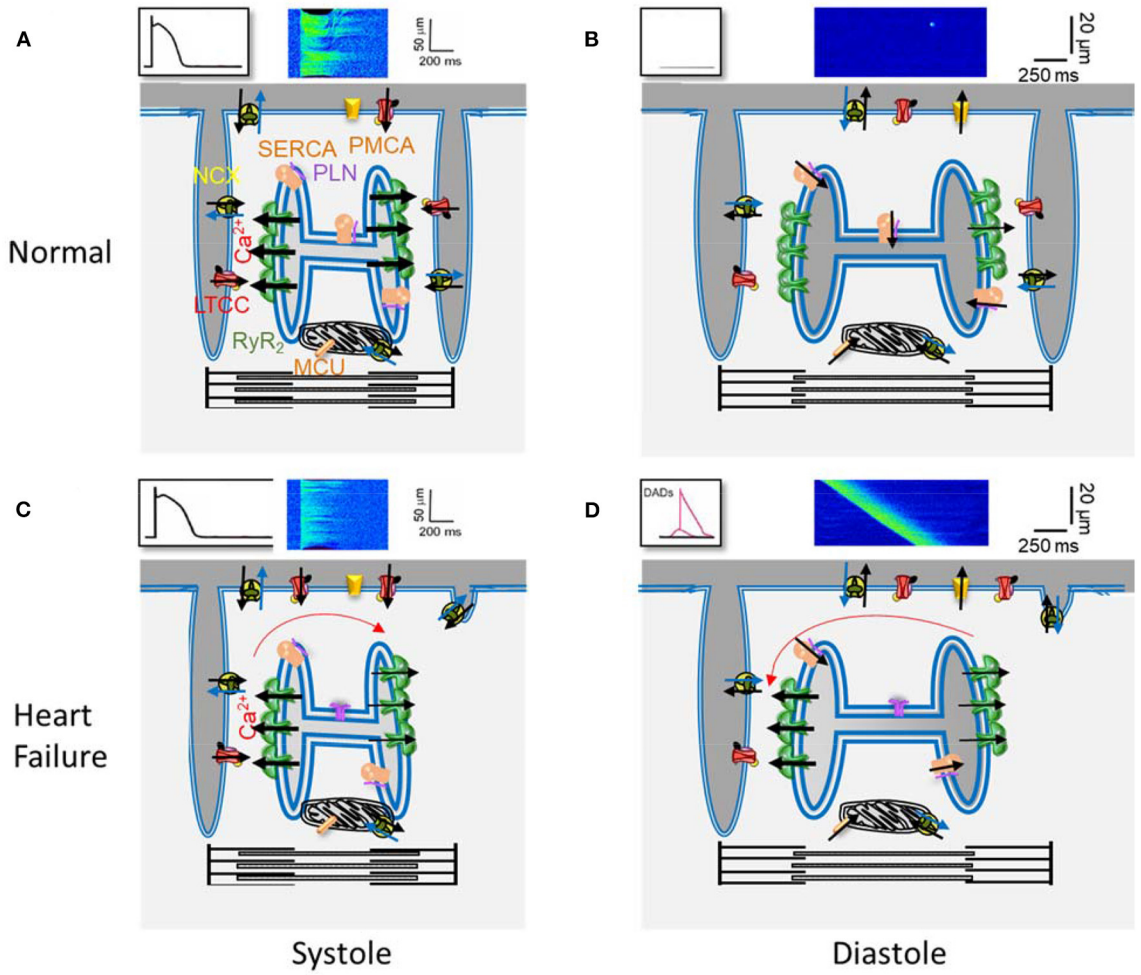

FIGURE 1 | Main elements of Ca^{2+} handling in excitation-contraction coupling in a ventricular cardiomyocyte. **(A)** Scheme of a portion of a ventricular cardiomyocyte showing two T-tubules, with L type Ca^{2+} channels (LTCC) and the Na^{+}/Ca^{2+} exchanger (NCX), and the junctional sarcoplasmic reticulum with Ryanodine Receptors (RyR2). Plasmalema and SarcoEndoplasmic Ca^{2+} ATPases (PMCA and SERCA) are also shown, with phospholamban (PLN) which slows SERCA activity, as well as the mitochondrial Ca^{2+} uniporter (MCU). The black arrows indicate Ca^{2+} movements during the action potential (drawing on top left), producing the $[Ca^{2+}]_i$ transient (confocal line scan image on top). **(B)** The same elements during rest. The LTCC are inactive, and the RyR2 closed, with small leak. **(C)** and **(D)** The same as in **(A)** and **(B)** but in heart failure: the density of T-tubules is decreased as well as SERCA expression; the RyR2 are more active.

The local increase in $[Ca^{2+}]_i$ in the dyads that follows activates the Ca^{2+} release channels, the ryanodine receptors (RyR2) located in the neighborhood, on the junctional sarcoplasmic reticulum (SR), resulting in the coordinated and global increase in the cell $[Ca^{2+}]_i$, by the Ca^{2+}-induced Ca^{2+}-release (CICR) mechanism, activating contractile myofibrils. Relaxation happens when the cytosolic $[Ca^{2+}]_i$ decreases, mainly by Ca^{2+} re-uptake into the SR through the SarcoEndoplasmic Reticulum Ca^{2+} ATPase (SERCA) and extrusion out of the cell through the Na^{+}/Ca^{2+} exchanger (NCX). Other systems, such as the plasmalemmal Ca^{2+} pump and the mitochondrial Ca^{2+} uniporter, play a minor role in cytosolic Ca^{2+} removal. The RyR2 are not so sensitive to Ca^{2+} so their activation probability depends on their proximity to the LTCCs, which determines the local Ca^{2+} concentration (Stern, 1992).

During diastole, some Ca^{2+} leaks outside the SR through the RyR2s, which have very low open probability at low cytosolic $[Ca^{2+}]_i$, but are also sensitive to luminal Ca^{2+}, what is high during diastole. The opening of a RyR2 cluster can be viewed visualized with a confocal microscope and adequate fluorescence dyes, as rapid (∼10 ms), brief (∼30 ms), and local (∼1.5 μm) elevations in cytosolic Ca^{2+}, named Ca^{2+} sparks (Cheng and Lederer, 2008). Ca^{2+} sparks analyses provide insight into RyR2 function in *situ*, while the incorporation of RyR2 into lipid bilayers provides direct information on the channel function in a non-cellular context. During excitation-contraction coupling (ECC), Ca^{2+} release units (CRU) formed by a cluster of RyR2s are activated by the LTCCs located in the T tubules in front of them, which open during the AP. The spatial and temporal summation of these coordinated Ca^{2+} sparks results in the whole

$[Ca^{2+}]_i$ transient. The efficacy of the LTCCs to activate CRUs has been referenced as CICR gain, and it has been studied in HF combining patch-clamp to measure L-type Ca^{2+} current (I_{Ca}) and confocal microscopy to visualize changes in $\ll Ca^{2+i}$.

In HF, there are alterations in contraction and relaxation, which may be related to alterations in cardiomyocyte Ca^{2+} cycling. Alterations have been reported in several cardiomyocyte Ca^{2+} cycling elements, such as SERCA, ratio phosphlamban (PLN)/SERCA, and single LTCCs, during both experimental and human HF. In this review, we will focus on alterations in the RyR2 function on left ventricular HF, although alterations in Ca^{2+} handling have also been found in right ventricular failure (Hautefort et al., 2019).

GAIN OF CICR

The first study of Ca^{2+} sparks in HF showed fewer Ca^{2+} sparks for a given amount of Ca^{2+} entry through LTCCs (I_{Ca}). This decrease in CICR gain was observed in experimental HF, due to chronic hypertension (Gomez et al., 1997) and after myocardial infarction (Gomez et al., 2001), and was reminiscent of pioneer work by Beuckelmann in human ventricular myocytes from explanted failing hearts, where they found a decrease in the global $[Ca^{2+}]_i$ transient but normal I_{Ca} density (Beuckelmann et al., 1992). One explanation of this decrease in CICR gain was that there could be an ultrastructural disarrangement, which physically increased the distance between CRU and LTCC. In fact, while I_{Ca} density is generally maintained in HF, higher activity of at the single channel level has been reported (Schroder et al., 1998). This finding suggests fewer LTCC in the T-tubules participating in CICR or a decrease in the T-tubules density, as observed in HF (Wagner et al., 2012; Guo et al., 2013; Jones et al., 2018). But this "uncoupling" of the ECC was also suggested in larger mammals, in which the T-tubular network is less developed. Following myocardial infarction, cardiomyocytes from pigs with HF had relatively more uncoupled RyR2s, which could underlie the decreased gain of CICR (Dries et al., 2018).

Besides this decrease in CICR gain, alterations in the RyR2 itself have been reported in different models of HF.

RYR2 POST TRANSLATIONAL MODIFICATIONS

During HF progression, the sympathetic nervous system and renin-angiotensin-aldosterone system are activated to compensate for the reduced contractile function of the heart and thus maintain a sufficient blood flow (Lymperopoulos et al., 2013). In this early stage of cardiac remodeling, ECC is enhanced, with an increased $[Ca^{2+}]_i$ transient amplitude and contraction, together with a faster relaxation (Ohkusa et al., 1997). However, chronic activation of both systems has deleterious effects on cardiomyocytes and is responsible for the decompensation of cardiac function. This decrease in cardiac contraction is associated with an alteration of ECC (Gomez et al., 1997, 2001), the $[Ca^{2+}]_i$ transient amplitude is decreased and its duration is increased. Besides, or on top of the ultrastructural remodeling mentioned above, the reduction in $[Ca^{2+}]_i$ transient amplitude can be explained by a reduction of Ca^{2+} stored in the sarcoplasmic reticulum (Piacentino et al., 2003; Lehnart et al., 2009). While the first analyses explained this decrease in SR Ca^{2+} load by a lower SERCA expression and function and/or a higher expression of its natural inhibitor PLN, or a decrease in its phosphorylation (Kranias and Hajjar, 2012), some authors attributed it to RyR2 hyperactivity, which enhances diastolic SR Ca^{2+} leak. Indeed, an increase of the spontaneous Ca^{2+} leak through RyR2 has been observed in HF (Fischer et al., 2014; Ho et al., 2014; Grimm et al., 2015; Fu et al., 2016; Uchinoumi et al., 2016; Walweel et al., 2017; Dries et al., 2018). This SR Ca^{2+} leak, together with the reduced SERCA activity, contributes to a decrease in SR Ca^{2+} stores and an increase of the propensity of Ca^{2+} waves (Cheng et al., 1996; Venetucci et al., 2008; Curran et al., 2010; Dries et al., 2018). This contrasted with a significant decrease in the Ca^{2+} spark frequency reported in isolated cardiomyocytes from patients with terminal HF compared with non-failing individuals (Lindner et al., 2002). As spontaneous Ca^{2+} sparks depend on the amount of SR Ca^{2+} stored and [ATP], which are both reduced in cardiomyocytes from failing hearts, these can mask the increased activity of RyR2, whereas this higher RyR2 activity can still favor Ca^{2+} waves once the Ca^{2+} spark is produced, as the neighboring RyR2 will be more sensitive (Ruiz-Hurtado et al., 2015). Extrusion of Ca^{2+} constituting the Ca^{2+} waves during diastole *via* the NCX can generate delays after depolarization and trigger new action potentials that can propagate and induce arrhythmias (Pogwizd et al., 2001; Venetucci et al., 2008; Belevych et al., 2011). All these modifications of Ca^{2+} release have not been associated with alterations of RyR2 expression during HF (Hasenfuss and Pieske, 2002), but with post-translational modifications such as phosphorylation and oxidation (Houser, 2014). We should also keep in mind that while post-translational alterations in RyR2 tends to increase its activity, other alterations in Ca^{2+}-handling proteins (such as SERCA reduction) and metabolic changes (that may curse with lower ATP levels) tend to reduce its activity (Ruiz-Hurtado et al., 2015).

In 2000, it was shown that hyperphosphorylation of RyR2 by PKA is responsible for the leaky RyR2 in failing hearts in humans. The authors claimed that PKA-mediated phosphorylation dissociates the FK506 binding protein (FKBP12.6) from the RyR2 leading to an increase in the channel open probability (Marx et al., 2000). FKBP12.6 is known to stabilize the RyR2 in a closed state and avoid aberrant Ca^{2+} leak (Brillantes et al., 1994; Gellen et al., 2008), but its removal may not affect RyR2 open probability (Xiao et al., 2007). In the early 90s, serine 2808 (S2808) was identified as the unique phosphorylation site of RyR2 (Witcher et al., 1991) and appeared to be a prominent target for PKA. In following publications, Marks' group highlighted the role of S2808 phosphorylation in the destabilization of the complex RyR2-FKBP12.6. They developed RyR2-S2808A knock-in mice, which prevent phosphorylation at this site. They showed that these mice are protected against RyR2-FKBP12.6 dissociation and leaky RyR2 in response to catecholamine stimulation (Shan et al., 2010a,b). Moreover, RyR2-S2808A knock-in mice seem to have a better cardiac function after myocardial infarction, which has been related again to the stabilization of the RyR2-FKBP12.6 complex in the absence of PKA phosphorylation (Wehrens et al.,

2006). They also confirmed this major role of S2808 using RyR2-S2808D knock-in mice, which mimicked hyperphosphorylation at that site and had a reduced association of FKBP12.6 to RyR2 (Shan et al., 2010a,b). However, other groups have not been able to confirm this major role of S2808 phosphorylation in the progression of HF (Jiang et al., 2002). Valdivia and Houser's groups also developed RyR2-S2808A knock-in mice. In these mice, response to β-adrenergic stimulation on $[Ca^{2+}]_i$ transient and ECC gain (MacDonnell et al., 2008) and progression of HF after myocardial infarction (Zhang et al., 2012) or aortic banding (Benkusky et al., 2007) were not affected no matter the genetic background of the mice (Alvarado et al., 2017). Moreover, it has also been shown that FKBP12.6 binding to RyR2 is not modified by acute β-adrenergic stimulation on wild-type mice or FKBP12.6 overexpressing mice in the heart (Gellen et al., 2008). Recently, evidences that S2808 is not the only target for RyR2 phosphorylation by PKA have been put forward; S2030 seems to be a potent target of PKA (Potenza et al., 2019) and can be involved in the progression of HF (Xiao et al., 2006; Benkusky et al., 2007). Taken together, these studies are in contradiction with Marks' group publications, and the controversy continues through the years (Bers, 2012; Alvarado and Valdivia, 2020; Dridi et al., 2020a,b). However, independently on RyR2 phosphorylation status, FKBP12.6 has been more consistently found decreased in HF (Ono et al., 2000; Gomez et al., 2009), which can by itself promote diastolic Ca^{2+} leak.

The Ca^{2+}/calmodulin-dependent protein kinase II (CaMKII) phosphorylation of S2814 (2815) has also been highlighted for its role in the increase in SR Ca^{2+} leak through RyR2 in HF. CaMKII is activated by catecholamine and by oxidation, which is high during HF (Erickson et al., 2008). It has been shown that in failing rabbit hearts, CaMKII phosphorylation of RyR2 decreases SR load and increases Ca^{2+} leak by increasing RyR2 open probability (Ai et al., 2005). In these rabbits, inhibition of CaMKII, but not of PKA, reduced SR Ca^{2+} leak (Ai et al., 2005). In human heart failure due to ischemic or dilated cardiomyopathy, CaMKII expression has been shown to increase, contributing to augmented SR Ca^{2+} leak (Fischer et al., 2014). Rats subjected to myocardial infarction treated with exendin-4, which reduced CaMKII activity, showed a decreased SR Ca^{2+} leak (Chen et al., 2020). This major effect of CaMKII in the development of HF has been confirmed in mice lacking CaMKII. After transverse aortic constriction, these mice were protected against HF progression together with a reduced SR Ca^{2+} leak and RyR2 phosphorylation at S2815 (Ling et al., 2009). Similarly to CaMKII Knock out mice, RyR2-S2814A knock-in mice were protected against abnormal SR Ca^{2+} leak and HF after transverse aortic constriction (TAC) (van Oort et al., 2010) but surprisingly not after myocardial infarction (MI) (Respress et al., 2012). To explain how CaMKII increases SR Ca^{2+} leak, Uchinoumi et al. hypothesize that phosphorylation of S2814 reduces CaM affinity for the RyR2, leading to a RyR2 conformational change and leakiness of the channel (Uchinoumi et al., 2016). Supporting this hypothesis, Dantrolene, which restores RyR2 CaM affinity, suppressed SR Ca^{2+} leak in RyR2 S2814D knock-in mice (Uchinoumi et al., 2016).

Among the 90 cysteines present in each of the four subunits of RyR2, 21 are in a free thiol state and accessible for redox modifications during oxidative stress (Xu et al., 1998). Oxidative stress is associated with the development of several pathologies, and excessive production of reactive oxygen species has deleterious effects on protein function and cell viability. To counter these deleterious effects, cells have their own specific antioxidants machinery, including superoxide dismutase, catalase, and glutathione peroxidase, and non-specific antioxidants reduced glutathione, which is ubiquitous and the most important antioxidant system in cardiac cells (Nikolaienko et al., 2018).

During HF ROS production is chronically increased due to the uncoupling of the mitochondrial electron transport chain, the increase in energy demand, the switch from fatty acids to glucose as an energy substrate in cardiomyocytes (Mak and Newton, 2001; Ventura-Clapier et al., 2004), upregulation of nitric oxide synthase (NOS), xanthine oxidase and NADPH oxidase (NOX), and decreased reduced glutathione (Zima and Mazurek, 2016; Nikolaienko et al., 2018). ROS are also known to activate SR Ca^{2+} leak (Terentyev et al., 2008) by increasing spontaneous Ca^{2+} sparks frequency (Yan et al., 2008; Prosser et al., 2011) and Ca^{2+} waves (Bovo et al., 2012). Indeed, part of the beneficial effect of carvedilol on HF has been attributed to its antioxidant action on RyR2 (Mochizuki et al., 2007). ROS oxidation of RyR2 during HF induces the dissociation of FKBP12.6 leading to the aberrant Ca^{2+} release (Shan et al., 2010a), although other groups showed that RyR2 oxidation induces CaM dissociation without changing FKBP12.6 binding (Ono et al., 2010; Oda et al., 2015). Increased NOX activity induced by tachycardia led to an increase in RyR2 *S*-glutathionylation associated with an increased SR Ca^{2+} leak (Sanchez et al., 2005), which has been suggested to be cardio protective during preconditioning with exercise. However, the role of NOX during HF is not well-documented. The increased activity of NOX during end-stage HF (Heymes et al., 2003) can participate in the increase in diastolic SR Ca^{2+} leak and SR Ca^{2+} depletion. Even if hypernitrosylation of RyR2 is supposed to increase Ca^{2+} leak, decreased *S*-nitrosylation has been associated with increased SR Ca^{2+} leak during HF (Gonzalez et al., 2007; 2010). In fact, it has been proposed that hyponitrosylation during HF favors the oxidation of RyR2 by ROS, leading to this aberrant Ca^{2+} release. In these studies, inhibition of xanthine oxidase decreased ROS production restoring *S*-nitrosylation and cardiac function (Gonzalez et al., 2010). Evidence of the cardio protective effect of RyR2 *S*-nitrosylation has been also highlighted in a mouse model where NOS1 overexpression prevents cardiac dysfunction and delays HF in response to pressure overload (Loyer et al., 2008). On a canine model of HF, it has been suggested that the disulfide oxidation is the predominant form of redox-sensitive modulation of RyR2 compared to *S*-nitrosylation and *S*-glutathionylation to influence the RyR2-mediated leak. On a rabbit model of HF, increased SR Ca^{2+} leak (Mazurek et al., 2014) and Ca^{2+} waves (Bovo et al., 2015) could be attributed to an increase in RyR2 intersubunit disulfide cross-linking (Mazurek et al., 2014; Bovo et al., 2015, 2018).

By accessing data from different laboratories, we can gather that the RyR2 itself may be more active in HF due to several

post-translational modifications such as oxidation, enhanced phosphorylation at the CaMKII site, as well as a depressed FKBP12.6 expression/binding to RyR2.

Figure 1 summarizes the key elements in Ca^{2+} handling in ventricular cardiomyocytes, as well as a representation of some of the reported findings in those elements, in different models of HF, which contribute to depressed contraction and pro-arrhythmogenic DADs production. The failing cell has a disruption in the T-tubular network, and a decreased SERCA expression (or augmented ratio PLN/SERCA), which together with more active RyR2 due to post-translational modifications, resulting in a drop of Ca^{2+} stored in the SR. As a result, and despite normal I_{Ca} density and prolonged AP, the triggered $[Ca^{2+}]_i$ transient is of lower amplitude, contributing to diminished cell contraction. During diastole, the higher RyR2 activity favors the probability of producing Ca^{2+} waves, generating an inward current through the NCX, when extruding Ca^{2+}, which produces DADs. When DADs reach the threshold, a triggered AP is generated, which may initiate arrhythmias.

HF WITH PRESERVED EJECTION FRACTION (HFPEF)

HF with preserved ejection fraction (HFpEF) has been identified as a subtype of HF in addition to HFrEF. HFpEF is more frequently found in older patients with comorbidities such as hypertension, obesity, diabetes, chronic kidney diseases (Redfield et al., 2003; Bhatia et al., 2006; Owan et al., 2006). HFpEF patients present normal left ventricular systolic function with impaired left ventricular relaxation and filling. Although HFpEF represents approximately 50% of HF patients (Dunlay et al., 2017), little is known about their specific mechanisms, in comparison to HFrEF, notably regarding RyR2 and Ca^{2+} release. A lack of knowledge is probably related to the difficulty in generating accurate experimental models or the diversity of associated comorbidities. As described previously, in HFrEF, cardiac systolic and diastolic changes are linked to Ca^{2+} mishandling. In HFpEF, Ca^{2+} alterations are not as clearly defined and seem to differ depending on the associated comorbidity. In a rat model in HFpEF with chronic pressure overload, a significant increase in diastolic SR Ca^{2+} release through RyR2s leading, as in HFrEF, to higher diastolic $[Ca^{2+}]$ and irregular $[Ca^{2+}]_i$ transients during pacing has been observed (Rouhana et al., 2019). This SR Ca^{2+} leak has been associated with an increase in PLN/SERCA ratio responsible for a delayed $[Ca^{2+}]_i$ transient decay and diastolic dysfunction, also seen in HFpEF with chronic kidney disease (Primessnig et al., 2016) and in human HF with EF > 45% (Hohendanner et al., 2013; Ljubojevic et al., 2014). Unlike HFrEF, a SR Ca^{2+} leak in HFpEF depends on PKA-dependent phosphorylation of RyR2 at S2808 (Durland, 2021) rather than CaMKII-dependent phosphorylation, alteration of FKBP12.6/RyR2 ratio, or RyR2s *S*-nitrosylation (Adeniran et al., 2015; Frisk et al., 2021). However, phosphorylation of RyR2 at S2808 was not significantly changed in Dahl salt-sensitive rats, with HFpEF, presenting both hypertension and insulin-resistance (Kilfoil et al., 2020). This discrepancy could be explained by insulin-resistance comorbidity not present in Durland's model (Durland, 2021). Although in HFrEF an increase in SR Ca^{2+} leak leads to SR Ca^{2+} depletion and lower $[Ca^{2+}]_i$ transient, in HFpEF, diastolic SR Ca^{2+} release does not induce SR Ca^{2+} load depletion or defective ECC. In fact, in HFpEF models, systolic Ca^{2+} release by the RyR2 is increased, probably as a compensatory mechanism to overcome the increased left ventricular stiffness associated with HFpEF (Selby et al., 2011; Adeniran et al., 2015; Durland, 2021). This enhanced SR Ca^{2+} release could be attributed to a more effective RyR2s recruitment by Ca^{2+} during the Ca^{2+} influx through the LTCC (Kilfoil et al., 2020) as well as an absence of T-tubules alteration (Durland, 2021). Indeed, in a Dahl-sensitive rat model of HFpEF (Kilfoil et al., 2020), a higher couplon recruitment improved ECC by increasing Ca^{2+} release synchronicity and lowering Ca^{2+} release latency. This should allow the heart to maintain an effective contraction besides higher ventricular wall stiffness. Moreover, T-tubule disorganization might also affect Ca^{2+} release effectiveness. However, the integrity of T-tubule structure in HFpEF depends on the comorbidities. Indeed, while T-tubule density is unchanged in Dahl salt-sensitive rats, in obese and diabetic Zucker rats or diabetic HFpEF patients, their density is increased in the ischemic model (post-MI with preserved EF but reduced E/A) (Frisk et al., 2021). This etiology-dependence is also found in proteins regulating SR Ca^{2+} release such as SERCA and NCX. In diabetic HFpEF, NCX expression and activity of SERCA decrease, which is not the case in ischemic or hypertensive disease models (Frisk et al., 2021). In type 1 diabetes, with subclinical diastolic dysfunction and normal systolic function, diastolic SR Ca^{2+} release and amplitude (measured as Ca^{2+} sparks frequency) decrease and is associated with a drop of SR Ca^{2+} load and $[Ca^{2+}]_i$ transient without affecting systolic function (Lagadic-Gossmann et al., 1996; Lacombe et al., 2007; Hamouda et al., 2015). In these diabetic models, SR Ca^{2+} uptake by the SERCA pump appears as the main responsible for the decrease in SR Ca^{2+} release with, in some models, an alteration of the SERCA2/PLN ratio (Miranda-Silva et al., 2020). It is deduced from the literature that the alterations in the RyR2s and Ca^{2+} release diverge between HFpEF depending on their diabetic or non-diabetic etiology, with a clear implication of SERCA alteration in the Ca^{2+} homeostasis underlying the diastolic function in diabetes.

Interestingly, in myocardial strips from patients with hypertrophy associated with hypertension and coronary artery disease, but normal ejection fraction (LVEF $\geq$ 50%), diastolic dysfunction is associated with an increase in SR Ca^{2+} load at high pacing rates (Selby et al., 2011). However, the impact of cellular changes in Ca^{2+} handling does not always transduce into *in vivo* alterations. Indeed, in isolated myocardial strips from animal models of hypertrophy induced by aortic banding, even though cellular Ca^{2+} extrusion was increased due to higher NCX and SERCA activities, *in vivo* relaxation remained slower (Roe et al., 2017). Similarly, exacerbated cellular Ca^{2+} handling has been described in a rat strain with cardiac hypertrophy despite the lack of hypertension, where the increased Ca^{2+} influx through the LTCCs seems to underlie the increased $[Ca^{2+}]_i$ transient amplitude and myocyte shortening. In this model, an increase in RyR2 phosphorylation by CaMKII leads to higher susceptibly to

in vivo arrhythmia and spontaneous SR Ca^{2+} release although RyR2 expression was decreased (Curl et al., 2018).

ALTERATION OF RYR2 IN HF SUPRAVENTRICULAR FUNCTION

RyR2 and Sinus Node Dysfunction

In addition to its role in governing cardiac contraction, the RyR2-mediated Ca^{2+} release of the pacemaker cardiomyocytes of the heart, located at the sinus node (SAN), contributes to heart automaticity. This observation was initiated in the late 80s by the finding that ryanodine slows down the final phase of diastolic depolarization, resulting in a significant increase in cellular pacemaker cycle length in cats (Rubenstein and Lipsius, 1989). Since then, and after intense debates, it is now of general agreement that spontaneous cyclical local Ca^{2+} releases named late Ca^{2+} release (LCR), are responsible for a net depolarizing current mediated by the NCX. This process drives pacemaker depolarization, which is referred to as the "Ca^{2+} clock," jointly with the "membrane or voltage clock" mediated by cyclic activation and deactivation of voltage-sensitive membrane ion channels [see for review (Carmeliet, 2019; Kohajda et al., 2020)]. This has been especially emphasized by the fact that RyR2 mutations associated with catecholaminergic polymorphic ventricular tachycardia (CPVT) induced SAN dysfunction (Neco et al., 2012; Wang et al., 2017).

Heart rate (HR) is an independent risk factor of all-cause mortality, cardiovascular mortality, and hospitalization for HF (Fox et al., 2007; Verrier and Tan, 2009). It has been long recognized that HF is associated with dysfunction of the SAN. Whereas, HR is commonly increased due to an excess of sympathetic activity and parasympathetic withdrawal, the intrinsic sinus rhythm in absence of autonomic nerve activity is depressed in HF. In the late 40s, a slower HR in isolated failing hearts was shown (Wollenberger, 1947; Wiggers, 1949). In animal models, and more importantly in humans with HF, the intrinsic HR is decreased with a reduction in SAN reserve and abnormal propagation of APs from the SAN, together with a caudal shift of the leading pacemaker site and fibrosis (Jose and Taylor, 1969; Jose and Collison, 1970; Vatner et al., 1974; Opthof et al., 2000; Verkerk et al., 2003; Sanders et al., 2004; Zicha et al., 2005; Packer et al., 2009; Swaminathan et al., 2011; Yanni et al., 2011). It has been suggested that this anatomic, structural, and functional SAN remodeling in HF might be an adaptive, protective response to improve cardiac oxygen supply to demand ratio (Mulder and Thuillez, 2006) and to prevent triggered arrhythmias enhanced by rapid HR (Opthof et al., 2000). However, reduced SAN automaticity, which favors the induction of early after-depolarization-triggered arrhythmias (Nuss et al., 1999), might translate into bradyarrhythmias or tachycardia-bradycardia syndrome (Mangrum and DiMarco, 2000). Indeed, bradyarrhythmias account for up to half of the deaths in HF (Luu et al., 1989; Stevenson et al., 1993; Uretsky and Sheahan, 1997; Faggiano et al., 2001; Packer et al., 2009; Bloch Thomsen et al., 2010; Gang et al., 2010; Glukhov et al., 2013; Lou et al., 2014). Moreover, in association with autonomic dysfunction (Colucci et al., 1989; Bristow et al., 1990; Samejima et al., 2003; Messias et al., 2016), slowing of the intrinsic HR by SAN remodeling might limit HR modulation to exercise (Sanders et al., 2004), the chronotropic incompetence observed during the HF process (Weber et al., 1982; Higginbotham et al., 1983; Brubaker et al., 2006; Brubaker and Kitzman, 2011; Benes et al., 2013).

To date, analysis of the Ca^{2+} clock in SAN dysfunction in HF has received little attention. In a canine model of HF induced by rapid pacing and using optical mapping, SAN bradycardia is associated with suppression of LCR together with the unresponsiveness of Ca^{2+} clock to isoproterenol and caffeine stimulation (Shinohara et al., 2010). In a similar rabbit HF model, alterations of SAN electro-pharmacological responses have been related to lower expression of RyR2, as well as inhibition of SERCA reuptake due to altered phosphorylation of PLN (Chang et al., 2017). By contrast, RyR2 expression, along with other Ca^{2+} handling proteins, is increased in the SAN but not in atrial tissue in a HF rat model (Yanni et al., 2011). The authors suggested that conjoint upregulation of RyR3 and calsequestrin 2 might however inhibit Ca^{2+} release resulting in slow automaticity. More recently, the same group (Yanni et al., 2020) reported that pressure overload-induced HF in mice did not change SAN mRNA for various components of the "Ca^{2+} clock," including RyR2, SERCA, calsequestrin, and NCX. This is consistent with a study in isolated SAN cells from rabbit HF model of pressure and volume overload, which concluded that SAN Ca^{2+} cycling properties are conserved despite bradycardic effects (Verkerk et al., 2015). However, the latest study did not take into account the presence of hierarchical pacemaker clustering within the SAN that might be modified in HF (Sanders et al., 2004; Lang and Glukhov, 2021). Preliminary data from our group, using TAC-induced HF in the mouse indicate impairment of "Ca^{2+} clock," characterized by slower spontaneous $[Ca^{2+}]_i$ transients, as well as less frequent and smaller Ca^{2+} sparks, supported by a mechanism including depression in the CaMKII signaling pathway (Xue et al., 2020). Taking into account that only a few (and somewhat controversial) studies have evaluated SAN Ca^{2+} clock function in HF to date, further studies are still clearly needed.

RyR2 and Atrial Fibrillation

Atrial fibrillation (AF) is a frequent complication of HF, and there is a reciprocal relationship between them. HF favors the development of AF (see below), and AF, because of its hemodynamic deleterious consequences, aggravates and may even generate HF. AF is defined as a rapid and disorganized electrical and mechanical activity of the atria, resulting in the loss of the synchronous contraction of atrial myocytes and myocardium normally occurring at end-diastole. The rapid anarchic electrical activity of the atria (around 300/min) is transmitted to the ventricle through the atrio-ventricular (AV) node, which plays the role of a filter, resulting in an irregular and nevertheless often rapid ventricular contraction rate. This has two deleterious consequences: first, the rapid irregular ventricular rate, together with the loss of atrial contraction, is responsible for a deterioration of ventricular filling, itself resulting in decreased cardiac output; second, the loss of atrial

contraction favors blood stasis in the atria and especially the auricles, with the risk of thrombus formation and its migration into a peripheral artery.

As with all cardiac arrhythmias, AF necessitates the coexistence of a substrate (functional or anatomic reentry circuits, and tissue remodeling) and a trigger (increased automaticity or triggered activities), both modulated by alterations of the autonomous nervous system tone (increase in the sympathetic tone in the case of HF) or other humoral alterations such as hypokalemia, hypoxia, or acidosis (Coumel, 1993, 1996). It is important to note that HF can not only participate in but even create these three conditions.

Even if, sometimes, it may appear somewhat artificial, one may distinguish two radically different forms of AF, at least for the sake of clarity. The pathophysiology of HF-induced AF is somewhat different and much less documented than that of the "loan AF" occurring in a presumed normal heart. In the latter, AF originates from the wall of the pulmonary veins (Haissaguerre et al., 1989), starts as rare episodes of short duration (paroxysmal AF) that become more and more frequent and of longer duration with time to then finally become persistent, i.e., unable to end spontaneously to return to sinus rhythm. In this pathophysiological scheme, the recurrence of AF episodes is responsible, with time, for a progressive cellular electrical, Ca^{2+} signaling, and tissue remodeling that favors new AF episodes and prevents the return to sinus rhythm: AF begets AF. A detailed description of this remodeling can be found in excellent recent reviews (Landstrom et al., 2017; Denham et al., 2018).

In HF-induced AF, the pathophysiological process starts from the increased ventricular filling pressure that creates a chronic mechanical overload of the atria, associated with various degrees of neurohumoral activation leading to the atrial remodeling creating a favorable ground (both the substrate and the trigger) for the occurrence of AF. Interestingly, HF generally develops an atrial pro-arrhythmic substrate before AF arises, that may therefore immediately present as persistent (Sisti et al., 2014).

Alterations in Ca^{2+} signaling are instrumental to the two pathophysiological mechanisms, showing several similarities, but also subtle differences. They are involved both in the triggering of AF and in the progression of the atrial substrate that facilitates AF. These alterations are impacted by the atrial nature of cardiomyocytes. Indeed, atrial myocytes have a much less developed T-tubular network than ventricular myocytes with less junctional SR, and RyR2 clusters disconnected from T-tubules (orphan clusters). This favors a more progressive rise and delayed peak of the $[Ca^{2+}]_i$ transient as compared to ventricular myocytes (Hatem et al., 1997; Caldwell et al., 2014). This also offers a greater opportunity for the development and propagation of Ca^{2+} waves. Thanks to significant technological advances in cell imaging, ECC of mice and human atrial myocytes has been recently clarified. Besides sparse T-tubule invaginations, which is associated with slow Ca^{2+} propagation, a voluminous axial tubular system develops extensive junctions with the SR comprising highly phosphorylated RyR2 clusters responsible, in mouse atrial myocytes, for a Ca^{2+} release approximately two times faster at the center of the cell than at its border, in agreement with the fast contractile activation of atrial myocytes (Brandenburg et al., 2016).

In contrast to the significant number of works exploring the role of Ca^{2+} mishandling in paroxysmal/persistent AF (Landstrom et al., 2017; Denham et al., 2018), far less has been published regarding the effects of HF on atrial Ca^{2+} handling. Studies have been carried out on various types of human atrial samples and two types of experimental models have been developed. The first uses long-lasting rapid ventricular pacing that finally results in increased atrial pressures and atrial dilation associated with various patterns of ventricular remodeling (Yeh et al., 2008; Dibb et al., 2009). More consistent with the actual HF pathophysiology, the second (e.g., MI in rat or rabbit, TAC in the mouse), aims to obtain left ventricular failure with only secondary impact on the left atrium (Boixel et al., 2001; Kettlewell et al., 2013; Brandenburg et al., 2016).

I_{Ca} is generally found to be decreased in atrial myocytes of HF models as well as in dilated atria or other pathological conditions associated with increased susceptibility to AF (Dinanian et al., 2008). In the rat MI model, the decrease in I_{Ca} density was related to a decrease in basal cAMP-dependent regulation of the current (Boixel et al., 2001). I_{Ca} density and the resulting $[Ca^{2+}]_i$ transient amplitude are also decreased under β-adrenergic stimulation in atrial myocytes isolated from rabbits with MI and increased susceptibility to AF (Kettlewell et al., 2013). In the tachypacing HF model in dogs, $[Ca^{2+}]_i$ transient amplitude and SR Ca^{2+} load were increased, associated with an increased diastolic Ca^{2+} concentration (Yeh et al., 2008). This was associated with decreased RyR2 and calsequestrin protein expression and increased CaMKII-dependent PLN phosphorylation whereas RyR2 phosphorylation was unchanged. In the mouse TAC model, left atrial hypertrophy is associated with marked proliferation of axial tubules and an increase in phosphorylated RyR2 at S2808, but not S2814, thereby accelerating SR Ca^{2+} release through non-junctional RyR2 cluster sites, despite decreases in RyR2 cluster density and RyR2 protein expression (Brandenburg et al., 2016). In a rabbit model of combined pressure and volume overload, diastolic Ca^{2+} concentration was also increased with $[Ca^{2+}]_i$ transient of larger amplitude due to enhanced IP3 receptor-induced Ca^{2+} release originating from central non-junctional SR, associated with increased frequency of spontaneous Ca^{2+} waves, increased activity of NCX, and Ca^{2+} wave-triggered action potentials (Hohendanner et al., 2015). Interestingly, reduced RyR2 expression associated with increased sensitivity to ryanodine occurs in the atrioventricular node and participate in the slowing of AV conduction observed with aging (Saeed et al., 2018). This process, probably enhanced in failing hearts, would increase the role of the filter assigned to the AV node and therefore protect the failing ventricles from the deleterious consequences of high beating rates.

As seen in paroxysmal/persistent AF, HF-induced AF is also associated with increased diastolic Ca^{2+} leak despite no change or even decreased RyR2 expression. However, in contrast to the former, in which RyR2 phosphorylation is increased at both the PKA and CaMKII sites, at the stage of persistent AF, RyR2 phosphorylation does not appear to change in HF-induced AF.

Therefore, the increased leak is more likely due to the increase in SR Ca^{2+} content, generally observed in models of HF in big mammals (Yeh et al., 2008; Clarke et al., 2015; Aistrup et al., 2017). The increased diastolic Ca^{2+} leak is often associated with increased NCX activity that favors the occurrence of DADs.

Recently, a striated muscle preferentially expressed protein kinase (SPEG) has been shown to play a role in the pathophysiology of paroxysmal/persistent AF (Campbell et al., 2020). Unlike PKA and CaMKII that increase RyR2 activity, SPEG phosphorylation at S2367 reduces RyR2-mediated SR Ca^{2+} release. SPEG protein levels, and RyR2 S2367 phosphorylation are decreased in atrial biopsies from patients with paroxysmal AF and transgenic RyR2-S2367A mice, in which the site cannot be phosphorylated, exhibited an increased susceptibility to pacing-induced AF. Whether such a pathophysiological mechanism exists in HF-induced AF remains to be established.

At last, it should be noted that HF also affects the pulmonary veins by increasing their electrical activity, thereby favoring the incidence of the trigger of paroxysmal/persistent AF in HF-induced AF (Lin et al., 2016).

In summary, the pathophysiology of HF-induced AF is complex and shares many features with paroxysmal/persistent AF, at least regarding alterations in Ca^{2+} signaling. More than in other fields of experimental cardiology, we often observed conflicting results due to differences in the species, experimental models, and disease stage studied. HF-induced AF pathophysiology may differ in humans according to the HF type considered. Indeed, HFpEF, in addition to the hemodynamic overload of the left atrium, may comprise specific pathophysiological mechanisms operating from the disease onset such as those of diabetes, inflammation, oxidation, etc., which may play a direct role simultaneously on the ventricles and atria through a "common atrial and ventricular myopathy" (Packer et al., 2020). Unequivocal information on the pathophysiology of HF-induced AF will be obtained from well-characterized standardized experimental models targeting left ventricular failure with secondary progressive atrial remodeling studied at the various stages of the pathological process.

CONCLUSION

In summary, alterations in RyR2 posttranslational modifications, location due to T-tubule remodeling, expression, and binding to accessory proteins have been all found in HF with variable conclusions depending on the experimental models or human etiology. What is clear is that RyR2 alteration contributes to the pathology of HF by participating in the depressed $[Ca^{2+}]_i$ transient, which is important for depression of cell contraction and in favoring arrhythmogenic Ca^{2+} waves during diastole.

AUTHOR CONTRIBUTIONS

All authors contributed to the conception of the manuscript, wrote, edited the manuscript, contributed to the article, and approved the submitted version.

FUNDING

This work was funded by Inserm, University Paris-Saclay, and grants from ANR (ANR-15-CE14–0005 and ANR-19-CE14-0031-01) and NIH (2R01HL055438-22).

REFERENCES

Adeniran, I., MacIver, D. H., Hancox, J. C., and Zhang, H. (2015). Abnormal calcium homeostasis in heart failure with preserved ejection fraction is related to both reduced contractile function and incomplete relaxation: an electromechanically detailed biophysical modeling study. *Front. Physiol.*6:78. doi: 10.3389/fphys.2015.00078

Ai, X., Curran, J. W., Shannon, T. R., Bers, D. M., and Pogwizd, S. M. (2005). Ca^{2+}/calmodulin-dependent protein kinase modulates cardiac ryanodine receptor phosphorylation and sarcoplasmic reticulum Ca^{2+} leak in heart failure. *Circ. Res.* 97, 1314–1322. doi: 10.1161/01.RES.0000194329.41863.89

Aistrup, G. L., Arora, R., Grubb, S., Yoo, S., Toren, B., Kumar, M., et al. (2017). Triggered intracellular calcium waves in dog and human left atrial myocytes from normal and failing hearts. *Cardiovasc. Res.* 113, 1688-1699. doi: 10.1093/cvr/cvx167

Alvarado, F. J., Chen, X., and Valdivia, H. H. (2017). Ablation of the cardiac ryanodine receptor phospho-site Ser2808 does not alter the adrenergic response or the progression to heart failure in mice. Elimination of the genetic background as critical variable. *J. Mol. Cell Cardiol.* 103, 40-47. doi: 10.1016/j.yjmcc.2017.01.001

Alvarado, F. J., and Valdivia, H. H. (2020). Mechanisms of ryanodine receptor 2 dysfunction in heart failure. *Nat. Rev. Cardiol.* 17:748. doi: 10.1038/s41569-020-00443-x

Belevych, A. E., Terentyev, D., Terentyeva, R., Nishijima, Y., Sridhar, A., Hamlin, R. L., et al. (2011). The relationship between arrhythmogenesis and impaired contractility in heart failure: role of altered ryanodine receptor function. *Cardiovasc. Res.* 90, 493-502. doi: 10.1093/cvr/cvr025

Benes, J., Kotrc, M., Borlaug, B. A., Lefflerova, K., Jarolim, P., Bendlova, B., et al. (2013). Resting heart rate and heart rate reserve in advanced heart failure have distinct pathophysiologic correlates and prognostic impact: a prospective pilot study. *JACC Heart Fail.* 1, 259-266. doi: 10.1016/j.jchf.2013.03.008

Benkusky, N. A., Weber, C. S., Scherman, J. A., Farrell, E. F., Hacker, T. A., John, M. C., et al. (2007). Intact beta-adrenergic response and unmodified progression toward heart failure in mice with genetic ablation of a major protein kinase A phosphorylation site in the cardiac ryanodine receptor. *Circ. Res.* 101, 819-829. doi: 10.1161/CIRCRESAHA.107.153007

Bers, D. M. (2012). Ryanodine receptor S2808 phosphorylation in heart failure: smoking gun or red herring. *Circ. Res.* 110, 796-799. doi: 10.1161/CIRCRESAHA.112.265579

Beuckelmann, D. J., Nabauer, M., and Erdmann, E. (1992). Intracellular calcium handling in isolated ventricular myocytes from patients with terminal heart failure. *Circulation.* 85, 1046-1055. doi: 10.1161/01.CIR.85.3.1046

Bhatia, R. S., Tu, J. V., Lee, D. S., Austin, P. C., Fang, J., Haouzi, A., et al. (2006). Outcome of heart failure with preserved ejection fraction in a population-based study. *N Engl. J. Med.* 355, 260-269. doi: 10.1056/NEJMoa051530

Bloch Thomsen, P. E., Jons, C., Raatikainen, M. J., Moerch Joergensen, R., Hartikainen, J., Virtanen, V., et al. (2010). Long-term recording of cardiac arrhythmias with an implantable cardiac monitor in patients with reduced ejection fraction after acute myocardial infarction: the cardiac Arrhythmias and risk stratification after acute myocardial infarction (CARISMA) study. *Circulation.* 122, 1258-1264. doi: 10.1161/CIRCULATIONAHA.109.902148

Boixel, C., Gonzalez, W., Louedec, L., and Hatem, S. N. (2001). Mechanisms of L-type Ca(2+) current downregulation in rat atrial myocytes during heart failure. *Circ. Res.* 89, 607-613. doi: 10.1161/hh1901.096702

Bovo, E., Lipsius, S. L., and Zima, A. V. (2012). Reactive oxygen species contribute to the development of arrhythmogenic Ca(2)(+) waves during beta-adrenergic receptor stimulation in rabbit cardiomyocytes. *J. Physiol.* 590, 3291-3304. doi: 10.1113/jphysiol.2012.230748

Bovo, E., Mazurek, S. R., Fill, M., and Zima, A. V. (2015). Cytosolic Ca(2)(+) buffering determines the intra-SR Ca(2)(+) concentration at which cardiac Ca(2)(+) sparks terminate. *Cell Calcium.* 58, 246-253. doi: 10.1016/j.ceca.2015.06.002

Bovo, E., Mazurek, S. R., and Zima, A. V. (2018). The role of RyR2 oxidation in the blunted frequency-dependent facilitation of Ca(2+) transient amplitude in rabbit failing myocytes. *Pflugers Arch.* 470, 959-968. doi: 10.1007/s00424-018-2122-3

Brandenburg, S., Kohl, T., Williams, G. S., Gusev, K., Wagner, E., Rog-Zielinska, E. A., et al. (2016). Axial tubule junctions control rapid calcium signaling in atria. *J. Clin. Invest.* 126, 3999-4015. doi: 10.1172/JCI88241

Brillantes, A. B., Ondrias, K., Scott, A., Kobrinsky, E., Ondriasova, E., Moschella, M. C., et al. (1994). Stabilization of calcium release channel (ryanodine receptor) function by FK506-binding protein. *Cell* 77, 513–523. doi: 10.1016/0092-8674(94)90214-3

Bristow, M. R., Hershberger, R. E., Port, J. D., Gilbert, E. M., Sandoval, A., Rasmussen, R., et al. (1990). Beta-adrenergic pathways in non-failing and failing human ventricular myocardium. *Circulation* 82, 12–25.

Brubaker, P. H., Joo, K. C., Stewart, K. P., Fray, B., Moore, B., and Kitzman, D. W. (2006). Chronotropic incompetence and its contribution to exercise intolerance in older heart failure patients. *J. Cardiopulm. Rehabil.* 26, 86-89. doi: 10.1097/00008483-200603000-00007

Brubaker, P. H., and Kitzman, D. W. (2011). Chronotropic incompetence: causes, consequences, and management. *Circulation* 123, 1010-1020. doi: 10.1161/CIRCULATIONAHA.110.940577

Caldwell, J. L., Smith, C. E., Taylor, R. F., Kitmitto, A., Eisner, D. A., Dibb, K. M., et al. (2014). Dependence of cardiac transverse tubules on the BAR domain protein amphiphysin II (BIN-1). *Circ. Res.* 115, 986-996. doi: 10.1161/CIRCRESAHA.116.303448

Campbell, H. M., Quick, A. P., Abu-Taha, I., Chiang, D. Y., Kramm, C. F., Word, T. A., et al. (2020). Loss of SPEG inhibitory phosphorylation of ryanodine receptor type-2 promotes atrial fibrillation. *Circulation* 142, 1159-1172. doi: 10.1161/CIRCULATIONAHA.120.045791

Carmeliet, E. (2019). Pacemaking in cardiac tissue. From IK2 to a coupled-clock system. *Physiol. Rep.* 7:e13862. doi: 10.14814/phy2.13862

Chang, S. L., Chuang, H. L., Chen, Y. C., Kao, Y. H., Lin, Y. K., Yeh, Y. H., et al. (2017). Heart failure modulates electropharmacological characteristics of sinoatrial nodes. *Exp. Ther. Med.* 13, 771-779. doi: 10.3892/etm.2016.4015

Chen, J., Xu, S., Zhou, W., Wu, L., Wang, L., and Li, W. (2020). Exendin-4 reduces ventricular arrhythmia activity and calcium sparks-mediated sarcoplasmic reticulum Ca leak in rats with heart failure. *Int. Heart J.* 61, 145-152. doi: 10.1536/ihj.19-327

Cheng, H., Lederer, M. R., Lederer, W. J., and Cannell, M. B. (1996). Calcium sparks and $[Ca^{2+}]$i waves in cardiac myocytes. *Am. J. Physiol.* 270, 148–159. doi: 10.1152/ajpcell.1996.270.1.C148

Cheng, H., and Lederer, W. J. (2008). Calcium sparks. *Physiol. Rev.* 88, 1491-1545. doi: 10.1152/physrev.00030.2007

Clarke, J. D., Caldwell, J. L., Horn, M. A., Bode, E. F., Richards, M. A., Hall, M. C., et al. (2015). Perturbed atrial calcium handling in an ovine model of heart failure: potential roles for reductions in the L-type calcium current. *J. Mol. Cell Cardiol.* 79, 169-179. doi: 10.1016/j.yjmcc.2014.11.017

Colucci, W. S., Ribeiro, J. P., Rocco, M. B., Quigg, R. J., Creager, M. A., Marsh, J. D., et al. (1989). Impaired chronotropic response to exercise in patients with congestive heart failure. Role of postsynaptic beta-adrenergic desensitization. *Circulation* 80, 314-323. doi: 10.1161/01.CIR.80.2.314

Coumel, P. (1993). Cardiac arrhythmias and the autonomic nervous system. *J. Cardiovasc. Electrophysiol.* 4, 338-355. doi: 10.1111/j.1540-8167.1993.tb01235.x

Coumel, P. (1996). Autonomic influences in atrial tachyarrhythmias. *J. Cardiovasc. Electrophysiol.* 7, 999-1007. doi: 10.1111/j.1540-8167.1996.tb00474.x

Curl, C. L., Danes, V. R., Bell, J. R., Raaijmakers, A. J. A., Ip, W. T. K., Chandramouli, C., et al. (2018). Cardiomyocyte functional etiology in heart failure with preserved ejection fraction is distinctive-a new preclinical model. *J. Am. Heart Assoc.* 7:e007451. doi: 10.1161/JAHA.117.007451

Curran, J., Brown, K. H., Santiago, D. J., Pogwizd, S., Bers, D. M., and Shannon, T. R. (2010). Spontaneous Ca waves in ventricular myocytes from failing hearts depend on Ca(2+)-calmodulin-dependent protein kinase II. *J. Mol. Cell Cardiol.* 49, 25-32. doi: 10.1016/j.yjmcc.2010.03.013

Denham, N. C., Pearman, C. M., Caldwell, J. L., Madders, G. W. P., Eisner, D. A., Trafford, A. W., et al. (2018). Calcium in the pathophysiology of atrial fibrillation and heart failure. *Front. Physiol.* 9:1380. doi: 10.3389/fphys.2018.01380

Dibb, K. M., Clarke, J. D., Horn, M. A., Richards, M. A., Graham, H. K., Eisner, D. A., et al. (2009). Characterization of an extensive transverse tubular network in sheep atrial myocytes and its depletion in heart failure. *Circ. Heart Fail.* 2, 482-489. doi: 10.1161/CIRCHEARTFAILURE.109.852228

Dinanian, S., Boixel, C., Juin, C., Hulot, J. S., Coulombe, A., Rucker-Martin, C., et al. (2008). Downregulation of the calcium current in human right atrial myocytes from patients in sinus rhythm but with a high risk of atrial fibrillation. *Eur. Heart J.* 29, 1190-1197. doi: 10.1093/eurheartj/ehn140

Dridi, H., Kushnir, A., Zalk, R., Yuan, Q., Melville, Z., and Marks, A. R. (2020a). Intracellular calcium leak in heart failure and atrial fibrillation: a unifying mechanism and therapeutic target. *Nat. Rev. Cardiol.* 17, 732-747. doi: 10.1038/s41569-020-0394-8

Dridi, H., Kushnir, A., Zalk, R., Yuan, Q., Melville, Z., and Marks, A. R. (2020b). Reply to "Mechanisms of ryanodine receptor 2 dysfunction in heart failure." *Nat. Rev. Cardiol.* 17, 749-750. doi: 10.1038/s41569-020-00444-w

Dries, E., Santiago, D. J., Gilbert, G., Lenaerts, I., Vandenberk, B., Nagaraju, C. K., et al. (2018). Hyperactive ryanodine receptors in human heart failure and ischaemic cardiomyopathy reside outside of couplons. *Cardiovasc. Res.* 114, 1512-1524. doi: 10.1093/cvr/cvy088

Dunlay, S. M., Roger, V. L., and Redfield, M. M. (2017). Epidemiology of heart failure with preserved ejection fraction. *Nat. Rev. Cardiol.* 14, 591-602. doi: 10.1038/nrcardio.2017.65

Durland, L. (2021). Distinguishing HF with reduced and preserved ejection fraction at the level of individual cardiomyocytes: implications for therapeutic development. *J. Physiol.* 599, 1027-1029. doi: 10.1113/JP280739

Erickson, J. R., Joiner, M. L., Guan, X., Kutschke, W., Yang, J., Oddis, C. V., et al. (2008). A dynamic pathway for calcium-independent activation of CaMKII by methionine oxidation. *Cell* 133, 462-474.. doi: 10.1016/j.cell.2008.02.048

Faggiano, P., d'Aloia, A., Gualeni, A., Gardini, A., and Giordano, A. (2001). Mechanisms and immediate outcome of in-hospital cardiac arrest in patients with advanced heart failure secondary to ischemic or idiopathic dilated cardiomyopathy. *Am. J. Cardiol.* 87, 655-657. doi: 10.1016/S0002-9149(00)01450-8

Fischer, T. H., Eiringhaus, J., Dybkova, N., Forster, A., Herting, J., Kleinwachter, A., et al. (2014). Ca(2+)/calmodulin-dependent protein kinase II equally induces sarcoplasmic reticulum Ca(2+) leak in human ischaemic and dilated cardiomyopathy. *Eur. J. Heart Fail.* 16, 1292-1300. doi: 10.1002/ejhf.163

Fox, K., Borer, J. S., Camm, A. J., Danchin, N., Ferrari, R., Lopez Sendon, J. L., et al. (2007). Resting heart rate in cardiovascular disease. *J. Am. Coll. Cardiol.* 50, 823-830. doi: 10.1016/j.jacc.2007.04.079

Frisk, M., Le C, Shen, X., Roe, A. T., Hou, Y., Manfra, O., Silva, G. J. J., et al. (2021). Etiology-dependent impairment of diastolic cardiomyocyte calcium homeostasis in heart failure with preserved ejection fraction. *J. Am. Coll. Cardiol.* 77, 405-419. doi: 10.1016/j.jacc.2020.11.044

Fu, Y., Shaw, S. A., Naami, R., Vuong, C. L., Basheer, W. A., Guo, X., et al. (2016). Isoproterenol promotes rapid ryanodine receptor movement to bridging integrator 1 (BIN1)-organized dyads. *Circulation* 133, 388-397. doi: 10.1161/CIRCULATIONAHA.115.018535

Gang, U. J., Jons, C., Jorgensen, R. M., Abildstrom, S. Z., Haarbo, J., Messier, M. D., et al. (2010). Heart rhythm at the time of death documented by an implantable loop recorder. *Europace* 12, 254-260. doi: 10.1093/europace/eup383

Gellen, B., Fernandez-Velasco, M., Briec, F., Vinet, L., LeQuang, K., Rouet-Benzineb, P., et al. (2008). Conditional FKBP12.6 overexpression in mouse cardiac myocytes prevents triggered ventricular tachycardia through specific alterations in excitation-contraction coupling. *Circulation* 117, 1778-1786. doi: 10.1161/CIRCULATIONAHA.107.731893

Glukhov, A. V., Hage, L. T., Hansen, B. J., Pedraza-Toscano, A., Vargas-Pinto, P., Hamlin, R. L., et al. (2013). Sinoatrial node reentry in a canine chronic left ventricular infarct model: role of intranodal fibrosis and

heterogeneity of refractoriness. *Circ. Arrhythm. Electrophysiol.* 6, 984-994. doi: 10.1161/CIRCEP.113.000404

Gomez, A. M., Guatimosim, S., Dilly, K. W., Vassort, G., and Lederer, W. J. (2001). Heart failure after myocardial infarction: altered excitation-contraction coupling. *Circulation* 104, 688-693. doi: 10.1161/hc3201.092285

Gomez, A. M., Rueda, A., Sainte-Marie, Y., Pereira, L., Zissimopoulos, S., Zhu, X., et al. (2009). Mineralocorticoid modulation of cardiac ryanodine receptor activity is associated with downregulation of FK506-binding proteins. *Circulation* 119, 2179-2187. doi: 10.1161/CIRCULATIONAHA.108.805804

Gomez, A. M., Valdivia, H. H., Cheng, H., Lederer, M. R., Santana, L. F., Cannell, M. B., et al. (1997). Defective excitation-contraction coupling in experimental cardiac hypertrophy and heart failure. *Science* 276, 800-806. doi: 10.1126/science.276.5313.800

Gonzalez, D. R., Beigi, F., Treuer, A. V., and Hare, J. M. (2007). Deficient ryanodine receptor S-nitrosylation increases sarcoplasmic reticulum calcium leak and arrhythmogenesis in cardiomyocytes. *Proc. Natl. Acad. Sci. U.S.A.* 104, 20612–20617. doi: 10.1073/pnas.0706796104

Gonzalez, D. R., Treuer, A. V., Castellanos, J., Dulce, R. A., and Hare, J. M. (2010). Impaired S-nitrosylation of the ryanodine receptor caused by xanthine oxidase activity contributes to calcium leak in heart failure. *J. Biol. Chem.* 285, 28938–28945. doi: 10.1074/jbc.M110.154948

Grimm, M., Ling, H., Willeford, A., Pereira, L., Gray, C. B., Erickson, J. R., et al. (2015). CaMKIIdelta mediates beta-adrenergic effects on RyR2 phosphorylation and SR Ca(2+) leak and the pathophysiological response to chronic beta-adrenergic stimulation. *J. Mol. Cell Cardiol.* 85, 282-291. doi: 10.1016/j.yjmcc.2015.06.007

Guo, A., Zhang, C., Wei, S., Chen, B., and Song, L. S. (2013). Emerging mechanisms of T-tubule remodelling in heart failure. *Cardiovasc. Res.* 98, 204-215. doi: 10.1093/cvr/cvt020

Haissaguerre, M., Warin, J. F., Lemetayer, P., Saoudi, N., Guillem, J. P., and Blanchot, P. (1989). Closed-chest ablation of retrograde conduction in patients with atrioventricular nodal reentrant tachycardia. *N. Engl. J. Med.* 320, 426-433. doi: 10.1056/NEJM198902163200704

Hamouda, N. N., Sydorenko, V., Qureshi, M. A., Alkaabi, J. M., Oz, M., and Howarth, F. C. (2015). Dapagliflozin reduces the amplitude of shortening and Ca(2+) transient in ventricular myocytes from streptozotocin-induced diabetic rats. *Mol. Cell Biochem.* 400, 7-68. doi: 10.1007/s11010-014-2262-5

Hasenfuss, G., and Pieske, B. (2002). Calcium cycling in congestive heart failure. *J. Mol. Cell Cardiol.* 34, 951-969. doi: 10.1006/jmcc.2002.2037

Hatem, S. N., Benardeau, A., Rucker-Martin, C., Marty, I., de Chamisso, P., Villaz, M., et al. (1997). Different compartments of sarcoplasmic reticulum participate in the excitation-contraction coupling process in human atrial myocytes. *Circ. Res.* 80, 345-353. doi: 10.1161/01.RES.80.3.345

Hautefort, A., Mendes-Ferreira, P., Sabourin, J., Manaud, G., Bertero, T., Rucker-Martin, C., et al. (2019). Bmpr2 mutant rats develop pulmonary and cardiac characteristics of pulmonary arterial hypertension. *Circulation* 139, 932-948. doi: 10.1161/CIRCULATIONAHA.118.033744

Heymes, C., Bendall, J. K., Ratajczak, P., Cave, A. C., Samuel, J. L., Hasenfuss, G., et al. (2003). Increased myocardial NADPH oxidase activity in human heart failure. *J. Am. Coll Cardiol.* 41, 2164-2171. doi: 10.1016/S0735-1097(03)00471-6

Higginbotham, M. B., Morris, K. G., Conn, E. H., Coleman, R. E., and Cobb, F. R. (1983). Determinants of variable exercise performance among patients with severe left ventricular dysfunction. *Am. J. Cardiol.* 51, 52-60. doi: 10.1016/S0002-9149(83)80010-1

Ho, H. T., Liu, B., Snyder, J. S., Lou, Q., Brundage, E. A., Velez-Cortes, F., et al. (2014). Ryanodine receptor phosphorylation by oxidized CaMKII contributes to the cardiotoxic effects of cardiac glycosides. *Cardiovasc. Res.* 101, 165-174. doi: 10.1093/cvr/cvt233

Hohendanner, F., Ljubojevic, S., MacQuaide, N., Sacherer, M., Sedej, S., Biesmans, L., et al. (2013). Intracellular dyssynchrony of diastolic cytosolic [Ca(2)(+)] decay in ventricular cardiomyocytes in cardiac remodeling and human heart failure. *Circ. Res.* 113, 527-538. doi: 10.1161/CIRCRESAHA.113.300895

Hohendanner, F., Walther, S., Maxwell, J. T., Kettlewell, S., Awad, S., Smith, G. L., et al. (2015). Inositol-1,4,5-trisphosphate induced Ca^{2+} release and excitation-contraction coupling in atrial myocytes from normal and failing hearts. *J. Physiol.* 593, 1459-1477. doi: 10.1113/jphysiol.2014.283226

Houser, S. R. (2014). Role of RyR2 phosphorylation in heart failure and arrhythmias: protein kinase A-mediated hyperphosphorylation of the ryanodine receptor at serine 2808 does not alter cardiac contractility or cause heart failure and arrhythmias. *Circ. Res.* 114, 1320-1327. doi: 10.1161/CIRCRESAHA.114.300569

Jiang, M. T., Lokuta, A. J., Farrell, E. F., Wolff, M. R., Haworth, R. A., and Valdivia, H. H. (2002). Abnormal Ca^{2+} release, but normal ryanodine receptors, in canine and human heart failure. *Circ. Res.* 91, 1015–1022. doi: 10.1161/01.RES.0000043663.08689.05

Jones, P. P., MacQuaide, N., and Louch, W. E. (2018). Dyadic Plasticity in Cardiomyocytes. *Front. Physiol.* 9:1773. doi: 10.3389/fphys.2018.01773

Jose, A. D., and Collison, D. (1970). The normal range and determinants of the intrinsic heart rate in man. *Cardiovasc. Res.* 4, 160-167. doi: 10.1093/cvr/4.2.160

Jose, A. D., and Taylor, R. R. (1969). Autonomic blockade by propranolol and atropine to study intrinsic myocardial function in man. *J. Clin. Invest.* 48, 2019-2031. doi: 10.1172/JCI106167

Kettlewell, S., Burton, F. L., Smith, G. L., and Workman, A. J. (2013). Chronic myocardial infarction promotes atrial action potential alternans, afterdepolarizations, and fibrillation. *Cardiovasc. Res.* 99, 215-224. doi: 10.1093/cvr/cvt087

Kilfoil, P. J., Lotteau, S., Zhang, R., Yue, X., Aynaszyan, S., Solymani, R. E., et al. (2020). Distinct features of calcium handling and beta-adrenergic sensitivity in heart failure with preserved versus reduced ejection fraction. *J. Physiol.* 598, 5091-5108. doi: 10.1113/JP280425

Kohajda, Z., Loewe, A., Toth, N., Varro, A., and Nagy, N. (2020). The cardiac pacemaker story-fundamental role of the Na(+)/Ca(2+) exchanger in spontaneous automaticity. *Front. Pharmacol.* 11:516. doi: 10.3389/fphar.2020.00516

Kranias, E. G., and Hajjar, R. J. (2012). Modulation of cardiac contractility by the phospholamban/SERCA2a regulatome. *Circ. Res.* 110, 1646-1660. doi: 10.1161/CIRCRESAHA.111.259754

Lacombe, V. A., Viatchenko-Karpinski, S., Terentyev, D., Sridhar, A., Emani, S., Bonagura, J. D., et al. (2007). Mechanisms of impaired calcium handling underlying subclinical diastolic dysfunction in diabetes. *Am. J. Physiol. Regul. Integr. Comp. Physiol.* 293, 1787-1797. doi: 10.1152/ajpregu.00059.2007

Lagadic-Gossmann, D., Buckler, K. J., Le Prigent, K., and Feuvray, D. (1996). Altered Ca^{2+} handling in ventricular myocytes isolated from diabetic rats. *Am. J. Physiol.* 270, 1529–1537. doi: 10.1152/ajpheart.1996.270.5.H1529

Landstrom, A. P., Dobrev, D., and Wehrens, X. H. T. (2017). Calcium signaling and cardiac arrhythmias. *Circ. Res.* 120, 1969-1993. doi: 10.1161/CIRCRESAHA.117.310083

Lang, D., and Glukhov, A. V. (2021). Cellular and molecular mechanisms of functional hierarchy of pacemaker clusters in the sinoatrial node: new insights into sick sinus syndrome. *J. Cardiovasc. Dev. Dis.* 8:43. doi: 10.3390/jcdd8040043

Lehnart, S. E., Maier, L. S., and Hasenfuss, G. (2009). Abnormalities of calcium metabolism and myocardial contractility depression in the failing heart. *Heart Fail. Rev.* 14, 213-224. doi: 10.1007/s10741-009-9146-x

Lin, Y. K., Chen, Y. C., Chen, Y. A., Yeh, Y. H., Chen, S. A., and Chen, Y. J. (2016). B-type natriuretic peptide modulates pulmonary vein arrhythmogenesis: a novel potential contributor to the genesis of atrial tachyarrhythmia in heart failure. *J. Cardiovasc. Electrophysiol.* 27, 1462-1471. doi: 10.1111/jce.13093

Lindner, M., Brandt, M. C., Sauer, H., Hescheler, J., Böhle, T., and Beuckelmann, D. J. (2002). Calcium sparks in human ventricular cardiomyocytes from patients with terminal heart failure. *Cell Calcium.* 31, 175-182. doi: 10.1054/ceca.2002.0272

Ling, H., Zhang, T., Pereira, L., Means, C. K., Cheng, H., Gu, Y., et al. (2009). Requirement for Ca^{2+}/calmodulin-dependent kinase II in the transition from pressure overload-induced cardiac hypertrophy to heart failure in mice. *J. Clin. Invest.* 119, 1230-1240. doi: 10.1172/JCI38022

Ljubojevic, S., Radulovic, S., Leitinger, G., Sedej, S., Sacherer, M., Holzer, M., et al. (2014). Early remodeling of perinuclear Ca^{2+} stores and nucleoplasmic Ca^{2+} signaling during the development of hypertrophy and heart failure. *Circulation* 130, 244-255. doi: 10.1161/CIRCULATIONAHA.114.008927

Lou, Q., Hansen, B. J., Fedorenko, O., Csepe, T. A., Kalyanasundaram, A., Li, N., et al. (2014). Upregulation of adenosine A1 receptors facilitates sinoatrial node dysfunction in chronic canine heart failure by exacerbating nodal conduction abnormalities revealed by novel dual-sided intramural optical mapping. *Circulation* 130, 315-324. doi: 10.1161/CIRCULATIONAHA.113.007086

Loyer, X., Gomez, A. M., Milliez, P., Fernandez-Velasco, M., Vangheluwe, P., Vinet, L., et al. (2008). Cardiomyocyte overexpression of neuronal nitric oxide synthase delays transition toward heart failure in response to pressure overload by preserving calcium cycling. *Circulation* 117, 3187–3198. doi: 10.1161/CIRCULATIONAHA.107.741702

Luu, M., Stevenson, W. G., Stevenson, L. W., Baron, K., and Walden, J. (1989). Diverse mechanisms of unexpected cardiac arrest in advanced heart failure. *Circulation* 80, 1675-1680. doi: 10.1161/01.CIR.80.6.1675

Lymperopoulos, A., Rengo, G., and Koch, W. J. (2013). Adrenergic nervous system in heart failure: pathophysiology and therapy. *Circ. Res.* 113, 739-753. doi: 10.1161/CIRCRESAHA.113.300308

MacDonnell, S. M., Garcia-Rivas, G., Scherman, J. A., Kubo, H., Chen, X., Valdivia, H., et al. (2008). Adrenergic regulation of cardiac contractility does not involve phosphorylation of the cardiac ryanodine receptor at serine 2808. *Circ. Res.* 102, 65-72. doi: 10.1161/CIRCRESAHA.108.174722

Mak, S., and Newton, G. E. (2001). The oxidative stress hypothesis of congestive heart failure: radical thoughts. *Chest* 120, 2035-2046. doi: 10.1378/chest.120.6.2035

Mangrum, J. M., and DiMarco, J. P. (2000). The evaluation and management of bradycardia. *N. Engl. J. Med.* 342, 703-709. doi: 10.1056/NEJM200003093421006

Marx, S. O., Reiken, S., Hisamatsu, Y., Jayaraman, T., Burkhoff, D., Rosemblit, N., et al. (2000). PKA phosphorylation dissociates FKBP12.6 from the calcium release channel (ryanodine receptor): defective regulation in failing hearts. *Cell* 101, 365–376. doi: 10.1016/S0092-8674(00)80847-8

Mazurek, S. R., Bovo, E., and Zima, A. V. (2014). Regulation of sarcoplasmic reticulum Ca(2+) release by cytosolic glutathione in rabbit ventricular myocytes. *Free Radic. Biol. Med.* 68, 159-167. doi: 10.1016/j.freeradbiomed.2013.12.003

Messias, L. R., Messias, A. C., de Miranda, S. M., Wiefels, C. C., Ferreira, A. G., Santos, L. M., et al. (2016). Abnormal adrenergic activation is the major determinant of reduced functional capacity in heart failure with preserved ejection fraction. *Int. J. Cardiol.* 203, 900-902. doi: 10.1016/j.ijcard.2015.10.224

Miranda-Silva, D., Wust, R. C. I., Conceicao, G., Goncalves-Rodrigues, P., Goncalves, N., Goncalves, A., et al. (2020). Disturbed cardiac mitochondrial and cytosolic calcium handling in a metabolic risk-related rat model of heart failure with preserved ejection fraction. *Acta Physiol (Oxf).* 228:e13378. doi: 10.1111/apha.13378

Mochizuki, M., Yano, M., Oda, T., Tateishi, H., Kobayashi, S., Yamamoto, T., et al. (2007). Scavenging free radicals by low-dose carvedilol prevents redox-dependent Ca^{2+} leak via stabilization of ryanodine receptor in heart failure. *J. Am. Coll. Cardiol.* 49, 1722-1732. doi: 10.1016/j.jacc.2007.01.064

Mulder, P., and Thuillez, C. (2006). Heart rate slowing for myocardial dysfunction/heart failure. *Adv. Cardiol.* 43, 97-105. doi: 10.1159/000095431

Neco, P., Torrente, A. G., Mesirca, P., Zorio, E., Liu, N., Priori, S. G., et al. (2012). Paradoxical effect of increased diastolic Ca(2+) release and decreased sinoatrial node activity in a mouse model of catecholaminergic polymorphic ventricular tachycardia. *Circulation* 126, 392-401. doi: 10.1161/CIRCULATIONAHA.111.075382

Nikolaienko, R., Bovo, E., and Zima, A. V. (2018). Redox dependent modifications of ryanodine receptor: basic mechanisms and implications in heart diseases. *Front. Physiol.* 9:1775. doi: 10.3389/fphys.2018.01775

Nuss, H. B., Kaab, S., Kass, D. A., Tomaselli, G. F., and Marbán, E. (1999). Cellular basis of ventricular arrhythmias and abnormal automaticity in heart failure. *Am. J. Physiol.* 277, 80–91. doi: 10.1152/ajpheart.1999.277.1.H80

Oda, T., Yang, Y., Uchinoumi, H., Thomas, D. D., Chen-Izu, Y., Kato, T., et al. (2015). Oxidation of ryanodine receptor (RyR) and calmodulin enhance Ca release and pathologically alter, RyR structure and calmodulin affinity. *J. Mol. Cell Cardiol.* 85, 240-248. doi: 10.1016/j.yjmcc.2015.06.009

Ohkusa, T., Hisamatsu, Y., Yano, M., Kobayashi, S., Tatsuno, H., Saiki, Y., et al. (1997). Altered cardiac mechanism and sarcoplasmic reticulum function in pressure overload-induced cardiac hypertrophy in rats. *J. Mol. Cell Cardiol.* 29, 45-54. doi: 10.1006/jmcc.1996.0250

Ono, K., Yano, M., Ohkusa, T., Kohno, M., Hisaoka, T., Tanigawa, T., et al. (2000). Altered interaction of FKBP12.6 with ryanodine receptor as a cause of abnormal Ca(2+) release in heart failure. *Cardiovasc. Res.* 48, 323-331. doi: 10.1016/S0008-6363(00)00191-7

Ono, M., Yano, M., Hino, A., Suetomi, T., Xu, X., Susa, T., et al. (2010). Dissociation of calmodulin from cardiac ryanodine receptor causes aberrant Ca(2+) release in heart failure. *Cardiovasc. Res.* 87, 609-617. doi: 10.1093/cvr/cvq108

Opthof, T., Coronel, R., Rademaker, H. M., Vermeulen, J. T., Wilms-Schopman, F. J., and Janse, M. J. (2000). Changes in sinus node function in a rabbit model of heart failure with ventricular arrhythmias and sudden death. *Circulation* 101, 2975-2980. doi: 10.1161/01.CIR.101.25.2975

Owan, T. E., Hodge, D. O., Herges, R. M., Jacobsen, S. J., Roger, V. L., and Redfield, M. M. (2006). Trends in prevalence and outcome of heart failure with preserved ejection fraction. *N. Engl. J. Med.* 355, 251-259. doi: 10.1056/NEJMoa052256

Packer, D. L., Prutkin, J. M., Hellkamp, A. S., Mitchell, L. B., Bernstein, R. C., Wood, F., et al. (2009). Impact of implantable cardioverter-defibrillator, amiodarone, and placebo on the mode of death in stable patients with heart failure: analysis from the sudden cardiac death in heart failure trial. *Circulation* 120, 2170-2176. doi: 10.1161/CIRCULATIONAHA.109.853689

Packer, M., Lam, C. S. P., Lund, L. H., and Redfield, M. M. (2020). Interdependence of atrial fibrillation and heart failure with a preserved ejection fraction reflects a common underlying atrial and ventricular myopathy. *Circulation* 141, 4-6. doi: 10.1161/CIRCULATIONAHA.119.042996

Piacentino, V. 3rd, Weber, C. R., Chen, X., Weisser-Thomas, J., Margulies, K. B., Bers, D. M., and Houser, S. R. (2003). Cellular basis of abnormal calcium transients of failing human ventricular myocytes. *Circ. Res.* 92, 651–658. doi: 10.1161/01.RES.0000062469.83985.9B

Pogwizd, S. M., Schlotthauer, K., Li, L., Yuan, W., and Bers, D. M. (2001). Arrhythmogenesis and contractile dysfunction in heart failure: Roles of sodium-calcium exchange, inward rectifier potassium current, and residual beta-adrenergic responsiveness. *Circ. Res.* 88, 1159-1167. doi: 10.1161/hh1101.091193

Potenza, D. M., Janicek, R., Fernandez-Tenorio, M., Camors, E., Ramos-Mondragon, R., Valdivia, H. H., et al. (2019). Phosphorylation of the ryanodine receptor 2 at serine 2030 is required for a complete beta-adrenergic response. *J. Gen. Physiol.* 151, 131-145. doi: 10.1085/jgp.201812155

Primessnig, U., Schonleitner, P., Holl, A., Pfeiffer, S., Bracic, T., Rau, T., et al. (2016). Novel pathomechanisms of cardiomyocyte dysfunction in a model of heart failure with preserved ejection fraction. *Eur. J. Heart Fail.* 18, 987-997. doi: 10.1002/ejhf.524

Prosser, B. L., Ward, C. W., and Lederer, W. J., (2011). X-ROS signaling: rapid mechano-chemo transduction in heart. *Science* 333, 1440-1445. doi: 10.1126/science.1202768

Redfield, M. M., Jacobsen, S. J., Burnett, J. C. Jr., Mahoney, D. W., Bailey, K. R., and Rodeheffer, R. J. (2003). Burden of systolic and diastolic ventricular dysfunction in the community: appreciating the scope of the heart failure epidemic. *JAMA* 289, 194-202. doi: 10.1001/jama.289.2.194

Respress, J. L., van Oort, R. J., Li, N., Rolim, N., Dixit, S. S., deAlmeida, A., et al. (2012). Role of RyR2 phosphorylation at S2814 during heart failure progression. *Circ. Res.* 110, 1474-1483. doi: 10.1161/CIRCRESAHA.112.268094

Roe, A. T., Aronsen, J. M., Skardal, K., Hamdani, N., Linke, W. A., Danielsen, H. E., et al. (2017). Increased passive stiffness promotes diastolic dysfunction despite improved Ca^{2+} handling during left ventricular concentric hypertrophy. *Cardiovasc. Res.* 113, 1161-1172. doi: 10.1093/cvr/cvx087

Rouhana, S., Farah, C., Roy, J., Finan, A., Rodrigues de Araujo, G., Bideaux, P., et al. (2019). Early calcium handling imbalance in pressure overload-induced heart failure with nearly normal left ventricular ejection fraction. *Biochim. Biophys. Acta. Mol. Basis Dis.* 1865, 230-242. doi: 10.1016/j.bbadis.2018.08.005

Rubenstein, D. S., and Lipsius, S. L. (1989). Mechanisms of automaticity in subsidiary pacemakers from cat right atrium. *Circ. Res.* 64, 648-657. doi: 10.1161/01.RES.64.4.648

Ruiz-Hurtado, G., Li, L., Fernandez-Velasco, M., Rueda, A., Lefebvre, F., Wang, Y., et al. (2015). Reconciling depressed Ca^{2+} sparks occurrence with enhanced RyR2 activity in failing mice cardiomyocytes. *J. Gen. Physiol.* 146, 295-306. doi: 10.1085/jgp.201511366

Saeed, Y., Temple, I. P., Borbas, Z., Atkinson, A., Yanni, J., Maczewski, M., et al. (2018). Structural and functional remodeling of the atrioventricular node with aging in rats: the role of hyperpolarization-activated cyclic nucleotide-gated and ryanodine 2 channels. *Heart Rhythm* 15, 752-760. doi: 10.1016/j.hrthm.2017.12.027

Samejima, H., Omiya, K., Uno, M., Inoue, K., Tamura, M., Itoh, K., et al. (2003). Relationship between impaired chronotropic response, cardiac output during

exercise, and exercise tolerance in patients with chronic heart failure. *Jpn. Heart J.* 44, 515-525. doi: 10.1536/jhj.44.515

Sanchez, G., Pedrozo, Z., Domenech, R. J., Hidalgo, C., and Donoso, P. (2005). Tachycardia increases NADPH oxidase activity and RyR2 S-glutathionylation in ventricular muscle. *J. Mol. Cell Cardiol.* 39, 982-991. doi: 10.1016/j.yjmcc.2005.08.010

Sanders, P., Kistler, P. M., Morton, J. B., Spence, S. J., and Kalman, J. M. (2004). Remodeling of sinus node function in patients with congestive heart failure: reduction in sinus node reserve. *Circulation* 110, 897-903. doi: 10.1161/01.CIR.0000139336.69955.AB

Schroder, F., Handrock, R., Beuckelmann, D. J., Hirt, S., Hullin, R., Priebe, L., et al. (1998). Increased availability and open probability of single L-type calcium channels from failing compared with non-failing human ventricle. *Circulation* 98, 969–976. doi: 10.1161/01.CIR.98.10.969

Selby, D. E., Palmer, B. M., LeWinter, M. M., and Meyer, M. (2011). Tachycardia-induced diastolic dysfunction and resting tone in myocardium from patients with a normal ejection fraction. *J. Am. Coll. Cardiol.* 58, 147-154. doi: 10.1016/j.jacc.2010.10.069

Shan, J., Betzenhauser, M. J., Kushnir, A., Reiken, S., Meli, A. C., Wronska, A., et al. (2010a). Role of chronic ryanodine receptor phosphorylation in heart failure and beta-adrenergic receptor blockade in mice. *J. Clin. Invest.* 120, 4375-4387. doi: 10.1172/JCI37649

Shan, J., Kushnir, A., Betzenhauser, M. J., Reiken, S., Li, J., Lehnart, S. E., et al. (2010b). Phosphorylation of the ryanodine receptor mediates the cardiac fight or flight response in mice. *J. Clin. Invest.* 120, 4388-4398. doi: 10.1172/JCI32726

Shinohara, T., Park, H. W., Han, S., Shen, M. J., Maruyama, M., Kim, D., et al. (2010). Ca^{2+} clock malfunction in a canine model of pacing-induced heart failure. *Am. J. Physiol. Heart Circ. Physiol.* 299, 1805-1811. doi: 10.1152/ajpheart.00723.2010

Sisti, A. D. E., Leclercq, J. F., Halimi, F., Fiorello, P., Bertrand, C., and Attuel, P. (2014). Evaluation of time course and predicting factors of progression of paroxysmal or persistent atrial fibrillation to permanent atrial fibrillation. *Pacing Clin. Electrophysiol.* 37, 345-355. doi: 10.1111/pace.12264

Stern, M. D. (1992). Theory of excitation-contraction coupling in cardiac muscle. *Biophys. J.* 63, 497-517. doi: 10.1016/S0006-3495(92)81615-6

Stevenson, W. G., Stevenson, L. W., Middlekauff, H. R., and Saxon, L. A. (1993). Sudden death prevention in patients with advanced ventricular dysfunction. *Circulation* 88, 2953-2961. doi: 10.1161/01.CIR.88.6.2953

Swaminathan, P. D., Purohit, A., Soni, S., Voigt, N., Singh, M. V., Glukhov, A. V., et al. (2011). Oxidized CaMKII causes cardiac sinus node dysfunction in mice. *J. Clin. Invest.* 121, 3277-3288. doi: 10.1172/JCI57833

Terentyev, D., Gyorke, I., Belevych, A. E., Terentyeva, R., Sridhar, A., Nishijima, Y., et al. (2008). Redox modification of ryanodine receptors contributes to sarcoplasmic reticulum Ca^{2+} leak in chronic heart failure. *Circ. Res.* 103, 1466-1472. doi: 10.1161/CIRCRESAHA.108.184457

Uchinoumi, H., Yang, Y., Oda, T., Li, N., Alsina, K. M., Puglisi, J. L., et al. (2016). CaMKII-dependent phosphorylation of RyR2 promotes targetable pathological RyR2 conformational shift. *J. Mol. Cell Cardiol.* 98, 62-72. doi: 10.1016/j.yjmcc.2016.06.007

Uretsky, B. F., and Sheahan, R. G. (1997). Primary prevention of sudden cardiac death in heart failure: will the solution be shocking? *J. Am. Coll. Cardiol.* 30, 1589-1597. doi: 10.1016/S0735-1097(97)00361-6

van Oort, R. J., McCauley, M. D., Dixit, S. S., Pereira, L., Yang, Y., Respress, J. L., et al. (2010). Ryanodine receptor phosphorylation by calcium/calmodulin-dependent protein kinase II promotes life-threatening ventricular arrhythmias in mice with heart failure. *Circulation* 122, 2669-2679. doi: 10.1161/CIRCULATIONAHA.110.982298

Vatner, S. F., Higgins, C. B., and Braunwald, E. (1974). Sympathetic and parasympathetic components of reflex tachycardia induced by hypotension in conscious dogs with and without heart failure. *Cardiovasc. Res.* 8, 153-161. doi: 10.1093/cvr/8.2.153

Venetucci, L. A., Trafford, A. W., O'Neill, S. C., and Eisner, D. A. (2008). The sarcoplasmic reticulum and arrhythmogenic calcium release. *Cardiovasc. Res.* 77, 285–292. doi: 10.1093/cvr/cvm009

Ventura-Clapier, R., Garnier, A., and Veksler, V. (2004). Energy metabolism in heart failure. *J. Physiol.* 555, 1-13. doi: 10.1113/jphysiol.2003.055095

Verkerk, A. O., van Borren, M. M., van Ginneken, A. C., and Wilders, R. (2015). Ca(2+) cycling properties are conserved despite bradycardic effects of heart failure in sinoatrial node cells. *Front. Physiol.* 6:18. doi: 10.3389/fphys.2015.00018

Verkerk, A. O., Wilders, R., Coronel, R., Ravesloot, J. H., and Verheijck, E. E. (2003). Ionic remodeling of sinoatrial node cells by heart failure. *Circulation* 108, 760-766. doi: 10.1161/01.CIR.0000083719.51661.B9

Verrier, R. L., and Tan, A. (2009). Heart rate, autonomic markers, and cardiac mortality. *Heart Rhythm* 6, 68-75. doi: 10.1016/j.hrthm.2009.07.017

Wagner, E., Lauterbach, M. A., Kohl, T., Westphal, V., Williams, G. S., Steinbrecher, J. H., et al. (2012). Stimulated emission depletion live-cell super-resolution imaging shows proliferative remodeling of T-tubule membrane structures after myocardial infarction. *Circ. Res.* 111, 402-414. doi: 10.1161/CIRCRESAHA.112.274530

Walweel, K., Molenaar, P., Imtiaz, M. S., Denniss, A., Dos Remedios, C., van Helden, D. F., et al. (2017). Ryanodine receptor modification and regulation by intracellular Ca(2+) and Mg(2+) in healthy and failing human hearts. *J. Mol. Cell Cardiol.* 104, 53-62. doi: 10.1016/j.yjmcc.2017.01.016

Wang, Y. Y., Mesirca, P., Marques-Sule, E., Zahradnikova, A. Jr., Villejoubert, O., D'Ocon, P., et al. (2017). RyR_2^{R420Q} catecholaminergic polymorphic ventricular tachycardia mutation induces bradycardia by disturbing the coupled clock pacemaker mechanism. *JCI Insight* 2:e91872. doi: 10.1172/jci.insight.91872

Weber, K. T., Kinasewitz, G. T., Janicki, J. S., and Fishman, A. P. (1982). Oxygen utilization and ventilation during exercise in patients with chronic cardiac failure. *Circulation* 65, 1213-1223. doi: 10.1161/01.CIR.65.6.1213

Wehrens, X. H., Lehnart, S. E., Reiken, S., Vest, J. A., Wronska, A., and Marks, A. R. (2006). Ryanodine receptor/calcium release channel PKA phosphorylation: a critical mediator of heart failure progression. *Proc. Natl. Acad. Sci. U.S.A.* 103, 511-518. doi: 10.1073/pnas.0510113103

Wiggers, C. J. (1949). *Physiology in Health and Disease. 5th Edn*, ed H. Kempton (London).

Witcher, D. R., Kovacs, R. J., Schulman, H., Cefali, D. C., and Jones, L. R. (1991). Unique phosphorylation site on the cardiac ryanodine receptor regulates calcium channel activity. *J. Biol. Chem.* 266, 11144-11152. doi: 10.1016/S0021-9258(18)99140-4

Wollenberger, A. (1947). On the energy-rich phosphate supply of the failing heart. *Am. J. Physiol.* 150, 733-745. doi: 10.1152/ajplegacy.1947.150.4.733

Xiao, B., Zhong, G., Obayashi, M., Yang, D., Chen, K., Walsh, M. P., et al. (2006). Ser-2030, but not Ser-2808, is the major phosphorylation site in cardiac ryanodine receptors responding to protein kinase A activation upon beta-adrenergic stimulation in normal and failing hearts. *Biochem. J.* 396, 7-16. doi: 10.1042/BJ20060116

Xiao, J., Tian, X., Jones, P. P., Bolstad, J., Kong, H., Wang, R., et al. (2007). Removal of FKBP12.6 does not alter the conductance and activation of the cardiac ryanodine receptor or the susceptibility to stress-induced ventricular arrhythmias. *J Biol Chem.* 282, 34828–34838. doi: 10.1074/jbc.M707423200

Xu, L., Eu, J. P., Meissner, G., and Stamler, J. S. (1998). Activation of the cardiac calcium release channel (ryanodine receptor) by poly-S-nitrosylation. *Science* 279, 234-237. doi: 10.1126/science.279.5348.234

Xue, J., Arbel Ganon, L., Gomez, S., Benitah, J. P., and Gomez, A. M. (2020). SAN function is altered in a mice model of heart failure. *J. Mol. Cell Cardiol.* 140:149. doi: 10.1016/j.yjmcc.2019.11.018

Yan, Y., Liu, J., Wei, C., Li, K., Xie, W., Wang, Y., et al. (2008). Bidirectional regulation of Ca^{2+} sparks by mitochondria-derived reactive oxygen species in cardiac myocytes. *Cardiovasc. Res.* 77, 432-441. doi: 10.1093/cvr/cvm047

Yanni, J., D'Souza, A., Wang, Y., Li, N., Hansen, B. J., Zakharkin, S. O., et al. (2020). Silencing miR-370-3p rescues funny current and sinus node function in heart failure. *Sci. Rep.* 10:11279. doi: 10.1038/s41598-020-67790-0

Yanni, J., Tellez, J. O., Maczewski, M., Mackiewicz, U., Beresewicz, A., Billeter, R., et al. (2011). Changes in ion channel gene expression underlying heart failure-induced sinoatrial node dysfunction. *Circ. Heart Fail.* 4, 496-508. doi: 10.1161/CIRCHEARTFAILURE.110.957647

Yeh, Y. H., Wakili, R., Qi, X. Y., Chartier, D., Boknik, P., Kaab, S., et al. (2008). Calcium-handling abnormalities underlying atrial arrhythmogenesis and contractile dysfunction in dogs with congestive heart failure. *Circ. Arrhythm. Electrophysiol.* 1, 93-102. doi: 10.1161/CIRCEP.107.754788

Zhang, H., Makarewich, C. A., Kubo, H., Wang, W., Duran, J. M., Li, Y., et al. (2012). Hyperphosphorylation of the cardiac ryanodine receptor at serine 2808

is not involved in cardiac dysfunction after myocardial infarction. *Circ. Res.* 110, 831-840. doi: 10.1161/CIRCRESAHA.111.255158

Zicha, S., Fernandez-Velasco, M., Lonardo, G., L'Heureux, N., and Nattel, S. (2005). Sinus node dysfunction and hyperpolarization-activated (HCN) channel subunit remodeling in a canine heart failure model. *Cardiovasc. Res.* 66, 472-481. doi: 10.1016/j.cardiores.2005.02.011

Zima, A. V., and Mazurek, S. R. (2016). Functional impact of ryanodine receptor oxidation on intracellular calcium regulation in the heart. *Rev. Physiol. Biochem. Pharmacol.* 171, 39-62. doi: 10.1007/112_2016_2

Conflict of Interest: The authors declare that the research was conducted in the absence of any commercial or financial relationships that could be construed as a potential conflict of interest.

Publisher's Note: All claims expressed in this article are solely those of the authors and do not necessarily represent those of their affiliated organizations, or those of the publisher, the editors and the reviewers. Any product that may be evaluated in this article, or claim that may be made by its manufacturer, is not guaranteed or endorsed by the publisher.

frontiers in Physiology

ORIGINAL RESEARCH
published: 12 October 2021
doi: 10.3389/fphys.2021.744730

Sarcoplasmic Reticulum Calcium Release Is Required for Arrhythmogenesis in the Mouse

*Andrew G. Edwards[1,2], Halvor Mørk[1], Mathis K. Stokke[1,3,4], David B. Lipsett[1], Ivar Sjaastad[1,3], Sylvain Richard[5], Ole M. Sejersted[1] and William E. Louch[1,3]**

[1] Institute for Experimental Medical Research, Oslo University Hospital, University of Oslo, Oslo, Norway, [2] Department of Pharmacology, University of California, Davis, Davis, CA, United States, [3] K.G. Jebsen Centre for Cardiac Research, University of Oslo, Oslo, Norway, [4] Department of Cardiology, Oslo University Hospital, Oslo, Norway, [5] Université de Montpellier, INSERM, CNRS, PhyMedExp, Montpellier, France

OPEN ACCESS

Edited by:
Daniel M. Johnson, The Open University, United Kingdom

Reviewed by:
Yanmin Zhang, Xi'an Jiaotong University, China
Yohannes Castro Shiferaw, California State University, Northridge, United States

***Correspondence:**
William E. Louch
w.e.louch@medisin.uio.no

Specialty section:
This article was submitted to Cardiac Electrophysiology, a section of the journal Frontiers in Physiology

Received: *20 July 2021*
Accepted: *20 September 2021*
Published: *12 October 2021*

Citation:
Edwards AG, Mørk H, Stokke MK, Lipsett DB, Sjaastad I, Richard S, Sejersted OM and Louch WE (2021) Sarcoplasmic Reticulum Calcium Release Is Required for Arrhythmogenesis in the Mouse. Front. Physiol. 12:744730. doi: 10.3389/fphys.2021.744730

Dysfunctional sarcoplasmic reticulum Ca^{2+} handling is commonly observed in heart failure, and thought to contribute to arrhythmogenesis through several mechanisms. Some time ago we developed a cardiomyocyte-specific inducible SERCA2 knockout mouse, which is remarkable in the degree to which major adaptations to sarcolemmal Ca^{2+} entry and efflux overcome the deficit in SR reuptake to permit relatively normal contractile function. Conventionally, those adaptations would also be expected to dramatically increase arrhythmia susceptibility. However, that susceptibility has never been tested, and it is possible that the very rapid repolarization of the murine action potential (AP) allows for large changes in sarcolemmal Ca^{2+} transport without substantially disrupting electrophysiologic stability. We investigated this hypothesis through telemetric ECG recording in the SERCA2-KO mouse, and patch-clamp electrophysiology, Ca^{2+} imaging, and mathematical modeling of isolated SERCA2-KO myocytes. While the SERCA2-KO animals exhibit major (and unique) electrophysiologic adaptations at both the organ and cell levels, they remain resistant to arrhythmia. A marked increase in peak L-type calcium (I_{CaL}) current and slowed I_{CaL} decay elicited pronounced prolongation of initial repolarization, but faster late repolarization normalizes overall AP duration. Early afterdepolarizations were seldom observed in KO animals, and those that were observed exhibited a mechanism intermediate between murine and large mammal dynamical properties. As expected, spontaneous SR Ca^{2+} sparks and waves were virtually absent. Together these findings suggest that intact SR Ca^{2+} handling is an absolute requirement for triggered arrhythmia in the mouse, and that in its absence, dramatic changes to the major inward currents can be resisted by the substantial K^+ current reserve, even at end-stage disease.

Keywords: early afterdepolarizations (EADs), delayed afterdepolarizations, species, triggered activity, repolarization

INTRODUCTION

Dysfunctional sarcoplasmic reticulum (SR) Ca^{2+} handling is known to destabilize cardiac electrophysiology in a broad range of arrhythmogenic diseases, from rare channelopathies (Priori et al., 2001, 2002) to prevalent acquired diseases such as heart failure (Pogwizd et al., 2001; Pogwizd and Bers, 2002). However, the role of the SR as an intracellular Ca^{2+} store able to drive cardiac contraction is fundamental to normal function of the heart, and evolutionary processes have carefully balanced the electrical stability of cardiac excitation-contraction (EC) coupling with the requirement for a high-gain intracellular Ca^{2+} release system. This balance has important implications for arrhythmia mechanisms in the heart, and these can be clearly illustrated by considering differences across mammalian species.

In healthy large mammals, approximately 30% of the Ca^{2+} that fuels cardiac contraction is obtained from L-type Ca^{2+} current (I_{CaL})-mediated Ca^{2+} influx (Shannon et al., 2004; Fearnley et al., 2011), and this can increase to near 50% in chronic diseases such as heart failure (Pogwizd and Bers, 2002). Such large transmembrane Ca^{2+} fluxes are permitted by a prolonged action potential (AP) plateau, which itself results from a relatively delicate balance of inward and outward currents in large mammals (Weiss et al., 2010). These characteristics of EC coupling in large mammals tend to favor repolarization instabilities, and potentiation of I_{CaL} by frequency, neurohormonal stimuli, and genetic abnormalities are well known to destabilize repolarization in humans (Piot et al., 1996; Splawski et al., 2004, 2005; Sato et al., 2009; Tran et al., 2009). Indeed, it is for exactly this reason that significant investments have been made to establish and study large animal models of human arrhythmogenic diseases thought to result from repolarization abnormalities (Brunner et al., 2008; Koren, 2009).

In contrast, the structure of murine EC coupling pushes the mouse heart toward arrhythmogenic mechanisms that rely upon unstable SR Ca^{2+} handling, and away from mechanisms that result directly from repolarization instabilities due to $I_{Ca,L}$ or other surface membrane currents. In particular, the large and rapidly activating outward K^+ currents in the mouse and rat permit only a very brief AP. This both limits the degree to which I_{CaL} can contribute to contractile Ca^{2+} and necessitates a larger contribution from the SR Ca^{2+} store (∼92%) (Bers, 2001). This promotes instability in both systolic and diastolic Ca^{2+} handling. Indeed, the mouse has proven to be a very useful model for studying arrhythmia phenotypes resulting from aberrant spontaneous SR Ca^{2+} release (Lehnart et al., 2008; Kashimura et al., 2010; Bai et al., 2013), and we have also shown that unstable triggered Ca^{2+} release recruits unique EAD dynamics in mice (Edwards et al., 2014). *In vivo* studies utilizing simultaneous ECG and surface mapping (monophasic AP or optical mapping) have suggested that the dominant mechanisms of arrhythmia in these mice are focal activity (perhaps originating from DADs in the His-Purkinje network), and APD alternans driven by aberrant SR Ca^{2+} handling (Lehnart et al., 2006; Cerrone et al., 2007). Together, these characteristics have led us to hypothesize that destabilized Ca^{2+} handling is a fundamental requirement for triggered arrhythmia in the mouse, and that in the absence of intact SR Ca^{2+} release, even a dramatically altered balance of sarcolemmal currents is not sufficient to elicit arrhythmia in response to commonly applied neurohormonal challenge.

To interrogate this hypothesis, we have examined *in vivo* and cellular arrhythmogenesis in a conditional SR Ca^{2+} ATPase type 2 (SERCA2) knockout mouse (KO). These mice progress to contractile failure in 7–10 weeks and display remarkable adaptations to the rapid loss of cardiac SR Ca^{2+} reuptake (Andersson et al., 2009; Liu et al., 2011; Li et al., 2012; Swift et al., 2012; Land et al., 2013). Most prominently, the Ca^{2+} fluxes responsible for supporting myofilament activation shift from the SR to the sarcolemma, with several fold increases in the inward currents attributable to I_{CaL} and forward mode Na^+-Ca^{2+} exchange (I_{NaCa}). In combination, these adaptations constitute a genetic model of extreme loss of I_{CaL} control in the mouse, and present a unique opportunity to directly dissect the role of sarcolemmal versus intracellular mechanisms in murine arrhythmia.

At end-stage life we found SERCA2 KO mice are remarkably resistant to arrhythmia, both at the cellular level and in intact conscious animals. This resistance exists in the face of large increases in both I_{CaL} and Na^+-Ca^{2+} exchange, both of which contribute to marked prolongation of the AP and are ordinarily interpreted as strongly proarrhythmic changes. In combination, these data strongly suggest that SR Ca^{2+} release is required for cellular arrhythmogenesis and tissue-level triggered events in the mouse.

MATERIALS AND METHODS

All experiments were performed in accordance with the Norwegian Animal Welfare Act, which conforms to NIH guidelines (NIH publication No 85-23, revised 1996).

Mouse Model

The SERCA2 knock out mouse (KO) has previously been described and studied in detail as a model of contractile failure (Andersson et al., 2009; Liu et al., 2011; Li et al., 2012; Swift et al., 2012; Land et al., 2013). Briefly, cardiac-specific SERCA2 KO excision was achieved by tamoxifen activation of Cre-recombinase (α-MHC driven MerCreMer) via a single tamoxifen injection at 8–12 weeks of age. Here we studied these animals near to their mean age of death at 7 weeks after tamoxifen injection, when they exhibit pronounced contractile dysfunction, and markedly reduced cardiac output (Andersson et al., 2009). Age-matched flox/flox mice (FF) were used as controls.

Electrocardiography

Telemetry transmitters (Physiotel ETA-F10, Data Sciences International, St. Paul, MN, United States) were used to record electrocardiograms in freely moving animals. Implantation was performed 6 weeks after tamoxifen injection, and as previously described (Manotheepan et al., 2016). Intraperitoneal

Xylazine hydrochloride and ketamine hydrochloride were administered in combination with isoflurane inhalation (1–4%) during the procedure, and subcutaneous buprenorphine was given toward the end of the procedure for postoperative analgesia. The transmitters were placed subcutaneously in the dorsal thoracolumbar region, and stabilized by ligatures to the dorsal muscles. Leads were attached to the pectoral muscles by ligatures in the upper left and lower right pectoral regions. Electrocardiograms were recorded after 7 days recovery from surgery, and recordings were analyzed for heart rate as well as ECG parameters during baseline conditions, and after a subsequent intraperitoneal injection of adrenalin (Epi, 0.5mg/kg). Analysis was performed manually and in fully-blinded fashion by the same experienced technician using both proprietary software (Matlab version 2013b, The Mathworks, Natick, MA, United States), and Ponemah (Data Sciences International, St. Paul, MN, United States). Steady state ECG analyses were performed by applying conventional definitions for all intervals. Of note, because the mouse often exhibits a pronounced J-wave we have defined QRS width (duration) as the time from first negative deflection after the P-wave to the first time after the S-wave minimum at which the ascending voltage signal crosses the isoelectric line. Rate dependent QT correction was performed by the Bazzet formula:

$$QTc = \frac{QT}{\sqrt{RR}}$$

Premature ventricular complexes (PVCs) were manually identified, and episodes of ventricular tachycardia (VT) were defined as 4 or more PVCs occurring in sequence. Runs of VT were defined as non-sustained (NSVT) if they lasted less than 20-s, and as sustained (SVT) if longer.

Cell Isolation

Cardiomyocytes were isolated from ventricles of FF and KO mice similarly to our prior studies (Ottesen et al., 2015; Manotheepan et al., 2016). Briefly, mice were isoflurane-anesthetized (98% oxygen, 2.0% isoflurane), and euthanized by cervical dislocation. Excised hearts were first rinsed in ice-cold isolation buffer containing (mM): 130 NaCl, 25 Hepes, 22 D-glucose, 5.4 KCl, 0.5 $MgCl_2$, 0.4 NaH_2PO4 (pH 7.4). Each heart was then retrograde-perfused under constant flow conditions (3 ml/min) with warmed (37°C) isolation buffer for 4 min, and then with the same buffer supplemented with 400 U/ml collagenase Type II (Worthington Biochemical Corporation, Lakewood, NJ, United States) and 0.015 mmol/L Ca^{2+}. After 10 min of enzyme perfusion, hearts were cut down and the left ventricle was removed, diced, and triturated in collagenase-free isolation buffer including 1% BSA and 0.02 U/L deoxyribonuclease I (Worthington), again at 37°C. The resulting cell suspension was filtered (200 μm nylon mesh) and sedimented, the cell pellet was washed in isolation buffer supplemented with 1% BSA, and Ca^{2+} was progressively reintroduced (0.05, 0.1, 0.2, and 0.5 mmol/L). The Ca^{2+}-tolerant cardiomyocytes were stored at room temperature until use, which occurred within 8 h of isolation.

Cell Electrophysiology

Single rod-shaped cardiomyocytes with clear striations were patch-clamped in whole-cell configuration using Axoclamp 2A and 2B amplifiers. Borosilicate patch-pipettes had resistances of 2–3 MOhms with the corresponding internal and external solutions. We used identical solutions for current clamp AP recordings and end-pulse K^+ currents in voltage clamp, where the internal solution contained (in mM: 120 K-Asp, 25 KCl, 0.5 $MgCl_2$, 6 NaCl, 4 K_2-ATP, 0.06 EGTA, 10 HEPES, and 10 D-Glucose, pH corrected to 7.2 with KOH), and external (in mM): NaCl 140, HEPES 5, KCl 5.4, $MgCl_2{\cdot}6H_2O$ 0.5, Glucose 5.5, $NaH_2PO_4H_2O$ 0.4, $CaCl_2$ 1. For voltage clamp recordings of the transient outward potassium current (I_{to}), the internal solution contained (in mM) 110 K-Asp, 20 KCl, 0.5 $MgCl_2$, 4 K_2-ATP, 5 EGTA, 5 HEPES, and 10 D-Glucose - pH 7.2 with KOH, with a Na^+ and Ca^{2+} free external solution (mM): 140 CholineCl, 1 $CdCl_2$, 0.5 $MgCl_2$, 5 HEPES, 5.5 Glucose, 5.4 KCl, pH 7.2 with KOH. For $I_{Ca,L}$ the internal solution was (mM) 130 CsCl, 0.33 $MgCl_2$, 4 Mg-ATP, 0.06 EGTA, 10 HEPES and 20 tetraethylammonium chloride - pH 7.2 with CsOH, and the bathing solution included (mM) 135 NaCl, 20 CsCl, 1 $MgCl_2$, 10 glucose, 10 HEPES, 1 $CaCl_2$, and 4 4-AP (pH 7.4).

Electrophysiologic Protocols

Cells were superfused with external solution in all experiments, and all current measurements were made during step-pulse protocols at 1 Hz. Following ten 50-ms conditioning pulses (also 1 Hz) to 0 mV from a holding potential of −70 mV, I_{CaL} was elicited by a 200-ms depolarizing voltage step (Mørk et al., 2009). Test potentials ranged from −40 to +50 mV with 10-mV increments from a post-train holding potential of −40 mV (to inactivate I_{Na}). Current amplitude was measured as the difference between peak inward current and steady-state current at the end of the test pulse. I_{to} (peak I_K) was elicited by 300-ms steps to test potentials between −40 and +60 mV in 10-mV increments from a holding potential of −70 mV (Louch et al., 2010a). Peak I_K was calculated as the peak outward current less the steady-state end pulse current from these 300-ms steps. The pedestal or plateau component of I_K (I_{Kp}) was calculated as the mean of the final 20-ms of 500-ms test-pulse steps between −100 and +60 mV, again at 10 mV increments from a –70 mV holding potential. All currents were normalized to capacitance, which was calculated as the integral of the transient current response to a 10-mV hyperpolarizing step (150 ms) from a holding potential of −70 mV.

Action potential waveforms were also recorded at 1 Hz in all experimental conditions, and at least 20 sequential beats were allowed to achieve steady state. In experiments assessing EAD and DAD susceptibility, Iso-containing superfusate (1 μM) was applied after 30-s of baseline recording, and maintained for at least 3 min further.

Mathematical Modeling

The computational models used here are modifications of those published by Li et al. (2012). Briefly, both the FF and KO models were constructed on the basis of extensive data collected in the FF

and KO mice at the same age and time after SERCA gene excision as studied here. Our modifications here were made sequentially to establish the requirements for the observed AP changes accompanying SERCA-KO. Thus, we describe them in that sequence in the results section. All parameter changes and details for code access are provided in the **Supplementary Material**.

Statistics

Steady state electrocardiographic parameters were assessed by repeated measures ANOVA (RMANOVA: Genotype × Epi) with repeated measures for Epi. ECG arrhythmia outcomes (PVC and NSVT frequency) were non-normally distributed, and interrogated by Kruskal-Wallis rank sum test after being separated into baseline and Epi recordings. Similarly, skewed data for EAD frequency were assessed via the Kruskal-Wallis test, and the Fisher exact test was used to determine differences in EAD incidence. Peak I_K, I_{Kp}, I_{CaL}, and AP durations at 20, 50, 70, and 90% repolarization were all tested by RMANOVA where step potential was repeated for current measurements, and treatment conditions (Ca^{2+} concentration, Nifedipine, or Isoproterenol) were repeated for AP recordings.

For all RMANOVAs, the Holm-Sidak test was used to identify pairwise effects *post hoc*. In the event that the sphericity assumption was not valid, RMANOVA was replaced by the Mann-Whitney-Wilcoxon test. Significant effects were defined at $p < 0.05$, and p-values are explicitly stated for all marginal results ($0.05 \leq p \leq 0.1$). All statistical analyses were performed either with SigmaPlot (Systat Software Inc., CA, United States), or R software (version 3.2.1, The R Foundation of Statistical Computing).

RESULTS

SERCA2-KO Mice Exhibit Unique but Stable Changes in Global Cardiac Electrophysiology

Seven weeks after gene excision, KO mice exhibit a range of electrophysiologic dysfunction as measured by telemetered ECG. The most pronounced effects are slowed ventricular activation observed as increased QRS width ($p < 0.01$, **Figure 1A**, left), and a much more prominent and positive-going T-wave than is normally measurable via standard lead II recordings in the mouse ($p < 0.0001$), particularly during epinephrine challenge (**Figures 1B,C**). Interestingly, these changes exist in the absence of significant rate-corrected QT prolongation ($p = 0.07$, **Figure 1A**, right), thus suggesting that terminal repolarization is not delayed in the KO mice. These outcomes will be discussed in more detail later, but are consistent with a markedly altered AP morphology in the KO myocytes.

The combined influence of these electrocardiographic abnormalities did not result in a higher frequency of either isolated PVCs or runs of non-sustained (or sustained) VT ($p > 0.1$). In fact, during Epi challenge we observed reduced frequency of PVCs ($p < 0.05$) and a tendency for reduced NSVT frequency in the KO group ($p = 0.09$, **Figure 1D**). Together, these observations suggest that while the KO mice exhibit clear disturbances to global cardiac electrophysiology, they remain resilient to arrhythmia.

SERCA2-KO Myocytes Have Prolonged Action Potentials Due to Markedly Increased Sarcolemmal Ca^{2+} Fluxes

Figure 2 shows the effect of SERCA2 loss on the cardiomyocyte AP and underlying currents. At the level of the AP (**Figure 2A**), the outstanding feature is a brief early plateau in KO myocytes, which is reminiscent of the phase 2 plateau in large mammals albeit much shorter (∼20 ms). Mechanistically, this plateau indicates that the balance of currents in early repolarization is shifted inwardly, particularly in the region between +20 and −20 mV. This effect was pronounced, and can be seen as a 273% longer APD_{50} and 230% longer APD_{70} in KO myocytes (both $p < 0.01$). Panels B and C show that this effect is due to modest potentiation of peak I_{CaL} (39% increase at 0 mV, $p < 0.001$), and dramatically slowed I_{CaL} inactivation (50% relaxation time at 0 mV is increased by 178% in KO, $p < 0.001$), which together result in a 200% increase in Ca^{2+} influx, measured as the I_{CaL} integral during the square-pulse voltage clamp protocol ($p < 0.001$). Exacerbating this gain in I_{CaL} was a moderate reduction of end-pulse potassium current (I_{Kp}) at positive potentials ($p < 0.05$). While we did not attempt to experimentally dissect the different components of this current, we used a computational model to assess the ability of those components to contribute to the observed changes in AP morphology. These analyses are described in further detail below.

In **Figure 3** we elaborate on the role of I_{CaL} in slowing early repolarization either by acutely changing superfusate Ca^{2+} concentration, or applying I_{CaL} blockade by Nifedipine (Nif, 1 μM). **Figure 3A** shows that the difference in APD_{50} and APD_{70} is removed when Ca^{2+} is excluded from the bath, and slightly exaggerated when it is increased to 1.8 mM (both $p < 0.05$). These alterations in extracellular $[Ca^{2+}]$ did not have statistically discernible effects on the kinetics of early repolarization in FF myocytes ($p > 0.1$). Because field-screening effects and non LCC-specific Ca fluxes^{2+} (such as Na^+/Ca^{2+} exchange) will be altered by modulation of extracellular Ca^{2+}, we also used Nifedipine to pharmacologically antagonize I_{CaL} (**Figure 3C**). As for removal of extracellular Ca^{2+}, this maneuver eliminated virtually all of the delay in early repolarization present in the KO myocytes – APD_{50} and APD_{70} were almost completely normalized (both $p < 0.01$ vs. control superfusion). This suggests that inward I_{CaL} is the major contributor to the small phase 2 plateau in KO cells. Finally, to determine whether maneuvers that ordinarily modulate Ca^{2+}-dependent I_{CaL} inactivation (via SR Ca^{2+} release) are ineffective in KO mice, we also assessed the frequency-dependence of peak I_{CaL} and I_{CaL} inactivation (**Supplementary Figure 1**). In moving from 0.1 to 1 Hz FF animals exhibit slowed I_{CaL} inactivation due to well-known Ca^{2+}-dependent facilitation, and this property is dependent on cytosolic Ca^{2+} (Fauconnier et al., 2003). In KO animals this frequency-dependent modulation of I_{CaL} inactivation is completely absent (given the already very

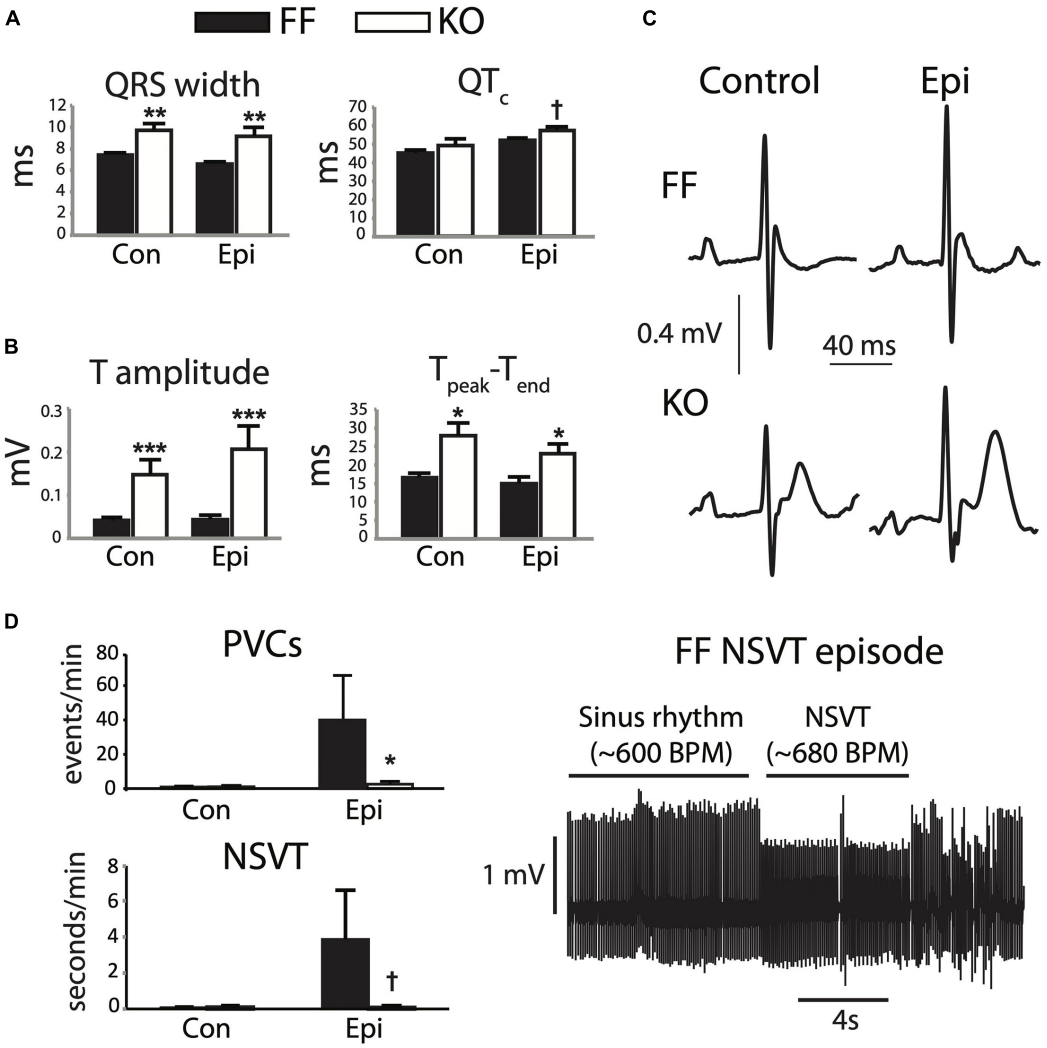

FIGURE 1 | SERCA2-KO mice exhibit unique alterations in global cardiac electrophysiology. Telemetered ECG recordings from 8 animals in each group were first analyzed for steady state characteristics from periods exhibiting only normal sinus activation sequence **(A,B)**. KO mice showed increased QRS width (**A**, left), and marked increases in T-wave amplitude and duration **(B)**. **(C)** Typical sinus waveforms recorded from FF and KO animals. Ectopic activity was also analyzed **(D)**, and KO animals surprisingly exhibited a reduced frequency of total ectopy (PVC frequency, top left), and a trend for fewer runs of non-sustained VT (bottom left), during Epi challenge. All panels: $^{\dagger}p < 0.1$ KO vs. FF, $^{*}p < 0.05$ KO vs. FF, $^{**}p < 0.01$ KO vs. FF, $^{***}p < 0.001$ KO vs. FF. Data are means ± SEM.

slow inactivation in KO myocytes), further indicating the loss of SR-dependent I_{CaL} control in KO animals.

Importantly, this shift in balance during early repolarization is not mirrored by slowed terminal repolarization. That is, the differences present at APD_{50} and APD_{70} are lost by 90% (APD_{90}) repolarization. The dominant inward currents modulating this late phase of repolarization in the mouse are I_{NaCa} and recovering I_{Na} (Edwards et al., 2014; Morotti et al., 2014). As described further below these inward currents compete with several components of I_K, particularly the inward rectifier K^+ current (I_{K1}) to shape terminal repolarization. While we have not directly assessed the balance of these currents during late repolarization in KO myocytes, the near complete absence of triggered Ca^{2+} release (Andersson et al., 2009) drastically reduces the potential for inward I_{NaCa}. The slower early repolarization would also be expected to limit I_{Na} recovery and the potential for I_{Na} reactivation.

EAD Dynamics in SERCA2-KO Myocytes Share Characteristics of Small and Large Mammals

In larger mammals, the increases in I_{CaL} peak current and 50% relaxation time would be expected to promote repolarization instabilities and EADs. To assess EAD susceptibility we challenged KO and FF myocytes with Isoproterenol (1 μM) for at least 3 min while pacing at 1 Hz in current clamp, and defined EADs as any upward deflection in the voltage signal exceeding 3 mV. **Figure 4A** shows that under these conditions EAD incidence and frequency were not increased in KO cells

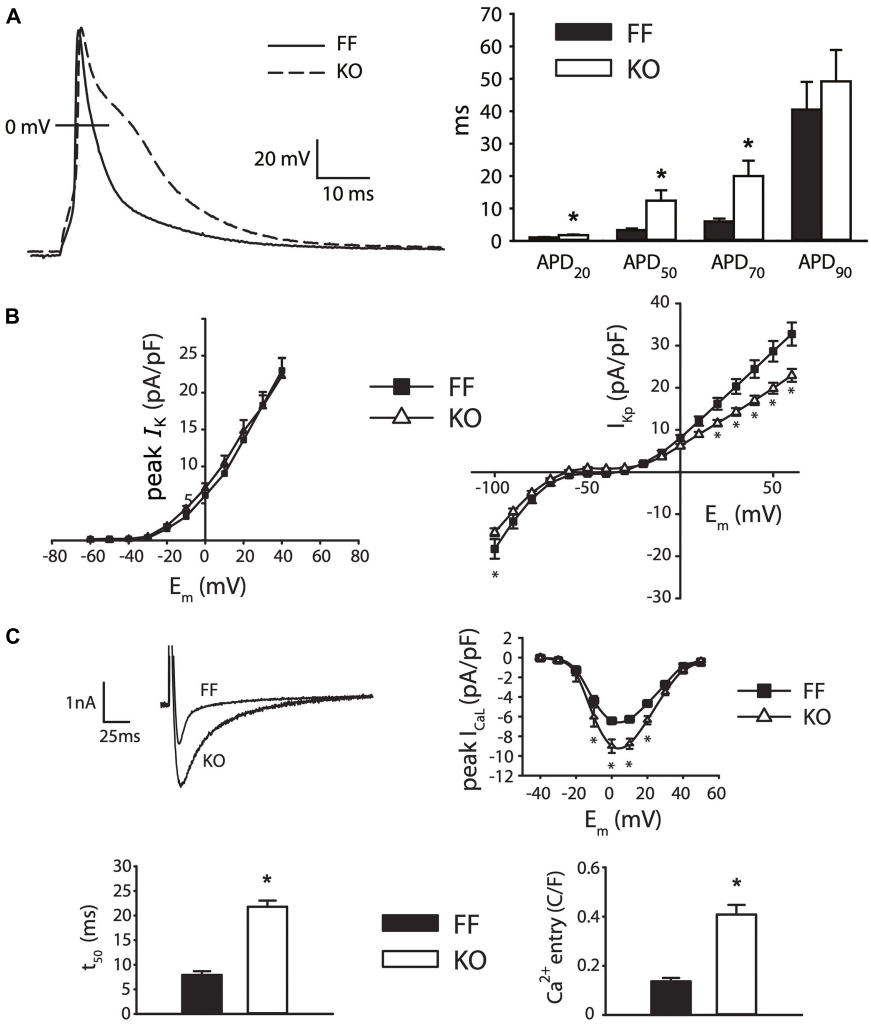

FIGURE 2 | Myocytes from failing SERCA2-KO hearts exhibit prolonged early repolarization due to exaggerated sarcolemmal calcium flux. **(A)** KO myocytes (n = 10) display marked prolongation of early repolarization compared to FF (n = 11), although this difference is normalized by 90% repolarization. **(B)** The dominant outward current during early repolarization (I_{to}), is unaltered in the failing KO myocytes relative to FF (n = 10, both groups; left panel), while slowly inactivating K^+ current components (measured as end-pulse, "pedestal" or "plateau," K^+ current – I_{Kp}) were slightly suppressed in KO cells (n = 17) relative to FF (n = 20). **(C)** However, peak I_{CaL} is potentiated and I_{CaL} inactivation is dramatically slowed in KO cells (n = 14) versus FF (n = 12), leading to a marked increase in calcium influx. All panels: *$p < 0.05$. Data are means ± SEM.

(both $p > 0.1$), rather EAD frequency tended to be higher (albeit non-significantly, $p > 0.05$) in the FF (9.3 ± 4.7%) than KO group (2.1 ± 1.8%). In FF cells, EADs exhibited signature properties identified in previous work (Sato et al., 2009; Tran et al., 2009). These features included periods with very high APD variability, indicating variable timing of terminal repolarization, but also intermittent beats that did not exhibit EADs. Furthermore, analysis of EAD take-off potentials (**Figure 4B**) suggests that EADs in the FF group exhibited very similar underlying dynamics to those we have described previously in the mouse, and different to those in larger mammals (Edwards et al., 2014). That is, they initiated at potentials too negative (−55 ± 7 mV) to be carried by I_{CaL}, and occurred too soon after stimulation (34.6 ± 2.7 ms; approximately coinciding with the peak of the bulk cytosolic Ca^{2+} transient) to result from subcellular Ca^{2+} waves. Thus, it is very likely that EADs in FF myocytes were carried almost entirely by non-equilibrium reactivation of the fast component of the sodium current (I_{Na}) (Edwards et al., 2014). In contrast, the EADs present in KO myocytes initiated at more positive take-off potentials (−41.8 ± 2 mV, $p < 0.001$), were much larger in amplitude (KO = 26.4 ± 9 mV vs. FF = 7.8 ± 2.6 mV; $p < 0.001$), and lasted much longer than EADs in the FF myocytes (KO = 124 ± 24 ms vs. FF = 55 ± 27 ms; $p < 0.001$). While these EADs initiated later than those in FF cells, because spontaneous SR Ca^{2+} release in KO cells is virtually negligible (**Supplementary Figure 2**), it is very unlikely that discoordinated SR Ca^{2+} release made any contribution to these events. Even after accounting for leftward shifts in I_{CaL} activation due to β-adrenergic activation (Bean et al., 1984; Tiaho et al., 1991; Kumari et al., 2018), the −40 mV take-off potentials are still

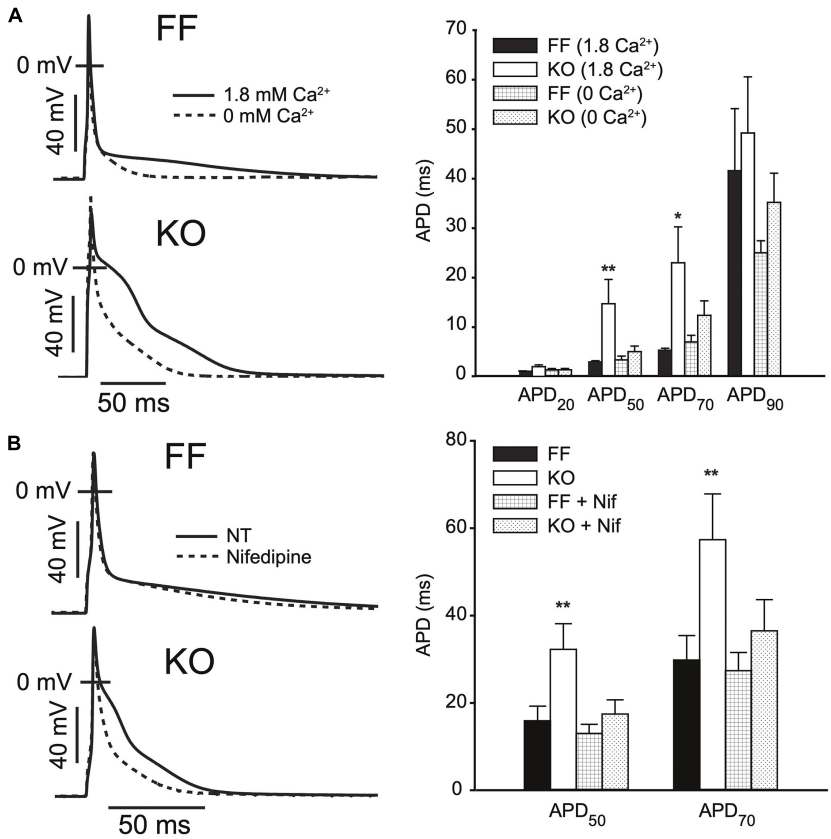

FIGURE 3 | AP prolongation in SERCA2-KO myocytes relies upon augmented L-type calcium current. **(A)** Superfusing FF (n = 7) and KO (n = 8) myocytes with nominally Ca^{2+} free extracellular solution abolishes early AP prolongation in KO myocytes, while elevating extracellular Ca^{2+} to 1.8 mM exaggerates the difference in APD_{50} and APD_{70} (**$p < 0.05$ FF vs. KO at 1.8 mM Ca^{2+}; and $p < 0.05$ KO at 1.8 mM vs. 0 mM Ca^{2+}, *$p < 0.0$ KO at 1.8 mM vs. 0 mM Ca^{2+}). **(B)** I_{CaL} blockade via Nifedipine (1 μM) achieves similar normalization of APD_{50} and APD_{70} in KO myocytes (n = 7) relative to FF (n = 7). **$p < 0.05$ FF vs. KO in control superfusate; and $p < 0.05$ KO in control vs. Nifedipine. All panels: data are means ± SEM.

only just approaching the lower limit of the I_{CaL} activation range, thus the ability for I_{CaL} to have directly contributed to initiation of these EADs is somewhat limited. However, once initiated, the large amplitude excursions of these EADs (see for example **Figure 4B** bottom left) suggest that I_{CaL} reactivation is pronounced and likely to be the dominant contributor to EAD dynamics, as it is in ventricular myocytes of large mammals (Weiss et al., 2010).

The Ability for Sarcolemmal Ca^{2+} Fluxes to Shape Murine Repolarization Depends on K^+ Current Activation Kinetics and Non-equilibrium Na^+ Current Dynamics

In considering the balance of currents shaping the trajectory of repolarization in the mouse, an important quantitative aspect is how rapid early repolarization favors I_{CaL} deactivation and limits the opportunity for Ca^{2+}-dependent I_{CaL} inactivation, which is prominent in larger species. Combining this with the known redundancy and different kinetic characteristics among the various K^+ currents active in this early phase of repolarization, it becomes much more difficult to predict or account for how changes in I_{CaL} regulation can contribute to modulating early repolarization. To interrogate these dynamics, we employed a published computational model of the mouse cardiomyocyte, which is specifically parameterized to incorporate the reduced SR Ca^{2+} handling and altered Na^+ balance in failing KO myocytes [16]. This model already incorporates the increased Cav1.2 and NCX1 expression in KO cells, which leads to exaggerated peak I_{CaL} and $I_{NaCa.}$ However, it does not fully capture the pronounced slowing of I_{CaL} inactivation we have observed in KO myocytes at 7 weeks of age, and incorporating this characteristic was our first alteration. **Figure 5A** shows the behavior of the reparameterized I_{CaL} model in square-pulse voltage-clamp protocols identical to our experiments (all parameter changes are provided in full in **Supplementary Table 1**). Even for its larger peak current and much slower inactivation, this I_{CaL} model was still overwhelmed by the fast component of the transient outward current ($I_{to,f}$) during early repolarization in both the FF and KO models, and had relatively little impact on the trajectory of early repolarization (APD_{20}, **Figure 5C**).

As mentioned above, KO myocytes also exhibit a reduction in the measurable total I_K at the end of our 500 ms test steps. The molecular identity of K^+ channels contributing to this

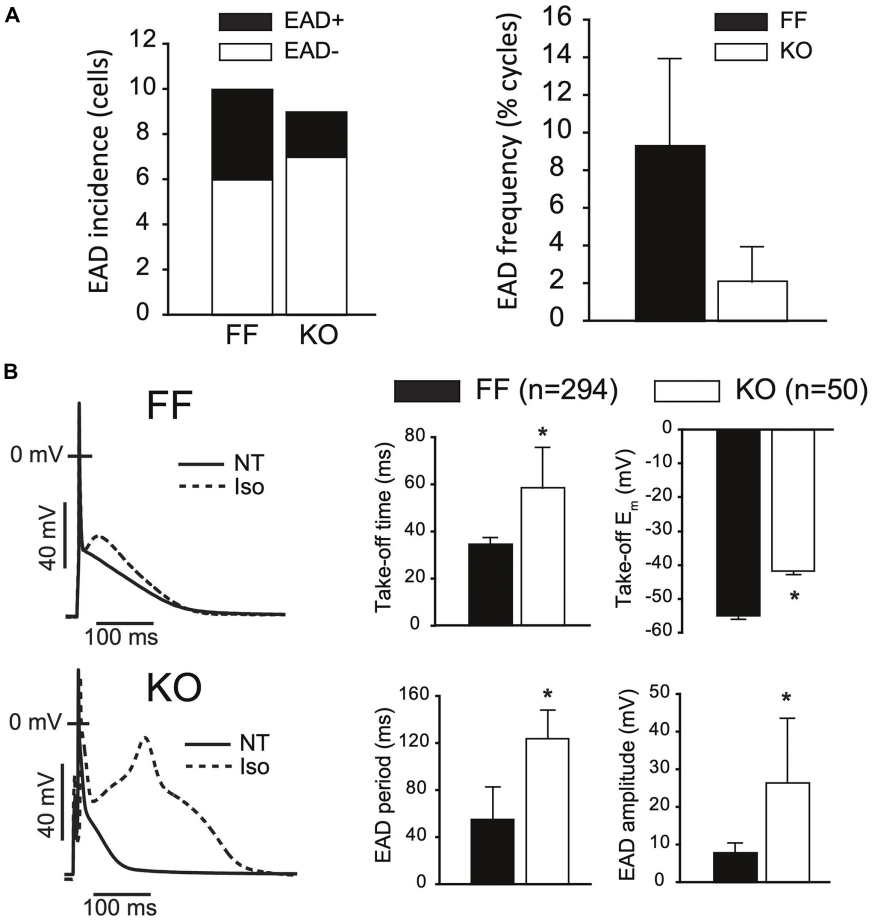

FIGURE 4 | SERCA2-KO myocytes are not more susceptible to EADs but exhibit altered EAD dynamics. **(A)** KO cells (n = 9) did not exhibit a higher incidence (left panel: 2/9 KO cells vs. 4/10 FF cells, $p > 0.01$), or frequency (right panel: 50/3037 total KO cycles vs. 293/2593 total FF cycles, $p > 0.01$) of EADs relative to FF (n = 10). **(B)** However, KO EADs exhibit altered dynamics as indicated by increased amplitude, period and time to initiation, and reduced (more positive) take-off potentials. All panels: $^*p < 0.05$. Data are means ± SEM.

slowly inactivating current are not fully reconciled, although it is clear that the slow component of the transient outward current (carried by the Kv1.4 alpha subunit) is minimally expressed in mice, and that currents carried by Kv1.5 and Kv2.1 make important contributions (Nerbonne, 2014). Together these channels carry the slowly inactivating current (I_{Kslow}), also commonly referred to as the ultrarapidly activating delayed rectifier (I_{Kur}) K^+ current. I_{Kslow} is a dominant contributor to the end-pulse K^+ current in mice. It combines with the steady state K^+ current (I_{Kss}, primarily carried by TASK1 and TREK1 channels (Nerbonne, 2014), and I_{K1} at more negative potentials, to comprise the compound end-pulse I_K that we term the "pedestal" or "plateau" I_{Kp}. Due to difficulties in separating the activation kinetics of the Kv1.5 and Kv2.1 contributions to I_{Kslow} in cardiac cells, most models have assumed that this current is a single functional entity, with very rapid activation and slow inactivation. One relatively recent model separated the currents for the purpose of implementing differing phosphoregulation and inactivation kinetics (Morotti et al., 2014). To simultaneously fit intermediate AP prolongation (APD_{50} and APD_{70}) and measured end pulse I_K with the KO model, we also had to employ the approach of Morotti et al. (2014) and separate I_{Kslow} into Kv1.5-($I_{Kslow,1}$) and Kv2.1-($I_{Kslow,2}$) specific components. However, unlike Morotti et al. (2014) we implemented slower activation kinetics for $I_{Kslow,2}$, as shown in **Figure 5B**, and which can be measured for Kv2.1 in heterologous systems (Gordon et al., 2006). These slower activation kinetics of Kv2.1 slowed the onset of I_{Kslow} enough to permit I_{CaL} modulation of intermediate repolarization, while also matching end-pulse I_K and permitting stable overall repolarization, as observed in our experiments.

EAD Dynamics in KO Myocytes Are a Mix of Mouse EAD Dynamics and Larger Mammal EAD Dynamics

We employed mathematical models specific to the KO and FF myocytes (Li et al., 2012) and challenged them with a simple model implementation of β-adrenergic stimulation, which is closely analogous to our experimental challenge. This strategy involves implementing established effects of

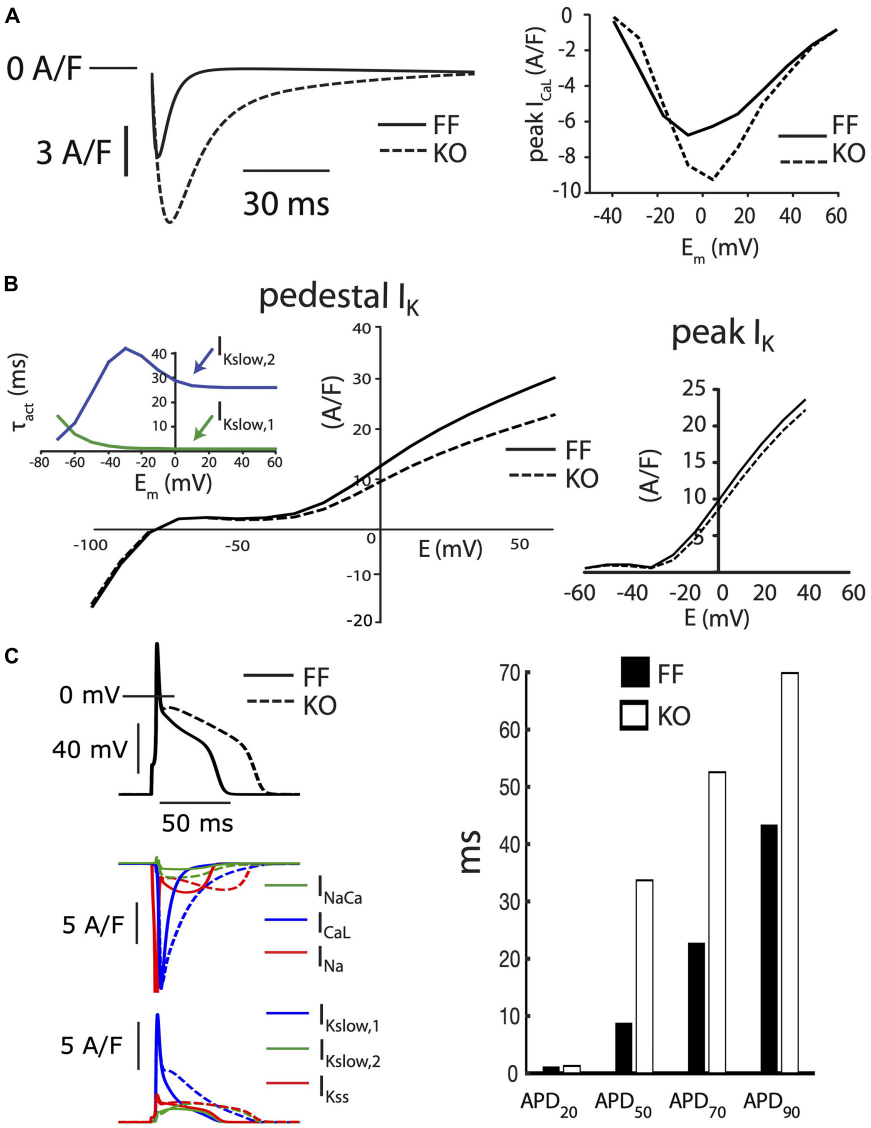

FIGURE 5 | Baseline FF and KO computational models. **(A)** I_{CaL} in the KO model was parameterized to permit the markedly slowed I_{CaL} inactivation accompanying loss of SR calcium release (left panel) and moderately increased peak current observed in KO myocytes (right panel). **(B)** Conductances for the slower activating component of I_{Kslow} (Kv2.1, $I_{Kslow,2}$) and the steady state K^+ current (I_{Kss}) were both reduced by 25% to fit end-pulse "pedestal" total I_K (main left panel). Simulated currents were assessed as the sum of all end-pulse K^+ currents as for the experimental measurements shown in **Figure 2**, where this compound current is referred to as I_{Kp}. To simultaneously fit the pedestal and peak components of the compound I_K, as well as differences in I_{CaL} and steady state APD, it was necessary to implement the slower activation kinetics of Kv2.1/$I_{Kslow,2}$ (inset left). Peak I_K was straightforwardly fit through scaling the conductance of $I_{to,f}$ in both the FF and KO models (right panel). **(C)** Together, these alterations resulted in slowed intermediate repolarization (APD_{50} and APD_{70}) similar to that observed for KO myocytes. However, the slower early repolarization and rapid late repolarization in KO cells were much more difficult to capture with models that remained faithful to the voltage-clamp measurements. See **Supplementary Table 1** for complete details of differences between these two baseline models.

β-adrenergic regulation at I_{CaL} (2–3 fold increased whole-cell permeability, P_{CaL}, and 5–10 mV left-shifted steady state activation), SERCA (50–60% reduction in the K_m for cytosolic Ca^{2+} binding), the Na^+-K^+ ATPase (25–30% reduction in the K_m for cytosolic Na^+ binding), and I_{Kur} (15–20% increase in whole cell conductance) (Edwards et al., 2014). The steady-state baseline models for the FF and KO myocytes were each simulated for 3 min at 1 Hz after applying these β-adrenergic parameter changes. Via this approach, EADs could be initiated in both the FF and KO models with identical changes to these key parameters, which remained wholly within the physiologic range. The EADs that result share several of the key features of EADs observed in our experiments during saturating Isoproterenol challenge. First the KO EADs exhibit greater I_{CaL} reactivation, and their dynamical characteristics (oscillation period and amplitude) are increased similarly to the experimental recordings (**Figure 4B**). These dynamic characteristics are similar to those of I_{CaL}-dominated EADs in large mammals (Sato et al., 2010).

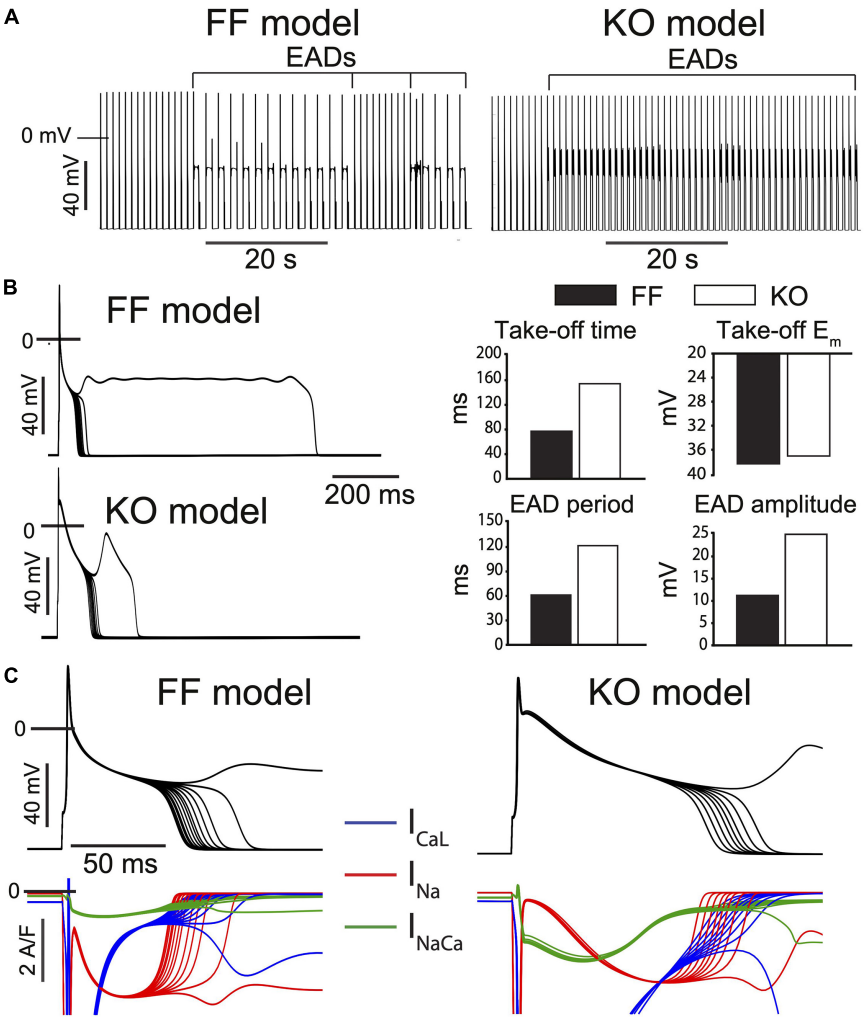

FIGURE 6 | Progressive β-adrenergic challenge was simulated in both the FF and KO models [13] and recapitulate the major differences in EAD dynamics observed experimentally. **(A)** Both models transition to an unstable repolarization regime involving EADs. **(B)** Analysis of the EAD oscillations suggest the model dynamics are similar to those observed experimentally, where EAD amplitude, period and time of initiation are all increased in KO cells, while take-off potential is only slightly more positive. **(C)** Somewhat surprisingly, EAD initiation and the transition into the unstable regime is driven by non-equilibrium reactivation of I_{Na} rather than reactivation of I_{CaL} in both models, although this dominant role for I_{Na} is slightly more clear for the FF model.

However, importantly, and somewhat surprisingly, even though the model EADs occurred at relatively positive potentials (approximately −38 mV) and relatively late (80 to 120 ms after the AP stimulus), they were initiated in both models by non-equilibrium reactivation of I_{Na} (Edwards et al., 2014) rather than I_{CaL} (**Figure 6C**). This suggests that even for EADs that initiate 120 ms after the AP peak, recovery from inactivation of I_{Na} is sufficient to permit an arrhythmogenic current reactivation.

DISCUSSION

The ability for SR Ca^{2+} release to act as a cellular driver of cardiac arrhythmia has been appreciated for at least 30 years (Lederer and Tsien, 1976), and is widely recognized as a mechanistic contributor to all major cellular arrhythmogenic behaviors (automaticity, EADs, DADs, and APD alternans). The relative importance of SR Ca^{2+} fluxes in each behavior is highly dependent on the electrophysiologic context, and in this study we highlight species-specificity. By studying the electrophysiologic characteristics of murine SERCA2 knock out, we have assessed the ability for membrane versus SR mechanisms to generate arrhythmia upon the background of the characteristically large repolarizing currents in the mouse. We report four findings that are likely to hold important implications for other studies assessing electrophysiologic outcomes in mice, both in health and disease: (1) Shifting the burden of contractile calcium flux away from the SR and toward the sarcolemma elicits a pronounced, positive, and prolonged T-wave that is not normally observable in mice. While these effects are substantial, they are not sufficient to destabilize cardiac activation or repolarization. (2) The major cellular effect underlying these global changes is a very large

increase in I_{CaL}-mediated Ca^{2+} influx, due largely to slowed current inactivation, and which results in a pronounced delay of early repolarization creating an unusual AP plateau around 0 mV. (3) This slowing of early repolarization is difficult to capture in models due to the rapid kinetics of the large measurable peak I_K, which is broadly thought to be carried by $I_{to,f}$ and $I_{Kur}/I_{Kslow,1}$. The manner in which K^+ current activation interacts with I_{CaL} inactivation to shape early repolarization of the murine AP in this way requires further review. (4) The overall shift in the balance of membrane currents in SERCA2-KO away from a mouse-like phenotype and toward a large mammalian phenotype recruits EAD dynamics that are closer to those in large mammals. However, this shift is not sufficient to increase EAD frequency or incidence, and initiation of infrequent EADs in KO myocytes still likely relies upon I_{Na} reactivation, which rarely drives EADs in large mammalian myocytes.

The appearance of gross ECG changes in KO mice, particularly in T-wave amplitude, was remarkable and somewhat surprising given that the T-wave is often virtually absent in mice (Liu et al., 2004). However, these effects are captured by other models of pronounced induction of I_{CaL} in mice and rats. Early rat studies of agonist dihydropiridines (Bay K 8644), which both potentiate and markedly prolong $I_{CaL,}$ noted similar overall changes and included additional ST segment elevation due to fusion of the QRS complex and T-wave (Abraham et al., 1987). Similarly in the mouse, β-adrenergic stimulation elicits a roughly twofold increase in T-wave amplitude (0.16 mV), and significant dispersion of repolarization as measured by T-wave decay time (Speerschneider and Thomsen, 2013). Finally here, one genetic model with very similar changes to macroscopic I_{CaL} is Timothy syndrome (formerly type 8 long QT syndrome). While mice have been generated for major mutations known to cause this channelopathy, and brief reports suggest QT prolongation and abnormal ECG characteristics (Bett et al., 2009), we are unaware of any comprehensive description of the changes in cardiac electrophysiology present in this mouse.

Our prior work with the SERCA2-KO mouse has clearly shown that 7 weeks after genetic ablation little to no SERCA expression remains, and the SR Ca^{2+} store is essentially eliminated (Andersson et al., 2009; Louch et al., 2010b). To verify that spontaneous SR Ca^{2+} release is similarly absent in the 7-week KO mice, we also measured Ca^{2+} sparks and waves in isolated myocytes and observed that both were essentially abolished (**Supplementary Figure 2**). This is key in the context of the arrhythmogenic outcomes of interest here because it eliminates at least one major class of triggered arrhythmia resulting from spontaneous Ca^{2+} release and DADs. With respect to EADs, the implications of SERCA-KO are more complex. Previous studies have suggested that SR Ca^{2+} release is involved in murine EADs (Pott et al., 2012; Edwards et al., 2014). Specifically, we have shown that exaggerated SR Ca^{2+} release is the critical proximal mechanism of slowed late repolarization in mouse ventricle, and that this in turn elicits EADs through non-equilibrium reactivation of I_{Na} (Edwards et al., 2014). By this mechanism it is predictable that EADs and their arrhythmogenic potential would be inhibited in the KO mice. However, the established and very large increases in sarcolemmal Ca^{2+} transport in these mice create a very different electrophysiologic context. One which shifts repolarization dynamics toward those present in larger mammalian myocytes, and in principle may predispose to EADs with large mammal-like dynamics. We have shown here that this remarkable degree of plasticity is not sufficient to induce such instability.

Two important examples of genetic mouse models that exhibit very different adaptations to the SERCA-KO mouse are provided by murine knock-out and transgenic overexpression of the cardiac Na^+-Ca^{2+} exchanger (NCX1). Henderson et al. (2004) developed a cardiac-specific NCX1 knock-out (NCX1-KO) mouse that lives to adulthood and exhibits 80-90% reduction in NCX1 expression. Through a set of (virtually opposite) adaptations to those resulting from SERCA-KO, the NCX1-KO mouse also retains remarkably viable contractile function. Unlike the SERCA-KO mice, these animals exhibit much reduced sarcolemmal Ca^{2+} transport but achieve sufficient contractile activation through very high gain EC coupling (Pott et al., 2005). While they exhibit clearly shortened APs (largely due to increased $I_{to,f}$) and QT intervals, they do not present an overt arrhythmia phenotype (Pott et al., 2007). In contrast, the NCX1-transgenic mouse developed by the same group exhibits pronounced slowing of terminal repolarization (prolonged APD_{90}), EADs, and an overt susceptibility to arrhythmia (Pott et al., 2012). Taken together, these studies strongly support the remarkable ability of cardiomyocytes to autonomously reconfigure their Ca^{2+} handling and electrophysiologic machinery to support the Ca^{2+} requirements for contraction. However, they also suggest that the gene regulatory programs governing those reconfigurations are not equally apt to defend electrophysiologic stability. That is, in response to certain perturbations, the regulatory adjustments made to defend contractile Ca^{2+} will be arrhythmogenic. Our SERCA-KO mouse can be considered fortunate in this respect.

LIMITATIONS

One immediately observable characteristic of the KO myocyte AP is marked slowing of early repolarization between +20 and −20 mV. While we did not attempt to broadly reparametrize the kinetics of the $I_{to,f}$ model to fit this characteristic, it proved challenging to reconcile with our peak I_K measurements, which readily overwhelmed even the large changes in peak I_{CaL} and I_{CaL} inactivation. While we are unaware of other studies that have systematically investigated the ability for altered I_{CaL} inactivation kinetics to prolong this early portion of the murine AP, this characteristic has been clearly observed in previous studies. For example, acutely evacuating the SR store via caffeine both markedly prolongs early repolarization and accelerates later repolarization in a manner that is remarkably consistent with the AP morphology in KO myocytes [see Figure 3C in Edwards et al., 2014)]. Because the dynamics of interaction between I_{CaL} and I_K during this phase of the AP are critical for determining Ca^{2+} influx, we suggest that they deserve further investigation.

Additionally, we had limited ability to reconcile the more rapid terminal repolarization (APD_{70} to APD_{90}) in KO myocytes while constraining I_{K1} to the measured inward

end-pulse current below E_K (**Figure 2B**, right panel). We (Edwards et al., 2014) and others (Yao et al., 1998; Pott et al., 2007, 2012; Ferreiro et al., 2012) have shown that SR Ca^{2+} release and resulting inward I_{NaCa} are major modulators of this phase of the murine AP. This suggests that more detailed accounting for components of I_K that are active and available between −80 and −40 mV (particularly I_{K1}), is likely necessary for properly capturing the interaction among I_{NaCa}, recovering I_{Na} and I_K in determining the trajectory of terminal repolarization in the mouse.

CONCLUSION

The major shifts in sarcolemmal Ca^{2+} transport resulting from cardiac specific SERCA2 knock out are clearly not sufficient to destabilize myocyte repolarization or global electrophysiology in the mouse. Furthermore, those shifts only alter EAD dynamics in a relatively subtle fashion. In sum, our data suggest that, in the mouse, the destabilizing influence of extreme changes to sarcolemmal Ca^{2+} influx and extrusion can be readily outweighed by the stabilizing influence of an absent SR Ca^{2+} store and dramatic reduction in spontaneous SR Ca^{2+} release. Of course, this characteristic relies on the very strong overall repolarization present in the mouse, and should not be interpreted to extend to humans or indeed any larger mammals exhibiting an AP plateau.

DATA AVAILABILITY STATEMENT

The raw data supporting the conclusions of this article will be made available by the authors, without undue reservation.

ETHICS STATEMENT

The animal study was reviewed and approved by the Norwegian National Committee for Animal Welfare.

AUTHOR CONTRIBUTIONS

AGE collected and analyzed data, performed computational analyses, conceived and designed aspects of the study, and wrote the manuscript. HM collected and analyzed data, conceived and designed aspects of the study, and reviewed the manuscript. MKS collected and analyzed data, and reviewed the manuscript. DBL collected and analyzed data. IS conceived and designed aspects of the study, and reviewed the manuscript. SR and WEL collected and analyzed data, conceived and designed aspects of the study, reviewed the manuscript, and contributed to funding the study. OMS conceived and designed aspects of the study, reviewed the manuscript, and contributed to funding the study. All authors contributed to the article and approved the submitted version.

FUNDING

This work was financially supported by the Norwegian Research Council (Grant No. 287395) and the South-Eastern Norway Regional Health Authority (Grant No. 2013075).

SUPPLEMENTARY MATERIAL

The Supplementary Material for this article can be found online at: https://www.frontiersin.org/articles/10.3389/fphys.2021.744730/full#supplementary-material

REFERENCES

Abraham, S., Amitai, G., Oz, N., and Weissman, B. A. (1987). Bay K 8644-induced changes in the ECG pattern of the rat and their inhibition by antianginal drugs. *Br. J. Pharmacol.* 92, 603–608. doi: 10.1111/j.1476-5381.1987.tb11362.x

Andersson, K. B., Birkeland, J. A., Finsen, A. V., Louch, W. E., Sjaastad, I., Wang, Y., et al. (2009). Moderate heart dysfunction in mice with inducible cardiomyocyte-specific excision of the Serca2 gene. *J. Mol. Cell. Cardiol.* 47:187.

Bai, Y., Jones, P. P., Guo, J., Zhong, X., Clark, R. B., Zhou, Q., et al. (2013). Phospholamban knockout breaks arrhythmogenic Ca^{2+}; waves and suppresses catecholaminergic polymorphic ventricular tachycardia in mice. *Circ. Res.* 113, 517–526. doi: 10.1161/circresaha.113.301678

Bean, B. P., Nowycky, M. C., and Tsien, R. W. (1984). β-Adrenergic modulation of calcium channels in frog ventricular heart cells. *Nature* 307, 371–375. doi: 10.1038/307371a0

Bers, D. M. (2001). Excitation-contraction coupling and cardiac contractile force. *J. Cardiova. Dis. Res.* 1:45.

Bett, G. C. L., Bondarenko, V. E., and Rasmusson, R. L. (2009). Cardiac characteristics of a mouse model of timothy syndrome. *Biophys. J.* 96, 665a–666a.

Brunner, M., Peng, X., Liu, G. X., Ren, X. Q., Ziv, O., Choi, B. R., et al. (2008). Mechanisms of cardiac arrhythmias and sudden death in transgenic rabbits with long QT syndrome. *J. Clin. Invest.* 118, 2246–2259.

Cerrone, M., Noujaim, S. F., Tolkacheva, E. G., Talkachou, A., O'Connell, R., Berenfeld, O., et al. (2007). Arrhythmogenic mechanisms in a mouse model of catecholaminergic polymorphic ventricular tachycardia. *Circ. Res.* 101, 1039–1048.

Edwards, A. G., Grandi, E., Hake, J. E., Patel, S., Li, P., Miyamoto, S., et al. (2014). Nonequilibrium reactivation of Na+ current drives early afterdepolarizations in mouse ventricle. *Circ. Arrhyt. Electrophys.* 7:1213.

Fauconnier, J., Bedut, S., Guennec, J.-Y. L., Babuty, D., and Richard, S. (2003). Ca^{2+} current-mediated regulation of action potential by pacing rate in rat ventricular myocytes. *Cardiovasc. Res.* 57, 670–680. doi: 10.1016/s0008-6363(02)00731-9

Fearnley, C. J., Roderick, H. L., and Bootman, M. D. (2011). Calcium signaling in cardiac myocytes. *CSH Perspect. Biol.* 3:a004242.

Ferreiro, M., Petrosky, A. D., and Escobar, A. L. (2012). Intracellular Ca^{2+} release underlies the development of phase 2 in mouse ventricular action potentials. *Am. J. Physiol. Heart C* 302, H1160–H1172.

Gordon, E., Roepke, T. K., and Abbott, G. W. (2006). Endogenous KCNE subunits govern Kv2.1K+ channel activation kinetics in xenopus oocyte studies. *Biophys. J.* 90, 1223–1231. doi: 10.1529/biophysj.105.072504

Henderson, S. A., Goldhaber, J. I., So, J. M., Han, T., Motter, C., Ngo, A., et al. (2004). Functional adult myocardium in the absence of Na+-Ca^{2+} exchange. *Circ. Res.* 95, 604–611.

Kashimura, T., Briston, S. J., Trafford, A. W., Napolitano, C., Priori, S. G., Eisner, D. A., et al. (2010). In the RyR2R4496C mouse model of CPVT, β-adrenergic stimulation induces CA waves by increasing SR Ca content and not by decreasing the threshold for Ca waves. *Circ. Res.* 107, 1483–1489. doi: 10.1161/circresaha.110.227744

Koren, G. (2009). Electrical remodeling and arrhythmias in long-QT syndrome: lessons from genetic models in mice. *Ann. Med.* 36, 22–27. doi: 10.1080/17431380410032643

Kumari, N., Gaur, H., and Bhargava, A. (2018). Cardiac voltage gated calcium channels and their regulation by β-adrenergic signaling. *Life Sci.* 194, 139–149. doi: 10.1016/j.lfs.2017.12.033

Land, S., Louch, W. E., Niederer, S. A., Aronsen, J. M., Christensen, G., Sjaastad, I., et al. (2013). Beta-adrenergic stimulation maintains cardiac function in serca2 knockout mice. *Biophys. J.* 104, 1349–1356. doi: 10.1016/j.bpj.2013.01.042

Lederer, W. J., and Tsien, R. W. (1976). Transient inward current underlying arrhythmogenic effects of cardiotonic steroids in Purkinje fibres. *J. Physiol.* 263, 73–100. doi: 10.1113/jphysiol.1976.sp011622

Lehnart, S. E., Mongillo, M., Bellinger, A., Lindegger, N., Chen, B. X., Hsueh, W., et al. (2008). Leaky Ca^{2+} release channel/ryanodine receptor 2 causes seizures and sudden cardiac death in mice. *J. Clin. Invest.* 118, 2230–2245.

Lehnart, S. E., Terrenoire, C., Reiken, S., Wehrens, X. H., Song, L. S., Tillman, E. J., et al. (2006). Stabilization of cardiac ryanodine receptor prevents intracellular calcium leak and arrhythmias. *Proc. Natl. Acad. Sci. U.S.A.* 103:7910.

Li, L., Louch, W. E., Niederer, S. A., Aronsen, J. M., Christensen, G., Sejersted, O. M., et al. (2012). Sodium accumulation in SERCA knockout-induced heart failure. *Biophys. J.* 102:2048.

Liu, G., Iden, J. B., Kovithavongs, K., Gulamhusein, R., Duff, H. J., and Kavanagh, K. M. (2004). In vivo temporal and spatial distribution of depolarization and repolarization and the illusive murine T wave. *J. Physiol.* 555, 267–279. doi: 10.1113/jphysiol.2003.054064

Liu, X. H., Zhang, Z. Y., Andersson, K. B., Husberg, C., Enger, U. H., Ræder, M. G., et al. (2011). Cardiomyocyte-specific disruption of Serca2 in adult mice causes sarco(endo)plasmic reticulum stress and apoptosis. *Cell Calcium* 49, 201–207. doi: 10.1016/j.ceca.2010.09.009

Louch, W. E., Hake, J., Jølle, G. F., Mørk, H. K., Sjaastad, I., Lines, G. T., et al. (2010a). Control of Ca^{2+} release by action potential configuration in normal and failing murine cardiomyocytes. *Biophys. J.* 99, 1377–1386. doi: 10.1016/j.bpj.2010.06.055

Louch, W. E., Hougen, K., Mørk, H. K., Swift, F., Aronsen, J. M., Sjaastad, I., et al. (2010b). Sodium accumulation promotes diastolic dysfunction in end-stage heart failure following Serca2 knockout. *J. Physiol.* 588:478.

Manotheepan, R., Danielsen, T. K., Sadredini, M., Anderson, M. E., Carlson, C. R., Lehnart, S. E., et al. (2016). Exercise training prevents ventricular tachycardia in CPVT1 due to reduced CaMKII-dependent arrhythmogenic Ca 2+ release. *Cardiovasc. Res.* 111, 295–306. doi: 10.1093/cvr/cvw095

Mørk, H. K., Sjaastad, I., Sejersted, O. M., and Louch, W. E. (2009). Slowing of cardiomyocyte Ca^{2+} release and contraction during heart failure progression in postinfarction mice. *Am. J. Physiol. Heart C* 296, H1069–H1079.

Morotti, S., Edwards, A. G., McCulloch, A. D., Bers, D. M., and Grandi, E. (2014). A novel computational model of mouse myocyte electrophysiology to assess the synergy between Na+ loading and CaMKII. *J. Physiol.* 592, 1181–1197. doi: 10.1113/jphysiol.2013.266676

Nerbonne, J. M. (2014). Mouse models of arrhythmogenic cardiovascular disease: challenges and opportunities. *Curr. Opin. Pharmacol.* 15, 107–114. doi: 10.1016/j.coph.2014.02.003

Ottesen, A. H., Louch, W. E., Carlson, C. R., Landsverk, O. J. B., Kurola, J., Johansen, R. F., et al. (2015). Secretoneurin is a novel prognostic cardiovascular biomarker associated with cardiomyocyte calcium handling. *J. Am. Coll. Cardiol.* 65:351.

Piot, C., LeMaire, S. A., Albat, B., Seguin, J., Nargeot, J., and Richard, S. (1996). High frequency–induced upregulation of human cardiac calcium currents. *Circulation* 93, 120–128. doi: 10.1161/01.cir.93.1.120

Pogwizd, S. M., and Bers, D. M. (2002). Calcium cycling in heart failure: the arrhythmia connection. *J. Cardiovasc. Electr.* 13, 88–91. doi: 10.1046/j.1540-8167.2002.00088.x

Pogwizd, S. M., Schlotthauer, K., Li, L., Yuan, W., and Bers, D. M. (2001). Arrhythmogenesis and contractile dysfunction in heart failure. *Circ. Res.* 88, 1159–1167. doi: 10.1161/hh1101.091193

Pott, C., Muszynski, A., Ruhe, M., Bögeholz, N., Schulte, J. S., Milberg, P., et al. (2012). Proarrhythmia in a non-failing murine model of cardiac-specific Na+/Ca 2+ exchanger overexpression: whole heart and cellular mechanisms. *Basic. Res. Cardiol.* 107:247.

Pott, C., Philipson, K. D., and Goldhaber, J. I. (2005). Excitation–contraction coupling in $Na+–Ca^{2+}$ exchanger knockout mice. *Circ. Res.* 97, 1288–1295.

Pott, C., Ren, X., Tran, D. X., Yang, M. J., Henderson, S., Jordan, M. C., et al. (2007). Mechanism of shortened action potential duration in $Na+-Ca^{2+}$ exchanger knockout mice. *Am. J. Physiol. Cell.* 292, C968–C973. doi: 10.1161/01.res.0000196563.84231.21

Priori, S. G., Napolitano, C., Memmi, M., Colombi, B., Drago, F., Gasparini, M., et al. (2002). Clinical and molecular characterization of patients with catecholaminergic polymorphic ventricular tachycardia. *Circulation* 106, 69–74.

Priori, S. G., Napolitano, C., Tiso, N., Memmi, M., Vignati, G., Bloise, R., et al. (2001). Mutations in the cardiac ryanodine receptor gene (hRyR2) underlie catecholaminergic polymorphic ventricular tachycardia. *Circulation* 103, 196–200. doi: 10.1161/01.cir.103.2.196

Sato, D., Xie, L. H., Sovari, A. A., Tran, D. X., Morita, N., Xie, F., et al. (2009). Synchronization of chaotic early afterdepolarizations in the genesis of cardiac arrhythmias. *Proc. Natl. Acad. Sci. U.S.A.* 106:2988.

Sato, D., Xie, L.-H., Nguyen, T. P., Weiss, J. N., and Qu, Z. (2010). Irregularly appearing early afterdepolarizations in cardiac myocytes: random fluctuations or dynamical chaos? *Biophys. J.* 99:773.

Shannon, T. R., Wang, F., Puglisi, J., Weber, C., and Bers, D. M. A. (2004). Mathematical treatment of integrated ca dynamics within the ventricular myocyte. *Biophys J.* 87, 3351–3371. doi: 10.1529/biophysj.104.047449

Speerschneider, T., and Thomsen, M. B. (2013). Physiology and analysis of the electrocardiographic T wave in mice. *Acta Physiol.* 209, 262–271. doi: 10.1111/apha.12172

Splawski, I., Timothy, K. W., Decher, N., Kumar, P., Sachse, F. B., Beggs, A. H., et al. (2005). Severe arrhythmia disorder caused by cardiac L-type calcium channel mutations. *Proc. Natl. Acad. Sci. U.S.A.* 102:8089 8096; discussion 8086-8088.

Splawski, I., Timothy, K. W., Sharpe, L. M., Decher, N., Kumar, P., Bloise, R., et al. (2004). Ca(V)1.2 calcium channel dysfunction causes a multisystem disorder including arrhythmia and autism. *Cell* 119:31.

Swift, F., Franzini-Armstrong, C., Øyehaug, L., Enger, U. H., Andersson, K. B., Christensen, G., et al. (2012). Extreme sarcoplasmic reticulum volume loss and compensatory T-tubule remodeling after Serca2 knockout. *Proc. Natl. Acad. Sci. U.S.A.* 109:4001.

Tiaho, F., Nargeot, J., and Richard, S. (1991). Voltage-dependent regulation of L-type cardiac Ca channels by isoproterenol. *Pflügers Arch.* 419, 596–602. doi: 10.1007/bf00370301

Tran, D. X., Sato, D., Yochelis, A., Weiss, J. N., Garfinkel, A., Qu, Z., et al. (2009). Bifurcation and chaos in a model of cardiac early afterdepolarizations. *Phys. Rev. Lett.* 102:258103.

Weiss, J. N., Garfinkel, A., Karagueuzian, H. S., Chen, P.-S., and Qu, Z. (2010). Early afterdepolarizations and cardiac arrhythmias. *Heart Rhythm.* 7, 1891–1899. doi: 10.1016/j.hrthm.2010.09.017

Yao, A., Su, Z., Nonaka, A., Zubair, I., Lu, L., Philipson, K. D., et al. (1998). Effects of overexpression of the $Na+-Ca^{2+}$ Exchanger on $[Ca^{2+}]i$ transients in murine ventricular myocytes. *Circ. Res.* 82, 657–665. doi: 10.1161/01.res.82.6.657

Conflict of Interest: The authors declare that the research was conducted in the absence of any commercial or financial relationships that could be construed as a potential conflict of interest.

Publisher's Note: All claims expressed in this article are solely those of the authors and do not necessarily represent those of their affiliated organizations, or those of the publisher, the editors and the reviewers. Any product that may be evaluated in this article, or claim that may be made by its manufacturer, is not guaranteed or endorsed by the publisher.

frontiers in Physiology

ORIGINAL RESEARCH
published: 29 October 2021
doi: 10.3389/fphys.2021.752940

KairoSight: Open-Source Software for the Analysis of Cardiac Optical Data Collected From Multiple Species

*Blake L. Cooper[1,2,3], Chris Gloschat[1,2], Luther M. Swift[1,2], Tomas Prudencio[1,2], Damon McCullough[1,2], Rafael Jaimes 3rd[1,2] and Nikki G. Posnack[1,2,3,4]**

[1] Sheikh Zayed Institute for Pediatric Surgical Innovation, Children's National Hospital, Washington, DC, United States, [2] Children's National Heart Institute, Children's National Hospital, Washington, DC, United States, [3] Department of Pharmacology and Physiology, George Washington University, Washington, DC, United States, [4] Department of Pediatrics, George Washington University, Washington, DC, United States

OPEN ACCESS

Edited by:
Daniel M. Johnson,
The Open University, United Kingdom

Reviewed by:
Christopher O'Shea,
University of Birmingham,
United Kingdom
Crystal M. Ripplinger,
University of California, Davis,
United States

***Correspondence:**
Nikki G. Posnack
nposnack@childrensnational.org

Specialty section:
This article was submitted to Cardiac Electrophysiology, a section of the journal Frontiers in Physiology

Received: 03 August 2021
Accepted: 27 September 2021
Published: 29 October 2021

Citation:
Cooper BL, Gloschat C, Swift LM, Prudencio T, McCullough D, Jaimes R 3rd and Posnack NG (2021) KairoSight: Open-Source Software for the Analysis of Cardiac Optical Data Collected From Multiple Species. Front. Physiol. 12:752940. doi: 10.3389/fphys.2021.752940

Cardiac optical mapping, also known as optocardiography, employs parameter-sensitive fluorescence dye(s) to image cardiac tissue and resolve the electrical and calcium oscillations that underly cardiac function. This technique is increasingly being used in conjunction with, or even as a replacement for, traditional electrocardiography. Over the last several decades, optical mapping has matured into a "gold standard" for cardiac research applications, yet the analysis of optical signals can be challenging. Despite the refinement of software tools and algorithms, significant programming expertise is often required to analyze large optical data sets, and data analysis can be laborious and time-consuming. To address this challenge, we developed an accessible, open-source software script that is untethered from any subscription-based programming language. The described software, written in python, is aptly named "*KairoSight*" in reference to the Greek word for "opportune time" (Kairos) and the ability to "see" voltage and calcium signals acquired from cardiac tissue. To demonstrate analysis features and highlight species differences, we employed experimental datasets collected from mammalian hearts (Langendorff-perfused rat, guinea pig, and swine) dyed with RH237 (transmembrane voltage) and Rhod-2, AM (intracellular calcium), as well as human induced pluripotent stem cell-derived cardiomyocytes (hiPSC-CM) dyed with FluoVolt (membrane potential), and Fluo-4, AM (calcium indicator). We also demonstrate cardiac responsiveness to ryanodine (ryanodine receptor modulator) and isoproterenol (beta-adrenergic agonist) and highlight regional differences after an ablation injury. *KairoSight* can be employed by both basic and clinical scientists to analyze complex cardiac optical mapping datasets without requiring dedicated computer science expertise or proprietary software.

Keywords: optical mapping of calcium and action potentials, cardiac electrophysiology, Langendorff model, excitation contraction coupling, human induced pluripotent stem cell derived cardiomyocytes, optocardiography, python, species differences

INTRODUCTION

Cardiovascular research has been advanced by the development of parameter-sensitive dyes, which can be used to monitor transmembrane voltage (V_m) and intracellular calcium (Ca^{2+}) within cardiac tissue (Jaimes et al., 2019a). Fluorescent reporters allow researchers to monitor action potentials and calcium transients in excitable cells and identify underlying alterations in ionic currents. Forty years ago, Salama and Morad acquired the first optical action potentials from heart muscle using Merocyanine-540 (Salama and Morad, 1976), and a decade later, Lee et al. (1987) directly measured intracellular calcium transients from heart preparations using the cytosolic calcium indicator Indo-1, AM. A variety of parameter-sensitive probes have since been incorporated into cardiac research, including ratiometric (e.g., Fura-2/4/8, Indo-1) and non-ratiometric calcium probes (e.g., Rhod-2/4, BAPTA-1, Fluo-2/3/4/8, Cal-520/590/630, Calbryte-520/590/630), and voltage sensitive dyes (e.g., RH237, Di-4-ANEPPS, Di-8-ANEPPS, Di-4-ANBDQPQ, Di-ANBDQBS, PGH-1, FluoVolt). Complementary probes can be used in dual-imaging approaches to simultaneously monitor action potentials and intracellular calcium handling (Choi and Salama, 2000; Salama and Hwang, 2009; Jaimes et al., 2019a). In optical mapping approaches, cardiac tissue preparations (or cells) are stained to monitor dynamic changes in fluorescent emission using scientific cameras with high spatiotemporal resolution. This offers the advantage of increased spatial resolution, compared with recordings from electrode arrays (Fluhler et al., 1985). Recent advances in cardiac imaging applications include: the development of probes with enhanced signal-to-noise characteristics or red-shifted dyes (Matiukas et al., 2007; Lee et al., 2019; Martišienė et al., 2020) to increase imaging depth, incorporation of mechanical uncouplers or motion tracking to reduce/remove motion artifact (Fedorov et al., 2007; Bourgeois et al., 2011; Jaimes et al., 2016b; Zhang et al., 2016; Kappadan et al., 2020), development of panoramic imaging techniques (Bray et al., 2000; Kay et al., 2004; Lee et al., 2017; Gloschat et al., 2018), and improvements in photodetector and light source technology (Grinvald et al., 1981; Fillette and Nassif, 1987; Salama et al., 1987).

To date, cardiac optical mapping, also known as optocardiography (Boukens and Efimov, 2014; George and Efimov, 2019; Swift et al., 2019), has been used to investigate changes in electrical activity, spiral wave formation (Jalife, 2003), excitation-contraction coupling (Christoph et al., 2017), sarcoplasmic reticulum-specific calcium cycling (Wang et al., 2014), metabolic status (Mercader et al., 2012; Wengrowski et al., 2014; Kuzmiak-Glancy et al., 2015; Jaimes et al., 2016a; Garrott et al., 2017), the efficacy of ablation therapies (Swift et al., 2014), stem-cell engraftment (Costa et al., 2012; Shiba et al., 2012; Filice et al., 2020), cardiotoxicity (Jaimes et al., 2019b), and the pathobiology of heart failure (Spragg and Kass, 2006; Ng et al., 2014; Zasadny et al., 2020). Due to differences in scientific inquiry, each optical mapping lab is unique in their focus and imaging approach. This manifests in the use of cameras with varying acquisition speeds (100–10,000 frames per second) and sensor size (100 × 100 to 2,000 × 2,000 pixels), simultaneous or interleaved light sources, and a variety of cardiac tissue preparations or distinct dye combinations with differing signal-to-noise profiles. Accordingly, individual laboratories often develop customized software tools to analyze the large volumes of spatial and temporal data produced by optical experiments (Laughner et al., 2012; Doshi et al., 2015; O'Shea et al., 2019). As a result, access to software analysis tools is limited and can impede the adoption of optical mapping techniques to the broader research community.

To increase accessibility to optical mapping approaches, a few software applications have been released as open-source packages with freely available code, installation instructions, and user manuals [e.g., Rhythm (Laughner et al., 2012; Gloschat et al., 2018), Orca (Doshi et al., 2015), ElectroMap (O'Shea et al., 2019), and Cosmas (Tomek et al., 2021)]. However, utilization of these analysis tools can be hindered by necessary software expertise, dependence on a programming language that is cost prohibitive, or significant investment in commercial software (e.g., Optiq—Cairn Research). To address these hurdles, we developed a new software solution with a condensed workflow (**Figure 1**) to analyze cardiac optical mapping data quickly and accurately. Notably, the presented software package is controlled by a graphical user interface, which can facilitate its use by individuals with limited data analysis expertise. The described software is aptly named "*KairoSight*" in reference to the Greek word for "opportune time" (Kairos) and the ability to "see" voltage or calcium signals acquired from cardiac tissue. Since this software package uses an open-source platform (Python), it does not require commercial or licensed components. In the described studies, we demonstrate the utility of our software application using experimental datasets collected from mammalian hearts (rat, guinea pig, swine) stained with RH237 (transmembrane voltage) and Rhod-2, AM (intracellular calcium), as well as hiPSC-CM stained with FluoVolt (membrane potential) and Fluo-4, AM (calcium indicator). We also demonstrate cardiac responsiveness to ryanodine (ryanodine receptor modulator) and isoproterenol (beta-adrenergic agonist)—two agents commonly used to monitor perturbations in calcium cycling—and highlight regional differences after an ablation injury. By reducing complexities associated with data analysis, *KairoSight* equips investigators with the necessary tools to evaluate cardiac physiology and pathophysiology without requiring dedicated computer science expertise or proprietary software.

Abbreviations: APD_{80}, action potential duration at 80% repolarization; AUF, arbitrary units of fluorescence; Ca^{2+}, intracellular calcium; CaD_{80}, calcium transient duration at 80% reuptake; dF/F0, change in fluorescence over baseline; hiPSC-CM, human induced pluripotent stem cell-derived cardiomyocytes; PCL, pacing cycle length; SNR, signal-to-noise ratio; V_m, transmembrane voltage.

MATERIALS AND METHODS

Acquisition and Generation of Optical Datasets

Animal procedures were approved by the Institutional Animal Care and Use Committee of the Children's Research Institute and

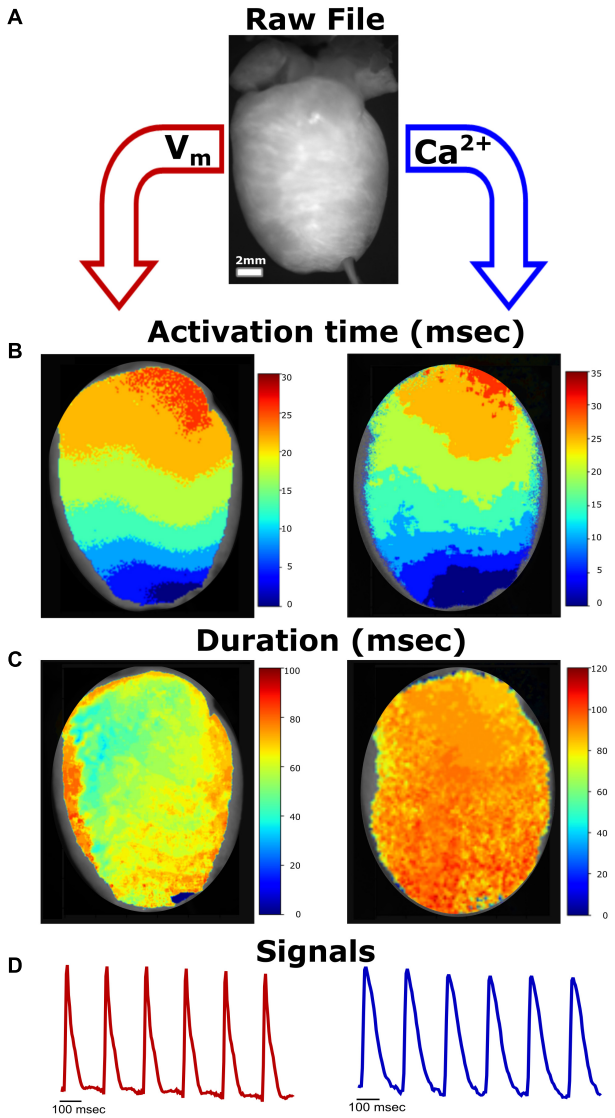

FIGURE 1 | Simplified Workflow. **(A)** Representative raw image file from a Langendorff-perfused rat heart study (*.tif stack). Image properties (e.g., frame rate) are defined by the user. In our experimental setup, voltage and calcium signals can be analyzed from the same heart preparation. **(B)** Activation maps generated from raw image file demonstrate propagation away from the pacing electrode at the apex (left—voltage, right—calcium). **(C)** Generated action potential duration (left) and calcium transient duration (right) maps. **(D)** Representative traces from the raw image file.

followed the National Institutes of Health's Guide for the Care and Use of Laboratory Animals. All animals were euthanized by exsanguination under anesthesia following heart excision, as previously described in detail (Jaimes et al., 2019a; Swift et al., 2019). Experimental data were acquired from isolated, intact hearts that were maintained on a temperature-controlled (37°C), constant-pressure (70 mmHg) Langendorff-perfusion system. To reduce motion artifact, Krebs-Henseleit perfusion buffer was supplemented with 10-15 μM (−/−) blebbistatin (Cayman Chemical) (Fedorov et al., 2007; Swift et al., 2012), or 10 mM 2, 3-butanedione monoxime (BDM; Sigma-Aldrich). Intact heart preparations were loaded with a calcium indicator dye (Rhod-2, AM: 100 μg rat, 100 μg guinea pig, 400 μg swine), which was added and allowed to stabilize for 10 min, followed by a potentiometric dye (RH237: 62 μg rat, 62 μg guinea pig, 248 μg swine). The epicardial surface was illuminated with filtered LED light (535 ± 25 nm), and emitted fluorescent light was split through a dichroic mirror (660 + nm) and directed through high-transmission filters to separate the V_m (710 nm long pass) and Ca^{2+} (585 ± 40 nm) signals. These simultaneous recordings were projected onto a single sensor with 2,016 × 2,016 pixel resolution and a pixel size of 11 × 11 μm (pco.dimax cs4), using an optosplit (Cairn Research) (Jaimes et al., 2019a; Swift et al., 2019). Adequate dye loading and signal detection was verified during the experiment using Fiji, an open-source image analysis software tool (Schindelin et al., 2012). Image stacks acquired from experimental data were saved in TIFF format (*.tif) for subsequent analysis.

Cryopreserved hiPSC-CMs (iCell cardiomyocytes; Cellular Dynamics International) were thawed and plated onto fibronectin-coated cover glass (~60,000 cells/cm^2), as previously described. Cells were maintained under standard cell culture conditions (37°C, 5% CO_2) in iCell cardiomyocyte maintenance medium (Cellular Dynamics International). Three days after plating, hiPSC-CMs formed a confluent monolayer, and were stained with either a potentiometric dye (FluoVolt; 1:1,000 dilution) or a calcium indicator dye (Fluo-4, AM; 10 μM) (Thermo Fisher Scientific) for 45 min at room temperature. Cell monolayers were then washed in dye-free Tyrode salt solution. Pace-induced action potentials and calcium transients were acquired at room temperature using a Nikon TiE microscope system, equipped with 470 nm excitation LED (SpectraX, Lumencor), 505–530 nm emission filter, and Photometrix 95B sCMOS back-illuminated camera. Cardiac monolayers were paced using field stimulation (monophasic, 10 ms pulse width, 1.5x threshold voltage, 0.3–0.7 Hz frequency).

Software Development, Installation, and Image Analysis

KairoSight source code was written in the Python programming language (Python 3.8). Files related to the user interface elements and layout were generated in Qt Designer and converted to *.py python script files, suitable for the PyQt library used to give interface elements their functionality. When available and appropriate, methods from the standard Python libraries were used for data handling and analysis. Steps were taken to minimize user input and error by taking advantage of existing optimized numerical libraries like NumPy, scikit-image, and SciPy, Python's core scientific computing library. The software is freely available to download as source code from https://github.com/kairosight/kairosight-2.0, which can be run and edited in either the Spyder IDE or from the command prompt using the Anaconda distribution of Python. For convenience, an installation video, graphical user interface usage video, README file, and sample image stacks (spatially binned due to file size limitations) are provided on GitHub.

Kairosight processes optical data by first importing an image stack and then applying the following steps (**Supplementary Figure 1**): (1) Image Properties (e.g., acquisition speed, cropping), (2) Processing (e.g., masking, spatial and temporal filtering, detrending, and signal normalization), and (3) Analysis (e.g., isolate action potential or calcium transient signal, compute relevant timepoints and durations, export results as pixel-wise values or pseudo-color maps). Data can be exported after the Analysis step as either pixel signals (*.csv), or optical maps (*.png).

Step 1—Image Properties

In the user interface, an image stack was imported, and key properties of the dataset were provided by the user [frame rate (fps), image scale (px/cm), and image type (V_m or Ca^{2+})]. When necessary, signal intensities were inverted along a central value to assure the analysis of relatively positive deflections from baseline intensities, based on the dye and filter combination. For our experimental dataset, upright signals were analyzed for calcium, while inverted signals were analyzed for voltage. An area of interest was isolated by cropping and rotating—which reduced the analysis of irrelevant pixels.

Step 2—Processing

Background regions or non-fluorescent tissue areas were masked to isolate pixels of interest. The default algorithm, Otsu, generates a threshold value based on Otsu's Method (Otsu, 1979; Lee et al., 2017) and classifies each pixel as "foreground" or "background." Thresholding uses an operator defined percentage value (between 0.0 and 1.0) and includes that percentage of pixels as sorted by their intensity in the mask, and uses an operator defined kernel size to perform morphological closing, opening, and dilation to smooth the mask. Random Walk (Grady, 2006) uses an Otsu approach to label pixels according to user-defined values. An algorithm solves diffusion equations initiated at defined pixels to label pixels of similar value, wherein unknown pixels are assigned the label they have the highest probability to reach during diffusion. Mean calculates the mean pixel intensity and labels all pixels below that threshold as background, and all pixels above the threshold as foreground (Glasbey, 1993). Using the first frame, background pixels were masked and assigned an intensity value of zero for the entire stack, and the dimensions of the stack were preserved throughout. Whether automated or user-guided, masking effectively isolated the brightest continuous region of a cardiac preparation independent of dynamic changes in the fluorescent signal from action potentials or calcium transients. Image stacks can also be convolved with a kernel, to blur or smooth the image by placing greater weight on pixels closer to the center pixel as described by a Gaussian curve, while minimizing spatial broadening of the optical signal (Laughner et al., 2012).

Voltage and calcium dyes often exhibit a small fractional change in fluorescence, which can result in a modest signal-to-noise ratio that impedes signal analysis without additional processing steps. Fluorescence signals regularly contain spatial noise, temporal noise, and baseline drift due to photobleaching. High-frequency temporal noise can be minimized, when needed, using a bidirectionally applied Butterworth filter with a user defined cutoff (e.g., 100 Hz). Spatial "salt-and-pepper" noise can be reduced by convolution with an image kernel filter (e.g., built-in box blur with adjustable kernel size). Signal drift can be removed by calculating and subtracting a least square fit polynomial curve of user-specified order for each pixel. Pixel intensity can be converted from arbitrary units of fluorescence (AUF) to normalized intensity (0 for minimum to 1 for maximum). Normalization from 0 to 1 scales all pixels to the same dynamic range, which facilitates subsequent workflow steps.

Step 3—Analysis

Analysis steps were performed to produce imaging results and maps from either individual or ensembled signals from suitable pixel(s). Specific timepoints and durations within the action potential or calcium transient signals were detected and calculated. The "start time" marker was placed prior to the upstroke of the signal and the "end time" marker was placed following the peak of the transient (activation time measurement) or following the return of the transient to baseline (duration time measurement; see **Supplementary Figure 1**). To identify inflections of interest, 1st and 2nd derivatives of each fluorescent signal were generated and smoothed. Maxima and minima of those derivations were used to identify the inflection points (timepoints) of interest within each action potential or calcium transient. For duration maps, the maximum expected time interval and the desired duration percentage (e.g., APD_{80}) was defined by the user.

Between the baseline period and the peak time, the activation time (dFmax) of the action potential or calcium transient were identified. Downstroke (dFmin) and end time (2nd dF2max) were identified after each peak time, but before the subsequent baseline period began (Laughner et al., 2012). Identification of fundamental time points enabled further computation of optical signal features (e.g., action potential or calcium transient durations (APD or CaD: time from activation to any% of Fmax), diastolic interval (DI: time from APD_{80} or CaD_{80} to the subsequent activation), the time for an action potential or calcium transient to reach 1-1/e amplitude (τ: mono-exponential decay time (Jaimes et al., 2016b)).

In addition to the temporal results derived from optical signals, spatial analysis was important for identifying tissue heterogeneities, voltage and calcium concordance, and the directionality of electrical and/or calcium wavefront propagation. Functional activation patterns were displayed using isochronal maps, in which an activation time was assigned to each pixel and presented simultaneously. Similarly, spatial distributions of durations (APD, CaD) were displayed in scaled maps.

Exporting Data

Images and text were exported through the user interface. A single frame or entire image stack was exported as a *.tif and a single frame or any generated map was exported as a *.png. Further, generated maps or corresponding temporal, spatial, or statistical results were exported as *.csv. Signal data was exported to obtain an (x, y) plot of action potential or calcium transient values. An array of fluorescence data was exported for each ROI

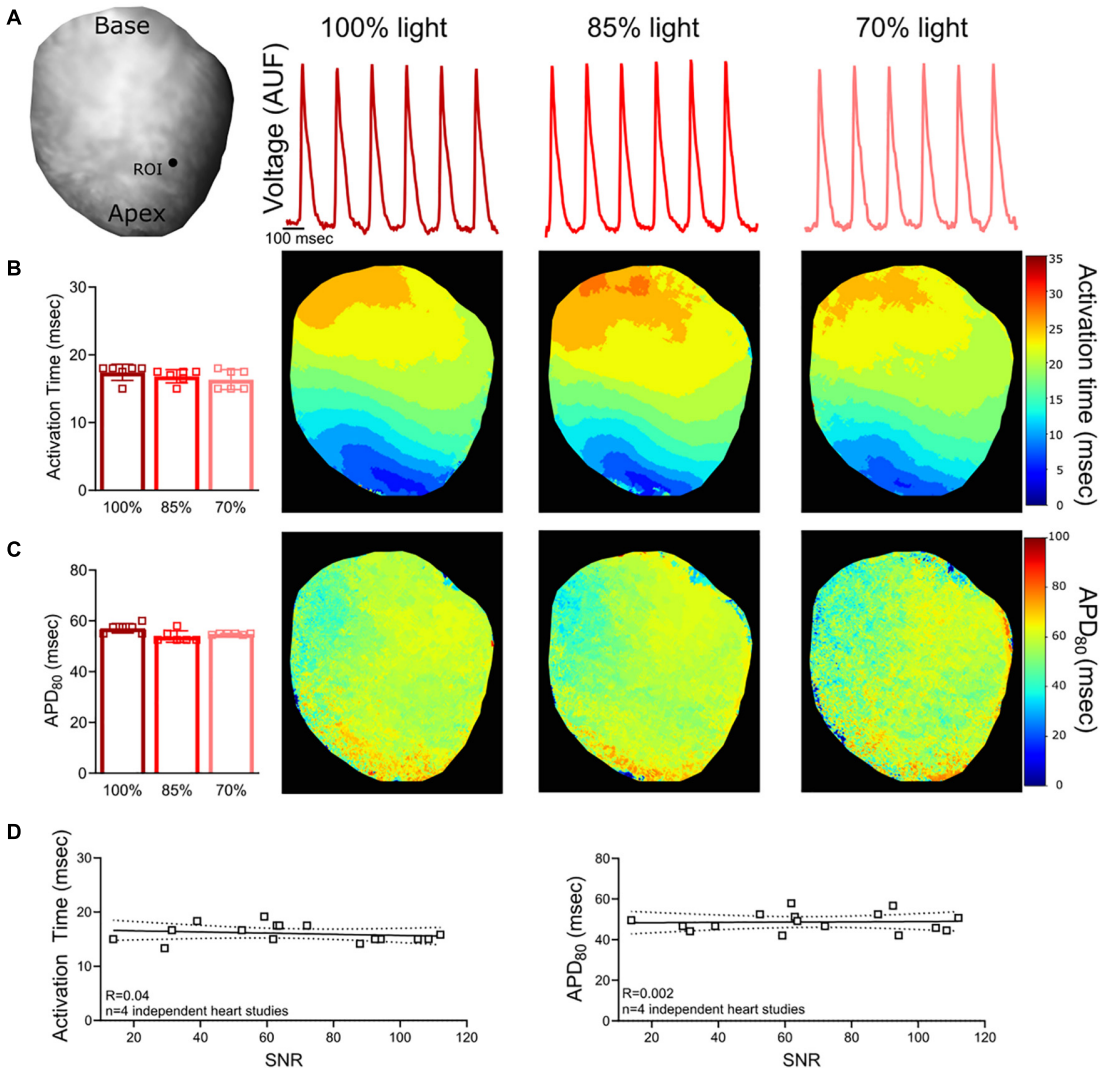

FIGURE 2 | Voltage Signal-to-Noise Ratio (SNR). **(A)** Representative rat heart loaded with voltage dye, RH237. Action potentials were analyzed from the same region of interest (ROI) on the epicardial surface (n = 6 action potentials, same heart with diminished light illumination). **(B)** No measurable change in activation time was noted when the excitation light intensity and SNR was reduced (n = 6 action potentials, same heart). **(C)** Calculated APD_{80} values also remained consistent (n = 6 action potentials, same heart). **(D)** Relationship between SNR and action potential measurements (n = 4 optical signals collected from n = 4 independent heart studies). Epicardial dynamic pacing (160 ms PCL) from the apex of the left ventricle.

over time, including intensity signals, analysis results (all values or mean ± SD) or calculated/mapped values as *.csv.

Statistical Analysis

Results were reported as mean ± standard deviation. Differences between group means were determined using two-tailed Student's t-test or analysis of variance (GraphPad Prism). Significance was defined as a p-value < 0.05, or an adjusted p-value ($q < 0.1$) after correction for multiple comparisons using two stage linear step-up procedure to control the false discovery rate (0.1), as described by Benjamini et al. (2006). Significance was denoted in the figures with an asterisk (*). Replicates were defined in each figure legend; independent optical signals were used from the same heart preparation (**Figures 2A–C**, **3A–C** signal-to-noise data), and independent heart preparations were used for other measurements (**Figures 4–8**).

RESULTS

KairoSight Workflow and User Interface

To provide a more accessible tool for optical mapping data analysis, we developed a novel, open-source software package with an intuitive user interface (**Supplementary Figure 1**) that directs users through a linear workflow (example shown in **Figure 1**). Image processing was accomplished by importing an image stack and applying the following steps: (1) Image Properties, (2) Processing, and (3) Analysis. The *KairoSight*

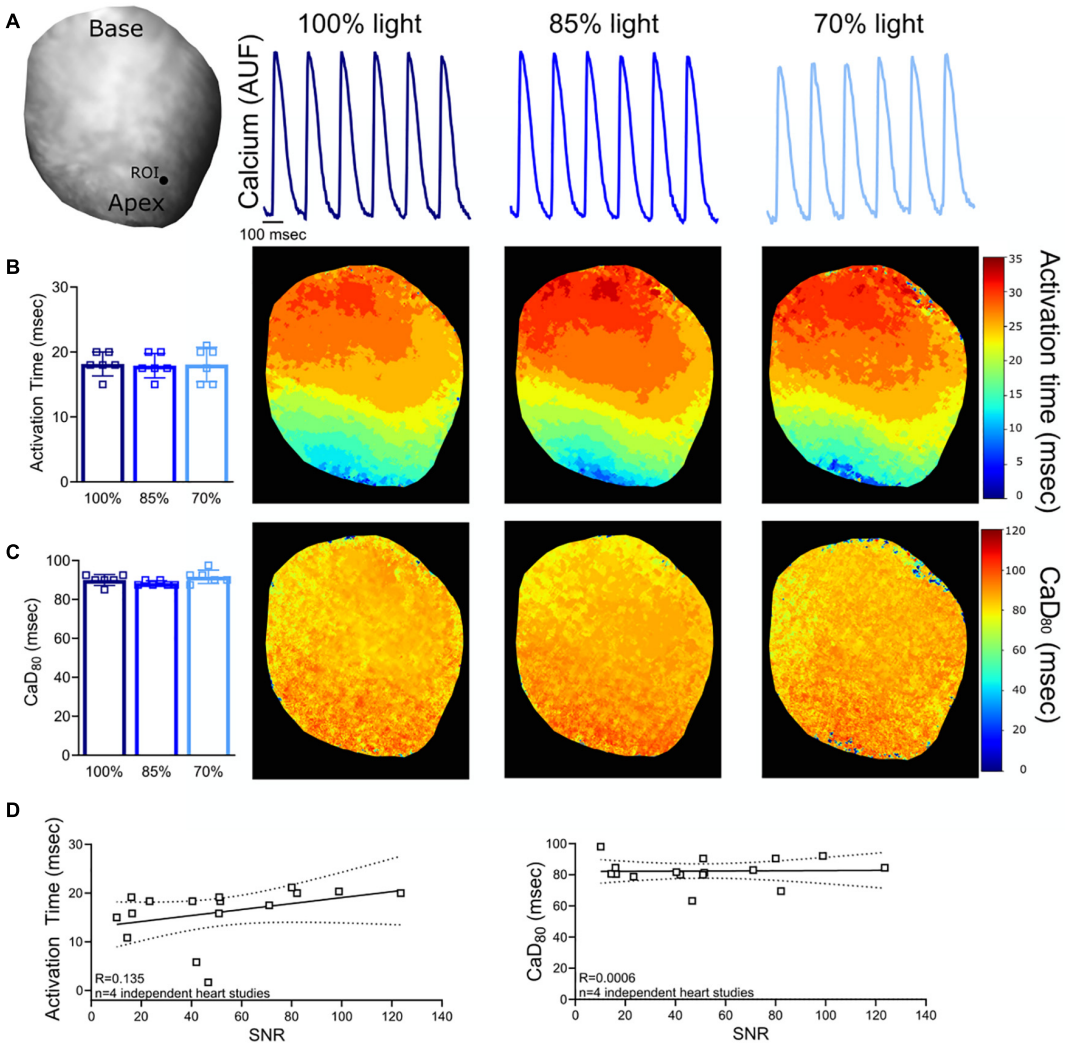

FIGURE 3 | Calcium Signal-to-Noise Ratio (SNR). **(A)** Representative rat heart loaded with calcium dye, Rhod-2, AM. Calcium transients were analyzed from the same region of interest (ROI) on the epicardial surface (n = 6 calcium transients, same heart with diminished light intensity). **(B)** No measurable change in activation time was noted when the excitation light intensity and SNR was reduced (n = 6 calcium transients, same heart). **(C)** Calculated CaD_{80} values also remain unchanged (n = 6 calcium transients, same heart). **(D)** Relationship between SNR and calcium transient measurements (n = 4 optical signals collected from n = 4 independent heart studies). Epicardial dynamic pacing (160 ms PCL) from the apex of the left ventricle.

interface used a workflow with very few input options, which minimized user error, maximized computational resources, and enabled new users to easily understand the methods to implement data analysis steps with accuracy. To illustrate the Image Properties step, cropping and masking were applied to an experimental dataset in **Figure 1**.

Analysis of Transmembrane Voltage and Intracellular Calcium

Multiparametric optical signals were acquired from Langendorff-perfused rat, guinea pig, and swine hearts, and hiPSC-CM, which were stained with fluorescent dyes. Using the cropping feature, the user isolated areas of interest and specified the type of signal (voltage—inverted signal, or calcium—upright signal) from the images loaded onto *KairoSight*. Activation maps, action potential, or calcium transient duration maps (**Figures 2–9**), as well as statistical results (e.g., action potential and calcium transient duration, amplitude, activation time, transient decay tau) were generated. The software identified and analyzed optical voltage and calcium signals from multiple species (**Figures 4**, **5**, **7**), with variations in signal shape and pacing frequency.

Suboptimal Signal-to-Noise Ratio

To confirm the consistency of the signal analysis software in the event of imperfect signals, experimental data was analyzed with varying degrees of noise. Optical signals were collected from hearts loaded with a voltage sensitive dye (RH237) and a calcium dye (Rhod-2, AM). The signal-to-noise ratio (SNR; calculated as the signal amplitude divided by the standard deviation of the

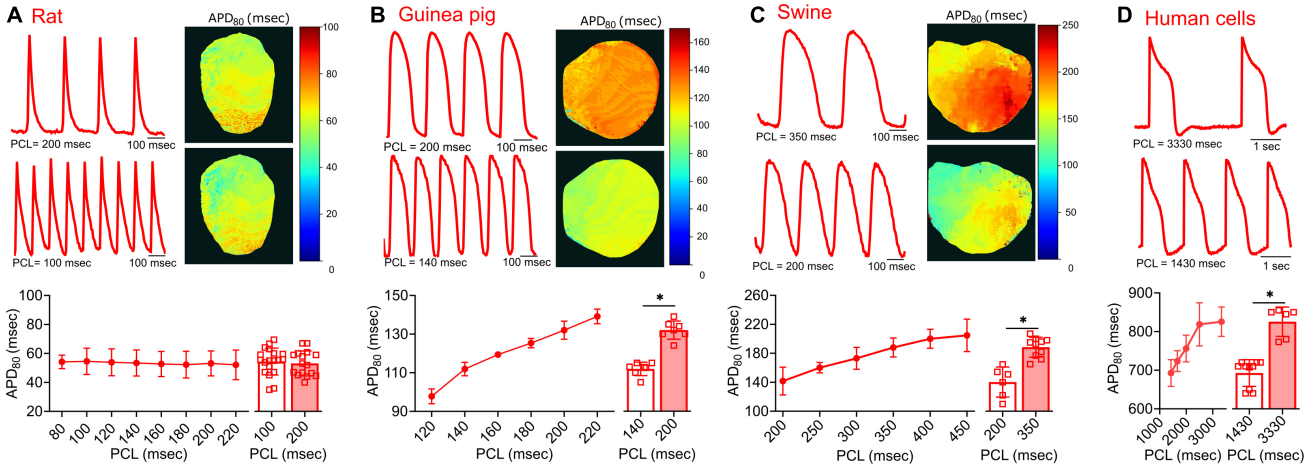

FIGURE 4 | Transmembrane voltage measurements acquired from four different species. **(A)** Representative signals and APD_{80} maps from a rat heart paced at 200 and 100 ms PCL (top). Compiled restitution curve of APD_{80}, in response to dynamic epicardial pacing (bottom left, n = 13–20 independent heart experiments). No change in APD_{80} was observed between 100 ms and 200 ms PCL (bottom right, n = 16–19 independent heart experiments). **(B)** Representative signals and APD_{80} maps from a guinea pig heart paced at 200 and 140 ms PCL (top). Compiled restitution curve of APD_{80}, in response to dynamic epicardial pacing (bottom left, n = 5–7 independent heart experiments). Longer APD_{80} values observed at slower rates (200 vs. 140 ms PCL, n = 7 independent heart experiments). **(C)** Representative signals and APD_{80} maps from a swine heart paced at 350 and 200 ms PCL (top). Compiled restitution curve of APD_{80}, in response to dynamic epicardial pacing (bottom left, n = 4–10 independent heart experiments). Longer APD_{80} values observed at slower rates (350 vs. 200 ms PCL, n = 6–10 independent heart experiments). **(D)** Representative signals from hiPSC-CM paced at 3330 and 1430 ms PCL (top). Compiled restitution curve of APD_{80}, in response to field potential stimulation (bottom left, n = 6–15 independent cell preparations). Longer APD_{80} values observed at slower rates (3330 vs. 1430 ms PCL, n = 6–10 independent cell preparations). Values reported as mean ± SD. *$p < 0.05$, as determined by an unpaired Student's t-test (two-tailed).

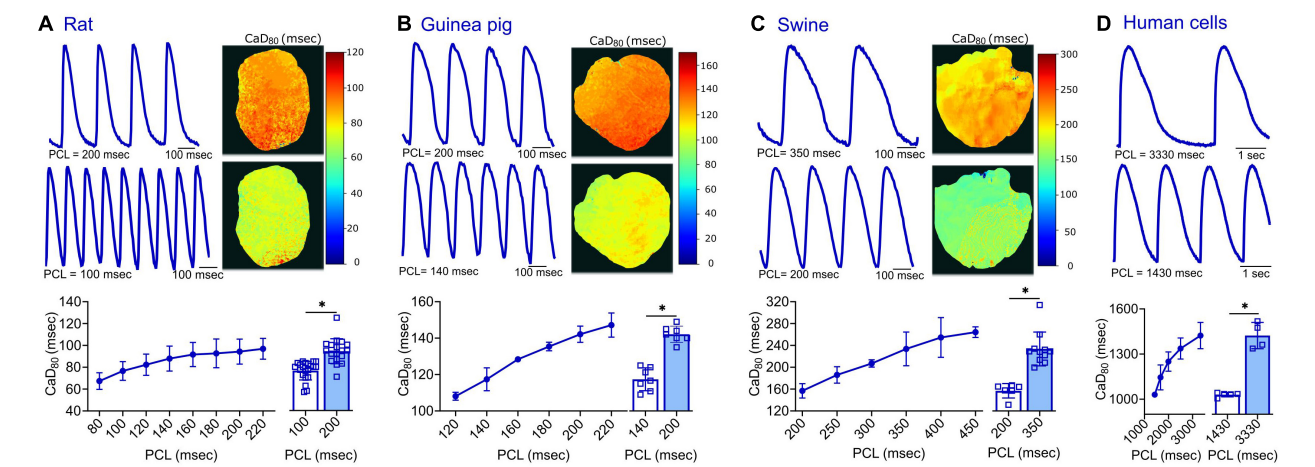

FIGURE 5 | Calcium transient measurements acquired from four different species. **(A)** Representative signals and CaD_{80} maps from a rat heart paced at 200 and 100 ms PCL (top). Compiled restitution curve of CaD_{80}, in response to dynamic epicardial pacing (bottom left, n = 11–19 independent heart preparations). Longer CaD_{80} values observed at slower rates (200 vs. 100 ms PCL, n = 18–21 independent heart preparations). **(B)** Representative signals and CaD_{80} maps from a guinea pig heart paced at 200 and 140 ms PCL (top). Compiled restitution curve of CaD_{80}, in response to dynamic epicardial pacing (bottom left, n = 5–7 independent heart preparations). Longer CaD_{80} values observed at slower rates (200 vs. 140 ms PCL, n = 7 independent heart preparations). **(C)** Representative signals and CaD_{80} maps from a swine heart paced at 350 and 200 ms PCL (top). Compiled restitution curve of CaD_{80}, in response to dynamic epicardial pacing (bottom left, n = 3–11 independent heart preparations). Longer CaD_{80} values observed at slower rates (350 vs. 200 ms PCL, n = 6–11 independent heart preparations). **(D)** Representative signals from hiPSC-CM paced at 3330 and 1430 ms PCL (top). Compiled restitution curve of CaD_{80}, in response to field potential stimulation (bottom left, n = 4–5 independent cell preparations). Longer CaD_{80} values observed at slower rates (3330 vs. 1430 ms PCL, n = 4–5 independent cell preparations). Values reported as mean ± SD. *$p < 0.05$, as determined by an unpaired Student's t-test (two-tailed).

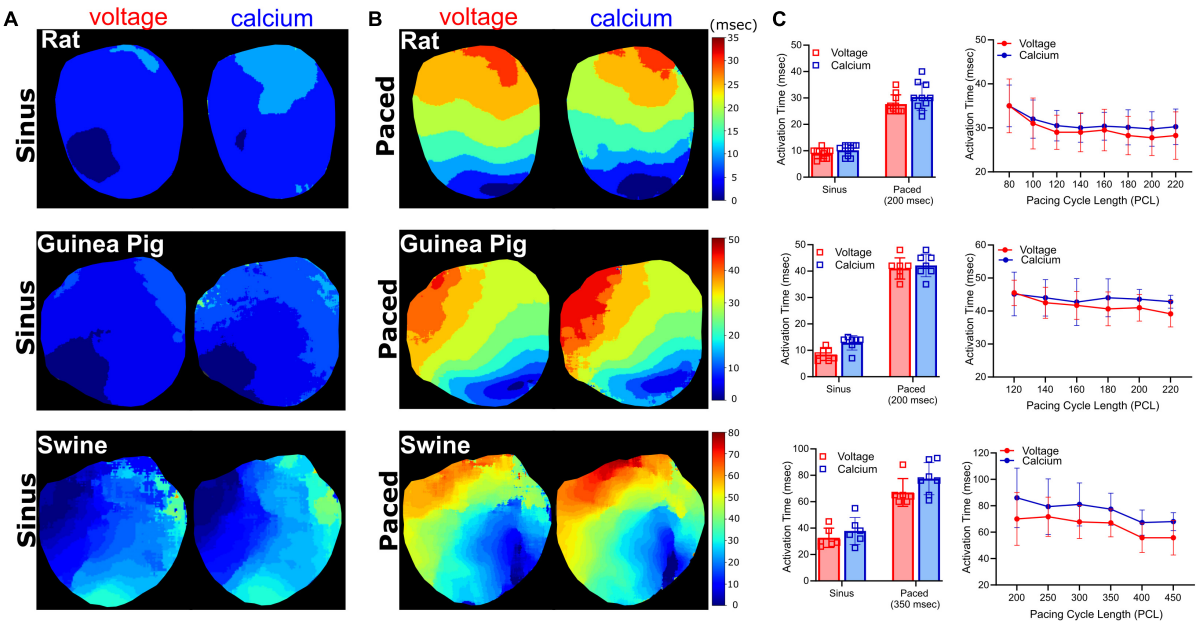

FIGURE 6 | Activation time measurements. Voltage and calcium activation maps generated from excised Langendorff-perfused hearts, during **(A)** sinus and **(B)** epicardial dynamic pacing applied to the left ventricle (rat: 200 ms, guinea pig: 200 ms, swine: 350 ms PCL). **(C)** Left: Average activation time delay during sinus rhythm, compared with dynamic epicardial pacing (n = 10 rat, n = 7 guinea pig, n = 6–8 swine independent heart preparations). Right: Activation time restitution curves for rat (n = 4–8), guinea pig (n = 6–7), and swine (n = 3–6 independent heart preparations).

baseline during the diastolic interval) was decreased by reducing LED illumination on the surface of the heart. Reducing LED illumination decreased voltage signal SNR (*100% light*: SNR 118.1 ± 19.1, *85% light*: 104.9 ± 10.6, *70% light*: 85.0 ± 4.5) and calcium signal SNR (*100% light*: SNR 118.9 ± 19.2, *85% light*: 104.0 ± 9.8, *70% light*: 82.3 ± 6.2). *Kairosight* was used to analyze corresponding voltage (**Figures 2A–C**) and calcium signals (**Figures 3A–C**) within the same heart, wherein only the degree of LED illumination was altered. Activation times for voltage (*100% light*: 17.4 ± 1.2, *85% light*: 16.8 ± 1, *70% light*: 16.3 ± 1.5 ms) and calcium (*100% light*: 18.2 ± 1.8, *85% light*: 17.9 ± 1.9, *70% light*: 18.1 ± 1.1 ms) were calculated from the middle of the epicardial surface, along with action potential duration time at 80% repolarization (APD_{80} *100% light*: 57.1 ± 1.9, *85% light*: 53.8 ± 2.3, *70% light*: 54.8 ± 0.3 ms) and calcium transient duration at 80% reuptake (CaD_{80}: *100% light*: 90 ± 2.7, *85% light*: 88.3 ± 1.3, *70% light*: 91.7 ± 3.4 ms); values were computed from n = 6 optical signals within the same heart. Experiments were then repeated (n = 4 independent heart preparations) under varying degrees of illumination to alter the SNR (**Figures 2D**, **3D**). We noted deviations in the activation time for the calcium signal ("calcium release") when SNR < 50, but calcium transient duration measurements remained consistent.

Multi-Species Analysis

To test the flexibility of the software in analyzing various signal morphologies, tissues from four source species were analyzed. Transmembrane voltage signals were collected from the hearts of rats, guinea pigs, and swine, as well as cultured hiPSC-CM layers. In comparing the morphology of the electrical and calcium traces between species, varying differences in the optical signals were detected (**Figures 4**, **5**). Rat action potential and calcium transient optical signals aligned with examples in the literature (Walton et al., 2013; Jaimes et al., 2016b; Zasadny et al., 2020). The corresponding electrical restitution curve showed little change when the dynamic pacing cycle length (PCL) was decremented from 200 to 100 ms (**Figure 4A**), however, the CaD_{80} shortened by 18.8% at the faster pacing rate (**Figure 5A**). Guinea pig signals and restitution values mirrored those reported in the literature (Guo et al., 2008; Lee et al., 2012), as well as those modeled by Edwards and Louch (2017). As expected, duration times were longer in the guinea pig heart, compared to the rat. Specifically, the APD_{80} and CaD_{80} shortened by approximately 15.2 and 17.4%, respectively, as the PCL was decremented from 200 to 140 ms (**Figures 4B**, **5B**). Likewise, swine APD_{80} and CaD_{80} exhibited even slower dynamics, in agreement with previous studies (Bourgeois et al., 2011; Walton et al., 2013; Lee et al., 2017). Decrementing the PCL from 350 to 200 ms shortened the APD_{80} by 25.5% (**Figure 4C**) and the CaD_{80} by 30.3% (**Figure 5C**). Although not directly comparable to an intact heart preparation, hiPSC-CM were also imaged and analyzed as proof of concept. Decrementing the PCL from 3,330 to 1,430 ms shortened the APD_{80} by 16.1% (**Figure 4D**) and CaD_{80} by 27.6% (**Figure 5D**).

Activation Time Measurements

Action potential and calcium transient activation maps were generated for rat, guinea pig, and swine hearts during both sinus

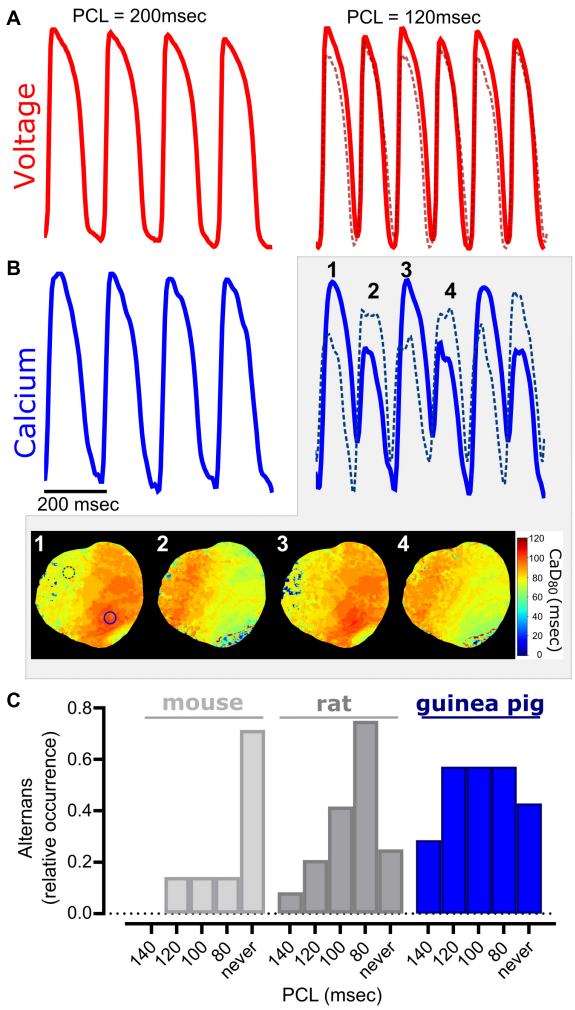

FIGURE 7 | Cardiac alternans occur at faster pacing cycle lengths. **(A)** Representative optical action potentials, and **(B)** calcium transients from a Langendorff-perfused guinea pig heart. Slower PCL (200 ms) produces uniform action potentials and calcium transients (left), while a faster PCL (140 ms) results in cardiac alternans (right). Traces were acquired from two different regions of interest (solid line—left ventricle, dotted line—right ventricle) and discordant alternans were readily observable in the calcium signal. Four sequential beats show regional differences in alternans in calcium duration maps. **(C)** Relative occurrence of cardiac alternans in different species (mouse, rat, guinea pig). Epicardial dynamic pacing applied to the left ventricle for all studies (n = 5–18 independent heart studies per species).

rhythm and in response to dynamic epicardial pacing (**Figure 6**). As expected, activation time measurements were faster during sinus rhythm (often occurring in the right ventricle before the left ventricle) and slower in response to external pacing. In the rat heart, activation time was 8.9 ± 1.9 ms (V_m) and 10.2 ± 2.1 ms (Ca^{2+}) during sinus rhythm (**Figure 6A**), which increased to 27.7 ± 3.5 ms (V_m) and 30.4 ± 5.2 ms (Ca^{2+}) with pacing (200 ms PCL; **Figures 6B,C**). Similar observations were noted in larger species; in the guinea pig heart activation time was 18.8 ± 5 ms (V_m) and 19.9 ± 6.3 ms (Ca^{2+}) during sinus rhythm (**Figure 6A**), which increased to 29.4 ± 3.4 ms (V_m) and 31.9 ± 4.8 ms (Ca^{2+}) with pacing (200 ms PCL, **Figures 6B,C**). Piglet heart activation time was 32.7 ± 7.3 ms (V_m) and 37.8 ± 10.2 ms (Ca^{2+}) during sinus rhythm (**Figure 6A**), which increased to 67.0 ± 10.5 (V_m) and 77.4 ± 12.2 ms (Ca^{2+}) with pacing (350 ms PCL, **Figures 6B,C**).

Cardiac Alternans and Demonstration of Regional Heterogeneity

Calcium flux plays a central role in excitation-contraction coupling, wherein perturbations in calcium handling (e.g., alternans, calcium leak from the sarcoplasmic reticulum) are associated with an array of cardiac dysfunctions, both electrical and mechanical (Weiss et al., 2011; Wang et al., 2014; Kanaporis and Blatter, 2015; Johnson et al., 2019; Sutanto et al., 2020). Calcium alternans are a potentially deleterious physiological oscillation, which are observable as alternating amplitude fluctuations in optical signals. The latter has been mechanistically linked to T-wave alternans that can segue into lethal ventricular arrhythmias (Weiss et al., 2011; Ng, 2017). Experimentally, cardiac alternans have been more commonly observed at faster heart rates and/or cooler temperatures (Egorov et al., 2012; Millet et al., 2021); accordingly, we utilized burst pacing to induce alternans in isolated, intact hearts (**Figures 7A–C**). Although not observed at slower pacing rates (200 ms PCL), intact guinea pig hearts displayed both APD alternans and calcium transient amplitude alternans at faster rates (120 ms PCL, **Figures 7A,B**). Further, calcium transient duration maps revealed spatially discordant alternans at faster rates, in which two regions of the tissue (right vs. left ventricle) were out of phase. When considering the occurrence of alternans between species, we observed variable susceptibility with increasing pacing frequency (relative occurrence at 100 ms PCL: 14% in mice, 42% in rats, and 57% in guinea pigs; **Figure 7C**).

Experimental Techniques to Demonstrate Responses to Pharmacological Agents and Myocardial Injury

Pharmacological agents are frequently employed to identify the mechanisms responsible for cardiac responses. As one example, isoproterenol is commonly used to induce heart failure through its positive chronotropic effects (Balakumar et al., 2007; Greer-Short and Poelzing, 2015; Chang et al., 2018). Using Langendorff-perfused rat hearts, we demonstrated that acute isoproterenol exposure (30 nM) results in a 40% increase in sinus rate (280.3 ± 32.4 baseline vs. 392.0 ± 37.7 BPM with isoproterenol), and 17.7% shortening of CaD_{80} with dynamic pacing at 120 ms PCL (89.9 ± 5.9 baseline vs. 74 ± 14.4 ms with isoproterenol; **Figures 8A,B**). Further, ryanodine (5 μM) modulates calcium release from the sarcoplasmic reticulum, and is often used to demonstrate signal specificity in dual optical mapping studies (Choi and Salama, 2000; Jaimes et al., 2019a). Using *KairoSight,* we demonstrated a marked 92% reduction in the calcium transient amplitude with minimal effects on optical action potentials collected from intact rat hearts (**Figure 8C**). Optical mapping studies are often used to monitor spiral wave

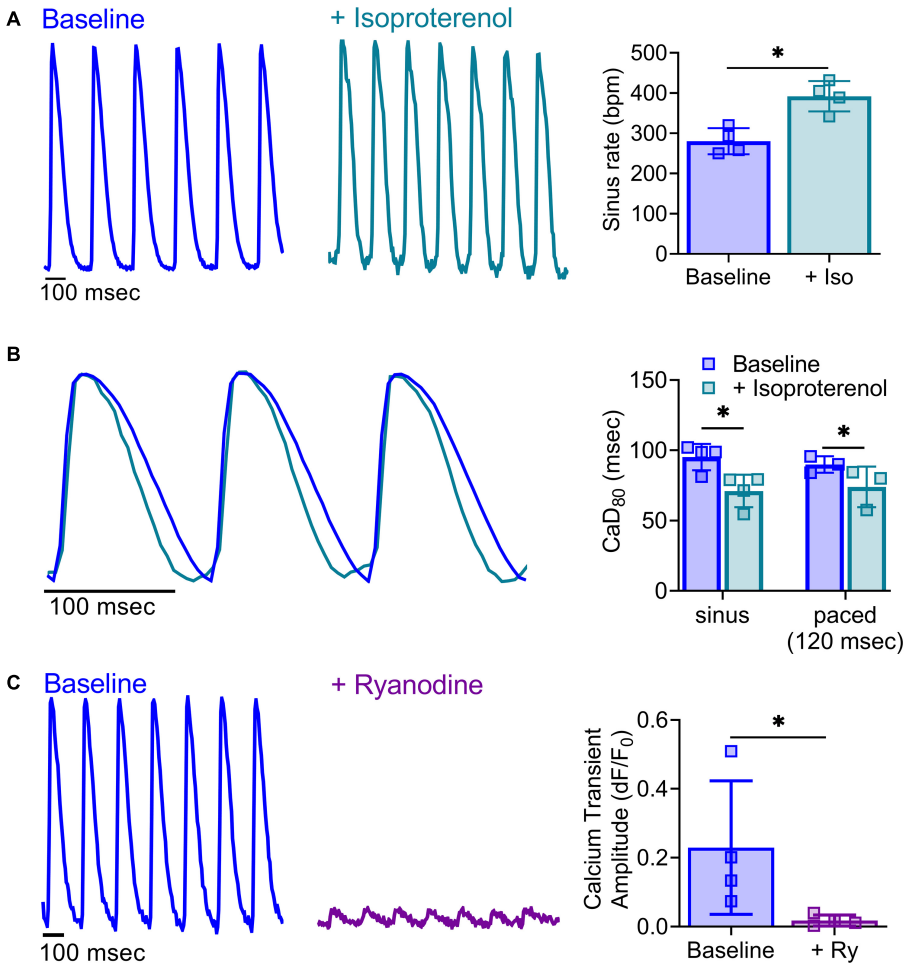

FIGURE 8 | Impact of pharmacological agents on calcium handling. **(A)** Representative calcium transients acquired from a Langendorff-perfused rat heart at baseline and after acute treatment with isoproterenol (30 nM). Isoproterenol increased sinus rate (right, $n = 4$ independent heart studies, $^*p < 0.05$ as determined by two-tailed Student's *t*-test). **(B)** Shorter calcium transient duration time in response to isoproterenol application was readily observable in calcium signals from a Langendorff-perfused rat heart during sinus rhythm and with external pacing for rate correction (120 ms PCL, $n = 3$–4 independent heart studies, $^*p < 0.05$ as determined by two-way ANOVA with multiple comparisons testing). **(C)** Representative calcium transients from a Langendorff-perfused rat heart at baseline and after acute treatment with ryanodine (5 μM), during external pacing (160 ms PCL). Ryanodine diminished calcium transient amplitude (right; $n = 4$ independent heart studies, $^*p < 0.05$ as determined by two-tailed Student's *t*-test). Values reported as mean ± SD. BPM = beats per minute, dF/F0 = change in fluorescence over baseline.

formation and re-entry arrhythmias (Moe and Jalife, 1977; Pumir et al., 2005), which may occur due to tissue heterogeneities from a myocardial infarction or incomplete cardiac ablation. To demonstrate the utility of our optical mapping approach and data analysis, an epicardial radiofrequency ablation was applied to mimic the physiological environment that can promote such arrhythmias (Mercader et al., 2012). Optical signals were collected before and after radiofrequency ablation, and the analyzed signals show a typical pattern of electrical activity and calcium fluctuations outside the ablated area (**Figure 9**). Within the ablated area, we observed irregular and diminished signals from both the voltage and calcium signals. Accordingly, optical signal analysis via *KairoSight* can be applied to other applications focused on pharmacological treatment, tissue injury, or pathophysiology.

DISCUSSION

Optical mapping is commonly used in cardiac research applications, as it allows one to resolve the electrical and calcium oscillations that underly cardiac function and dysfunction (Jaimes et al., 2016b; George and Efimov, 2019). Nevertheless, there are important technical limitations and constraints that should be considered. Although optical mapping can be employed *in situ* (Lee et al., 2019; Martišienė et al., 2020)—this technique is more commonly applied *ex vivo*, using Langendorff-perfused heart preparations that are maintained with a crystalloid buffer. To avoid signal distortion, the motion of the heart is often suppressed using mechanical constraint or excitation-contraction uncoupling agents (Fedorov et al., 2007; Swift et al., 2012). In the latter, the secondary effects of uncoupling agents

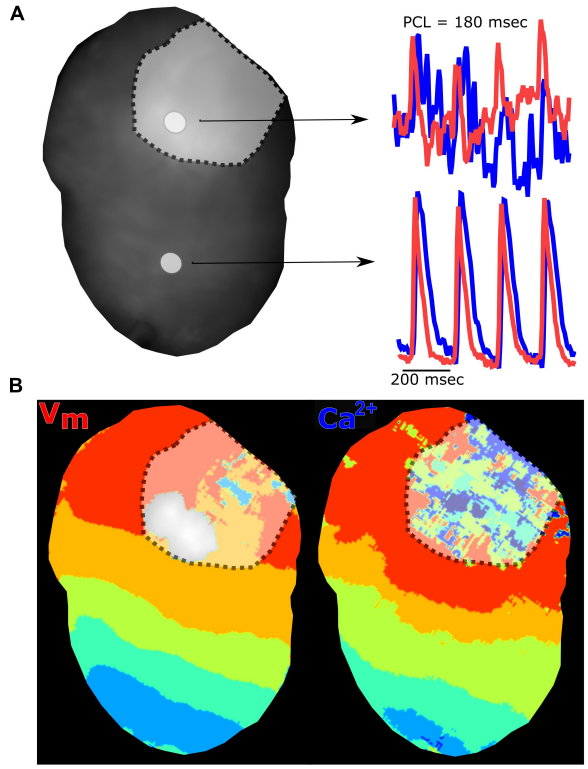

FIGURE 9 | Myocardial injury via radiofrequency ablation diminishes electrical and calcium signals. **(A)** Langendorff-perfused rat heart after radiofrequency ablation showing two regions of interest and corresponding traces. The voltage signal (red) and calcium signal (blue) are collected from the ablation site (denoted with dotted line) and non-ablated tissue. **(B)** Voltage and calcium isochronal maps display activation time across the heart, with disruption at the site of ablation injury. Epicardial dynamic pacing from the apex of the heart.

should be considered (e.g., reduced metabolic demand, altered electrical activity). Moreover, in Langendorff-perfused heart preparations, optical mapping is limited to the surface of the tissue and endocardial activity can only be surmised by what is "seen" on the epicardium. Similarly, measurements of activation time and conduction velocity are monitored in response to external pacing—rather than under sinus rhythm. Despite these limitations, optical mapping remains a powerful tool for studying the spatiotemporal dynamics of cardiac electrophysiology and excitation-contraction coupling.

Optical mapping techniques have evolved over the last few decades, with continuous advancements in voltage and calcium-sensitive dyes, light source and photodetector technology. As just one example, in 1975 the first fully digital camera took 23 s to record a 100 × 100 pixel image, while newly developed CMOS sensors have offered improved spatiotemporal resolution with acquisition speeds that can exceed 2,000 frames per second. Despite these immense technical improvements, data analysis remains an obstacle for new investigators entering the field of optical mapping, as many groups still develop their own custom software. To help address this barrier to entry, we have developed an accessible and functional software platform to prepare, process, and analyze optical action potentials and calcium signals collected from cardiac preparations. In the presented article, we document the utility of *KairoSight* in analyzing optical data sets collected under conditions of variable SNR, demonstrate species-specific differences in action potentials and calcium transients, showcase cardiac responses to varying pacing frequencies and/or pharmacological agents, and highlight tissue heterogeneities in the context of discordant alternans and cardiac injury. Our open-source software was developed using Python, as it has consistently been ranked as a "top 10" programming language by industry analysts (Stephens, 2020). Due to its flexibility and widespread adoption, we fully anticipate the research community to utilize *KairoSight* for image analysis applications—and also modify and tailor this tool for their own research aims. For example, future updates to the software could include measurements of conduction velocity, automated detection of electrical or calcium alternans, and/or the generation of signal:noise ratio maps.

DATA AVAILABILITY STATEMENT

Datasets are available from the corresponding author on reasonable request.

ETHICS STATEMENT

The animal study was reviewed and approved by Institutional Animal Care and Use Committee of the Children's Research Institute.

AUTHOR CONTRIBUTIONS

BC, CG, LS, TP, DM, RJ, and NP performed the experiments and approved the manuscript. BC, CG, LS, and NP analyzed the data. BC, LS, and NP prepared the figures. BC, LS, DM, and NP drafted the manuscript. BC, LS, CG, RJ, DM, and NP conceived and designed the experiments. All authors contributed to the article and approved the submitted version.

FUNDING

This work was supported by the National Institutes of Health (R01HL139472 to NP), Children's Research Institute, and Children's National Heart Institute.

ACKNOWLEDGMENTS

We gratefully acknowledge Ritvik Muralidharan, Marissa Reilly, and Nina Ciccarelli for helpful discussions and technical input on this project.

SUPPLEMENTARY MATERIAL

The Supplementary Material for this article can be found online at: https://www.frontiersin.org/articles/10.3389/fphys.2021.752940/full#supplementary-material

Supplementary Figure 1 | Example User Interface. Representative TIFF stack (*.tif) loaded into the *KairoSight* interface, with "Image Properties" including frame rate defined by the user. During "Processing," background was removed, pixels were box blurred 3 × 3, 100 Hz filter was applied, signal drift was removed, and traces were normalized (0–1). During "Analysis," the start and end of a signal upstroke was defined by the user to measure activation time.

REFERENCES

Balakumar, P., Singh, A. P., and Singh, M. (2007). Rodent models of heart failure. *J. Pharmacol. Toxicol. Methods* 56, 1–10. doi: 10.1016/j.vascn.2007.01.003

Benjamini, Y., Krieger, A. M., and Yekutieli, D. (2006). Adaptive linear step-up procedures that control the false discovery rate. *Biometrika* 93, 491–507. doi: 10.1093/biomet/93.3.491

Boukens, B. J., and Efimov, I. R. (2014). A century of optocardiography. *IEEE Rev. Biomed. Eng.* 7, 115–125. doi: 10.1109/rbme.2013.2286296

Bourgeois, E. B., Bachtel, A. D., Huang, J., Walcott, G. P., and Rogers, J. M. (2011). Simultaneous optical mapping of transmembrane potential and wall motion in isolated, perfused whole hearts. *J. Biomed. Opt.* 16:096020. doi: 10.1117/1.3630115

Bray, M. A., Lin, S. F., and Wikswo, J. P. (2000). Three-dimensional surface reconstruction and flourescent visualization of cardiac activation. *IEEE Trans. Biomed. Eng.* 47, 1382–1391. doi: 10.1109/10.871412

Chang, S. C., Ren, S., Rau, C. D., and Wang, J. J. (2018). Isoproterenol-induced heart failure mouse model using osmotic pump implantation. *Methods Mol. Biol.* 1816, 207–220. doi: 10.1007/978-1-4939-8597-5_16

Choi, B. R., and Salama, G. (2000). Simultaneous maps of optical action potentials and calcium transients in guinea-pig hearts: mechanisms underlying concordant alternans. *J. Physiol.* 529, 171–188. doi: 10.1111/j.1469-7793.2000.00171.x

Christoph, J., Schröder-Schetelig, J., and Luther, S. (2017). Electromechanical optical mapping. *Prog. Biophys. Mol. Biol.* 130, 150–169. doi: 10.1016/j.pbiomolbio.2017.09.015

Costa, A., Panda, N., Yong, S., Mayorga, M., Gp, P., Fan, K., et al. (2012). Optical mapping of cryoinjured rat myocardium grafted with mesenchymal stem cells. *Am. J. Physiol. Heart Circ. Physiol.* 302, H270–H277.

Doshi, A. N., Walton, R. D., Krul, S. P., de Groot, J. R., Bernus, O., Efimov, I. R., et al. (2015). Feasibility of a semi-automated method for cardiac conduction velocity analysis of high-resolution activation maps. *Comput. Biol. Med.* 65, 177–183. doi: 10.1016/j.compbiomed.2015.05.008

Edwards, A. G., and Louch, W. E. (2017). Species-dependent mechanisms of cardiac arrhythmia: a cellular focus. *Clin. Med. Insights Cardiol.* 11:1179546816686061.

Egorov, Y. V., Glukhov, A. V., Efimov, I. R., and Rosenshtraukh, L. V. (2012). Hypothermia-induced spatially discordant action potential duration alternans and arrhythmogenesis in nonhibernating versus hibernating mammals. *Am. J. Physiol. Heart Circ. Physiol.* 303, H1035–H1046.

Fedorov, V. V., Lozinsky, I. T., Sosunov, E. A., Anyukhovsky, E. P., Rosen, M. R., Balke, C. W., et al. (2007). Application of blebbistatin as an excitation-contraction uncoupler for electrophysiologic study of rat and rabbit hearts. *Heart Rhythm.* 4, 619–626. doi: 10.1016/j.hrthm.2006.12.047

Filice, D., Dhahri, W., Solan, J. L., Lampe, P. D., Steele, E., Milani, N., et al. (2020). Optical mapping of human embryonic stem cell-derived cardiomyocyte graft electrical activity in injured hearts. *Stem Cell Res. Ther.* 11:417.

Fillette, F., and Nassif, G. (1987). A study of electrical activation of the heart by laser spectrometry - an optical study of cellular action potentials. *Int. J. Card. Imaging* 2, 165–172. doi: 10.1007/bf01784304

Fluhler, E., Burnham, V. G., and Loew, L. M. (1985). Spectra, membrane binding, and potentiometric reponses of new charge shift probes†. *Biochemistry* 24, 5749–5755. doi: 10.1021/bi00342a010

Garrott, K., Kuzmiak-Glancy, S., Wengrowski, A., Zhang, H., Rogers, J., and Kay, M. W. (2017). KATP channel inhibition blunts electromechanical decline during hypoxia in left ventricular working rabbit hearts. *J. Physiol.* 595, 3799–3813. doi: 10.1113/jp273873

George, S. A., and Efimov, I. R. (2019). Optocardiography: a review of its past, present, and future. *Curr. Opin. Biomed. Eng.* 9, 74–80. doi: 10.1016/j.cobme.2019.03.001

Glasbey, C. A. (1993). An analysis of histogram-based thresholding algorithms. *CVGIP Graph Model Image Process.* 55, 532–537. doi: 10.1006/cgip.1993.1040

Gloschat, C., Aras, K., Gupta, S., Faye, N. R., Zhang, H., Syunyaev, R. A., et al. (2018). RHYTHM: an open source imaging toolkit for cardiac panoramic optical mapping. *Sci. Rep.* 8:2921.

Grady, L. (2006). Random walks for image segmentation. *IEEE Trans. Pattern Anal. Mach. Intell.* 28, 1768–1783.

Greer-Short, A., and Poelzing, S. (2015). Temporal response of ectopic activity in guinea pig ventricular myocardium in response to isoproterenol and acetylcholine. *Front. Physiol.* 6:278. doi: 10.3389/fphys.2015.00278

Grinvald, A., Cohen, L. B., Lesher, S., and Boyle, M. B. (1981). Simultaneous optical monitoring of activity of many neurons in invertebrate ganglia using a 124-element photodiode array. *J. Neurophysiol.* 45, 829–840. doi: 10.1152/jn.1981.45.5.829

Guo, D., Zhou, J., Zhao, X., Gupta, P., Kowey, P. R., Martin, J., et al. (2008). L-type calcium current recovery versus ventricular repolarization: preserved membrane-stabilizing mechanism for different QT intervals across species. *Heart Rhythm.* 5, 271–279. doi: 10.1016/j.hrthm.2007.09.025

Jaimes, R., Walton, R. D., Pasdois, P. L. C. P., Bernus, O., Efimov, I. R., Kay, M. W., et al. (2016b). A technical review of optical mapping of intracellular calcium within myocardial tissue. *Am. J. Physiol. Circ. Physiol.* 310, H1388–H1401.

Jaimes, R., Kuzmiak-Glancy, S., Brooks, D. M., Swift, L. M., Posnack, N. G., and Kay, M. W. (2016a). Functional response of the isolated, perfused normoxic heart to pyruvate dehydrogenase activation by dichloroacetate and pyruvate. *Pflügers Arch.* 468, 131–142. doi: 10.1007/s00424-015-1717-1

Jaimes, R., McCullough, D., Siegel, B., Swift, L., Hiebert, J., McInerney, D., et al. (2019a). Lights, camera, path splitter: a new approach for truly simultaneous dual optical mapping of the heart with a single camera. *BMC Biomed. Eng.* 1:25. doi: 10.1186/s42490-019-0024-x

Jaimes, R., McCullough, D., Siegel, B., Swift, L., McInerney, D., Hiebert, J., et al. (2019b). Plasticizer interaction with the heart: chemicals used in plastic medical devices can interfere with cardiac electrophysiology. *Circ. Arrhythmia Electrophysiol.* 12:e007294.

Jalife, J. (2003). Rotors and spiral waves in atrial fibrillation. *J. Cardiovasc. Electrophysiol.* 14, 776–780.

Johnson, D. M., Mugelli, A., and Cerbai, E. (2019). Editorial: the role of calcium handling in heart failure and heart failure associated arrhythmias. *Front. Physiol.* 10:1. doi: 10.3389/fphys.2019.00001

Kanaporis, G., and Blatter, L. A. (2015). The mechanisms of calcium cycling and action potential dynamics in cardiac alternans. *Circ. Res.* 116, 846–856. doi: 10.1161/circresaha.116.305404

Kappadan, V., Telele, S., Uzelac, I., Fenton, F., Parlitz, U., Luther, S., et al. (2020). High-resolution optical measurement of cardiac restitution, contraction, and fibrillation dynamics in beating vs. blebbistatin-uncoupled isolated rabbit hearts. *Front. Physiol.* 11:464. doi: 10.3389/fphys.2020.00464

Kay, M. W., Amison, P. M., and Rogers, J. M. (2004). Three-dimensional surface reconstruction and panoramic optical mapping of large hearts. *IEEE Trans. Biomed. Eng.* 51, 1219–1229. doi: 10.1109/tbme.2004.827261

Kuzmiak-Glancy, S., Jaimes, R., Wengrowski, A. M., and Kay, M. W. (2015). Oxygen demand of perfused heart preparations: how electromechanical function and inadequate oxygenation affect physiology and optical measurements. *Exp. Physiol.* 100, 603–616. doi: 10.1113/ep085042

Laughner, J. I., Ng, F. S., Sulkin, M. S., Arthur, R. M., and Efimov, I. R. (2012). Processing and analysis of cardiac optical mapping data obtained with potentiometric dyes. *Am. J. Physiol. Circ. Physiol.* 303, H753–H765.

Lee, H. C., Smith, N., Mohabir, R., and Clusin, W. T. (1987). Cytosolic calcium transients from the beating mammalian heart. *Proc. Natl. Acad. Sci. U.S.A.* 84, 7793–7797. doi: 10.1073/pnas.84.21.7793

Lee, P., Calvo, C. J., Alfonso-Almazán, J. M., Quintanilla, J. G., Chorro, F. J., Yan, P., et al. (2017). Low-cost optical mapping systems for panoramic imaging of complex arrhythmias and drug-action in translational heart models. *Sci. Rep*. 7:43217.

Lee, P., Quintanilla, J. G., Alfonso-Almazán, J. M., Galán-Arriola, C., Yan, P., Sánchez-González, J., et al. (2019). In vivo ratiometric optical mapping enables high-resolution cardiac electrophysiology in pig models. *Cardiovasc. Res*. 115, 1659–1671.

Lee, P., Wang, K., Woods, C., Yan, P., Kohl, P., Ewart, P., et al. (2012). Cardiac electrophysiological imaging systems scalable for high-throughput drug testing. *Pflugers Arch*. 464, 645–656. doi: 10.1007/s00424-012-1149-0

Martišienė, I., Karèiauskas, D., Navalinskas, A., Maèianskienė, R., Kuèinskas, A., Treinys, R., et al. (2020). Optical mapping of the pig heart in situ under artificial blood circulation. *Sci. Rep*. 10, 8548.

Matiukas, A., Mitrea, B. G., Qin, M., Pertsov, A. M., Shvedko, A. G., Warren, M. D., et al. (2007). Near-infrared voltage-sensitive fluorescent dyes optimized for optical mapping in blood-perfused myocardium. *Heart Rhythm*. 4, 1441–1451. doi: 10.1016/j.hrthm.2007.07.012

Mercader, M., Swift, L., Sood, S., Asfour, H., Kay, M., and Sarvazyan, N. (2012). Use of endogenous NADH fluorescence for real-time in situ visualization of epicardial radiofrequency ablation lesions and gaps. *Am. J. Physiol. Circ. Physiol*. 302, H2131–H2138.

Millet, J., Aguilar-Sanchez, Y., Kornyeyev, D., Bazmi, M., Fainstein, D., Copello, J. A., et al. (2021). Thermal modulation of epicardial Ca2+ dynamics uncovers molecular mechanisms of Ca2+ alternans. *J. Gen. Physiol*. 153:e202012568.

Moe, G. K., and Jalife, J. (1977). Reentry and ectopic mechanisms in the genesis of arrhythmias. *Arch. Inst. Cardiol. Mex*. 47, 206–211.

Ng, F. S., Holzem, K. M., Koppel, A. C., Janks, D., Gordon, F., Wit, A. L., et al. (2014). Adverse remodeling of the electrophysiological response to ischemia–reperfusion in human heart failure is associated with remodeling of metabolic gene expression. *Circ. Arrhythmia Electrophysiol*. 7, 875–882. doi: 10.1161/circep.113.001477

Ng, G. (2017). Feasibility of selection of antiarrhythmic drug treatment on the basis of arrhythmogenic mechanism - relevance of electrical restitution, wavebreak and rotors. *Pharmacol. Ther*. 176, 1–12. doi: 10.1016/j.pharmthera.2016.10.002

O'Shea, C., Holmes, A. P., Yu, T. Y., Winter, J., Wells, S. P., Correia, J., et al. (2019). ElectroMap: high-throughput open-source software for analysis and mapping of cardiac electrophysiology. *Sci. Rep*. 9:1389.

Otsu, N. (1979). Threshold selection method from gray-level histograms. *IEEE Trans. Syst. Man. Cybern*. 9, 62–66. doi: 10.1109/tsmc.1979.4310076

Pumir, A., Arutunyan, A., Krinsky, V., and Sarvazyan, N. (2005). Genesis of ectopic waves: role of coupling, automaticity, and heterogeneity. *Biophys. J*. 89, 2332–2349. doi: 10.1529/biophysj.105.061820

Salama, G., and Hwang, S. (2009). Simultaneous optical mapping of intracellular free calcium and action potentials from Langendorff perfused hearts. *Curr. Protoc. Cytom*. [Epub ahead of print].

Salama, G., and Morad, M. (1976). Merocyanine 540 as an optical probe of transmembrane electrical activity in the heart. *Science* 191, 485–487.

Salama, G., Lombardi, R., and Elson, J. (1987). Maps of optical action potentials and NADH fluorescence in intact working hearts. *Am. J. Physiol*. 252, H384–H394.

Schindelin, J., Arganda-Carreras, I., Frise, E., Kaynig, V., Longair, M., Pietzsch, T., et al. (2012). Fiji: an open-source platform for biological-image analysis. *Nat. Methods* 9, 676–682.

Shiba, Y., Fernandes, S., Zhu, W. Z., Filice, D., Muskheli, V., Kim, J., et al. (2012). Human ES-cell-derived cardiomyocytes electrically couple and suppress arrhythmias in injured hearts. *Nature* 489, 322–325. doi: 10.1038/nature11317

Spragg, D., and Kass, D. (2006). Pathobiology of left ventricular dyssynchrony and resynchronization. *Prog. Cardiovasc. Dis*. 49, 26–41. doi: 10.1016/j.pcad.2006.05.001

Stephens, R. (2020). *RedMonk Top 20 Languages Over Time*. Available online at: https://redmonk.com/rstephens/2020/07/27/redmonk-top-20-languages-over-time-june-2020/ (accessed July 1, 2021).

Sutanto, H., Lyon, A., Lumens, J., Schotten, U., Dobrev, D., and Heijman, J. (2020). Cardiomyocyte calcium handling in health and disease: insights from in vitro and in silico studies. *Prog. Biophys. Mol. Biol*. 157, 54–75. doi: 10.1016/j.pbiomolbio.2020.02.008

Swift, L. M., Asfour, H., Posnack, N. G., Arutunyan, A., Kay, M. W., and Sarvazyan, N. (2012). Properties of blebbistatin for cardiac optical mapping and other imaging applications. *Pflugers Arch. Eur. J. Physiol*. 464, 503–512. doi: 10.1007/s00424-012-1147-2

Swift, L., Gil, D. A. B., Jaimes, R., Kay, M., Mercader, M., and Sarvazyan, N. (2014). Visualization of epicardial cryoablation lesions using endogenous tissue fluorescence. *Circ. Arrhythm. Electrophysiol*. 7, 929–937. doi: 10.1161/circep.114.001750

Swift, L., Jaimes, R., McCullough, D., Burke, M., Reilly, M., Maeda, T., et al. (2019). Optocardiography and electrophysiology studies of ex vivo langendorff-perfused hearts. *J. Vis. Exp*. [Epub ahead of print].

Tomek, J., Wang, Z. J., Burton, R.-A. B., Herring, N., and Bub, G. (2021). COSMAS: a lightweight toolbox for cardiac optical mapping analysis. *Sci. Rep*. 11:9147.

Walton, R. D., Benson, A. P., Hardy, M. E., White, E., and Bernus, O. (2013). Electrophysiological and structural determinants of electrotonic modulation of repolarization by the activation sequence. *Front. Physiol*. 4:281. doi: 10.3389/fphys.2013.00281

Wang, L., Myles, R. C., De Jesus, N. M., Ohlendorf, A. K. P., Bers, D. M., and Ripplinger, C. M. (2014). Optical mapping of sarcoplasmic reticulum Ca2+ in the intact heart: ryanodine receptor refractoriness during alternans and fibrillation. *Circ. Res*. 114, 1410–1421. doi: 10.1161/circresaha.114.302505

Weiss, J. N., Nivala, M., Garfinkel, A., and Qu, Z. (2011). Alternans and arrhythmias: from cell to heart. *Circ. Res*. 108, 98–112. doi: 10.1161/circresaha.110.223586

Wengrowski, A. M., Kuzmiak-Glancy, S., Jaimes, R., and Kay, M. W. (2014). NADH changes during hypoxia, ischemia, and increased work differ between isolated heart preparations. *Am. J. Physiol. Heart Circ. Physiol*. 306, H529–H537.

Zasadny, F. M., Dyavanapalli, J., Maritza Dowling, N., Mendelowitz, D., and Kay, M. W. (2020). Cholinergic stimulation improves electrophysiological rate adaptation during pressure overload-induced heart failure in rats. *Am. J. Physiol*. 319, H1358–H1368.

Zhang, H., Iijima, K., Huang, J., Walcott, G. P., and Rogers, J. M. (2016). Optical mapping of membrane potential and epicardial deformation in beating hearts. *Biophys. J*. 111, 438–451. doi: 10.1016/j.bpj.2016.03.043

Conflict of Interest: The authors declare that the research was conducted in the absence of any commercial or financial relationships that could be construed as a potential conflict of interest.

Publisher's Note: All claims expressed in this article are solely those of the authors and do not necessarily represent those of their affiliated organizations, or those of the publisher, the editors and the reviewers. Any product that may be evaluated in this article, or claim that may be made by its manufacturer, is not guaranteed or endorsed by the publisher.

frontiers in Physiology

REVIEW
published: 05 November 2021
doi: 10.3389/fphys.2021.752370

Potential Mechanisms of SGLT2 Inhibitors for the Treatment of Heart Failure With Preserved Ejection Fraction

*Steffen Pabel[1], Nazha Hamdani[2,3], Jagdeep Singh[4] and Samuel Sossalla[1,5]**

[1] Department of Internal Medicine II, University Hospital Regensburg, Regensburg, Germany, [2] Department of Molecular and Experimental Cardiology, Institut für Forschung und Lehre (IFL), Ruhr University Bochum, Bochum, Germany, [3] Department of Cardiology, St. Josef-Hospital, Ruhr University Bochum, Bochum, Germany, [4] The Heart Centre, Royal Infirmary of Edinburgh, Edinburgh, United Kingdom, [5] Clinic for Cardiology and Pneumology, Georg-August University Göttingen, DZHK (German Centre for Cardiovascular Research), Partner Site Göttingen, Göttingen, Germany

OPEN ACCESS

Edited by:
Elisabetta Cerbai, University of Florence, Italy

Reviewed by:
Coert J. Zuurbier, Academic Medical Center, Netherlands
Michele Ciccarelli, University of Salerno, Italy
RaffaEle Coppini, University of Florence, Italy

***Correspondence:**
Samuel Sossalla
samuel.sossalla@ukr.de

Specialty section:
This article was submitted to Cardiac Electrophysiology, a section of the journal Frontiers in Physiology

Received: *02 August 2021*
Accepted: *07 October 2021*
Published: *05 November 2021*

Citation:
Pabel S, Hamdani N, Singh J and Sossalla S (2021) Potential Mechanisms of SGLT2 Inhibitors for the Treatment of Heart Failure With Preserved Ejection Fraction. Front. Physiol. 12:752370. doi: 10.3389/fphys.2021.752370

Heart failure with preserved ejection fraction (HFpEF) is an unsolved and growing concern in cardiovascular medicine. While no treatment options that improve prognosis in HFpEF patients has been established so far, SGLT2 inhibitors (SGLT2i) are currently being investigated for the treatment of HFpEF patients. SGLT2i have already been shown to mitigate comorbidities associated with HFpEF such as type 2 diabetes and chronic renal disease, however, more recently there has been evidence that they may also directly improve diastolic function. In this article, we discuss some potential beneficial mechanisms of SGLT2i in the pathophysiology of HFpEF with focus on contractile function.

Keywords: heart failure, HFpEF—heart failure with preserved ejection fraction, SGLT2 inhibitors, diastolic function, inflammation, oxidative stress

INTRODUCTION: HEART FAILURE WITH PRESERVED EJECTION FRACTION—AN UNMET CLINICAL NEED

Heart failure (HF) with preserved ejection fraction (HFpEF) is diagnosed in a growing proportion of patients presenting with symptoms of HF (Redfield, 2016). Patients with HFpEF are characterized by clinical signs of HF with evidence of diastolic dysfunction, while systolic function is preserved. Clinical data indicate that morbidity and mortality in HFpEF patients is comparable to those with HFrEF (Redfield, 2016). Until very recently, in contrast to HFrEF, no prognostically relevant treatment strategy could be established for HFpEF patients; many efficacious drugs used in HFrEF failed to improve prognosis in HFpEF patients. Current and future pharmacological endeavors face the difficulties of a highly heterogenous HFpEF population, involving a variety of comorbidities and pathomechanisms. While HFpEF is a complex and multifaceted disease, different effects of sodium-glucose-cotransporter 2 inhibitors (SGLT2i) on mechanisms considered to be involved in HFpEF pathophysiology have been reported. Very recently, the EMPEROR-Preserved trial was the first positive study reporting a reduction of the combined risk of cardiovascular death or hospitalization for HF in patients with HFpEF after treatment with empagliflozin

(Anker et al., 2021a). This review will discuss the potential mechanisms of SGLT2i in HFpEF patients, paving the way for a novel pharmacological option for HFpEF patients.

CLINICAL EVIDENCE OF SGLT2 INHIBITORS FOR THE TREATMENT OF HEART FAILURE WITH PRESERVED EJECTION FRACTION PATIENTS

SGLT2i were initially used as oral anti-diabetes agents via blood glucose reduction from the inhibition of SGLT2 transporters in the kidney. Remarkably, SGLT2i showed distinct beneficial effects on cardiovascular outcomes in patients with type 2 diabetes mellitus (T2DM) but also in patients with HF independent of T2DM (Zinman et al., 2015; Neal et al., 2017; McMurray et al., 2019; Wiviott et al., 2019; Packer et al., 2020). The DAPA-HF trial was the first phase 3, placebo-controlled trial, which randomly assigned 4744 patients with New York Heart Association class II to IV HF with an ejection fraction of 40% or less to receive either dapagliflozin or placebo, on top of guideline recommended therapy. The primary outcome, a composite of worsening HF or cardiovascular death, was significantly and remarkably reduced in patients treated with dapagliflozin (McMurray et al., 2019). Similarly, empagliflozin significantly diminished cardiovascular death and hospitalization for HF in patients with HFrEF (Packer et al., 2020). Importantly, these improved hard outcomes in HF patients were independent of T2DM in both trials (McMurray et al., 2019; Packer et al., 2020; Petrie et al., 2020; Anker et al., 2021b). This has led to the redefinition of the pharmacological landscape in HFrEF, with SGLT2i now being recommended by clinical guidelines for HF (Cosentino et al., 2020; McDonagh et al., 2021; Writing et al., 2021).

Given the favorable cardiovascular outcomes of SGLT2i in patients with T2DM and established cardiovascular disease or at high risk and in patients with HFrEF, SGLT2i are currently being investigated in HFpEF. The recently published EMPEROR-Preserved trial investigated the effect of empagliflozin on the composite endpoint of cardiovascular death or HF hospitalization in 5988 patients with HF and an EF $>$ 40% (NYHA II-IV, elevated NT-proBNP, structural heart disease or HF hospitalization). Empagliflozin significantly reduced the primary endpoint, which was mainly driven by a ∼29% reduced risk of hospitalization for HF (Anker et al., 2021a). Although the effect was more pronounced in patients with mildly reduced EF, the effect was still present up to an EF of $<$ 60%. Therefore, SGLT2i showed to be the first evidence-proved drug for these respective patients in the absence of HFrEF. In addition to the EMPEROR-Preserved trial, the randomized controlled DELIVER trial is studying the effects of dapagliflozin on cardiovascular death or HF events in patients with HFpEF (EF $>$ 40%, structural heart disease, Elevated NT-pro BNP levels, NYHA II-IV). Both these trials undoubtedly define the role of SGLT2i in HFpEF. Of note, it has to be mentioned that the inclusion criteria of an EF $>$ 40% in both clinical trials lack the typical HFpEF definition (preserved EF). This has, however, to be discussed elsewhere. Additionally, there has been some previous evidence pointing toward favorable effects of SGLT2i in HFpEF patients.

A recent meta-analysis of randomized controlled studies regarding effects of SGLT2i in ∼16,000 patients with HF with or without T2DM, indicated that the subgroup of patients with HFpEF may also achieve a risk reduction of the composite endpoint of cardiovascular death or HF hospitalization (Singh et al., 2021). The SOLOIST-WHF trial investigated the effects of the dual SGLT1 and SGLT2 inhibitor sotagliflozin in 1222 T2DM patients recently hospitalized for worsening of HF. The investigation of sotagliflozin is of particular interest as it also inhibits SGLT1, which is, in contrast to SGLT2, expressed in the myocardium (Di Franco et al., 2017). Sotagliflozin reduced the composite of cardiovascular death, HF hospitalization and urgent HF visit consistently across different subgroups including patients with an EF $>$ 50% (Bhatt et al., 2021). Whereas pooled data from the SCORED and the SOLOIST-WHF trial showed a reduction in the composite of cardiovascular death, HF hospitalization and urgent HF visit after treatment with sotagliflozin compared to placebo (Bhatt et al., 2021), in 739 patients with HFpEF (EF $>$ 50%). Another exploratory analysis of the data from the DECLARE-TMI 58 trial, the VERTIS CV and pooled data from the SOLOIST−WHF and the SCORED study also suggests favorable effects SGLT2i on the composite of HF hospitalization and cardiovascular death in patients with HFpEF (Butler et al., 2020). Moreover, one could assume in the early cardiovascular outcome trials of SGLT2i in patients with T2DM (i.e., EMPA-REG Outcome trial, CANVAS trial, DECLARE-TIMI 58 trial), a substantial proportion of patients may have had undiagnosed HFpEF due to the comorbidities and risk profile of the trial participants (Zinman et al., 2015; Neal et al., 2017; Wiviott et al., 2019). Finally, existing evidence of the effects of SGLT2i on comorbidities relevant to HFpEF pathophysiology lends credence to the investigation of SGLT2i in HFpEF.

EFFECTS OF SODIUM-GLUCOSE-COTRANSPORTER 2 INHIBITORS ON HEART FAILURE WITH PRESERVED EJECTION COMORBIDITIES: CUTTING THE ROOTS INSTEAD OF CUTTING THE TREE?

Inhibition of SGLT2 transporters in the kidney causes glucosuria, natriuresis, and osmotic diuresis. This results in lower blood glucose levels, obesity, blood pressure and improved lipid metabolism (Abdul-Ghani et al., 2016; Mancia et al., 2016; Benham et al., 2021). All of these are typical comorbidities in HFpEF patients and are associated with increased morbidity and mortality in HFpEF (Mentz et al., 2014). Therefore, it is tempting to speculate that SGLT2i may be beneficial in HFpEF patients because their pleiotropic effects target the multifaceted pathophysiology of HFpEF.

However, some arguments against a major contribution of classical cardiovascular risk factors for the improvement of clinical outcomes should be discussed. It has been suggested that

at least in diabetic patients the reduction of cardiovascular risk factors like blood pressure (Benham et al., 2021), cholesterol (Langslet et al., 2020), or blood glucose (Fitchett et al., 2017, 2018, 2019) are unlikely to be responsible for the prognostic benefits seen with SGLT2i. It is also known that improvement of atherosclerotic risk is not considered as main mechanism to improve prognosis in diabetic patients (Fitchett et al., 2019; Zelniker et al., 2019; Arnott et al., 2020). This is also supported by the early time course of the prognostic effects of SGLT2i in clinical trials in patients with T2DM and high cardiovascular risk (Verma et al., 2017; Berg et al., 2021). However, a contribution to the later separation of the curves cannot be ruled out.

Another important consideration is cardiorenal syndrome: The hallmark feature of HF is salt and water retention, both of which are regulated by the kidneys, therefore the intimate interaction between the heart and kidneys cannot be discounted. The Study to Evaluate the Effect of Dapagliflozin on Renal Outcomes and Cardiovascular Mortality in Patients With Chronic Kidney Disease (Dapa-CKD) and Evaluation of the Effects of Canagliflozin on Renal and Cardiovascular Outcomes in Participants With Diabetic Nephropathy (CREDENCE) trials both showed striking benefits in hard renal outcomes including progression of CKD, end stage renal disease and death (Perkovic et al., 2019; Heerspink et al., 2020). Interestingly, even in these "renal outcome trials" the benefits to HF outcomes remained very robust. The putative mechanism of renal benefits stem from a reduction in trans-glomerular pressure, thereby preserving glomerular longevity. This results from renal afferent arteriolar vasoconstriction due to tubuloglomerular feedback from increased sodium delivery to the macula densa following inhibition of the SGLT2 transporter (Lytvyn et al., 2017). It follows that preservation of renal function will have salutary cardiac effects given the kidneys are the downstream target organ of the natriuretic peptide and renin-angiotensin-aldosterone systems, which play critical roles in HF.

It is known that patients with either clinically stable HFpEF, or at hospital admission due to HFpEF, worsening of renal function is independently associated with all-cause mortality (Roth et al., 2017; Kang et al., 2018). Taken together, renoprotection is therefore very likely one of the key extra-cardiac benefits of SGLT2i therapy which may lead to improved outcomes in HFpEF patients.

EFFECTS OF SODIUM-GLUCOSE-COTRANSPORTER 2 INHIBITORS ON DIASTOLIC FUNCTION

HFpEF on the myocardial level is characterized by diastolic dysfunction with impaired relaxation leading to compromised filling of the ventricles. Thus, improving diastolic function should theoretically be the ultimate treatment strategy for patients with HFpEF. While there is currently no approved therapy for the specific treatment of diastolic dysfunction, there is growing evidence suggesting that SGLT2i may directly target diastolic function. In small but prospective clinical studies in patients with T2DM and normal EF, SGLT2i improved diastolic function as determined by echocardiography after 3 (Matsutani et al., 2018) and 6 months of treatment (Shim et al., 2021). Likewise, in another small prospective but uncontrolled trial in patients with T2DM and high atherosclerotic risk, an improvement of diastolic function after 3 months empagliflozin treatment was reported (Verma et al., 2016). These clinical findings are supported by experimental evidence; in different diabetic mice models chronic treatment with empagliflozin mitigated diastolic dysfunction as measured by echocardiography (Habibi et al., 2017; Hammoudi et al., 2017) or pressure catheter (Moellmann et al., 2020). Of note, SGLT2i-treated and untreated diabetic animal models might have higher differences in blood glucose levels depending on the treatment with SGLT2i compared to patients in clinical trials with already established antidiabetic therapy. In obese diabetic rats that are characterized by diastolic dysfunction, treatment with empagliflozin acutely shortened isovolumetric relaxation time and increased the E/A ratio indicating improved diastolic function (Pabel et al., 2018). Notably, also in a DOCA-salt induced rodent HFpEF model, empagliflozin improved pathological diastolic parameters and relaxation measured by echocardiography and pressure-volume loops (Connelly et al., 2019).

As SGLT2i have broad systemic effects, investigations excluding different confounders are needed to further clarify the effects of SGLT2i on diastolic function. Our group provided first evidence of favorable effects of empagliflozin on diastolic function in human ventricular trabecula from patients with HFrEF (Pabel et al., 2018). Empagliflozin acutely mitigated pathological diastolic stiffness in the human specimens. The study firstly showed that these effects were independent of T2DM. Importantly, the human trabeculae were studied *in vitro*, in the absence of systemic confounders (e.g., alterations of blood pressure or volume shift) as may occur in any *in vivo* model. Thus, these experiments indicate a direct cardiac effect of SGLT2i-induced improvement of diastolic function (Pabel et al., 2018).

To understand the potential mechanism of action of SGLT2i-induced improvement in diastolic function, one must appreciate that diastolic function is determined by (1) the myocardial stiffness based on the viscoelastic properties mediated largely by myofilament stiffness as well as structural remodeling of the extracellular matrix and (2) myocardial relaxation mediated by Ca^{2+} dissociation from troponin C and reuptake into the sarcoplasmic reticulum (Franssen and González Miqueo, 2016). The following paragraphs will discuss the potential effects of SGLT2i on these different aspects of diastolic function and their pathophysiological implications in HFpEF.

Effects of Sodium-Glucose-Cotransporter 2 Inhibitors on Myofilament Function

Myofilament function critically determines diastolic cardiomyocyte stiffness, and myofilament stiffness is abnormally increased in HFpEF patients (Borbely et al., 2005). The giant elastic protein titin is known to influence passive stiffness via isoform shift (N2BA/N2B ratio) and posttranslational

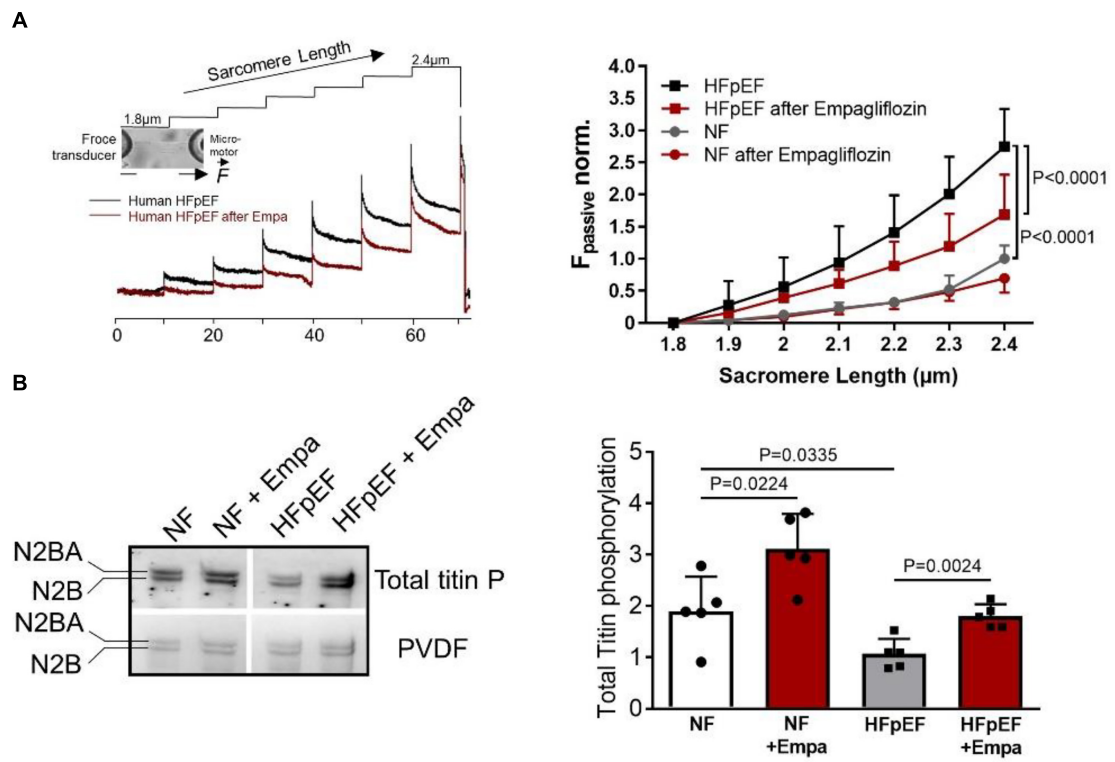

FIGURE 1 | (A) Force response to stepwise cardiomyocyte stretches showing the effects of empagliflozin on passive myofilament stiffness of human skinned cardiomyocytes from HFpEF patients or controls (non-failing, NF) and **(B)** phosphorylation levels of titin in human HFpEF myocardium and controls ± empagliflozin treatment (Pabel et al., 2018); with permission.

modifications such as oxidation and/or phosphorylation (Linke and Hamdani, 2014). In animal and human HFpEF myocardia, altered phosphorylation of titin and other small regulatory myofilament proteins have been shown to increase passive cardiomyocyte stiffness (Hamdani et al., 2013a,b,c; Linke and Hamdani, 2014). Our previous findings demonstrated that in human HFpEF myocardium, empagliflozin restores the pathologically altered phosphorylation of titin (**Figure 1**) and the small regulatory proteins troponin I and myosin binding protein C (Pabel et al., 2018). Consequently, empagliflozin treatment led to a reduction of pathological cardiomyocyte stiffness in human HFpEF myocardium (Pabel et al., 2018). Furthermore, we revealed that these observations were mediated by an improvement of cyclic guanosine monophosphate (cGMP)-dependent protein kinase or protein kinase G (PKG) signaling, which is typically diminished in HFpEF myocardium and is known to underlie diastolic stiffness in HFpEF (Paulus and Tschöpe, 2013). Accordingly, the improvement of cGMP pool, which regulates PKG activity, is thus considered as a potential therapeutic target in HFpEF (Greene et al., 2013). Interestingly, empagliflozin enhanced the NO-cGMP-PKG pathway after 8 weeks of treatment in diabetic mice (Xue et al., 2019). In human and rodent HFpEF myocardium we showed that nitric oxide bioavailability increased upon acute empagliflozin treatment resulting in elevated cGMP levels and increased PKG activity. As a consequence, PKG-dependent phosphorylation of myofilament proteins was restored (Kolijn et al., 2021). Recently, in pigs with myocardial infarction induced HFrEF 2 months of treatment with empagliflozin also resulted in an improved diastolic function in invasive and non-invasive analyses, which was associated with increased NO availability and PKG signaling (Santos-Gallego et al., 2021). As PKG is centrally involved in HFpEF pathophysiology, the impact of SGLT2i on PKG signaling and myofilament function could therefore be a key-stone effect in improving diastolic function in HFpEF hearts (**Figure 2**), thereby resulting in material change the disease trajectory (Pabel et al., 2020a).

Effects of Sodium-Glucose-Cotransporter 2 Inhibitors on Myocardial Fibrosis

Increased cardiac fibrosis adversely affects diastolic function and is a common feature in HFpEF patients (Zile et al., 2015). The etiology of fibrosis is heterogenous and the development of fibrotic tissue presumably takes place at later disease stages

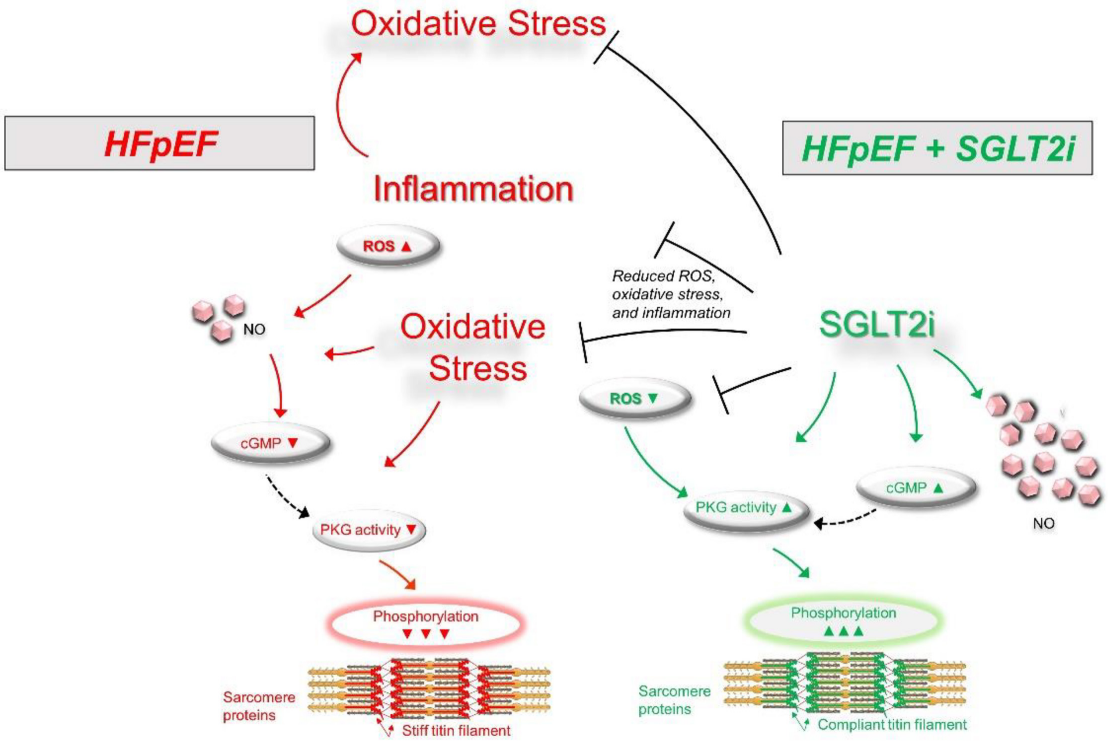

FIGURE 2 | Scheme for the signaling pathways in HFpEF (left) showing an oxidative condition with impaired signaling pathways via increased inflammation and oxidative stress (Upward arrows = increase; downward arrows = decrease). SGLT2i treatment (right) may result in a significant improvement of signaling pathways via decreased inflammation and oxidative stress. cGMP, cyclic guanosine monophosphate; HFpEF, heart failure with preserved ejection fraction; NO, nitric oxide; PKG, protein kinase G; ROS, reactive oxygen species.

(Sweeney et al., 2020). Increased fibrosis reduces myocardial compliance thereby limiting diastolic filling (de Souza, 2002; Kasner et al., 2011; Sweeney et al., 2020). Limited evidence of the impact of SGLT2i on myocardial fibrosis has been reported. In a hypertensive HF model, 12 weeks of treatment with empagliflozin resulted in reduced cardiac remodeling with less atrial as well as ventricular fibrosis (Lee et al., 2019). In another rat model of myocardial infarction, dapagliflozin reduced myofibroblast and macrophages infiltration and thereby demonstrating antifibrotic properties (Lee et al., 2017). Reduced fibrotic content upon SGLT2i treatment was also observed in diabetic (Li et al., 2019) and afterload induced HFrEF mice (Shi et al., 2019). A possible mechanism has been provided in a diabetic mouse model, where dapagliflozin reduced myocardial fibrosis and proinflammatory markers, which was associated with regulation of AMPK (Ye et al., 2017). Accordingly, dapagliflozin increased AMPK phosphorylation in cardiac fibroblasts, which also resulted in a reduction of NHE1 mRNA expression (Ye et al., 2018).

Preventing the development of cardiac fibrosis using SGLT2i likely impedes the progression of myocardial stiffness and may therefore be advantageous for the causal treatment HFpEF patients. Nevertheless, evidence of these specific and direct mechanisms of SGLT2i on fibrosis is limited. Moreover, the effect of these agents on myocardial fibrosis may be confounded by their other cardiovascular effects which may deter disease progression via different mechanisms.

Effects of Sodium-Glucose-Cotransporter 2 Inhibitors on Cardiac Hypertrophy

In patients presenting with HFpEF, diastolic dysfunction and cardiac hypertrophy are often concomitantly found. While the interaction of hypertrophy, diastolic function and HFpEF is complex, increased left ventricular hypertrophy impairs chamber geometry and may induce diastolic dysfunction *per se* (Heinzel et al., 2015). Along with the SGLT2i-induced improvement of diastolic function in different patient populations, an impact of SGLT2i on left ventricular hypertrophy has been demonstrated. Clinical data of a randomized placebo-controlled trial of 97 patients with preserved EF and T2DM as well as coronary artery disease demonstrated using cardiac MRI that empagliflozin reduced LV mass index after 6 months of treatment (Verma et al., 2019). A reduction of LV mass following SGLT2i therapy was also observed in echocardiographic measurements of patients with T2DM (Verma et al., 2016; Brown et al., 2020). However, in these clinical trials it is impossible to separate direct cardiac effects from secondary mechanisms such as changes of blood pressure or pre- and

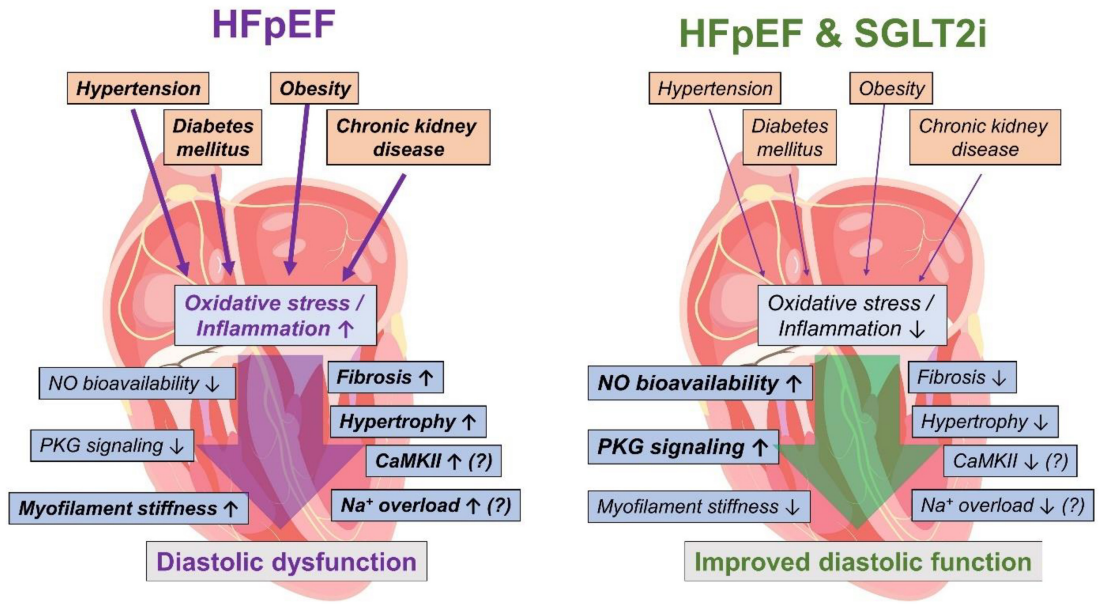

FIGURE 3 | Pathophysiology involved in HFpEF leading to diastolic dysfunction (left) and possible beneficial mechanisms of SGLT2i in HFpEF (right). HFpEF, heart failure with preserved ejection fraction; NO, nitric oxide; PKG, protein kinase G; CaMKII, Ca^{2+}/calmodulin-dependent protein kinase IIδ; SGLT2i, sodium-glucose-cotransporter 2 inhibitors. The heart image is licensed by Shutterstock.com/Usama Nasir MD.

afterload. As of now, the mechanisms of the regression in hypertrophy warrants further investigation, in particular in HFpEF patients.

Effects of Sodium-Glucose-Cotransporter 2 Inhibitors on Cardiomyocyte Na^+ and Ca^{2+} Homeostasis

Cardiomyocyte Ca^{2+} homeostasis mediates excitation-contraction coupling, thereby determining myocardial contraction and relaxation. During diastole cytosolic Ca^{2+} moves back into the sarcoplasmic reticulum via the SERCA2a transporter which is modulated by phospholamban. Ca^{2+} is also eliminated from the cardiomyocyte via the Na^+/Ca^{2+} exchanger. As cytosolic Ca^{2+} levels decrease, the passive dissociation from Troponin C changes tropomyosin conformation resulting in myocardial relaxation (Bers, 2002). Thus, Ca^{2+} homeostasis plays a critical role for diastolic function. However, data on Ca^{2+} handling in HFpEF are scarce due to limited availability of human samples and limitations of HFpEF-like animal models. Reports from HFpEF-like animal models (i.e., via age, metabolic disorders or transverse aortic constriction) indicate that systolic Ca^{2+} release and cell shortening could be unaltered or increased, while Ca^{2+} reuptake and relaxation may be impaired along with elevated diastolic Ca^{2+} depending on the model studied (Peana and Domeier, 2017; Frisk et al., 2021). SGLT2i have been reported to influence cardiomyocyte Na^+ homeostasis and thereby Ca^{2+} handling (firstly reported by Baartscheer et al., 2017), thus potentially modulating diastolic function. In failing ventricular murine and human cardiomyocytes treated *in vitro* with empagliflozin (24 h) Ca^{2+}/calmodulin-dependent protein kinase IIδ (CaMKII) activity has been found to be diminished (Mustroph et al., 2018). Consequently, aberrant diastolic sarcoplasmic reticulum Ca^{2+} leak, which elevates cytosolic Ca^{2+} levels and thereby adversely increasing diastolic tension (Fischer et al., 2013) was reduced after exposure to empagliflozin (Mustroph et al., 2018). It has therefore been speculated that this mechanism could also be involved in HFpEF pathophysiology (Eisner et al., 2020). Interestingly, in obese diabetic mice, the improvement of diastolic function was associated with an increased phospholamban phosphorylation and thus SERCA2a activity (Hammoudi et al., 2017). However, the effects of SGLT2i on cardiomyocyte Ca^{2+} homeostasis are in part controversial and difficult to interpret as experimental protocols and (disease) models varied. In human cardiomyocytes from patients with HFrEF acute treatment with empagliflozin did not change systolic Ca^{2+} transient or diastolic cytosolic Ca^{2+} (Pabel et al., 2018). Likewise, we performed a blinded experimental long-term study of human induced pluripotent stem cell cardiomyocytes from healthy subjects as clinical effects occur after weeks or months which is in contrast to many experimental study designs where acute exposure to these drugs have been performed. In our respective study 2 months of treatment with empagliflozin showed no impact on Ca^{2+} homeostasis and EC-coupling proteins (Pabel et al., 2020b). In a study based on Dahl salt-sensitive rats with high-salt diet serving as a HFpEF model, the authors reported that dapagliflozin beneficially affects Ca^{2+} and Na^+ overload after *in vivo* treatment but not after direct treatment of cardiomyocytes (Cappetta et al., 2020). Therefore, also non-cardiomyocyte targets might be involved in possible effects of SGLT2i on EC-coupling.

Besides Ca^{2+} cycling, Na^+ homeostasis has shown to influence diastolic function. As an increased Na^+ influx is counterbalanced via Na^+/Ca^{2+} exchanger, mechanisms elevating cytosolic Na^+ levels may also increase Ca^{2+} concentration. We have demonstrated that inhibition of the late Na^+ current reduces increased cellular Na^+ in HF and secondary diastolic Ca^{2+} which indeed led to a reduced diastolic dysfunction in human HF preparations (Sossalla et al., 2008). This mechanism may theoretically also reduce the arrhythmia potential and could explain the early mortality benefit seen (i.e., less sudden cardiac deaths) in this otherwise high risk population. Thus, distorted Na^+/Ca^{2+} interplay detrimentally contributes to diastolic dysfunction in HFrEF (Sossalla et al., 2008).

Interestingly, SGLT2i has been recently reported to inhibit the late Na^+ current in murine HF cardiomyocytes, which constitutes an abnormal Na^+ influx throughout the action potential (Philippaert et al., 2021). In molecular docking simulations these effects were proposed to be driven by binding of empagliflozin on major cardiac Na^+ channel isoform $Na_V1.5$ (Philippaert et al., 2021). While the role of SGLT2i for late Na^+ current needs to be further investigated in HFpEF, the reduction of late Na^+ current could favorably impact diastolic function (Sossalla et al., 2011). Interestingly, in patients with hypertrophic cardiomyopathy, typically characterized by normal systolic function but severely disturbed myocardial relaxation, the late Na^+ current has been demonstrated to deteriorate cardiomyocyte Na^+ and thus Ca^{2+} balance as a mechanism for impaired diastolic function (Coppini et al., 2013; Ferrantini et al., 2018). On the other hand, in patients with HFpEF and hypertensive heart disease an increased diastolic Ca^{2+} with impaired relaxation was found, which was, however, not caused by elevated Na^+ levels in this model (Runte et al., 2017). Thus, further studies of cardiomyocyte Na^+ homeostasis with respect to SGLT2i are needed, in particular in HFpEF myocardium.

Another mechanism by which SGLT2i may influence myocardial Na^+ homeostasis are inhibitory effects on the Na^+/H^+ exchanger 1 (NHE1), which were first reported for rabbit myocardium (Baartscheer et al., 2017), and later confirmed for murine cardiomyocytes (Uthman et al., 2018) and human atrial tissue (Trum et al., 2020). A study in healthy rabbit cardiomyocytes reported a consecutive acute reduction in cytosolic Ca^{2+} and Na^+ by empagliflozin (Baartscheer et al., 2017). On the contrary the effects on Na^+ homeostasis via NHE1 inhibition have been questioned in a study using healthy rat cardiomyocytes (Chung et al., 2020).

Finally, overall cytosolic Na^+ levels were also decreased by empagliflozin after 30 min and 24 h treatment in murine wild-type mice (Mustroph et al., 2018). Therefore, SGLT2i-dependent changes in myocardial Na^+ might constitute an important cardiac mechanism potentially also in HFpEF (Trum et al., 2021). In conclusion, studies in different experimental models reported an involvement of SGLT2i in cellular Ca^{2+} and Na^+ homeostasis. Yet, the role of cellular Ca^{2+} and Na^+ alterations with respect to treatment with SGLT2i in HFpEF is rather speculative and further studies in HFpEF myocardium are required to clarify this important question.

Inflammation and Oxidative Stress: The Joint Mechanism of Sodium-Glucose-Cotransporter 2 Inhibitors?

In HFpEF, inflammation and oxidative stress play a key role for the progression of structural and functional diastolic dysfunction and are associated with comorbidities typically found in HFpEF patients (**Figure 3**) such as chronic kidney disease or metabolic syndrome (Franssen et al., 2016; Zhazykbayeva et al., 2020). In particular in cardiorenal syndrome, kidney injury-associated chronic inflammation and oxidative activation may impair cardiac function as shown in different models of renal failure (Rangaswami et al., 2019). Thus, oxidative stress and inflammation are considered as central mechanisms linking the cardiac HFpEF phenotype with the multifaceted comorbidities in the HFpEF patient (Zhazykbayeva et al., 2020). Growing evidence demonstrates that SGLT2i attenuate inflammation and oxidative stress (Yaribeygi et al., 2019). In diabetic mice with myocardial infarction SGLT2i reduced oxidative stress and inflammatory markers (Ye et al., 2017; Yurista et al., 2019). Likewise, 4 weeks of treatment with ipragliflozin diminished oxidative stress and inflammation in diabetic mice (Tahara et al., 2013, 2014).

In HFpEF, also inflammation/oxidative stress-mediated endothelial dysfunction may impair cardiomyocyte function (Franssen et al., 2016). A recent work demonstrated that empagliflozin may reduce inflammation-dependent endothelial dysfunction resulting in improved cardiomyocyte contractility (Juni et al., 2019). In line with that, dapagliflozin reduced endothelial dysfunction and inflammation in a HFpEF rat model (Dahl salt-sensitive rats with high-salt diet) resulting in an improved diastolic function (Cappetta et al., 2020). Moreover, we showed that empagliflozin attenuated pathologically elevated levels of oxidative stress (H_2O_2, GSH, LPO) and inflammation (ICAM, VCAM, TNFα, and IL-6) in human HFpEF myocardium after *in vitro* treatment (Kolijn et al., 2021).

As empagliflozin reduced oxidative stress and inflammation in human HFpEF myocardium, NO bioavailability and PKG signaling were improved upon exposure to empagliflozin leading to lower myofilament stiffness and thereby improved diastolic function in human myocardium (Pabel et al., 2018; Kolijn et al., 2021). Thus, the attenuation of oxidative stress and inflammation due to SGLT2i treatment could be potentially helpful in HFpEF patients (**Figure 3**) at least via an improvement of contractility (Pabel et al., 2020a). Also, other potential secondary effects of SGLT2i driven by a reduction of oxidative stress and inflammation are conceivable. A potential oxidative CaMKII activation (Erickson et al., 2008) might be diminished as SGLT2i reduce oxidative stress, which could result in lower diastolic sarcoplasmic reticulum Ca^{2+} leak as well as reduced late Na^+ current (Mustroph et al., 2018; Philippaert et al., 2021). Finally, hypertrophy and fibrosis are a common detrimental outcome of chronic inflammation and oxidative stress, and could thereby be ameliorated upon anti-oxidative and anti-inflammatory effects of SGLT2i (Zhazykbayeva et al., 2020). However, the molecular mechanisms need to be explored further.

CONCLUSION

As we are on the cusp of welcoming the first prognostically beneficial drug class in HFpEF, understanding the mechanistic effects of SGLT2i on the myocardium will be key in maximizing its potential in this important patient population. While some putative targets and pathways are still rather speculative, evidence from human myocardium including human HFpEF hearts indicate direct favorable effects on diastolic function via reduced myofilament stiffness due to improved PKG signaling. While this review discusses some potentially relevant mechanisms of SGLT2i in HFpEF, also other pleiotropic effects of SGLT2i have been described as discussed elsewhere (Packer, 2020). Both the EMPEROR-Preserved and the DELIVER trials will, undoubtedly, provide further insight into the extent to which SGLT2i will have an impact on the treatment of HFpEF patients in the near future.

AUTHOR CONTRIBUTIONS

SP, NH, JS, and SS drafted and revised the manuscript. All authors contributed to the article and approved the submitted version.

FUNDING

SP and SS were funded by the Else-Kröner-Fresenius Stiftung via research grants (2017_A137 and 2019_A84). SP was funded by the German Society of Internal Medicine. NH was funded by DFG (HA 7512/2-1, HA 7512/2-4) and the European HCEMM.

REFERENCES

Abdul-Ghani, M., Del Prato, S., Chilton, R., and DeFronzo, R. A. (2016). SGLT2 inhibitors and cardiovascular risk: lessons learned from the EMPA-REG OUTCOME study. *Diab. Care* 39, 717–725. doi: 10.2337/dc16-0041

Anker, S. D., Butler, J., Filippatos, G., Ferreira, J. P., Bocchi, E., Bohm, M., et al. (2021a). Empagliflozin in heart failure with a preserved ejection fraction. *N. Engl. J. Med.* Online ahead of print. doi: 10.1056/NEJMoa2107038

Anker, S. D., Butler, J., Filippatos, G., Khan, M. S., Marx, N., Lam, C. S. P., et al. (2021b). Effect of empagliflozin on cardiovascular and renal outcomes in patients with heart failure by baseline diabetes status: results from the EMPEROR-Reduced trial. *Circulation* 143, 337–349. doi: 10.1161/CIRCULATIONAHA.120.051824

Arnott, C., Li, Q., Kang, A., Neuen, B. L., Bompoint, S., Lam, C. S. P., et al. (2020). Sodium-Glucose Cotransporter 2 inhibition for the prevention of cardiovascular events in patients with Type 2 diabetes mellitus: a systematic review and meta-analysis. *J. Am. Heart Assoc.* 9:e014908. doi: 10.1161/JAHA.119.014908

Baartscheer, A., Schumacher, C. A., Wust, R. C., Fiolet, J. W., Stienen, G. J., Coronel, R., et al. (2017). Empagliflozin decreases myocardial cytoplasmic Na(+) through inhibition of the cardiac Na(+)/H(+) exchanger in rats and rabbits. *Diabetologia* 60, 568–573. doi: 10.1007/s00125-016-4134-x

Benham, J. L., Booth, J. E., Sigal, R. J., Daskalopoulou, S. S., Leung, A. A., and Rabi, D. M. (2021). Systematic review and meta-analysis: SGLT2 inhibitors, blood pressure and cardiovascular outcomes. *Int. J. Cardiol. Heart Vasc.* 33:100725. doi: 10.1016/j.ijcha.2021.100725

Berg, D. D., Jhund, P. S., Docherty, K. F., Murphy, S. A., Verma, S., Inzucchi, S. E., et al. (2021). Time to clinical benefit of dapagliflozin and significance of prior heart failure hospitalization in patients with heart failure with reduced ejection fraction. *JAMA Cardiol.* 6, 499–507. doi: 10.1001/jamacardio.2020.7585

Bers, D. M. (2002). Cardiac excitation-contraction coupling. *Nature* 415, 198–205. doi: 10.1038/415198a

Bhatt, D. L., Szarek, M., Steg, P. G., Cannon, C. P., Leiter, L. A., McGuire, D. K., et al. (2021). Sotagliflozin in patients with diabetes and recent worsening heart failure. *N. Engl. J. Med.* 384, 117–128. doi: 10.1056/NEJMoa2030183

Borbely, A., van der Velden, J., Papp, Z., Bronzwaer, J. G., Edes, I., Stienen, G. J., et al. (2005). Cardiomyocyte stiffness in diastolic heart failure. *Circulation* 111, 774–781. doi: 10.1161/01.CIR.0000155257.33485.6D

Brown, A. J. M., Gandy, S., McCrimmon, R., Houston, J. G., Struthers, A. D., and Lang, C. C. (2020). A randomized controlled trial of dapagliflozin on left ventricular hypertrophy in people with type two diabetes: the DAPA-LVH trial. *Eur. Heart J.* 41, 3421–3432. doi: 10.1093/eurheartj/ehaa419

Butler, J., Usman, M. S., Khan, M. S., Greene, S. J., Friede, T., Vaduganathan, M., et al. (2020). Efficacy and safety of SGLT2 inhibitors in heart failure: systematic review and meta-analysis. *ESC Heart Fail* 7, 3298–3309. doi: 10.1002/ehf2.13169

Cappetta, D., De Angelis, A., Ciuffreda, L. P., Coppini, R., Cozzolino, A., Micciche, A., et al. (2020). Amelioration of diastolic dysfunction by dapagliflozin in a non-diabetic model involves coronary endothelium. *Pharmacol. Res.* 157:104781. doi: 10.1016/j.phrs.2020.104781

Chung, Y. J., Park, K. C., Tokar, S., Eykyn, T. R., Fuller, W., Pavlovic, D., et al. (2020). Off-target effects of SGLT2 blockers: empagliflozin does not inhibit Na+/H+ exchanger-1 or lower [Na+]i in the heart. *Cardiovasc. Res.* Online ahead of print. doi: 10.1093/cvr/cvaa323

Connelly, K. A., Zhang, Y., Visram, A., Advani, A., Batchu, S. N., Desjardins, J. F., et al. (2019). Empagliflozin improves diastolic function in a nondiabetic rodent model of heart failure with preserved ejection fraction. *JACC Basic Transl. Sci.* 4, 27–37. doi: 10.1016/j.jacbts.2018.11.010

Coppini, R., Ferrantini, C., Yao, L., Fan, P., Del Lungo, M., Stillitano, F., et al. (2013). Late sodium current inhibition reverses electromechanical dysfunction in human hypertrophic cardiomyopathy. *Circulation* 127, 575–584. doi: 10.1161/CIRCULATIONAHA.112.134932

Cosentino, F., Grant, P. J., Aboyans, V., Bailey, C. J., Ceriello, A., Delgado, V., et al. (2020). 2019 ESC guidelines on diabetes, pre-diabetes, and cardiovascular diseases developed in collaboration with the EASD. *Eur. Heart J.* 41, 255–323. doi: 10.1093/eurheartj/ehz486

de Souza, R. R. (2002). Aging of myocardial collagen. *Biogerontology* 3, 325–335. doi: 10.1023/A:1021312027486

Di Franco, A., Cantini, G., Tani, A., Coppini, R., Zecchi-Orlandini, S., Raimondi, L., et al. (2017). Sodium-dependent glucose transporters (SGLT) in human ischemic heart: a new potential pharmacological target. *Int. J. Cardiol.* 243, 86–90. doi: 10.1016/j.ijcard.2017.05.032

Eisner, D. A., Caldwell, J. L., Trafford, A. W., and Hutchings, D. C. (2020). The control of diastolic calcium in the heart: basic mechanisms and functional implications. *Circ. Res.* 126, 395–412. doi: 10.1161/CIRCRESAHA.119.315891

Erickson, J. R., Joiner, M. L., Guan, X., Kutschke, W., Yang, J., Oddis, C. V., et al. (2008). A dynamic pathway for calcium-independent activation of CaMKII by methionine oxidation. *Cell* 133, 462–474. doi: 10.1016/j.cell.2008.02.048

Ferrantini, C., Pioner, J. M., Mazzoni, L., Gentile, F., Tosi, B., Rossi, A., et al. (2018). Late sodium current inhibitors to treat exercise-induced obstruction in hypertrophic cardiomyopathy: an in vitro study in human myocardium. *Br. J. Pharmacol.* 175, 2635–2652. doi: 10.1111/bph.14223

Fischer, T. H., Maier, L. S., and Sossalla, S. (2013). The ryanodine receptor leak: how a tattered receptor plunges the failing heart into crisis. *Heart Fail. Rev.* 18, 475–483. doi: 10.1007/s10741-012-9339-6

Fitchett, D., Butler, J., van de Borne, P., Zinman, B., Lachin, J. M., Wanner, C., et al. (2018). Effects of empagliflozin on risk for cardiovascular death and heart failure hospitalization across the spectrum of heart failure risk in the EMPA-REG OUTCOME(R) trial. *Eur. Heart J.* 39, 363–370. doi: 10.1093/eurheartj/ehx511

Fitchett, D., Inzucchi, S. E., Cannon, C. P., McGuire, D. K., Scirica, B. M., Johansen, O. E., et al. (2019). Empagliflozin reduced mortality and hospitalization for heart failure across the spectrum of cardiovascular risk in the EMPA-REG OUTCOME trial. *Circulation* 139, 1384–1395. doi: 10.1161/CIRCULATIONAHA.118.037778

Fitchett, D., Mcknight, J., Lee, J., George, J. T., Mattheus, M., Woerle, H. J., et al. (2017). Empagliflozin (EMPA) reduces heart failure irrespective of control of blood pressure (BP), low density lipoprotein cholesterol (LDL-C), and HbA1c. *Diabetes* 66, A312–A313. doi: 10.1016/j.cjca.2017.07.336

Franssen, C., Chen, S., Unger, A., Korkmaz, H. I., De Keulenaer, G. W., Tschope, C., et al. (2016). Myocardial microvascular inflammatory endothelial activation in heart failure with preserved ejection fraction. *JACC Heart Fail* 4, 312–324. doi: 10.1016/j.jchf.2015.10.007

Franssen, C., and González Miqueo, A. (2016). The role of titin and extracellular matrix remodelling in heart failure with preserved ejection fraction. *Neth Heart J.* 24, 259–267. doi: 10.1007/s12471-016-0812-z

Frisk, M., Le, C., Shen, X., Roe, A. T., Hou, Y., Manfra, O., et al. (2021). Etiology-Dependent impairment of diastolic cardiomyocyte calcium homeostasis in heart failure with preserved ejection fraction. *J. Am. Coll. Cardiol.* 77, 405–419. doi: 10.1016/j.jacc.2020.11.044

Greene, S. J., Gheorghiade, M., Borlaug, B. A., Pieske, B., Vaduganathan, M., Burnett, J. C., et al. (2013). The cGMP signaling pathway as a therapeutic target in heart failure with preserved ejection fraction. *J. Am. Heart Assoc.* 2:e000536. doi: 10.1161/JAHA.113.000536

Habibi, J., Aroor, A. R., Sowers, J. R., Jia, G., Hayden, M. R., Garro, M., et al. (2017). Sodium glucose transporter 2 (SGLT2) inhibition with empagliflozin improves cardiac diastolic function in a female rodent model of diabetes. *Cardiovasc. Diabetol.* 16:9. doi: 10.1186/s12933-016-0489-z

Hamdani, N., Bishu, K. G., von Frieling-Salewsky, M., Redfield, M. M., and Linke, W. A. (2013a). Deranged myofilament phosphorylation and function in experimental heart failure with preserved ejection fraction. *Cardiovasc. Res.* 97, 464–471. doi: 10.1093/cvr/cvs353

Hamdani, N., Franssen, C., Lourenco, A., Falcao-Pires, I., Fontoura, D., Leite, S., et al. (2013b). Myocardial titin hypophosphorylation importantly contributes to heart failure with preserved ejection fraction in a rat metabolic risk model. *Circ. Heart Fail* 6, 1239–1249. doi: 10.1161/CIRCHEARTFAILURE.113.000539

Hamdani, N., Krysiak, J., Kreusser, M. M., Neef, S., Dos Remedios, C. G., Maier, L. S., et al. (2013c). Crucial role for Ca2(+)/calmodulin-dependent protein kinase-II in regulating diastolic stress of normal and failing hearts via titin phosphorylation. *Circ. Res.* 112, 664–674. doi: 10.1161/CIRCRESAHA.111.300105

Hammoudi, N., Jeong, D., Singh, R., Farhat, A., Komajda, M., Mayoux, E., et al. (2017). Empagliflozin improves left ventricular diastolic dysfunction in a genetic model of Type 2 diabetes. *Cardiovasc. Drugs. Ther.* 31, 233–246. doi: 10.1007/s10557-017-6734-1

Heerspink, H. J. L., Stefansson, B. V., Correa-Rotter, R., Chertow, G. M., Greene, T., Hou, F. F., et al. (2020). Dapagliflozin in patients with chronic kidney disease. *N. Engl. J. Med.* 383, 1436–1446. doi: 10.1056/NEJMoa2024816

Heinzel, F. R., Hohendanner, F., Jin, G., Sedej, S., and Edelmann, F. (2015). Myocardial hypertrophy and its role in heart failure with preserved ejection fraction. *J. Appl. Physiol.* 119, 1233–1242. doi: 10.1152/japplphysiol.00374.2015

Juni, R. P., Kuster, D. W. D., Goebel, M., Helmes, M., Musters, R. J. P., van der Velden, J., et al. (2019). Cardiac microvascular endothelial enhancement of cardiomyocyte function is impaired by inflammation and restored by empagliflozin. *JACC Basic Transl. Sci.* 4, 575–591. doi: 10.1016/j.jacbts.2019.04.003

Kang, J., Park, J. J., Cho, Y. J., Oh, I. Y., Park, H. A., Lee, S. E., et al. (2018). Predictors and prognostic value of worsening renal function during admission in HFpEF versus HFrEF: data from the KorAHF (Korean Acute Heart Failure) registry. *J. Am. Heart Assoc.* 7:e007910. doi: 10.1161/JAHA.117.007910

Kasner, M., Westermann, D., Lopez, B., Gaub, R., Escher, F., Kuhl, U., et al. (2011). Diastolic tissue Doppler indexes correlate with the degree of collagen expression and cross-linking in heart failure and normal ejection fraction. *J. Am. Coll. Cardiol.* 57, 977–985. doi: 10.1016/j.jacc.2010.10.024

Kolijn, D., Pabel, S., Tian, Y., Lodi, M., Herwig, M., Carrizzo, A., et al. (2021). Empagliflozin improves endothelial and cardiomyocyte function in human heart failure with preserved ejection fraction via reduced pro-inflammatory-oxidative pathways and protein kinase Galpha oxidation. *Cardiovasc. Res.* 117, 495–507. doi: 10.1093/cvr/cvaa123

Langslet, G., Zinman, B., Wanner, C., Hantel, S., Espadero, R. M., Fitchett, D., et al. (2020). Cardiovascular outcomes and LDL-cholesterol levels in EMPA-REG OUTCOME((R)). *Diab. Vasc. Dis. Res.* 17:1479164120975256. doi: 10.1177/1479164120975256

Lee, H. C., Shiou, Y. L., Jhuo, S. J., Chang, C. Y., Liu, P. L., Jhuang, W. J., et al. (2019). The sodium-glucose co-transporter 2 inhibitor empagliflozin attenuates cardiac fibrosis and improves ventricular hemodynamics in hypertensive heart failure rats. *Cardiovasc. Diabetol.* 18:45. doi: 10.1186/s12933-019-0849-6

Lee, T. M., Chang, N. C., and Lin, S. Z. (2017). Dapagliflozin, a selective SGLT2 Inhibitor, attenuated cardiac fibrosis by regulating the macrophage polarization via STAT3 signaling in infarcted rat hearts. *Free Radic Biol. Med.* 104, 298–310. doi: 10.1016/j.freeradbiomed.2017.01.035

Li, C., Zhang, J., Xue, M., Li, X., Han, F., Liu, X., et al. (2019). SGLT2 inhibition with empagliflozin attenuates myocardial oxidative stress and fibrosis in diabetic mice heart. *Cardiovasc. Diabetol.* 18:15. doi: 10.1186/s12933-019-0816-2

Linke, W. A., and Hamdani, N. (2014). Gigantic business: titin properties and function through thick and thin. *Circ. Res.* 114, 1052–1068. doi: 10.1161/CIRCRESAHA.114.301286

Lytvyn, Y., Bjornstad, P., Udell, J. A., Lovshin, J. A., and Cherney, D. Z. I. (2017). Sodium glucose Cotransporter-2 inhibition in heart failure: potential mechanisms, clinical applications, and summary of clinical trials. *Circulation* 136, 1643–1658. doi: 10.1161/CIRCULATIONAHA.117.030012

Mancia, G., Cannon, C. P., Tikkanen, I., Zeller, C., Ley, L., Woerle, H. J., et al. (2016). Impact of empagliflozin on blood pressure in patients with Type 2 diabetes mellitus and hypertension by background antihypertensive medication. *Hypertension* 68, 1355–1364. doi: 10.1161/HYPERTENSIONAHA.116.07703

Matsutani, D., Sakamoto, M., Kayama, Y., Takeda, N., Horiuchi, R., and Utsunomiya, K. (2018). Effect of canagliflozin on left ventricular diastolic function in patients with type 2 diabetes. *Cardiovasc. Diabetol.* 17:73. doi: 10.1186/s12933-018-0717-9

McDonagh, T. A., Metra, M., Adamo, M., Gardner, R. S., Baumbach, A., Bohm, M., et al. (2021). 2021 ESC guidelines for the diagnosis and treatment of acute and chronic heart failure. *Eur. Heart J.* 42, 3599–3726. doi: 10.1093/eurheartj/ehab368

McMurray, J. J. V., Solomon, S. D., Inzucchi, S. E., Kober, L., Kosiborod, M. N., Martinez, F. A., et al. (2019). Dapagliflozin in patients with heart failure and reduced ejection fraction. *N. Engl. J. Med.* 381, 1995–2008. doi: 10.1056/NEJMoa1911303

Mentz, R. J., Kelly, J. P., von Lueder, T. G., Voors, A. A., Lam, C. S., Cowie, M. R., et al. (2014). Noncardiac comorbidities in heart failure with reduced versus preserved ejection fraction. *J. Am. Coll. Cardiol.* 64, 2281–2293. doi: 10.1016/j.jacc.2014.08.036

Moellmann, J., Klinkhammer, B. M., Droste, P., Kappel, B., Haj-Yehia, E., Maxeiner, S., et al. (2020). Empagliflozin improves left ventricular diastolic function of db/db mice. *Biochim Biophys. Acta Mol. Basis Dis.* 1866:165807. doi: 10.1016/j.bbadis.2020.165807

Mustroph, J., Wagemann, O., Lucht, C. M., Trum, M., Hammer, K. P., Sag, C. M., et al. (2018). Empagliflozin reduces Ca/calmodulin-dependent kinase II activity in isolated ventricular cardiomyocytes. *ESC Heart Fail* 5, 642–648. doi: 10.1002/ehf2.12336

Neal, B., Perkovic, V., Mahaffey, K. W., de Zeeuw, D., Fulcher, G., Erondu, N., et al. (2017). Canagliflozin and cardiovascular and renal events in Type 2 diabetes. *N. Engl. J. Med.* 377, 644–657. doi: 10.1056/NEJMoa1611925

Pabel, S., Hamdani, N., and Sossalla, S. (2020a). A mechanistic rationale for the investigation of sodium-glucose co-transporter 2 inhibitors in heart failure with preserved ejection fraction. letter regarding the article 'Baseline characteristics of patients with heart failure with preserved ejection fraction in the EMPEROR-Preserved trial'. *Eur. J. Heart Fail.* 23:841. doi: 10.1002/ejhf.2091

Pabel, S., Reetz, F., Dybkova, N., Shomroni, O., Salinas, G., Mustroph, J., et al. (2020b). Long-term effects of empagliflozin on excitation-contraction-coupling in human induced pluripotent stem cell cardiomyocytes. *J. Mol. Med. (Berl)* 98, 1689–1700. doi: 10.1007/s00109-020-01989-6

Pabel, S., Wagner, S., Bollenberg, H., Bengel, P., Kovacs, A., Schach, C., et al. (2018). Empagliflozin directly improves diastolic function in human heart failure. *Eur. J. Heart Fail.* 20, 1690–1700. doi: 10.1002/ejhf.1328

Packer, M. (2020). Autophagy stimulation and intracellular sodium reduction as mediators of the cardioprotective effect of sodium-glucose cotransporter 2 inhibitors. *Eur. J. Heart Fail.* 22, 618–628. doi: 10.1002/ejhf.1732

Packer, M., Anker, S. D., Butler, J., Filippatos, G., Pocock, S. J., Carson, P., et al. (2020). Cardiovascular and renal outcomes with empagliflozin in heart failure. *N. Engl. J. Med.* 383, 1413–1424. doi: 10.1056/NEJMoa2022190

Paulus, W. J., and Tschöpe, C. (2013). A novel paradigm for heart failure with preserved ejection fraction: comorbidities drive myocardial dysfunction and remodeling through coronary microvascular endothelial inflammation. *J. Am. Coll. Cardiol.* 62, 263–271. doi: 10.1016/j.jacc.2013.02.092

Peana, D., and Domeier, T. L. (2017). Cardiomyocyte Ca(2+) homeostasis as a therapeutic target in heart failure with reduced and preserved ejection fraction. *Curr. Opin. Pharmacol.* 33, 17–26. doi: 10.1016/j.coph.2017.03.005

Perkovic, V., Jardine, M. J., Neal, B., Bompoint, S., Heerspink, H. J. L., Charytan, D. M., et al. (2019). Canagliflozin and renal outcomes in Type 2 diabetes and nephropathy. *N. Engl. J. Med.* 380, 2295–2306. doi: 10.1056/NEJMoa1811744

Petrie, M. C., Verma, S., Docherty, K. F., Inzucchi, S. E., Anand, I., Belohlavek, J., et al. (2020). Effect of dapagliflozin on worsening heart failure and cardiovascular death in patients with heart failure with and without diabetes. *JAMA* 323, 1353–1368. doi: 10.1001/jama.2020.1906

Philippaert, K., Kalyaanamoorthy, S., Fatehi, M., Long, W., Soni, S., Byrne, N. J., et al. (2021). Cardiac late sodium channel current is a molecular target for the Sodium/Glucose Cotransporter 2 inhibitor empagliflozin. *Circulation* 143, 2188–2204. doi: 10.1161/CIRCULATIONAHA.121.053350

Rangaswami, J., Bhalla, V., Blair, J. E. A., Chang, T. I., Costa, S., Lentine, K. L., et al. (2019). Cardiorenal syndrome: classification, pathophysiology, diagnosis, and treatment strategies: a scientific statement from the american heart association. *Circulation* 139, e840–e878. doi: 10.1161/CIR.0000000000000664

Redfield, M. M. (2016). Heart failure with preserved ejection fraction. *New England J. Med.* 375, 1868–1877. doi: 10.1056/NEJMcp1511175

Roth, G. A., Johnson, C., Abajobir, A., Abd-Allah, F., Abera, S. F., Abyu, G., et al. (2017). Global, regional, and national burden of cardiovascular diseases for 10 causes, 1990 to 2015. *J. Am. Coll. Cardiol.* 70, 1–25. doi: 10.1016/j.jacc.2017.04.052

Runte, K. E., Bell, S. P., Selby, D. E., Haussler, T. N., Ashikaga, T., LeWinter, M. M., et al. (2017). Relaxation and the role of calcium in isolated contracting myocardium from patients with hypertensive heart disease and heart failure with preserved ejection fraction. *Circ. Heart Fail* 10:e004311. doi: 10.1161/CIRCHEARTFAILURE.117.004311

Santos-Gallego, C. G., Requena-Ibanez, J. A., San Antonio, R., Garcia-Ropero, A., Ishikawa, K., Watanabe, S., et al. (2021). Empagliflozin ameliorates diastolic dysfunction and left ventricular fibrosis/stiffness in nondiabetic heart failure: a multimodality study. *JACC Cardiovasc. Imaging* 14, 393–407. doi: 10.1016/j.jcmg.2020.07.042

Shi, L., Zhu, D., Wang, S., Jiang, A., and Li, F. (2019). Dapagliflozin attenuates cardiac remodeling in mice model of cardiac pressure overload. *Am. J. Hypertens.* 32, 452–459. doi: 10.1093/ajh/hpz016

Shim, C. Y., Seo, J., Cho, I., Lee, C. J., Cho, I. J., Lhagvasuren, P., et al. (2021). Randomized, controlled trial to evaluate the effect of dapagliflozin on left ventricular diastolic function in patients with Type 2 diabetes mellitus: the IDDIA trial. *Circulation* 143, 510–512. doi: 10.1161/CIRCULATIONAHA.120.051992

Singh, A. K., Singh, R., and Misra, A. (2021). Do SGLT-2 inhibitors exhibit similar cardiovascular benefit in patients with heart failure with reduced or preserved ejection fraction? *J. Diab.* 13, 596–600. doi: 10.1111/1753-0407.13182

Sossalla, S., Maurer, U., Schotola, H., Hartmann, N., Didie, M., Zimmermann, W. H., et al. (2011). Diastolic dysfunction and arrhythmias caused by overexpression of CaMKIIdelta(C) can be reversed by inhibition of late Na(+) current. *Basic Res. Cardiol.* 106, 263–272. doi: 10.1007/s00395-010-0136-x

Sossalla, S., Wagner, S., Rasenack, E. C., Ruff, H., Weber, S. L., Schondube, F. A., et al. (2008). Ranolazine improves diastolic dysfunction in isolated myocardium from failing human hearts–role of late sodium current and intracellular ion accumulation. *J. Mol. Cell Cardiol.* 45, 32–43. doi: 10.1016/j.yjmcc.2008.03.006

Sweeney, M., Corden, B., and Cook, S. A. (2020). Targeting cardiac fibrosis in heart failure with preserved ejection fraction: mirage or miracle? *EMBO Mol. Med.* 12:e10865. doi: 10.15252/emmm.201910865

Tahara, A., Kurosaki, E., Yokono, M., Yamajuku, D., Kihara, R., Hayashizaki, Y., et al. (2013). Effects of SGLT2 selective inhibitor ipragliflozin on hyperglycemia, hyperlipidemia, hepatic steatosis, oxidative stress, inflammation, and obesity in type 2 diabetic mice. *Eur. J. Pharmacol.* 715, 246–255. doi: 10.1016/j.ejphar.2013.05.014

Tahara, A., Kurosaki, E., Yokono, M., Yamajuku, D., Kihara, R., Hayashizaki, Y., et al. (2014). Effects of sodium-glucose cotransporter 2 selective inhibitor ipragliflozin on hyperglycaemia, oxidative stress, inflammation and liver injury in streptozotocin-induced type 1 diabetic rats. *J. Pharm. Pharmacol.* 66, 975–987. doi: 10.1111/jphp.12223

Trum, M., Riechel, J., Lebek, S., Pabel, S., Sossalla, S. T., Hirt, S., et al. (2020). Empagliflozin inhibits Na(+) /H(+) exchanger activity in human atrial cardiomyocytes. *ESC Heart Fail* 7, 4429–4437. doi: 10.1002/ehf2.13024

Trum, M., Riechel, J., and Wagner, S. (2021). Cardioprotection by SGLT2 inhibitors-does it all come down to Na(+)? *Int. J. Mol. Sci.* 22:7976. doi: 10.3390/ijms22157976

Uthman, L., Baartscheer, A., Bleijlevens, B., Schumacher, C. A., Fiolet, J. W. T., Koeman, A., et al. (2018). Class effects of SGLT2 inhibitors in mouse cardiomyocytes and hearts: inhibition of Na(+)/H(+) exchanger, lowering of cytosolic Na(+) and vasodilation. *Diabetologia* 61, 722–726. doi: 10.1007/s00125-017-4509-7

Verma, S., Garg, A., Yan, A. T., Gupta, A. K., Al-Omran, M., Sabongui, A., et al. (2016). Effect of empagliflozin on left ventricular mass and diastolic function in individuals with diabetes: an important clue to the EMPA-REG OUTCOME trial? *Diabetes Care* 39, e212–e213. doi: 10.2337/dc16-1312

Verma, S., Mazer, C. D., Yan, A. T., Mason, T., Garg, V., Teoh, H., et al. (2019). Effect of empagliflozin on left ventricular mass in patients with Type 2 diabetes mellitus and coronary artery disease: the EMPA-HEART CardioLink-6 randomized clinical trial. *Circulation* 140, 1693–1702. doi: 10.1161/CIRCULATIONAHA.119.042375

Verma, S., McMurray, J. J. V., and Cherney, D. Z. I. (2017). The metabolodiuretic promise of sodium-dependent glucose Cotransporter 2 inhibition: the search for the sweet spot in heart failure. *JAMA Cardiol.* 2, 939–940. doi: 10.1001/jamacardio.2017.1891

Wiviott, S. D., Raz, I., Bonaca, M. P., Mosenzon, O., Kato, E. T., Cahn, A., et al. (2019). Dapagliflozin and cardiovascular outcomes in Type 2 diabetes. *N. Engl. J. Med.* 380, 347–357. doi: 10.1056/NEJMoa1812389

Writing, C., Maddox, T. M., Januzzi, J. L. Jr., Allen, L. A., Breathett, K., et al. (2021). 2021 update to the 2017 ACC expert consensus decision pathway for optimization of heart failure treatment: answers to 10 pivotal issues about heart failure with reduced ejection fraction: a report of the american college of cardiology solution set oversight committee. *J. Am. Coll. Cardiol.* 77, 772–810. doi: 10.1016/j.jacc.2020.11.022

Xue, M., Li, T., Wang, Y., Chang, Y., Cheng, Y., Lu, Y., et al. (2019). Empagliflozin prevents cardiomyopathy via sGC-cGMP-PKG pathway in type 2 diabetes mice. *Clin. Sci. (Lond)* 133, 1705–1720. doi: 10.1042/CS20190585

Yaribeygi, H., Atkin, S. L., Butler, A. E., and Sahebkar, A. (2019). Sodium-glucose cotransporter inhibitors and oxidative stress: an update. *J. Cell. Physiol.* 234, 3231–3237. doi: 10.1002/jcp.26760

Ye, Y., Bajaj, M., Yang, H. C., Perez-Polo, J. R., and Birnbaum, Y. (2017). SGLT-2 inhibition with dapagliflozin reduces the activation of the Nlrp3/ASC inflammasome and attenuates the development of diabetic cardiomyopathy in mice with Type 2 diabetes. further augmentation of the effects with saxagliptin, a DPP4 inhibitor. *Cardiovasc. Drugs Ther.* 31, 119–132. doi: 10.1007/s10557-017-6725-2

Ye, Y., Jia, X., Bajaj, M., and Birnbaum, Y. (2018). Dapagliflozin attenuates Na(+)/H(+) exchanger-1 in cardiofibroblasts via AMPK activation. *Cardiovasc. Drugs. Ther.* 32, 553–558. doi: 10.1007/s10557-018-6837-3

Yurista, S. R., Sillje, H. H. W., Oberdorf-Maass, S. U., Schouten, E. M., Pavez Giani, M. G., Hillebrands, J. L., et al. (2019). Sodium-glucose co-transporter 2 inhibition with empagliflozin improves cardiac function in non-diabetic rats with left ventricular dysfunction after myocardial infarction. *Eur. J. Heart Fail.* 21, 862–873. doi: 10.1002/ejhf.1473

Zelniker, T. A., Wiviott, S. D., Raz, I., Im, K., Goodrich, E. L., Bonaca, M. P., et al. (2019). SGLT2 inhibitors for primary and secondary prevention of cardiovascular and renal outcomes in type 2 diabetes: a systematic review and meta-analysis of cardiovascular outcome trials. *Lancet* 393, 31–39. doi: 10.1016/S0140-6736(18)32590-X

Zhazykbayeva, S., Pabel, S., Mugge, A., Sossalla, S., and Hamdani, N. (2020). The molecular mechanisms associated with the physiological responses to inflammation and oxidative stress in cardiovascular diseases. *Biophys. Rev.* 12, 947–968. doi: 10.1007/s12551-020-00742-0

Zile, M. R., Baicu, C. F., Ikonomidis, J. S., Stroud, R. E., Nietert, P. J., Bradshaw, A. D., et al. (2015). Myocardial stiffness in patients with heart failure and a preserved ejection fraction: contributions of collagen and titin. *Circulation* 131, 1247–1259. doi: 10.1161/CIRCULATIONAHA.114.013215

Zinman, B., Wanner, C., Lachin, J. M., Fitchett, D., Bluhmki, E., Hantel, S., et al. (2015). Empagliflozin, cardiovascular outcomes, and mortality in Type 2 diabetes. *N. Engl. J. Med.* 373, 2117–2128. doi: 10.1056/NEJMoa1504720

Conflict of Interest: SP received speaker's honoraria from AstraZeneca. JS has received speaker's honoraria from Boehringer Ingelheim Pharma GmbH and AstraZeneca. SS received speaker's/consultancy honoraria from Boehringer Ingelheim Pharma GmbH and AstraZeneca.

The remaining author declares that the research was conducted in the absence of any commercial or financial relationships that could be construed as a potential conflict of interest.

Publisher's Note: All claims expressed in this article are solely those of the authors and do not necessarily represent those of their affiliated organizations, or those of the publisher, the editors and the reviewers. Any product that may be evaluated in this article, or claim that may be made by its manufacturer, is not guaranteed or endorsed by the publisher.

frontiers in Pharmacology

MINI REVIEW
published: 09 November 2021
doi: 10.3389/fphar.2021.718496

Navigating Calcium and Reactive Oxygen Species by Natural Flavones for the Treatment of Heart Failure

Tianhao Yu[1]†, Danhua Huang[2]†, Haokun Wu[1], Haibin Chen[1], Sen Chen[1] and Qingbin Cui[2]*

[1]Department of Cardiology, Guangdong Second Provincial General Hospital, Guangzhou, China, [2]School of Public Health, Guangzhou Medical University, Guangzhou, China

Heart failure (HF), the leading cause of death among men and women world-wide, causes great health and economic burdens. HF can be triggered by many factors, such as coronary artery disease, heart attack, cardiomyopathy, hypertension, obesity, etc., all of which have close relations with calcium signal and the level of reactive oxygen species (ROS). Calcium is an essential second messenger in signaling pathways, playing a pivotal role in regulating the life and death of cardiomyocytes via the calcium-apoptosis link mediated by the cellular level of calcium. Meanwhile, calcium can also control the rate of energy production in mitochondria that are the major resources of ROS whose overproduction can lead to cell death. More importantly, there are bidirectional interactions between calcium and ROS, and such interactions may have therapeutic implications in treating HF through finely tuning the balance between these two by certain drugs. Many naturally derived products, e.g., flavones and isoflavones, have been shown to possess activities in regulating calcium and ROS simultaneously, thereby leading to a balanced microenvironment in heart tissues to exert therapeutic efficacies in HF. In this mini review, we aimed to provide an updated knowledge of the interplay between calcium and ROS in the development of HF. In addition, we summarized the recent studies (*in vitro*, *in vivo* and in clinical trials) using natural isolated flavones and isoflavones in treating HF. Critical challenges are also discussed. The information collected may help to evoke multidisciplinary efforts in developing novel agents for the potential prevention and treatment of HF.

Keywords: heart failure, calcium overload, ROS, flavones, treatment

OPEN ACCESS

Edited by:
Alessandro Mugelli,
University of Florence, Italy

Reviewed by:
Elisabetta Bigagli,
University of Florence, Italy
Laura Pucci,
National Research Council (CNR), Italy

***Correspondence:**
Tianhao Yu
eshldr@126.com

†These authors have contributed equally to this work

Specialty section:
This article was submitted to Cardiovascular and Smooth Muscle Pharmacology, a section of the journal Frontiers in Pharmacology

Received: *24 June 2021*
Accepted: *18 October 2021*
Published: *09 November 2021*

Citation:
Yu T, Huang D, Wu H, Chen H, Chen S and Cui Q (2021) Navigating Calcium and Reactive Oxygen Species by Natural Flavones for the Treatment of Heart Failure. Front. Pharmacol. 12:718496. doi: 10.3389/fphar.2021.718496

INTRODUCTION

Heart diseases, including cardiovascular diseases, the world's leading cause of death, are composed with a class of chronic, progressive, and/or lethal diseases, such as high blood pressure, high blood cholesterol, abnormal heart rhythms, coronary artery disease, ischemic heart disease, stroke, heart attacks, etc. (Virani et al., 2021). Heart failure (HF), the late stage of heart diseases, is a condition in which there is a dramatically reduced supply of blood pumped by the muscle of the heart (Dryer et al., 2021). While HF is a chronic and progressive disease, its onset and consequence are acute and prominent (Weintraub et al., 2010). In China, there are approximately 14 million patients suffering from HF, with a prevalence rate of 1.3% (0.9% in 2000). As in the United States, approximately 1.5 million people experience HF every year, causing over 690,000 deaths in 2019 (Ahmad and Anderson, 2021), indicating a great burden to health and finance.

While varied therapeutics for heart diseases that may lead to HF are available, such as nitrates, calcium channel blockers, angiotensin-converting enzyme (ACE) inhibitors, angiotensin II receptor blockers, and 3-hydroxy-3-methylglutaryl coenzyme A (HMG-CoA) reductase inhibitors, etc., novel agents, including those effective in preventing HF, are in urgent need to reduce the high morbidity, and mortality. Growing evidence has suggested that the prevention of HF is quite imperative (Horwich and Fonarow, 2017; Wang, 2019). Among all the newly developed regimens, nature-derived products can exert huge potential because of their unique properties and multiple functions such as regulating calcium and reactive oxygen species (ROS) levels in cells.

Here, we attempted to summarize the interactions between calcium cation (Ca^{2+}) signaling and ROS level, both of which contribute to the progression of heart disease as well as HF (Bertero and Maack, 2018). Calcium can work as a direct signaling transductor or a second messenger in regulating neuronal transmission, electrical excitation and contractile function of myocytes (Landstrom et al., 2017; Terrar, 2020), or in promoting the growth, life or death of cells such as proliferation and apoptosis (Rizzuto et al., 2003; Lemos and Ehrlich, 2018) which has an intimate connection with the level of cellular ROS (Orrenius et al., 2003). Meanwhile, similar to high levels of ROS, high levels of cytoplasmic calcium, a term called calcium overload, can also induce cell death (Zhivotovsky and Orrenius, 2011). Therefore, it is feasible that the close interaction between ROS and calcium in inducing cell death can be endowed with therapeutic implications (Münzel et al., 2017). Interestingly, there are many natural products that can simultaneously reduce calcium overload and ROS over-production, exerting cardiovascular protective, and HF-preventing effects (Jiang et al., 2016; Mohiuddin, 2019). Flavones including isoflavones, which are one of the most abundant components in plants and fruits, have been intensely studied and applied in markets as a dietary supplement to prevent the incidence of heart diseases including HF (Dixon and Pasinetti, 2010; McCullough et al., 2012; Zamora-Ros et al., 2013). Therefore, we also attempted to summarize the current status (those studies conducted in the past decade) and challenges in using flavones as therapeutic agents in HF via the dual-regulation of calcium and ROS. The information gained may serve as a foundation for further in-depth study, including pharmacological and chemical modification research, and the development of flavones in clinical use.

THE INTERPLAY BETWEEN CALCIUM AND ROS IN INDUCING CARDIOMYOCYTES DEATH

ROS over-production and calcium accumulation in acute myocardial ischemic injury can be attributed to be the major causes of damage to the heart (Shen and Jennings, 1972). Calcium plays key roles in multiple aspects of heart tissue and cell biology. In this review, we highlighted its role in inducing cell death. Calcium concentrations in the outside and inside of cells, in endoplasmic reticulum (ER), and mitochondria are pivotal for maintaining cell functions, and its alterations could lead to cell death (Bagur and Hajnóczky, 2017). Calcium overload, especially in the mitochondria of cardiomyocytes, can cause HF as shown in cell-based models and mouse models (Luo and Anderson, 2013; Santulli et al., 2015; Mora et al., 2018). The malfunctional mitochondria due to calcium overload can further produce more ROS, which may also finally contribute to HF (Luo and Anderson, 2013; Santulli et al., 2015; Bertero and Maack, 2018).

ROS are one of the main inducers of cell death (Ryter et al., 2007). Normally, the ROS level remains in a controllable condition mediated by the producing systems and the active antioxidant enzymes (eliminating systems) in cells, and they, when working as signal transductors, can closely participate in almost every aspect of cell biology (Cui et al., 2018a; Bock and Tait, 2020). Under stress and malfunctioning conditions, the ROS level in cells can be increased due to varied reasons, leading to the apoptosis initiation (Cui et al., 2018a). Oxidative stress due to over-produced ROS is one of the hallmarks of cardiovascular disease, which has close connections with the progression of ischemia-reperfusion damage and atherosclerosis, both of which can eventually lead to HF (Panth et al., 2016).

There are bidirectional interactions between calcium and ROS as shown in **Figure 1** (Görlach et al., 2015). Briefly, calcium can modulate the formation and production of ROS. First, ER and mitochondria are two major producers of various ROS; and calcium can induce ER stress, and enhance ATP production in mitochondria that requires oxygen, resulting in over-produced ROS. Second, NADPH oxidases (NOXs) that are calcium dependent, are another major source of ROS such as H_2O_2 and O_2^- (Rastogi et al., 2016; Burtenshaw et al., 2017). Calcium can either activate NOXs *via* directly binding to NOXs at certain domains or in an indirect way through signal transduction, leading to ROS over-production (Bánfi et al., 2004). Endothelial nitric oxide synthase (eNOS), one of three isoforms that synthesize nitric oxide (NO) (Cui et al., 2019), is another enzyme that is calcium dependent (Aoyagi et al., 2003; Devika and Jaffar Ali, 2013). Calcium can activate calmodulin, which then binds to eNOS, leading to its efficient NO production (Sessa, 2004). Furthermore, calcium can also induce ROS generation by impacting other key ROS-maintaining enzymes such as voltage dependent anion channels (VDAC) (Feno et al., 20192019), or certain complexes form the electron transporting chain (ETC) located in the inner mitochondrial membrane (Adam-Vizi and Starkov, 2010), etc.

Meanwhile, ROS can also negatively influence myocardial calcium handling, causing arrhythmia, and augmenting cardiac remodeling by inducing hypertrophic signaling and apoptosis, which later contributes to HF (Senoner and Dichtl, 2019). ROS are ready to attack cellular biomolecules including calcium transporters on cell membranes or organelles' membranes including ER and mitochondria, therefore affecting the calcium homeostasis (Zimmerman et al., 2011). Free radical H_2O_2 can bind to the residue of Cys674 at the sarcoplasmic reticulum Ca^{2+} ATPase (SERCA), leading to disturbed cardiac myocyte in a rat heart (Qin et al., 2013).

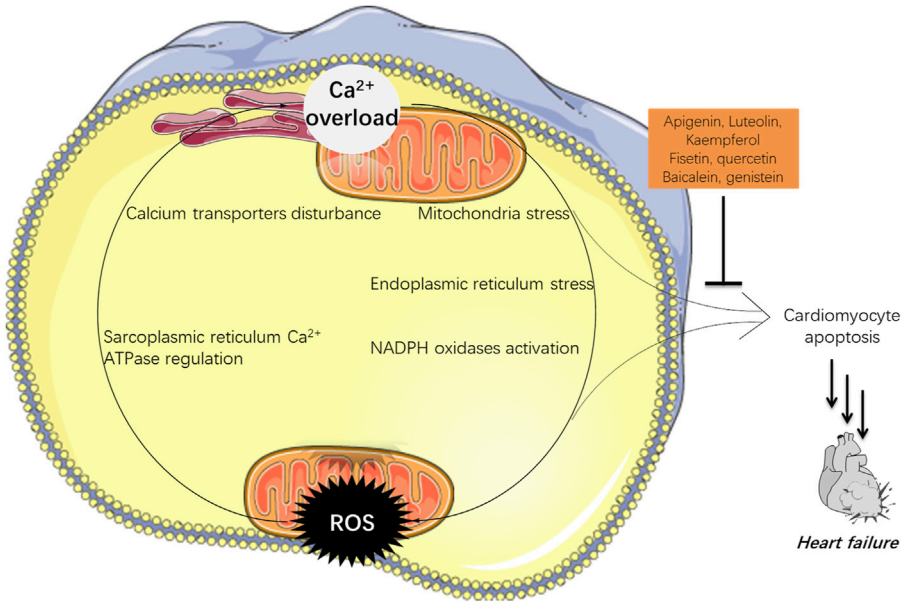

FIGURE 1 | The interactions between calcium and ROS in HF. Over-loaded calcium could not only induce apoptosis, but also stimulate the production of ROS which may initiate cell death. Flavones hold potential in navigating both of them which can be adopted in HF treatment.

In a word, high levels of ROS can increase the uptake of calcium in cells; meanwhile the calcium level in cells can also stimulate the production of ROS. These two events working together can finally induce cardiomyocyte death and eventually HF.

NATURAL FLAVONES EXHIBIT POTENTIAL IN TREATING HF VIA DUAL REGULATION OF CALCIUM AND ROS

Flavones, including isoflavones, are a class of natural products categorized as flavonoids, sharing a common backbone of 2-phenylchromen-4-one (flavone) or 3-phenylchromen-4-one (isoflavone) (**Figure 2**) (Hostetler et al., 2017). Natural flavones are rich in fruits, vegetables, soybean, herbal plants, honey, and they have been used as herbal medicines for over 1,000 years. Importantly, the isolated/purified components have been used as supplemental nutrients for decades (Singh et al., 2014). Currently, dozens of flavones are under clinical trials for the treatment of diseases associated with cardiovascular dysfunction and other diseases including neurodegenerative diseases, diabetes mellitus, cancers, etc., suggesting their huge potentials (Hostetler et al., 2017; Cui et al., 2018b). Flavones are known as multi-targeting or multi-functional compounds since they can regulate/target multiple enzymes *in vivo* (Qiu et al., 2018; Ye et al., 2019), such as silent mating type information regulation 2 homolog (SIRT) (Kang et al., 2018), ABC transporters (Li and Paxton, 2013), cyclin-dependent kinases (CDKs) (Khuntawee et al., 2012), and certain microRNA (Lin et al., 2018), etc. In addition to their multi-functional property, flavones also exert medical efficacies *via* multi-mechanisms including the regulation of both ROS and calcium that contribute significantly to HF. A retrospective clinical meta-analysis of 23 years among 56,048 Danish people has indicated that the consumption of certain flavonoids (500 mg/day) can reduce the incidence and mortality of cardiovascular diseases (Bondonno et al., 2019), and such efficacies have been validated by other studies as well (Ponzo et al., 2015; Dalgaard et al., 2019), suggesting the beneficial effects of flavonoids in treating HF. Indeed, growing *in vitro* and *in vivo* studies have proven such effects (Mozaffarian and Wu, 2018). Here, we focus on those flavones and isoflavones (**Figure 2**) that exert their heart protective effects *via* dual regulating ROS and calcium signal.

Apigenin (4′,5,7-trihydroxyflavone), a dietary supplement that has demonstrated the ability to regulate both ROS and calcium (Maher and Hanneken, 2005; Wu et al., 2021), suggesting its potential in treating HF. Li et al. (2017) reported that apigenin (50 mg/kg) could relieve myocardial injury induced by endotoxin and decrease the death rate of cardiomyocytes in mice, suggesting a cardioprotective effect (Li et al., 2017). Apigenin worked *via* reducing oxidative stress as confirmed by increased cardiac glutathione (GSH) level, oxidative stress markers, and pro-inflammatory cytokines including tumor necrosis factor (TNF-α), interleukin 1β (IL-1β), macrophage inflammatory protein-2 (MIP-2) which have intimate networks with Ca^{2+}-associated signals (Hendy and Canaff, 2016; Li et al., 2017).

Luteolin (3′,4′,5,7-tetrahydroxyflavone) is a flavone that has been serving as a supplemental nutrient for decades for improving memory and brain health (Swaminathan et al., 2019; Wang et al., 2021). Luteolin can protect heart from damage caused by over-produced ROS and over-loaded calcium (Wang et al., 2012; Yan et al., 2018). Wang et al.

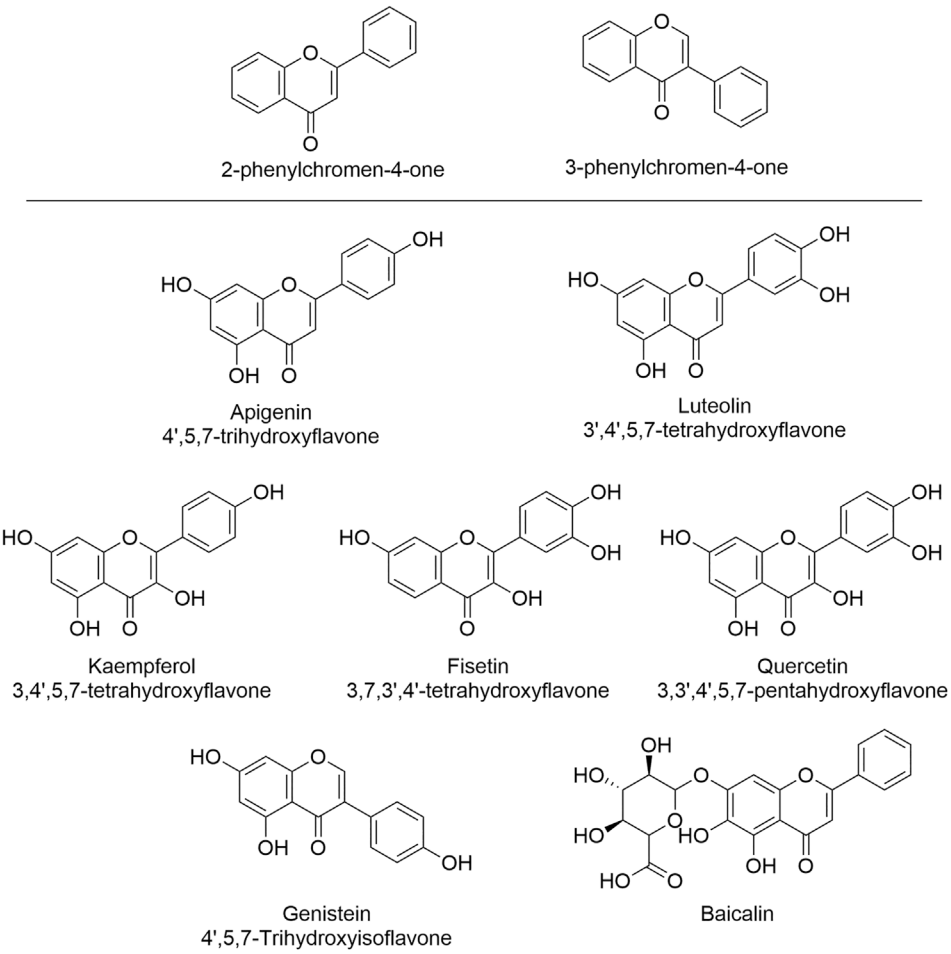

FIGURE 2 | The structures of flavones and isoflavone that show HF-treating/preventing effects *via* the regulation of both ROS and calcium signal. These natural products can serve as leading compounds that can undergo structural modification to achieve the selective regulation of ROS and calcium.

(2012) found that in an animal model of type I diabetic cardiomyopathy, luteolin (200 mg/kg) maintained certain cardiac functions as measured by the left ventricular systolic pressure, left ventricular developed pressure, left ventricular end diastolic pressure, and maximal rate of rise/fall left ventricle pressure development (Wang et al., 2012). They also found that luteolin worked by reducing oxidative stress as confirmed by decreased ROS-producing proteins and signal pathways (Wang et al., 2012). Madhesh and Vaiyapuri (2005 and 2012) found that luteolin (0.3 mg/kg/day) could protect cardiac function and prevent myocardial infarction by reducing mitochondrial lipid peroxidation (a route that produce ROS *in vivo*) and increasing the mitochondrial antioxidant levels as shown in isoproterenol induced myocardial infarction model in rats (Manju et al., 2005; Madhesh and Vaiyapuri, 2012). Luteolin appears to be an inhibitor of L-type calcium channels as confirmed by Yan et al. (2018), Yan et al. (2019). Luteolin (7.5, 15, or 30 μM) ameliorated calcium overload in freshly isolated cardiomyocytes, accompanied by suppressed Protein Kinase A (PKA) activity and enhanced Ca^{2+}-Mg^{2+}-ATPase activity (Yan et al., 2018). Luteolin's regulatory role in calcium was also confirmed by Li et al.'s studies in 2015 and 2017 (Nai et al., 2015; Hu et al., 2017a).

Kaempferol is another widely used dietary supplement with a chemical name of 3,4′,5,7-tetrahydroxyflavone, and it can protect heart *via* the navigation of both ROS and calcium (An and Kim, 2015; Guo et al., 2015). An *in vitro* study by Guo et al. (2015) showed that in A/R-induced injury model, kaempferol (10, 20, or 40 μM) inhibited mitochondria-mediated apoptosis and increased the cell viability of cardiomyocytes *via* reducing ROS production mediated by activating SIRT1 (Guo et al., 2015). Calmodulin kinase II (CaMKII), a key player in calcium signaling pathways, can be activated by higher levels of ROS, thereby resulting in abnormally slow heart rhythm or cardiomyocytes death (Di Carlo et al., 2014; Santalla et al., 2014). Kaempferol (15 mM) significantly reduced the CaMKII oxidization and sinus nodal cell death, warranting further *in vivo* verification (An and Kim, 2015). It is also worth noting that the concentration used in this study is 15 mM, which is much higher than the other studies that fall in submicromolar concentrations. Such high concentrations may cause problems in clinical trials when translating the *in vitro*

doses into those in humans, requiring an in-depth pharmacokinetic study.

Fisetin (3,7,3′,4′-tetrahydroxyflavone) is an abundant flavone existing in strawberry, apple, persimmon, grape, onion, and cucumber. Fisetin demonstrated multiple health benefits including preventing HF via regulating ROS and calcium (Rodius et al., 2020). Shanmugam et al. (2018) confirmed the cardiovascular protective effect of fisetin using a Langendorff isolated heart perfusion system (Shanmugam et al., 2018). Fisetin pretreatment (20 mg/kg) showed a strong protective effect against the damage induced by myocardial ischemia reperfusion in the isolated rat heart. Fisetin improved mitochondrial physiology, biogenesis, and functions including maintaining the ETC and reducing superoxide (O_2^-) generated in mitochondria, suggesting a mitochondria-mediated mechanism (Shanmugam et al., 2018). The further *in silico* analysis and computer-aided docking study showed that fisetin might be a potent glycogen synthase kinase 3β (GSK3β) inhibitor (Shanmugam et al., 2018), warranting further study.

Quercetin (3,3′,4′,5,7-pentahydroxyflavone) is an important dietary flavone in fruits and vegetables, and it possesses anti-inflammatory and anti-oxidative properties which may benefit the patients with cardiovascular diseases (Patel et al., 2018). Jing et al. (2016) found that quercetin pretreatment (20 mg/kg) reversed cardiomyocytes apoptosis induced by posttraumatic stress and it restored cardiac function as shown in a rat model (Jing et al., 2016). *In vitro* study of pretreatment with quercetin at 20 μM showed that it can obviously maintain the cell viability, decreased TNF-α, ROS level and calcium overload in H9c2 cells, suggesting the beneficial effects of quercetin in treating cardiac injury (Jing et al., 2016). Quercetin can also protect the heart from myocardial ischemia reperfusion injury via the dual regulation of ROS level and calcium overload (Zhang et al., 2020). Furthermore, a meta-analysis of clinical trials showed that the consumption of quercetin (at the dose of more than 500 mg/day) exhibited significant reduction of blood pressure, suggesting a beneficial effect of quercetin in HF (Serban et al., 2016).

Baicalein, enriched in natural products and herbal medicines, is a glycosylated flavone that regulates ROS and calcium in cells (Xin et al., 2020), showing promising therapeutic effects in treating and preventing HF (Zhao et al., 2016). Zhao et al. (2016) found that in HF *in vivo* model established by abdominal aorta constriction in rats and *in vitro* isoproterenol-induced H9C2 cells, baicalein (50, 100, and 200 mg/kg *in vivo* or 5, 10, 20 μM *in vitro*) significantly alleviated HF syndromes by improving heart function as confirmed by hematoxylin-eosin and ELISA measuring the pathomorphological changes and down-regulated TNF-α, angiotensin II, and BNP in peripheral blood (Zhao et al., 2016). Baicalein reduced myocardial fibrosis *in vivo* through inhibiting the expression and activities of matrix metalloproteinase-2 and -9 (MMP-2/9). Furthermore, baicalein was found to suppress isoproterenol-induced cardiomyocytes hypertrophy and apoptosis *in vivo* and *in vitro*, probably via regulating calcium related proteins such as the phosphorylated Ca^{2+}/calmodulin-dependent protein kinase II (CaMKII), Na^+/Ca^{2+}-exchangers (NCX1) and sarcoplasmic reticulum Ca^{2+} ATPase 2 (SERCA2) (Zhao et al., 2016).

Genistein (4′,5,7-trihydroxyisoflavone) is an isoflavone that is found in soy-based products, being widely used as a supplemental nutrient for years (Williamson-Hughes et al., 2006; Mamagkaki et al., 2021). Genistein is also a dual regulator of ROS and calcium (Uddin and Kabir, 2019). Matori et al. (2012) found that genistein (1 mg/kg/day for 9 days) could restore cardiopulmonary structure and function, and reverse the loss of capillaries induced by pulmonary hypertension in the rat model, demonstrating its potential in preventing HF (Matori et al., 2012). In addition, a randomized double-blind case-control study conducted among postmenopausal women with metabolic syndrome showed that genistein (54 mg/day) significantly improved heart functions measured by the left ventricular ejection fraction and remodeling, suggesting a favorable outcome when applied in human with cardiovascular diseases (De Gregorio et al., 2017).

Other potential flavones such as rutin, quercetin-3-O-rutinoside which is the glycosylated quercetin (Chu et al., 2014; Lv et al., 2018), chrysin (5,7-Dihydroxyflavone) (Farkhondeh et al., 2019; Xingyue et al., 2021), wogonin (5,7-Dihydroxy-8-methoxyflavone) (Khan et al., 2016; Khan and Kamal, 2019), also possess cardiovascular protective and HF-preventing efficacies *via* an ROS-calcium associated mechanism, rendering them as attractive drug candidates or dietary supplements.

DISCUSSION AND FUTURE PERSPECTIVE

The information discussed above has indicated that 1) there is a vicious cycle between overloaded calcium and over-produced ROS, and both contribute to HF; 2) certain flavones can protect cardiovascular *via* down-regulating both intracellular calcium content and ROS level, thereby demonstrating potentials in preventing/treating HF as summarized in **Table 1**. As shown in the original studies, luteolin, kaempferol, and baicalein, demonstrated a dose-dependent mode of action; while the other four including apigenin, fisetin, quercetin, and genistein, were tested with one dose/concentration to exert the HF-treating/preventing effects, warranting further pharmacological study *in vivo*. In addition, combinational strategies of certain flavones and conventional drugs can also be developed and applied in HF treatment via synergistic effects (Guerrero et al., 2012; Zeka et al., 2017).

Meanwhile, cautions should also be made. Firstly, these flavones are not specific regulators of ROS or calcium, undermining their potential as drug candidates which require the selective targeting of certain pathogenic mechanisms/proteins. As for these small-molecule flavones, it appears to be true that none of them has a selective bio-target *in vivo*, and it is well accepted that most of them might exert their bioactivities *via* interacting with membrane proteins (Cyboran et al., 2012; Ingólfsson et al., 2014; Phan et al., 2014), requiring more studies such as medicinal chemical modification to improve the selectivity and druglikeness (Boniface and Elizabeth, 2019).

TABLE 1 | Summary of the discussed flavones.

Flavones	Experimental model	Doses/Effects	Mechanisms	References
Apigenin	*In vivo* myocardial injury	Relieving myocardial injury at 50 mg/kg	Reducing ROS and negatively regulating calcium-related signal	Li et al. (2017)
Luteolin	*In vivo* type I diabetic cardiomyopathy	Maintaining cardiac functions at 200 mg/kg	Reducing oxidative stress	Yan et al. (2018)
	In vivo myocardial infarction model	Protecting cardiac function at 0.3 mg/kg/day	Reducing mitochondrial lipid peroxidation	Manju et al. (2005), Madhesh and Vaiyapuri (2012)
Kaempferol	*In vitro* anoxia/reoxygenation induced injury model	Inhibiting apoptosis at 10, 20, or 40 μM	Reducing ROS production mediated by activating SIRT1	Guo et al. (2015)
	Isolated Langendorff heart	Protecting sinus node	Reducing CaMKII oxidization	An and Kim (2015)
Fisetin	The Langendorff isolated heart perfusion system	Protective effect against myocardial ischemia reperfusion at 20mg/kg	Decreasing ROS and calcium	Shanmugam et al. (2018)
Quercetin	*In vivo* posttraumatic cardiac injury model	Preventing apoptosis and cardiac dysfunction at 20 mg/kg	Decreasing ROS and calcium	Jing et al. (2016)
	In vitro H9c2 cardiomyoblasts	Maintaining cell viability at 20 μM	Decreasing ROS and calcium	Jing et al. (2016)
Baicalein	*In vivo* HF model and *In vitro* in H9C2 cells	Alleviating HF syndromes and reducing myocardial fibrosis at 50, 100, and 200 mg/kg and inhibiting apoptosis at 5–20 μM	Inhibiting MMP-2/9, reducing ROS, and regulating calcium signal	Zhao et al. (2016)
Genistein	*In vivo* pulmonary hypertension model	restore the structure and function of heart and lung at 1 mg/kg/day for 9 days	Decreasing ROS and calcium	Matori et al. (2012)

As far as the authors concerned, it seems to be more reasonable to develop them as supplemental nutrients in preventing HF.

Secondly, the dual-regulation of ROS and calcium might not be the mere mechanism that leads to cardio-protective effects by flavones (Najjar and Feresin, 2021). HF, the late stage of heart diseases, can be triggered by various factors; consequently, flavones can also exert HF-preventing efficacies *via* multiple mechanisms which have been intensively studied over the past decade (Grassi et al., 2013; Choy et al., 2019; Ciumărnean et al., 2020a; Ciumărnean et al., 2020b; Fusi et al., 2020; Yamagata and Yamori, 2020; Jiang et al., 2021). This fact can further support the strategy of developing flavones as supplemental nutrients.

Last, in spite of the fact that the aforementioned flavones can generally reduce the level of ROS in cardiomyocytes, a significant proportion of them (at varied concentrations) can also induce the production, leading to cell death which can be applied in cancer treatment (Lu et al., 2007; Lin et al., 2011; Shih et al., 2017; Souza et al., 20172017; Cui et al., 2018b; Cataneo et al., 2019; Korga et al., 2019). Thus, the therapeutic windows of each flavone should be determined before their application (or trials) in humans.

Multiple clinical trials are ongoing and several conducted previously have been completed as shown in the **Supplemental Table S1**. It is worth noting that quercetin, whose name has been used since 1857, has been widely tested in clinical trials for the treatment of different diseases including heart diseases. As one of the most abundant, and widely studied and applied as nutritional supplement (Jing et al., 2016; Patel et al., 2018), it is the authors' opinion that quercetin has a greater potential in treating/preventing HF among all the others. However, by far, using flavones as drug candidates in HF treatment/prevention is still in its early stage. One of the major obstacles that refrain the effects *in vivo* and in clinical trials is that the stability, selectivity, and overall poor bioavailability that fails to reach consistent exposure levels, etc. (Ross and Kasum, 2002; Wu et al., 2011; Thilakarathna and Rupasinghe, 2013; Hu et al., 2017b). Bioavailability of certain flavones has been tested in human, and the results indicated that only a small proportion can be absorbed (Meyer et al., 2006; Kanaze et al., 2007), such as15–24% of genistein (Lu and Anderson, 1998). Such low bioavailability may require high doses in humans, and a typical dose is 500 mg/day, and doses below this may not benefit patients with heart diseases/conditions (Kirienko and Radak, 2016; Serban et al., 2016; Bondonno et al., 2019). Therefore, to achieve the full potential in HF, further *in vitro* and *in vivo* studies are required to determine the dose, administration methods, safety, and pharmacokinetic and pharmacodynamics profiles.

CONCLUSION

Overload of calcium and elevated ROS production can form a vicious cycle to induce cardiomyocytes death that may finally lead to HF. A number of flavones show the dual-regulation of calcium and ROS, demonstrating their therapeutic potential in HF.

AUTHOR CONTRIBUTIONS

Conceptualization: TY, DH, and QC. Writing: TY, DH, HC, SC, and HW. Review and editing: TY and DH. All authors contributed to the article and approved the submitted version.

SUPPLEMENTARY MATERIAL

The Supplementary Material for this article can be found online at: https://www.frontiersin.org/articles/10.3389/fphar.2021.718496/full#supplementary-material

REFERENCES

Adam-Vizi, V., and Starkov, A. A. (2010). Calcium and Mitochondrial Reactive Oxygen Species Generation: How to Read the Facts. *J. Alzheimers Dis.* 20 (Suppl. 2), S413–S426. doi:10.3233/JAD-2010-100465

Ahmad, F. B., and Anderson, R. N. (2021). The Leading Causes of Death in the US for 2020. *JAMA* 325 (18), 1829–1830. doi:10.1001/jama.2021.5469

An, M., and Kim, M. (2015). Protective Effects of Kaempferol against Cardiac Sinus Node Dysfunction via CaMKII Deoxidization. *Anat. Cel. Biol.* 48 (4), 235–243. doi:10.5115/acb.2015.48.4.235

Aoyagi, M., Arvai, A. S., Tainer, J. A., and Getzoff, E. D. (2003). Structural Basis for Endothelial Nitric Oxide Synthase Binding to Calmodulin. *EMBO J.* 22 (4), 766–775. doi:10.1093/emboj/cdg078

Bagur, R., and Hajnóczky, G. (2017). Intracellular Ca2+ Sensing: Its Role in Calcium Homeostasis and Signaling. *Mol. Cel.* 66 (6), 780–788. doi:10.1016/j.molcel.2017.05.028

Bánfi, B., Tirone, F., Durussel, I., Knisz, J., Moskwa, P., Molnár, G. Z., et al. (2004). Mechanism of Ca2+ Activation of the NADPH Oxidase 5 (NOX5). *J. Biol. Chem.* 279 (18), 18583–18591. doi:10.1074/jbc.M310268200

Bertero, E., and Maack, C. (2018). Calcium Signaling and Reactive Oxygen Species in Mitochondria. *Circ. Res.* 122 (10), 1460–1478. doi:10.1161/CIRCRESAHA.118.310082

Bock, F. J., and Tait, S. W. G. (2020). Mitochondria as Multifaceted Regulators of Cell Death. *Nat. Rev. Mol. Cel. Biol.* 21 (2), 85–100. doi:10.1038/s41580-019-0173-8

Bondonno, N. P., Dalgaard, F., Kyrø, C., Murray, K., Bondonno, C. P., Lewis, J. R., et al. (2019). Flavonoid Intake Is Associated with Lower Mortality in the Danish Diet Cancer and Health Cohort. *Nat. Commun.* 10 (1), 3651. doi:10.1038/s41467-019-11622-x

Boniface, P. K., and Elizabeth, F. I. (2019). Flavones as a Privileged Scaffold in Drug Discovery: Current Developments. *Curr. Org. Synth.* 16 (7), 968–1001. doi:10.2174/1570179416666190719125730

Burtenshaw, D., Hakimjavadi, R., Redmond, E. M., and Cahill, P. A. (2017). Nox, Reactive Oxygen Species and Regulation of Vascular Cell Fate. *Antioxidants (Basel)* 6 (4). doi:10.3390/antiox6040090

Cataneo, A. H. D., Tomiotto-Pellissier, F., Miranda-Sapla, M. M., Assolini, J. P., Panis, C., Kian, D., et al. (2019). Quercetin Promotes Antipromastigote Effect by Increasing the ROS Production and Anti-amastigote by Upregulating Nrf2/HO-1 Expression, Affecting Iron Availability. *Biomed. Pharmacother.* 113, 108745. doi:10.1016/j.biopha.2019.108745

Choy, K. W., Murugan, D., Leong, X. F., Abas, R., Alias, A., and Mustafa, M. R. (2019). Flavonoids as Natural Anti-inflammatory Agents Targeting Nuclear Factor-Kappa B (NFκB) Signaling in Cardiovascular Diseases: A Mini Review. *Front. Pharmacol.* 10, 1295. doi:10.3389/fphar.2019.01295

Chu, J. X., Li, G. M., Gao, X. J., Wang, J. X., and Han, S. Y. (2014). Buckwheat Rutin Inhibits AngII-Induced Cardiomyocyte Hypertrophy via Blockade of CaN-dependent Signal Pathway. *Iran. J. Pharm. Res.* 13 (4), 1347–1355.

Ciumărnean, L., Milaciu, M. V., Runcan, O., Vesa, Ș. C., Răchișan, A. L., Negrean, V., et al. (2020). The Effects of Flavonoids in Cardiovascular Diseases. *Molecules* 25 (18). doi:10.3390/molecules25184320

Ciumărnean, L., Milaciu, M. V., Runcan, O., Vesa, Ș. C., Răchișan, A. L., Negrean, V., et al. (2020). The Effects of Flavonoids in Cardiovascular Diseases. *Molecules* 25 (18). doi:10.3390/molecules25184320

Cui, Q., Wang, J. Q., Assaraf, Y. G., Ren, L., Gupta, P., Wei, L., et al. (2018). Modulating ROS to Overcome Multidrug Resistance in Cancer. *Drug Resist. Updat.* 41, 1–25. doi:10.1016/j.drup.2018.11.001

Cui, Q., Yang, D. H., and Chen, Z. S. (2018). Special Issue: Natural Products: Anticancer and beyond. *Molecules* 23 (6), 1246–1249. doi:10.3390/molecules23061246

Cui, Q., Yang, Y., Ji, N., Wang, J. Q., Ren, L., Yang, D. H., et al. (2019). Gaseous Signaling Molecules and Their Application in Resistant Cancer Treatment: from Invisible to Visible. *Future Med. Chem.* 11 (4), 323–336. doi:10.4155/fmc-2018-0403

Cyboran, S., Oszmiański, J., and Kleszczyńska, H. (2012). Interaction between Plant Polyphenols and the Erythrocyte Membrane. *Cell. Mol. Biol. Lett.* 17 (1), 77–88. doi:10.2478/s11658-011-0038-4

Dalgaard, F., Bondonno, N. P., Murray, K., Bondonno, C. P., Lewis, J. R., Croft, K. D., et al. (2019). Associations between Habitual Flavonoid Intake and Hospital Admissions for Atherosclerotic Cardiovascular Disease: a Prospective Cohort Study. *Lancet Planet. Health* 3 (11), e450–59. doi:10.1016/S2542-5196(19)30212-8

De Gregorio, C., Marini, H., Alibrandi, A., Di Benedetto, A., Bitto, A., Adamo, E. B., et al. (2017). Genistein Supplementation and Cardiac Function in Postmenopausal Women with Metabolic Syndrome: Results from a Pilot Strain-Echo Study. *Nutrients* 9 (6). doi:10.3390/nu9060584

Devika, N. T., and Jaffar Ali, B. M. (2013). Analysing Calcium Dependent and Independent Regulation of eNOS in Endothelium Triggered by Extracellular Signalling Events. *Mol. Biosyst.* 9 (11), 2653–2664. doi:10.1039/c3mb70258h

Di Carlo, M. N., Said, M., Ling, H., Valverde, C. A., De Giusti, V. C., Sommese, L., et al. (2014). CaMKII-dependent Phosphorylation of Cardiac Ryanodine Receptors Regulates Cell Death in Cardiac Ischemia/reperfusion Injury. *J. Mol. Cel. Cardiol.* 74, 274–283. doi:10.1016/j.yjmcc.2014.06.004

Dixon, R. A., and Pasinetti, G. M. (2010). Flavonoids and Isoflavonoids: from Plant Biology to Agriculture and Neuroscience. *Plant Physiol.* 154 (2), 453–457. doi:10.1104/pp.110.161430

Dryer, C., Cotter, E. K., and Flynn, B. (2021). Overview of the 2021 Update to the 2017 ACC Expert Consensus Decision Pathway for Optimization of Heart Failure with Reduced Ejection Fraction. *J. Cardiothorac. Vasc. Anesth.* doi:10.1053/j.jvca.2021.03.041

Farkhondeh, T., Samarghandian, S., and Bafandeh, F. (2019). The Cardiovascular Protective Effects of Chrysin: A Narrative Review on Experimental Researches. *Cardiovasc. Hematol. Agents Med. Chem.* 17 (1), 17–27. doi:10.2174/1871525717666190114145137

Feno, S., Butera, G., Vecellio Reane, D., Rizzuto, R., and Raffaello, A. (20192019). Crosstalk between Calcium and ROS in Pathophysiological Conditions. *Oxid. Med. Cel. Longev.* 2019, 9324018. doi:10.1155/2019/9324018

Fusi, F., Trezza, A., Tramaglino, M., Sgaragli, G., Saponara, S., and Spiga, O. (2020). The Beneficial Health Effects of Flavonoids on the Cardiovascular System: Focus on K+ Channels. *Pharmacol. Res.* 152, 104625. doi:10.1016/j.phrs.2019.104625

Görlach, A., Bertram, K., Hudecova, S., and Krizanova, O. (2015). Calcium and ROS: A Mutual Interplay. *Redox Biol.* 6, 260–271. doi:10.1016/j.redox.2015.08.010

Grassi, D., Desideri, G., Di Giosia, P., De Feo, M., Fellini, E., Cheli, P., et al. (2013). Tea, Flavonoids, and Cardiovascular Health: Endothelial protection. *Am. J. Clin. Nutr.* 98 (6 Suppl. l), 1660S–1666S. doi:10.3945/ajcn.113.058313

Guerrero, L., Castillo, J., Quiñones, M., Garcia-Vallvé, S., Arola, L., Pujadas, G., et al. (2012). Inhibition of Angiotensin-Converting Enzyme Activity by Flavonoids: Structure-Activity Relationship Studies. *PLoS One* 7 (11), e49493. doi:10.1371/journal.pone.0049493

Guo, Z., Liao, Z., Huang, L., Liu, D., Yin, D., and He, M. (2015). Kaempferol Protects Cardiomyocytes against Anoxia/reoxygenation Injury via Mitochondrial Pathway Mediated by SIRT1. *Eur. J. Pharmacol.* 761, 245–253. doi:10.1016/j.ejphar.2015.05.056

Hendy, G. N., and Canaff, L. (2016). Calcium-sensing Receptor, Proinflammatory Cytokines and Calcium Homeostasis. *Semin. Cel. Dev. Biol.* 49, 37–43. doi:10.1016/j.semcdb.2015.11.006

Horwich, T. B., and Fonarow, G. C. (2017). Prevention of Heart Failure. *JAMA Cardiol.* 2 (1), 116. doi:10.1001/jamacardio.2016.3394

Hostetler, G. L., Ralston, R. A., and Schwartz, S. J. (2017). Flavones: Food Sources, Bioavailability, Metabolism, and Bioactivity. *Adv. Nutr.* 8 (3), 423–435. doi:10.3945/an.116.012948

Hu, M., Wu, B., and Liu, Z. (2017). Bioavailability of Polyphenols and Flavonoids in the Era of Precision Medicine. *Mol. Pharm.* 14 (9), 2861–2863. doi:10.1021/acs.molpharmaceut.7b00545

Hu, W., Xu, T., Wu, P., Pan, D., Chen, J., Chen, J., et al. (2017). Luteolin Improves Cardiac Dysfunction in Heart Failure Rats by Regulating Sarcoplasmic Reticulum Ca2+-ATPase 2a. *Sci. Rep.* 7, 41017. doi:10.1038/srep41017

Ingólfsson, H. I., Thakur, P., Herold, K. F., Hobart, E. A., Ramsey, N. B., Periole, X., et al. (2014). Phytochemicals Perturb Membranes and Promiscuously Alter Protein Function. *ACS Chem. Biol.* 9 (8), 1788–1798. doi:10.1021/cb500086e

Jiang, Y. Q., Chang, G. L., Wang, Y., Zhang, D. Y., Cao, L., and Liu, J. (2016). Geniposide Prevents Hypoxia/Reoxygenation-Induced Apoptosis in H9c2 Cells: Improvement of Mitochondrial Dysfunction and Activation of

GLP-1R and the PI3K/AKT Signaling Pathway. *Cell. Physiol. Biochem.* 39 (1), 407–421. doi:10.1159/000445634

Jiang, Y., Sun-Waterhouse, D., Chen, Y., Li, F., and Li, D. (2021). Epigenetic Mechanisms Underlying the Benefits of Flavonoids in Cardiovascular Health and Diseases: Are Long Non-coding RNAs Rising Stars? *Crit. Rev. Food Sci. Nutr.*, 1–19. doi:10.1080/10408398.2020.1870926

Jing, Z., Wang, Z., Li, X., Li, X., Cao, T., Bi, Y., et al. (2016). Protective Effect of Quercetin on Posttraumatic Cardiac Injury. *Sci. Rep.* 6, 30812. doi:10.1038/srep30812

Kanaze, F. I., Bounartzi, M. I., Georgarakis, M., and Niopas, I. (2007). Pharmacokinetics of the Citrus Flavanone Aglycones Hesperetin and Naringenin after Single Oral Administration in Human Subjects. *Eur. J. Clin. Nutr.* 61 (4), 472–477. doi:10.1038/sj.ejcn.1602543

Kang, H. W., Lee, S. G., Otieno, D., and Ha, K. (2018). Flavonoids, Potential Bioactive Compounds, and Non-shivering Thermogenesis. *Nutrients* 10 (9). doi:10.3390/nu10091168

Khan, S., and Kamal, M. A. (2019). Can Wogonin Be Used in Controlling Diabetic Cardiomyopathy? *Curr. Pharm. Des.* 25 (19), 2171–2177. doi:10.2174/1381612825666190708173108

Khan, S., Zhang, D., Zhang, Y., Li, M., and Wang, C. (2016). Wogonin Attenuates Diabetic Cardiomyopathy through its Anti-inflammatory and Anti-oxidative Properties. *Mol. Cel. Endocrinol.* 428, 101–108. doi:10.1016/j.mce.2016.03.025

Khuntawee, W., Rungrotmongkol, T., and Hannongbua, S. (2012). Molecular Dynamic Behavior and Binding Affinity of Flavonoid Analogues to the Cyclin Dependent Kinase 6/cyclin D Complex. *J. Chem. Inf. Model.* 52 (1), 76–83. doi:10.1021/ci200304v

Kirienko, A., and Radak, D. (2016). Clinical Acceptability Study of Once-Daily versus Twice-Daily Micronized Purified Flavonoid Fraction in Patients with Symptomatic Chronic Venous Disease: a Randomized Controlled Trial. *Int. Angiol.* 35 (4), 399–405.

Korga, A., Ostrowska, M., Jozefczyk, A., Iwan, M., Wojcik, R., Zgorka, G., et al. (2019). Apigenin and Hesperidin Augment the Toxic Effect of Doxorubicin against HepG2 Cells. *BMC Pharmacol. Toxicol.* 20 (1), 22. doi:10.1186/s40360-019-0301-2

Landstrom, A. P., Dobrev, D., and Wehrens, X. H. T. (2017). Calcium Signaling and Cardiac Arrhythmias. *Circ. Res.* 120 (12), 1969–1993. doi:10.1161/CIRCRESAHA.117.310083

Lemos, F. O., and Ehrlich, B. E. (2018). Polycystin and Calcium Signaling in Cell Death and Survival. *Cell Calcium* 69, 37–45. doi:10.1016/j.ceca.2017.05.011

Li, F., Lang, F., Zhang, H., Xu, L., Wang, Y., Zhai, C., et al. (2017). Apigenin Alleviates Endotoxin-Induced Myocardial Toxicity by Modulating Inflammation, Oxidative Stress, and Autophagy. *Oxid. Med. Cel. Longev.* 2017, 2302896. doi:10.1155/2017/2302896

Li, Y., and Paxton, J. W. (2013). The Effects of Flavonoids on the ABC Transporters: Consequences for the Pharmacokinetics of Substrate Drugs. *Expert Opin. Drug Metab. Toxicol.* 9 (3), 267–285. doi:10.1517/17425255.2013.749858

Lin, C. C., Kuo, C. L., Lee, M. H., Lai, K. C., Lin, J. P., Yang, J. S., et al. (2011). Wogonin Triggers Apoptosis in Human Osteosarcoma U-2 OS Cells through the Endoplasmic Reticulum Stress, Mitochondrial Dysfunction and Caspase-3-dependent Signaling Pathways. *Int. J. Oncol.* 39 (1), 217–224. doi:10.3892/ijo.2011.1027

Lin, C. M., Wang, B. W., Pan, C. M., Fang, W. J., Chua, S. K., Hou, S. W., et al. (2018). Effects of Flavonoids on MicroRNA 145 Regulation through Klf4 and Myocardin in Neointimal Formation *In Vitro* and *In Vivo*. *J. Nutr. Biochem.* 52, 27–35. doi:10.1016/j.jnutbio.2017.08.016

Lu, H. F., Hsueh, S. C., Ho, Y. T., Kao, M. C., Yang, J. S., Chiu, T. H., et al. (2007). ROS Mediates Baicalin-Induced Apoptosis in Human Promyelocytic Leukemia HL-60 Cells through the Expression of the Gadd153 and Mitochondrial-dependent Pathway. *Anticancer Res.* 27 (1A), 117–125.

Lu, L. J., and Anderson, K. E. (1998). Sex and Long-Term Soy Diets Affect the Metabolism and Excretion of Soy Isoflavones in Humans. *Am. J. Clin. Nutr.* 68 (6 Suppl. l), 1500S–1504S. doi:10.1093/ajcn/68.6.1500S

Luo, M., and Anderson, M. E. (2013). Mechanisms of Altered Ca^{2+} Handling in Heart Failure. *Circ. Res.* 113 (6), 690–708. doi:10.1161/CIRCRESAHA.113.301651

Lv, L., Yao, Y., Zhao, G., and Zhu, G. (2018). Rutin Inhibits Coronary Heart Disease through ERK1/2 and Akt Signaling in a Porcine Model. *Exp. Ther. Med.* 15 (1), 506–512. doi:10.3892/etm.2017.5365

Madhesh, M., and Vaiyapuri, M. (2012). Effect of Luteolin on Lipid Peroxidation and Antioxidants in Acute and Chronic Periods of Isoproterenol Induced Myocardial Infarction in Rats. *J. Acute Med.* 2 (3), 70–76. doi:10.1016/j.jacme.2012.06.001

Maher, P., and Hanneken, A. (2005). Flavonoids Protect Retinal Ganglion Cells from Oxidative Stress-Induced Death. *Invest. Ophthalmol. Vis. Sci.* 46 (12), 4796–4803. doi:10.1167/iovs.05-0397

Mamagkaki, A., Bouris, I., Parsonidis, P., Vlachou, I., Gougousi, M., and Papasotiriou, I. (2021). Genistein as a Dietary Supplement; Formulation, Analysis and Pharmacokinetics Study. *PLoS One* 16 (4), e0250599. doi:10.1371/journal.pone.0250599

Manju, V., Balasubramaniyan, V., and Nalini, N. (2005). Rat Colonic Lipid Peroxidation and Antioxidant Status: the Effects of Dietary Luteolin on 1,2-dimethylhydrazine challenge. *Cel. Mol. Biol. Lett.* 10 (3), 535–551.

Matori, H., Umar, S., Nadadur, R. D., Sharma, S., Partow-Navid, R., Afkhami, M., et al. (2012). Genistein, a Soy Phytoestrogen, Reverses Severe Pulmonary Hypertension and Prevents Right Heart Failure in Rats. *Hypertension* 60 (2), 425–430. doi:10.1161/HYPERTENSIONAHA.112.191445

McCullough, M. L., Peterson, J. J., Patel, R., Jacques, P. F., Shah, R., and Dwyer, J. T. (2012). Flavonoid Intake and Cardiovascular Disease Mortality in a Prospective Cohort of US Adults. *Am. J. Clin. Nutr.* 95 (2), 454–464. doi:10.3945/ajcn.111.016634

Meyer, H., Bolarinwa, A., Wolfram, G., and Linseisen, J. (2006). Bioavailability of Apigenin from Apiin-Rich Parsley in Humans. *Ann. Nutr. Metab.* 50 (3), 167–172. doi:10.1159/000090736

Mohiuddin, A. (2019). Natural Foods and Indian Herbs of Cardiovascular Interest. *Pharm. Pharmacol. Int. J.* 7 (2), 60–84. doi:10.15406/ppij.2019.07.00235

Mora, M. T., Ferrero, J. M., Gomez, J. F., Sobie, E. A., and Trenor, B. (2018). Ca2+ Cycling Impairment in Heart Failure Is Exacerbated by Fibrosis: Insights Gained from Mechanistic Simulations. *Front. Physiol.* 9, 1194. doi:10.3389/fphys.2018.01194

Mozaffarian, D., and Wu, J. H. Y. (2018). Flavonoids, Dairy Foods, and Cardiovascular and Metabolic Health: A Review of Emerging Biologic Pathways. *Circ. Res.* 122 (2), 369–384. doi:10.1161/CIRCRESAHA.117.309008

Münzel, T., Camici, G. G., Maack, C., Bonetti, N. R., Fuster, V., and Kovacic, J. C. (2017). Impact of Oxidative Stress on the Heart and Vasculature: Part 2 of a 3-Part Series. *J. Am. Coll. Cardiol.* 70 (2), 212–229. doi:10.1016/j.jacc.2017.05.035

Nai, C., Xuan, H., Zhang, Y., Shen, M., Xu, T., Pan, D., et al. (2015). Luteolin Exerts Cardioprotective Effects through Improving Sarcoplasmic Reticulum Ca(2+)-ATPase Activity in Rats during Ischemia/Reperfusion *In Vivo*. *Evid. Based Complement. Alternat Med.* 2015, 365854.

Najjar, R. S., and Feresin, R. G. (2021). Protective Role of Polyphenols in Heart Failure: Molecular Targets and Cellular Mechanisms Underlying Their Therapeutic Potential. *Int. J. Mol. Sci.* 22 (4). doi:10.3390/ijms22041668

Orrenius, S., Zhivotovsky, B., and Nicotera, P. (2003). Regulation of Cell Death: the Calcium-Apoptosis Link. *Nat. Rev. Mol. Cel. Biol.* 4 (7), 552–565. doi:10.1038/nrm1150

Panth, N., Paudel, K. R., and Parajuli, K. (2016). Reactive Oxygen Species: A Key Hallmark of Cardiovascular Disease. *Adv. Med.* 2016, 9152732. doi:10.1155/2016/9152732

Patel, R. V., Mistry, B. M., Shinde, S. K., Syed, R., Singh, V., and Shin, H. S. (2018). Therapeutic Potential of Quercetin as a Cardiovascular Agent. *Eur. J. Med. Chem.* 155, 889–904. doi:10.1016/j.ejmech.2018.06.053

Phan, H. T., Yoda, T., Chahal, B., Morita, M., Takagi, M., and Vestergaard, M. C. (2014). Structure-dependent Interactions of Polyphenols with a Biomimetic Membrane System. *Biochim. Biophys. Acta* 1838 (10), 2670–2677. doi:10.1016/j.bbamem.2014.07.001

Ponzo, V., Goitre, I., Fadda, M., Gambino, R., De Francesco, A., Soldati, L., et al. (2015). Dietary Flavonoid Intake and Cardiovascular Risk: a Population-Based Cohort Study. *J. Transl. Med.* 13, 218. doi:10.1186/s12967-015-0573-2

Qin, F., Siwik, D. A., Lancel, S., Zhang, J., Kuster, G. M., Luptak, I., et al. (2013). Hydrogen Peroxide-Mediated SERCA Cysteine 674 Oxidation Contributes to Impaired Cardiac Myocyte Relaxation in Senescent Mouse Heart. *J. Am. Heart Assoc.* 2 (4), e000184. doi:10.1161/JAHA.113.000184

Qiu, T., Wu, D., Yang, L., Ye, H., Wang, Q., Cao, Z., et al. (2018). Exploring the Mechanism of Flavonoids through Systematic Bioinformatics Analysis. *Front. Pharmacol.* 9, 918. doi:10.3389/fphar.2018.00918

Rastogi, R., Geng, X., Li, F., and Ding, Y. (2016). NOX Activation by Subunit Interaction and Underlying Mechanisms in Disease. *Front. Cel. Neurosci.* 10, 301. doi:10.3389/fncel.2016.00301

Rizzuto, R., Pinton, P., Ferrari, D., Chami, M., Szabadkai, G., Magalhães, P. J., et al. (2003). Calcium and Apoptosis: Facts and Hypotheses. *Oncogene* 22 (53), 8619–8627. doi:10.1038/sj.onc.1207105

Rodius, S., de Klein, N., Jeanty, C., Sánchez-Iranzo, H., Crespo, I., Ibberson, M., et al. (2020). Fisetin Protects against Cardiac Cell Death through Reduction of ROS Production and Caspases Activity. *Sci. Rep.* 10 (1), 2896. doi:10.1038/s41598-020-59894-4

Ross, J. A., and Kasum, C. M. (2002). Dietary Flavonoids: Bioavailability, Metabolic Effects, and Safety. *Annu. Rev. Nutr.* 22, 19–34. doi:10.1146/annurev.nutr.22.111401.144957

Ryter, S. W., Kim, H. P., Hoetzel, A., Park, J. W., Nakahira, K., Wang, X., et al. (2007). Mechanisms of Cell Death in Oxidative Stress. *Antioxid. Redox Signal.* 9 (1), 49–89. doi:10.1089/ars.2007.9.49

Santalla, M., Valverde, C. A., Harnichar, E., Lacunza, E., Aguilar-Fuentes, J., Mattiazzi, A., et al. (2014). Aging and CaMKII Alter Intracellular Ca2+ Transients and Heart Rhythm in *Drosophila melanogaster*. *PLoS One* 9 (7), e101871. doi:10.1371/journal.pone.0101871

Santulli, G., Xie, W., Reiken, S. R., and Marks, A. R. (2015). Mitochondrial Calcium Overload Is a Key Determinant in Heart Failure. *Proc. Natl. Acad. Sci. U S A.* 112 (36), 11389–11394. doi:10.1073/pnas.1513047112

Senoner, T., and Dichtl, W. (2019). Oxidative Stress in Cardiovascular Diseases: Still a Therapeutic Target? *Nutrients* 11 (9), 11. doi:10.3390/nu11092090

Serban, M. C., Sahebkar, A., Zanchetti, A., Mikhailidis, D. P., Howard, G., Antal, D., et al. (2016). Effects of Quercetin on Blood Pressure: A Systematic Review and Meta-Analysis of Randomized Controlled Trials. *J. Am. Heart Assoc.* 5 (7). doi:10.1161/JAHA.115.002713

Sessa, W. C. (2004). eNOS at a Glance. *J. Cel. Sci.* 117 (Pt 12), 2427–2429. doi:10.1242/jcs.01165

Shanmugam, K., Ravindran, S., Kurian, G. A., and Rajesh, M. (2018). Fisetin Confers Cardioprotection against Myocardial Ischemia Reperfusion Injury by Suppressing Mitochondrial Oxidative Stress and Mitochondrial Dysfunction and Inhibiting Glycogen Synthase Kinase 3β Activity. *Oxid. Med. Cel. Longev.* 2018, 9173436. doi:10.1155/2018/9173436

Shen, A. C., and Jennings, R. B. (1972). Kinetics of Calcium Accumulation in Acute Myocardial Ischemic Injury. *Am. J. Pathol.* 67 (3), 441–452.

Shih, Y. L., Hung, F. M., Lee, C. H., Yeh, M. Y., Lee, M. H., Lu, H. F., et al. (2017). Fisetin Induces Apoptosis of HSC3 Human Oral Cancer Cells through Endoplasmic Reticulum Stress and Dysfunction of Mitochondria-Mediated Signaling Pathways. *In Vivo* 31 (6), 1103–1114. doi:10.21873/invivo.11176

Singh, M., Kaur, M., and Silakari, O. (2014). Flavones: an Important Scaffold for Medicinal Chemistry. *Eur. J. Med. Chem.* 84, 206–239. doi:10.1016/j.ejmech.2014.07.013

Souza, R. P., Bonfim-Mendonça, P. S., Gimenes, F., Ratti, B. A., Kaplum, V., Bruschi, M. L., et al. (20172017). Oxidative Stress Triggered by Apigenin Induces Apoptosis in a Comprehensive Panel of Human Cervical Cancer-Derived Cell Lines. *Oxid. Med. Cel. Longev.* 2017, 1512745. doi:10.1155/2017/1512745

Swaminathan, A., Basu, M., Bekri, A., Drapeau, P., and Kundu, T. K. (2019). The Dietary Flavonoid, Luteolin, Negatively Affects Neuronal Differentiation. *Front. Mol. Neurosci.* 12, 41. doi:10.3389/fnmol.2019.00041

Terrar, D. A. (2020). Calcium Signaling in the Heart. *Adv. Exp. Med. Biol.* 1131, 395–443. doi:10.1007/978-3-030-12457-1_16

Thilakarathna, S. H., and Rupasinghe, H. P. (2013). Flavonoid Bioavailability and Attempts for Bioavailability Enhancement. *Nutrients* 5 (9), 3367–3387. doi:10.3390/nu5093367

Uddin, M. S., and Kabir, M. T. (2019). Emerging Signal Regulating Potential of Genistein against Alzheimer's Disease: A Promising Molecule of Interest. *Front. Cel. Dev. Biol.* 7, 197. doi:10.3389/fcell.2019.00197

Virani, S. S., Alonso, A., Aparicio, H. J., Benjamin, E. J., Bittencourt, M. S., Callaway, C. W., et al. (2021). Heart Disease and Stroke Statistics-2021 Update: A Report from the American Heart Association. *Circulation* 143 (8), e254–743. doi:10.1161/CIR.0000000000000950

Wang, D. D. (2019). Dietary Patterns and Precision Prevention of Heart Failure. *J. Am. Coll. Cardiol.* 73 (16), 2046–2048. doi:10.1016/j.jacc.2019.02.037

Wang, G., Li, W., Lu, X., Bao, P., and Zhao, X. (2012). Luteolin Ameliorates Cardiac Failure in Type I Diabetic Cardiomyopathy. *J. Diabetes Complications* 26 (4), 259–265. doi:10.1016/j.jdiacomp.2012.04.007

Wang, Z., Zeng, M., Wang, Z., Qin, F., Chen, J., and He, Z. (2021). Dietary Luteolin: A Narrative Review Focusing on its Pharmacokinetic Properties and Effects on Glycolipid Metabolism. *J. Agric. Food Chem.* 69 (5), 1441–1454. doi:10.1021/acs.jafc.0c08085

Weintraub, N. L., Collins, S. P., Pang, P. S., Levy, P. D., Anderson, A. S., Arslanian-Engoren, C., et al. (2010). Acute Heart Failure Syndromes: Emergency Department Presentation, Treatment, and Disposition: Current Approaches and Future Aims: a Scientific Statement from the American Heart Association. *Circulation* 122 (19), 1975–1996. doi:10.1161/CIR.0b013e3181f9a223

Williamson-Hughes, P. S., Flickinger, B. D., Messina, M. J., and Empie, M. W. (2006). Isoflavone Supplements Containing Predominantly Genistein Reduce Hot Flash Symptoms: a Critical Review of Published Studies. *Menopause* 13 (5), 831–839. doi:10.1097/01.gme.0000227330.49081.9e

Wu, B., Kulkarni, K., Basu, S., Zhang, S., and Hu, M. (2011). First-pass Metabolism via UDP-Glucuronosyltransferase: a Barrier to Oral Bioavailability of Phenolics. *J. Pharm. Sci.* 100 (9), 3655–3681. doi:10.1002/jps.22568

Wu, Q., Li, W., Zhao, J., Sun, W., Yang, Q., Chen, C., et al. (2021). Apigenin Ameliorates Doxorubicin-Induced Renal Injury via Inhibition of Oxidative Stress and Inflammation. *Biomed. Pharmacother.* 137, 111308. doi:10.1016/j.biopha.2021.111308

Xin, L., Gao, J., Lin, H., Qu, Y., Shang, C., Wang, Y., et al. (2020). Regulatory Mechanisms of Baicalin in Cardiovascular Diseases: A Review. *Front. Pharmacol.* 11, 583200. doi:10.3389/fphar.2020.583200

Xingyue, L., Shuang, L., Qiang, W., Jinjuan, F., and Yongjian, Y. (2021). Chrysin Ameliorates Sepsis-Induced Cardiac Dysfunction through Upregulating Nfr2/Heme Oxygenase 1 Pathway. *J. Cardiovasc. Pharmacol.* 77 (4), 491–500. doi:10.1097/FJC.0000000000000989

Yamagata, K., and Yamori, Y. (2020). Inhibition of Endothelial Dysfunction by Dietary Flavonoids and Preventive Effects against Cardiovascular Disease. *J. Cardiovasc. Pharmacol.* 75 (1), 1–9. doi:10.1097/FJC.0000000000000757

Yan, Q., Li, Y., Yan, J., Zhao, Y., Liu, Y., and Liu, S. (2018). Effects of Luteolin on Regulatory Proteins and Enzymes for Myocyte Calcium Circulation in Hypothermic Preserved Rat Heart. *Exp. Ther. Med.* 15 (2), 1433–1441. doi:10.3892/etm.2017.5514

Yan, Q., Li, Y., Yan, J., Zhao, Y., Liu, Y., and Liu, S. (2019). Luteolin Improves Heart Preservation through Inhibiting Hypoxia-dependent L-type Calcium Channels in Cardiomyocytes. *Exp. Ther. Med.* 17 (3), 2161–2171. doi:10.3892/etm.2019.7214

Ye, Q., Liu, K., Shen, Q., Li, Q., Hao, J., Han, F., et al. (2019). Reversal of Multidrug Resistance in Cancer by Multi-Functional Flavonoids. *Front. Oncol.* 9, 487. doi:10.3389/fonc.2019.00487

Zamora-Ros, R., Jiménez, C., Cleries, R., Agudo, A., Sánchez, M. J., Sánchez-Cantalejo, E., et al. (2013). Dietary Flavonoid and Lignan Intake and Mortality in a Spanish Cohort. *Epidemiology* 24 (5), 726–733. doi:10.1097/EDE.0b013e31829d5902

Zeka, K., Ruparelia, K., Arroo, R. R. J., Budriesi, R., and Micucci, M. (2017). Flavonoids and Their Metabolites: Prevention in Cardiovascular Diseases and Diabetes. *Diseases* 5 (3). doi:10.3390/diseases5030019

Zhang, Y. M., Zhang, Z. Y., and Wang, R. X. (2020). Protective Mechanisms of Quercetin against Myocardial Ischemia Reperfusion Injury. *Front. Physiol.* 11, 956. doi:10.3389/fphys.2020.00956

Zhao, F., Fu, L., Yang, W., Dong, Y., Yang, J., Sun, S., et al. (2016). Cardioprotective Effects of Baicalein on Heart Failure via Modulation of Ca(2+) Handling Proteins *In Vivo* and *In Vitro*. *Life Sci.* 145, 213–223. doi:10.1016/j.lfs.2015.12.036

Zhivotovsky, B., and Orrenius, S. (2011). Calcium and Cell Death Mechanisms: a Perspective from the Cell Death Community. *Cell Calcium* 50 (3), 211–221. doi:10.1016/j.ceca.2011.03.003

Zimmerman, M. C., Takapoo, M., Jagadeesha, D. K., Stanic, B., Banfi, B., Bhalla, R. C., et al. (2011). Activation of NADPH Oxidase 1 Increases Intracellular Calcium and Migration of Smooth Muscle Cells. *Hypertension* 58 (3), 446–453. doi:10.1161/HYPERTENSIONAHA.111.177006

Conflict of Interest: The authors declare that the research was conducted in the absence of any commercial or financial relationships that could be construed as a potential conflict of interest.

Publisher's Note: All claims expressed in this article are solely those of the authors and do not necessarily represent those of their affiliated organizations, or those of the publisher, the editors and the reviewers. Any product that may be evaluated in this article, or claim that may be made by its manufacturer, is not guaranteed or endorsed by the publisher.

frontiers in Physiology

REVIEW
published: 07 February 2022
doi: 10.3389/fphys.2022.806366

Basic Research Approaches to Evaluate Cardiac Arrhythmia in Heart Failure and Beyond

Max J. Cumberland[1], Leto L. Riebel[2], Ashwin Roy[1], Christopher O'Shea[1], Andrew P. Holmes[1,3], Chris Denning[4], Paulus Kirchhof[1,5], Blanca Rodriguez[2] and Katja Gehmlich[1,6]**

[1]Institute of Cardiovascular Sciences, College of Medical and Dental Sciences, University of Birmingham, Birmingham, United Kingdom, [2]Department of Computer Science, University of Oxford, Oxford, United Kingdom, [3]Institute of Clinical Sciences, College of Medical and Dental Sciences, University of Birmingham, Birmingham, United Kingdom, [4]Stem Cell Biology Unit, Biodiscovery Institute, British Heart Foundation Centre for Regenerative Medicine, University of Nottingham, Nottingham, United Kingdom, [5]University Heart and Vascular Center, University Medical Center Hamburg-Eppendorf, Hamburg, Germany, [6]Cardiovascular Medicine, Radcliffe Department of Medicine, University of Oxford and British Heart Foundation Centre of Research Excellence Oxford, Oxford, United Kingdom

OPEN ACCESS

Edited by:
Elisabetta Cerbai, University of Florence, Italy

Reviewed by:
Leonardo Sacconi, University of Florence, Italy
Markéta Bébarová, Masaryk University, Czechia

***Correspondence:**
Max J. Cumberland
MJC487@student.bham.ac.uk
Katja Gehmlich
k.gehmlich@bham.ac.uk

Specialty section:
This article was submitted to Cardiac Electrophysiology, a section of the journal Frontiers in Physiology

Received: *31 October 2021*
Accepted: *10 January 2022*
Published: *07 February 2022*

Citation:
Cumberland MJ, Riebel LL, Roy A, O'Shea C, Holmes AP, Denning C, Kirchhof P, Rodriguez B and Gehmlich K (2022) Basic Research Approaches to Evaluate Cardiac Arrhythmia in Heart Failure and Beyond. Front. Physiol. 13:806366. doi: 10.3389/fphys.2022.806366

Patients with heart failure often develop cardiac arrhythmias. The mechanisms and interrelations linking heart failure and arrhythmias are not fully understood. Historically, research into arrhythmias has been performed on affected individuals or *in vivo* (animal) models. The latter however is constrained by interspecies variation, demands to reduce animal experiments and cost. Recent developments in *in vitro* induced pluripotent stem cell technology and *in silico* modelling have expanded the number of models available for the evaluation of heart failure and arrhythmia. An agnostic approach, combining the modalities discussed here, has the potential to improve our understanding for appraising the pathology and interactions between heart failure and arrhythmia and can provide robust and validated outcomes in a variety of research settings. This review discusses the state of the art models, methodologies and techniques used in the evaluation of heart failure and arrhythmia and will highlight the benefits of using them in combination. Special consideration is paid to assessing the pivotal role calcium handling has in the development of heart failure and arrhythmia.

Keywords: heart failure, *in vivo* cardiac models, human induced pluripotent stem cells, methods, *in silico* modelling, cardiac arrhythmias

INTRODUCTION

Heart failure and cardiac arrhythmias are intrinsically linked in a complex interplay of cause and effect. Cardiac arrhythmias can promote left ventricular systolic dysfunction through rapid ventricular rates which disrupt atrial and ventricular output (Prabhu et al., 2017). Moreover, heart failure is an independent risk factor for arrhythmogenesis, due to its deleterious impact on atrial remodelling (Heijman et al., 2014). Heart failure and arrhythmias have shared physiological and genetic causes. Furthermore, many of the methods and systems used to

evaluate the electrophysiological changes that occur in cardiac arrhythmias are common to those used in heart failure research.

Advancements in medical therapies have led to the survival of patients with heart failure and arrhythmias for longer, increasing the prevalence of both conditions (Schmitt et al., 2009). Furthermore, in patients with inherited cardiac conditions, arrhythmias are common and represent a significant financial and clinical burden (Verheugt et al., 2010). The number of people living with chronic heart failure is increasing, estimated to be 64.3 million worldwide in 2020 (Groenewegen et al., 2020). An increased prevalence of atrial fibrillation (AF; 3.29% in 2016) in the United Kingdom over the past decade has compounded the issue, as it predisposes many to the development of heart failure and ischaemic stroke (Pozzoli et al., 1998; Eckardt et al., 2016; Adderley et al., 2019).

Research into the diagnosis, aetiology, prevention and treatment of cardiac arrhythmias has the potential to provide substantive clinical benefit to a significant proportion of the population and is particularly pertinent to those suffering from heart failure. Despite recent advances in cardiology, the mechanisms underpinning the multitude of different types of cardiac arrhythmias are still not fully understood.

Historically, researchers have been heavily reliant upon electrophysiological data obtained from clinical cases and animal models. Obtaining human experimental data, such as electrocardiograms and echocardiograms, is relatively inexpensive, available and non-invasive to the patient (Davie et al., 1996). However, the procurement and subsequent use of human tissue in cardiac arrhythmia research is often limited by stringent ethical approval and a lack of availability (Price, 2005).

Cardiovascular research requiring the use of animal models, such as mice, rabbit, goat and pig, is often highly invasive and consequently carries a substantial ethical burden. Moreover, although heart failure and cardiac arrhythmias have been successfully modelled *in vivo*, distinct interspecies differences in cardiac electrophysiology (e.g., heart rate of mice being approximately 10 times faster than in humans) limits the translation of these findings into the clinical setting. Recent developments in human-based methodologies, including induced pluripotent stem cells (iPSC) and computational cardiac modelling and simulation, present exciting prospects to supplement and augment experimental and clinical investigations (Rodriguez et al., 2015).

In the following text, we will outline many of the models and techniques most commonly used to evaluate cardiac arrhythmias in heart failure research. They are summarised in **Table 1**. For a broader description of the experimental models available for cardiac electrophysiology research, and their suitability for use in evaluating specific arrhythmogenic syndromes, the reader is directed to the excellently written review by Odening et al. (2021). Heart failure can arise from a multitude of aetiologies, including but not limited to inherited genetics, environment (including chemotherapy) and age (Ziaeian and Fonarow, 2016). While only present in a sub-group of patients with heart failure, this review will often use arrhythmias linked to genetic variation as a prime example, as this area of research has made significant advances within recent years.

MODELS AND TECHNIQUES USED TO EVALUATE ARRHYTHMIA IN HEART FAILURE

In vivo/*Ex vivo* Model Systems

Genetically Modified Animals

Following the pioneering work by Thomas and Capecchi (1987) on the site directed mutagenesis of mouse embryonic derived stem cells, genetically modified animal models have become a staple method commonly used in disease modelling. A myriad of genetic variations can be inserted into the embryos of animals to cause the overexpression, inactivation, conditional expression and modification of cardiac genes (Low et al., 2016). Modern genome editing techniques, such as clustered regularly interspaced short palindromic repeat (CRISPR) Cas9 editing, have allowed the engineering of animal genomes to be performed with unprecedented ease (Ran et al., 2013; Zarei et al., 2019). This has consequently led to the widespread use of genetically engineered animals in cardiovascular research (Ding et al., 2014; Carroll et al., 2016; Tessadori et al., 2018).

A variety of genetically modified animals have been used to study heart failure and arrhythmias, including but not limited to rabbits, pigs, dogs and rats (Clauss et al., 2019). **Figure 1** outlines the most commonly used animals in arrhythmia and heart failure research, their differences in electrophysiology in relation to humans and the methods used in their evaluation. The prevalence of large animals in arrhythmia research is comparatively small when contrasted to that of the mouse and zebrafish. Genetically modified mice, containing loss of function variants in the gap junction protein connexin43, frequently develop severe ventricular arrhythmias and have been used to model the arrhythmogenic substrates behind sudden cardiac death (Gutstein et al., 2001). Heart failure in *in vivo* models can be promoted in a variety of ways, including coronary artery ligation, aortic banding, chronic rapid pacing and isoproterenol infusion treatment (Chen et al., 2017a; Bosch et al., 2020). Many of these methods are detailed in Halapas et al. (2008) and can be performed on animal models possessing arrhythmogenic variants to study the complex pathogenesis of arrhythmias in chronic heart failure.

Channelopathies, such as long QT syndrome, have been recapitulated in mice, by the targeted mutagenesis of genes encoding subunits of inward rectifier potassium channels and *SCN5A* (Salama and London, 2007). However distinct differences in the ion channels predominantly responsible for cellular repolarisation in adult human and mouse cardiomyocytes exemplify how contrasts in interspecies cardiac electrophysiology limits the use of data obtained from such models (Wang et al., 1996).

Arrhythmogenic cardiomyopathies, often caused by genetic alterations, have been successfully modelled in genetically modified mice to assess the impact they have on the development of heart failure. The micropeptide phospholamban helps regulate intracellular calcium handling in cardiomyocytes by inhibiting the sarcoplasmic reticulum Ca^{2+}-ATP-ase SERCA2 (MacLennan and Kranias, 2003). Pathogenic variants of the *PLN* gene have

TABLE 1 | Methods used to evaluate cardiac arrhythmia in heart failure.

Approach	Method	Description	Invasiveness	Advantages	Limitations
In vivo	Electrocardiogram (ECG)	Measuring voltage versus time from electrodes placed on the skin	Non-invasive	• Easy to perform • Can be used to detect most sustained arrhythmias	• Provides limited information on mechanism of arrhythmia • Struggles to detect intermittent arrhythmias
In vivo	Echocardiography	Using sound waves to facilitate live imaging of the heart. This can be used to indirectly estimate measurements of the cardiac cycle	Non-invasive	• Provides detailed structural information on the heart • Relatively easy to perform	• Cardiac cycle is estimated • High interobserver variability
Ex vivo	Monophasic and transmembrane action potentials	The recording of action potentials from either a single or group of cardiomyocytes using intracellular and extracellular electrodes	Invasive/Non-invasive	• Direct recoding of transmembrane voltage changes • Can be recorded in freely beating heart/preparations • Ideally suited for arrhythmia induction and testing	• Low spatial resolution • Direct electrode contact can damage tissue • Hearts/tissue samples often require preparation, e.g., Langendorff perfusion
Ex vivo	Voltage and calcium optical mapping	Using voltage and/or calcium-sensitive dyes to analyse action potential propagation and calcium transients	Partially invasive	• High spatial resolution allows visualisation of propagation patterns present in complex arrhythmias • Enables the electrophysiological assessment of samples following electrical shocks which may be elicited to induce arrhythmogenesis or mimic defibrillation	• Hearts/tissue samples often require preparation, e.g., Langendorff perfusion • Motion artefacts can occur if samples are uncoupled • High skill level required • Dye toxicity and photobleaching
Ex vivo/In vitro	Patch clamping	Microelectrodes are used to interrogate membrane potential and ion current channel function in excitable cardiac cells and preparations	Invasive	• Enables electrophysiological characterisation of a subset of individual ion channel(s) (voltage clamp) • Enables the direct recording of action potentials (current clamp) • Enables the comprehensive characterisation of electrophysiological events at a single-cell level under controlled conditions	• High skill level required • Cannot detect electrophysiological events related to re-entry • Low throughput
In vitro	Multi-electrode arrays (MEA)	A surface containing embedded electrodes acts as a neural interface to assay the electrical activity of cultured cells	Non-invasive	• High-throughput multiplexed reads • Relatively unharmful to the cells, allowing experiments to be performed over a long period of time	• Low spatial resolution • An extracellular field potential is recorded rather than the action potential itself
In vitro	Intracellular calcium imaging	A fluorescent calcium indicator is either added to the cells or endogenously expressed to visualise calcium transients	Partially invasive	• High spatial resolution allows assessment of intracellular calcium handling • Can be performed in conjunction with voltage-sensitive dyes	• Dyes can be toxic to the cells • Skill required to determine the appropriate indicator/dye for imaging
In silico	Human-based computational models and simulations	Simulations using mathematical models of human cardiac pathophysiology yield high spatio-temporal resolution data, including time course of ionic currents, action potentials, calcium transients, conduction velocity and the ECG.	Non-invasive	• Fast and cost-effective way of evaluating arrhythmias • Can be used to generate predictions on arrhythmia mechanisms which would be imperceptible using solely experimental data	• Can be reliant on experimental data • Computational power is limited requiring researchers to balance the complexity of their model against its performance

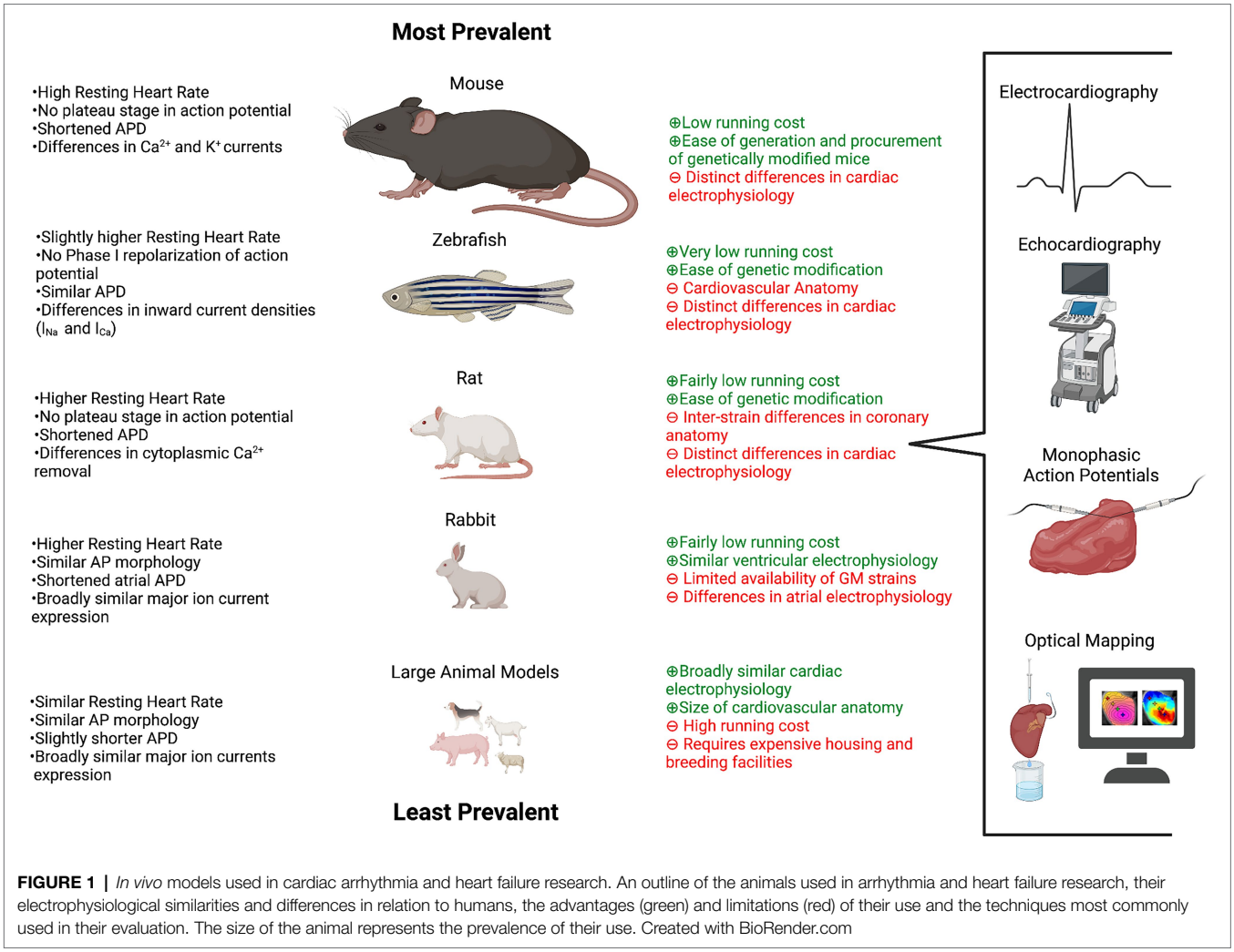

FIGURE 1 | *In vivo* models used in cardiac arrhythmia and heart failure research. An outline of the animals used in arrhythmia and heart failure research, their electrophysiological similarities and differences in relation to humans, the advantages (green) and limitations (red) of their use and the techniques most commonly used in their evaluation. The size of the animal represents the prevalence of their use. Created with BioRender.com

been linked to the development of arrhythmogenic cardiomyopathies and severe heart failure and have been successfully modelled in mice to assess arrhythmia susceptibility and response to standard heart failure therapy (Fish et al., 2016; Eijgenraam et al., 2020). Another example of cardiomyopathies being modelled in mouse models is evidenced in Geisterfer-Lowrance et al. (1996), where the group generated a *Myh6* p. Arg403Gln variant in the orthologous α cardiac myosin heavy chain (MHC) gene to explore the pathological effects of the variant in familial hypertrophic cardiomyopathy.

Common single nucleotide variants, identified in genome-wide association studies of AF and heart failure, are frequently found located in non-coding regions of the genome (Shah et al., 2020). The association between the variant and the disease is often unclear and can consequently require further elucidation using *in vivo* models. Genetic variants located in the 4q25 region, which lies adjacent to the *PITX2* gene, have been strongly linked to the development of AF (Gudbjartsson et al., 2007). The precise mechanism by which this genomic region affects the expression of *PITX2* and the development of AF remains cryptic. Genetically modified mouse models have proven powerful tools to validate disease association. The insertion of fragments of the 4q25 region attached to a reporter gene, into the genome of mouse embryos, has helped researchers explore the functional role variants in this cis-regulatory region have on cardiac development (Aguirre et al., 2015).

The use of genetically modified mouse models in arrhythmia and heart failure research poses a difficult challenge. Although mice and humans share approximately 85% sequence homology in protein coding regions, fundamental differences remain in the sequence composition of many key genes and their relative expression levels (Makałowski et al., 1996). Disparities in the compartment-specific expression of transient outward K^+ current (I_{to}), as well as voltage-gated sodium and calcium channel isoform expression causes stark differences in the formation of the cardiac action potential (Blechschmidt et al., 2008; Niwa and Nerbonne, 2010; Björling et al., 2013). Consequently, results obtained from mice often require translation when interpreted for humans (Tanner and Beeton, 2018).

The generation of humanised mouse models has attempted to mitigate differences in sequence homology through the

replacement of the mouse gene with the orthologous human counterpart (Zhu et al., 2019). However, the complexity of gene expression regulation in higher eukaryotes makes precise transcriptional emulation difficult. The cost and time needed to generate genetically modified mouse models limits their use in investigating rare inherited variants associated with cardiomyopathies, arrhythmias and heart failure. Furthermore, genetically modified animal models struggle to emulate the environmental stressors and comorbidities of individuals with heart failure and arrhythmia and therefore struggle to capture the phenotypic spectrum of either disease (Colbert et al., 1997; Vakrou et al., 2018).

Ex vivo Cardiac Preparations

Pioneered by Oskar Langendorff, the retrogradely perfused heart allows prolonged experimental interrogation in a context independent of confounding non-cardiac organ function (Bell et al., 2011). The Langendorff heart is a cornerstone of basic cardiology research. It allows precise control of physiological and pharmacological interventions and facilitates programmed stimulation for arrhythmia induction. The effect that these interventions as well as genetic and environmental stressors have on the isolated heart, can be studied using several methodologies (section "Electrophysiological Study of *ex vivo* Model Systems"). The Langendorff heart is a non-working system which fails to fully recapitulate *in vivo* conditions due to its retrograde perfusion. The Langendorff model can be modified into the orthogradely perfused working model developed by Neely et al. (1967), to better characterise pump function. Further information on isolated heart models can be derived from Olejnickova et al. (2015).

Additional preparations of the animal heart have been developed from the whole heart to answer specific experimental questions. The innervated heart technique, originally developed by Ng et al. (2001) for use in the rabbit, has been applied in several animal models to enable study of autonomic influences on cardiac electrophysiology (Winter et al., 2018; Wang et al., 2019). Isolated atrial preparations enable detailed study of the atria and sinoatrial node without confounding ventricular influences, while slice and wedge preparations allow transmural properties of the mouse heart to be investigated (Lang et al., 2015; Holmes et al., 2016; Wen et al., 2018; Dong et al., 2019; Brennan et al., 2020).

Electrocardiography in *in vivo* Model Systems

Fundamentals of Electrocardiography in Animal Models

The electrical changes that occur during the cardiac cycle can be plotted in a voltage versus time graph, commonly known as an ECG (Geselowitz, 1989). Recognisable complexes within the ECG, such as the P wave, QRS complex and T wave, correspond to the depolarisation of the atria (P) and ventricles (QRS) and the repolarisation of the latter (T). Willem Einthoven is credited with the invention of electrocardiography and the contemporary ECG (Barold, 2003). Historically, the use of electrocardiography was integral in defining many of the fundamental mechanisms behind clinically important arrhythmias (Fye, 1994). Today the technique underpins a significant proportion of modern cardiovascular research and is pervasively used to phenotype genetically modified animal models.

Heart rate and heart rate variability are two of the most important metrics determined from an ECG. Researchers use animal heart rates to characterise cardiac function in response to hemodynamic, pharmacologic and environmental stressors (Appel et al., 1989). Variation in heart rate, which arises from differential sinoatrial node stimulation, is influenced by the animal's temperature, activity, stress level and sleep cycle (Thireau et al., 2008). It can be used as a measurement of how adaptive the animal is to cardiac stress, with a decreased variation in heart rate being linked to an increased risk of mortality following myocardial infarction (Kleiger et al., 1987). Intervals between recognisable complexes within the ECG, such as the QT, PR and RR, can be calculated and compared between animals with relative ease. Perturbation of such complexes can be used to identify structural abnormalities within the heart and can be prognostically important in the evaluation of heart failure and arrhythmia. For example, the RR interval can be plotted in Poincaré plots to identify the presence of AF (Park et al., 2009).

ECGs of genetically modified animals are often used to assess the pathogenic impact gene variants have on arrhythmogenesis. This has proven particularly pertinent when exploring variants associated with channelopathies and arrhythmogenic syndromes, such as those in the calcium ryanodine receptors (Zhao et al., 2015). Despite the overwhelming prevalence of the animal in cardiovascular research, the surface ECG of the zebrafish has and continues to be relatively underutilised. Further information on the practicalities of electrocardiography in zebrafish can be found in Zhao et al. (2019). The coming paragraphs will focus on electrocardiography in mice, due to their aforementioned common use in arrhythmia and heart failure research.

Experimental Methods for Electrocardiography in Mouse

The arrhythmias common in patients with heart failure are often sporadic and present inconsistently, therefore the induction of arrhythmias in mice is often required. Arrhythmias can be induced in a variety of ways including burst/S1-S2 pacing, intense endurance exercise and the administration of pro-arrhythmic agents (Schrickel et al., 2002; Spurney et al., 2011; Aschar-Sobbi et al., 2015). Electrocardiography can be performed on conscious or sedated mice, with the latter being disadvantageous as disruption of cardiac function can be caused by many of the commonly used sedatives (Chaves et al., 2003).

There are three established systems for the recording of ECGs from mice: non-invasive, tethered and implanted telemetry ECG (Ho et al., 2011). Non-invasive ECGs involve placing the mouse in a constraint so that three small surface electrodes make contact with the paws of the animal. As anaesthesia is not required and the technique is quick and easy to do, non-invasive electrocardiography facilitates "high-throughput"

screening of mice; however, the technique is not suitable for long term ECG recordings.

Tethered electrocardiography involves attaching four small electrodes into the back of the mouse. The electrodes are tethered to a swivel device to enable unrestricted movement. ECGs can be recorded without the need of an often stress inducing restraining cage and for longer periods of time. General anaesthesia is however required to insert the electrodes into the mouse and may consequently lead to abnormal cardiac function. Mice must be monitored during the recording of the ECG to prevent agitation of the tethered electrode wires, limiting the use of the technique in long term experimental studies.

Implanted telemetry electrocardiography involves inserting a radio transmitter connected to two electrodes into the mouse. Signals are received wirelessly by a nearby amplifier and computer system. The technique enables ECGs to be recorded over a prolonged continuum, enabling heart rate variability to be monitored and arrhythmia frequency to be calculated (Knollmann et al., 2003). Implanted telemetry electrocardiography allows researchers to determine whether arrhythmic events were responsible for cause of death. The surgery required for implanted telemetry ECGs poses significant risk of mortality and morbidity to the mouse (Schuler et al., 2009). A recovery period is required following the surgery, making the technique more suited to use in long term electrophysiological studies.

Utility of Electrocardiography in Mouse

Electrocardiography is often described as the "gold standard" technique for the electrophysiological analysis of the heart. It lacks the spatio-temporal resolution afforded to optical mapping but exceeds in its capacity for comprehensive *in vivo* characterisation. Alternative methods, such as echocardiography, which indirectly determines heart rate, provide limited information on the electrophysiology of the cardiac cycle and is unable to discriminate between sinus and ectopic heartbeats. This consequently constrains its use in the evaluation of complex ventricular arrhythmias associated with chronic heart failure. Echocardiography is extensively used in cardiovascular research to characterise the structural cardiac phenotype of genetically modified animal models; however, due to its restricted use in arrhythmia research, it will not be covered in detail in this review. Further information on the role echocardiography has in basic and clinical cardiovascular research can be obtained from Scherrer-Crosbie and Thibault (2008).

Comparing ECGs generated from mice to those derived from humans is not straightforward but is essential when assessing arrhythmogenesis of heart failure models. Bazett's formula, which is commonly used to equate QT intervals measured from contrasting heart rates, fails to account for the differences present in mice sedated by certain anaesthetics (Boukens et al., 2014). The distinct differences in the cardiac electrophysiology of mice and humans are evidenced by both the heart rate and action potential duration (Kaese and Verheule, 2012). Further contrasts are evidenced by morphological changes in complexes of the ECG, such as an ambiguous ST segment and an additional J wave. The J wave arises in the mouse (and other rodents) ECG due to the lack of a plateau phase in the action potential, meaning early repolarisation is visible as a positive deflection shortly after the QRS complex (Offerhaus et al., 2021). It is for this reason also that the mouse ECG has a less pronounced T wave.

As well as morphological changes present in the sinus rhythm of mice and humans, patho-anatomical changes can cause varying responses in the ECG of humans and mice. Acute myocardial ischemia is represented by the elevation of the ST segment in humans, while in mice it is conversely shown as a reduction in S wave amplitude followed by an abnormal J wave and inverted T wave (Janse, 1986; Gehrmann et al., 2001). The potential of the surface ECG in mice is largely restricted by the size of the animal. Although not limited to its use in mice, electrocardiography is still performed comparatively little in larger, more electrophysiologically analogous mammals, such as pigs and dogs. This is mainly due to the cost associated with the animals housing and upkeep and the more stringent ethical restrictions covering their use in research.

Further to surface ECG recording, methods have been developed to directly record electrical activity of the *in vivo* mouse heart at the epicardial surface (*via* an open torso approach) and intracardially (*via* transvenous catheters; Berul et al., 1996; VanderBrink et al., 1999). Such approaches are advantageous over the surface ECG as they enable recording of an ECG to be taken under programmed stimulation elicited to unearth arrhythmia in animal models with altered myocardial structure (Maguire et al., 2000; Saba et al., 2000; Sawaya et al., 2007). However, they are limited by the relatively low spatio-temporal resolution associated with indirect extracellular ECG recordings.

Electrophysiological Study of *ex vivo* Model Systems

Monophasic and Transmembrane Action Potential Recordings

Electrode-based methods allow the recording of action potentials from the isolated heart and other *ex vivo* cardiac preparations. Intracellular microelectrodes can be used to record transmembrane action potentials from a single cell within the intact preparation or indeed from isolated cardiomyocytes (section "Cellular Systems: Primary Cells"). By using one electrode in the intracellular space and another extracellular electrode, the difference between the two signals facilitates the recording of the transmembrane action potential (Holmes et al., 2016).

Larger electrodes (>.1 mm diameter), positioned firmly against cardiac tissue, can be used to record extracellular activity originating from several cells (Kirchhof et al., 1998; Fabritz et al., 2003; Iravanian et al., 2020). These recordings are known as monophasic action potentials (MAPs) and are routinely recorded from Langendorff perfused animal hearts to directly assess cardiac electrophysiology. Freundt et al. (2019) recorded MAPs from rabbits following treatment with the histone deacetylase inhibitor, entinostat, to demonstrate that the drug could prevent heart failure associated early after depolarisations

(EADs) and structural remodelling. The setup required to record these signals consist of a proximal and distal electrode, neither of which crosses the cellular membrane. The exact mechanisms behind the origin of monophasic action potential recordings are not fully understood; however, they are thought to rely on proximal inactivation of one part of the tissue (Franz, 1991; Tse et al., 2016).

Ex vivo Optical Mapping

Overview

Electrode techniques inherently have low spatial resolution due to the physical constraint of electrode placement. Cardiac excitation however involves the coordinated (or uncoordinated in the case of some arrythmias) propagation of action potentials across the tissue. Furthermore, tissue heterogeneities, such as activation or repolarisation dispersion and areas of ectopic activity, are often fundamental mechanisms for arrythmia induction in patients with heart failure. Therefore, higher spatial resolution mapping techniques are required for mechanistic research of cardiac preparations. These include multielectrode array techniques (section "Multi Electrode Arrays") and optical mapping.

Cardiac optical mapping is a method used to investigate the electrical properties of cardiac tissue preparations through the excitation of fluorescent dyes (Zhang et al., 2016; O'Shea et al., 2020). Staining with voltage-sensitive indicators, such as potentiometric Di-4-ANEPPs, enables adjustments in membrane potential to be monitored with greater spatial resolution than electrode-based methods. Calcium-sensitive indicators are utilised to visualise intracellular calcium handling. Furthermore, co-staining with voltage and calcium-sensitive indicators allows concurrent mapping of both calcium transients and action potential propagation (O'Shea et al., 2019b). The information in the following section pertains to the optical imaging of *ex vivo* heart samples, although much of it remains highly relevant to the optical imaging of *in vitro* models, discussed in section "Calcium Imaging in *in vitro* Model Systems."

Optical mapping was first developed to study the membrane potentials of neuronal cells by Salzberg et al. (1973). The extension of its use to cardiac research by Salama and Morad (1976), enabled the electrophysiological characterisation of cell samples which were previously awkward to assay by traditional microelectrode-based methods. The further development of optical mapping techniques enabled the imaging of retrogradely perfused animal hearts and other *ex vivo* preparations (Salama and Choi, 2000).

Optical mapping has become a routinely performed experimental technique used to evaluate arrhythmogenesis in isolated perfused hearts and *ex vivo* cardiac preparations. The basic setup for the optical mapping of an *ex vivo* cardiac tissue preparation consists of three main parts: a sample to image, equipment designed to elicit fluorescent excitation and a detector for the recording of spectral emission. Optical mapping of cardiac tissue samples facilitates the visualisation and recording of action potential propagation and duration. The significantly greater spatial resolution afforded to optical mapping has enabled the visualisation of complex propagation patterns present during cardiac arrhythmia and has helped to identify both the macro- and micromechanisms behind them (Girouard et al., 1996). Optical mapping has proven particularly pertinent in the research of re-entrant arrhythmias enriched in patients with chronic heart failure, such as atrial and ventricular fibrillation, where it has enabled the visualisation of spiral waves in isolated epicardial muscle (Pertsov et al., 1993; Masarone et al., 2017).

Optical mapping has been used to investigate mechanisms behind atrial fibrillation in age-related heart failure with preserved ejection fraction (Mesquita et al., 2020). The group used *ex vivo* preparations derived from aged rats prone to heart failure with preserved ejection fraction to demonstrate slowed conduction velocities and perturbed β-adrenergic response. In contrast to microelectrode-based monitoring, the output of cardiac optical mapping remains broadly unaffected by high-voltage shocks. This allows the electrophysiological response of samples to be determined following the elicitation of electrical shocks designed to mimic defibrillation or induce arrhythmogenesis (Chattipakorn et al., 2001; Fast and Cheek, 2002).

Limitations of Optical Mapping

Optical mapping however has its limitations. Contractile movements from the cardiac sample can distort pixel imaging and create artefacts in the measured signal. Motion suppression can be achieved using uncoupling agents, such as blebbistatin. However, although useful, uncoupling agents can cause significant disruption to the electrophysiology of the cells and can shroud important interactions that occur due to mechano-electrical feedback. Significant prolongation of the action potential and an increase in ventricular fibrillation have been reported following the treatment of rabbit hearts with blebbistatin, demonstrating possible limitations with its use (Brack et al., 2013; Kappadan et al., 2020). Other reports however have suggested that blebbistatin exerts little direct influence on cardiac electrophysiology (Fedorov et al., 2007).

Methods have therefore been developed to image mechanically coupled cardiac preparations. Ratiometric optical mapping involves recording signals using two different excitation or emission wavelengths. In this approach, two signals are recorded which are differentially altered by calcium concentration or voltage, but similarly corrupted by motion. Therefore, the ratio between the signals can be used to mitigate the impact of motion artefacts (Knisley et al., 2000; Bachtel et al., 2011). Sophisticated motion tracking algorithms, developed to reduce noise in mechanically coupled hearts, can be used effectively in conjunction with ratiometric optical mapping to further reduce motion artefacts (Rodriguez and Nygren, 2014; Garrott et al., 2017; Christoph and Luther, 2018). Analysis of optical mapping data requires highly specialised algorithms. This originally restricted use to laboratories that could develop these in-house. Recently however the emergence of open-source, versatile and high-throughput software by several different laboratories has meant that this is no longer a significant limitation (Gloschat et al., 2018; O'Shea et al., 2019a; Tomek et al., 2021).

In vitro Model Systems

Cellular Systems: Primary Cells

In vitro models consisting of excitable, functional primary cardiomyocytes can be derived from enzymatically treated cardiac tissue using Langendorff perfusion, the newly developed Langendorff-free method and the so-called "chunk method", which is commonly used on isolated human heart tissue (Yue et al., 1996; Workman et al., 2001; Louch et al., 2011; Holmes et al., 2021). Cell culture models consisting of primary cardiomyocytes offer an easily manipulated and physiologically relevant model for heart failure and arrhythmia research. The cells used are often derived from the explanted hearts of patients with end-stage heart disease (Zhang et al., 2021). Such models have proven particularly useful in investigating the fundamental cellular mechanisms behind arrhythmia due to physiological ion channel expression within the cells. Pérez-Hernández et al. (2016) were able to demonstrate that increased expression of *PITX2c*, which is commonly seen in the atrial appendages derived from patients with AF, could alter the densities of the slow delayed rectifier potassium channel (I_{Ks}) and L-type calcium channel (I_{CaL}) in human atrial myocytes (Gudbjartsson et al., 2007).

The inaccessibility of healthy human reference tissue and the limited proliferation potential of the cells derived in culture have however impeded the widespread use of primary human cardiac cells in heart failure research (Ikenishi et al., 2012). Primary cardiac preparations derived from small laboratory animals, such as mice and rats, are comparatively abundant and consequently their use in arrhythmia and heart failure research is common. Non-human primary cardiomyocytes were first used to study the effects that inotropic agents had on the membrane potential of single cells (Iijima et al., 1985). Patch clamping, a technique used to record the membrane voltage and ion channel activity in isolated cells or tissue sections, was often utilised in such experiments (section "Patch Clamp"). Advancements in the optical imaging of calcium- and voltage-sensitive dyes (section "Calcium Imaging in *in vitro* Model Systems") expanded the utility of primary non-human cardiomyocyte models in arrhythmia research and enabled, for the first time, the visualisation of spontaneous re-entrant waves in myocyte monolayers (Bub et al., 1998).

The development of 3D engineered heart tissue models from primary neonatal rat cardiomyocytes has allowed greater phenotypic maturation and the generation of a system particularly well suited to cardiotoxicity drug screening (Krause et al., 2018). Significant electrophysiological differences in action potential duration and intracellular calcium handling in human and rodent species however continues to limit the validity of results obtained using animal cardiomyocytes (**Figure 2**).

Cardiovascular research using human and non-human primary cardiomyocytes is hampered by the cells lack of propensity for proliferation. In spite of this, they have been used with great effect in understanding the electrophysiological changes that occur during heart failure. Maltsev et al. (2007) demonstrated that the cardiomyocytes derived from failing human and dog hearts were prone to early after depolarisations due to increased variation in action potential duration. An increase in late sodium current (I_{Na}) activity was identified as a potential cause, with inhibition of the current reducing action potential duration variability and the presence of early after depolarisations.

Cellular Systems: Immortalised Cardiac Cells

Immortalised cardiomyocyte cell lines can be generated from human and non-human cardiac tissue. They can be readily expanded *in vitro*, theoretically circumventing one of the major limitations associated with primary cardiac cells (Davidson et al., 2005). In reality, the proliferative capacity of immortalised cardiomyocytes can limit their use as a viable cardiac model. This is due to the instability of their myofibrils, which are continually undergoing disassembly during cell division (Ahuja et al., 2004; Onódi et al., 2022). Immortalised cardiac cell lines can be generated through the ectopic expression of the oncogene *SV40*, which allows mitotically arrested cells to re-enter the cell cycle and proliferate (Ramkisoensing et al., 2021).

HL-1, a renowned mouse cardiac (atrial) cell line, has been successfully used to model the effects of structural and electrical remodelling in AF development (Wiersma et al., 2017; Zhang et al., 2018). More recently, it has been used to investigate the effect overexpression of microRNAs (mRNAs) have in patients with heart failure with reduced ejection fraction and AF (Garcia-Elias et al., 2021). The group demonstrated that exposure of HL-1 cells to the mRNAs identified in patients with heart failure and AF caused disruption to calcium handling and cell to cell communication.

One major limitation of immortalised cardiac cells is that the uncontrolled expression of oncogenes can cause the generation of a population of cells with desynchronised cell cycles. Over time, this can lead to a heterogenous population of cells with disparate electrophysiological and functional properties. The development of conditionally immortalised cell lines, in which the SV40 oncogene is under the control of an inducible promoter, has partially addressed this limitation and has enabled the generation of models with greater electrophysiological maturity and homogeneity (Liu et al., 2018). The non-cardiac cell line human embryonic kidney 293 is used in cardiac research to explore the effect pathogenic variants have on the activity of specific ion channels. Pathogenic variants of ion channel genes can be transiently expressed in the cells to elucidate cellular mechanisms behind cardiac disease (Prakash et al., 2021). The reader is directed to Odening et al. (2021) for a more detailed description on the role such cells play in cardiac electrophysiology research.

Cellular Systems: Induced Pluripotent Stem Cells

Generation of Cardiomyocytes From Induced Pluripotent Stem Cells

Following the pioneering work by Takahashi and Yamanaka (2006) in identifying transcription factors capable of inducing pluripotency in somatic cells, cellular reprogramming technology has revolutionised disease modelling. The generation of induced pluripotent stem cell (iPSCs) lines from genetically diverse

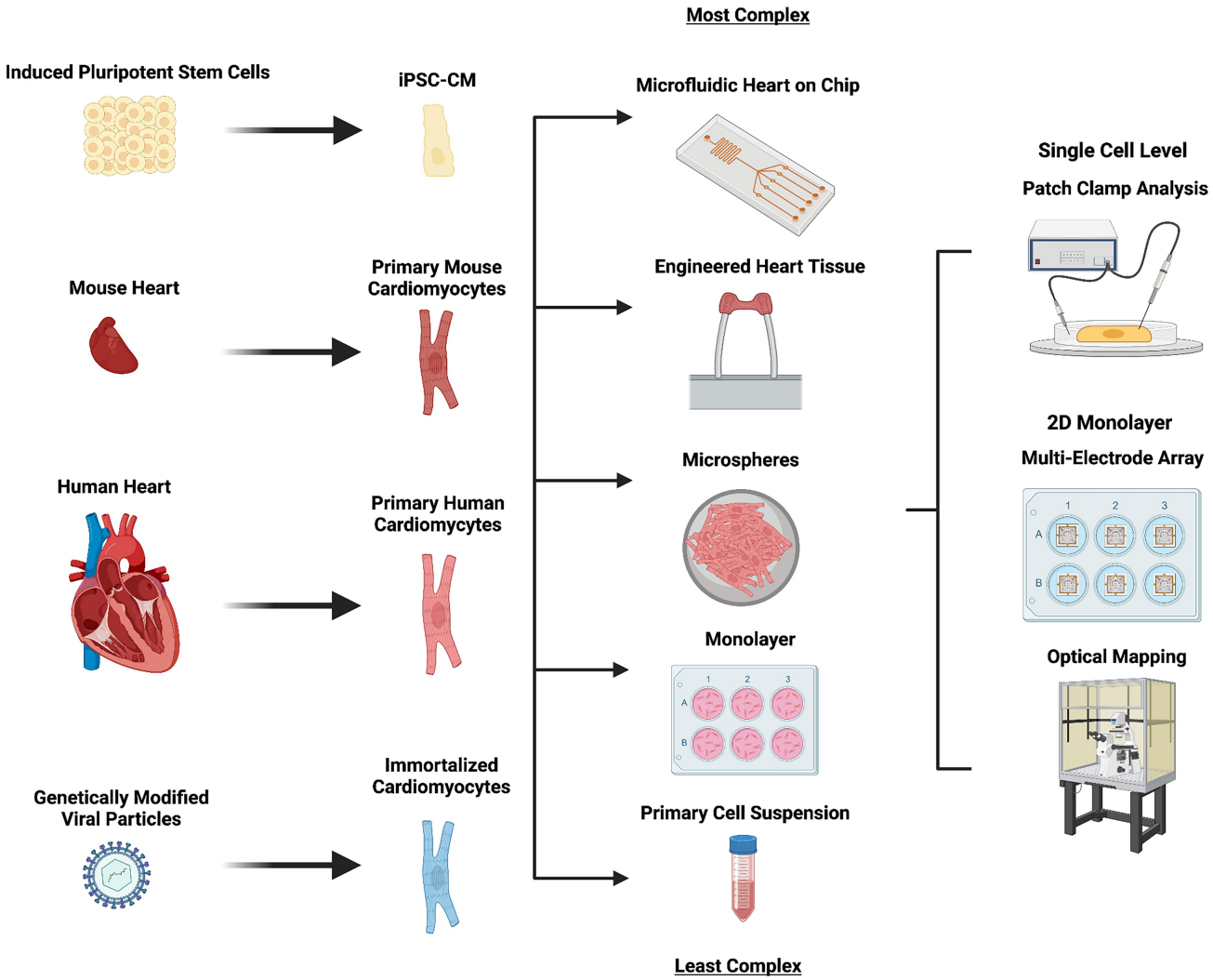

FIGURE 2 | *In vivo* models used in cardiac arrhythmia and heart failure research. An outline of the *in vitro* cell models used in arrhythmia and heart failure research, how they are derived (left), the format in which they can be used (middle right) and the techniques most commonly used in their evaluation (right). Complexity of the model used increases from bottom (primary cell suspension) to top (microfluidic heart on chip). Created with BioRender.com

individuals has enabled researchers to explore the impact common and rare genetic variants have on complex disease.

The relative ease in which genetic engineering can be performed on iPSCs is unparalleled in primary and immortalised cell lines. This can consequently facilitate the "high-throughput" screening of pathogenic variants. Cultures of iPSCs can be differentiated into cardiomyocytes by the manipulation of the Wnt signalling pathway. This allows the generation of a variety of cardiac cell types, including ventricular, atrial and nodal cardiomyocytes (Burridge et al., 2014; Schweizer et al., 2017; Cyganek et al., 2018).

In contrast to primary and immortalised cardiac cells, iPSCs act as both a renewable and reliable source of cells. Free from the ethical restrictions concomitant with embryonic stem cells and capable of being derived from individuals that vary in age, sex, race and disease state, the versatility afforded to iPSCs has led to their routine use in arrhythmia and heart failure research.

Cardiovascular Research Using iPSC-Derived Cardiomyocytes

The adoption of induced pluripotent stem cell models into arrhythmia and heart failure disease modelling has not come without challenges. Inefficient differentiation protocols yielding heterogeneous and often phenotypically immature cardiac cells has hindered the use of iPSCs in the modelling of many complex cardiovascular diseases (Goedel et al., 2017). Despite this, iPSC-derived cardiomyocytes (iPSC-CMs) have been successfully used to model channelopathies including long QT and Brugada syndrome (Savla et al., 2014). The monogenic aetiology of many channelopathies means that phenotypic variation can often be adequately assessed in single-cell assays.

This circumvents the need for vast quantities of homogenous cardiac myocytes.

In contrast to some of the other physiological properties of the iPSC-CM, the activity of many of the key ion currents (inward sodium current, inward calcium current, delayed rectifier current, transient outward current) is broadly similar to human adult cardiomyocytes (Knollmann, 2013). Itzhaki et al. (2011) used multi-electrode arrays and patch clamping (sections "Patch Clamp" and "Multi Electrode Arrays") to analyse iPSC-CMs derived from a patient with congenital long QT syndrome. The patient possessed a missense variant in the potassium voltage-gated ion channel subunit gene *KCNH2*. The cells demonstrated EADs and prolonged action potentials, due to a reduction in rapid delayed rectifier (I_{Kr}) current activity.

Genetic variants identified in patients with cardiomyopathies and/or arrhythmias have been successfully modelled in iPSC-CM to investigate the molecular mechanisms behind their pathogenesis. Mutations within the *TTN* gene, that encodes the sarcomeric protein titin, are strongly linked to the development of familial dilated cardiomyopathy and atrial fibrillation (Herman et al., 2012; Choi et al., 2018). They have been successfully modelled in iPSC-CM to deepen our understanding of the pathogenic impact titin variants have on sarcomere organisation and calcium handling (Schick et al., 2018).

Challenges of iPSC-Derived Cardiomyocytes

The greatest challenge associated with the widespread employment of iPSC models in cardiovascular research remains the phenotypic immaturity of the derived cardiac cells. This is evidenced by the automaticity, reduction of inwardly rectifying potassium current (I_{K1}) density and relatively positive diastolic membrane potential present in many populations of iPSC-CM (Goversen et al., 2018). The problem is further exacerbated when considering the age-related dependency of many cardiovascular diseases and arrhythmogenic syndromes. There is a myriad of methods used to enhance maturation of iPSC-CM. These can range from mechanical and electrical stimulation of the cells to the construction of 3D organoids. Many of these methods are comprehensively described in Machiraju and Greenway (2019).

Current differentiation protocols can generate cells that demonstrate tissue-specific expression of atrial, ventricular and nodal ion channels, transporters and connexins (Schweizer et al., 2017; Cyganek et al., 2018). Current protocols, however, often generate mixed populations of cells and are to our knowledge unable to specify the generation of cells from either the left or right chambers of the heart. This is of particular importance when considering the compartmental origin of the different types of heart failure. The optimisation of cellular differentiation protocols is often limited by the onerous and expensive nature of cellular differentiation and characterisation. The recent incorporation of genetically encoded calcium sensors (section "Genetically Encoded Calcium Indicators") into commonly used iPSC lines has helped ameliorate this by facilitating high-throughput phenotypic screening of iPSC-CM following cellular differentiation (Chen et al., 2017b).

Re-entrant arrhythmias commonly seen in patients with heart failure often present due to structural differences in the 3D anatomy of the heart. This is challenging to model *in vitro* in 2D monolayers. The integration of iPSC-derived cardiac cells in co-culture and three-dimensional culture systems can provide models that demonstrate significantly greater phenotypic maturity and physiological relevance (Lemoine et al., 2017). However, they are still some way off recapitulating the intricacies of the cardiac micro-anatomy and intra-chamber regional variability which are important to both arrhythmia and heart failure development (Holmes et al., 2016). Furthermore, pathophysiological stressors including diabetes, hypertension, hypoxia, ageing, obesity and reduced cardiac blood flow, which act as major drivers for arrhythmogenesis and heart failure, are difficult to recapitulate, even in 3D iPSC-CM cultures (Yildirir et al., 2002; Lau et al., 2013; Chow et al., 2014; Pathak et al., 2015; Morand et al., 2018).

Emerging Strategies to Improve iPSC-Derived Cardiomyocyte Models

In recent years, an amalgamation between iPSC disease modelling and tissue engineering has fathered the generation of three-dimensional iPSC-CM models, such as cardiac microspheres and engineered heart tissue (**Figure 2**; Schaaf et al., 2011; Beauchamp et al., 2015). Such models are capable of demonstrating improved intracellular calcium handling and I_{K1} current densities (Buikema et al., 2013; Amano et al., 2016; Silbernagel et al., 2020). A comprehensive description of three-dimensional *in vitro* cardiac models is beyond the scope of this review, the reader is directed to Salem et al. (2021) for a current report describing such models.

The incorporation of co-culture and three-dimensional culture systems into microfluidic "heart on chip" platforms is an exciting prospect. In-built optical and electrical sensors allow data to be generated on calcium handling and contractility (Cho et al., 2020). Furthermore, microfluidic chips enable greater control over culture conditions, such as pH and substrate stiffness, with future iterations possibly permitting researchers to adjust parameters to consider pathophysiological stressors important in heart failure, including hypoxia and reduced blood flow (Beauchamp et al., 2020).

As is the case with primary and immortalised cell lines, the maintenance cost required for the use of iPSCs in arrhythmia and heart failure research is substantially lower than that of maintaining *in vivo* models, such as mice and zebrafish. Pathological variants of genes that cause embryonic lethality in mouse models can be modelled in iPSC models without the design and generation of complex conditional expression systems (Nishii et al., 2014). Despite this, there is scepticism about the *in vivo* reproducibility of experimental data derived from iPSC models. Presently, validation of such experimental data is often required in small rodent animals. The development of more efficient differentiation protocols and maturation strategies will likely facilitate the generation of iPSC-derived cardiomyocytes that are phenotypically much closer to adult cardiac myocytes. Furthermore, future iterations of co-culture model systems will provide greater accuracy in replicating the cardiac micro-anatomy.

Electrophysiological Study of *in vitro* Model Systems

Patch Clamp

Overview

Patch clamping is the definitive technique used to study ionic currents and membrane potential in tissue samples, isolated cells and expression systems. Patch clamping has and continues to be the gold standard for studying ion channel activity in excitable cells including cardiomyocytes and neurones (Guinamard et al., 2004; Alloui et al., 2006). There are a myriad of patch clamping setups used to monitor the electrophysiology of cells under a variety of controlled conditions. The reader is directed to Kornreich (2007) for an in-depth description of patch clamping setups and their suitability in addressing specific research questions.

Patch clamping can be broadly separated into two types. Voltage clamping involves "clamping" cardiac myocytes at different defined membrane potentials, in order to elicit specific currents of interest which can then be recorded. This often takes place in the presence of numerous pharmacological agents which block other ion channels allowing for the isolation of a single current. Conversely, in the current clamp setup, the researcher controls the current being injected into the cell and records the membrane potential. This is usually in the form of an action potential. Both setups are routinely used in heart failure and arrhythmia research to understand the impact genetic variants, drug treatment and hypoxia have on ionic current, action potential morphology and resting membrane potential (Chavali et al., 2019; Plant et al., 2020).

Patch Clamping in Arrhythmia and Heart Failure Research

Patch clamping is used in heart failure research to investigate cardiac electrical remodelling in a variety of *in vitro* model systems including primary, immortalised and iPSC-derived cardiomyocytes. Hallmarks of arrhythmia in heart failure, which can be detected in *in vitro* cardiac cell models using patch clamping, include but are not limited to depolarised resting membrane potentials (largely due to a reduction in I_{K1}), delayed after depolarisations (due to spontaneous Ca^{2+} leak from the SR and activation of the depolarising sodium-calcium exchanger), early after depolarisations (subsequent to reactivation of I_{CaL} and possibly I_{Na}), prolongation of the action potential duration [primarily dependent on a decrease in major repolarising currents including I_{to}, I_{Ks} and I_{Kr}, but also due to enhanced late sodium current (I_{NaL})], ectopic automaticity, sinus node dysfunction and calcium handling disruption, recently reviewed in full by Husti et al. (2021). That said, ion channel remodelling in heart failure can display significant variation between individuals likely dependent on the different underlying origins and types of heart failure and the extent of disease progression. Shemer et al. (2021) used patch clamping techniques to interrogate the electrophysiology of iPSC-CM derived from two patients with *LMNA*-related dilated cardiomyopathy. Patients with *LMNA*-related dilated cardiomyopathy are at risk of severe heart failure and sudden cardiac death (Pasotti et al., 2008). The group identified delayed and early after depolarisations, as well as prolonged action potential durations in the iPSC-CM. This consequently increased our understanding of the mechanisms causing severe ventricular arrhythmias in patients with *LMNA*-related dilated cardiomyopathy.

Patch clamping is a technique that offers researchers unparalleled interrogation of the intracellular electrophysiology of cardiac cell models. However, patch clamping is relatively low throughput, with recordings being obtained from a single cell for a short period of time. The technique is highly skilled and consequently requires extensive time to master. Finally, there is still considerable subjectivity involved in choosing which cell to record from. This is exacerbated when patching iPSC-CM which are often heterogeneous, varying in shape, size and electrophysiological phenotype. Many of these limitations are being overcome using easy-to-handle automated patch clamp systems, which can improve throughput and standardisation and are comprehensively described in Suk et al. (2019), Obergrussberger et al. (2021), and Bell and Fermini (2021).

Multi-Electrode Arrays

Overview

Multi-electrode arrays (MEAs) are a non-invasive methodology used to assess the regional electrophysiology activity/heterogeneity in multicellular preparations. They have been used to measure electrical propagation in primary cardiac tissue, cultured monolayers of neonatal cardiac myocytes, immortalised cardiac cell lines and iPSC-derived cardiomyocytes (Wells et al., 2019). Cells are cultured on a surface embedded with dot-like electrodes to monitor regional extracellular field potentials at different points across the preparation, over a prolonged period (Spira and Hai, 2013). Changes in extracellular voltage occur due to the propagation of a spontaneous or stimulated action potential through the cell monolayer. The recorded field potential can be subsequently used to directly measure or estimate key electrical parameters including activation patterns, conduction velocity, spontaneous beating frequency, field/action potential duration and field/action potential amplitude (Halbach et al., 2003; Wells et al., 2019). Further information on the fundamentals behind MEA technology and the practicalities behind its use with cardiac cell types is beyond the scope of this review but can be obtained from Clements (2016) and Kussauer et al. (2019).

MEAs in Arrhythmia and Heart Failure Research

The adoption of MEAs into cardiac electrophysiology research has occurred relatively recently, with systems previously being designed for use in assessing the electrical activity of neural networks (Erickson et al., 2008). MEAs are broadly used on *in vitro* cell models to provide an overall assessment on the electrophysiological state of cardiomyocytes, in a way not dissimilar to the use of ECGs in *in vivo* models. MEAs have been used to ascertain the effectiveness of anti-arrhythmic therapies. For example, a study by Kim et al. (2022) used MEAs to evaluate the potential use of cardiac radioablation

in the treatment of refractory ventricular arrhythmias, commonly seen in patients with heart failure (Peichl et al., 2021). The group monitored the electrical activity of iPSC-CM following irradiation, to further understand the electrophysiological response of the cells to the treatment. Despite this, MEAs are currently most often employed in assessing cardiotoxicity of pharmacological therapeutics. The effect the drug has on the field potential can be translated onto the action potential and subsequently used to predict *in vivo* cardiotoxicity (Braam et al., 2010; Colatsky et al., 2016; Tertoolen et al., 2018). Further information on the role MEAs play in *in vitro* drug research is beyond the scope of this review but can be obtained from Andrysiak et al. (2021). The main advantages of MEAs are that they are high-throughput and allow experimentation over prolonged periods, unlike patch clamping based methodologies. However, they are unsuitable for assessing the electrophysiology of single cells and lack the signal complexity afforded to intracellular interrogation. An exciting prospect for the future is the amalgamation of MEA technology into microfluidic heart on chip models. This may allow the electrophysiological response of cardiac cells to be monitored under pathological conditions associated with heart failure, such as hypoxia and hypokalaemia (Liu et al., 2020).

Calcium Imaging in *in vitro* Model Systems

Calcium (Ca^{2+}) flux is the principal determinant of contraction in cardiac myocytes (Bers, 2002). Intracellular calcium handling underlies excitation–contraction coupling and is commonly perturbed in patients with cardiac arrhythmia and end-stage heart failure (Gwathmey et al., 1987; Ter Keurs and Boyden, 2007). Detailed information regarding the role intracellular calcium handling plays in cardiac arrhythmia and heart failure is beyond the scope of this review but is excellently summarised by Landstrom et al. (2017). Disruption to calcium handling can be caused by a number of mechanisms. Genetic variants of key ion channels, such as Ryanodine receptor 2, are one such example and can predispose individuals to arrhythmogenic syndromes and heart failure (Swan et al., 1999; Dridi et al., 2020).

The most dynamic and recognisable process in intracellular calcium handling is the release and subsequent re-sequestration of Ca^{2+} by the sarcoplasmic reticulum. This is known as a whole-cell calcium transient and commonly occurs prior to the contraction of a cardiac myocyte. It can be measured in primary, immortalised and iPSC-derived cardiac cell models. The spatial analysis of calcium transient kinetics has been used to explore mechanisms behind pathogenic variant driven arrhythmias and chronic heart failure in *in vitro* cell models. Lehnart et al. (2006) demonstrated diastolic Ca^{2+} leak from the sarcoplasmic reticulum of cardiomyocytes derived from mice deficient in calstabin-2, a protein key to ryanodine receptor 2 stabilisation, while Yin et al. (2014) used calcium imaging to elucidate the effect arrhythmogenic calmodulin variants had on intracellular calcium handling. It is worth noting that calcium imaging is a skilled technique, where careful consideration of the appropriate indicator is required.

Calcium Dyes and Indicators

Chemical Calcium Indicators. A range of light emitting dyes have been used to image Ca^{2+} in *in vitro* cardiac models. The dyes can be broadly categorised as being ratiometric or non-ratiometric. Ratiometric dyes display a shift in excitation or emission spectra following the binding of Ca^{2+}. The ratio between the spectra allows the calculation of the absolute concentration of Ca^{2+} which is pertinent when measuring the amplitude of Ca^{2+} transients (Van Meer et al., 2016). An increase in fluorescence from non-ratiometric dyes corresponds to an increase in the relative concentration of cytosolic Ca^{2+}. As no spectral shift is observed when a non-ratiometric dye is bound to Ca^{2+}, variability in dye loading and cell permeability can cause a greater susceptibility to inter-assay variation. While ratiometric dyes are advantageous in capturing contractile behaviour for arrhythmia research, many imaging setups do not support their use (Jaimes et al., 2016).

Tetracarboxylate-based probes, synthesised by Tsien (1983), acted as blueprints for the fabrication of contemporarily used ratiometric and non-ratiometric calcium probes. Cyclically fluorescent and capable of traversing the sarcolemma, the dyes enabled the prolonged imaging of intracellular Ca^{2+} in cells derived from myocardial tissue without the inconvenience of cellular microinjection. Further iterations of the dyes led to the development of the 1,2-bis(2-aminophenoxy)ethane-*N,N,N′,N′*-tetraacetic acid (BAPTA) based probes fura-1 and fura-2. The BAPTA based dyes resolved limitations associated with previous tetracarboxylate-based probes, including narrow excitation/emission spectra and autofluorescence. Furthermore, they provided additional benefits including improved Ca^{2+} selectivity and the use of ratiometry (Grynkiewicz et al., 1985).

The synthesis of fluorescent indicators based on the chromophores rhodamine and fluorescein by Minta et al. (1989) facilitated the imaging of cytosolic Ca^{2+} transients at greater resolutions. Probes derived from these chromophores, such as rhod 1 and fluo 1, are non-ratiometric and display a lower affinity for Ca^{2+}. This consequently confers improved dynamic range and increased sensitivity during calcium imaging. Properties, such as these, make the dyes particularly suitable for the imaging of ephemeral Ca^{2+} flux and intracellular diastolic calcium removal (Lock et al., 2015). Although still widely used, phototoxicity has limited the use of chemical calcium indicators in exploring intracellular calcium handling of *in vitro* models under prolonged investigation (Shinnawi et al., 2015).

Genetically Encoded Calcium Indicators. Genomic engineering has provided novel and innovative tools for the intracellular imaging of calcium ions. The use of ratiometric dyes, such as fura-2, can impair the contractility of cardiomyocytes through unwanted Ca^{2+} chelation and can produce uneven and erroneous dye loading (Robinson et al., 2018). Genetically encoded Ca^{2+} indicators (GECI) offer numerous advantages over small molecule dyes including cell type-specific calcium imaging, homogenous indicator expression and reduced levels of unintentional compartmentalisation (Bassett and Monteith, 2017).

The recombinant gene for the sensor, which is usually a derivative of green fluorescent protein, can be cloned into commonly used laboratory animals or expressed within *in vitro* cell lines following transfection or viral transduction. The precise mechanisms behind the delivery and design of genetically encoded calcium indicators are beyond the scope of this review. Further information can be obtained from Kaestner et al. (2014). Genetically encoded Ca^{2+} sensors are emerging as a promising tool for high-throughput anti-arrhythmic drug development (Wu et al., 2019). However, their use is currently limited by narrow spectral bands and putative disruption of endogenous signalling cascades.

Intracellular calcium imaging using small molecule and genetically encoded indicators have proven insightful in exploring the effects pathogenic variants have on excitation–contraction coupling, arrhythmia and heart failure. When used in conjunction with the optical imaging of voltage-sensitive dyes, it enables a comprehensive assessment of the electrophysiological state of *in vitro* cell models. This is evidenced in Pierre et al. (2021), where both optical action potentials and calcium transients were recorded to assess the impact of a $Na_V1.5$ knock-out in iPSC-CM monolayers.

Calcium Spark Analysis

Calcium sparks are small areas of localised fluorescence caused by the ephemeral release of Ca^{2+} from the ryanodine receptors of the sarcoplasmic reticulum (Cheng et al., 1993). In contrast to the calcium transient, the calcium spark is a sudden and unsustained release of Ca^{2+} which cannot independently trigger the contraction of the cell. Calcium sparks are the building blocks of the calcium transient and excitation–contraction coupling (Cheng et al., 1996). Highly sensitive calcium indicators that confer a high signal to noise ratio, such as the non-ratiometric dyes fluo-3 and fluo-4, are used to image calcium sparks.

Increases in angiotensin II activity are commonly observed during the development of AF (Goette et al., 2000). The analysis of calcium sparks in atrial cardiomyocytes by Gassanov et al. (2006) helped demonstrate the pro-arrhythmic effects of angiotensin II. Primary atrial cardiomyocytes that were incubated in angiotensin II demonstrated increased frequencies of spontaneous calcium spark production. Such an increase is linked to abnormal cell membrane depolarisation and is thought to contribute to the re-initiation of AF.

Compartment-Specific Calcium Imaging

The compartmentalisation of Ca^{2+} sensitive indicators in intracellular organelles was reported as a common problem during early attempts at calcium imaging (Malgaroli et al., 1987). Recently however, indicators have been used specifically to image the flux of Ca^{2+} in organelles including the mitochondria, endoplasmic reticulum and nucleus. Mitochondrial calcium signalling causes the formation of a dynamic buffer which helps control the concentration of cytosolic Ca^{2+} and it is essential for the generation of the ATP required for cardiac contraction (Dedkova and Blatter, 2013; Boyman et al., 2014). Dysfunction of mitochondrial calcium handling can cause oxidative stress and is strongly associated with the development of chronic heart failure and AF (Luo and Anderson, 2013; Xie et al., 2015; Wiersma et al., 2019). Mitochondrial calcium imaging was used effectively by Santulli et al. (2015) to assess the importance of mitochondrial calcium overload in murine post-myocardial infarction heart failure. Cardiomyocytes derived from the mice demonstrated significant increases in cardiac mitochondrial Ca^{2+} and reactive oxygen species levels following myocardial infarction.

Genetically encoded calcium indicators have been particularly useful for calcium imaging in specific organelles, such as the endoplasmic reticulum, Golgi apparatus and mitochondria (Suzuki et al., 2016).

Computational Cardiac Modelling and Simulations

Fundamentals of Computational Cardiac Modelling and Simulation

Computational (*in silico*) cardiac modelling and simulation is a widely used technique to investigate the biophysical processes underlying cardiac pathophysiology, arrhythmias and heart failure at a multiscale level. They provide unique mechanistic insights at high spatio-temporal resolution, to augment experimental and clinical investigations. Detailed experimental characterisation of cardiac electrophysiology mechanisms by techniques, such as voltage clamping, has enabled the generation of mathematical models capable of describing action potential, excitation–contraction coupling and underlying ionic currents of human atrial, ventricular, Purkinje and iPSC-CMs (Courtemanche et al., 1998; Tomek et al., 2019a; Paci et al., 2020; Trovato et al., 2020; freely available https://www.cs.ox.ac.uk/insilicocardiotox/model-repository). Models, such as these, are based upon the pioneering work performed by Hodgkin and Huxley (1952) and Noble (1960) for the neuronal and cardiac action potential, respectively. The models consist of a set of equations characterising the dynamics of transmembrane and sarcoplasmic reticulum ion channels, pumps and transporters.

Ventricular and Atrial Cardiac Computational Models

The ToR-ORd model (Tomek et al., 2019a) is the most recent human ventricular cardiomyocyte model and was derived from the O'Hara-Rudy (ORd) model (O'Hara et al., 2011). The ToR-ORd model includes formulations of key current dynamics and can express repolarisation abnormalities promoting the arrhythmic substrate. The models' parameters can be varied to represent intersubject variability and disease conditions promoting arrhythmogenesis (Dutta et al., 2017; Passini et al., 2017; Zile and Trayanova, 2017; Muszkiewicz et al., 2018). Specifically, simulation studies using human ventricular single-cell models have provided novel insights into the mechanisms behind heart failure associated arrhythmogenicity (Gomez et al., 2014; Mora et al., 2021; Szlovák et al., 2021). Models have also been developed to study the effect of heart failure-associated

changes in sub-cellular structures including t-tubules (Hrabcová et al., 2013; Poláková and Sobie, 2013).

Cardiac computational simulations of atrial electrophysiology are commonly performed using models derived from Nygren et al. (1998), Courtemanche et al. (1998) and Grandi et al. (2011). Such models have been used extensively to study the underlying mechanisms behind the most common sustained type of arrhythmia, AF (Grandi et al., 2019). Genetic variation in the two-pore domain acid-sensitive potassium channel TASK-1 (I_{TASK}) has been linked to an increased susceptibility of AF and has been shown to cause prolongation of the action potential duration in animal models (Petric et al., 2012; Liang et al., 2014). Schmidt et al. (2015) used a version of the Grandi model to demonstrate that upregulation of I_{TASK} facilitated the pro-arrhythmic shortening of action potential duration *in silico* and that pharmacological inhibition of the channel represented a viable anti-arrhythmic strategy. Tools incorporating single-cell models of different cell types have been developed to predict pro-arrhythmic cardiotoxicity and inform clinical risk stratification of different drugs, specifically anti-arrhythmic drugs (Passini et al., 2017; Sutanto et al., 2019).

Applications of Cardiac Computational Modelling and Simulation

Cardiac computational models can be used to comprehensively investigate the mechanisms behind genetic variant associated arrhythmogenicity. Robust models of atrial, ventricular and sinoatrial nodal cellular electrophysiology can be used in conjunction to help researchers reveal the effect that pathogenic variants confer in multiple cardiac cell types. Gain of function variants in the voltage-gated potassium channel gene *KCNQ1* are associated with the development of complex phenotypes including AF and QT prolongation (Hasegawa et al., 2014). Paradoxically, pathogenic variants in *KCNQ1* have also been identified in patients with short QT syndrome 2 (Wu et al., 2015). Zhou et al. (2019) conducted experimentally informed *in silico* simulations using a selection of human atrial, ventricular and sinus nodal models to identify the pathological mechanism behind a gain of function variant of *KCNQ1*. The simulations implicated the elongation of the ventricular action potential duration as a possible cause of conduction delays and QT prolongation.

Integrating biophysical cellular models into anatomical whole-organ and electrical propagation models enables multiscale simulations of cardiac electrophysiology from ionic current to the ECG (Sánchez et al., 2018; Martinez-Navarro et al., 2019; Mincholé et al., 2019). Incorporating experimental mechanistic insights and data on the mechanics of tension development in human cardiomyocytes allows for the construction of human-based electromechanical models capable of representing abnormalities in the ECG and mechanical function caused by disease conditions, such as myocardial infarction (Land et al., 2017; Margara et al., 2021; Wang et al., 2021). They have also been used to investigate mechanical function in a biventricular model under heart failure conditions (Park et al., 2018). Furthermore, three-dimensional *in silico* modelling and simulation has been employed to study arrhythmogenicity of cell therapy using stem cell-derived cardiomyocytes, exploring the effects of graft size, location, anisotropy and ectopic beat propagation (Yu et al., 2019, 2021). Organ level computational studies have furthermore been conducted on the atria, with a specific focus on mechanisms and treatment of AF (Aslanidi et al., 2011; Zhao et al., 2017; Roney et al., 2018). A study by Dux-Santoy et al. (2011) highlighted the relevance of including the cardiac conduction system in whole heart simulations, the absence of which presents a considerable limitation in some three-dimensional studies.

Machine Learning

The use of artificial intelligence (AI) and machine learning (ML) presents an exciting opportunity to increase the predictive power of computational models in clinical and experimental arrhythmia research. Definitions of key concepts including deep learning, ML and artificial neural networks as well as examples by which the implementation of AI could change clinical research in cardiac electrophysiology and disease can be drawn from Feeny et al. (2020). In recent years, the generation of clinical data, including cardiac images, ECGs and DNA sequencing status, has occurred at an unprecedented rate. AI methods enable large quantities of complex data to be filtered and analysed to identify causal links that may not be immediately evident.

Supervised machine learning (SML) has been the most widely used form of AI applied to arrhythmia and heart failure research. SML techniques have been employed to categorise iPSC-CM from patients with catecholaminergic polymorphic ventricular tachycardia, long QT syndrome and hypertrophic cardiomyopathy (Juhola et al., 2018). Another study has employed machine learning techniques to classify different phenotypes of hypertrophic cardiomyopathy, the mechanisms behind their heterogeneities and differences in arrhythmic risks (Lyon et al., 2019). These studies highlight the exciting development in applying ML techniques to experimental data and could facilitate significant change in the ways we currently evaluate genetic variants and the increased risk they confer on arrhythmogenesis.

Impact and Benefit of Computational Cardiac Modelling and Simulations in Arrhythmia and Heart Failure Research

In summary, computational modelling and simulation has improved our current understanding of cardiac electrophysiology, the development of arrhythmia and the mechanisms underlying heart failure. Experimental and clinical studies are time-consuming, require biological resources and overall can be extremely costly. *In silico* simulation studies provide a cost-effective and complementary technique, which can reduce the amount of necessary *in vitro* and animal models used in the interrogation of cardiac mechanisms. Computational modelling and simulation studies can also precede and drive large scale experimental or clinical studies by predicting a drug's optimal dose or identifying groups at risk of adverse treatment effects.

In silico models and simulations are scalable, detailed and biophysically accurate and can give insights into arrhythmia mechanisms which would be otherwise imperceptible to

researchers using experimental data solely. Since computational studies are informed by and based on real data to ensure their clinical relevance, they can sometimes be restricted by the availability of suitable data. Furthermore, computational power is limited, implying that researchers must balance the complexity of their model against its performance. Parallel computing and advances in computer architecture have made advances in addressing these issues (Sachetto Oliveira et al., 2018).

DISCUSSION

The Benefit of Combining Research Modalities

The relationship between heart failure and arrhythmias is complex and often manifests through diverse aetiologies. Hence, there is benefit in a varied approach to study them, combining the use of *in vitro*, *in vivo* and *in silico* models and using a wide array of experimental techniques. This will overcome the limitations present when using only a single model or a limited toolbox of techniques. However, it requires pulling expertise from various areas and the collaboration of specialists in a "Team Science" approach. The benefits of this approach are outlined in **Figure 3**. Similarly, Odening et al. (2021) advocate "strategies that combine different methodological approaches" in cardiac electrophysiology research.

In vivo and *in vitro* models have been used in conjunction to generate complementary data sets. This is evidenced in Gesmundo et al. (2017), where the group used a number of the models and techniques discussed above to investigate the beneficial effect growth hormone-releasing hormone had on cardiac hypertrophy and heart failure. Elicitation of the drug in immortalised H9c2 cardiac cells (section "Cellular Systems: Immortalised Cardiac Cells"), adult rat ventricular cardiac myocytes (section "Cellular Systems: Primary Cells") and iPSC-CM (section "Cellular Systems: Induced Pluripotent Stem Cells") counteracted phenylephrine-induced hypertrophy and reduced expression of hypertrophic genes, such as *Epac1* (Ulucan et al., 2007). *In vivo*,

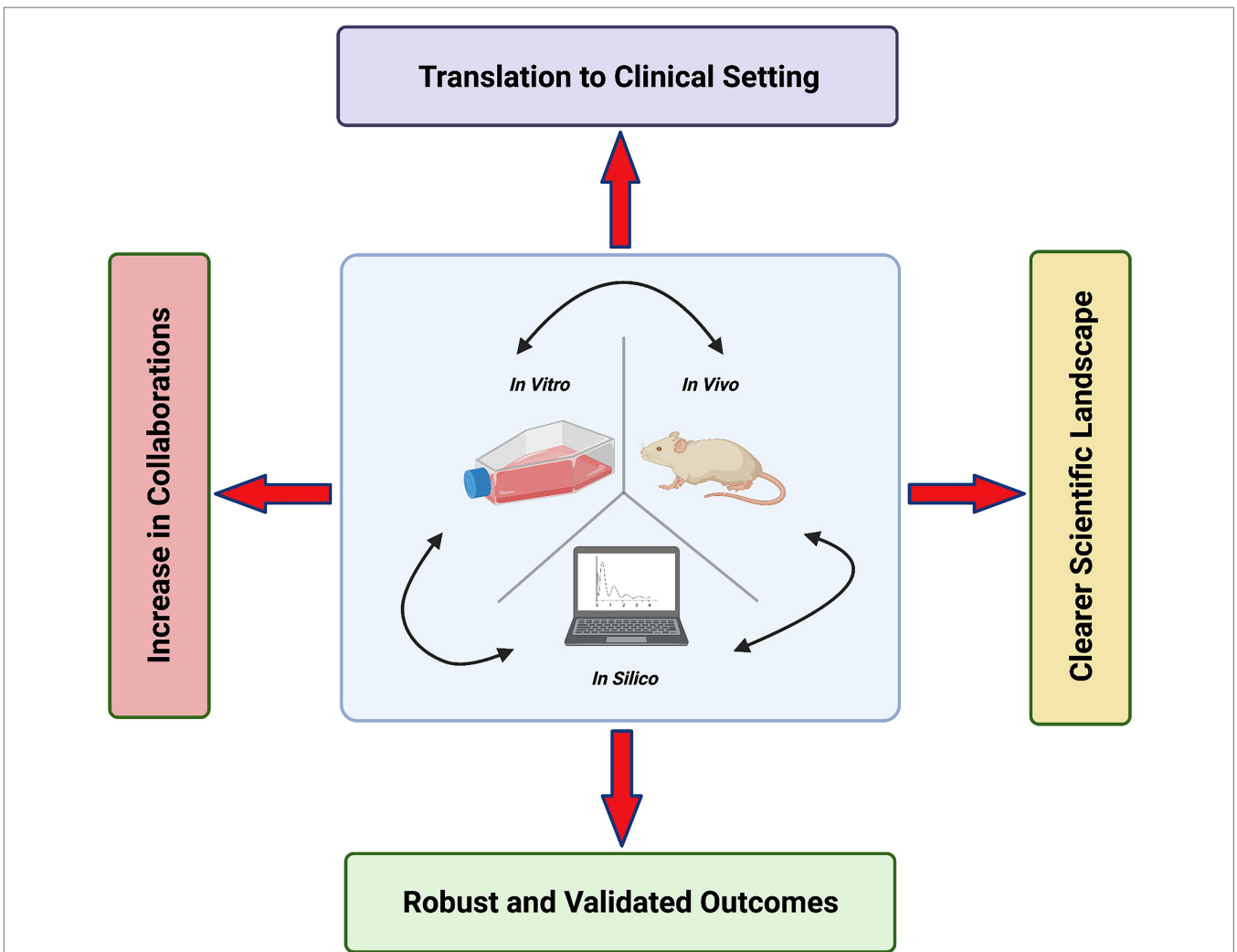

FIGURE 3 | The benefits of a "Team Science" approach in cardiac arrhythmia and heart failure research. Created with Biorender.com.

an agonist of the hormone provided complementary results and was able to improve cardiac function and alleviate cardiac hypertrophy in mice with transverse aortic constriction.

The synergistic use of computational modelling and wet-lab experiments is an emerging area with potential to achieve robust, mechanistic and interpretable results. It is exemplified by the combined use of *in vivo* and *in silico* models in Tomek et al. (2019b) where optical mapping data was derived from Langendorff perfused post-myocardial infarction (MI) rat hearts (section "*Ex vivo* Cardiac Preparations"). An increased liability to alternans formation was observed at the border zone when paced at longer cycle lengths. β-Adrenergic receptor stimulation with norepinephrine reduced alternans formation by approximately 60% when elicited in the infarct border zone of retrogradely perfused rat hearts. Results were subsequently reproduced in computer models of the border zone informed on intracellular calcium handling and ion channels. The results obtained in the study, using both *ex vivo* and *in silico* models, supported clinical imaging studies which predict border zone denervation as being pro-arrhythmic (Malhotra et al., 2015). While previous data obtained from animal models have conversely demonstrated sympathetic reinnervation of the border zone post-myocardial infarction as being pro-arrhythmic (Shen and Zipes, 2014). Understanding the effect β-adrenergic receptor stimulation has on the border zone of healed myocardial infarctions (MI) is clinically important, as it can inform treatment. It is routine for patients to be prescribed beta blockers post-MI and for chronic heart failure, as they reduce heart rate and blood pressure and thus decrease myocardial workload (Lange et al., 1983). These examples highlight the relevance of combining different experimental and computational techniques to validate findings and ensure the robustness of predictions for a clinical setting.

Conclusion

This review has outlined state-of-the-art experimental and computational methods and their relative strengths and weaknesses. The authors conclude that there is not one ideal model or methodology for all studies. Instead, research into arrhythmia and heart failure requires a careful consideration of its goals, resources and scope. Previous studies have shown that a combination of experimental and computational models can provide robust and validated outcomes in a variety of research settings. Such an approach will help to gain detailed mechanistic insights, which are a prerequisite for developing targeted therapies to prevent or at least ameliorate arrhythmias in heart failure patients.

AUTHOR CONTRIBUTIONS

All authors listed have made a substantial, direct, and intellectual contribution to the work, and approved it for publication.

FUNDING

This work was funded by the National Centre for the Replacement, Refinement and Reduction of Animals in Research (NC3Rs; NC/T001747/1 to KG and MC). Work in KG's laboratory is funded by the British Heart Foundation (BHF) (PG/19/45/34419 and FS/12/40/29712); the Medical Research Council (MR/V009540/1); and the Wellcome Trust (201543/B/16/Z and 204846/Z/16/Z to UoB). LR is funded by a BBSRC PhD scholarship in collaboration with AstraZeneca (BB/V509395/1). BR is funded by a Wellcome Trust Senior Research Fellowship in Basic Biomedical Sciences (214290/Z/18/Z) and an NC3Rs Infrastructure for Impart Award (NC/P001076/1). AH is funded by the BHF Project grant (PG/17/30/32961) and a BHF Studentship (FS/PhD/20/29093). The Institute of Cardiovascular Sciences, University of Birmingham, has received an Accelerator Award by the British Heart Foundation (AA/18/2/34218). CO'S is funded by a Wellcome Trust (Sir Henry Wellcome Fellowship 221650/Z/20/Z). AR is funded by a BHF Accelerator (AA/18/2/34218). CD is funded by the British Heart Foundation (CRMR/21/290009, PG/21/10545) and the National Centre for the Replacement, Refinement, and Reduction of Animals in Research (35911–259146, NC/K000225/1, NC/S001808/1).

REFERENCES

Adderley, N. J., Ryan, R., Nirantharakumar, K., and Marshall, T. (2019). Prevalence and treatment of atrial fibrillation in UK general practice from 2000 to 2016. *Heart* 105, 27–33. doi: 10.1136/heartjnl-2018-312977

Aguirre, L. A., Alonso, M. E., Badía-Careaga, C., Rollán, I., Arias, C., Fernández-Miñán, A., et al. (2015). Long-range regulatory interactions at the 4q25 atrial fibrillation risk locus involve PITX2c and ENPEP. *BMC Biol.* 13:26. doi: 10.1186/s12915-015-0138-0

Ahuja, P., Perriard, E., Perriard, J. C., and Ehler, E. (2004). Sequential myofibrillar breakdown accompanies mitotic division of mammalian cardiomyocytes. *J. Cell Sci.* 117, 3295–3306. doi: 10.1242/jcs.01159

Alloui, A., Zimmermann, K., Mamet, J., Duprat, F., Noel, J., Chemin, J., et al. (2006). TREK-1, a K^+ channel involved in polymodal pain perception. *EMBO J.* 25, 2368–2376. doi: 10.1038/sj.emboj.7601116

Amano, Y., Nishiguchi, A., Matsusaki, M., Iseoka, H., Miyagawa, S., Sawa, Y., et al. (2016). Development of vascularised iPSC derived 3D-cardiomyocyte tissues by filtration layer-by-layer technique and their application for pharmaceutical assays. *Acta Biomater.* 33, 110–121. doi: 10.1016/j.actbio.2016.01.033

Andrysiak, K., Stępniewski, J., and Dulak, J. (2021). Human-induced pluripotent stem cell-derived cardiomyocytes, 3D cardiac structures, and heart-on-a-chip as tools for drug research. *Pflug. Arch. Eur. J. Phy.* 473, 1061–1085. doi: 10.1007/s00424-021-02536-z

Appel, M. L., Berger, R. D., Saul, J. P., Smith, J. M., and Cohen, R. J. (1989). Beat to beat variability in cardiovascular variables: noise or music? *J. Am. Coll. Cardiol.* 14, 1139–1148. doi: 10.1016/0735-1097(89)90408-7

Aschar-Sobbi, R., Izaddoustdar, F., Korogyi, A. S., Wang, Q., Farman, G. P., Yang, F., et al. (2015). Increased atrial arrhythmia susceptibility induced by intense endurance exercise in mice requires TNFα. *Nat. Commun.* 6:6018. doi: 10.1038/ncomms7018

Aslanidi, O. V., Colman, M. A., Stott, J., Dobrzynski, H., Boyett, M. R., Holden, A. V., et al. (2011). 3D virtual human atria: a computational platform for studying clinical atrial fibrillation. *Prog. Biophys. Mol. Biol.* 107, 156–168. doi: 10.1016/j.pbiomolbio.2011.06.011

Bachtel, A. D., Gray, R. A., Stohlman, J. M., Bourgeois, E. B., Pollard, A. E., and Rogers, J. M. (2011). A novel approach to dual excitation ratiometric optical mapping of cardiac action potentials with di-4-ANEPPS using pulsed LED excitation. *IEEE Trans. Biomed. Eng.* 58, 2120–2126. doi: 10.1109/TBME.2011.2148719

Barold, S. S. (2003). Willem Einthoven and the birth of clinical electrocardiography a hundred years ago. *Card. Electrophysiol. Rev.* 7, 99–104. doi: 10.1023/A:1023667812925

Bassett, J. J., and Monteith, G. R. (2017). Genetically encoded calcium indicators as probes to assess the role of calcium channels in disease and for high-throughput drug discovery. *Adv. Pharmacol.* 79, 141–171. doi: 10.1016/bs.apha.2017.01.001

Beauchamp, P., Jackson, C. B., Ozhathil, L. C., Agarkova, I., Galindo, C. L., Sawyer, D. B., et al. (2020). 3D co-culture of hiPSC-derived cardiomyocytes with cardiac fibroblasts improves tissue-like features of cardiac spheroids. *Front. Mol. Biosci.* 7:14. doi: 10.3389/fmolb.2020.00014

Beauchamp, P., Moritz, W., Kelm, J. M., Ullrich, N. D., Agarkova, I., Anson, B. D., et al. (2015). Development and characterization of a scaffold-free 3D spheroid model of induced pluripotent stem cell-derived human cardiomyocytes. *Tissue Eng. Part C Methods* 21, 852–861. doi: 10.1089/ten.tec.2014.0376

Bell, D. C., and Fermini, B. (2021). Use of automated patch clamp in cardiac safety assessment: past, present and future perspectives. *J. Pharmacol. Toxicol. Methods* 110:107072. doi: 10.1016/j.vascn.2021.107072

Bell, R. M., Mocanu, M. M., and Yellon, D. M. (2011). Retrograde heart perfusion: the Langendorff technique of isolated heart perfusion. *J. Mol. Cell. Cardiol.* 50, 940–950. doi: 10.1016/j.yjmcc.2011.02.018

Bers, D. M. (2002). Cardiac excitation–contraction coupling. *Nature* 415, 198–205. doi: 10.1038/415198a

Berul, C. I., Aronovitz, M. J., Wang, P. J., and Mendelsohn, M. E. (1996). In vivo cardiac electrophysiology studies in the mouse. *Circulation* 94, 2641–2648. doi: 10.1161/01.CIR.94.10.2641

Björling, K., Morita, H., Olsen, M. F., Prodan, A., Hansen, P. B., Lory, P., et al. (2013). Myogenic tone is impaired at low arterial pressure in mice deficient in the low-voltage-activated CaV3.1 T-type $Ca^{(2+)}$ channel. *Acta Physiol.* 207, 709–720. doi: 10.1111/apha.12066

Blechschmidt, S., Haufe, V., Benndorf, K., and Zimmer, T. (2008). Voltage-gated Na^{+} channel transcript patterns in the mammalian heart are species-dependent. *Prog. Biophys. Mol. Biol.* 98, 309–318. doi: 10.1016/j.pbiomolbio.2009.01.009

Bosch, L., de Haan, J. J., Bastemeijer, M., van der Burg, J., van der Worp, E., Wesseling, M., et al. (2020). The transverse aortic constriction heart failure animal model: a systematic review and meta-analysis. *Heart Fail. Rev.* 26, 1515–1524. doi: 10.1007/s10741-020-09960-w

Boukens, B. J., Rivaud, M. R., Rentschler, S., and Coronel, R. (2014). Misinterpretation of the mouse ECG: 'musing the waves of Mus musculus'. *J. Physiol.* 592, 4613–4626. doi: 10.1113/jphysiol.2014.279380

Boyman, L., Chikando, A. C., Williams, G. S., Khairallah, R. J., Kettlewell, S., Ward, C. W., et al. (2014). Calcium movement in cardiac mitochondria. *Biophys. J.* 107, 1289–1301. doi: 10.1016/j.bpj.2014.07.045

Braam, S. R., Tertoolen, L., van de Stolpe, A., Meyer, T., Passier, R., and Mummery, C. L. (2010). Prediction of drug-induced cardiotoxicity using human embryonic stem cell-derived cardiomyocytes. *Stem Cell Res.* 4, 107–116. doi: 10.1016/j.scr.2009.11.004

Brack, K. E., Narang, R., Winter, J., and Ng, G. A. (2013). The mechanical uncoupler blebbistatin is associated with significant electrophysiological effects in the isolated rabbit heart. *Exp. Physiol.* 98, 1009–1027. doi: 10.1113/expphysiol.2012.069369

Brennan, J. A., Chen, Q., Gams, A., Dyavanapalli, J., Mendelowitz, D., Peng, W., et al. (2020). Evidence of superior and inferior sinoatrial nodes in the mammalian heart. *Clin. Electrophysiol.* 6, 1827–1840. doi: 10.1016/j.jacep.2020.09.012

Bub, G., Glass, L., Publicover, N. G., and Shrier, A. (1998). Bursting calcium rotors in cultured cardiac myocyte monolayers. *Proc. Natl. Acad. Sci.* 95, 10283–10287. doi: 10.1073/pnas.95.17.10283

Buikema, J. W., Van Der Meer, P., Sluijter, J. P., and Domian, I. J. (2013). Concise review: engineering myocardial tissue: the convergence of stem cells biology and tissue engineering technology. *Stem Cells* 31, 2587–2598. doi: 10.1002/stem.1467

Burridge, P. W., Matsa, E., Shukla, P., Lin, Z. C., Churko, J. M., Ebert, A. D., et al. (2014). Chemically defined generation of human cardiomyocytes. *Nat. Methods* 11, 855–860. doi: 10.1038/nmeth.2999

Carroll, K. J., Makarewich, C. A., McAnally, J., Anderson, D. M., Zentilin, L., Liu, N., et al. (2016). A mouse model for adult cardiac-specific gene deletion with CRISPR/Cas9. *Proc. Natl. Acad. Sci.* 113, 338–343. doi: 10.1073/pnas.1523918113

Chattipakorn, N., Banville, I., Gray, R. A., and Ideker, R. E. (2001). Mechanism of ventricular defibrillation for near-defibrillation threshold shocks: a whole-heart optical mapping study in swine. *Circulation* 104, 1313–1319. doi: 10.1161/hc3601.094295

Chavali, N. V., Kryshtal, D. O., Parikh, S. S., Wang, L., Glazer, A. M., Blackwell, D. J., et al. (2019). The patient-independent human iPSC model–a new tool for rapid determination of genetic variant pathogenicity in long QT syndrome. *Heart Rhythm* 16, 1686–1695. doi: 10.1016/j.hrthm.2019.04.031

Chaves, A. A., Dech, S. J., Nakayama, T., Hamlin, R. L., Bauer, J. A., and Carnes, C. A. (2003). Age and anesthetic effects on murine electrocardiography. *Life Sci.* 72, 2401–2412. doi: 10.1016/s0024-3205(03)00137-1

Chen, J., Ceholski, D. K., Liang, L., Fish, K., and Hajjar, R. J. (2017a). Variability in coronary artery anatomy affects consistency of cardiac damage after myocardial infarction in mice. *Am. J. Phys. Heart Circ. Phys.* 313, H275–H282. doi: 10.1152/ajpheart.00127.2017

Chen, Z., Xian, W., Bellin, M., Dorn, T., Tian, Q., Goedel, A., et al. (2017b). Subtype-specific promoter-driven action potential imaging for precise disease modelling and drug testing in hiPSC-derived cardiomyocytes. *Eur. Heart J.* 38, 292–301. doi: 10.1093/eurheartj/ehw189

Cheng, H., Lederer, W. J., and Cannell, M. B. (1993). Calcium sparks: elementary events underlying excitation-contraction coupling in heart muscle. *Science* 262, 740–744. doi: 10.1126/science.8235594

Cheng, H., Lederer, M. R., Lederer, W. J., and Cannell, M. B. (1996). Calcium sparks and $[Ca^{2+}]$ i waves in cardiac myocytes. *Am. J. Phys. Cell Phys.* 270, C148–C159. doi: 10.1152/ajpcell.1996.270.1.C148

Cho, K. W., Lee, W. H., Kim, B. S., and Kim, D. H. (2020). Sensors in heart-on-a-chip: a review on recent progress. *Talanta* 219:121269. doi: 10.1016/j.talanta.2020.121269

Choi, S. H., Weng, L. C., Roselli, C., Lin, H., Haggerty, C. M., Shoemaker, M. B., et al. (2018). Association between titin loss-of-function variants and early-onset atrial fibrillation. *JAMA* 320, 2354–2364. doi: 10.1001/jama.2018.18179

Chow, E., Bernjak, A., Williams, S., Fawdry, R. A., Hibbert, S., Freeman, J., et al. (2014). Risk of cardiac arrhythmias during hypoglycemia in patients with type 2 diabetes and cardiovascular risk. *Diabetes* 63, 1738–1747. doi: 10.2337/db13-0468

Christoph, J., and Luther, S. (2018). Marker-free tracking for motion artifact compensation and deformation measurements in optical mapping videos of contracting hearts. *Front. Physiol.* 9:1483. doi: 10.3389/fphys.2018.01483

Clauss, S., Bleyer, C., Schuettler, D., Tomsits, P., Renner, S., Klymiuk, N., et al. (2019). Animal models of arrhythmia: classic electrophysiology to genetically modified large animals. *Nat. Rev. Cardiol.* 16, 457–475. doi: 10.1038/s41569-019-0179-0

Clements, M. (2016). Multielectrode array (mea) assay for profiling electrophysiological drug effects in human stem cell-derived cardiomyocytes. *Curr. Protoc. Toxicol.* 68, 22.4.1–22.4.32. doi: 10.1002/cptx.2

Colatsky, T., Fermini, B., Gintant, G., Pierson, J. B., Sager, P., Sekino, Y., et al. (2016). The comprehensive in vitro proarrhythmia assay (CiPA) initiative—update on progress. *J. Pharmacol. Toxicol. Methods* 81, 15–20. doi: 10.1016/j.vascn.2016.06.002

Colbert, M. C., Hall, D. G., Kimball, T. R., Witt, S. A., Lorenz, J. N., Kirby, M. L., et al. (1997). Cardiac compartment-specific overexpression of a modified retinoic acid receptor produces dilated cardiomyopathy and congestive heart failure in transgenic mice. *J. Clin. Invest.* 100, 1958–1968. doi: 10.1172/JCI119727

Courtemanche, M., Ramirez, R. J., and Nattel, S. (1998). Ionic mechanisms underlying human atrial action potential properties: insights from a mathematical model. *Am. J. Phys. Heart Circ. Phys.* 275, H301–H321. doi: 10.1152/ajpheart.1998.275.1.H301

Cyganek, L., Tiburcy, M., Sekeres, K., Gerstenberg, K., Bohnenberger, H., Lenz, C., et al. (2018). Deep phenotyping of human induced pluripotent stem cell–derived atrial and ventricular cardiomyocytes. *JCI Insight* 3:e99941. doi: 10.1172/jci.insight.99941

Davidson, M. M., Nesti, C., Palenzuela, L., Walker, W. F., Hernandez, E., Protas, L., et al. (2005). Novel cell lines derived from adult human ventricular cardiomyocytes. *J. Mol. Cell. Cardiol.* 39, 133–147. doi: 10.1016/j.yjmcc.2005.03.003

Davie, A. P., Francis, C. M., Love, M. P., Caruana, L., Starkey, I. R., Shaw, T. R. D., et al. (1996). Value of the electrocardiogram in identifying heart failure

due to left ventricular systolic dysfunction. *Brit. Med. J.* 312:222. doi: 10.1136/bmj.312.7025.222

Dedkova, E. N., and Blatter, L. A. (2013). Calcium signaling in cardiac mitochondria. *J. Mol. Cell. Cardiol.* 58, 125–133. doi: 10.1016/j.yjmcc.2012.12.021

Ding, Q., Strong, A., Patel, K. M., Ng, S. L., Gosis, B. S., Regan, S. N., et al. (2014). Permanent alteration of PCSK9 with in vivo CRISPR-Cas9 genome editing. *Circ. Res.* 115, 488–492. doi: 10.1161/CIRCRESAHA.115.304351

Dong, R., Mu-U-Min, R., Reith, A. J., O'Shea, C., He, S., Duan, K., et al. (2019). A protocol for dual calcium-voltage optical mapping in murine sinoatrial preparation with optogenetic pacing. *Front. Physiol.* 10:954. doi: 10.3389/fphys.2019.00954

Dridi, H., Kushnir, A., Zalk, R., Yuan, Q., Melville, Z., and Marks, A. R. (2020). Intracellular calcium leak in heart failure and atrial fibrillation: a unifying mechanism and therapeutic target. *Nat. Rev. Cardiol.* 17, 732–747. doi: 10.1038/s41569-020-0394-8

Dutta, S., Chang, K. C., Beattie, K. A., Sheng, J., Tran, P. N., Wu, W. W., et al. (2017). Optimization of an in silico cardiac cell model for proarrhythmia risk assessment. *Front. Physiol.* 8:1025. doi: 10.3389/fphys.2017.01025

Dux-Santoy, L., Sebastian, R., Felix-Rodriguez, J., Ferrero, J. M., and Saiz, J. (2011). Interaction of specialised cardiac conduction system with antiarrhythmic drugs: a simulation study. *IEEE Trans. Biomed. Eng.* 58, 3475–3478. doi: 10.1109/TBME.2011.2165213

Eckardt, L., Häusler, K. G., Ravens, U., Borggrefe, M., and Kirchhof, P. (2016). ESC guidelines on atrial fibrillation 2016: summary of the most relevant recommendations and modifications. *Herz* 41, 677–683. doi: 10.1007/s00059-016-4503-8

Eijgenraam, T. R., Boukens, B. J., Boogerd, C. J., Schouten, E. M., van de Kolk, C. W., Stege, N. M., et al. (2020). The phospholamban p.(Arg14del) pathogenic variant leads to cardiomyopathy with heart failure and is unresponsive to standard heart failure therapy. *Sci. Rep.* 10:16710. doi: 10.1038/s41598-020-66656-9

Erickson, J., Tooker, A., Tai, Y. C., and Pine, J. (2008). Caged neuron MEA: a system for long-term investigation of cultured neural network connectivity. *J. Neurosci. Methods* 175, 1–16. doi: 10.1016/j.jneumeth.2008.07.023

Fabritz, L., Kirchhof, P., Franz, M. R., Eckardt, L., Mönnig, G., Milberg, P., et al. (2003). Prolonged action potential durations, increased dispersion of repolarization, and polymorphic ventricular tachycardia in a mouse model of proarrhythmia. *Basic Res. Cardiol.* 98, 25–32. doi: 10.1007/s00395-003-0386-y

Fast, V. G., and Cheek, E. R. (2002). Optical mapping of arrhythmias induced by strong electrical shocks in myocyte cultures. *Circ. Res.* 90, 664–670. doi: 10.1161/01.RES.0000013403.24495.CC

Fedorov, V. V., Lozinsky, I. T., Sosunov, E. A., Anyukhovsky, E. P., Rosen, M. R., Balke, C. W., et al. (2007). Application of blebbistatin as an excitation–contraction uncoupler for electrophysiologic study of rat and rabbit hearts. *Heart Rhythm* 4, 619–626. doi: 10.1016/j.hrthm.2006.12.047

Feeny, A. K., Chung, M. K., Madabhushi, A., Attia, Z. I., Cikes, M., Firouznia, M., et al. (2020). Artificial intelligence and machine learning in arrhythmias and cardiac electrophysiology. *Circ. Arrhythm. Electrophysiol.* 13:e007952. doi: 10.1161/CIRCEP.119.007952

Fish, M., Shaboodien, G., Kraus, S., Sliwa, K., Seidman, C. E., Burke, M. A., et al. (2016). Mutation analysis of the phospholamban gene in 315 south Africans with dilated, hypertrophic, peripartum and arrhythmogenic right ventricular cardiomyopathies. *Sci. Rep.* 6, 1–8. doi: 10.1038/srep22235

Franz, M. R. (1991). Method and theory of monophasic action potential recording. *Prog. Cardiovasc. Dis.* 33, 347–368. doi: 10.1016/0033-0620(91)90002-4

Freundt, J. K., Frommeyer, G., Spieker, T., Wötzel, F., Grotthoff, J. S., Stypmann, J., et al. (2019). Histone deacetylase inhibition by Entinostat for the prevention of electrical and structural remodeling in heart failure. *BMC Pharmacol. Toxicol.* 20:16. doi: 10.1186/s40360-019-0294-x

Fye, W. B. (1994). A history of the origin, evolution, and impact of electrocardiography. *Am. J. Card.* 73, 937–949.

Garcia-Elias, A., Tajes, M., Yañez-Bisbe, L., Enjuanes, C., Comín-Colet, J., Serra, S. A., et al. (2021). Atrial fibrillation in heart failure is associated with high levels of circulating microRNA-199a-5p and 22–5p and a defective regulation of intracellular calcium and cell-to-cell communication. *Int. J. Mol. Sci.* 22:10377. doi: 10.3390/ijms221910377

Garrott, K., Kuzmiak-Glancy, S., Wengrowski, A., Zhang, H., Rogers, J., and Kay, M. W. (2017). KATP channel inhibition blunts electromechanical decline during hypoxia in left ventricular working rabbit hearts. *J. Physiol.* 595, 3799–3813. doi: 10.1113/JP273873

Gassanov, N., Brandt, M. C., Michels, G., Lindner, M., Er, F., and Hoppe, U. C. (2006). Angiotensin II-induced changes of calcium sparks and ionic currents in human atrial myocytes: potential role for early remodeling in atrial fibrillation. *Cell Calcium* 39, 175–186. doi: 10.1016/j.ceca.2005.10.008

Gehrmann, J., Frantz, S., Maguire, C. T., Vargas, M., Ducharme, A., Wakimoto, H., et al. (2001). Electrophysiological characterization of murine myocardial ischemia and infarction. *Basic Res. Cardiol.* 96, 237–250. doi: 10.1007/s003950170054

Geisterfer-Lowrance, A. A., Christe, M., Conner, D. A., Ingwall, J. S., Schoen, F. J., Seidman, C. E., et al. (1996). A mouse model of familial hypertrophic cardiomyopathy. *Science* 272, 731–734. doi: 10.1126/science.272.5262.731

Geselowitz, D. B. (1989). On the theory of the electrocardiogram. *Proc. IEEE* 77, 857–876. doi: 10.1109/5.29327

Gesmundo, I., Miragoli, M., Carullo, P., Trovato, L., Larcher, V., Di Pasquale, E., et al. (2017). Growth hormone-releasing hormone attenuates cardiac hypertrophy and improves heart function in pressure overload-induced heart failure. *Proc. Natl. Acad. Sci.* 114, 12033–12038. doi: 10.1073/pnas.1712612114

Girouard, S. D., Pastore, J. M., Laurita, K. R., Gregory, K. W., and Rosenbaum, D. S. (1996). Optical mapping in a new Guinea pig model of ventricular tachycardia reveals mechanisms for multiple wavelengths in a single reentrant circuit. *Circulation* 93, 603–613. doi: 10.1161/01.CIR.93.3.603

Gloschat, C., Aras, K., Gupta, S., Faye, N. R., Zhang, H., Syunyaev, R. A., et al. (2018). RHYTHM: an open source imaging toolkit for cardiac panoramic optical mapping. *Sci. Rep.* 8, 1–12. doi: 10.1038/s41598-018-21333-w

Goedel, A., My, I., Sinnecker, D., and Moretti, A. (2017). Perspectives and challenges of pluripotent stem cells in cardiac arrhythmia research. *Curr. Cardiol. Rep.* 19:23. doi: 10.1007/s11886-017-0828-z

Goette, A., Arndt, M., Röcken, C., Spiess, A., Staack, T., Geller, J. C., et al. (2000). Regulation of angiotensin II receptor subtypes during atrial fibrillation in humans. *Circulation* 101, 2678–2681. doi: 10.1161/01.CIR.101.23.2678

Gomez, J. F., Cardona, K., Romero, L., Ferrero, J. M. Jr., and Trenor, B. (2014). Electrophysiological and structural remodeling in heart failure modulate arrhythmogenesis. 1D simulation study. *PLoS One* 9:e106602. doi: 10.1371/journal.pone.0111730

Goversen, B., van der Heyden, M. A., van Veen, T. A., and de Boer, T. P. (2018). The immature electrophysiological phenotype of iPSC-CMs still hampers in vitro drug screening: special focus on IK1. *Pharmacol. Ther.* 183, 127–136. doi: 10.1016/j.pharmthera.2017.10.001

Grandi, E., Dobrev, D., and Heijman, J. (2019). Computational modeling: what does it tell us about atrial fibrillation therapy? *Int. J. Cardiol.* 287, 155–161. doi: 10.1016/j.ijcard.2019.01.077

Grandi, E., Pandit, S. V., Voigt, N., Workman, A. J., Dobrev, D., Jalife, J., et al. (2011). Human atrial action potential and Ca^{2+} model: sinus rhythm and chronic atrial fibrillation. *Circ. Res.* 109, 1055–1066. doi: 10.1161/CIRCRESAHA.111.253955

Groenewegen, A., Rutten, F. H., Mosterd, A., and Hoes, A. W. (2020). Epidemiology of heart failure. *Eur. J. Heart Fail.* 22, 1342–1356. doi: 10.1002/ejhf.1858

Grynkiewicz, G., Poenie, M., and Tsien, R. Y. (1985). A new generation of Ca^{2+} indicators with greatly improved fluorescence properties. *J. Biol. Chem.* 260, 3440–3450. doi: 10.1016/S0021-9258(19)83641-4

Gudbjartsson, D. F., Arnar, D. O., Helgadottir, A., Gretarsdottir, S., Holm, H., Sigurdsson, A., et al. (2007). Variants conferring risk of atrial fibrillation on chromosome 4q25. *Nature* 448, 353–357. doi: 10.1038/nature06007

Guinamard, R., Chatelier, A., Demion, M., Potreau, D., Patri, S., Rahmati, M., et al. (2004). Functional characterization of a Ca^{2+}-activated non-selective cation channel in human atrial cardiomyocytes. *J. Physiol.* 558, 75–83. doi: 10.1113/jphysiol.2004.063974

Gutstein, D. E., Morley, G. E., Tamaddon, H., Vaidya, D., Schneider, M. D., Chen, J., et al. (2001). Conduction slowing and sudden arrhythmic death in mice with cardiac-restricted inactivation of connexin43. *Circ. Res.* 88, 333–339. doi: 10.1161/01.RES.88.3.333

Gwathmey, J. K., Copelas, L., MacKinnon, R., Schoen, F. J., Feldman, M. D., Grossman, W., et al. (1987). Abnormal intracellular calcium handling in myocardium from patients with end-stage heart failure. *Circ. Res.* 61, 70–76. doi: 10.1161/01.RES.61.1.70

Halapas, A., Papalois, A., Stauropoulou, A., Philippou, A., Pissimissis, N., Chatzigeorgiou, A., et al. (2008). In vivo models for heart failure research. *In Vivo* 22, 767–780.

Halbach, M., Egert, U., Hescheler, J., and Banach, K. (2003). Estimation of action potential changes from field potential recordings in multicellular mouse cardiac myocyte cultures. *Cell. Physiol. Biochem.* 13, 271–284. doi: 10.1159/000074542

Hasegawa, K., Ohno, S., Ashihara, T., Itoh, H., Ding, W. G., Toyoda, F., et al. (2014). A novel KCNQ1 missense mutation identified in a patient with juvenile-onset atrial fibrillation causes constitutively open IKs channels. *Heart Rhythm* 11, 67–75. doi: 10.1016/j.hrthm.2013.09.073

Heijman, J., Voigt, N., Nattel, S., and Dobrev, D. (2014). Cellular and molecular electrophysiology of atrial fibrillation initiation, maintenance, and progression. *Circ. Res.* 114, 1483–1499. doi: 10.1161/CIRCRESAHA.114.302226

Herman, D. S., Lam, L., Taylor, M. R., Wang, L., Teekakirikul, P., Christodoulou, D., et al. (2012). Truncations of titin causing dilated cardiomyopathy. *N. Engl. J. Med.* 366, 619–628. doi: 10.1056/NEJMoa1110186

Ho, D., Zhao, X., Gao, S., Hong, C., Vatner, D. E., and Vatner, S. F. (2011). Heart rate and electrocardiography monitoring in mice. *Curr. Protoc. Mouse Biol.* 1, 123–139. doi: 10.1002/9780470942390.mo100159

Hodgkin, A. L., and Huxley, A. F. (1952). A quantitative description of membrane current and its application to conduction and excitation in nerve. *J. Physiol.* 117, 500–544. doi: 10.1113/jphysiol.1952.sp004764

Holmes, A. P., Saxena, P., Kabir, S. N., O'Shea, C., Kuhlmann, S. M., Gupta, S., et al. (2021). Atrial resting membrane potential confers sodium current sensitivity to propafenone, flecainide and dronedarone. *Heart Rhythm* 18, 1212–1220. doi: 10.1016/j.hrthm.2021.03.016

Holmes, A. P., Yu, T. Y., Tull, S., Syeda, F., Kuhlmann, S. M., O'Brien, S. M., et al. (2016). A regional reduction in Ito and IKACh in the murine posterior left atrial myocardium is associated with action potential prolongation and increased ectopic activity. *PLoS One* 11:e0154077. doi: 10.1371/journal.pone.0154077

Hrabcová, D., Pásek, M., Šimurda, J., and Christé, G. (2013). Effect of ion concentration changes in the limited extracellular spaces on sarcolemmal ion transport and Ca^{2+} turnover in a model of human ventricular cardiomyocyte. *Int. J. Mol. Sci.* 14, 24271–24292. doi: 10.3390/ijms141224271

Husti, Z., Varró, A., and Baczkó, I. (2021). Arrhythmogenic remodeling in the failing heart. *Cell* 10:3203. doi: 10.3390/cells10113203

Iijima, T., Irisawa, H., and Kameyama, M. (1985). Membrane currents and their modification by acetylcholine in isolated single atrial cells of the Guinea-pig. *J. Physiol.* 359, 485–501. doi: 10.1113/jphysiol.1985.sp015598

Ikenishi, A., Okayama, H., Iwamoto, N., Yoshitome, S., Tane, S., Nakamura, K., et al. (2012). Cell cycle regulation in mouse heart during embryonic and postnatal stages. *Develop. Growth Differ.* 54, 731–738. doi: 10.1111/j.1440-169X.2012.01373.x

Iravanian, S., Uzelac, I., Herndon, C., Langberg, J. J., and Fenton, F. H. (2020). Generation of monophasic action potentials and intermediate forms. *Biophys. J.* 119, 460–469. doi: 10.1016/j.bpj.2020.05.039

Itzhaki, I., Maizels, L., Huber, I., Zwi-Dantsis, L., Caspi, O., Winterstern, A., et al. (2011). Modelling the long QT syndrome with induced pluripotent stem cells. *Nature* 471, 225–229. doi: 10.1038/nature09747

Jaimes, R. III, Walton, R. D., Pasdois, P., Bernus, O., Efimov, I. R., and Kay, M. W. (2016). A technical review of optical mapping of intracellular calcium within myocardial tissue. *Am. J. Phys. Heart Circ. Phys.* 310, H1388–H1401. doi: 10.1152/ajpheart.00665.2015

Janse, M. J. (1986). Electrophysiological effects of myocardial ischaemia. Relationship with early ventricular arrhythmias. *Eur. Heart J.* 7(Suppl A), 35–43

Juhola, M., Joutsijoki, H., Penttinen, K., and Aalto-Setälä, K. (2018). Detection of genetic cardiac diseases by Ca^{2+} transient profiles using machine learning methods. *Sci. Rep.* 8:9355. doi: 10.1038/s41598-018-27695-5

Kaese, S., and Verheule, S. (2012). Cardiac electrophysiology in mice: a matter of size. *Front. Physiol.* 3:345. doi: 10.3389/fphys.2012.00345

Kaestner, L., Scholz, A., Tian, Q., Ruppenthal, S., Tabellion, W., Wiesen, K., et al. (2014). Genetically encoded Ca^{2+} indicators in cardiac myocytes. *Circ. Res.* 114, 1623–1639. doi: 10.1161/CIRCRESAHA.114.303475

Kappadan, V., Telele, S., Uzelac, I., Fenton, F., Parlitz, U., Luther, S., et al. (2020). High-resolution optical measurement of cardiac restitution, contraction, and fibrillation dynamics in beating vs. blebbistatin-uncoupled isolated rabbit hearts. *Front. Physiol.* 11:464. doi: 10.3389/fphys.2020.00464

Kim, J. S., Choi, S. W., Park, Y. G., Kim, S. J., Choi, C. H., Cha, M. J., et al. (2022). Impact of high-dose irradiation on human iPSC-derived cardiomyocytes using multi-electrode arrays: implications for the antiarrhythmic effects of cardiac radioablation. *Int. J. Mol. Sci.* 23:351. doi: 10.3390/ijms23010566

Kirchhof, P. F., Fabritz, C. L., and Franz, M. R. (1998). Phase angle convergence of multiple monophasic action potential reordings precedes spontaneous termination of ventricular fibrillation. *Basic Res. Cardiol.* 93, 412–421. doi: 10.1007/s003950050110

Kleiger, R. E., Miller, J. P., Bigger, J. T. Jr., and Moss, A. J. (1987). Decreased heart rate variability and its association with increased mortality after acute myocardial infarction. *Am. J. Cardiol.* 59, 256–262. doi: 10.1016/0002-9149(87)90795-8

Knisley, S. B., Justice, R. K., Kong, W., and Johnson, P. L. (2000). Ratiometry of transmembrane voltage-sensitive fluorescent dye emission in hearts. *Am. J. Phys. Heart Circ. Phys.* 279, H1421–H1433. doi: 10.1152/ajpheart.2000.279.3.H1421

Knollmann, B. C. (2013). Induced pluripotent stem cell–derived cardiomyocytes: boutique science or valuable arrhythmia model? *Circ. Res.* 112, 969–976. doi: 10.1161/CIRCRESAHA.112.300567

Knollmann, B. C., Kirchhof, P., Sirenko, S. G., Degen, H., Greene, A. E., Schober, T., et al. (2003). Familial hypertrophic cardiomyopathy-linked mutant troponin T causes stress-induced ventricular tachycardia and Ca^{2+}-dependent action potential remodeling. *Circ. Res.* 92, 428–436. doi: 10.1161/01.RES.0000059562.91384.1A

Kornreich, B. G. (2007). The patch clamp technique: principles and technical considerations. *J. Vet. Cardiol.* 9, 25–37. doi: 10.1016/j.jvc.2007.02.001

Krause, J., Löser, A., Lemoine, M. D., Christ, T., Scherschel, K., Meyer, C., et al. (2018). Rat atrial engineered heart tissue: a new in vitro model to study atrial biology. *Basic Res. Cardiol.* 113:41. doi: 10.1007/s00395-018-0701-2

Kussauer, S., David, R., and Lemcke, H. (2019). hiPSCs derived cardiac cells for drug and toxicity screening and disease modeling: what micro-electrode-array analyses can tell us. *Cell* 8:1331. doi: 10.3390/cells8111331

Land, S., Park-Holohan, S. J., Smith, N. P., Dos Remedios, C. G., Kentish, J. C., and Niederer, S. A. (2017). A model of cardiac contraction based on novel measurements of tension development in human cardiomyocytes. *J. Mol. Cell. Cardiol.* 106, 68–83. doi: 10.1016/j.yjmcc.2017.03.008

Landstrom, A. P., Dobrev, D., and Wehrens, X. H. (2017). Calcium signaling and cardiac arrhythmias. *Circ. Res.* 120, 1969–1993. doi: 10.1161/CIRCRESAHA.117.310083

Lang, D., Holzem, K., Kang, C., Xiao, M., Hwang, H. J., Ewald, G. A., et al. (2015). Arrhythmogenic remodeling of β2 versus β1 adrenergic signaling in the human failing heart. *Circ. Arrhythm. Electrophysiol.* 8, 409–419. doi: 10.1161/CIRCEP.114.002065

Lange, R., Kloner, R. A., and Braunwald, E. (1983). First ultra-short-acting beta-adrenergic blocking agent: its effect on size and segmental wall dynamics of reperfused myocardial infarcts in dogs. *Am. J. Cardiol.* 51, 1759–1767. doi: 10.1016/0002-9149(83)90224-2

Lau, D. H., Shipp, N. J., Kelly, D. J., Thanigaimani, S., Neo, M., Kuklik, P., et al. (2013). Atrial arrhythmia in ageing spontaneously hypertensive rats: unraveling the substrate in hypertension and ageing. *PLoS One* 8:e72416. doi: 10.1371/journal.pone.0072416

Lehnart, S. E., Terrenoire, C., Reiken, S., Wehrens, X. H., Song, L. S., Tillman, E. J., et al. (2006). Stabilization of cardiac ryanodine receptor prevents intracellular calcium leak and arrhythmias. *Proc. Natl. Acad. Sci.* 103, 7906–7910. doi: 10.1073/pnas.0602133103

Lemoine, M. D., Mannhardt, I., Breckwoldt, K., Prondzynski, M., Flenner, F., Ulmer, B., et al. (2017). Human iPSC-derived cardiomyocytes cultured in 3D engineered heart tissue show physiological upstroke velocity and sodium current density. *Sci. Rep.* 7:5464. doi: 10.1038/s41598-017-05600-w

Liang, B., Soka, M., Christensen, A. H., Olesen, M. S., Larsen, A. P., Knop, F. K., et al. (2014). Genetic variation in the two-pore domain potassium channel, TASK-1, may contribute to an atrial substrate for arrhythmogenesis. *J. Mol. Cell. Cardiol.* 67, 69–76. doi: 10.1016/j.yjmcc.2013.12.014

Liu, H., Bolonduro, O. A., Hu, N., Ju, J., Rao, A. A., Duffy, B. M., et al. (2020). Heart-on-a-chip model with integrated extra-and intracellular bioelectronics for monitoring cardiac electrophysiology under acute hypoxia. *Nano Lett.* 20, 2585–2593. doi: 10.1021/acs.nanolett.0c00076

Liu, J., Volkers, L., Jangsangthong, W., Bart, C. I., Engels, M. C., Zhou, G., et al. (2018). Generation and primary characterization of iAM-1, a versatile

new line of conditionally immortalised atrial myocytes with preserved cardiomyogenic differentiation capacity. *Cardiovasc. Res.* 114, 1848–1859. doi: 10.1093/cvr/cvy134

Lock, J. T., Parker, I., and Smith, I. F. (2015). A comparison of fluorescent Ca^{2+} indicators for imaging local Ca^{2+} signals in cultured cells. *Cell Calcium* 58, 638–648. doi: 10.1016/j.ceca.2015.10.003

Louch, W. E., Sheehan, K. A., and Wolska, B. M. (2011). Methods in cardiomyocyte isolation, culture, and gene transfer. *J. Mol. Cell. Cardiol.* 51, 288–298. doi: 10.1016/j.yjmcc.2011.06.012

Low, B. E., Kutny, P. M., and Wiles, M. V. (2016). "Simple, efficient CRISPR-Cas9-mediated gene editing in mice: strategies and methods," in *Mouse Models for Drug Discovery. Methods in Molecular Biology. Vol. 1438.* eds. G. Proetzel and M. Wiles (New York, NY: Humana Press), 19–53.

Luo, M., and Anderson, M. E. (2013). Mechanisms of altered Ca^{2+} handling in heart failure. *Circ. Res.* 113, 690–708. doi: 10.1161/CIRCRESAHA.113.301651

Lyon, A., Mincholé, A., Bueno-Orovio, A., and Rodriguez, B. (2019). Improving the clinical understanding of hypertrophic cardiomyopathy by combining patient data, machine learning and computer simulations: a case study. *Morphologie* 103, 169–179. doi: 10.1016/j.morpho.2019.09.001

Machiraju, P., and Greenway, S. C. (2019). Current methods for the maturation of induced pluripotent stem cell-derived cardiomyocytes. *World J. Stem Cells* 11, 33–43. doi: 10.4252/wjsc.v11.i1.33

MacLennan, D. H., and Kranias, E. G. (2003). Phospholamban: a crucial regulator of cardiac contractility. *Nat. Rev. Mol. Cell Biol.* 4, 566–577. doi: 10.1038/nrm1151

Maguire, C. T., Bevilacqua, L. M., Wakimoto, H., Gehrmann, J., and Berul, C. I. (2000). Maturational atrioventricular nodal physiology in the mouse. *J. Cardiovasc. Electrophysiol.* 11, 557–564. doi: 10.1111/j.1540-8167.2000.tb00009.x

Makałowski, W., Zhang, J., and Boguski, M. S. (1996). Comparative analysis of 1196 orthologous mouse and human full-length mRNA and protein sequences. *Genome Res.* 6, 846–857. doi: 10.1101/gr.6.9.846

Malgaroli, A., Milani, D., Meldolesi, J., and Pozzan, T. (1987). Fura-2 measurement of cytosolic free Ca^{2+} in monolayers and suspensions of various types of animal cells. *J. Cell Biol.* 105, 2145–2155. doi: 10.1083/jcb.105.5.2145

Malhotra, S., Fernandez, S. F., Fallavollita, J. A., and Canty, J. M. (2015). Prognostic significance of imaging myocardial sympathetic innervation. *Curr. Cardiol. Rep.* 17:62. doi: 10.1007/s11886-015-0613-9

Maltsev, V. A., Silverman, N., Sabbah, H. N., and Undrovinas, A. I. (2007). Chronic heart failure slows late sodium current in human and canine ventricular myocytes: implications for repolarization variability. *Eur. J. Heart Fail.* 9, 219–227. doi: 10.1016/j.ejheart.2006.08.007

Margara, F., Wang, Z. J., Levrero-Florencio, F., Santiago, A., Vázquez, M., Bueno-Orovio, A., et al. (2021). In-silico human electro-mechanical ventricular modelling and simulation for drug-induced pro-arrhythmia and inotropic risk assessment. *Prog. Biophys. Mol. Biol.* 159, 58–74. doi: 10.1016/j.pbiomolbio.2020.06.007

Martinez-Navarro, H., Mincholé, A., Bueno-Orovio, A., and Rodriguez, B. (2019). High arrhythmic risk in antero-septal acute myocardial ischemia is explained by increased transmural reentry occurrence. *Sci. Rep.* 9:168031. doi: 10.1038/s41598-019-53221-2

Masarone, D., Limongelli, G., Rubino, M., Valente, F., Vastarella, R., Ammendola, E., et al. (2017). Management of arrhythmias in heart failure. *J. Cardiovasc. Dis. Res.* 4:3. doi: 10.3390/jcdd4010003

Mesquita, T. R. R., Zhang, R., de Couto, G., Valle, J., Sanchez, L., Rogers, R. G., et al. (2020). Mechanisms of atrial fibrillation in aged rats with heart failure with preserved ejection fraction. *Heart Rhythm* 17, 1025–1033. doi: 10.1016/j.hrthm.2020.02.007

Mincholé, A., Zacur, E., Ariga, R., Grau, V., and Rodriguez, B. (2019). MRI-based computational torso/biventricular multiscale models to investigate the impact of anatomical variability on the ECG QRS complex. *Front. Physiol.* 10:1103. doi: 10.3389/fphys.2019.01103

Minta, A., Kao, J. P., and Tsien, R. Y. (1989). Fluorescent indicators for cytosolic calcium based on rhodamine and fluorescein chromophores. *J. Biol. Chem.* 264, 8171–8178. doi: 10.1016/S0021-9258(18)83165-9

Mora, M. T., Gong, J. Q., Sobie, E. A., and Trenor, B. (2021). The role of β-adrenergic system remodeling in human heart failure: a mechanistic investigation. *J. Mol. Cell. Cardiol.* 153, 14–25. doi: 10.1016/j.yjmcc.2020.12.004

Morand, J., Arnaud, C., Pepin, J. L., and Godin-Ribuot, D. (2018). Chronic intermittent hypoxia promotes myocardial ischemia-related ventricular arrhythmias and sudden cardiac death. *Sci. Rep.* 8:2997. doi: 10.1038/s41598-018-21064-y

Muszkiewicz, A., Liu, X., Bueno-Orovio, A., Lawson, B. A., Burrage, K., Casadei, B., et al. (2018). From ionic to cellular variability in human atrial myocytes: an integrative computational and experimental study. *Am. J. Phys. Heart Circ. Phys.* 314, H895–H916. doi: 10.1152/ajpheart.00477.2017

Neely, J. R., Liebermeister, H., Battersby, E. J., and Morgan, H. E. (1967). Effect of pressure development on oxygen consumption by isolated rat heart. *Am. J. Physiol.* 212, 804–814. doi: 10.1152/ajplegacy.1967.212.4.804

Ng, G. A., Brack, K. E., and Coote, J. H. (2001). Effects of direct sympathetic and vagus nerve stimulation on the physiology of the whole heart-a novel model of isolated Langendorff perfused rabbit heart with intact dual autonomic innervation. *Exp. Physiol.* 86, 319–329. doi: 10.1113/eph8602146

Nishii, K., Shibata, Y., and Kobayashi, Y. (2014). Connexin mutant embryonic stem cells and human diseases. *World J. Stem Cells* 6, 571–578. doi: 10.4252/wjsc.v6.i5.571

Niwa, N., and Nerbonne, J. M. (2010). Molecular determinants of cardiac transient outward potassium current (Ito) expression and regulation. *J. Mol. Cell. Cardiol.* 48, 12–25. doi: 10.1016/j.yjmcc.2009.07.013

Noble, D. (1960). Cardiac action and pacemaker potentials based on the Hodgkin-Huxley equations. *Nature* 188, 495–497. doi: 10.1038/188495b0

Nygren, A., Fiset, C., Firek, L., Clark, J. W., Lindblad, D. S., Clark, R. B., et al. (1998). Mathematical model of an adult human atrial cell: the role of K^+ currents in repolarization. *Circ. Res.* 82, 63–81. doi: 10.1161/01.RES.82.1.63

O'Hara, T., Virág, L., Varró, A., and Rudy, Y. (2011). Simulation of the undiseased human cardiac ventricular action potential: model formulation and experimental validation. *PLoS Comput. Biol.* 7:e1002061. doi: 10.1371/journal.pcbi.1002061

O'Shea, C., Holmes, A. P., Ting, Y. Y., Winter, J., Wells, S. P., Correia, J., et al. (2019a). ElectroMap: high-throughput open-source software for analysis and mapping of cardiac electrophysiology. *Sci. Rep.* 9, 1–13. doi: 10.1038/s41598-018-38263-2

O'Shea, C., Holmes, A. P., Winter, J., Correia, J., Ou, X., Dong, R., et al. (2019b). Cardiac optogenetics and optical mapping–overcoming spectral congestion in all-optical cardiac electrophysiology. *Front. Physiol.* 10:182. doi: 10.3389/fphys.2019.00182

O'Shea, C., Kabir, S. N., Holmes, A. P., Lei, M., Fabritz, L., Rajpoot, K., et al. (2020). Cardiac optical mapping–state-of-the-art and future challenges. *Int. J. Biochem. Cell Biol.* 126:105804. doi: 10.1016/j.biocel.2020.105804

Obergrussberger, A., Rinke-Weiß, I., Goetze, T. A., Rapedius, M., Brinkwirth, N., Becker, N., et al. (2021). The suitability of high throughput automated patch clamp for physiological applications. *J. Physiol.* 600, 277–297. doi: 10.1113/JP282107

Odening, K. E., Gomez, A. M., Dobrev, D., Fabritz, L., Heinzel, F. R., Mangoni, M. E., et al. (2021). ESC working group on cardiac cellular electrophysiology position paper: relevance, opportunities, and limitations of experimental models for cardiac electrophysiology research. *EP Eur.* 23, 1795–1814. doi: 10.1093/europace/euab142

Offerhaus, J. A., Snelderwaard, P. C., Algül, S., Faber, J. W., Riebel, K., Jensen, B., et al. (2021). High heart rate associated early repolarization causes J-waves in both zebra finch and mouse. *Phys. Rep.* 9:e14775. doi: 10.14814/phy2.14775

Olejnickova, V., Novakova, M., and Provaznik, I. (2015). Isolated heart models: cardiovascular system studies and technological advances. *Med. Biol. Eng. Comput.* 53, 669–678. doi: 10.1007/s11517-015-1270-2

Onódi, Z., Visnovitz, T., Kiss, B., Hambalkó, S., Koncz, A., Ágg, B., et al. (2022). Systematic transcriptomic and phenotypic characterization of human and murine cardiac myocyte cell lines and primary cardiomyocytes reveals serious limitations and low resemblances to adult cardiac phenotype. *J. Mol. Cell. Cardiol.* 165, 19–30. doi: 10.1016/j.yjmcc.2021.12.007

Paci, M., Passini, E., Klimas, A., Severi, S., Hyttinen, J., Rodriguez, B., et al. (2020). All-optical electrophysiology refines populations of in silico human iPSC-CMs for drug evaluation. *Biophys. J.* 118, 2596–2611. doi: 10.1016/j.bpj.2020.03.018

Park, J. I., Heikhmakhtiar, A. K., Kim, C. H., Kim, Y. S., Choi, S. W., Song, K. S., et al. (2018). The effect of heart failure and left ventricular assist device treatment on right ventricular mechanics: a computational study. *Biomed. Eng. Online* 17:62. doi: 10.1186/s12938-018-0498-0

Park, J., Lee, S., and Jeon, M. (2009). Atrial fibrillation detection by heart rate variability in Poincare plot. *Biomed. Eng. Online* 8, 1–12. doi: 10.1186/1475-925X-8-38

Pasotti, M., Klersy, C., Pilotto, A., Marziliano, N., Rapezzi, C., Serio, A., et al. (2008). Long-term outcome and risk stratification in dilated cardiolaminopathies. *J. Am. Coll. Cardiol.* 52, 1250–1260. doi: 10.1016/j.jacc.2008.06.044

Passini, E., Britton, O. J., Lu, H. R., Rohrbacher, J., Hermans, A. N., Gallacher, D. J., et al. (2017). Human in silico drug trials demonstrate higher accuracy than animal models in predicting clinical pro-arrhythmic cardiotoxicity. *Front. Physiol.* 8:668. doi: 10.3389/fphys.2017.00668

Pathak, R. K., Mahajan, R., Lau, D. H., and Sanders, P. (2015). The implications of obesity for cardiac arrhythmia mechanisms and management. *Can. J. Cardiol.* 31, 203–210. doi: 10.1016/j.cjca.2014.10.027

Peichl, P., Rafaj, A., and Kautzner, J. (2021). Management of ventricular arrhythmias in heart failure: current perspectives. *Heart Rhythm* 2, 796–806. doi: 10.1016/j.hroo.2021.08.007

Pérez-Hernández, M., Matamoros, M., Barana, A., Amorós, I., Gómez, R., Núñez, M., et al. (2016). Pitx2c increases in atrial myocytes from chronic atrial fibrillation patients enhancing I Ks and decreasing I Ca, L. *Cardiovasc. Res.* 109, 431–441. doi: 10.1093/cvr/cvv280

Pertsov, A. M., Davidenko, J. M., Salomonsz, R., Baxter, W. T., and Jalife, J. (1993). Spiral waves of excitation underlie reentrant activity in isolated cardiac muscle. *Circ. Res.* 72, 631–650. doi: 10.1161/01.RES.72.3.631

Petric, S., Clasen, L., van Wessel, C., Geduldig, N., Ding, Z., Schullenberg, M., et al. (2012). *In vivo* electrophysiological characterization of TASK-1 deficient mice. *Cell. Physiol. Biochem.* 30, 523–537. doi: 10.1159/000341435

Pierre, M., Djemai, M., Poulin, H., and Chahine, M. (2021). NaV1. 5 knockout in iPSCs: a novel approach to study NaV1. 5 variants in a human cardiomyocyte environment. *Sci. Rep.* 11, 1–16. doi: 10.1038/s41598-021-96474-6

Plant, L. D., Xiong, D., Romero, J., Dai, H., and Goldstein, S. A. (2020). Hypoxia produces pro-arrhythmic late sodium current in cardiac myocytes by SUMOylation of NaV1. 5 channels. *Cell Rep.* 30, 2225.e4–2236.e4. doi: 10.1016/j.celrep.2020.01.025

Poláková, E., and Sobie, E. A. (2013). Alterations in T-tubule and dyad structure in heart disease: challenges and opportunities for computational analyses. *Cardiovasc. Res.* 98, 233–239. doi: 10.1093/cvr/cvt026

Pozzoli, M., Cioffi, G., Traversi, E., Pinna, G. D., Cobelli, F., and Tavazzi, L. (1998). Predictors of primary atrial fibrillation and concomitant clinical and hemodynamic changes in patients with chronic heart failure: a prospective study in 344 patients with baseline sinus rhythm. *J. Am. Coll. Cardiol.* 32, 197–204. doi: 10.1016/S0735-1097(98)00221-6

Prabhu, S., Voskoboinik, A., Kaye, D. M., and Kistler, P. M. (2017). Atrial fibrillation and heart failure—cause or effect? *Heart Lung Circ.* 26, 967–974. doi: 10.1016/j.hlc.2017.05.117

Prakash, O., Held, M., McCormick, L. F., Gupta, N., Lian, L. Y., Antonyuk, S., et al. (2021). CPVT-associated calmodulin variants N53I and A102V dysregulate calcium signalling via different mechanisms. *J. Cell Sci.* doi: 10.1242/jcs.258796 Epub ahead of print

Price, D. (2005). The human tissue act 2004. *Mod. Law Rev.* 68, 798–821. doi: 10.1111/j.1468-2230.2005.00561.x

Ramkisoensing, A. A., Zhang, J., Harlaar, N., Pijnappels, D. A., and De Vries, A. A. F. (2021). Formation of human cardiomyocytes is impaired in a fibrotic environment: unravelling human cardiac regeneration. *Eur. Heart J.* 42(Supplement_1):ehab724-3271. doi: 10.1093/eurheartj/ehab724.3271

Ran, F. A., Hsu, P. D., Wright, J., Agarwala, V., Scott, D. A., and Zhang, F. (2013). Genome engineering using the CRISPR-Cas9 system. *Nat. Protoc.* 8, 2281–2308. doi: 10.1038/nprot.2013.143

Robinson, P., Sparrow, A.J., Broyles, C.N., Sievert, K., Chang, Y.F., Brook, F.A., et al. (2018). Measurement of myofilament calcium in living cardiomyocytes using a targeted genetically encoded indicator. bioRxiv. doi: 10.1101/268003.

Rodriguez, B., Carusi, A., Abi-Gerges, N., Ariga, R., Britton, O., Bub, G., et al. (2015). Human-based approaches to pharmacology and cardiology: an interdisciplinary and intersectorial workshop. *EP Eur.* 18, 1287–1298. doi: 10.1093/europace/euv320

Rodriguez, M. P., and Nygren, A. (2014). Motion estimation in cardiac fluorescence imaging with scale-space landmarks and optical flow: a comparative study. *IEEE Trans. Biomed. Eng.* 62, 774–782. doi: 10.1109/TBME.2014.2364959

Roney, C. H., Williams, S. E., Cochet, H., Mukherjee, R. K., O'Neill, L., Sim, I., et al. (2018). Patient-specific simulations predict efficacy of ablation of interatrial connections for treatment of persistent atrial fibrillation. *EP Eur.* 20(Suppl 3), iii55–iii68. doi: 10.1093/europace/euy232

Saba, S., Wang, P. J., and Estes, N. M. III (2000). Invasive cardiac electrophysiology in the mouse: techniques and applications. *Trends Cardiovasc. Med.* 10, 122–132. doi: 10.1016/S1050-1738(00)00060-8

Sachetto Oliveira, R., Martins Rocha, B., Burgarelli, D., Meira, W. Jr., Constantinides, C., and Weber dos Santos, R. (2018). Performance evaluation of GPU parallelization, space-time adaptive algorithms, and their combination for simulating cardiac electrophysiology. *Int. J. Numer. Methods Biomed. Eng.* 34:e2913. doi: 10.1002/cnm.2913

Salama, G., and Choi, B. R. (2000). Images of action potential propagation in heart. *Physiology* 15, 33–41. doi: 10.1152/physiologyonline.2000.15.1.33

Salama, G., and London, B. (2007). Mouse models of long QT syndrome. *J. Physiol.* 578, 43–53. doi: 10.1113/jphysiol.2006.118745

Salama, G., and Morad, M. (1976). Merocyanine 540 as an optical probe of transmembrane electrical activity in the heart. *Science* 191, 485–487. doi: 10.1126/science.191.4226.485

Salem, T., Frankman, Z., and Churko, J. M. (2021). Tissue engineering techniques for induced pluripotent stem cell derived three-dimensional cardiac constructs. *Tissue Eng. Part B Rev.* doi: 10.1089/ten.teb.2021.0088 Epub ahead of print

Salzberg, B. M., Davila, H. V., and Cohen, L. B. (1973). Optical recording of impulses in individual neurones of an invertebrate central nervous system. *Nature* 246, 508–509. doi: 10.1038/246508a0

Sánchez, C., d'Ambrosio, G., Maffessanti, F., Caiani, E. G., Prinzen, F. W., Krause, R., et al. (2018). Sensitivity analysis of ventricular activation and electrocardiogram in tailored models of heart-failure patients. *Med. Biol. Eng. Comput.* 56, 491–504. doi: 10.1007/s11517-017-1696-9

Santulli, G., Xie, W., Reiken, S. R., and Marks, A. R. (2015). Mitochondrial calcium overload is a key determinant in heart failure. *Proc. Natl. Acad. Sci.* 112, 11389–11394. doi: 10.1073/pnas.1513047112

Savla, J. J., Nelson, B. C., Perry, C. N., and Adler, E. D. (2014). Induced pluripotent stem cells for the study of cardiovascular disease. *J. Am. Coll. Cardiol.* 64, 512–519. doi: 10.1016/j.jacc.2014.05.038

Sawaya, S. E., Rajawat, Y. S., Rami, T. G., Szalai, G., Price, R. L., Sivasubramanian, N., et al. (2007). Downregulation of connexin40 and increased prevalence of atrial arrhythmias in transgenic mice with cardiac-restricted overexpression of tumor necrosis factor. *Am. J. Phys. Heart Circ. Phys.* 292, H1561–H1567. doi: 10.1152/ajpheart.00285.2006

Schaaf, S., Shibamiya, A., Mewe, M., Eder, A., Stöhr, A., Hirt, M. N., et al. (2011). Human engineered heart tissue as a versatile tool in basic research and preclinical toxicology. *PLoS One* 6:e26397. doi: 10.1371/journal.pone.0026397

Scherrer-Crosbie, M., and Thibault, H. B. (2008). Echocardiography in translational research: of mice and men. *J. Am. Soc. Echocardiogr.* 21, 1083–1092. doi: 10.1016/j.echo.2008.07.001

Schick, R., Mekies, L. N., Shemer, Y., Eisen, B., Hallas, T., Ben Jehuda, R., et al. (2018). Functional abnormalities in induced pluripotent stem cell-derived cardiomyocytes generated from titin-mutated patients with dilated cardiomyopathy. *PLoS One* 13:e0205719. doi: 10.1371/journal.pone.0205719

Schmidt, C., Wiedmann, F., Voigt, N., Zhou, X. B., Heijman, J., Lang, S., et al. (2015). Upregulation of K2P3. 1 K^+ current causes action potential shortening in patients with chronic atrial fibrillation. *Circulation* 132, 82–92. doi: 10.1161/CIRCULATIONAHA.114.012657

Schmitt, J., Duray, G., Gersh, B. J., and Hohnloser, S. H. (2009). Atrial fibrillation in acute myocardial infarction: a systematic review of the incidence, clinical features and prognostic implications. *Eur. Heart J.* 30, 1038–1045. doi: 10.1093/eurheartj/ehn579

Schrickel, J. W., Bielik, H., Yang, A., Schimpf, R., Shlevkov, N., Burkhardt, D., et al. (2002). Induction of atrial fibrillation in mice by rapid transesophageal atrial pacing. *Basic Res. Cardiol.* 97, 452–460. doi: 10.1007/s003950200052

Schuler, B., Rettich, A., Vogel, J., Gassmann, M., and Arras, M. (2009). Optimised surgical techniques and postoperative care improve survival rates and permit accurate telemetric recording in exercising mice. *BMC Vet. Res.* 5, 1–11. doi: 10.1186/1746-6148-5-28

Schweizer, P. A., Darche, F. F., Ullrich, N. D., Geschwill, P., Greber, B., Rivinius, R., et al. (2017). Subtype-specific differentiation of cardiac pacemaker cell clusters

from human induced pluripotent stem cells. *Stem Cell Res Ther* 8:229. doi: 10.1186/s13287-017-0681-4

Shah, S., Henry, A., Roselli, C., Lin, H., Sveinbjörnsson, G., Fatemifar, G., et al. (2020). Genome-wide association and Mendelian randomisation analysis provide insights into the pathogenesis of heart failure. *Nat. Commun.* 11:163. doi: 10.1038/s41467-019-13690-5

Shemer, Y., Mekies, L. N., Ben Jehuda, R., Baskin, P., Shulman, R., Eisen, B., et al. (2021). Investigating LMNA-related dilated cardiomyopathy using human induced pluripotent stem cell-derived cardiomyocytes. *Int. J. Mol. Sci.* 22:7874. doi: 10.3390/ijms22157874

Shen, M. J., and Zipes, D. P. (2014). Role of the autonomic nervous system in modulating cardiac arrhythmias. *Circ. Res.* 114, 1004–1021. doi: 10.1161/CIRCRESAHA.113.302549

Shinnawi, R., Huber, I., Maizels, L., Shaheen, N., Gepstein, A., Arbel, G., et al. (2015). Monitoring human-induced pluripotent stem cell-derived cardiomyocytes with genetically encoded calcium and voltage fluorescent reporters. *Stem Cell Rep.* 5, 582–596. doi: 10.1016/j.stemcr.2015.08.009

Silbernagel, N., Körner, A., Balitzki, J., Jaggy, M., Bertels, S., Richter, B., et al. (2020). Shaping the heart: structural and functional maturation of iPSC-cardiomyocytes in 3D-micro-scaffolds. *Biomaterials* 227:119551. doi: 10.1016/j.biomaterials.2019.119551

Spira, M. E., and Hai, A. (2013). Multi-electrode array technologies for neuroscience and cardiology. *Nat. Nanotechnol.* 8, 83–94. doi: 10.1038/nnano.2012.265

Spurney, C. F., Guerron, A. D., Yu, Q., Sali, A., van der Meulen, J. H., Hoffman, E. P., et al. (2011). Membrane sealant Poloxamer P188 protects against isoproterenol induced cardiomyopathy in dystrophin deficient mice. *BMC Cardiovasc. Disord.* 11:20. doi: 10.1186/1471-2261-11-20

Suk, H. J., Boyden, E. S., and van Welie, I. (2019). Advances in the automation of whole-cell patch clamp technology. *J. Neurosci. Methods* 326:108357. doi: 10.1016/j.jneumeth.2019.108357

Sutanto, H., Laudy, L., Clerx, M., Dobrev, D., Crijns, H. J., and Heijman, J. (2019). Maastricht antiarrhythmic drug evaluator (MANTA): a computational tool for better understanding of antiarrhythmic drugs. *Pharmacol. Res.* 148:104444. doi: 10.1016/j.phrs.2019.104444

Suzuki, J., Kanemaru, K., and Iino, M. (2016). Genetically encoded fluorescent indicators for organellar calcium imaging. *Biophys. J.* 111, 1119–1131. doi: 10.1016/j.bpj.2016.04.054

Swan, H., Piippo, K., Viitasalo, M., Heikkilä, P., Paavonen, T., Kainulainen, K., et al. (1999). Arrhythmic disorder mapped to chromosome 1q42–q43 causes malignant polymorphic ventricular tachycardia in structurally normal hearts. *J. Am. Coll. Cardiol.* 34, 2035–2042. doi: 10.1016/S0735-1097(99)00461-1

Szlovák, J., Tomek, J., Zhou, X., Tóth, N., Veress, R., Horváth, B., et al. (2021). Blockade of sodium-calcium exchanger via ORM-10962 attenuates cardiac alternans. *J. Mol. Cell. Cardiol.* 153, 111–122. doi: 10.1016/j.yjmcc.2020.12.015

Takahashi, K., and Yamanaka, S. (2006). Induction of pluripotent stem cells from mouse embryonic and adult fibroblast cultures by defined factors. *Cell* 126, 663–676. doi: 10.1016/j.cell.2006.07.024

Tanner, M. R., and Beeton, C. (2018). Differences in ion channel phenotype and function between humans and animal models. *Front. Biosci.* 23, 43–64. doi: 10.2741/4581

Ter Keurs, H. E., and Boyden, P. A. (2007). Calcium and arrhythmogenesis. *Physiol. Rev.* 87, 457–506. doi: 10.1152/physrev.00011.2006

Tertoolen, L. G. J., Braam, S. R., Van Meer, B. J., Passier, R., and Mummery, C. L. (2018). Interpretation of field potentials measured on a multi electrode array in pharmacological toxicity screening on primary and human pluripotent stem cell-derived cardiomyocytes. *Biochem. Biophys. Res. Commun.* 497, 1135–1141. doi: 10.1016/j.bbrc.2017.01.151

Tessadori, F., Roessler, H. I., Savelberg, S. M., Chocron, S., Kamel, S. M., Duran, K. J., et al. (2018). Effective CRISPR/Cas9-based nucleotide editing in zebrafish to model human genetic cardiovascular disorders. *Dis. Model. Mech.* 11:dmm035469. doi: 10.1242/dmm.035469

Thireau, J., Zhang, B. L., Poisson, D., and Babuty, D. (2008). Heart rate variability in mice: a theoretical and practical guide. *Exp. Physiol.* 93, 83–94. doi: 10.1113/expphysiol.2007.040733

Thomas, K. R., and Capecchi, M. R. (1987). Site-directed mutagenesis by gene targeting in mouse embryo-derived stem cells. *Cell* 51, 503–512. doi: 10.1016/0092-8674(87)90646-5

Tomek, J., Bueno-Orovio, A., Passini, E., Zhou, X., Minchole, A., Britton, O., et al. (2019a). Development, calibration, and validation of a novel human ventricular myocyte model in health, disease, and drug block. *Elife* 8:e48890. doi: 10.7554/eLife.48890

Tomek, J., Hao, G., Tomková, M., Lewis, A., Carr, C., Paterson, D. J., et al. (2019b). β-Adrenergic receptor stimulation and alternans in the border zone of a healed infarct: an ex vivo study and computational investigation of arrhythmogenesis. *Front. Physiol.* 10:350. doi: 10.3389/fphys.2019.00350

Tomek, J., Wang, Z. J., Burton, R. A. B., Herring, N., and Bub, G. (2021). COSMAS: a lightweight toolbox for cardiac optical mapping analysis. *Sci. Rep.* 11:9147. doi: 10.1038/s41598-021-87402-9

Trovato, C., Passini, E., Nagy, N., Varró, A., Abi-Gerges, N., Severi, S., et al. (2020). Human Purkinje in silico model enables mechanistic investigations into automaticity and pro-arrhythmic abnormalities. *J. Mol. Cell. Cardiol.* 142, 24–38. doi: 10.1016/j.yjmcc.2020.04.001

Tse, G., Wong, S. T., Tse, V., and Yeo, J. M. (2016). Monophasic action potential recordings: which is the recording electrode? *J. Basic Clin. Physiol. Pharmacol.* 27, 457–462. doi: 10.1515/jbcpp-2016-0007

Tsien, R. Y. (1983). Intracellular measurements of ion activities. *Annu. Rev. Biophys. Bioeng.* 12, 91–116. doi: 10.1146/annurev.bb.12.060183.000515

Ulucan, C., Wang, X., Baljinnyam, E., Bai, Y., Okumura, S., Sato, M., et al. (2007). Developmental changes in gene expression of Epac and its upregulation in myocardial hypertrophy. *Am. J. Phys. Heart Circ. Phys.* 293, H1662–H1672. doi: 10.1152/ajpheart.00159.2007

Vakrou, S., Fukunaga, R., Foster, D. B., Sorensen, L., Liu, Y., Guan, Y., et al. (2018). Allele-specific differences in transcriptome, miRNome, and mitochondrial function in two hypertrophic cardiomyopathy mouse models. *JCI Insight* 3:e94493. doi: 10.1172/jci.insight.94493

Van Meer, B. J., Tertoolen, L. G., and Mummery, C. L. (2016). Concise review: measuring physiological responses of human pluripotent stem cell derived cardiomyocytes to drugs and disease. *Stem Cells* 34, 2008–2015. doi: 10.1002/stem.2403

VanderBrink, B. A., Link, M. S., Aronovitz, M. J., Saba, S., Sloan, S. B., Homoud, M. K., et al. (1999). Assessment of atrioventricular nodal physiology in the mouse. *J. Interv. Card. Electrophysiol.* 3, 207–212. doi: 10.1023/A:1009842105146

Verheugt, C. L., Uiterwaal, C. S., van der Velde, E. T., Meijboom, F. J., Pieper, P. G., Sieswerda, G. T., et al. (2010). The emerging burden of hospital admissions of adults with congenital heart disease. *Heart* 96, 872–878. doi: 10.1136/hrt.2009.185595

Wang, L., Feng, Z. P., Kondo, C. S., Sheldon, R. S., and Duff, H. J. (1996). Developmental changes in the delayed rectifier K^+ channels in mouse heart. *Circ. Res.* 79, 79–85. doi: 10.1161/01.RES.79.1.79

Wang, L., Morotti, S., Tapa, S., Francis Stuart, S. D., Jiang, Y., Wang, Z., et al. (2019). Different paths, same destination: divergent action potential responses produce conserved cardiac fight-or-flight response in mouse and rabbit hearts. *J. Physiol.* 597, 3867–3883. doi: 10.1113/JP278016

Wang, Z. J., Santiago, A., Zhou, X., Wang, L., Margara, F., Levrero-Florencio, F., et al. (2021). Human biventricular electromechanical simulations on the progression of electrocardiographic and mechanical abnormalities in post-myocardial infarction. *EP Eur.* 23(Supplement_1), i143–i152. doi: 10.1093/europace/euaa405

Wells, S. P., Waddell, H. M., Sim, C. B., Lim, S. Y., Bernasochi, G. B., Pavlovic, D., et al. (2019). Cardiomyocyte functional screening: interrogating comparative electrophysiology of high-throughput model cell systems. *Am. J. Phys. Cell Phys.* 317, C1256–C1267. doi: 10.1152/ajpcell.00306.2019

Wen, Q., Gandhi, K., Capel, R. A., Hao, G., O'Shea, C., Neagu, G., et al. (2018). Transverse cardiac slicing and optical imaging for analysis of transmural gradients in membrane potential and Ca^{2+} transients in murine heart. *J. Physiol.* 596, 3951–3965. doi: 10.1113/JP276239

Wiersma, M., Meijering, R. A., Qi, X. Y., Zhang, D., Liu, T., Hoogstra-Berends, F., et al. (2017). Endoplasmic reticulum stress is associated with autophagy and cardiomyocyte remodeling in experimental and human atrial fibrillation. *J. Am. Heart Assoc.* 6:e006458. doi: 10.1161/JAHA.117.006458

Wiersma, M., van Marion, D., Wüst, R. C., Houtkooper, R. H., Zhang, D., de Groot, N., et al. (2019). Mitochondrial dysfunction underlies cardiomyocyte remodeling in experimental and clinical atrial fibrillation. *Cell* 8:1202. doi: 10.3390/cells8101202

Winter, J., Bishop, M. J., Wilder, C. D., O'Shea, C., Pavlovic, D., and Shattock, M. J. (2018). Sympathetic nervous regulation of calcium and action potential alternans in the intact heart. *Front. Physiol.* 9:16. doi: 10.3389/fphys.2018.00016

Workman, A. J., Kane, K. A., and Rankin, A. C. (2001). The contribution of ionic currents to changes in refractoriness of human atrial myocytes associated with chronic atrial fibrillation. *Cardiovasc. Res.* 52, 226–235. doi: 10.1016/S0008-6363(01)00380-7

Wu, Z. J., Huang, Y., Fu, Y. C., Zhao, X. J., Zhu, C., Zhang, Y., et al. (2015). Characterization of a Chinese KCNQ1 mutation (R259H) that shortens repolarization and causes short QT syndrome 2. *J. Geriatr. Cardiol.* 12, 378–382. doi: 10.11909/j.issn.1671-5411.2015.04.009

Wu, N., Nishioka, W. K., Derecki, N. C., and Maher, M. P. (2019). High-throughput-compatible assays using a genetically-encoded calcium indicator. *Sci. Rep.* 9:12692. doi: 10.1038/s41598-019-49070-8

Xie, W., Santulli, G., Reiken, S. R., Yuan, Q., Osborne, B. W., Chen, B. X., et al. (2015). Mitochondrial oxidative stress promotes atrial fibrillation. *Sci. Rep.* 5:11427. doi: 10.1038/srep18115

Yildirir, A., Batur, M. K., and Oto, A. (2002). Hypertension and arrhythmia: blood pressure control and beyond. *Europace* 4, 175–182. doi: 10.1053/eupc.2002.0227

Yin, G., Hassan, F., Haroun, A. R., Murphy, L. L., Crotti, L., Schwartz, P. J., et al. (2014). Arrhythmogenic calmodulin mutations disrupt intracellular cardiomyocyte Ca^{2+} regulation by distinct mechanisms. *J. Am. Heart Assoc.* 3:e000996. doi: 10.1161/JAHA.114.000996

Yu, J. K., Franceschi, W., Huang, Q., Pashakhanloo, F., Boyle, P. M., and Trayanova, N. A. (2019). A comprehensive, multiscale framework for evaluation of arrhythmias arising from cell therapy in the whole post-myocardial infarcted heart. *Sci. Rep.* 9:9238. doi: 10.1038/s41598-019-45684-0

Yu, J. K., Liang, J. A., Weinberg, S. H., and Trayanova, N. A. (2021). Computational modeling of aberrant electrical activity following remuscularization with intramyocardially injected pluripotent stem cell-derived cardiomyocytes. *J. Mol. Cell. Cardiol.* 162, 97–109. doi: 10.1016/j.yjmcc.2021.08.011

Yue, L., Feng, J., Li, G. R., and Nattel, S. (1996). Transient outward and delayed rectifier currents in canine atrium: properties and role of isolation methods. *Am. J. Phys. Heart Circ. Phys.* 270, H2157–H2168. doi: 10.1152/ajpheart.1996.270.6.H2157

Zarei, A., Razban, V., Hosseini, S. E., and Tabei, S. M. B. (2019). Creating cell and animal models of human disease by genome editing using CRISPR/Cas9. *J. Gene Med.* 21:e3082. doi: 10.1002/jgm.3082

Zhang, D., Hu, X., Li, J., Hoogstra-Berends, F., Zhuang, Q., Esteban, M. A., et al. (2018). Converse role of class I and class IIa HDACs in the progression of atrial fibrillation. *J. Mol. Cell. Cardiol.* 125, 39–49. doi: 10.1016/j.yjmcc.2018.09.010

Zhang, H., Iijima, K., Huang, J., Walcott, G. P., and Rogers, J. M. (2016). Optical mapping of membrane potential and epicardial deformation in beating hearts. *Biophys. J.* 111, 438–451. doi: 10.1016/j.bpj.2016.03.043

Zhang, H., Viveiros, A., Nikhanj, A., Nguyen, Q., Wang, K., Wang, W., et al. (2021). The human explanted heart program: a translational bridge for cardiovascular medicine. *Biochim. Biophys. Acta Mol. Basis Dis.* 1867:165995. doi: 10.1016/j.bbadis.2020.165995

Zhao, J., Hansen, B. J., Wang, Y., Csepe, T. A., Sul, L. V., Tang, A., et al. (2017). Three-dimensional integrated functional, structural, and computational mapping to define the structural "fingerprints" of heart-specific atrial fibrillation drivers in human heart ex vivo. *J. Am. Heart Assoc.* 6:e005922. doi: 10.1161/JAHA.117.005922

Zhao, Y. T., Valdivia, C. R., Gurrola, G. B., Hernández, J. J., and Valdivia, H. H. (2015). Arrhythmogenic mechanisms in ryanodine receptor channelopathies. *Sci. China Life Sci.* 58, 54–58. doi: 10.1007/s11427-014-4778-z

Zhao, Y., Yun, M., Nguyen, S. A., Tran, M., and Nguyen, T. P. (2019). In vivo surface electrocardiography for adult Zebrafish. *J. Vis. Exp.* 150:e60011. doi: 10.3791/60011

Zhou, X., Bueno-Orovio, A., Schilling, R. J., Kirkby, C., Denning, C., Rajamohan, D., et al. (2019). Investigating the complex arrhythmic phenotype caused by the gain-of-function mutation KCNQ1-G229D. *Front. Physiol.* 10:259. doi: 10.3389/fphys.2019.00259

Zhu, F., Nair, R. R., Fisher, E. M., and Cunningham, T. J. (2019). Humanising the mouse genome piece by piece. *Nat. Commun.* 10:1845. doi: 10.1038/s41467-019-09716-7

Ziaeian, B., and Fonarow, G. C. (2016). Epidemiology and aetiology of heart failure. *Nat. Rev. Cardiol.* 13, 368–378. doi: 10.1038/nrcardio.2016.25

Zile, M. A., and Trayanova, N. A. (2017). Myofilament protein dynamics modulate EAD formation in human hypertrophic cardiomyopathy. *Prog. Biophys. Mol. Biol.* 130, 418–428. doi: 10.1016/j.pbiomolbio.2017.06.015

Conflict of Interest: The authors declare that the research was conducted in the absence of any commercial or financial relationships that could be construed as a potential conflict of interest.

Publisher's Note: All claims expressed in this article are solely those of the authors and do not necessarily represent those of their affiliated organizations, or those of the publisher, the editors and the reviewers. Any product that may be evaluated in this article, or claim that may be made by its manufacturer, is not guaranteed or endorsed by the publisher.

frontiers in Physiology

ORIGINAL RESEARCH
published: 14 February 2022
doi: 10.3389/fphys.2021.741317

Long-Term Endurance Exercise Training Alters Repolarization in a New Rabbit Athlete's Heart Model

Péter Kui[1†], Alexandra Polyák[1,2,3†], Nikolett Morvay[1], László Tiszlavicz[4], Norbert Nagy[1,3], Balázs Ördög[1], Hedvig Takács[2], István Leprán[1], András Farkas[2], Julius Gy. Papp[1,3], Norbert Jost[1,3], András Varró[1,3,5], István Baczkó[1,5‡] and Attila S. Farkas[2‡]*

[1] Department of Pharmacology and Pharmacotherapy, Albert Szent-Györgyi Medical School, University of Szeged, Szeged, Hungary, [2] Department of Internal Medicine, Albert Szent-Györgyi Medical School, University of Szeged, Szeged, Hungary, [3] ELKH-SZTE Working Group of Cardiovascular Pharmacology, Szeged, Hungary, [4] Department of Pathology, Albert Szent-Györgyi Medical School, University of Szeged, Szeged, Hungary, [5] Department of Pharmacology and Pharmacotherapy, Interdisciplinary Excellence Centre, Albert Szent-Györgyi Medical School, University of Szeged, Szeged, Hungary

OPEN ACCESS

Edited by:
Elisabetta Cerbai, University of Florence, Italy

Reviewed by:
Matthew Hardy, University of Bradford, United Kingdom
Sanjay Ram Kharche, Western University, Canada

***Correspondence:**
András Varró
varro.andras@med.u-szeged.hu

†These authors share first authorship
‡These authors share last authorship

Specialty section:
This article was submitted to Cardiac Electrophysiology, a section of the journal Frontiers in Physiology

Received: *14 July 2021*
Accepted: *22 October 2021*
Published: *14 February 2022*

Citation:
Kui P, Polyák A, Morvay N, Tiszlavicz L, Nagy N, Ördög B, Takács H, Leprán I, Farkas A, Papp JG, Jost N, Varró A, Baczkó I and Farkas AS (2022) Long-Term Endurance Exercise Training Alters Repolarization in a New Rabbit Athlete's Heart Model. Front. Physiol. 12:741317. doi: 10.3389/fphys.2021.741317

In the present study, the effect of long-term exercise training was investigated on myocardial morphological and functional remodeling and on proarrhythmic sensitivity in a rabbit athlete's heart model. New-Zealand white rabbits were trained during a 12-week long treadmill running protocol and compared with their sedentary controls. At the end of the training protocol, echocardiography, *in vivo* and *in vitro* ECG recordings, proarrhythmic sensitivity with dofetilide (nM) were performed in isolated hearts, and action potential duration (APD) measurements at different potassium concentrations (4.5 and 2 mM) were made in the isolated papillary muscles. Expression levels of the slow component of delayed rectifier potassium current and fibrosis synthesis and degradation biomarkers were quantified. Echocardiography showed a significantly dilated left ventricle in the running rabbits. ECG PQ and RR intervals were significantly longer in the exercised group (79 ± 2 vs. 69 ± 2 ms and 325 ± 11 vs. 265 ± 6 ms, $p < 0.05$, respectively). The *in vivo* heart rate variability (HRV) (SD of root mean square: 5.2 ± 1.4 ms vs. 1.4 ± 0.2 ms, $p < 0.05$) and Tpeak-Tend variability were higher in the running rabbits. Bradycardia disappeared in the exercised group *in vitro*. Dofetilide tended to increase the QTc interval in a greater extent, and significantly increased the number of arrhythmic beats in the trained animals *in vitro*. APD was longer in the exercised group at a low potassium level. Real-time quantitative PCR (RT-qPCR) showed significantly greater messenger RNA expression of fibrotic biomarkers in the exercised group. Increased repolarization variability and higher arrhythmia incidences, lengthened APD at a low potassium level, increased fibrotic biomarker gene expressions may indicate higher sensitivity of the rabbit "athlete's heart" to life-threatening arrhythmias.

Keywords: athlete's heart, physical endurance, arrhythmia, ventricular remodeling, biological markers, repolarization abnormality

INTRODUCTION

Strong physical exercise induces hemodynamic changes in competitive athletes, which leads to adaptive morphological and functional remodeling of the heart described as "athlete's heart" (O'Keefe et al., 2012). Sports activities improve quality of life and life expectancy, however, a number of tragic sudden cardiac death (SCD) events involving young competitive athletes have been recently reported conveying a devastating emotional impact on families and on the community. While SCD among athletes is rare, approximately 1–2:100,000, it is still 2–4 times more frequent in athletes than in their age-matched controls (Maron et al., 2009).

Numerous pathological anomalies have been associated with SCD in athletes (hypertrophic cardiomyopathy, arrhythmogenic right ventricular cardiomyopathy, etc.), although autopsy findings were inconclusive and normal hearts were demonstrated in 3–6% of the SCD cases among top athletes (Maron et al., 2009). In a review article, Varró and Baczkó proposed a mechanism underlying SCD in athletes that are based on repolarization abnormalities due to potassium channel downregulation, and the concurrent presence of several additional factors, such as cardiac muscle remodeling with the increase of collagen deposits, left ventricular hypertrophy, autonomous nervous system imbalance, genetic defects, electrolyte imbalance (e.g., hypokalemia and hypomagnesemia), certain drugs, doping agents, and dietary ingredients. These factors together can increase the repolarization heterogeneity leading to life-threatening arrhythmias (Varro and Baczko, 2010).

It would be crucial to accurately distinguish benign physiological, morphological, and electrical alterations from those considered to represent potentially serious diseases. The career of athletes is secondary to their lives, although the prevention of the unnecessary termination of career of an athlete and to minimize the risk of SCD are important. However, insights into the electrophysiological features of human athlete's heart are limited. Thus, it is necessary to obtain further information from appropriate animal models to fortify current knowledge.

As preliminary results, we have recently introduced a long-term endurance training induced rabbit athlete's heart model, which shares some properties with the human athlete's heart (Polyak et al., 2018). In the present study, we investigated whether sustained intensive exercise training-induced potentially adverse myocardial morphological and functional remodeling and increased the arrhythmia sensitivity in isolated rabbit "athlete's hearts."

MATERIALS AND METHODS

Ethical Statement

Animal maintenance and research were conducted in accordance with the National Institutes of Health Guide for the Care and Use of Laboratory Animals. All procedures using animals were approved by the local ethics committee (including the Ethical Committee for the Protection of Animals in Research at the University of Szeged, Hungary) and conformed to the rules and principles of the 86/609/EEC Directive.

Experimental Protocol

New Zealand white rabbits from either sex, weighing 3,500–4,000 g, were randomized into sedentary ("Sed," n = 7, 4 male rabbits and 3 female rabbits) and exercised ("Ex," n = 7, 5 male rabbits and 2 female rabbits) groups. "Ex rabbits" underwent a 12-week-long training session, while the "Sed" group did not participate in the training protocol. Running sessions were performed on a self-developed treadmill system, with two separated corridors for the animals and a control panel to modulate speed intensity. The protocol started with a 2-week-long warm-up period, thereafter animals were trained for 5 days/week with 40 min daily running sessions for 12 weeks. The speed intensity of the treadmill was increased progressively and set to 2.5 km/h. Rabbits were supervised continuously throughout the training protocol.

In vivo Echocardiography and ECG

Echocardiography was performed at 0 and 12 weeks of the training protocol. Rabbits were anesthetized with intramuscular ketamine injected into thigh muscle (50 mg/kg). Then, they were shaved at the chest and kept in a supine position on a heating pad. M-mode parasternal long-axis view was applied using an 11.5 MHz transducer (GE 10S-RS, GE Healthcare, Chicago, IL, United States), connected to an echocardiographic imaging unit (Vivid S5, GE Healthcare, Chicago, IL, United States). All parameters were analyzed by an investigator in a randomized and blinded manner. The diameter of ascending aorta, left ventricle (LVID), thickness of the left ventricular posterior wall (LVPW), and interventricular septum (IVS) at systole and diastole were measured in M-mode images. A more extended echocardiography analysis description is shown in **Supplementary Material**.

After completing the 12-week training protocol, *in vivo* ECG recording was made with needle electrodes that were placed subcutaneously in all four limbs. ECGs were recorded simultaneously with the National Instruments data acquisition hardware (PC card, National Instruments, Austin, TX, United States) and SPEL Advanced Hemosys software (version 3.26, Experimetria Ltd. and Logirex Software Laboratory, Budapest, Hungary).

Proarrhythmia Protocol in Isolated Hearts

Langendorff-perfusion of the hearts was performed after completion of the *in vivo* ECG at 12th week, as described earlier (Farkas et al., 2006). Briefly, rabbits were anticoagulated with sodium heparin and anesthetized with sodium pentobarbital (∼80 mg/kg) injected into the marginal ear vein. Hearts were rapidly removed *via* thoracotomy and rinsed in ice-cold modified Krebs-Henseleit buffer, which contains (in mM): NaCl 118.5, glucose 11.1, $MgSO_4$ 0.5, NaH_2PO_4 1.2, KCl 3, $NaHCO_3$ 25, and $CaCl_2$ 1.8. The aorta was cannulated and hanged on a Langendorff apparatus. All hearts were retrogradely

perfused with modified Krebs-Henseleit buffer for 15 min ("initial perfusion" period), followed by a 30-min perfusion with dofetilide (a selective blocker of the rapid delayed rectifier potassium current) at a concentration of 50 nM ("Dof" period). Our previous examinations showed that dofetilide at this concentration did not provoke Torsades de Pointes (TdP) in healthy isolated rabbit hearts (in contrast to 100 nM) (Farkas et al., 2006), which offered scope for the examination of additional effects that can further increase the incidence of this arrhythmia. In the third period of the protocol, hearts were perfused with modified Krebs-Henseleit buffer again for 30 min to remove the effect of the dofetilide ("washout" period). Volume-conducted ECG was recorded with the National Instruments data acquisition hardware and SPEL Advanced Hemosys software (MDE Gmbh, Heidelberg, Germany).

Recording Action Potentials in Multicellular Papillary Muscles

Action potentials were recorded at 37°C from the surface of right ventricular papillary muscles using conventional microelectrode techniques. The preparations were mounted in a custom made plexiglass chamber, allowing continuous superfusion with O_2 saturated Locke solution (containing in mM: NaCl 118.5, KCl 4.5, $CaCl_2$ 2.0, $MgSO_4$ 1.0, NaH_2PO_4 1.2, NaHCO3 25.0, and glucose 10.0, the pH of this solution was set to 7.35 ± 0.05 when saturated with a mixture of 95% O_2 and 5% CO_2) and stimulated with constant current pulses of 1 ms duration at a rate of 1 Hz through a pair of bipolar platinum electrodes using an electrostimulator (Hugo-Sachs Elektronic, modell 215/II, March, Germany). Sharp microelectrodes with tip resistance of 10–20 MΩ, when filled with 3 M KCl, were connected to an amplifier (BioLogic amplifier, model VF 102, Claix, France). The voltage output from the amplifier was sampled using an AD converter (NI 6025, Unisip Ltd, Budapest, Hungary). APD, determined at 25 and 90% level of repolarization, was obtained using Evokewave v1.49 (Unisip Ltd., Budapest, Hungary). After a 30 min of equilibration, 10 consecutive pulses with a cycle length of 400 ms were applied before the hypokalemic (2 mM) Locke solution and the pacing protocol was repeated. Triangulation was calculated as a difference between APD_{90} and APD_{25}. Efforts were also made to maintain the same impalement throughout the whole experiment. When the impalement was dislodged, an adjustment was attempted. The measurements were only continued if the action potential characteristics of the re-established impalement deviated less than 5% from the previous one.

Measurement of the ECG Intervals *in vivo* and *in vitro*

After the 12 weeks training protocol under ketamine (50 mg/kg im.) anesthesia, 20 min of ECG was registered with four limb needle ECG electrodes. *In vivo* ECG intervals were measured at the 10th min after initiation of the recording according to Farkas et al. (2004). *In vitro* ECG parameters of the Langendorff perfused rabbit hearts were evaluated in sinus rhythm 1 min before the end of "initial perfusion" period and 10 min after the start of the "Dof" period (as shown in **Supplementary Material**). RR, PQ, QRS, QT, and Tpeak-Tend (interval between the peak and end of the T wave) intervals were measured by manual positioning on screen markers of 40 consecutive sinus beats, and mean values were calculated. The QT interval was defined as the time from the first deviation from the isoelectric line during the PR interval until the end of the T wave. Where the T wave overlapped the following P wave or the QRS complex of the subsequent beat, the extrapolation method was applied to measure the length of the QT interval, that is, the end of the T wave was extrapolated from the curve of the T wave to the isoelectric line under the P wave or the QRS complex. Since the QT interval is influenced by the heart rate, the rate corrected QT interval (QTc) was calculated with a correction method described earlier (Farkas et al., 2009; Polyak et al., 2018). Baseline data in sinus rhythm for QT intervals together with the corresponding RR intervals were obtained from *in vitro* and

TABLE 1 | Echocardiography parameters.

	Before training protocol			After training protocol		
	"Sedentary" group	"Exercised" group	*p*-value	"Sedentary" group	"Exercised" group	*p*-value
IVSd, mm	3.28 ± 0.16	3.18 ± 0.15	0.646	3.24 ± 0.21	3.03 ± 0.16	0.437
IVSs, mm	4.69 ± 0.15	4.79 ± 0.05	0.525	4.75 ± 0.23	4.20 ± 0.24	0.129
LVIDd, mm	14.70 ± 0.54	15.80 ± 0.32	0.104	14.44 ± 0.62	17.25 ± 0.31	**0.002***
LVIDs, mm	10.58 ± 0.36	10.84 ± 0.21	0.537	10.57 ± 0.58	11.81 ± 0.29	0.078
LVPWd, mm	3.13 ± 0.13	3.07 ± 0.13	0.141	3.13 ± 0.20	2.94 ± 0.13	0.447
LVPWs, mm	4.74 ± 0.24	4.95 ± 0.27	0.577	4.59 ± 0.22	4.96 ± 0.42	0.447
Ao, mm	8.64 ± 0.29	9.02 ± 0.28	0.374	7.98 ± 0.16	9.09 ± 0.41	**0.027***
EF,%	64.29 ± 3.09	61.57 ± 1.85	0.466	57.43 ± 3.17	64.29 ± 2.47	0.113
FS,%	32.43 ± 2.42	30.43 ± 1.25	0.477	27,86 ± 2.04	32.71 ± 1.7	0.092

The effect of exercise training on echocardiographic cardiac dimensions and performance values were measured before (at 0th week, control measurements) and after (at 12th week) the training protocol.

IVSs and IVSd, interventricular septum in systole and diastole; LVIDs and LVIDd, left ventricular internal diameter in systole and diastole; LVPWs and LVPWd, left ventricular posterior wall in systole and diastole; Ao, aortic root diameter; EF, ejection fraction; FS, fractional shortening.

*All values are means ± SEM. *P < 0.05 vs. 'Sedentary' (embolded in the text).*

in vivo pooled ECG data of our laboratory (containing hundreds of *in vitro* and *in vivo* rabbit experiments). Rate corrected QT interval (QTc) was calculated both at *in vivo* [$QTc_n = QT_n - 0.354 \cdot (RR_{n-1} - 295)$] (Polyak et al., 2018) and *in vitro* [$QTc_n = QT_n - 0.326 \cdot (RR_{n-1} - 404)$] (Farkas et al., 2009) using formulas developed by our laboratory.

The T_{peak}-T_{end} interval was measured according to Antzelevitch and Oliva (2006) in the standard limb Lead II of the ECG. When the end of the T_{peak}-T_{end} interval overlapped the following P wave, the extrapolation method (Farkas et al., 2004) was applied.

Measurement of the Beat-to-Beat Variability and Instability of the ECG Intervals in Sinus Rhythm

Beat-to-beat variability and instability (BVI) parameters of the RR, PQ, QRS, QT, and Tpeak-Tend intervals were calculated from 40 consecutive sinus beats at the same time points where mean ECG intervals were measured according to Farkas et al. (2009) and Orosz et al. (2014). A computer program was developed in a.NET environment to obtain the BVI parameters. The calculation of BVI parameters is summarized in **Supplementary Material**.

Arrhythmia Analysis

In vitro ECG recordings were replayed offline and arrhythmia incidences were calculated throughout the whole experiment ("initial perfusion," "dofetilide period," and "wash-out period"). Ventricular tachyarrhythmia definitions of Lambeth Conventions I (Walker et al., 1988) were applied together with all other (non-tachyarrhythmia) ventricular arrhythmia definitions of Lambeth Conventions II (Curtis et al., 2013). Runs of 4 or more consecutive ventricular premature beats without the TdP-like twisting QRS morphology were differentiated from TdP and were defined as ventricular tachycardia (Farkas et al., 2009). The total number of arrhythmic beats was calculated as the sum of all ventricular premature beats (i.e., arrhythmic beats in any kind of arrhythmia).

Histology and Morphometry

Total cardiac mass was measured after finishing the Langendorff protocol, then the atria were removed from the hearts, and ventricles were weighed to calculate heart-weight-to-body weight and ventricular-weight-to-body weight ratio.

Samples were taken from the left ventricular free wall for histological studies. Heart sections were stained with Crossman-trichrome to identify collagen deposition. Semiquantitative analysis was performed by a pathologist to score the degree of the interstitial fibrosis with the following criteria: 0 = negative; 1 = mild; and 2 = moderate. The pathologist was blinded to the training protocol of the animals.

Real-Time Quantitative PCR of Gene Expressions of Fibrotic Biomarkers and I_{Kr} and I_{Ks}

RNA was isolated from left ventricular free wall samples with the Direct-zol RNA MiniPrep (Zymo Research, Irvine, CA, United States, Cat. No. R2051). cDNA molecules were synthesized from mRNA templates by reverse transcription, using High-Capacity cDNA Reverse Transcription Kit (Applied Biosystems, Waltham, MA, United States, Cat. No. 4368814). Real-time PCR was conducted with gene-specific primers and SYBR green (Thermo Fisher Scientific, Waltham, MA, United States, Cat. No. K0222) on ABI PRISM® 7000 Sequence Detection System (Thermo Fisher Scientific, Waltham, MA, United States, Cat. No. K0222). After each run, a melting point analysis was performed by measuring fluorescence intensity. The expression levels of fibrotic biomarker encoding genes were examined (transforming growth factor-β1, TGF-β; fibronectin-1, FN-1; pro-alpha1 chain of type I collagen, COL1A1; pro-alpha1 chain of type III collagen, COL3A1; matrix metalloproteinase-2, MMP-2; and tissue inhibitor of metalloproteinase-1, TIMP-1), as well as ion channel subunit expression underlying the rapidly and the slowly activating component of I_K channel: I_{Kr} (KCNH2) and I_{Ks} (KCNQ1), respectively. We calculated the relative copy numbers of mRNAs by normalizing each cDNA to the geometric average of β-actin (ACTB), signal-recognition-particle assembly 14 (SRP14), and ribosomal protein S5 (RPS5) expression.

Statistical Analysis

Continuous data were expressed as mean ± SEM. Independent variables from echocardiographic parameters, ECG intervals, BVI parameters, arrhythmia numbers, and fibrosis scores were compared with Mann–Whitney *U*-test as independent variables between the groups. The repeated measure of ANOVA was applied to compare the prolongation of the QTc interval. Relative gene expression was evaluated by using *t*-test type 3. $p < 0.05$ was taken as indicative of a statistically significant difference between values.

RESULTS

Echocardiography

At the end of the protocol, endurance training resulted in significantly greater internal end-diastolic diameter of the left ventricle (LVIDd) (**Table 1**). The thickness of the LVPW and the IVS did not differ between the groups neither in systole nor in diastole (**Table 1**). Thus, the left ventricle became dilated due to the endurance training without ventricular hypertrophy. The diameter of the aorta became significantly greater in the "Ex" group compared with that in the "Sed" group. After long-term training, ejection fraction and fractional shortening did not differ between the "Ex" and "Sed" groups. The complete list of measured echocardiographic parameters is shown in **Table 1**.

ECG Intervals *in vivo* and *in vitro*

The intervals PQ and RR were significantly longer in running rabbits possibly indicating an increased vagal tone. QT and T_{peak}-T_{end} intervals were significantly longer in the "Ex" group compared with those measured in the control rabbits. However, the heart rate corrected QT (QTc) values did not differ between the "Ex" and "Sed" groups indicating a

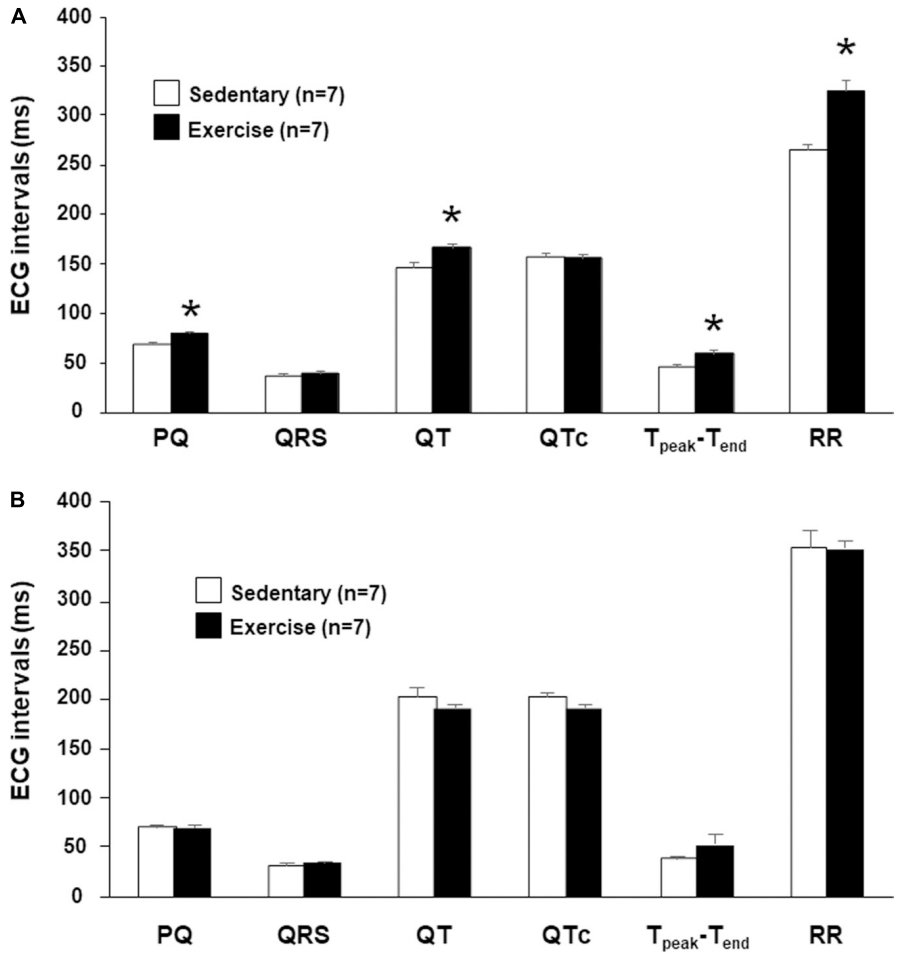

FIGURE 1 | The mean *in vivo* **(A)** and *in vitro* **(B)** ECG intervals at 12th week. Values were derived from 40 consecutive ventricular complexes during sinus rhythm. All values are shown as mean ± SEM. *$p < 0.05$ vs. "Sedentary."

frequency dependency of the length of repolarization. There was no significant difference in the QRS intervals, thus the ventricular depolarization was not affected by the intensive training (**Figure 1A**).

In isolated perfused hearts, the heart rate (RR interval) and the atrioventricular propagation time (PQ interval) were not different in the two groups (**Figure 1B**). Therefore, increased parasympathetic tone disappeared in the "Ex" group due to the denervation. No significant differences were found in any baseline ECG intervals at the beginning of the *in vitro* proarrhythmia protocol (**Figure 1B**).

Beat-to-Beat Variability and Instability Parameters *in vivo*

Most of the calculated BVI parameters of the RR intervals (heart rate variability [HRV]) showed a marked and significant increase in running rabbits in comparison with the control group (**Figure 2A**), which indicates an increased vagal tone in the exercised animals. Analysis of repolarization variability parameters showed a significant increase in all the T_{peak}-T_{end} BVI parameters in trained animals compared with the sedentary group (**Figure 2B**). Interestingly, no significant differences were found between the "Ex" and "Sed" groups regarding QT variability (**Figure 2C**).

Beat-to-Beat Variability and Instability Parameters *in vitro,* the Effect of Dofetilide

Importantly, the HRV parameters (RR variability parameters) markedly decreased when the hearts were removed and Langendorff perfused, which indicates the cessation of parasympathetic tone (**Table 2**).

The I_{Kr} inhibitor dofetilide at a concentration of 50 nM was applied to test the sensitivity of repolarization of the rabbit athletes' hearts in the Langendorff preparation, *in vitro*. Dofetilide markedly increased the QTc interval in the hearts of "Ex" and "Sed" groups too, however, the QTc prolongation was more pronounced in the exercised hearts (**Figure 3A**). Mean values of the PQ, QRS, and T_{peak}-T_{end} intervals did not differ

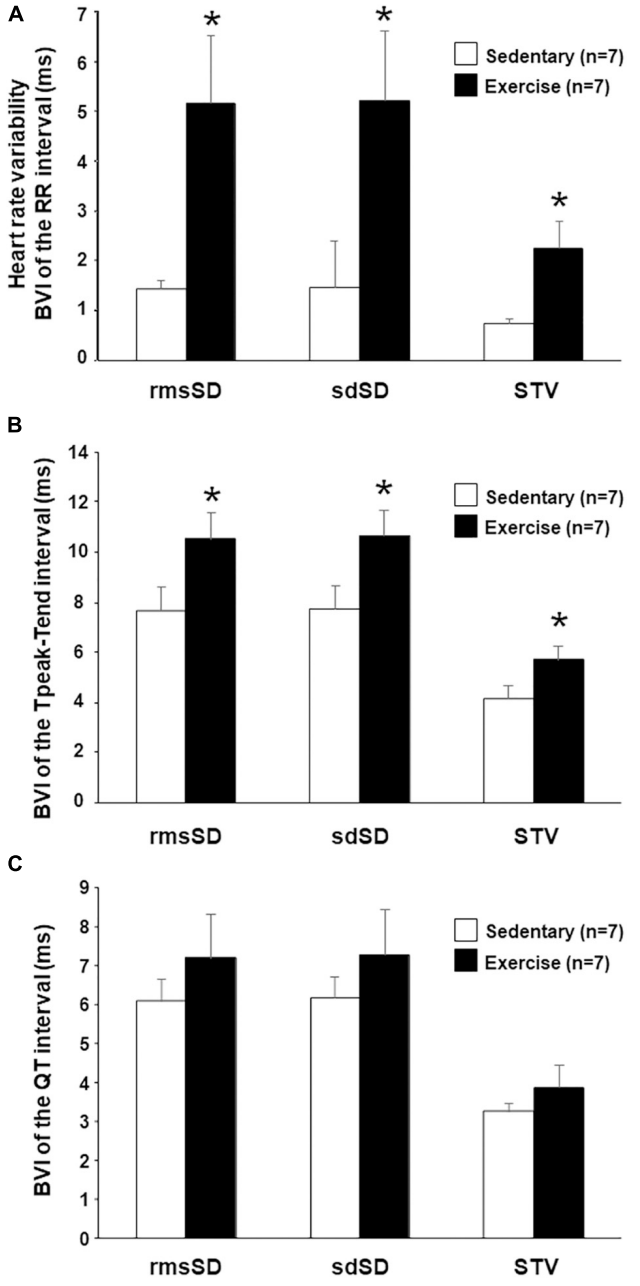

FIGURE 2 | *In vivo* beat-to-beat variability parameters (BVI) of the RR interval **(A)**, T_{peak}-T_{end} **(B)**, and QT intervals **(C)** at 12th week. RMS, root mean square; rmsSD, root mean square of successive differences; sdSD, SD of successive differences; STV, short-term variability. All values are shown as mean ± SEM. *$p < 0.05$ vs. "Sedentary."

significantly between the groups in either experimental period (data not shown).

No significant difference was found in the BVI parameters of any ECG intervals between the "Ex" and "Sed" groups at the beginning and at the end of the initial drug-free perfusion. Dofetilide perfusion tended to increase the QT and $T_{peak}T_{end}$ variability parameters in the hearts of "Ex" and "Sed" groups too, but no significant differences were found in these parameters between the groups (data not shown).

Arrhythmia Susceptibility Analysis in Isolated Hearts

The number of arrhythmic beats did not differ between the "Ex" and "Sed" groups during drug-free "Initial perfusion." However, dofetilide perfusion significantly increases the number of arrhythmic beats in the "Ex" group as compared with the "Sed" group (**Figure 3B**). The previous endurance training had a tendency to increase the number or ventricular tachycardias during dofetilide perfusion in the hearts of the "Ex group," but this parameter did not differ significantly between the "Sed" and "Ex" group (**Figure 3C**). TdP ventricular tachycardia did not develop during dofetilide perfusion in any groups. There was no significant difference in any arrhythmia parameters between the groups during the washout period (data not shown).

Action Potential Duration Measurements in Multicellular Papillary Muscle Preparations

The durations of the action potentials were compared in papillary muscles obtained from exercised and sedentary animals under normal and lower potassium levels (**Figures 4A,B**). No difference was found in the APDs between the "Ex" and "Sed" groups under normal potassium (4.5 mM) level (**Figure 4C**). However, under low potassium (2.0 mM) circumstances, the APD was significantly longer in exercised papillary muscles than that measured in the sedentary ones (**Figure 4C**). Also, when low potassium solution was applied, the rate of triangulation was significantly larger in the exercised group than that measured in the sedentary group (**Figure 4D**).

Relative Gene Expression Analysis

After 12-week of endurance training, the relative gene expression of fibrosis synthesis and degradation biomarkers of the left ventricle free wall was assessed. The level of mRNA expression of COL3A1, MMP-2, and TIMP-1 were significantly increased in the "Ex" group as compared with that measured in the "Sed" group. COL1A1 and FN-1 expression showed a moderate, but not significant increase in the exercised group (**Figure 5A**). The expression level of TGF-ß was similar in the "Ex" and "Sed" groups (**Figure 5A**).

The *KCNH2* (hERG, the main pore-forming subunit responsible for I_{Kr}) gene was expressed at approximately the same level in the "Ex" and "Sed" groups (**Figure 5B**). The expression level of the I_{Ks}-related channel encoding *KCNQ1* was slightly lower in the exercised hearts, but the difference proved to be not statistically significant between the "Ex" and "Sed" groups (**Figure 5B**).

Morphometry and Histology

The total heart weight, ventricular weight, and their ratios to body weight were determined after the completion of the Langendorff perfusion protocol. The long-term exercise increased these

TABLE 2 | Heart rate variability parameters.

	In vivo			*In vitro*		
	"Sedentary" group	**"Exercised" group**	***p*-value**	**"Sedentary" group**	**"Exercised" group**	***p*-value**
$Mean_{RR}$, ms	265.5 ± 5.7	324.5 ± 10.5	**0.001***	354.2 ± 17.9	352.5 ± 8.3	0.930
SD_{RR}, ms	1.5 ± 0.2	4.4 ± 0.8	**0.026***	1.6 ± 0.7	3.4 ± 1.7	0.360
RMS_{RR}, ms	265.5 ± 5.7	324.5 ± 10.5	**0.001***	354.2 ± 17.9	352.5 ± 8.3	0.931
$rmsSD_{RR}$, ms	1.4 ± 0.2	5.2 ± 1.4	**0.035***	2.2 ± 1.2	5.0 ± 2.8	0.401
$sdSD_{RR}$, ms	1.5 ± 0.2	5.2 ± 1.4	**0.047***	2.2 ± 1.2	5.1 ± 2.8	0.401
STV_{RR}, ms	0.7 ± 0.1	2.2 ± 0.5	**0.016***	0.7 ± 0.2	2.0 ± 0.9	0.199
LTV_{RR}, ms	1.4 ± 0.2	3.4 ± 0.8	**0.049***	1.0 ± 0.3	2.0 ± 0.8	0.317
TI_{RR}, ms	1.8 ± 0.2	4.1 ± 1.0	**0.047***	1.0 ± 0.2	2.3 ± 0.5	**0.032***

Heart rate variability (HRV) parameters in vivo and in vitro.
RMS, root mean square; rmsSD, root mean square of successive differences; sdSD, SD of successive differences; STV, short-term variability; LTV, long-term variability; TI, total instability.
*All values are means ± SEM. *P < 0.05 vs. 'Sedentary' (embolded in the text).*

parameters (except bodyweight), however, the difference was not significant (**Figure 6A**).

To assess the level of collagen deposition in the left ventricle, Crossman's trichrome staining was performed. Similarly, to the relative gene expression results, semiquantitative score analysis showed an increased level of fibrosis in the "Ex" group compared with that in the "Sed" group (**Figures 6B,C**).

DISCUSSION

This study is the extension of our earlier long-term endurance training-induced rabbit athlete's heart model study (Polyak et al., 2018) giving more insights into the electrophysiological properties of the model. Long-term physical exercise decreased the resting heart rate and increased the HRV, which indicates an increased parasympathetic tone as a result of long-term training. Morphological adaptations, such as left ventricle end-diastolic and relative aortic diameter dilation were found, which was accompanied by a close to significant left ventricular fibrosis together with a significantly increased fibrotic gene expression.

Additionally, the present study tested the proarrhythmic sensitivity of isolated rabbit athlete's hearts. An increased arrhythmic beat activity and a close to significant QTc prolongation were observed in exercised isolated hearts challenged with the I_{Kr} inhibitor dofetilide. In addition, papillary muscles from exercised hearts were more sensitive to the APD-prolonging and triangulation-increasing effects of dofetilide under low potassium concentrations. These results imply an increased proarrhythmic sensitivity in the exercised rabbit hearts. Based on these results, our rabbit animal model with the applied training protocol may be a useful experimental model for further investigations of the cardiovascular effects of long-term physical exercise.

A Rabbit Model to Mimic the Human Athlete's Heart

To our knowledge, our recently introduced rabbit model is the first to mimic a human athlete's heart, especially on the cardiac electrophysiological level (Polyak et al., 2018). Radovits et al. (2013) developed a rat training model where swimming-induced left ventricular hypertrophy was found by echocardiography and histomorphometry. Chen et al. (2000) and Benito et al. (2011) applied a treadmill system for long-term endurance training of rats. It must be emphasized that mouse and rat have distinctly different potassium channel expression patterns than other mammals including humans. Rat and mouse myocytes lack functional sarcolemmal I_{Kr} and I_{Ks} potassium currents (Tamargo et al., 2004), thus repolarization-related arrhythmias cannot be examined in these species, and results cannot be extrapolated to humans. Some acute and chronic endurance training rabbit models have been described, although less of them investigated the cardiovascular effects of exercise, especially on the electrophysiological level (Lozano et al., 2020). Gaustad et al. (2010) tested a VO2max protocol in rabbits and found that rabbit is a suitable species for studying responses to training and could be of great importance for showing novel cellular cardiac adaptations for training. Hexeberg et al. (1995) found a structural myocardial remodeling and increased contractile reserve after a 10-week exercise training program on rabbits. They concluded that rabbits can be used to study the myocardial effects of endurance training. Considering the ion channel kinetic properties, the I_{Ks} measured in dog (Liu and Antzelevitch, 1995) and rabbit ventricles (Lengyel et al., 2001) best resemble that measured in human hearts. In this respect, the present study investigated the effects of endurance exercise training on cardiac remodeling in the rabbit that shares similar cardiac electrophysiological and autonomic neural properties with humans.

Based on recent studies, the treadmill running model seems to be the preferred option to investigate the effect of chronic physical exercise since it allows uniform and well-controlled exercise workloads (Hoydal et al., 2007). Previous studies demonstrated that rabbits could obtain a documented cardiovascular training effect by using the proper intensity, duration, and frequency of exercise (DiCarlo and Bishop, 1990; Liu et al., 2000). Carroll and Kyser (2002) used a rabbit model to determine the effects of exercise training during the development of obesity, by 12-week-long treadmill protocol at 18–20 m/min (1.2 km/h) of maximum speed and 50–60-min daily running

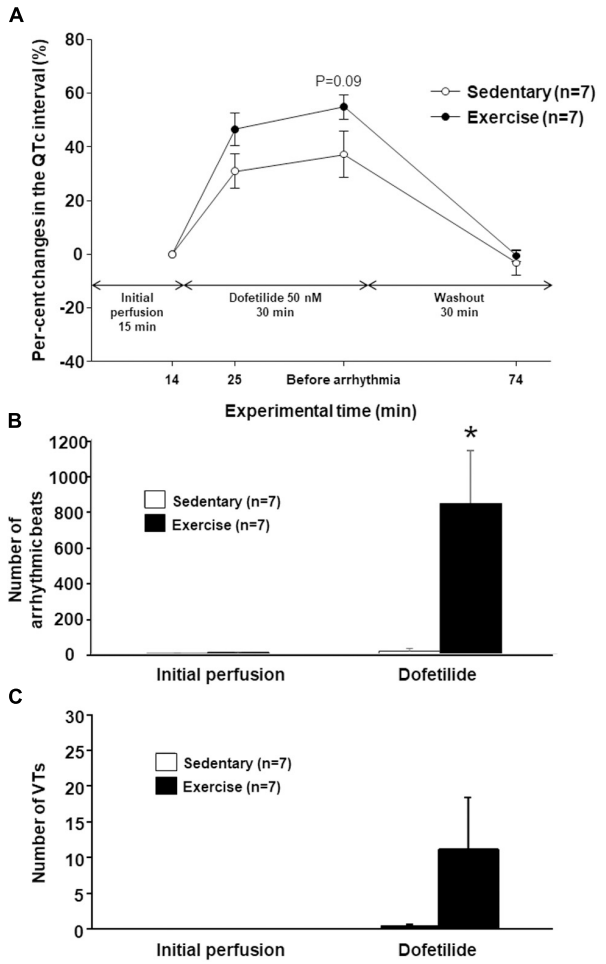

FIGURE 3 | The percentage change in the mean heart rate-corrected QT (QTc) interval under dofetilide challenge *in vitro* in the last minute before dofetilide administration (14th min), 10 min after the start of dofetilide infusion (25th min), immediately before arrhythmia occurred, and after "Washout" (74th min) **(A)**. The total number of arrhythmic beats **(B)** and the number of ventricular tachycardia episodes **(C)** under dofetilide challenge *in vitro*. All values are shown as mean ± SEM. *$p < 0.05$ vs. "Sedentary."

sessions. Exercise-trained rabbits had slower resting heart rates in both lean and obese animals (Carroll and Kyser, 2002). Such et al. (2008) found lower resting heart rates and longer ventricular effective refractory periods at similar workload in rabbits.

The applied running protocol in our model made the participating rabbits physically tired and sometimes exhausted. As the New Zealand white rabbit is a relatively physically inactive species, this workload is thought to be convenient to mimic regular, high-intensity human training activity.

Morphological Adaptations of the Cardiovascular System to Long-Term Exercise

Strongly related to the type of sports activity, Morganroth et al. (1975) arbitrarily classified the athletic endeavors into "isometric" and "isotonic" varieties, based on the presumptive hemodynamic stresses of the two types of activity. In "isotonic exercise" activities (e.g., long-distance running, cycling, and swimming), the change in LV architecture might be considered a form of eccentric remodeling in that both chamber size and LV mass are increased, similar to those in chronic volume overloads (Kim and Baggish, 2016). Recently, D'Andrea et al. (2010b) reported significantly greater LV end-diastolic diameter in endurance-trained athletes than in the strength-trained athletes and control participants.

Similar to these earlier findings in athletes, increased cardiac LV end-diastolic diameter was detected in the exercised rabbit group, which indicates a structural response to the increased cardiac volume load and corresponds to the effect of long-term endurance training. Our endurance-trained rabbits presented a relatively greater aortic root diameter compared with the control group, which implies the effect of cardiac volume overload in these exercised animals. These results are in a good accordance with the results of a large cohort study of competitive athletes, where male endurance athletes showed greater aortic and LV cavity dimensions than sex-matched strength athletes (Pelliccia et al., 1999). Significantly greater aortic root diameter was found in elite strength-trained athletes (D'Andrea et al., 2010a). Neither IVS, nor posterior wall thickening was detected, LV contractile function (EF and FS) remained normal in this model that represents a physiologic adaptation to vigorous exercise training. Similarly, Such et al. (2008) did not observe differences between sedentary and exercised rabbit hearts in terms of hypertrophy. However, endurance-trained athletes may show LV wall thickening, parallel with the extreme LV dilatation (Pelliccia et al., 1999). The reason for different echocardiography results concerning hypertrophy might be the outcome of the different hemodynamic and loading conditions of the heart depending on various training activities. This indicates that myocardial adaptations may depend on the cardiac pressure loads and exercise-related cardiac blood volumes in different sports activities (Hoogsteen et al., 2004).

Cardiac Fibrotic Changes and Lower I_{Ks}-Related Gene Expression Associated With Long-Term Physical Exercise

Myocardial extracellular matrix (ECM) is a complex microenvironment containing a large portfolio of matrix proteins, signaling molecules, proteases, and cell types that play a fundamental role in the myocardial remodeling process (Spinale, 2007). Fibrosis and inflammatory infiltrates have been identified in well-trained athletes (Tahir et al., 2017) and forced swimming rats (Chen et al., 2000). Benito et al. (2011) demonstrated an increase in atrial and ventricular inflammation and fibrosis and a greater risk of ventricular arrhythmias in the "marathon rats" after treadmill exercise. Our significantly increased MMP-2 and TIMP-1 gene expressions, which play an important role in the degradation of cardiac ECM (Brown et al., 2005), indicate higher fibrotic activity in exercised hearts. The balance of MMPs and TIMP determine the maintenance of interstitial tissue homeostasis. Similarly, to our results, increased levels of MMP-2 and TIMP-1 were found in rats after acute exhaustive swimming (Olah et al., 2015). Polyakova et al. (2011) found higher levels of Collagen type I and II, TIMP1, MMP2 in

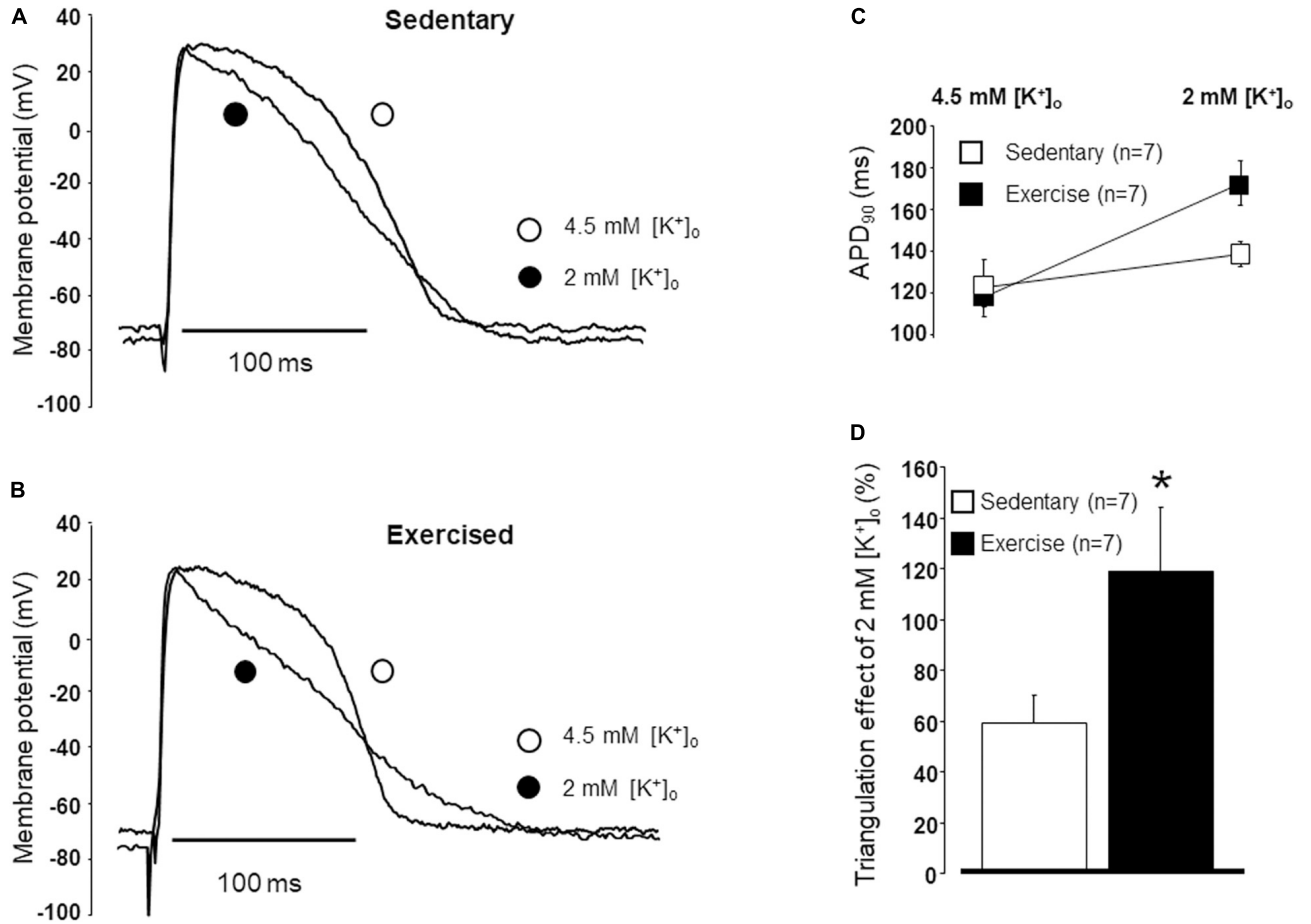

FIGURE 4 | Representative examples of the action potentials in papillary muscles obtained from hearts excised from sedentary **(A)** and exercised **(B)** animals under normal and low potassium levels. The duration of the action potential measured at 90% repolarization (APD_{90}) in papillary muscles obtained from hearts excised from sedentary and exercised animals under normal (4.5 mM) and low (2.0 mM) potassium levels **(C)**. Triangulation measured in papillary muscles obtained from hearts excised from sedentary and exercised animals under low potassium levels **(D)**. All values are shown as mean ± SEM. $^*p < 0.05$ vs. "Sedentary."

explanted human hearts with heart failure due to either dilated, ischemic or inflammatory cardiomyopathy (myocarditis) as compared with controls. Collagen type I and collagen type III are the two major components of the cardiac ECM (Polyakova et al., 2011). The relative gene expression of type III collagen in our study was significantly greater in the exercised group in our study. Similar results were found in cardiac remodeling in heart failure (Zannad et al., 2010) and in spontaneous hypertensive rats, where the ratio of collagen type I/III was decreased after 10 weeks compared with normotensive control rats, meanwhile the collagen concentration did not differ between the groups (Mukherjee and Sen, 1990). Since collagen type III is a major component of the cardiac ECM, its qualitative-quantitative changes may have an important role in cardiac pathophysiology. The higher collagen synthesis promotes higher expression of TIMP and MMP. The histological analysis of the hearts of the rabbits in our study implies that long-term exercise-induced fibrosis in the myocardium. These histology results were strongly corroborated by our gene expression data. The collagen deposition and consequent myocardial fibrosis is a result of an imbalance of synthetic/degradative events. Fibrotic changes affect impulse conduction in the heart, and thus fibrosis may increase the risk of the development of ventricular arrhythmias (Morita et al., 2014).

It was postulated in some reviews that potassium channel downregulation may be present in an athlete's heart (Varro and Baczko, 2010). The current study has examined the most common long QT syndrome-susceptibility genes encoding key ion channel subunits *KCNQ1* (LQT1) and *KCNH2* (LQT2). We found slightly decreased I_{Ks}-related channel *KCNQ1* levels in the exercised hearts. I_{Ks} downregulation accompanied by an incorrect QT adaptation may result in higher arrhythmic risk especially during sympathetic stress (i.e., high-level exercise) (Tseng and Xu, 2015). I_{Ks} downregulation might contribute to the higher dispersion facilitating the development of reentry circuits (Varro and Baczko, 2010). Interestingly, I_{Ks} downregulation was found in the chronic AV blocked dog model, which shares some similar properties with the athlete's heart in terms of cardiac adaptation (Volders et al., 1999). In addition, hypokalemia is known to increase I_{Ks} and decrease I_{Kr} (Varro et al., 2021).

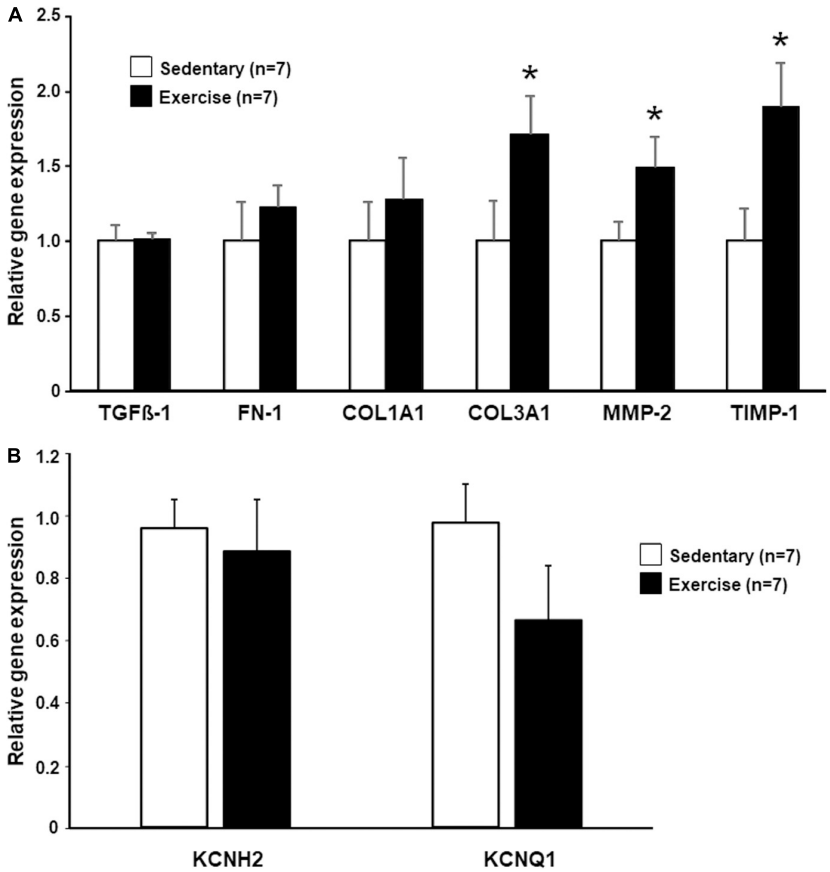

FIGURE 5 | The relative expression levels of different fibrosis synthesis and degradation biomarker genes **(A)** and I_{Kr}- and I_{Ks}-related genes **(B)** determined by real-time quantitative PCR (qRT-PCR). The mRNA levels were quantified in tissue samples collected from the left ventricle (LV). The data were normalized to the expression level of β-actin (ACTB), SRP14, and RPS5, and are presented as mean ± SEM. *$p < 0.05$ vs. "Sedentary."

Therefore, the application of dofetilide which inhibits I_{Kr} can produce a more robust effect on repolarization in case I_{Ks} is downregulated and thereby the hypokalemia cannot properly compensate for the loss of I_{Kr} density.

Exercise Training Increased Parasympathetic Activity

Reduced heart rate and HRV, i.e., the beat-to-beat variability of the cycle length (RR interval) in sinus rhythm *in vivo,* are considered parameters of parasympathetic activity (Aubert et al., 2003). Accordingly, exercise training elicited significant reductions in baseline heart rate accompanied by significant increases in almost all examined sinus HRV parameters in our running rabbits. With regards to atrial electrophysiological properties, exercise training increased PQ interval (atrioventricular conduction time) *in vivo*. These results correlate well with the increased time-domain indices of HRV presented in competitive athletes (Langdeau et al., 2001). Studies using a canine model of sudden death demonstrate that endurance exercise training (treadmill running) enhanced cardiac parasympathetic regulation (increased heart rate variability) and protected against ventricular fibrillation induced by acute myocardial ischemia (Billman, 2009). Bilateral vagotomy prevents the development of TdP in rabbits *in vivo* (Farkas et al., 2008). Furthermore, bradycardia in the absence of increased vagal tone contributes to the arrhythmogenesis. Thus, the increased vagal tone and bradycardia might have importance in the arrhythmia development.

Recently, Boyett et al. (2013) have shown that training-induced bradycardia in rats resulted from the reduced expression of the *HCN4* gene, i.e., downregulation of the channels conducting the pacemaker I_f current rather than as a consequence of changes in the cardiac autonomic regulation. In our study, exercise training might have had only a minor effect on intrinsic heart rate since heart rate and HRV differences disappeared in isolated hearts. The difference between the results can be accounted for methodological and species differences. Since we have not investigated *HCN4* expression in our present study, some downregulation of I_f in our model cannot be ruled out.

Ventricular Repolarization in the Rabbit Athlete's Heart

Previous studies found longer QTc in endurance athletes compared with age-matched controls (Lengyel et al., 2011). However, several authors have demonstrated a prolonged QTc

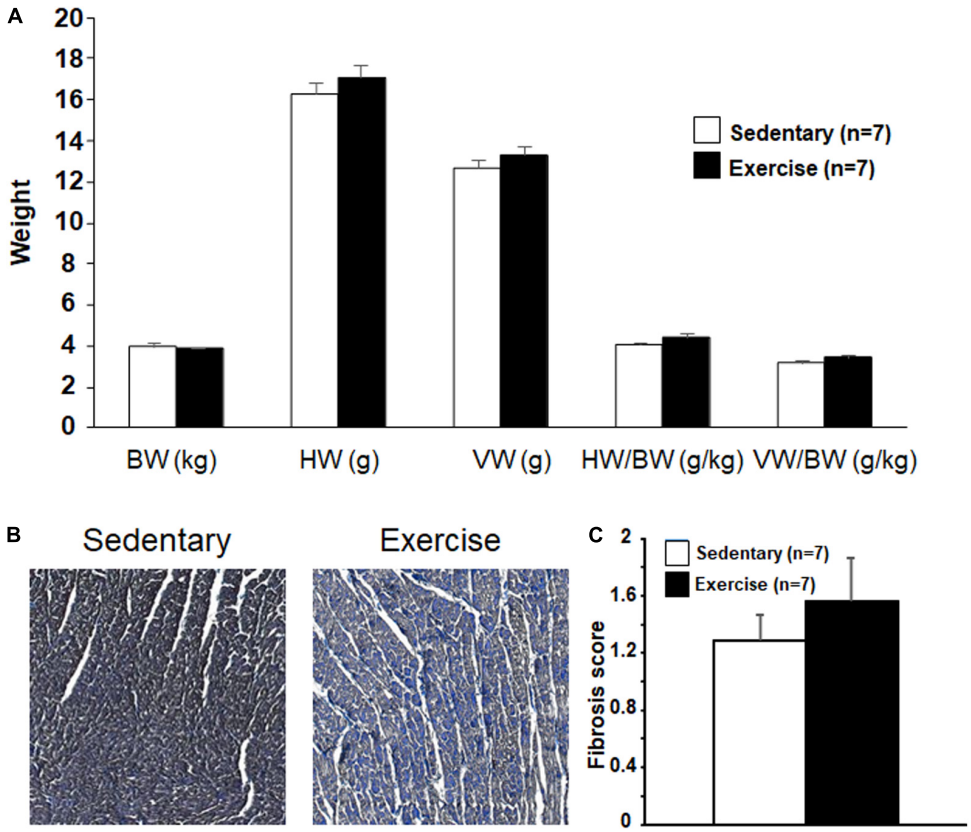

FIGURE 6 | The mean values for body weight (BW), heart weight (HW), ventricular weight (VW), HW/BW, and VW/BW ratio at 12th week **(A)** and representative Crossman's trichrome stains taken from histological sections of "Sedentary" and "Exercised" left ventricle **(B)** and the mean microscopic fibrosis scores for "Exercised" and "Sedentary" groups **(C)**. Pronounced interstitial fibrosis **(A)** and slightly increased fibrosis score **(B)** are present in the "Exercised" group. Heart weight and ventricular weight are in g and body weight in kg. All values are shown as mean ± SEM.

interval duration in athletes as an uncommon observation, and QTc prolongation was considered to be unrelated to sports activities (Basavarajaiah et al., 2007). These data correspond to our findings, since native QT values were significantly longer in the running rabbits, although the difference disappeared when QT intervals were corrected to heart rate (QTc).

The T_{peak}-T_{end} could forecast the development of TdP in LV wedge preparations (Fish et al., 2004) and in patients with LQT syndrome (Yamaguchi et al., 2003). Our experiments showed that long-term exercise significantly increased the duration of the T_{peak}-T_{end} interval *in vivo*, which may imply an increased proarrhythmic sensitivity of the exercised animals. Interestingly, the T_{peak}-T_{end} interval did not differ significantly between the "Ex" and "Sed" groups in Langendorff hearts, which indicates that the exercise-induced prolongation of the T_{peak}-T_{end} interval seen *in vivo* was caused by either bradycardia or activity of the autonomic nervous system.

Results of human investigations and *in vivo* and *in vitro* animal experiments (Hinterseer et al., 2010) pointed out that repolarization BVI parameters increase during electrical remodeling. Lengyel et al. (2011) found increased STV QT values in competitive soccer players raising the possibility of an increased propensity for ventricular arrhythmias in that population. In our study, BVI parameters of QT intervals tended to be increased in the exercised group *in vivo*. Moreover, BVI of T_{peak}-T_{end} intervals was significantly increased in the running rabbits *in vivo*, indicating altered repolarization due to long-term exercise.

Higher instability (ECG BVI parameter) and increased triangulation increase the proarrhythmic activity of drugs in isolated rabbit hearts even in the presence of lengthened or shortened ADP (Hondeghem et al., 2001). Thus, these parameters are regarded as proarrhythmia biomarkers. APD and triangulation were significantly prolonged in low K^+ conditions in exercised hearts in our study. Exercise-induced hypokalemia was observed after strenuous exercise (Lindinger, 1995; Atanasovska et al., 2018). Hypokalemia is generally thought to be due to the reuptake of potassium into the muscle after exercise perhaps as the result of the continuation of catecholamine stimulation of the sarcolemmal sodium/potassium ATPase without anaerobic metabolism or muscle ischemia. Hypokalemia can be more serious if the electrolyte supplementation was not adequate or use of diuretics (e.g., for hypertension treatment). Hypokalemia, particularly when acute, contributes to the direct suppression of cardiac K^+ channels and to the activation of Na^+ and Ca^{2+} channels that contribute to impaired

repolarization (Podrid, 1990; Weiss et al., 2017). Our results show that APD can lengthen, and triangulation may develop under hypokalemia in the myocardium after long-term exercise, which may have a role in arrhythmia development as a substrate.

Higher arrhythmic beat activity in the presence of I_{Kr} inhibition showed higher repolarization sensitivity in our model. The higher arrhythmic beat activity might provide triggers for re-entrant tachyarrhythmia, e.g., polymorphic tachycardia, under various conditions (Farkas and Nattel, 2010).

Limitation of Our Study

It has to be mentioned that our study has some limitations. First, rabbits do not tolerate well heavy exercise, and accordingly the exercise-induced changes in our study were rather modest. In addition, QTc measurements in rabbit are rather uncertain since rabbit has distinctly different frequency-dependent repolarization relations than those of human (Arpadffy-Lovas et al., 2020), which may cause problems to accurately detect small alterations. As rabbit myocardium differs from the human in terms of ionic channel profile (e.g., lower expression of I_{Ks} in rabbits) (Lu et al., 2002; Dumaine and Cordeiro, 2007), electrophysiological remodeling might have different effects on repolarization in humans. However, it should be kept in mind that rigorous endurance training sometimes fails to produce pronounced electrophysiological effects in humans and the enhanced proarrhythmic risk is only evident if other predisposing factors, such as HCM, hypokalemia, doping, or QT-prolonging drugs are present. The Langendorff protocol may influence the dry weight of the heart and ventricles due to edema. Male gender dominance in the experimental groups might influence the severity of the structural, functional, and electrophysiological remodeling. As the mRNA level does not always reflect the protein level, different protein levels as compared with the mRNA levels cannot be excluded.

CONCLUSION

In the present study, we extended our preliminarily published novel rabbit exercise-induced athlete's heart model (Polyak et al., 2018). The detected echocardiography changes and signs of increased parasympathetic activity resemble those of the human athlete's heart. The detected structural and functional changes in exercised rabbit hearts, e.g., increased fibrotic gene expression and alterations in repolarization, may directly contribute to the higher risk of the development of life-threatening arrhythmias in athletes, and the question that how enhanced vagal tone can contribute to the repolarization changes and possible enhanced proarrhythmic risk after heavy endurance training still needs further investigations.

DATA AVAILABILITY STATEMENT

The original contributions presented in the study are included in the article/**Supplementary Material**, further inquiries can be directed to the corresponding author/s.

ETHICS STATEMENT

All procedures using animals were approved by the local ethics committee (including the Ethical Committee for the Protection of Animals in Research at the University of Szeged, Hungary) and conformed to the rules and principles of the 86/609/EEC Directive.

AUTHOR CONTRIBUTIONS

PK and HT performed the treadmill experiments and data collection. AP and BÖ performed the mRNA experiments. NN performed the APD experiments. LT managed the histology. IL, ArF, JP, and NJ managed the project and prepared the manuscript. AV, IB, and ASF performed the data collection, project management, and manuscript preparation. All authors contributed to the article and approved the submitted version.

FUNDING

This work was supported by the National Research Development and Innovation Office (NKFIH K-135464, NKFIH K-128851, FK-129117, and GINOP-2.3.2-15-2016-00047), the Ministry of Human Capacities Hungary (20391-3/2018/FEKUSTRAT and EFOP3.6.2-16-2017-00006), and from the Eötvös Loránd Research Network.

SUPPLEMENTARY MATERIAL

The Supplementary Material for this article can be found online at: https://www.frontiersin.org/articles/10.3389/fphys.2021.741317/full#supplementary-material

REFERENCES

Antzelevitch, C., and Oliva, A. (2006). Amplification of spatial dispersion of repolarization underlies sudden cardiac death associated with catecholaminergic polymorphic VT, long QT, short QT and Brugada syndromes. *J. Intern. Med.* 259, 48–58. doi: 10.1111/j.1365-2796.2005.01587.x

Arpadffy-Lovas, T., Baczko, I., Balati, B., Bitay, M., Jost, N., Lengyel, C., et al. (2020). Electrical restitution and its modifications by antiarrhythmic drugs in undiseased human ventricular muscle. *Front. Pharmacol.* 11:479. doi: 10.3389/fphar.2020.00479

Atanasovska, T., Smith, R., Graff, C., Tran, C. T., Melgaard, J., Kanters, J. K., et al. (2018). Protection against severe hypokalemia but impaired cardiac repolarization after intense rowing exercise in healthy humans receiving salbutamol. *J. Appl. Physiol.* 125, 624–633. doi: 10.1152/japplphysiol.00680.2017

Aubert, A. E., Seps, B., and Beckers, F. (2003). Heart rate variability in athletes. *Sports Med.* 33, 889–919. doi: 10.2165/00007256-200333120-00003

Basavarajaiah, S., Wilson, M., Whyte, G., Shah, A., Behr, E., and Sharma, S. (2007). Prevalence and significance of an isolated long QT interval in elite athletes. *Eur. Heart J.* 28, 2944–2949. doi: 10.1093/eurheartj/ehm404

Benito, B., Gay-Jordi, G., Serrano-Mollar, A., Guasch, E., Shi, Y., Tardif, J. C., et al. (2011). Cardiac arrhythmogenic remodeling in a rat model of long-term intensive exercise training. *Circulation* 123, 13–22. doi: 10.1161/CIRCULATIONAHA.110.938282

Billman, G. E. (2009). Cardiac autonomic neural remodeling and susceptibility to sudden cardiac death: effect of endurance exercise training. *Am. J. Physiol. Heart Circ. Physiol.* 297, H1171–H1193. doi: 10.1152/ajpheart.00534.2009

Boyett, M. R., D'Souza, A., Zhang, H., Morris, G. M., Dobrzynski, H., and Monfredi, O. (2013). Viewpoint: is the resting bradycardia in athletes the result of remodeling of the sinoatrial node rather than high vagal tone? *J. Appl. Physiol.* 114, 1351–1355. doi: 10.1152/japplphysiol.01126.2012

Brown, R. D., Ambler, S. K., Mitchell, M. D., and Long, C. S. (2005). The cardiac fibroblast: therapeutic target in myocardial remodeling and failure. *Annu. Rev. Pharmacol. Toxicol.* 45, 657–687. doi: 10.1146/annurev.pharmtox.45.120403.095802

Carroll, J. F., and Kyser, C. K. (2002). Exercise training in obesity lowers blood pressure independent of weight change. *Med .Sci. Sports Exerc.* 34, 596–601. doi: 10.1097/00005768-200204000-00006

Chen, Y., Serfass, R. C., Mackey-Bojack, S. M., Kelly, K. L., Titus, J. L., and Apple, F. S. (2000). Cardiac troponin T alterations in myocardium and serum of rats after stressful, prolonged intense exercise. *J. Appl. Physiol.* 88, 1749–1755. doi: 10.1152/jappl.2000.88.5.1749

Curtis, M. J., Hancox, J. C., Farkas, A., Wainwright, C. L., Stables, C. L., Saint, D. A., et al. (2013). The lambeth conventions (II): guidelines for the study of animal and human ventricular and supraventricular arrhythmias. *Pharmacol. Ther.* 139, 213–248. doi: 10.1016/j.pharmthera.2013.04.008

D'Andrea, A., Cocchia, R., Riegler, L., Scarafile, R., Salerno, G., Gravino, R., et al. (2010a). Aortic root dimensions in elite athletes. *Am. J. Cardiol.* 105, 1629–1634. doi: 10.1016/j.amjcard.2010.01.028

D'Andrea, A., Cocchia, R., Riegler, L., Scarafile, R., Salerno, G., Gravino, R., et al. (2010b). Left ventricular myocardial velocities and deformation indexes in top-level athletes. *J. Am. Soc. Echocardiogr.* 23, 1281–1288. doi: 10.1016/j.echo.2010.09.020

DiCarlo, S. E., and Bishop, V. S. (1990). Regional vascular resistance during exercise: role of cardiac afferents and exercise training. *Am. J. Physiol.* 258(3 Pt 2), H842–H847. doi: 10.1152/ajpheart.1990.258.3.H842

Dumaine, R., and Cordeiro, J. M. (2007). Comparison of K+ currents in cardiac Purkinje cells isolated from rabbit and dog. *J. Mol. Cell Cardiol.* 42, 378–389. doi: 10.1016/j.yjmcc.2006.10.019

Farkas, A. S., Acsai, K., Tóth, A., Dézsi, L., Orosz, S., Forster, T., et al. (2006). Importance of extracardiac alpha1-adrenoceptor stimulation in assisting dofetilide to induce torsade de pointes in rabbit hearts. *Eur. J. Pharmacol.* 537, 118–125. doi: 10.1016/j.ejphar.2006.03.014

Farkas, A. S., and Nattel, S. (2010). Minimizing repolarization-related proarrhythmic risk in drug development and clinical practice. *Drugs* 70, 573–603. doi: 10.2165/11535230-000000000-00000

Farkas, A. S., Makra, P., Csík, N., Orosz, S., Shattock, M. J., Fülöp, F., et al. (2009). The role of the Na+/Ca2+ exchanger, I(Na) and I(CaL) in the genesis of dofetilide-induced torsades de pointes in isolated, AV-blocked rabbit hearts. *Br. J. Pharmacol.* 156, 920–932. doi: 10.1111/j.1476-5381.2008.00096.x

Farkas, A., Batey, A. J., and Coker, S. J. (2004). How to measure electrocardiographic QT interval in the anaesthetized rabbit. *J. Pharmacol. Toxicol. Methods* 50, 175–185. doi: 10.1016/j.vascn.2004.05.002

Farkas, A., Dempster, J., and Coker, S. J. (2008). Importance of vagally mediated bradycardia for the induction of torsade de pointes in an in vivo model. *Br. J. Pharmacol.* 154, 958–970. doi: 10.1038/bjp.2008.154

Fish, J. M., Di Diego, J. M., Nesterenko, V., and Antzelevitch, C. (2004). Epicardial activation of left ventricular wall prolongs QT interval and transmural dispersion of repolarization: implications for biventricular pacing. *Circulation* 109, 2136–2142. doi: 10.1161/01.CIR.0000127423.75608.A4

Gaustad, S. E., Rolim, N., and Wisloff, U. (2010). A valid and reproducible protocol for testing maximal oxygen uptake in rabbits. *Eur. J. Cardiovasc. Prev. Rehabil.* 17, 83–88. doi: 10.1097/HJR.0b013e32833090c4

Hexeberg, E., Westby, J., Hessevik, I., and Hexeberg, S. (1995). Effects of endurance training on left ventricular performance: a study in anaesthetized rabbits. *Acta Physiol. Scand.* 154, 479–488. doi: 10.1111/j.1748-1716.1995.tb09933.x

Hinterseer, M., Beckmann, B. M., Thomsen, M. B., Pfeufer, A., Ulbrich, M., Sinner, M. F., et al. (2010). Usefulness of short-term variability of QT intervals as a predictor for electrical remodeling and proarrhythmia in patients with nonischemic heart failure. *Am. J. Cardiol.* 106, 216–220. doi: 10.1016/j.amjcard.2010.02.033

Hondeghem, L. M., Carlsson, L., and Duker, G. (2001). Instability and triangulation of the action potential predict serious proarrhythmia, but action potential duration prolongation is antiarrhythmic. *Circulation* 103, 2004–2013. doi: 10.1161/01.cir.103.15.2004

Hoogsteen, J., Hoogeveen, A., Schaffers, H., Wijn, P. F., van Hemel, N. M., and van der Wall, E. E. (2004). Myocardial adaptation in different endurance sports: an echocardiographic study. *Int. J. Cardiovasc. Imaging* 20, 19–26. doi: 10.1023/b:caim.0000013160.79903.19

Hoydal, M. A., Wisloff, U., Kemi, O. J., and Ellingsen, O. (2007). Running speed and maximal oxygen uptake in rats and mice: practical implications for exercise training. *Eur. J. Cardiovasc. Prev. Rehabil.* 14, 753–760. doi: 10.1097/HJR.0b013e3281eacef1

Kim, J. H., and Baggish, A. L. (2016). Physical activity, endurance exercise, and excess-can one overdose? *Curr. Treat. Options Cardiovasc. Med.* 18:68. doi: 10.1007/s11936-016-0490-6

Langdeau, J. B., Blier, L., Turcotte, H., O'Hara, G., and Boulet, L. P. (2001). Electrocardiographic findings in athletes: the prevalence of left ventricular hypertrophy and conduction defects. *Can. J. Cardiol.* 17, 655–659.

Lengyel, C., Iost, N., Virag, L., Varro, A., Lathrop, D. A., and Papp, J. G. (2001). Pharmacological block of the slow component of the outward delayed rectifier current (I(Ks)) fails to lengthen rabbit ventricular muscle QT(c) and action potential duration. *Br. J. Pharmacol.* 132, 101–110. doi: 10.1038/sj.bjp.0703777

Lengyel, C., Orosz, A., Hegyi, P., Komka, Z., Udvardy, A., Bosnyak, E., et al. (2011). Increased short-term variability of the QT interval in professional soccer players: possible implications for arrhythmia prediction. *PLoS One* 6:e18751. doi: 10.1371/journal.pone.0018751

Lindinger, M. I. (1995). Potassium regulation during exercise and recovery in humans: implications for skeletal and cardiac muscle. *J. Mol. Cell Cardiol.* 27, 1011–1022. doi: 10.1016/0022-2828(95)90070-5

Liu, D. W., and Antzelevitch, C. (1995). Characteristics of the delayed rectifier current (IKr and IKs) in canine ventricular epicardial, midmyocardial, and endocardial myocytes. A weaker IKs contributes to the longer action potential of the M cell. *Circ. Res.* 76, 351–365. doi: 10.1161/01.res.76.3.351

Liu, J. L., Irvine, S., Reid, I. A., Patel, K. P., and Zucker, I. H. (2000). Chronic exercise reduces sympathetic nerve activity in rabbits with pacing-induced heart failure: a role for angiotensin II. *Circulation* 102, 1854–1862. doi: 10.1161/01.cir.102.15.1854

Lozano, W. M., Parra, G., Arias-Mutis, O. J., and Zarzoso, M. (2020). Exercise training protocols in rabbits applied in cardiovascular research. *Animals* 10:1263. doi: 10.3390/ani10081263

Lu, H. R., Vlaminckx, E., Van Ammel, K., and De Clerck, F. (2002). Drug-induced long QT in isolated rabbit Purkinje fibers: importance of action potential duration, triangulation and early afterdepolarizations. *Eur. J. Pharmacol.* 452, 183–192. doi: 10.1016/s0014-2999(02)02246-x

Maron, B. J., Doerer, J. J., Haas, T. S., Tierney, D. M., and Mueller, F. O. (2009). Sudden deaths in young competitive athletes: analysis of 1866 deaths in the United States, 1980-2006. *Circulation* 119, 1085–1092. doi: 10.1161/CIRCULATIONAHA.108.804617

Morganroth, J., Maron, B. J., Henry, W. L., and Epstein, S. E. (1975). Comparative left ventricular dimensions in trained athletes. *Ann. Intern. Med.* 82, 521–524. doi: 10.7326/0003-4819-82-4-521

Morita, N., Mandel, W. J., Kobayashi, Y., and Karagueuzian, H. S. (2014). Cardiac fibrosis as a determinant of ventricular tachyarrhythmias. *J. Arrhythm.* 30, 389–394. doi: 10.1016/j.joa.2013.12.008

Mukherjee, D., and Sen, S. (1990). Collagen phenotypes during development and regression of myocardial hypertrophy in spontaneously hypertensive rats. *Circ. Res.* 67, 1474–1480. doi: 10.1161/01.res.67.6.1474

O'Keefe, J. H., Patil, H. R., Lavie, C. J., Magalski, A., Vogel, R. A., and McCullough, P. A. (2012). Potential adverse cardiovascular effects from excessive

endurance exercise. *Mayo Clin. Proc.* 87, 587–595. doi: 10.1016/j.mayocp.2012.04.005

Olah, A., Nemeth, B. T., Matyas, C., Horvath, E. M., Hidi, L., Birtalan, E., et al. (2015). Cardiac effects of acute exhaustive exercise in a rat model. *Int. J. Cardiol.* 182, 258–266. doi: 10.1016/j.ijcard.2014.12.045

Orosz, S., Sarusi, A., Csík, N., Papp, J. G., Varró, A., Farkas, S., et al. (2014). Assessment of efficacy of proarrhythmia biomarkers in isolated rabbit hearts with attenuated repolarization reserve. *J. Cardiovasc. Pharmacol.* 64, 266–276. doi: 10.1097/FJC.0000000000000116

Pelliccia, A., Culasso, F., Di Paolo, F. M., and Maron, B. J. (1999). Physiologic left ventricular cavity dilatation in elite athletes. *Ann. Intern. Med.* 130, 23–31.

Podrid, P. J. (1990). Potassium and ventricular arrhythmias. *Am. J. Cardiol.* 65, 33E–44E. doi: 10.1016/0002-9149(90)90250-5

Polyak, A., Kui, P., Morvay, N., Lepran, I., Agoston, G., Varga, A., et al. (2018). Long-term endurance training-induced cardiac adaptation in new rabbit and dog animal models of the human athlete's heart. *Rev. Cardiovasc. Med.* 19, 135–142. doi: 10.31083/j.rcm.2018.04.4161

Polyakova, V., Loeffler, I., Hein, S., Miyagawa, S., Piotrowska, I., Dammer, S., et al. (2011). Fibrosis in endstage human heart failure: severe changes in collagen metabolism and MMP/TIMP profiles. *Int. J. Cardiol.* 151, 18–33. doi: 10.1016/j.ijcard.2010.04.053

Radovits, T., Olah, A., Lux, A., Nemeth, B. T., Hidi, L., Birtalan, E., et al. (2013). Rat model of exercise-induced cardiac hypertrophy: hemodynamic characterization using left ventricular pressure-volume analysis. *Am. J. Physiol. Heart Circ. Physiol.* 305, H124–H134. doi: 10.1152/ajpheart.00108.2013

Spinale, F. G. (2007). Myocardial matrix remodeling and the matrix metalloproteinases: influence on cardiac form and function. *Physiol. Rev.* 87, 1285–1342. doi: 10.1152/physrev.00012.2007

Such, L., Alberola, A. M., Such-Miquel, L., Lopez, L., Trapero, I., Pelechano, F., et al. (2008). Effects of chronic exercise on myocardial refractoriness: a study on isolated rabbit heart. *Acta Physiol.* 193, 331–339. doi: 10.1111/j.1748-1716.2008.01851.x

Tahir, E., Starekova, J., Muellerleile, K., von Stritzky, A., Munch, J., Avanesov, M., et al. (2017). Myocardial fibrosis in competitive triathletes detected by contrast-enhanced CMR correlates with exercise-induced hypertension and competition history. *JACC Cardiovasc. Imaging* 11, 1260–1270. doi: 10.1016/j.jcmg.2017.09.016

Tamargo, J., Caballero, R., Gomez, R., Valenzuela, C., and Delpon, E. (2004). Pharmacology of cardiac potassium channels. *Cardiovasc. Res.* 62, 9–33. doi: 10.1016/j.cardiores.2003.12.026

Tseng, G. N., and Xu, Y. (2015). Understanding the microscopic mechanisms for LQT1 needs a global view of the I(Ks) channel. *Heart Rhythm* 12, 395–396. doi: 10.1016/j.hrthm.2014.11.008

Varro, A., and Baczko, I. (2010). Possible mechanisms of sudden cardiac death in top athletes: a basic cardiac electrophysiological point of view. *Pflugers Arch.* 460, 31–40. doi: 10.1007/s00424-010-0798-0

Varro, A., Tomek, J., Nagy, N., Virag, L., Passini, E., Rodriguez, B., et al. (2021). Cardiac transmembrane ion channels and action potentials: cellular physiology and arrhythmogenic behavior. *Physiol. Rev.* 101, 1083–1176. doi: 10.1152/physrev.00024.2019

Volders, P. G., Sipido, K. R., Vos, M. A., Spatjens, R. L., Leunissen, J. D., Carmeliet, E., et al. (1999). Downregulation of delayed rectifier K(+) currents in dogs with chronic complete atrioventricular block and acquired torsades de pointes. *Circulation* 100, 2455–2461. doi: 10.1161/01.cir.100.24.2455

Walker, M. J., Curtis, M. J., Hearse, D. J., Campbell, R. W., Janse, M. J., Yellon, D. M., et al. (1988). The lambeth conventions: guidelines for the study of arrhythmias in ischaemia infarction, and reperfusion. *Cardiovasc. Res.* 22, 447–455. doi: 10.1093/cvr/22.7.447

Weiss, J. N., Qu, Z., and Shivkumar, K. (2017). Electrophysiology of hypokalemia and hyperkalemia. *Circ. Arrhythm. Electrophysiol.* 10:e004667. doi: 10.1161/CIRCEP.116.004667

Yamaguchi, M., Shimizu, M., Ino, H., Terai, H., Uchiyama, K., Oe, K., et al. (2003). T wave peak-to-end interval and QT dispersion in acquired long QT syndrome: a new index for arrhythmogenicity. *Clin. Sci.* 105, 671–676. doi: 10.1042/CS20030010

Zannad, F., Rossignol, P., and Iraqi, W. (2010). Extracellular matrix fibrotic markers in heart failure. *Heart Fail. Rev.* 15, 319–329. doi: 10.1007/s10741-009-9143-0

Conflict of Interest: The authors declare that the research was conducted in the absence of any commercial or financial relationships that could be construed as a potential conflict of interest.

Publisher's Note: All claims expressed in this article are solely those of the authors and do not necessarily represent those of their affiliated organizations, or those of the publisher, the editors and the reviewers. Any product that may be evaluated in this article, or claim that may be made by its manufacturer, is not guaranteed or endorsed by the publisher.

frontiers | Frontiers in Physiology

ORIGINAL RESEARCH
published: 19 April 2022
doi: 10.3389/fphys.2022.864547

Genotype-Driven Pathogenesis of Atrial Fibrillation in Hypertrophic Cardiomyopathy: The Case of Different *TNNT2* Mutations

Josè Manuel Pioner[1], *Giulia Vitale*[2], *Francesca Gentile*[2], *Beatrice Scellini*[2], *Nicoletta Piroddi*[2], *Elisabetta Cerbai*[3], *Iacopo Olivotto*[2], *Jil Tardiff*[4], *Raffaele Coppini*[3], *Chiara Tesi*[2], *Corrado Poggesi*[2] *and Cecilia Ferrantini*[2]*

[1]Department of Biology, University of Florence, Florence, Italy, [2]Department of Experimental and Clinical Medicine, University of Florence, Florence, Italy, [3]Department NeuroFarBa, University of Florence, Florence, Italy, [4]Department of Medicine and Biomedical Engineering, University of Arizona, Tucson, AZ, United States

OPEN ACCESS

Edited by:
Fabien Brette,
Institut National de la Santé et de la Recherche Médicale (INSERM), France

Reviewed by:
Olivier Cazorla,
Université de Montpellier, France
Charles Redwood,
University of Oxford, United Kingdom
Bogdan Iorga,
Hannover Medical School, Germany

***Correspondence:**
Cecilia Ferrantini
cecilia.ferrantini@unifi.it

Specialty section:
This article was submitted to Cardiac Electrophysiology, a section of the journal Frontiers in Physiology

Received: 28 January 2022
Accepted: 28 March 2022
Published: 19 April 2022

Citation:
Pioner JM, Vitale G, Gentile F, Scellini B, Piroddi N, Cerbai E, Olivotto I, Tardiff J, Coppini R, Tesi C, Poggesi C and Ferrantini C (2022) Genotype-Driven Pathogenesis of Atrial Fibrillation in Hypertrophic Cardiomyopathy: The Case of Different TNNT2 Mutations. Front. Physiol. 13:864547. doi: 10.3389/fphys.2022.864547

Atrial dilation and atrial fibrillation (AF) are common in Hypertrophic CardioMyopathy (HCM) patients and associated with a worsening of prognosis. The pathogenesis of atrial myopathy in HCM remains poorly investigated and no specific association with genotype has been identified. By re-analysis of our cohort of thin-filament HCM patients (Coppini et al. 2014) AF was identified in 10% of patients with sporadic mutations in the cardiac Troponin T gene (*TNNT2*), while AF occurrence was much higher (25–75%) in patients carrying specific "hot-spot" *TNNT2* mutations. To determine the molecular basis of arrhythmia occurrence, two HCM mouse models expressing human *TNNT2* variants (a "hot-spot" one, R92Q, and a "sporadic" one, E163R) were selected according to the different pathophysiological pathways previously demonstrated in ventricular tissue. Echocardiography studies showed a significant left atrial dilation in both models, but more pronounced in the R92Q. In E163R atrial trabeculae, in line with what previously observed in ventricular preparations, the energy cost of tension generation was markedly increased. However, no changes of twitch amplitude and kinetics were observed, and there was no atrial arrhythmic propensity. R92Q atrial trabeculae, instead, displayed normal ATP consumption but markedly increased myofilament calcium sensitivity, as previously observed in ventricular preparations. This was associated with reduced inotropic reserve and slower kinetics of twitch contractions and, importantly, with an increased occurrence of spontaneous beats and triggered contractions that represent an intrinsic arrhythmogenic mechanism promoting AF. The association of specific *TNNT2* mutations with AF occurrence depends on the mutation-driven pathomechanism (i.e., increased atrial myofilament calcium sensitivity rather than increased myofilament tension cost) and may influence the individual response to treatment.

Keywords: hypertrophic cardiomyopathy, atrial myopathy, atrial fibrillation, sarcomere mechanics, sarcomere energetics, excitation-contraction coupling, cardiac troponin T

INTRODUCTION

Although Hypertrophic CardioMyopathy (HCM) is mostly manifested as a disease of the left ventricle (LV), atria are often involved. In a community-based HCM population, atrial fibrillation (AF) is extremely common, with a 22% prevalence over 9 years, and is associated with an increased risk of heart failure-related mortality, stroke and severe functional disability, particularly in patients with LV outflow obstruction (Olivotto et al., 2008). The genes most frequently responsible for HCM (i.e. *MYH7* encoding for β-myosin heavy chains, *MYBPC3* encoding for myosin binding protein C and the gene encoding for the thin filament protein troponin T (*TNNT2*) (Olivotto et al., 2008; Biagini et al., 2014)) are not equally and uniformly expressed in the four cardiac chambers (Piroddi et al., 2007; Belus et al., 2010)). For instance, the β-myosin heavy chain (β-MHC:*MYH7*) isoform, target of HCM-related mutations, is poorly expressed in the atria (Walklate et al., 2021), while cardiac Troponin T (cTnT) is present in both chambers with the same isoform. cTnT, in particular, is a protein closely associated to the motor function and its calcium regulation. A few case reports describing the clinical phenotype of families with severe *TNNT2*-associated HCM highlighted a high incidence of ventricular and atrial arrhythmias, including AF, despite relatively mild ventricular hypertrophy (Tardiff, 2005). These anecdotal reports suggest that mutations in specific *TNNT2* gene hot-spots may trigger sarcomere-driven mechanisms (e.g., association with increased myofilament calcium sensitivity and changes of intracellular calcium buffering) that create an arrhythmogenic substrate in both atrial and ventricular chambers (Tardiff et al., 1999).

In 2014 (Coppini et al., 2014) we assessed the clinical features and outcomes in a large cohort of patients with HCM associated with thin-filament mutations. All participants were unrelated index patients, with *TNNT2* defects being the most common (53% of the thin-filament cohort). Other thin-filament genes were *TNNI3* (30%), *TPM1* (9%), and *ACTC* (8%). None carried double thin-filament mutations. Patients carrying mutations in the most represented genes, *TNNT2* and *TNNI3*, showed remarkably similar clinical features and outcome profile compared to the thick-filament: less prominent and atypically distributed LV hypertrophy, increased LV fibrosis, higher likelihood of adverse LV remodeling leading to functional deterioration, and more frequent occurrence of triphasic LV filling, reflecting profound diastolic dysfunction. Importantly, the occurrence of ventricular and atrial arrhythmias (particularly AF) in the thin-filament and thick-filament genes appears comparable. Of note, in the thin-filament group AF was most frequently treated in an aggressive way through chateher ablation. In this study no internal comparison was made among different thin-filament genes and specific mutations in a given gene.

A mutation-specific atrial remodeling in HCM was described in cTnT mutant mice carrying different mutations in the same spot of *TNNT2* (R92W, R92L, and R92Q) (Tardiff, 2005). The R92W mouse showed a severe biatrial dilation since birth while the R92L had normal atrial dimensions with a late-onset atrial dilation at 1 year of age. In the R92Q mutants (transgenic mouse lines expressing 30, 67, and 92% of their total cTnT protein as the R92Q mutant), atria were dilated at early disease stages and, importantly, atrial dimensions increased proportionally with the level of transgenic protein expression (Tardiff et al., 1999). By employing the 67% R92Q mutant, we recently showed that atrial dilation can be prevented in the R92Q mice, if treated with ranolazine since birth (Coppini et al., 2017).

In the present work 1) we described the association of individual *TNNT2* mutations with AF by revising the clinical atrial data from 45 *TNNT2*-HCM index patients 2) to clarify the cellular basis of atrial pro-arrhythmogenic substrate we studied the energetics, mechanics and contractility of atrial myocardium from two well known HCM mouse models expressing *TNNT2* mutations (R92Q and E163R) selected because of their likely different association to AF. In our patient cohort R92Q is a hot spot mutation whereas E163R (like the ΔE163 in our cohort) is much likely a sporadic mutation. The combined clinical and biophysical analysis presented in this work supports the hypothesis that mutations in specific *TNNT2* hot-spots are more frequently associated with AF, triggered by intrinsic cellular mechanisms, than sporadic *TNNT2* mutations. The difference may affect the individual response to different treatment options.

METHODS

Patients with *TNNT2* Mutations: Genetic Testing and Atrial Phenotype

Patient data collection is as described in Coppini et al., 2014. In brief, after informed consent, patients were screened for mutations in protein-coding exons and splice sites of 8 myofilament genes, including the thin-filament genes *TNNT2*, *TNNI3*, *TPM1*, and *ACTC*; the thick-filament genes *MYBPC3*, *MYH7*, *MYL2,* and *MYL3*. Genetic testing using established methods available at screening was performed by Clinical Laboratory Improvement Amendments (CLIA)–certified laboratories in the United States and at the Genetics Unit of the Careggi University Hospital in Florence. Presence of AF (either proximal and sustained) and Non Sustained Ventricular Tachycardia (NSVT) were evaluated by ECG analysis. Atrial dimensions and additional echocardiographic parameters were assessed using commercially available instruments.

TnT Mutant Transgenic Mouse Lines

All experimental protocols on mice were performed in agreement with current Italian and European regulations and were approved by the local institutional review board and by the animal-welfare committee of the Italian Ministry of Health. We used a total of 27 6-to-8 month-old male C57BL/6N transgenic mice carrying the R92Q (Tardiff et al., 1999; Javadpour et al., 2003) or the E163R (Moore et al., 2014) mutation in the *TNNT2* gene, as well as Wild-Type (WT) littermates: 8 R92Q, 9 E163R and 10 WT mice were used for the experiments described below. The mouse colonies were housed in the animal facility of the University of Florence and all experiments were conducted locally. Transgenic protein expression levels of the R92Q and E163R lines were

determined in the whole heart to be 67 and 50% mutant forms, respectively (Tardiff et al., 1999; Moore et al., 2014).

Echocardiography

Echocardiographic studies were performed on isoflurane-anesthetized mice as previously described (Pistner et al., 2010) to characterize left-atrium (LA) morphology and LV diastolic function, using a Vevo 2,100 small animal echocardiography setup (Fujifilm Visualsonics). In brief, mice were anesthetised with 1.5% isoflurane and imaged in the supine position using a Vevo 2,100 Imaging System with a 40-MHz linear probe (Visualsonics, Canada). Core temperature was maintained at 37°C. Heart rates were kept consistent between experimental groups (400–500 bpm). ECG monitoring was obtained using limb electrodes. A standard 2D echocardiographic study was initially performed in the parasternal long-axis view for assessment of LV dimensions and LA diameter. The maximal anteroposterior LA diameter was measured using the M-mode. Doppler flow profiles were acquired using pulsed wave Doppler in the apical 4-chamber view. The sample volume was placed close to the tip of the mitral leaflets in the mitral orifice parallel to the blood flow in order to record maximal transmitral flow velocities. To assess the Isovolumic Relaxation Time (IVRT), a simultaneous mitral inflow and aortic outflow profile was recorded, allowing measurement of the time interval between aortic valve closure and mitral valve opening. Left atrial area was quantified in the apical 4-chamber view by tracing the border of the left atrium. Measurement was performed in end-systole before opening of the mitral valve.

Mechanics and Energetics of LA Trabeculae

To prepare *intact atrial trabeculae*, we used methods solutions and protocols previously described for intact ventricular trabeculae (Ferrantini et al., 2014; Ferrantini et al., 2015). Briefly, mice were heparinized (5000 UI/ml) and anesthetized by inhaled isoflurane. The heart was rapidly excised, perfused retrogradely via the proximal aorta with a modified Krebs-Henseleit solution and placed in a dissection dish. The LA was opened and thin unbranched trabeculae were dissected by removing a portion of the LA wall on both ends. LA intact trabeculae were mounted between the basket-shaped platinum end of a force transducer and a motor, both connected to micromanipulators, in a glass-bottomed heated horizontal tissue bath with platinum wires for field stimulation. Sarcomere length was measured by laser5 diffraction. A custom-made Labview software was used for motor control, stimulation and force and length signal recording. Muscles were allowed to stabilize under our control conditions (30°C, 2 mM extracellular [Ca^{2+}]], 1 Hz stimulation frequency) and were gradually stretched to optimal initial sarcomere length (2.15 ± 0.03 μm) before starting the experimental protocol. LA intact trabeculae were used to record isometric force during electrical stimulation with different pacing protocols and experimental conditions (Ferrantini et al., 2014; Crocini et al., 2016; Ferrantini et al., 2017). The cross-sectional area of the trabecula was calculated with the assumption of an ellipsoid shape.

LA trabeculae, dissected as described above, were permeabilized by overnight incubation in relaxing solution added with 0.5% Triton X100. Triton was then removed and the *atrial permeabilized trabeculae* were mounted horizontally between a force transducer and a motor by means of T-clips. The length of the preparations was adjusted to a sarcomere length of ~2.15 μm. Tension-pCa curves (where pCa is equal to $-\log_{10}$ [Ca^{2+}]) were obtained as previously described (Chandra et al., 2001). Muscles were activated by transferring them manually between baths containing different pCa solutions and the pCa-tension relationship was determined. The tension-pCa data were fit using the equation, $P/Po = 1/[1 + 10^{n} \times (pCa_{50}\text{-}pCa)]$, where P is tension Po is maximum tension at saturating [Ca^{2+}], n is the Hill coefficient, and pCa_{50} is equal to $-\log_{10}$ [Ca^{2+}] required for producing half-maximal tension.

Sarcomere energetics was assessed in permeabilized trabeculae by simultaneous measurement of isometric tension and ATPase activity with an enzyme-coupled assay. The experimental procedures, solutions, and equipment used were as described previously (Witjas-Paalberends et al., 2014a; Witjas-Paalberends et al., 2014b). Isometric force and ATPase activity were measured at maximal and submaximal [Ca^{2+}] at 20°C. The Ca^{2+}-activated ATPase activity was calculated by subtracting the basal ATPase activity (measured in relaxing solution) from the total ATPase activity measured during contraction and normalized to the volume of the trabecula. LA trabecula volume was calculated as the sum of a cylinder (central body) and two elliptical cones (side) (see **Figure 3A**). The tension cost (energy cost of tension generation) was determined either from the ratio between ATPase activity and tension measured at maximal Ca^{2+} activation or as the slope of the relationship between ATPase activity and active tension measured at various pCa's.

Statistical Analysis

Unpaired Student t tests were used to compare normally distributed data from patients with different *TNNT2* mutations. Chi-square test was used to compare non-continuous variables expressed as proportions (Coppini et al., 2017).

Data from the mouse models are expressed as mean ± SEM (number of preparations and animals are indicated in the respective Figure legends). Statistical analysis was performed as previously described (Coppini et al., 2013; Coppini et al., 2017), using SPSS 23.0 (IBM, United States) and STATA 12.0 (StataCorp, United States). The three different groups (WT, R92Q, and E163R) were compared using One-Way ANOVA with Tukey correction (for normally-distributed homoscedastic datasets).

Overall, $p < 0.05$ was considered statistically significant. The range of calculated p values for each comparison ($0.05 > p > 0.01$, $0.01 > p > 0.001$ or $p < 0.001$) is indicated in the respective figure panels using symbols: red symbols refer to R92Q vs. WT comparisons, blue symbols to E163R vs. WT comparison, and purple symbols to R92Q vs. E163R comparison.

RESULTS

Different Association of Individual *TNNT2* Mutations With AF in HCM Patients

Here, 45 cTnT-HCM patients, mostly those recruited in (Coppini et al., 2014) are reanalysed to assess the association of specific

TNNT2 mutations with AF (**Figure 1** and **Table 1**). We indeed identified 10 patients with 9 mutations (D86A, R94H, K97N, ΔE160, ΔE163, L178F, N262S, N269K, and ΔW287) that are sparse in the *TNNT2* gene and "unexpectedly" sporadic (only 1/2 patients per each mutation among the 45 was found). They overall represent less than one fourth of the entire cTnT-HCM group (**Figure 1**). Of note, the prevalence of some mutations (ΔE160, ΔE163) appears rather low compared to previous description (Watkins et al., 1995) likely because we confined the analysis to index patients. The remaining 35 cTnT-HCM patients are carriers of mutations clustered in six "hot-spot" sites: I79N, R92Q/W, F110L, R130C, R278C, and R286C. For each mutation, 4 to 9 index patients were identified (**Figure 1**; **Table 1**).

The overall arrhythmic burden (quantified as the occurrence of any type of atrial or ventricular arrhythmia) was significantly higher in patients with mutations in the "hot-spot" sites (17 of 35) compared to those with mutations in the "sporadic" sites (1 of 10, $p < 0.05$, see **table 1**). By analysing separately atrial and ventricular episodes, we found that 1) among patients with mutations in the sporadic sites, none had NSVT episodes while NSVTs were described in 12/35 patients in the hot-spot group ($p < 0.05$), 2) AF was identified in only 1 out of 10 patients with sporadic mutations, while the occurrence of AF was much higher (from 25 to 75%) in patients with hot-spot mutations.

Interestingly, none of the patients in the sporadic group showed both AF and NSVT, while among the 35 with mutations in the hot-spot sites, eight were positive for both AF and NSVT, potentially unveiling a common mutation-driven substrate for arrhythmias in both cardiac chambers.

We selected the mutation site E163 (rarely associated to AF) and R92 (more frequently associated to AF) to investigate mutation-driven arrhythmogenic mechanisms of atrial myocardium in the R92Q and E163R mouse models that were available for *in vivo* and *in vitro* functional studies.

Left Atrial Dilation Is More Severe in R92Q Compared to E163R Transgenic Mice

Echocardiographic measurements were performed in anesthetized male mice from the three study groups (WT, R92Q, and E163R), using a standardized protocol (Merx et al., 2014) and focussing on the atrial characteristics and LV diastolic function. Representative images of four-chamber long axis views are reported in **Figure 2A**. The highlighted perimeter of LA was used to estimate the LA circumferential area, while atrial anteroposterior diameter was measured in the parasternal long axis view (**Figure 2B**). In both R92Q and E163R, the LA areas and diameters were significantly increased compared to WT (**Figure 2B**), demonstrating the presence of atrial dilation in both HCM models. However, it is important to note that the extent of atrial dilation was minimal in the E163R (+15%) but markedly severe in the R92Q (+125%). This was paralleled by a markedly worse diastolic function in R92Q mice, when compared with E163 (**Figure 2B**), as previously observed (Ferrantini et al., 2018). Indeed, the isovolumic relaxation time (IVRT) was markedly increased and the E/A ratio decreased in the R92Q mice compared to WT while they were less affected in the E163R hearts. Interestingly, the marked decrease of the E/A ratio in the R92Q mice was mainly driven by a larger A wave, corresponding to transmitral flow during atrial contraction (see **Figure 2B**).

Energy Cost of Tension Generation and Calcium Sensitivity of R92Q and E163R Atrial Myocardium: The Sarcomere Changes Are Similar to Those Observed in the Corresponding Ventricles

Direct demonstration of the energetic impact of E163R-cTnT and R92Q-cTnT, expressed at 50 and 67% respectively in atrial sarcomere, was obtained by simultaneously measuring isometric tension and ATPase activity in permeabilized LA trabeculae (**Figure 3A**) at 20°C. Representative recordings are reported in **Figure 3B**. Both cTnT mutated strains generated maximal Ca^{2+}-activated tension similar to WT but the maximal ATPase activity was markedly increased in the E163R permeabilized LA trabeculae (**Table 2**). The ratio between maximal Ca^{2+}-activated ATPase and active tension, that represents the energetic cost of tension generation, was markedly higher in the E163R trabeculae while it was comparable to WT in the R92Q trabeculae (**Table 2**). The different behaviour of the tension cost in the E163R atrial muscle compared to WT and R92Q was confirmed by measuring tension and ATPase activity at sub-maximal [Ca^{2+}] (**Figure 3C**). Tension cost measured by the slope of the relation between Ca^{2+}-activated ATPase activity and tension was significantly higher in the E163R compared to WT and R92Q (**Figure 3C**; **Table 2**). It is worth noting that increased tension cost has been associated with an increased cross-bridge detachment rate (Vitale et al., 2021; Ferrantini et al., 2017).

The average pCa-tension relationships obtained from the same permeabilized trabeculae showed a marked left shift in the R92Q preparations compared to both WT and E163R trabeculae (**Figure 3D**). The results in **Figure 3D**; **Table 2** clearly show that myofilament Ca^{2+}-sensitivity was significantly increased in the R92Q atrial trabeculae compared to WT while no difference was present in the E163R compared to WT mice. Interestingly, like in other cases of increased Ca^{2+} sensitivity in cardiac muscle (Kreutziger et al., 2011) the Hill coefficient (n_h) of the pCa-tension relation is significantly decreased in the R92Q atrial trabeculae compared to both WT and E163R (**Table 2**).

Increased tension cost in the E163R atrial myocardium and increased myofilament Ca^{2+}-sensitivity in the R92Q atrial myocardium are key alterations also identified in permeabilized ventricular trabeculae of the same mouse strains (Ferrantini et al., 2017). This suggests that these changes are most likely the direct, specific, consequences of the mutations that impact the sarcomere function of both cardiac chambers.

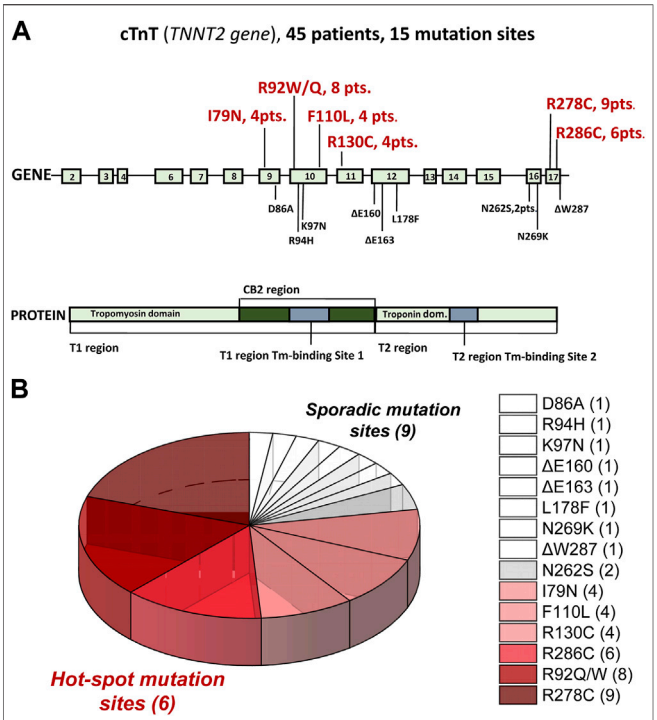

FIGURE 1 | Sites and carrier numerosity of individual mutations in 45 *TNNT2*-positive Hypertrophic CardioMyopathy patients (HCM). **(A)** Representation of *TNNT2* exons (top panel) and structural and functional cTnT protein domains (bottom panel) showing hot (big red bold numbers) and sporadic (small black numbers) mutation sites. For mutations carried by more than one patient, the total number of carriers is indicated. **(B)** Pie chart of data reported in A: Six hot-spot mutation sites and nine sporadic ones are identified. Data modified and updated from Coppini et al., 2014.

Twitch Relaxation Is Prolonged and Spontaneous Activity Increased Only in R92Q Atrial Myocardium

Isometric force was measured from intact LA trabeculae during field-stimulation at 30°C under different stimulation protocols and various inotropic stimuli (i.e. Isoproterenol 1 μM (ISO), 6 mM extracellular [Ca^{2+}] and post rest potentiation) (**Figure 4**). Under our control experimental condition, i.e. 1 Hz, 2 mM extracellular [Ca^{2+}], the amplitude of twitch contractions was similar in WT, R92Q, and E163R trabeculae (**Figure 4A**). The plot relating twitch tension to stimulation frequency in **Figure 4A** shows that at low pacing frequency (0.5 Hz), R92Q atrial trabeculae developed lower twitch tension than E163R and WT. The overall force frequency relation seems to be blunted in the R92Q atrial trabeculae. In addition, the R92Q atrial trabeculae showed prolonged twitch duration compared to WT, due to a significant prolongation of both contraction and relaxation times (**Figure 4B**). No major variations of contraction kinetics, instead, were observed in the E163R preparations, although contraction peak time at low pacing rates was significantly faster in the E163R compared to WT trabeculae (**Figure 4B**).

To further evaluate the impact of the mutation on the mechanics of intact atrial trabeculae, we applied inotropic interventions (ISO, high extracellular [Ca^{2+}], post rest potentiation) (**Figure 4C**). Under ISO, high extracellular [Ca^{2+}] or post rest potentiation, R92Q preparations showed lower tension levels than WT indicating reduced inotropic response. Contrarily, E163R trabeculae showed a positive inotropic response under all inotropic interventions tested (**Figure 4C**) similar to that of WT atrial trabeculae.

Finally, the arrhythmogenic propensity associated with each of the two mutations was assessed (**Figure 5A**). To increase the

TABLE 1 | *TNNT2* sporadic and hot spot mutations associated to Hypertrophic CardioMyopathy (HCM) and prevalence of arrhythmias and clinical phenotype.

cTnT Mutations	N° of patients	Positive Arrhythmic burden	AF	NSVT	AF and NSVT	Atrial dilation	Final NYHA class III or IV
Sporadic sites							
D86A (1)	1	0	0	0	0	0	1
R94H (1)	1	0	0	0	0	1	1
K97N (1)	1	0	0	0	0	0	0
ΔE160 (1)	1	0	0	0	0	0	2
ΔE163 (1)	1	0	0	0	0	0	1
L178F (1)	1	0	0	0	0	0	1
N262S (2)	2	0	0	0	0	0	1
N269K (1)	1	0	0	0	0	0	1
ΔW287 (1)	1	1	1	0	0	0	1
Total	10	1	1	0	0	1	9
Hot-spot sites							
I79N (4)	4	2	2	2	2	2	2
R92Q/W (8)	8	3	2	2	1	2	0
F110L (4)	4	2	1	2	1	1	1
R130C (4)	4	3	3	1	1	2	1
R278C (9)	9	4	3	3	2	3	2
R286C (6)	6	3	2	2	1	2	1
Total	35	17	13	12	8	12	7
p(Chi-square)		**0.0281**	0.1020	**0.0306**	0.0955	0.1351	**0.0001**

AF, atrial fibrillation, NSVT, non-sustained ventricular tachycardia. Data modified and updated from Coppini et al., 2014.

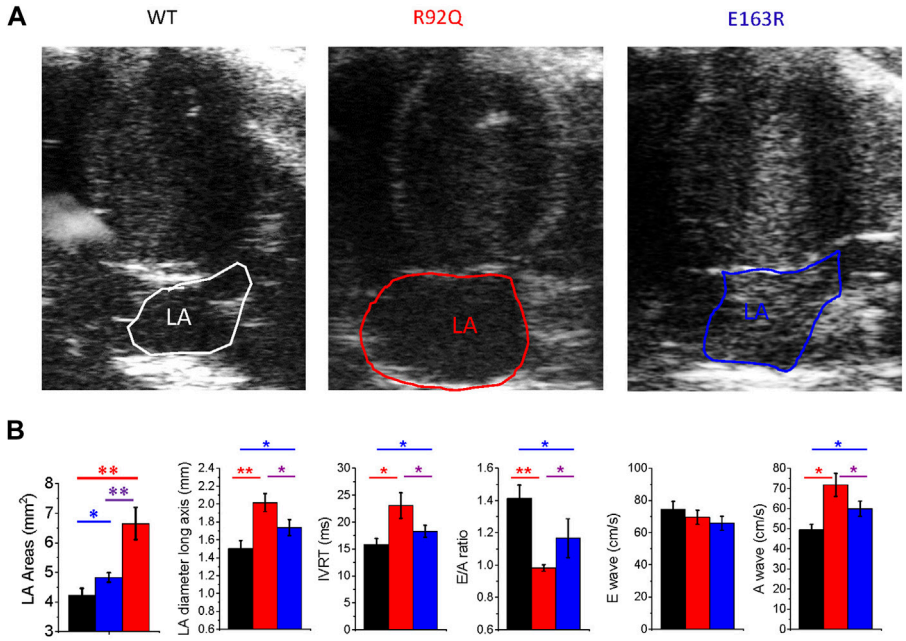

FIGURE 2 | Echocardiographic measurements in WT and cTnT mutant mouse models. **(A)** Representative echocardiographic images of left atrial area (LA) of WT, R92Q and E163R mice. **(B)** Comparison of LA areas, maximal anteroposterior left atrial diameter measured from parasternal long axis view, ratio between E and A waves (E/A ratio), isovolumic relaxation time (IVRT), E-wave and A wave in mice from the three study cohorts. Statistical tests: One-way ANOVA with Tukey correction. Data are Means ± S.E.M. from 10 mice per group. * = 0.05>p > 0.01; ** = 0.01 > p > 0.001.

probability of spontaneous events, we applied a combination of ISO and a burst of high-rate (3 Hz) stimuli followed by a 30 s simulation pause. With this protocol, spontaneous activity occurred in more than 60% of the R92Q atrial trabeculae, while premature contractions occurred in less than 10% of the E163R and WT atrial trabeculae (**Figure 5B**).

DISCUSSION

The prevalence of AF in HCM was initially described to be independent from the underlying disease genotype. Olivotto et al., 2008 was the first report showing no difference between myofilament positive and myofilament negative patients in terms of AF prevalence (Olivotto et al., 2008). Furthermore, no differences were found between patients carrying mutations in thick or thin filament-related genes in more recent studies (Coppini et al., 2014; Bongini et al., 2016). However, in the thin filament subgroup, AF tends to onset at younger age (Bongini et al., 2016) and is more often aggressively treated with catheter ablation (Coppini et al., 2014). Indeed, in a recent prospective observational cohort study on more than 1,200 patients with early-onset AF (<66 years) (Yoneda et al., 2021), the cardiomyopathy-gene panel test identified a pathogenic sarcomere mutation in 10% of patients. This pivotal study supports the use of genetic testing in early-onset AF, although the clinical association between sarcomere mutation and AF remains controversial.

Approximately, 9–13% of HCM is caused by mutations in the *TNNT2* gene coding for cTnT (Coppini et al., 2017), a sarcomeric protein that anchors the cardiac ternary troponin (cTn) complex to tropomyosin (Tm) contributing to the modulation of calcium-induced activation of the cardiac thin filament. The cTnT protein comprises two functional domains: the Tm-binding T1 domain and the calcium-sensitive T2 domain, which binds cardiac troponin I (cTnI), cardiac troponin C (cTnC), and Tm (Gordon et al., 2000). A long (~50-amino acids) flexible linker connecting the T1 and T2 domains (**Figure 1A**) is essential for transmitting the calcium-induced conformational changes from the C-terminal end of cTnT to the N terminus. Although cTnT is a relatively small protein (34.6 kDa), distinct regions have individual and specific functions. Thus, the molecular pathogenesis of HCM induced by mutations in different regions can be different and associated to different phenotypic manifestations in terms of degree of LV hypertrophy, diastolic dysfunction and propensity towards ventricular arrhythmias as well as, importantly, occurrence of AF and severity of atrial remodelling.

Hot-Spot *TNNT2* Mutations Associated to High AF-Prevalence can be Identified in HCM Patients

Initial clinical phenotype descriptions of *TNNT2* mutations were from families with severe HCM (cTnT-HCM), characterized by mild hypertrophy and high incidence of sudden cardiac death (SCD). More recently the severity of cTnT-HCM has been

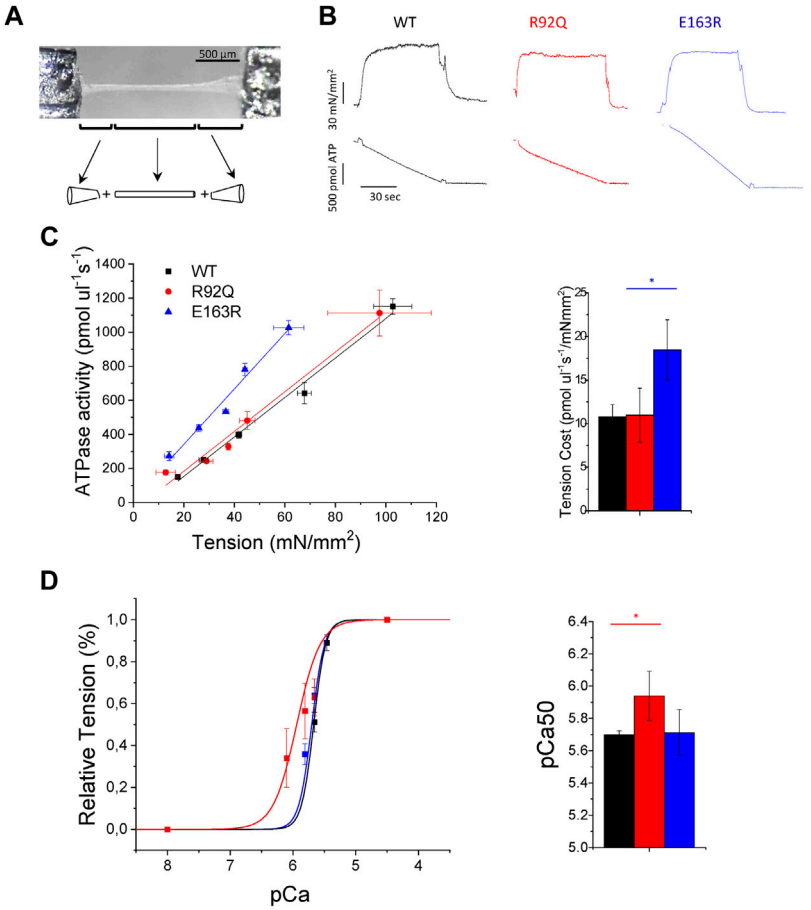

FIGURE 3 | Mechanics and energetics of permeabilized atrial trabeculae from WT and cTnT mutant mouse models. **(A)** Picture of one permeabilized atrial trabecula with a scheme of the method used to calculate the volume of the trabecula assumed to be a cylinder between two elliptical cones **(B)** Representative tension (top) and ATPase activity (bottom) traces from wild-type (WT), R92Q, and E163R trabeculae that were maximally Ca^{2+}-activated (pCa 4.5) at 20°C. Tension cost can be estimated as the ratio between the maximal Ca^{2+}-activated ATPase activity and isometric tension (see **Table 2**). **(C)** Relationship between isometric tension and ATPase activity measured at different pCa's in permeabilized atrial trabeculae from the three groups of mice. The tension cost can be measured from the slope of the ATPase-tension relationship; mean tension cost values are reported at the right. Mean ± SE of tension cost was calculated at 20°C. from WT (N = 6, *n* = 10), R92Q (N = 3, *n* = 6) and E163R (N = 4, n = 8) mice: N = number of animals, n = number of trabeculae. Statistical test see below **(D)** pCa-Tension curves (left) and mean values of pCa at half-maximal activation (pCa_{50}, right) from WT (N = 5, n = 10), R92Q (N = 3, n = 7) and E163R (N = 4, n = 9) trabeculae. Statistical tests for all measurements: One-way ANOVA with Tukey correction. * = 0.05 > *p* > 0.01; ** = 0.01 > *p* > 0.001.

TABLE 2 | Mechanical energetic and myofilament Ca^{2+}-sensitivity parameters of permeabilized atrial trabeculae from WT, E163R, and R92Q mice.

	P_o (mN/mm^2)	$ATPase_{MAX}$ ($pmol\ ul^{-1}\ s^{-1}$)	$ATPase_{rest}$ ($pmol\ ul^{-1}\ s^{-1}$)	TC (slope) ($pmol\ ul^{-1}\ s^{-1}/mN/mm^2$)	TC (Max) ($pmol\ ul^{-1}\ s^{-1}/mN/mm^2$)	pCa_{50}	n_H Cooperativity
WT (N = 7)	65.31 ± 6.22 (*n = 10*)	655.89 ± 93.49 (*n = 15*)	136.13 ± 11.02 (*n = 10*)	10.779 ± 1.40 (*n = 10*)	9.47 ± 1.39 (*n = 8*)	5.7 ± 0.02 (*n = 10*)	4.23 ± 0,8 (*n = 10*)
E163R (N = 2)	59.92 ± 6.75 (*n = 8*)	771.91 ± 90.9* (*n = 8*)	189.47 ± 41.63 (*n = 8*)	18.46 ± 3.47* (*n = 8*)	19.03 ± 4.5* (*n = 8*)	5.67 ± 0.14 (n = 7)	4.54 ± 0.62 (*n = 7*)
R92Q (N = 2)	58.16 ± 12.3 (n = 8)	603.87 ± 187.3 (n = 7)	142.34 ± 30.10 (n = 7)	10.98 ± 3.10 (n = 7)	9.12 ± 4.48 (*n = 8*)	5.94 ± 0.15* (n = 7)	2.33 ± 1.05* (n = 7)

Tension cost (TC) data are measured from ATPase and isometric tension values measured at maximal activation (TC max) or from the slope of the ATPase tension relationship measured at different pCa's (TC slope); see ***Figure 3****. Po maximal isometric tension. pCa_{50}, –log10 [Ca^{2+}] required to get half maximal tension; n_H, Hill coefficient. Statistical test: one-way ANOVA with Tukey correction ("*" indicates a statistically significant difference).*

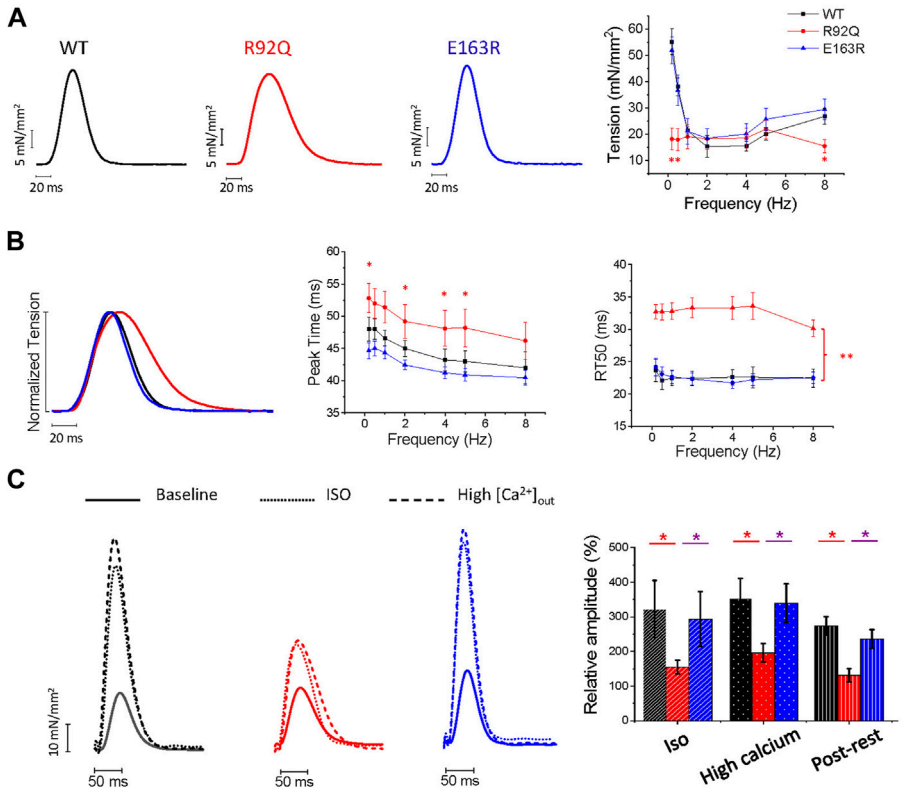

FIGURE 4 | Comparison of isometric twitch amplitude and kinetics of intact atrial trabeculae from WT, R92Q and E163Rmice. **(A)** Left: representative tension traces of twitches from intact atrial trabeculae of WT, R92Q and E163R mice under control experimental conditions (30°C, 2 mM external [Ca^{2+}], stimulation frequency 1 Hz). Right: relationship between stimulation frequency and peak isometric twitch tension in the three groups of intact atrial trabeculae. **(B)** Left: normalized superimposed twitches at 1 Hz stimulation frequency to highlight kinetics differences. Center: average time to peak at different stimulation frequencies in atrial trabeculae from the three groups. Right: average time from peak to 50% relaxation (RT_{50}) in atrial trabeculae from the three groups. **(C)** Inotropic interventions in atrial trabeculae. Left: superimposed traces under control conditions and following addition of isoproterenol 1 μM (ISO) or 6 mM external [Ca^{2+}] in trabeculae from WT, R92Q, and E163R mice. Right: variation of the peak twitch force from our control conditions following ISO, 6 mM external [Ca^{2+}] and post rest potentiation. * = $p < 0.05$ ** = $p < 0.01$; One-way ANOVA with Tukey correction. WT (N = 9, *n* = 14), R92Q (N = 4, *n* = 10) and E163R (N = 5, *n* = 10) mice. N = number of animals, *n* = number of trabeculae.

reconsidered in light of large patient-populations (Coppini et al., 2014). Despite the occurrence of life-threatening ventricular arrhythmias that always catches the attention of clinicians and basic scientists, the most common sustained arrhythmia in HCM, including cTnT-HCM, is AF (Olivotto et al., 2001). Identification of hot-spot mutations in the *TNNT2* gene that are highly associated to AF is therefore potentially relevant to clinical decision-making, including risk stratification for AF prophylaxis.

In the present work we show that the association between *TNNT2* mutations and AF is variable.

In our cohort of HCM patients, we identified an association of individual *TNNT2* mutations with AF. AF was identified in 10% of patients with sporadic *TNNT2* mutations (D86A, R94H, K97N, ΔE160, ΔE163, L178F, N262S, N269K, and ΔW287), while AF occurrence was much higher (25–75%) in patients carrying specific "hot-spot" mutations (I79N, R92Q/W, F110L, R130C, R278C, and R286C). Interestingly, only in patients with hot-spot mutations we observed a positive association between AF and ventricular arrhythmias in the form of NSVT, that may unveil a common mutation-driven substrate. In fact, in both cardiac chambers, highly enhanced cellular automaticity can be the cause of arrythmia onset and recurrences, promoting both AF and NSVT.

R92Q vs. E163R TNNT2 Mouse Models: Severity of Atrial Myopathy and Propensity Towards Arrhythmias Depend on Genotype

Two HCM mouse models with R92Q and E163R cTnT mutations were studied with *in vivo* echocardiography and *in vitro* biophysical measurements to assess the extent of LA remodeling and the relative roles of myofilament dysfunction and excitation-contraction coupling changes in HCM pathophysiology. This choice was related to the availability of two mouse models with mutations at sites corresponding to a human hot (92) or sporadic (163) spot in the *TNNT2* gene respectively.

In our previous study on ventricular myocardium we showed that both R92Q and E163R mouse models exhibited ventricular hypertrophy, with prolonged twitch contractions, and increased

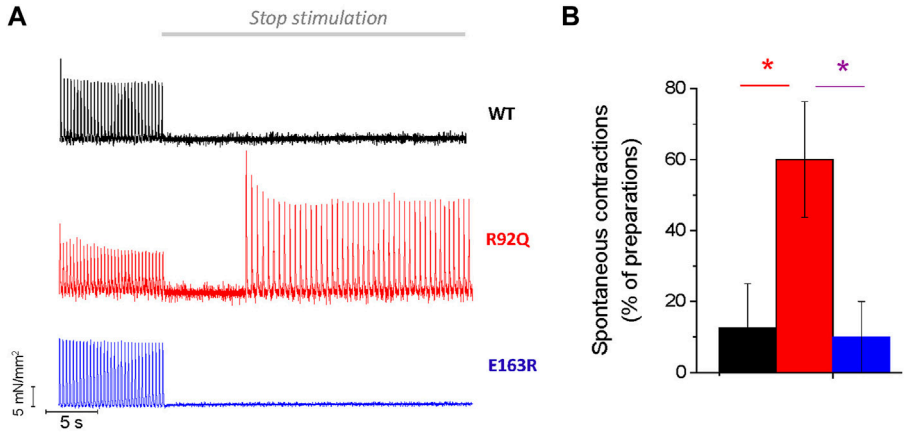

FIGURE 5 | Spontaneous activity in R92Q atrial trabeculae. **(A)** Representative traces showing the stimulation protocol that may induce spontaneous activity upon stimulation pauses following a train of high frequency stimuli. R92Q but not E163R and WT trabeculae showed significant occurrence of spontaneous triggered activity during the resting pauses. **(B)** Percentage of trabeculae showing spontaneous activity during long pauses. One-way ANOVA with Tukey correction. * = $p < 0.05$. WT (N = 9, n = 14), R92Q (N = 4, n = 10) and E163R (N = 5, n = 10) mice. N = number of animals, n = number of trabeculae.

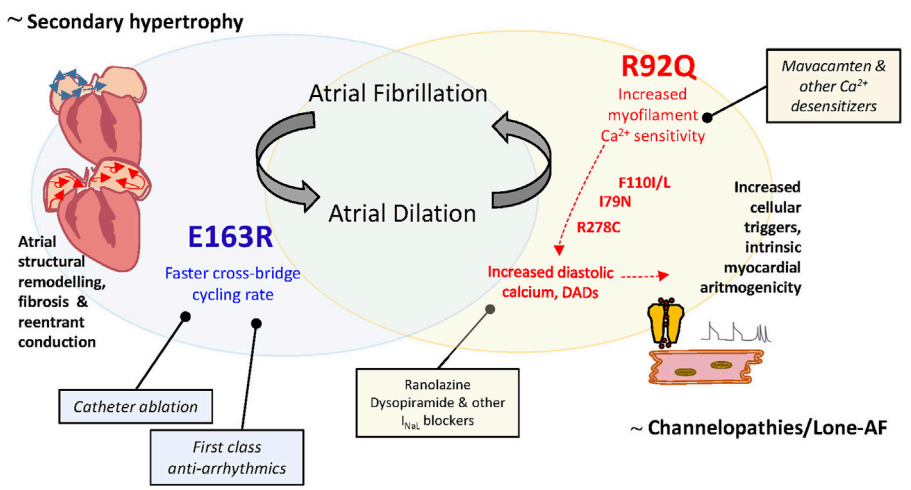

FIGURE 6 | Atrial myopathy in cTnT-HCM: different pathogenesis of atrial cardiomyopathy, different genotype-driven therapeutical strategies for AF. Left: Atrial myopathy in E163R cTnT-HCM is likely a consequence of increased LV filling pressures as in secondary hypertrophy and other chronic LV conditions. In this case, AF would be predominantly sustained by atrial tissue structural remodeling and associated micro and macro reentrant conduction and first class antiarrhythmics to slow down conduction velocity and catheter ablation could be the recommended first choice treatments. Right: Atrial myopathy in R92Q cTnT-HCM is likely a direct effect of the mutation as in other genetic-based forms of AF. We identified the increased atrial and ventricular myofilament calcium sensitivity associated to this mutation as the trigger for cellular arrhythmias determined by calcium handling dysregulation, as previously demonstrated for other cTnT mutations. In this case drugs that directly decrease sarcomere calcium sensitivity or ameliorate cell calcium homeostasis can be more beneficial compared to classical antiarrhythmics and invasive treatments.

arrhythmogenicity (Ferrantini et al., 2017; Vitale et al., 2021). At the sarcomere level, the two mutant proteins lead to the same effects in the atria as observed in the ventricles. Indeed, in E163R atrial myocardium the energy cost of tension generation is increased, likely due to increased cross-bridge cycling rate (Ferrantini et al., 2017) (with no significant variation of calcium sensitivity), while in the R92Q atrial myocardium we observed a rather large increase in calcium sensitivity (with no variation of cross-bridge energetics and cycling rates).

LA systolic function is typically an auxotonic contraction with much lower after-load and much higher shortening velocity compared to the LV contraction. For this reason, increased isometric cross-bridge cycling rates and ATP consumption in the E163R atrial myocardium may not represent a significant disadvantage for the

atrial chambers. Consistently, in E163R intact atrial trabeculae twitch contraction parameters are normal or even slightly faster at low pacing rates (peak time), likely reflecting faster cross-bridge cycling rate during force development. Because of the different working conditions of the LA with respect to the LV, determining lower ATP consumption per unit of myocardial mass, the increased tension cost of E163R atrial myocardium may not significantly affect global cardiomyocyte energy balance, at variance with ventricular tissue. Therefore, the E163R mutation in atrial tissue may be unable to activate the pathological signalling pathways of cardiomyocytes that are most likely responsible for the slower twitch duration and the increased propensity to arrhythmias observed in the ventricular myocardium. The most relevant signalling pathway involved is likely the Ca-calmodulin Kinase II (CaMKII) pathway. Indeed, increased CaMKII activation has been observed in the ventricular tissue of HCM patients (Coppini et al., 2013; Coppini et al., 2018) and is associated with the severity of disease presentation (Helms et al., 2016) and with the occurrence of arrhythmogenic remodelling (Coppini et al., 2017) of HCM ventricles. In E163R atria, however, the occurrence of spontaneous contractions was not different from that of WT. These results seem to exclude the idea that the E163R mutation itself, by changing cross-bridge cycling rates, may represent a direct trigger towards atrial arrhythmias. The mild increase of E163R atrial dimensions observed *in-vivo* may not be related to the mutation itself but, rather it may be related to hemodynamic factors and diastolic dysfunction, that explain the late-onset of atrial dilation, governed by the severity of the LV disease. Only at late stages of the disease, atrial dilation due to LV dysfunction can promote and sustain AF.

In R92Q atrial myocardium, instead, increased myofilament calcium sensitivity can directly impair atrial contraction and predispose towards arrhythmias, similarly to the ventricular myocardium (Ferrantini et al., 2017). Again, increased CaMKII activity due to diastolic Ca^{2+} accumulation in the cytosol (a direct consequence of increased myofilament Ca^{2+}-sensitivity) may explain the increased arrhythmic propensity and the extended functional alterations observed in the R92Q atrial myocardium (Coppini et al., 2018). Twitch contractions are severely prolonged (particularly in the relaxation phase) and the occurrence of spontaneous beats (likely related to Delayed After Depolarizations (DADs)) is markedly increased. In R92Q ventricular myocytes, we previously found that altered Ca^{2+}-transient kinetics and increased Ca^{2+}-dependent arrhythmogenesis are linked with increased CaMKII activation (Coppini et al., 2017). Although we did not directly measure calcium fluxes or CaMKII activity in R92Q atrial myocardium, the results unveil an intrinsic sarcomere mutation-driven mechanism associated to a higher occurrence of arrhythmias in both cardiac chambers.

Previous studies on I79N, F110I, R278C *TNNT2* mutations (all hot-spot sites for AF, according to our analysis in HCM patients) clearly demonstrated that increased myofilament Ca^{2+}-sensitivity, by modifying cytosolic Ca^{2+} buffering, promotes DADs and triggered activity (Schober et al., 2012), representing a direct cause of arrythmias in both atrial and ventricular cardiomyocytes. In agreement, crossing transgenic mice expressing pathogenic cTnT mutants with opposite effects on myofilament Ca^{2+} sensitivity attenuates cardiomyopathy phenotypes and propensity to arrythmias in mice (Dieseldorff Jones et al., 2019).

Clinical and Therapeutical Implications

The principal role of the LA is to modulate LV filling and cardiovascular performance by operating as a reservoir for venous return during LV systole, a conduit for venous return during early LV diastole, and as a booster pump that augments LV filling during LV diastole. Thus, while LA compliance (or its inverse, stiffness) is the major determinant of reservoir function and conduit function, atrial booster-pump function reflects the magnitude and timing of atrial contraction, that occurs against a low after-load (<20 mmHg, compared to more than 100 mmHg in the ventricle) with a relatively large percentage change in chamber volume (>20–30). Here we demonstrate that increased isometric cross-bridge detachment rates and ATP consumption in the E163R atrial myocardium may not represent a significant disadvantage for the atrial chambers and is unlikely to initiate/promote E-C coupling alterations. In fact, twitch contraction amplitude and kinetics are preserved in E163R and no premature contractions were observed, suggesting no major changes in cardiomyocyte calcium handling. Indeed, in our E163R mouse model, atrial myopathy is manifested only as a mild dilation, likely a consequence of increased LV filling pressures due to LV diastolic dysfunction. This consideration in the murine model does not exclude that in selected patients carrying the E163R mutation, LV remodelling over time may lead to severe LV hypertrophy. In this case, as in secondary hypertrophy and other chronic LV conditions, AF may occur and would be predominantly sustained by tissue structural remodeling, fibrosis, micro and macro reentrant conduction (**Figure 6**). In this scenario, catheter ablation could be a recommended treatment.

According to the results reported here and in Ferrantini et al. (2017), increased cross bridge cycling rates and the energetic dysfunction associated with the E163R mutation affect contractility only when high-pressure generation is required (i.e. in the ventricles and not in the atria). As mentioned, we cannot exclude that -over timeprogressive LV remodelling trough mechanisms that are not specifically related to the mutation (e.g. fibrosis, myocardial disarray) causes LA remodeling, with increased LA pressures to levels that are critical for the E163R myocadium cross bridge cycling and energetic requirements.

On the contrary, atrial myopathy in R92Q cTnT-HCM is manifested as moderate-to-severe atrial dilation associated to atrial arrhythmias. In this case both the loss of atrial inotropic reserve (promoting dilation) and the membrane instability (premature contractions) are direct effects of the mutation. In this sense the R92Q cTnT-associated AF cannot be reconducted to mechanisms of secondary hypertrophy but rather resemble other genetic-based forms of AF associated to increased cellular arrithmogenicity (e.g. channelopathies, lone-AF (**Figure 6**). We identified the increased myofilament calcium sensitivity associated to R92Q cTnT mutation as the key trigger for calcium handling dysregulation, as previously demonstrated for other cTnT mutations and largely highlighted in R92Q cTnT ventricular myocardium (Ferrantini et al., 2017). From the therapeutical standpoint, we can hypothesize that, in the presence of these mutations, drugs that decrease sarcomere calcium sensitivity (including the novel first-in-class myosin inhibitors) or drugs that

ameliorate cell calcium homeostasis can be more effective on atrial arrhythmogenesis compared to classical pharmacological approaches or invasive catheter treatments. We previously observed that ranolazine, by blocking late Na current, has the ability to normalize Ca-handling in human HCM myocardium (Coppini et al., 2013) and in the ventricles of R92Q mice (Coppini et al., 2017), and may thus reduce Ca-dependent arrhythmias in R92Q atria as well. Ranolazine also has the ability to selectively inhibit peak Na current in the atria destabilizing atrial reentry circuits (Burashnikov et al., 2007). These observations prompt towards further tests of ranolazine as a drug to prevent AF in selected HCM patients with high risk mutations.

Limitations

To study the link between AF and *TNNT2* mutation, we used two mouse models (R92Q and E163R) that, based on our patient data, were not the best models to use. It may be difficult to accept that R92 mutations in cTnT are highly associated with AF when only 2 patients out of 8 (i.e. 25%) had AF and to generalize that patients with E163 mutations don't do AF when we had only one patient, without AF, with a truncation mutation in the 163 site. According to the patient data, other mutations, like the R130C and the N262S (representative of the hot spot and sporadic spot mutations respectively), could have been better models of investigation. We used the R92Q and the E163R simply because of their availability and because in the patient study the cTnT sites 92 and 163 were associated to hot spot and sporadic mutations. This choice may have not been the best one but it was our only realistic possibility.

In the present study we did not perform long term ECG analysis by telemetry in conscious animals to detect or induce AF or other arrhythmias. This had been done for the R92Q model by Jimenez and Tardiff (2011) who demonstrated abnormalities in conduction, ventricular ectopy and a prolonged P duration after isoproterenol injections. The conclusion that the increased myofilament calcium sensitivity associated to *TNNT2* hot spot mutations is the key trigger for the calcium handling dysregulation that promotes arrhythmias may be limited by the difficulties of relating *in vivo* patient (and animal) propensity to arrhythmias to *in vitro* data that measure the propensity to spontaneous activity.

It may have not been sound to conclude that the differences in atrial phenotype associated to hot spot and sporadic *TNNT2* mutations are due to different biophysical mechanisms based upon just the data from a single mouse model (likely not the best one) for each category of mutation. There is, however, a wealth of biophysical data in the literature examining the effects of various cTnT mutations in different experimental systems. Some of these data can actually be used to support the argument of our study. For instance, Chandra et al. (2005) found that different mutations (R92 W/L) at the 92 site, that we classified as a hot spot site, markedly increased calcium sensitivity while a truncation mutation (delta E160) in a site, that we classified as a sporadic site, increased myofilament calcium sensitivity only very slightly while it specifically increased sarcomere energetics and cross bridge cycling rates. These findings and additional reports confirming that a marked increase of myofilament calcium sensitivity occurs in all the hot spot mutations that have been investigated so far (at least to our knowledge, e.g. Miller et al., 2001 for the I79N; Groen et al., 2020 for the R130C; Schuldt et al., 2021 for the R278C) support the conclusion of our study.

Contractile function of cardiomyocytes depends on isoform types of key sarcomeric proteins (e.g., alpha/beta-MyHC, MLC-1a/v, MLC-2a/v) and the phosphorylation status of some of them (e.g., cTnT, cTnI, MLC-2, cMyBP-C). In the present study the potential contribution of differences in sarcomeric protein isoforms and phosphorylation levels to the mouse model phenotypes has not been investigated. Therefore, we cannot rule out that isoform shifts and post-translational changes in some of the sarcomeric proteins may have been involved in the changes of myofilament calcium sensitivity and/or cross bridge cycling rates found in this study. Additional work is needed to address this point.

CONCLUSION

Overall, this work sets the stage for a reconsideration of patient genotype as a criterion for predicting AF in HCM patients. We suggest that the correlation is not gene-specific, not even mutation-specific, but rather "biophysical mechanism"-specific. Mutations that affect cross-bridge cycling are likely to be "E163R"-like (that do not directly promote AF and loss of atrial contractility), while mutations affecting myofilament calcium sensitivity are likely to be "R92Q"-like (that directly promote cellular arrhyhtmogeneicity). Moreover, if the association of *TNNT2* mutations with AF occurrence depends on the underlying mutation-driven pathomechanisms, then tailored preventive treatments for AF can be identified (including Mavacamten and Ranolazine) and tested in selected genotyped HCM subgroups ("R92Q"-like).

DATA AVAILABILITY STATEMENT

The raw data supporting the conclusion of this article will be made available by the authors, without undue reservation.

ETHICS STATEMENT

The animal study was reviewed and approved by the Ministero della Salute.

AUTHOR CONTRIBUTIONS

JP, CP and CF devised the project, perfomed experiments, analyzed data and drafted the manuscript. GV, FG, BS, and NP performed and analyzed experiments. EC, IO, JT, RC, and CT contributed to data analysis and interpretation and critically reviewed the manuscript.

ACKNOWLEDGMENTS

This work was supported by the Italian Ministry of Health (Ricerca Finalizzata Giovani Ricercatori GR-2011-02350583) and by the European Union's Horizon 2020 research and innovation programme under grant agreements no. 952166 (REPAIR) and no. 777204 (SILICO FCM).

REFERENCES

Belus, A., Piroddi, N., Ferrantini, C., Tesi, C., Cazorla, O., Toniolo, L., et al. (2010). Effects of Chronic Atrial Fibrillation on Active and Passive Force Generation in Human Atrial Myofibrils. *Circ. Res.* 107, 144–152. doi:10.1161/circresaha.110.220699

Biagini, E., Olivotto, I., Iascone, M., Parodi, M. I., Girolami, F., Frisso, G., et al. (2014). Significance of Sarcomere Gene Mutations Analysis in the End-Stage Phase of Hypertrophic Cardiomyopathy. *Am. J. Cardiol.* 114, 769–776. doi:10.1016/j.amjcard.2014.05.065

Bongini, C., Ferrantini, C., Girolami, F., Coppini, R., Arretini, A., Targetti, M., et al. (2016). Impact of Genotype on the Occurrence of Atrial Fibrillation in Patients with Hypertrophic Cardiomyopathy. *Am. J. Cardiol.* 117, 1151–1159. doi:10.1016/j.amjcard.2015.12.058

Burashnikov, A., Di Diego, J. M., Zygmunt, A. C., Belardinelli, L., and Antzelevitch, C. (2007). Atrium-Selective Sodium Channel Block as a Strategy for Suppression of Atrial Fibrillation. *Circulation* 116, 1449–1457. doi:10.1161/circulationaha.107.704890

Chandra, M., Rundell, V. L., Tardiff, J. C., Leinwand, L. A., De Tombe, P. P., and Solaro, R. J. (2001). $Ca(^{2+})$ activation of myofilaments from transgenic mouse hearts expressing R92Q mutant cardiac troponin T. *Am. J. Physiol. Heart Circ. Physiol.* 280(2), H705–H713. doi:10.1152/ajpheart.2001.280.2.H705

Chandra, M., Tschirgi, M. L., and Tardiff, J. C. (2005). Increase in Tension-dependent ATP Consumption Induced by Cardiac Troponin T Mutation. *Am. J. Physiology-Heart Circulatory Physiol.* 289, H2112–H2119. doi:10.1152/ajpheart.00571.2005

Coppini, R., Mazzoni, L., Ferrantini, C., Gentile, F., Pioner, J. M., Laurino, A., et al. (2017). Ranolazine Prevents Phenotype Development in a Mouse Model of Hypertrophic Cardiomyopathy. *Circ. Heart Fail.* 10, e003565. doi:10.1161/CIRCHEARTFAILURE.116.003565

Coppini, R., Ferrantini, C., Mugelli, A., Poggesi, C., and Cerbai, E. (2018). Altered Ca2+ and Na+ Homeostasis in Human Hypertrophic Cardiomyopathy: Implications for Arrhythmogenesis. *Front. Physiol.* 9, 1391. doi:10.3389/fphys.2018.01391

Coppini, R., Ferrantini, C., Yao, L., Fan, P., Del Lungo, M., Stillitano, F., et al. (2013). Late Sodium Current Inhibition Reverses Electromechanical Dysfunction in Human Hypertrophic Cardiomyopathy. *Circulation* 127, 575–584. doi:10.1161/circulationaha.112.134932

Coppini, R., Ho, C. Y., Ashley, E., Day, S., Ferrantini, C., Girolami, F., et al. (2014). Clinical Phenotype and Outcome of Hypertrophic Cardiomyopathy Associated with Thin-Filament Gene Mutations. *J. Am. Coll. Cardiol.* 64, 2589–2600. doi:10.1016/j.jacc.2014.09.059

Crocini, C., Ferrantini, C., Scardigli, M., Coppini, R., Mazzoni, L., Lazzeri, E., et al. (2016). Novel Insights on the Relationship between T-Tubular Defects and Contractile Dysfunction in a Mouse Model of Hypertrophic Cardiomyopathy. *J. Mol. Cell. Cardiol.* 91, 42–51. doi:10.1016/j.yjmcc.2015.12.013

Dieseldorff Jones, K. M., Koh, Y., Weller, R. S., Turna, R. S., Ahmad, F., Huke, S., et al. (2019). Pathogenic Troponin T Mutants with Opposing Effects on Myofilament Ca2+ Sensitivity Attenuate Cardiomyopathy Phenotypes in Mice. *Arch. Biochem. Biophys.* 661, 125–131. doi:10.1016/j.abb.2018.11.006

Ferrantini, C., Coppini, R., Sacconi, L., Tosi, B., Zhang, M. L., Wang, G. L., et al. (2014). Impact of Detubulation on Force and Kinetics of Cardiac Muscle Contraction. *J. Gen. Physiol.* 143, 783–797. doi:10.1085/jgp.201311125

Ferrantini, C., Coppini, R., Scellini, B., Ferrara, C., Pioner, J. M., Mazzoni, L., et al. (2015). R4496C RyR2 mutation impairs atrial and ventricular contractility. *J. Gen. Physiol.* 147(1), 39–52. doi:10.1085/jgp.201511450

Ferrantini, C., Coppini, R., Pioner, J. M., Gentile, F., Tosi, B., Mazzoni, L., et al. (2017). Pathogenesis of Hypertrophic Cardiomyopathy Is Mutation rather Than Disease Specific: A Comparison of the Cardiac Troponin T E163R and R92Q Mouse Models. *J. Am. Heart Assoc.* 6, e005407. doi:10.1161/JAHA.116.005407

Ferrantini, C., Pioner, J. M., Mazzoni, L., Gentile, F., Tosi, B., Rossi, A., et al. (2018). Late sodium current inhibitors to treat exercise-induced obstruction in hypertrophic cardiomyopathy: an in vitro study in human myocardium. *Br. J. Pharmacol.* 175(13), 2635–2652. doi:10.1111/bph.14223

Gordon, A. M., Homsher, E., and Regnier, M. (2000). Regulation of Contraction in Striated Muscle. *Physiol. Rev.* 80, 853–924. doi:10.1152/physrev.2000.80.2.853

Groen, M., López-Dávila, A. J., Zittrich, S., Pfitzer, G., and Stehle, R. (2020). Hypertrophic and Dilated Cardiomyopathy-Associated Troponin T Mutations R130C and ΔK210 Oppositely Affect Length-dependent Calcium Sensitivity of Force Generation. *Front. Physiol.* 11, 516. doi:10.3389/fphys.2020.00516

Helms, A. S., Alvarado, F. J., Yob, J., Tang, V. T., Pagani, F., Russell, M. W., et al. (2016). Genotype-Dependent and -Independent Calcium Signaling Dysregulation in Human Hypertrophic Cardiomyopathy. *Circulation* 134, 1738–1748. doi:10.1161/circulationaha.115.020086

Javadpour, M. M., Tardiff, J. C., Pinz, I., and Ingwall, J. S. (2003). Decreased Energetics in Murine Hearts Bearing the R92Q Mutation in Cardiac Troponin T. *J. Clin. Invest.* 112, 768–775. doi:10.1172/jci15967

Jimenez, J., and Tardiff, J. C. (2011). Abnormal Heart Rate Regulation in Murine Hearts with Familial Hypertrophic Cardiomyopathy-Related Cardiac Troponin T Mutations. *Am. J. Physiology-Heart Circulatory Physiol.* 300, H627–H635. doi:10.1152/ajpheart.00247.2010

Kreutziger, K. L., Piroddi, N., McMichael, J. T., Tesi, C., Poggesi, C., and Regnier, M. (2011). Calcium Binding Kinetics of Troponin C Strongly Modulate Cooperative Activation and Tension Kinetics in Cardiac Muscle. *J. Mol. Cell. Cardiol.* 50, 165–174. doi:10.1016/j.yjmcc.2010.10.025

Merx, M. W., Gorressen, S., Sandt, A. M., Cortese-Krott, M. M., Ohlig, J., Stern, M., et al. (2014). Depletion of Circulating Blood NOS3 Increases Severity of Myocardial Infarction and Left Ventricular Dysfunction. *Basic Res. Cardiol.* 109, 398. doi:10.1007/s00395-013-0398-1

Miller, T., Szczesna, D., Housmans, P. R., Zhao, J., de Freitas, F., Gomes, A. V., et al. (2001). Abnormal Contractile Function in Transgenic Mice Expressing a Familial Hypertrophic Cardiomyopathy-Linked Troponin T (I79N) Mutation. *J. Biol. Chem.* 276, 3743–3755. doi:10.1074/jbc.m006746200

Moore, R. K., Abdullah, S., and Tardiff, J. C. (2014). Allosteric Effects of Cardiac Troponin TNT1 Mutations on Actomyosin Binding: a Novel Pathogenic Mechanism for Hypertrophic Cardiomyopathy. *Arch. Biochem. Biophys.* 552, 21–28. doi:10.1016/j.abb.2014.01.016

Olivotto, I., Cecchi, F., Casey, S. A., Dolara, A., Traverse, J. H., and Maron, B. J. (2001). Impact of Atrial Fibrillation on the Clinical Course of Hypertrophic Cardiomyopathy. *Circulation* 104, 2517–2524. doi:10.1161/hc4601.097997

Olivotto, I., Girolami, F., Ackerman, M. J., Nistri, S., Bos, J. M., Zachara, E., et al. (2008). Myofilament Protein Gene Mutation Screening and Outcome of Patients with Hypertrophic Cardiomyopathy. *Mayo Clinic Proc.* 83, 630–638. doi:10.1016/s0025-6196(11)60890-2

Piroddi, N., Belus, A., Scellini, B., Tesi, C., Giunti, G., Cerbai, E., et al. (2007). Tension Generation and Relaxation in Single Myofibrils from Human Atrial

and Ventricular Myocardium. *Pflugers Arch. - Eur. J. Physiol.* 454, 63–73. doi:10.1007/s00424-006-0181-3

Pistner, A., Belmonte, S., Coulthard, T., and Blaxall, B. (2010). Murine Echocardiography and Ultrasound Imaging. *J. Vis. Exp.: JoVE* 8(42), 2100. doi:10.3791/2100

Schober, T., Huke, S., Venkataraman, R., Gryshchenko, O., Kryshtal, D., Hwang, H. S., et al. (2012). Myofilament Ca Sensitization Increases Cytosolic Ca Binding Affinity, Alters Intracellular Ca Homeostasis, and Causes Pause-dependent Ca-Triggered Arrhythmia. *Circ. Res.* 111, 170–179. doi:10.1161/circresaha.112.270041

Schuldt, M., Johnston, J. R., He, H., Huurman, R., Pei, J., Harakalova, M., et al. (2021). Mutation Location of HCM-Causing Troponin T Mutations Defines the Degree of Myofilament Dysfunction in Human Cardiomyocytes. *J. Mol. Cell. Cardiol.* 150, 77–90. doi:10.1016/j.yjmcc.2020.10.006

Tardiff, J. C., Hewett, T. E., Palmer, B. M., Olsson, C., Factor, S. M., Moore, R. L., et al. (1999). Cardiac Troponin T Mutations Result in Allele-specific Phenotypes in a Mouse Model for Hypertrophic Cardiomyopathy. *J. Clin. Invest.* 104, 469–481. doi:10.1172/jci6067

Tardiff, J. C. (2005). Sarcomeric Proteins and Familial Hypertrophic Cardiomyopathy: Linking Mutations in Structural Proteins to Complex Cardiovascular Phenotypes. *Heart Fail. Rev.* 10, 237–248. doi:10.1007/s10741-005-5253-5

Vitale, G., Ferrantini, C., Piroddi, N., Scellini, B., Pioner, J. M., Colombini, B., et al. (2021). The Relation between Sarcomere Energetics and the Rate of Isometric Tension Relaxation in Healthy and Diseased Cardiac Muscle. *J. Muscle Res. Cel Motil* 42, 47–57. doi:10.1007/s10974-019-09566-2

Walklate, J., Ferrantini, C., Johnson, C. A., Tesi, C., Poggesi, C., and Geeves, M. A. (2021). Alpha and Beta Myosin Isoforms and Human Atrial and Ventricular Contraction. *Cell. Mol. Life Sci.* 78, 7309–7337. doi:10.1007/s00018-021-03971-y

Watkins, H., McKenna, W. J., Thierfelder, L., Suk, H. J., Anan, R., O'Donoghue, A., et al. (1995). Mutations in the Genes for Cardiac Troponin T and α-Tropomyosin in Hypertrophic Cardiomyopathy. *N. Engl. J. Med.* 332, 1058–1065. doi:10.1056/nejm199504203321603

Witjas-Paalberends, E. R., Ferrara, C., Scellini B, B., Piroddi, N., Montag, J., Tesi, C., et al. (2014a). Faster cross-bridge detachment and increased tension cost in human hypertrophic cardiomyopathy with the R403Q MYH7 mutation. *J. Physiol.* 592(15), 3257–3272. doi:10.1113/jphysiol.2014.274571

Witjas-Paalberends, E. R., Güçlü, A., Germans, T., Knaapen, P., Harms, H. J., Vermeer, A. M., et al. (2014b). Gene-specific increase in the energetic cost of contraction in hypertrophic cardiomyopathy caused by thick filament mutations. *Cardiovasc. Res.* 103(2), 248–257. doi:10.1093/cvr/cvu127

Yoneda, Z. T., Anderson, K. C., Quintana, J. A., O'Neill, M. J., Sims, R. A., Glazer, A. M., et al. (2021). Early-Onset Atrial Fibrillation and the Prevalence of Rare Variants in Cardiomyopathy and Arrhythmia Genes. *JAMA Cardiol.* 6, 1371–1379. doi:10.1001/jamacardio.2021.3370

Conflict of Interest: The authors declare that the research was conducted in the absence of any commercial or financial relationships that could be construed as a potential conflict of interest.

Publisher's Note: All claims expressed in this article are solely those of the authors and do not necessarily represent those of their affiliated organizations, or those of the publisher, the editors and the reviewers. Any product that may be evaluated in this article, or claim that may be made by its manufacturer, is not guaranteed or endorsed by the publisher.

Advantages of publishing in Frontiers

OPEN ACCESS
Articles are free to read for greatest visibility and readership

FAST PUBLICATION
Around 90 days from submission to decision

HIGH QUALITY PEER-REVIEW
Rigorous, collaborative, and constructive peer-review

TRANSPARENT PEER-REVIEW
Editors and reviewers acknowledged by name on published articles

Frontiers
Avenue du Tribunal-Fédéral 34
1005 Lausanne | Switzerland

Visit us: www.frontiersin.org
Contact us: frontiersin.org/about/contact

REPRODUCIBILITY OF RESEARCH
Support open data and methods to enhance research reproducibility

DIGITAL PUBLISHING
Articles designed for optimal readership across devices

FOLLOW US
@frontiersin

IMPACT METRICS
Advanced article metrics track visibility across digital media

EXTENSIVE PROMOTION
Marketing and promotion of impactful research

LOOP RESEARCH NETWORK
Our network increases your article's readership